29th

TRY-U2023

empowering young researchers for a better future

THE FUTURE OF ENVIRONMENTAL SUSTAINABILITY AND INNOVATION IN AGRICULTURE

POPULATION FOOD ENERGY ENVIRONMENT AGRICULTURE INNOVATION

at Maejo University, Chiang Mai, Thailand.

21-23 December 2023

Organized by: MJU-IC Maejo University International College

Conference Proceedings

The 29th Tri-U International Joint Seminar and Symposium

21st to 24th December 2023

Maejo University, Chiang Mai, Thailand

Conference Proceeding Book of the 29th Tri-U International Joint Seminar and Symposium

Published by
Maejo University International College,
63 Sansai-Phrao Road, Nongharn Sub-District, Sansai District, Chiang Mai Province 50290, Thailand
Website: https://triu2023-mju.com/
Email: maejointernationalcollege@gmail.com

Welcome to the 29th Tri-U International Joint Seminar and Symposium

Young scientists are future world leaders who must be prepared to overcome global problems. This idea was the primary concern that led Prof. Nobutaka ITO and Prof. Seizo KATO from the Faculty of Bio Engineering – Mie University, Japan, to initiate a forum called "The Tri-U International Joint Seminar & Symposium (Tri-U IJSS)" in 1994. This annual event is conducted to expose young scientists to international experiences while enriching their knowledge and widening their views through information exchanges of scientific and cultural backgrounds. Through intensive interaction and a friendly atmosphere, the participants representing young scientists from various countries are expected to be able to create peace in the world by having mutual respect and understanding (culture, religion, and customs/behavior).

The global problem faced worldwide has been the dramatic increase in population, which has led to issues of food security and sufficiency, as well as increasing energy demand and a disturbed environment. Thus, these four critical issues are the annual topics discussed at Tri-U IJSS: population, food, energy, and environment. Every year, there are five topics covered in the Tri-U IJSS. The host decides on the fifth topic.

The 29th Tri-University International Joint Seminar & Symposium program is 5 days program in the theme of The Future of Environmental Sustainability and Innovation in Agriculture. It is designed to enable member institutions to send student representatives to study agriculture and other fields at Maejo University. It is conducted through a series of lectures about current developments, practices, and technologies in agriculture and related fields at Maejo University. Students can visit farms, research facilities, and experiment stations during the program. They also attend and participate in discussions practicum of an existing class offered on the campus. They are also exposed to the culture and traditions of Chiang Mai city.

Table of content

18	Tianhong Yang	Reasons and Ripples of China's Population Decline
19	Yao Mengjiao	A method of seedling conveying and picking for automatic transplanter
20	Arthit Dankathok	Characteristics and properties of emulsion-based film coating from chitosan incorporated with carnauba wax
21	Wei Zhang	Agricultural product marketing strategy driven by digital and intelligent marketing concepts：a case study of Zi Chang New Farmers Association
22	Yao Feng	Current Status and Solutions of Energy and Environmental Problems
23	Liu Chengxin	Environmental Education and Public Awareness
24	Yiming Peng	Experimental Study on High Pressure Sealing Performance of Water-filled Impedance Tube
25	Tanwutta Thaisuntad	Innovation Agricultural Museum of the Maejo University
26	Supamas Thaweesuk	Assessment of the energy potential of residue materials from pineapple cultivation in the northern region of Thailand
27	Yufei Gu	Self-cleaning Integrative Aerogel for Stable Solar-assisted Desalination
28	Senaka Bandara	Sustainability evaluation of broiler waste management practices in Thailand using AHP analysis
29	Jidapa Chanjaroen	A Comprehensive Approach to Standard Time and Sustainable Waste Reduction in Granola Manufacturing for SMEs
30	Jaturong Kongwutthivech	Extraction of humic acid from Mae Moh leonardite for sustainable agriculture
31	Wahyu Nurkholis Hadi Syahputra	Integrating Advanced Neural Networks and Computer Vision for Precision Classification of Palm Oil Fresh Fruit Bunches
32	Ziyan Leung	The Environmental Governance on Dairy Cattle Breeding in Xinjiang Uygur Autonomous Region From the Perspective of Animal Welfare-Based on the Field Research with Local Farms
33	Xiaoyun Li	Climate-Related Disclosure Standards and China's Strategic Choices
34	Hongyu Zhu	Low-carbon Optimization Operation Strategy for Multi-Energy System
35	Krit Sujarittam	Recent advances in therapeutic ultrasound
36	Thitipong Thiansem	Designing Modified Covered Lagoon System for Biogas Production from Cassava Starch Wastewater
37	Yizhou Yang	Experimental Study on the Effect of Elliptical Hole Nozzle on Flash Boiling Spray of High Pressure Liquid Ammonia
38	Nipathon Wilailak	Innovation technology for encapsulation of bioactive compounds from marigold extract.
39	Li Ruihan	Medicaments Recovery and Recycling Efforts to Avoid Ecosystem Pollution Caused by the Inappropriate Disposal of Unused/Expired Pharmaceuticals.

40	Min Zhu	The Cross-species Adaptation of Influenza A Virus from Pet Dogs
41	Kritsada Sompan	New Method for Measuring Water Flow Rate in Plant Stems Using Thermoelectric Cooling Techniques
42	Sengdaeth Touysimeuang	Guidelines for Potential Management of the Natural Tourism Destination: Tad-Kamuet Waterfall, Nong Luang Village, Paksong District, Champasak Province, Lao People's Democratic Republic
43	Chimhan Panyacha	Understanding Non-Communicable Disease Risks in Buddhist Monks: A Review of Lifestyle Factors and Community-Based Solutions
44	Sarawut Polvongsri	Optimizing hot water mass flow rates into a heat exchanger for temperature control in a cricket breeding container
45	Wang Meng	The improvement of agricultural production technology can help to solve the problem of food shortage caused by the rapid increase of population
46	Tian Jinrong	Green Tourism Development and Practical Types--The Case of Tourist Spots in Guangxi Zhuang Autonomous Region
47	Theeraphol Senphan	Change in phytochemical properties of Kombucha beverage infused with Assam tea and longan juice
48	Samuel Kwesi Dunyo	The organic economy model: Nurturing sustainability and harmony
49	Fei Gao	Uncovering the potentials of long-term straw return and nitrogen supply on subtropical maize (Zea mays L.) photosynthesis and grain yield
50	Xinyi Lu	Experimental Study on the Effect of Stepped Vertical Greening Based on the Spray System on Outdoor Thermal Environment: A Case Study of Nanning City, China
51	Wang Qianyun	Food Loss and Waste in Supply Chain: Challenges and Solutions
52	Boonchai Sae-Yang	Variation of leaf architecture within F1 maize population for high-density planting
53	Wenjian Gao	Calorie Detection in Dishes Based on Deep Learning and 3D Reconstruction
54	Zhou Qiaotong	The Localization of Thailand Cuisine in China from the Perspective of Globalization-Taking Thai Restaurants in N City as an Example
55	Yannan Chen	Turning waste into treasure: An eco-friendly cellulose-based hybrid membrane derived from waste bagasse for wearable applications
56	Jidapa Chanjaroen	A Comprehensive Approach to Standard Time and Sustainable Waste Reduction in Granola Manufacturing for SMEs

The 29th Tri-U International Joint Seminar and Symposium
Maejo University, Chiang Mai, Thailand, 21–24, December 2023

Study of ozone treatment process for contaminated dried kaffir lime leaf instead of steam sterilization to reduce energy use in the re-production process

Samat Phromma[1], Parin Khongkrapan[1, *], Rotjapun Nirunsin[1] and Yardfon Tanongkankit[2]

[1]School of Renewable Energy, Maejo University, Chiang Mai, 50290 Thailand
[2]Faculty of Engineering and Agro-Industry, Maejo University, Chiang Mai, 50290 Thailand
**Corresponding author, E-mail: parin.khongkrapan@gmail.com*

Abstract: Dried kaffir lime leaf products contaminated with *Escherichia coli* (*E. coli*) are not eligible for export. To comply with safety standards, such products must undergo reprocessing processes that consist of steam sterilization followed by drying. This reprocessing method, while necessary, incurs significant costs and energy consumption. Additionally, it leads to a decrease in the nutritional quality of the food. Therefore, instead of steaming, this study investigated the application of the ozone treatment procedure to contaminated dried kaffir lime leaf. According to the findings of an experiment involving 200 kg of dried kaffir lime leaf contaminated with *E. coli* at 200 CFU/g, which were stored in a chamber for 5 to 120 min, ozone treatment procedures can reduce the amount of *E. coli* contaminants in dried kaffir lime leaf products by 10.00% to 97.50%. The ozone sterilization method can reduce the time and specific energy consumption of the reprocess processing by up to 78.57% and 99.47%, respectively. This approach is capable of significantly reducing both time and energy costs for manufacturers. Therefore, this strategy is suitable for expansion into larger food industries.

Keywords: Dried Kaffir lime leaf, Reprocessing, *E. coli*, Ozone treatment

1. Introduction

The leaves of the *Citrus hystrix* D.C. tree, commonly referred to as kaffir limes, are utilized in culinary preparations and valued for their aromatic properties. In order to ensure preservation, it is necessary to subject them to a drying process [1]. In 2003, the Ministry of Public Health (Issue 273) established guidelines stating that dried kaffir lime leaf products must have a moisture content of less than 8.00%wb, following the Standard for Food Contaminants (Version 2).

The product must not be contaminated with *E. coli* exceeding 10 CFU/g (Total Plate Count; TPC $1x10^5$ CFU/g). This announcement is the primary source of manufacturing issues that result in goods that exceed export requirements. When the product fails to meet the requirements, it cannot be exported for sale in international markets. For the reasons stated, entrepreneurs must reprocess products that do not meet the standards to ensure compliance with the law and the safety of consumers and international markets because it is shorter than making a new one. The traditional reprocessing process for contaminated dried kaffir lime leaf products involves two main steps: 1. sterilizing with a steam; and 2. drying with hot air. Both subprocesses mentioned require a substantial amount of energy and time. Moreover, the reprocessed products lose quality because of the steam sterilization, including color and aroma, which lowers the product's selling price. There is abundant research addressing the elimination of microbial contaminants in food products, with some discussing the use of ozone gas. Ozone is a powerful oxidizing agent and can be a non-chemical disinfectant because it can kill microorganisms, viruses, bacteria, and spores [2]. Cho et al. [3] reported the effect of using ozone (O_3) on the survival of *E. coli* and compared it with the use of chemicals (chlorine) and ultraviolet. The results indicated that ozone is a more effective way to reduce the amount of *E. coli* than both chlorine and ultraviolet (UV) radiation. Because the ozone stimulates bacterial cell membranes to undergo an oxidation reaction, which results in the osmotic bursting of the cells. The results of laboratory experiments by Arita et al. [4], Murakami et al. [5], and Estrela et al. [6] also found that ozone affects many types of bacteria, such as *Streptococcus mutans*, Methicillin-resistant *Staphylococcus aureus* (MRSA), and Candida albicans. Moreover, the research by Murray et al. [7] indicates that ozone therapy

can eliminate a broad range of viruses, including both enveloped and non-enveloped viruses [8]. Additionally, studies conducted by Thabet et al. [9] suggest that ozone treatment may destroy parasite eggs, such as *Schistosomiasis mansoni*, the name of the infection that causes blood flukes.

Considering how applying ozone affects the physical characteristics of crops. Rodoni et al. [10] studied the ozone application for postharvest disinfection of tomatoes at a concentration of 10 ppm for a period of 5 to 20 min. It was found that disinfection using this method did not affect the color, sugar content, acidity, or antioxidant capacity of the tested tomatoes because the number of phenolic compounds, which have antioxidant properties, increased significantly. From the above research, it can be concluded that ozone can be used to kill pathogenic microorganisms and parasites and reduce chemical contamination without causing ozone residue, which reduces the use of chemicals in washing raw materials. And, using ozone can reduce energy consumption from steaming, boiling, or heating in various sterilization processes, which benefits entrepreneurs [11]. In order to reduce the excessive specific energy consumption (SEC) of steam sterilization in the reprocessing process, this study will examine the use of the ozone treatment process on dried kaffir lime leaf contaminated with *E. coli* to compare SEC with the traditional reprocess processing that requires steam for sterilization and subsequent drying, which is both energy and time-consuming due to the two-step procedure.

2. Materials and methods

2.1 Feedstock characteristics

The experimental example used is 200 kg of the exceed standard dried kaffir lime leaf with a moisture content less than 8 % wb, contaminated with E. coli at a level of 2 0 0 CFU/g (total 5.2 x 10^5 CFU/g). They were divided into two groups. Group 1 gets treated with the traditional reprocess processing method, while Group 2 will be undergoing the ozone treatment process.

2.2 Experimental setup

2.2.1 Traditional reprocess processing method

The traditional reprocessing processing for contaminated dried kaffir lime leaf consists of two main steps. Step 1: In this phase, the contaminated dried kaffir lime leaf will be transported via a conveyor belt into a chamber for sterilization using steam at a temperature of around 100°C for 5 min. This stream sterilizer system requires an electrical power of 5.65 kW for the electrical motors and a water pump. Step 2: The moisture-sterilized kaffir lime leaf will be moved to the five dryers (40 kg per dryer), where they will undergo drying with hot air at a temperature of 50°C for about 120 min or until the moisture content of the kaffir lime leaf is below 8.00 %wb. These five dryers require an electrical power of 5.46 kW for the electrical fans and control system. The heat source of both equipment is a stream boiler that utilizes liquid petroleum gas (LPG) as a fuel, with a fuel consumption rate of approximately 25 kg/h for the stream sterilizer system and 20 kg/h for the drying system. The capacity of this reprocessing system is 28.57 kg/h.

2.2.2 Ozone treatment method

The ozone treatment process for contaminated dried kaffir lime leaf, which do not meet contamination standards in this study, involves subjecting the 200 kg of contaminated products to the same drying system used in traditional reprocessing (40 kg per dryer for 5 dryers), albeit without the sterilization step. The ozone generator for each dryer requires a power of 1.10 kW, and it can generate ozone gas at a rate of 320 g/h. Ozone gas is introduced into the drying chamber by utilizing a ¾ hp circulation fan within the dryer. The comprehensive electrical power demand for the ozone treatment process across five drying chambers is determined to be 8.31 kW.

2.3 Data analysis

For microbial analysis, 100 g of sample was randomly selected from five positions on each drying tray. Subsequently, the samples obtained were combined and sent to the Central Laboratory (Thailand) Company Limited (CLT), which is a government laboratory. Total plate count was determined following the Association of Official Analytical Chemists (AOAC) standard method (2000). For energy analysis, specific energy consumption (SEC) is the value that represents the amount of energy utilized per mass of the produced product as given by SEC= E/m [9]; where E is the energy consumption of the process (MJ), and m is the mass of contaminated dried kaffir lime leaf (kg) that passed the process.

3. Results and discussion

From the experimental results, it was found that the dried kaffir lime leaf contaminated with *E. coli* at a level of 200 CFU/g and subjected to the traditional reprocessing method exhibited specific energy consumption for the steam sterilization and drying stages of 31.90 and 10.24 kJ/kg, respectively, resulting in a total SEC of 42.14 kJ/kg. As a result, the quantity of *E. coli* contamination in the dried kaffir lime leaf processed through this method was found to be lower than 10 CFU/g, which is by the standards established by the Ministry of Public Health [2]. The production rate of this method is around 29 kg/h. According to the results of an experiment involving 200 kg of contaminated dried kaffir lime leaf (40 kg per dryer for 5 dryers), subjected to ozone treatment procedures in a chamber for 5 to 90 min, it was found that the procedures can reduce the levels of E. coli contaminants in dried kaffir lime leaf products by 30% to 85%, as shown in Figure 1.

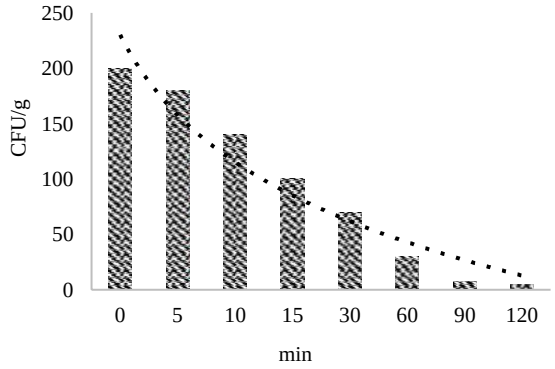

Figure 1. Number of *E. coli* at difference ozone treatment time

From Figure 1 , it can be observed that *E. coli* decreased from 200 CFU/g to below 10 CFU/g after 90 minutes. This can be calculated as a production rate of approximately 133 kg/h, approximately five times faster than the traditional method. The specific energy consumption of ozone treatment method is only 0.22 MJ/kg [3-10]. From the earlier mention, it can be observed that the ozone sterilization method can reduce the reprocessing process's time and specific energy consumption by up to 78.57% and 99.47%, respectively. The energy data, production rates, and production costs for each method are presented in Table 1.

Table 1. Energy data, production rates, and production costs for each method

Reprocessing Method		Mass	Time	Production Rate	Electricity*		Fuel (LPG)**	SEC	Cost
		(kg)	(min)	(kg/h)	(kW)	(MJ)	(MJ)	(MJ/kg)	(Baht/kg)
Traditional	Step1. Stream Sterilization	200	300	28.57	5.65	101.70	6,277.50	31.90	17.29
	Step 2. Drying		120		5.46	39.33	2,008.80	10.24	5.58
				total	11.11	141.03	8,286.30	42.14	22.88
This study	Ozone Treatment	200	90	133.33	8.31	44.89	-	0.22	0.31

* Electricity 5 Baht/kWh; **LPG 26.54 Baht/kg

4. Conclusion

The ozone treatment system in this study can effectively reduce the amount of *E. coli* in dried kaffir lime leaf products that do not meet the food standards specified by the Ministry of Public Health of Thailand. This approach can significantly reduce both time and energy costs for manufacturers. Therefore, this strategy is suitable for expansion into larger food industries.

References

[1] Pradechboon, T., Dussadee, N., Unpaprom, Y., & Chindaraksa, S. (2022). Effect of rotary microwave drying on quality characteristics and physical properties of Kaffir lime leaf (*Citrus hystrix* DC). Biomass Conversion and Biorefinery. https://doi.org/10.1007/s13399-022-02722-8 1-10.

[2] Yuliantol, E., Restiwijayal, M., Sasmital, E. et al., (2019). Power analysis of ozone generator for high-capacity production. Journal of Physics: Conf. Series, 1170, 1-7.

[3] Cho, M., Kim, J., Kim, J. Y., Yoon, J., and Kim, J. H. (2010). Mechanisms of Escherichia coli inactivation by several disinfectants. Water Research, 44(11), 3410-3418.

[4] Arita, M., Nagayoshi, M., Fukuizumi, T., et al., (2005). Microbicidal efficacy of ozonated water against Candida albicans adhering to acrylic denture plates. Oral Microbiology and Immunology, 20(4), 206-210.

[5] Murakami, H., Mizuguchi, M., Hattori, M., Ito, Y., Kawai, T., and Hasegawa, J. (2002). Effect of denture cleaner using ozone against methicillin-resistant *Staphylococcus aureus* and E. coli T1 phage. Dental Materials Journal, 21(1), 53–60.
[6] Estrela, C., Estrela, C. R., Decurcio, D. A., Silva, J. A., and Bammann, L. L., (2006). Antimicrobial potential of ozone in an ultrasonic cleaning system against *Staphylococcus aureus*. Brazilian Dental Journal, 17(2), 134–138.
[7] Murray, B. K., Ohmine, S., Tomer, D. P., Jensen, K. J., Johnson, F. B., Kirsi, J. J., Robison, R. A., and O'Neill, K. L. (2008). Virion disruption by ozone-mediated reactive oxygen species. Journal of Virological Methods, 153(1), 74-77.
[8] Pradechboon, T., Ramaraj, R., Dussadee, N., & Chindaraksa, S. (2022). Advances application of a newly developed microwave rotary dryer for drying agricultural products of red chili pepper. Biomass Conversion and Biorefinery. https://doi.org/10.1007/s13399-022-02876-5
[9] Thabet, S. S., Thabet, H. S., and Atalla, S. S. (2007). Efficacy of medical ozone in attenuation of murine *Schistosomiasis mansoni* infection morbidity. Journal of the Egyptian Society of Parasitology, 37(3), 915-944.
[10] Rodoni, L., Casadei, N., Concellon, A., Alicia, A. R. C., and Vicente, A. R., (2010). Effect of short-term ozone treatments on tomato (*Solanum lycopersicum* L.) fruit quality and cell wall degradation. Journal of Agricultural and Food Chemistry, 58(1), 594–599.
[11] Peesel, R. H., Philippa, M., Schumm, G. et al., (2016). Energy efficiency measures for batch retort sterilization in the food processing industry. Chemical Engineering Transactions, 52, 163-168.

Mr. Samat Phromma
Dehydrated Food Entrepreneur
Master Student in
Renewable Energy Engineering Program,
School of Renewable Energy,
Maejo University, Thailand.

Dr. Rotjapun Nirunsin
B.Ed., M.Ed., Ph.D.
Assistant Professor
School of Renewable Energy,
Maejo University, Thailand.
Research Interests:
Biogas Technology (Community and Industrial Scale), Biodiesel Technology, Energy Engineering.

Dr. Parin Khongkrapan
B.Eng., M.Eng., D.Eng.
Assistant Professor
School of Renewable Energy,
Maejo University, Thailand.
Research Interests:
Plasma Technology, Drying Technology, Machine Design, Energy Engineering.

Dr. Yardfon Tanongkankit
B.Sc., M.Sc., D.Eng.
Assistant Professor
Faculty of Engineering and Agro-Industry,
Maejo University, Thailand.
Research Interests:
Drying Technology, Extraction of Phytochemical Compounds, Thermal and Non-thermal Processing.

The effect of record-high gasoline prices on the consumers'new energy vehicle purchase intention: Evidence from the uniform experimental design

Huiqian Sun, Peng Jing*, Baihui Wang, Yunhao Cai, Jie Ye, Bichen Wang

School of Traffic and Automation Engineering, Jiangsu University, China, 212013
**Corresponding author, E-mail: jingpeng@ujs.edu.cn*

Abstract: Geopolitical conflicts and military actions pushed gasoline prices in China into the highest from March to April 2022 for the first time. We aim to quantitatively understand how the rising gasoline and vehicle prices affect consumers' vehicle purchase intention with different demographic characteristics simultaneously. The study applies Wilcoxon signed-rank test and Panel Data Mixed Logit model to analyze the data from the uniform experimental design. We subdivide the respondents into three groups: fuel vehicle owners, new energy vehicle owners, and car-free individuals. The findings show that if the maximum increase price of pure energy vehicles does not exceed 27,000 CNY, fuel vehicle owners will still be inclined to purchase pure energy vehicles, accompanied by China's 95 gasoline rising from 8.44 on February 18th to 9.41 CNY per liter on April 1st, 2022. However, the increasing prices are 25,000 and 22,000 CNY, which will offset the impact of rising gasoline prices on new energy vehicle owners and car-free individuals. The results have implications for introducing fuel tax to cope with adverse changes in consumers' vehicle purchase intention. The study provides theoretical support for analyzing consumers' travel behavior and vehicle purchase intention when gasoline prices have huge fluctuations in the future.

Keywords: record-high gasoline prices; rising vehicle prices; vehicle purchase intention; travel behavior; new energy vehicles

1. Introduction

Crude oil is regarded as a scarce and non-renewable resource whose price significantly impacts countries' economic development and political stability worldwide. Events such as economic changes, political upheavals, military actions, and terrorist attacks have frequently affected international crude oil prices since 2000 (Antonakakis et al., 2017; Monge and Cristóbal, 2021; Selmi et al., 2020; Song et al., 2022). In particular, military action caused by geopolitical conflicts pushed international crude oil prices to the highest in March 2022 since 2008. Volatile international markets have greatly influenced China's oil prices as China actively engages in the world oil market and depends on imports over 70% (Ma, 2020). The highest growth rates were recorded for gasoline prices from March to April 2022 in China for the first time. The sharp rising oil prices increase the cost of motorized travel and may lead to changes in travel behavior and vehicle choices (Burke and Nishitateno, 2013; Ozgur et al., 2021). Travelers may have the intention to switch from driving the vehicle to other modes, such as buses and e-bikes, due to the record-high gasoline prices. New energy vehicles with low or even independent fuel consumption provide consumers with a substitutable travel mode when gasoline prices peak.

New energy vehicle sales exceed 3.5 million in China, accounting for13.4% of total sales in 2021 (China Development Network, 2022; Liu et al., 2023), and becoming more potential in China's vehicle market (General Office of the State Council, 2020). China's passenger vehicle market has gradually formed a new-competitive situation among traditional fuel vehicles (FVs), plug-in hybrid (including extended-range) vehicles (PHVs), and pure electric vehicles (PEVs). Promoting new energy vehicles has significantly contributed to energy conservation and emission reduction. China's gasoline prices have continued to rise sharply because of the international geopolitical conflicts from March 4th to May 1st, 2022. Topics related to "new energy vehicles," "travel mode changes," and "higher driving costs" have been discussed on social media platforms widely. We made a text network analysis graph using co-word analysis based on 6,500 comments collected from

Chinese mainstream social media platforms, such as Sina Weibo and Tik Tok, from March 4th to May 1st, 2022. The results showed in Figure 1 that topics like "oil price," "electric vehicle," and "vehicle price" have become hotspots. The "rising" "oil prices" would increase consumers' willingness to use "buses" and "e-bikes." Consumers were inclined to purchase "electric vehicles" and "hybrid" vehicles compared with "fuel vehicles" during the "rising" "oil prices." Meanwhile, with concerns about the vehicle price, range, and charging piles of electric vehicles, the media have reported that consumers may change their travel behavior and purchase electric vehicles (China Economic Net, 2022; Scroll, 2022; Sina, 2022). Are the travel behavior and purchase intention in these reports consistent with the public's genuine willingness? If yes, it is still unclear to what extent consumers' travel behavior and purchase intention changed during the rising gasoline prices. Are the changes distinguished among groups of different demographic characteristics?

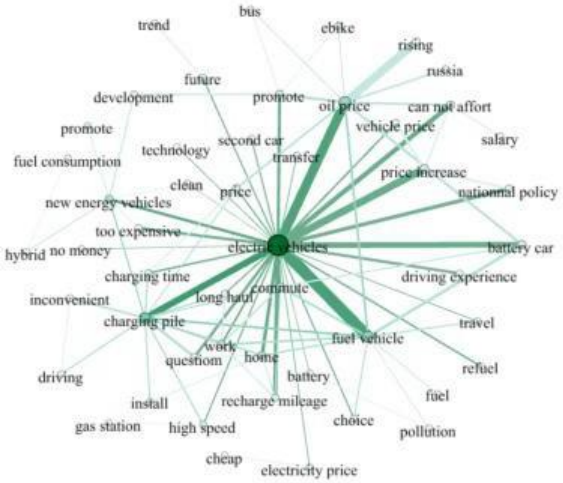

Figure 1 Text network analysis based on social media data during oil price rose (Source: Constructed by authors) Previous studies tried to quantitatively observe the changes in consumers' travel behavior and purchase intention when oil prices increased. Consumers may adopt low-cost and resource-saving travel modes with record-high gasoline prices. Song et al. (2022) and Goetzke (2021) found that the rising oil prices caused car mileage to decline significantly based on the National Household Traffic Survey data in 2009 and 2017. Du and Lin (2017) divided respondents into low and high-income categories and found that low-income consumers would drive less. The changes in oil prices are more significant than the research period mentioned above since March 4th, 2022. In addition, the research focusing on the influence of different types of owned vehicles on travel behavior is limited, including fuel vehicle owners (only with fuel vehicles), new energy vehicle owners (only with new energy vehicles), and hybrid vehicle owners (both fuel vehicles and new energy vehicles). How do record-high gasoline prices affect the travel behavior of owners with different vehicles? The share of new energy vehicles has increased sharply in China recently, making the new energy vehicle a competitive alternative when people intend to change their travel mode, especially during the record-high gasoline prices. Wang et al. (2022) assessed the connection between oil prices and vehicle sales in each subsector of the automobile market. Du and Lin (2017) analyzed how the rising oil prices impacted the vehicle purchase intention of different income groups when 95 gasoline was about 6 CNY per liter. The above studies imaged a high oil prices scenario to investigate consumers' vehicle purchase intention, which may not represent the authentic intention changes under the record-high gasoline prices. China's 95 gasoline entered the "9 CNY era" and even reached 10 CNY in some provinces on March 17th, 2022, which marks the "high gasoline prices era." Although Jing et al. (2022) explored consumers' vehicle purchase intention in the "high gasoline prices era," they neglected the impact of rising gasoline prices on travel behavior. This study addresses how consumers' travel behavior and vehicle purchase intention change in "the high gasoline prices era" simultaneously, which underlines the theoretical implications for understanding mode choice behavior and automobile market trends.Besides gasoline prices, vehicle attributes and policies also have various degrees of influence on consumers' vehicle purchase intention. Shafiei et al. (2012) found that consumers prefer new energy vehicles with rising oil prices, falling new energy vehicle prices, and increasing mileage. However, the vehicle prices of most new energy vehicle brands also increased in 2022 compared with 2021.

For example, the prices of the Tesla Model 3 all-wheel-drive version, BYD Yuan Pro series, and Xiaopeng series have increased by 28,000 CNY, 6,000 CNY, and 10,000-20,000 CNY, respectively in "the high gasoline prices era" (Li et al., 2022; Xu, 2022; Yu, 2022). Meanwhile, China's subsidy policy for purchasing new energy vehicles will be entirely abolished at the end of 2022. In addition, mileage and charging time are essential factors in consumers' purchase intention for new energy vehicles (Egbue and Long, 2012). In conclusion, the impacts of record-high gasoline prices on consumers are twofold. Firstly, adjustments in gasoline prices could affect consumers' travel behavior. Secondly,

signed-rank test to compare consumers' travel behavior before and during the record-high oil prices (Study 1). Moreover, the Panel Data Mixed Logit model investigated attributes related to consumers' vehicle purchase intention, including vehicle attributes,

individual attributes, and travel frequency changes (Study 2). It is of great significance to accurately understand consumers' travel behavior and vehicle purchase intention. This study focuses on the following questions:

(1) How will the unprecedented record-high gasoline prices simultaneously affect consumers' travel behavior and vehicle purchase intention?

(2) How will consumers' purchase intention change with the high-rise in both gasoline and vehicle prices?

(3) Will these changes differ among groups of consumers with different demographic characteristics?

The remainder of the study was organized as follows: Section 2 conducted a literature review, Section 3 described the data collection and survey design, Section 4 and Section 5 about study 1 and study 2, including their methods and results, and Section 6 discussed the findings according to the results, conclusion, implications, and limitations were detailed in Section 7.

2. Literature review

Previous studies focused on the impact of oil prices on consumers' travel behavior and vehicle purchase intention. We reviewed the relevant literature as follows.

2.1 Oil prices

Golden rain tree (*Cassia fistula*) was grown at Maejo University campus, Chiang Mai, Thailand). The ripened pods of rain tree and golden rain tree that fell on the ground were collected durng March to April of 2018. Then, the samples were dried at 50 °C for 48 hours in an oven to prevent mold growth, seed germination, and rotting. Dried samples were stored in plastic bags until experiments are performed. Batch fermentation was carried out in 100 ml bottles. Rain tree and golden rain tree pods thermal extraction as carbon sources were rapidly inoculated with 10% (v/v) actively growing RCM cell suspension. The initial pH of the medium was adjusted to 6.5 using 2 M NaOH and 1 M HCl. To generate an anaerobic condition, the medium was spared with oxygen-free nitrogen gas for 4 min Before inoculation, the medium was sterilized at 121 °C for 15 min, followed by inoculation with inoculum culture (OD660 = 1.5~2.0) of *C. acetobutylicum* TISTR 2375 (4.5 ml cell suspension in 45 ml medium). The fermentation was operated at 35 °C for 120 hour [9-12]. The samples were withdrawn at time intervals of 24 hours for analysis. Prior to analysis, the samples were centrifuged at 8,000 rpm for 15 min. Events such as economic changes, political upheavals, military actions, and terrorist attacks have frequently affected international crude oil and China's gasoline prices. We analyzed 5,253 international crude oil prices (dollars/barrel) and 229 China's gasoline prices (CNY/ton) with box plots from 2003 to 2022 to ensure data integrity and continuity, as shown
in Figures 2 and 3.

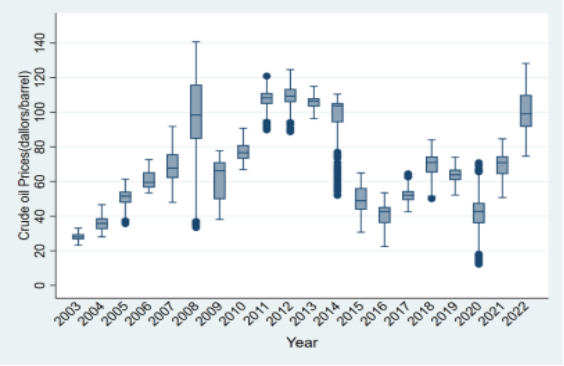

Figure 2. International crude oil prices from 2003 to 2022 (Source: Constructed by authors and the data from "https://www.opec.org/basket/basketDayArchives.xml") International crude oil prices reached the peak affected by falling inventories, strong demand from emerging economies, and geopolitical tensions in 2008. The median international crude oil price was 98.38 dollars/barrel in 2008, and the maximum data reached a record level of 140.73 dollars/barrel on July 3rd. In 2022, geopolitical conflicts and military actions also pushed international crude oil prices to the highest, except in 2008. The maximum, median, and minimum data value of international crude oil prices was 128.27, 99.13, and 74.66 dollars/barrel, respectively. The median value of international crude oil price in 2022 was slightly higher than in 2008, but the magnitude of the change was smaller.

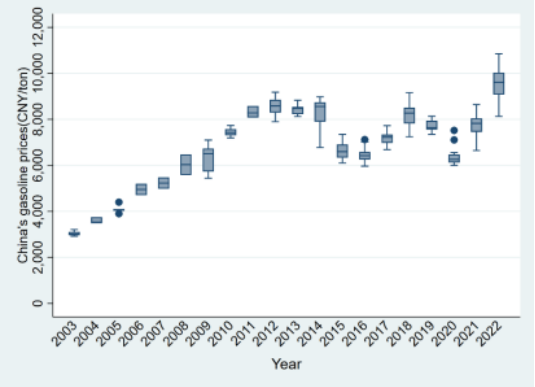

Figure 3. China's gasoline prices from 2003 to 2022
(Source: Constructed by authors and the data from "https://data.eastmoney.com/cjsj/yjtz/default.html")

Figure 3 shows that China's gasoline prices reached the highest level and exceeded 10,000 CNY per ton for the first time in 2022, influenced by geopolitical conflicts and military actions. In 2022, the maximum (10,850 CNY/ton), median (9,610 CNY/ton), and minimum data (8,130 CNY/ton) of China's gasoline prices almost recorded their highest values. Specifically, we presented China's gasoline prices in 2022 with a bar graph (Figure 4) using the 24 data and analyzed the changes in gasoline prices over the data collection emphatically.

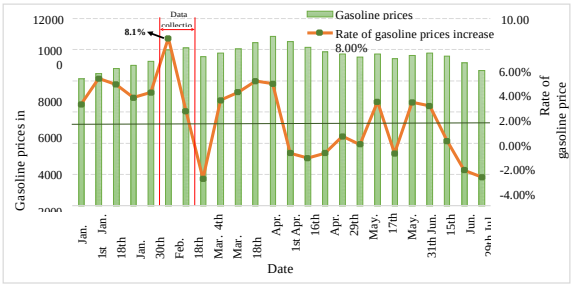

Figure 4. China's gasoline prices fluctuation in 2022
(Source: Constructed by authors and the data from "https://data.eastmoney.com/cjsj/yjtz/default.html")

China's gasoline prices fluctuated almost every 10 working days in 2022, except in October. The gasoline prices in China increased continuously during data collection from March to April 2022. The record-high gasoline prices and the time lag with consumers' responses were considered in our study. China's gasoline prices exceeded 10,000 CNY/ton for the first time on March 18th and increased by 750 CNY/ton compared to the price on March 4th. The gasoline prices recorded the highest growth rate (8.1%) in 2022 on March 18th and continued to increase on April 1st, reaching 10,115 CNY/ton.

Researchers have paid extensive attention to the impact of oil prices on consumers' travel behavior and new energy vehicle purchase intention. Khoo et al. (2012) found a potential travel mode shift from private vehicles to public transport with rising oil prices. Du and Lin (2017) examined the impact of oil price changes on Chinese consumers' purchase intention due to a slight increase in 2016. The results showed that only when the gasoline price rose above 10 CNY per liter would high-income consumers with potential purchase intention choose low-emission vehicles. The sharp rising gasoline prices are not only related to the consumers' travel behavior but also affect their vehicle purchase intention.

2.2 Travel behavior

Oil prices would affect consumers' travel behavior inevitably. Lee and Lovellette (2011) revealed that oil price fluctuations significantly impacted fuel vehicle owners more than pure electric vehicle owners. Hu et al. (2011) illustrated that consumers prefer public transport as high oil prices reduce consumers' demand for

fuel vehicle travel. Zhao and Miao (2012) found that owners with higher annual income and longer annual mileage were less sensitive to high oil prices. Consumers are more likely to start reducing the usage of private vehicles when gasoline prices rise above 10 CNY per liter. Wang et al. (2013) found that reducing the vehicle travel frequency, changing travel mode, and avoiding traveling during peak hours are the most frequent choices in response to increasing oil prices. Fluctuations in oil prices have different impacts on consumers' travel behavior.

The National Development and Reform Commission (NDRC) indicates that China's gasoline and diesel oil prices would reach a ceiling if the international crude oil prices rose to 130 dollars per barrel from the notice of "Oil Price Management Measures." (National Development and Reform Commission, 2016). The international crude oil price was 128.42 dollars/barrel on March 9th, 2022 (Organization of the Petroleum Exporting Countries, 2023). At the same time, China's 95 gasoline prices were generally close to 10 and even exceeded 10 CNY per liter in Hainan and Xizang. Previous studies have focused on the impact of 95 gasoline prices below 10 CNY per liter on consumers' travel behavior. However, the 95 gasoline prices exceeded 10 CNY per liter in April 2022, which is the ceiling in history. Consumers' travel behavior may change significantly due to record-high gasoline prices. It is significant to investigate consumers' travel behavior when 95 gasoline prices are about to break through 10 CNY per liter massively. The study will provide theoretical support for analyzing consumers' travel behavior when gasoline prices fluctuate significantly in future major events.

2.3 Vehicle purchase intention

Besides oil prices, vehicle prices also significantly impact consumers' purchase intention. Qian and Soopramanien (2011) used the discrete choice model to analyze the purchase intention of Chinese consumers for traditional fuel vehicles, hybrid electric vehicles, and pure electric vehicles. The results showed that vehicle prices significantly affect consumers' purchase intention. Rasouli and Timmermans (2016) found that when pure electric vehicle prices are much higher than traditional fuel vehicle prices, there is an exceptionally high heterogeneity of consumers' vehicle purchase intention. Wang et al. (2013) revealed that vehicle price is one of the most critical factors affecting Chinese consumers' purchase intention of new energy vehicles. The average vehicle prices of the vast majority of the top 15 new energy vehicle brands in China increased in 2022 compared to 2021, except Tesla and Geely had a slight reduction (as shown in Table 1). Further analysis showed that the average price of Tesla also increased in April 2022. The effect of new energy vehicle prices on consumers' vehicle purchase intention in the previous studies may not apply to the situation as the gasoline and vehicle prices are rising simultaneously in China.

Table 1 New energy vehicle prices of the top 15 brands in 2021 and 2022

Brands	Price in 2022 (1,000 CNY)	Price in 2021 (1,000 CNY)	The ratio of price rise or decline in 2022	Market share (2022)
BYD	207.0	176.5	+17.3%	34.73%
SGMW	89.6	62.2	+44.1%	9.89%
Tesla	304.1	319.3	-4.8%	9.69%
Changan	92.5	88.3	+4.8%	4.93%
AION	177.3	164.7	+7.7%	4.69%
Chery	165.5	154.5	+7.1%	4.01%
Geely	148.5	158.7	-6.4%	3.47%
NIO	461.5	432.3	+6.8%	2.64%
Leapmotor	155.4	144.1	+7.8%	2.39%
Greatwall	266.8	259.8	+2.7%	2.34%
SAIC	178.4	145.3	+22.8%	2.06%
Volkswage	257.1	242.5	+6.0%	2.05%

Note: the data from "https://car.autohome.com.cn/price/series"

In addition to the vehicle prices, the cruising range and charging time of new energy vehicles also influence the consumer's purchase intention (Qi et al., 2021; Sierzchula et al., 2014). Dimitropoulos et al. (2013) examined that new energy vehicles with a more extended range will push consumers to purchase them. At present, most fuel vehicles can be refueled in about 5 minutes. However, new energy vehicles need about 30 minutes to be fully charged at a fast-charging station, and it even takes more than 10 hours to charge from a 110V or 220V socket. Compared with traditional vehicles, new energy vehicles have a longer charging time, which will hinder people from purchasing new energy vehicles. However, rising gasoline prices may reduce the expectations for cruising range and charging time, thus increasing the consumers' purchase intention of new energy vehicles.

In conclusion, this study examined the impacts of consumers' travel behavior and vehicle purchase intention due to record-high gasoline prices. Besides, we explored the combined effects of rising gasoline and vehicle prices on consumers' vehicle purchase intention. Understanding the changes in consumers' travel behavior and vehicle purchase intention is valuable to formulating vehicle prices and emissions mitigation policies.

3. Data collection and survey design

We designed a questionnaire to investigate the effect of record-high gasoline prices on consumers' travel behavior and vehicle purchase intention in China. The key factors that affect consumers' vehicle purchase intention are measured through the uniform design in the Stated Preference survey, such as vehicle prices and subsidies.

3.1 Survey methods

This questionnaire was divided into two parts. The first part investigated individual socioeconomic attributes, such as age, gender, occupation, education level, and travel frequency for various modes before and during the record-high gasoline prices. The second part was the Stated Preference survey, which aimed to understand the key factors influencing consumers' vehicle purchase intention.

The purpose of the Stated Preference survey was to obtain consumers' subjective preferences for multiple scenarios under hypothetical conditions. Jing et al. (2012) indicated that the questionnaire is usually designed by mathematical methods such as orthogonal design and uniform design to reduce the correlation between the questionnaire's options. The uniform experimental design method requires that the test points are "evenly dispersion" and the number is small, which can make up for the deficiency of orthogonal design (Jing et al., 2012). The smaller the centralization L2 deviation is, the more reasonable the uniform design table is (Fang, 2004). The centralized L2 deviation of our experiments is at least 0.0437, which indicates that the uniform experimental design table is reasonable. We referred to the vehicle attributes released by Autohome and Yiche to determine vehicle attributes to ensure that the scenario is consistent with the actual situation (Autohome, 2022; Yiche, 2022). Our study focused on three critical attributes of PHVs and PEVs: vehicle prices, maximum cruising range, and charging time. Combined with the uniform experimental design table of six factors and five levels, the survey scheme was obtained, as shown in Table 2.

We added preconditions for 95 gasoline prices to each survey scheme to analyze the impact of rising gasoline prices on consumers' vehicle purchase intention, which were 6, 8, and 10 CNY per liter, respectively. Five schemes and three 95 gasoline prices formed fifteen survey scenarios. According to the schemes, we divided the second part of the questionnaire (five schemes as shown in Table 1) into three sets to avoid respondents' boredom and guarantee the reliability of the results. One of the schemes was randomly assigned to two questionnaires, each containing two schemes (6 scenarios). We randomly distributed these questionnaires to respondents; each questionnaire could obtain six observations.

Table 2 Stated Preference survey schemes

Scheme	FVs			PHVs			PEVs		
	Vehicle price/CNY	Charging time/min	Maximum cruising range/km	Vehicle price/CNY	Charging time/min	Maximum cruising range/km	Vehicle price/CNY	Charging time/min	Maximum cruising range/km
1	150,000	5	700	150,000	40	1200	250,000	70	400
2	150,000	5	700	250,000	30	1000	200,000	30	700
3	150,000	5	700	300,000	60	900	300,000	60	500
4	150,000	5	700	100,000	50	800	100,000	50	600
5	150,000	5	700	200,000	70	1100	150,000	40	300

3.2 Data collection

We recruited participants from Sojump, one of the largest online survey platforms in China, with more than 60 million registered users with diverse demographic backgrounds in 2022. The data from Sojump has been widely used in Chinese consumer studies (Akhtar et al., 2020; Chu and Chen, 2019; Sheng et al., 2019). The detailed process of questionnaire collection is as follows in Figure 5.

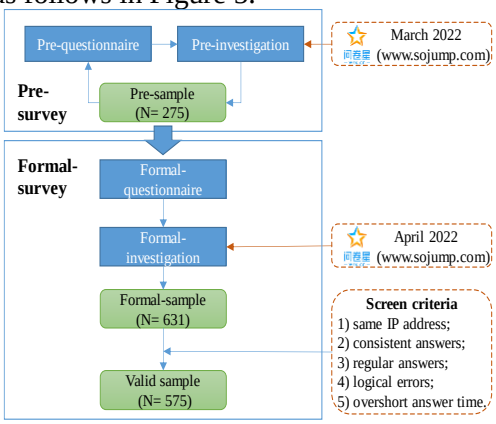

A pre-investigation was conducted through Sojump, and obtained 275 samples on March 19th and 20th, 2022, to evaluate the feasibility and readability of the questionnaire. The questionnaire was adjusted based on the feedback from the data analysis of the pre-investigation. A formal survey using the revised questionnaire was also carried out through Sojump from April 9th to 12th, 2022. A total of 631 questionnaires were collected. We screened out 56 invalid questionnaires according to the five criteria: 1) same IP address; 2) consistent answers; 3) regular answers; 4) logical errors; 5) overshort answer time.

For example, sixteen respondents reported consistent or regular answers; twelve respondents selected the primary school graduate and below as their education level, but the occupation choice was still a full-time student. Finally, 575 valid questionnaires were obtained with a recovery rate of 91.1%. A total of 3450 observations were collected as each questionnaire obtained six observations.

Figure 5. The process of questionnaire collection (Source: Constructed by authors). Our survey engaged in paid sample service to randomly deliver questionnaires to ensure data quality and representativeness from the Sojump sample database in China. Participants who completed the questionnaire successfully would get a monetary reward. The questionnaires were distributed on non-working days to reduce the possibility that workers do not have time to fill them in. Moreover, to avoid participants' boredom and guarantee the reliability of the survey data, the five schemes in the Stated Preference survey were assigned to three questionnaires randomly. We also determined the criteria for screening invalid questionnaires

to ensure data quality when processing the data.

3.3 Descriptive statistical analysis

The socioeconomic attributes of the respondents are shown in Table 3.

Table 3 shows that the proportion of male and female respondents was 54.61% and 45.39%, respectively. The respondents were between 18 and 65 years old, with 69.57% being between 26 and 34 years old. Most respondents have a bachelor's degree or above, accounting for 83.30%. Regarding occupation, management staff accounted for the highest proportion at 27.48%, and technical R&D staff followed at 13.04%. The vast majority (57.91%) of respondents only owned fuel vehicles, and 14.26% only owned new energy vehicles. Respondents with fuel and new energy vehicles simultaneously accounted for 17.57%. The results of the data analysis indicated that the questionnaires were collected from 29 provincial regions, accounting for 29/34 as a total of 34 provincial administrative regions in China. The male/female ratio of respondents (1.2:1) was close to that of data from the Seventh National Population Census in China (1.1:1) (National Bureau of Statistics, 2021). However, our sample overrepresented young-aged, middle-aged, and well-educated groups, which may be due to the skew of Sojump's participant pool. The sample limitation will be highlighted again in the Conclusion and policy implication.

We conducted two studies based on the survey data: Study 1 analyzed vehicle travel frequency to capture the impact of gasoline prices on travel behavior, and Study 2 explored the effect of the vehicle attributes, environment attributes, individual characteristics, and travel behavior (changes obtained from study 1) on consumers' vehicle purchase intention.

Variable	Categories	Sample size	Percent/%
Gender	Male	314	54.61
	Female	261	45.39
Age	≤25	101	17.57
	26-35	400	69.57
	36-45	57	9.91
	46-55	14	2.43
	≥56	3	0.52
Marital status	Married	442	76.87
	Unmarried	133	23.13
Education	College graduate and below	96	16.70
	Bachelor graduate	444	77.21
	Graduate student and above	35	6.09
Occupation	Student	32	5.57
	Production staff	37	6.43
	Sales staff	31	5.39
	Marketing/public relations staff	28	4.87
	Administrative/logistics staff	42	7.30
	Human resources	26	4.52
	Finance staff	42	7.30
	Clerical staff	48	8.35
	Technical R&D staff	75	13.04
	Management staff	158	27.48
	Other	56	9.74
Monthly income	≤3000 CNY	41	7.13
	3001-5000 CNY	69	12.00
	5001-10000 CNY	274	47.65
	10001-15000 CNY	125	21.74
	15001-20000 CNY	39	6.78
	≥20001 CNY	27	4.70
Driving license	Yes	549	95.48
	No	26	4.525
Types of vehicles owned	No vehicle	59	10.26
	Only fuel vehicles	333	57.91
	Only new energy vehicles	82	14.26
	Own fuel vehicles and new energy vehicles	101	17.57

4. Study 1

Study 1 explored the changes in consumers' travel behavior affected by record-high gasoline prices in China, using survey data on travel frequency.

4.1 Method

The Wilcoxon signed-rank test was named for Frank Wilcoxon, who also proposed the Wilcoxon-rank-sum test (Wilcoxon, 1945). Wilcoxon signed-rank test is a non-parametric statistical test used to analyze the matched-pair data on a single sample (Woolson, 2007). Wilcoxon signed-rank test is suitable for handling small sample sizes, non-normal distribution, and ordered measurements compared with other statistical tests, such as t-test (Bowerman, 2017). Thus, the Wilcoxon signed-rank test is suitable for analyzing ordinal categorical variables (Keller, 2022). The responses to question items about travel frequency in our survey ("how often do you currently travel per week in each of the following travel modes?" and "before the surge in China's gasoline prices (By February 24, 2022), how often do you currently travel per week in each of the following travel modes?") were divided into five categories: 0 times a week; 1~2 times a week; 3~4 times a week; 5~6 times a week; and 7 times a week or more.

Therefore, the Wilcoxon signed-rank test was compatible with comparing vehicle travel frequency for respondents before and during the record-high gasoline prices. The null hypothesis is stated as H0: $\theta=0$ means that the distribution of vehicle travel frequency differences before and during the record-high gasoline prices symmetry to 0 corresponds to no difference between the two samples.

Respondents are divided into three groups according to the types of vehicles they own: fuel vehicle owners (only with fuel vehicles), new energy vehicle owners (only with new energy vehicles), and hybrid vehicle owners (both fuel vehicles and new energy vehicles). According to the descriptive statistical analysis in Table 3, 59 respondents without a vehicle were excluded from study 1. Finally, study 1 contained 516 individuals: fuel vehicle owners (N=333), new energy vehicle owners (N=82), and hybrid vehicle owners (N=101).

Results

The Wilcoxon signed-rank test results of the record-high gasoline prices' impact on the vehicle usage frequency in the three groups are shown in Table 4. The Wilcoxon signed-rank test results showed that the sharp rising gasoline prices had a significantly negative effect on the travel frequency (Z=-4.275, P<0.001) and led to a reduction in the average vehicle travel frequency for the fuel vehicle owners.

Table 4 The impact of the record-high gasoline prices on the vehicle usage frequency

	Travel frequency	Before the rising/%	During the rising/%	*Z* value	*P* value
Fuel vehicle owners	0 times a week	1.14	2.28	-4.275	0.0000
	1-2 times a week	17.38	18.23		
	3-4 times a week	24.5	29.34		
	5-6times a week	31.34	33.62		
	7 times a week or more	25.64	16.52		
New energy vehicle owners	0 times a week	2.44	3.66	0.682	0.4921
	1-2 times a week	23.17	13.41		
	3-4 times a week	21.95	25.61		
	5-6times a week	34.15	45.12		
	7 times a week or more	18.29	12.2		
Hybrid vehicle owners	0 times a week	2.7	1.8	1.142	0.2765
	1-2 times a week	15.32	9.91		
	3-4 times a week	20.72	25.23		
	5-6times a week	34.23	36.04		
	7 times a week or more	27.03	27.03		

However, there was no significant change in the vehicle usage frequency of new energy owners (Z=0.682, P>0.1) and hybrid vehicle owners (Z=1.142, P>0.1). Do the changes in vehicle travel frequency affect consumers' purchase intention among FVs, PHVs, and PEVs in "the high gasoline prices era"? Study 2 was conducted to test the relationship between travel behavior and purchase intention.

5. Study 2

Study 2 estimated the impact of vehicle attributes, environment attributes, individual characteristics, and vehicle travel frequency on consumers' purchase intention among FVs, PHVs, and PEVs.

5.1 Method

The Panel Data Mixed Logit (PDML) model is one of the widely used discrete choice models, which could handle data with panel effects effectively (Ali et al., 2021; Bliemer and Rose, 2010; Chen et al., 2018; Grigolon et al., 2013). The model accounts for individual heterogeneity of preferences and explains the decision process among a set of alternatives. The PDML model generally serves panel data, which is the data for multiple entities that observe each entity at two or more periods (Stock and Watson, 2003). The panel data can also be understood as consisting of multiple observations on each sampling unit and observed at repeated points in time (Badi, 1998). Therefore, the PDML model is applicable to Stated Preference survey data containing multiple scenarios, which can not only horizontally compare the change of selection Table 5 Calibration results of the PDML model behavior in different scenarios, but also excavate the factors affecting the selection behavior in the same scenario (Yang et al., 2016). In the Stated Preference survey of this study, respondents are required to make repeated choices for five scenarios with 95 gasoline prices of 6, 8, and 10 CNY per liter. Overall, the PDML model is suitable for the experimental data of 15 different scenarios in our study.

5.2 Results

Based on the PDML model, we chose vehicle attributes, environment attributes, and individual characteristics as variables for an alternative selection. The effects of these variables on consumers' intention to purchase FVs, PHVs, and PEVs were also estimated. The FVs were set as the base category in the PDML model, and the estimated parameters indicate the difference between the corresponding category (PHVs or PEVs) and the base category. We recovered 575 valid samples in 15 scenarios by Stated Preference survey, containing a total of 3450 observations. The results are summarized in Table 5..

As shown in Table 5, the respondents with bachelor's or higher levels degrees preferred to purchase PHVs (β=1.056, p<0.01; β=0.896, p<0.05) and PEVs (β=1.457, p<0.01; β=0.840, p<0.1) compared with FVs. Specifically, the respondents' travel frequency affected by record-high gasoline prices was also a significant factor that negatively impacted the PHVs' purchase intention (β=-0.261, p<0.05). Moreover, vehicle prices significantly impacted the respondents' purchase preferences (β=-0.382, p<0.01). Recharge mileage significantly affected vehicle purchase intention (β=0.001, p<0.01). The higher the gasoline prices, the more the respondents were inclined to purchase PHVs (β=1.036, p<0.01) and PEVs (β=1.874, p<0.01). Meanwhile, we found that the subsidy policy significantly affected consumers' purchase intention for PHVs (β=0.135, p<0.01) and PEVs (β=0.048, p<0.01). In terms of charging convenience, the popularity of charging stations was related to the purchase intention of PHVs (β=0.255, p<0.1) and PEVs (β=0.396, p<0.05) positively.

6. Discussion

The study of consumers' travel behavior and purchase intention is particularly significant now that China's record-high gasoline prices are spreading from March 4th to May 1st, 2022. Our study examined consumers' travel behavior changes before and during record-high gasoline prices. Moreover, consumers' vehicle purchase intention was analyzed under the complex scenario within the booming new energy vehicle market, record-high gasoline prices, rising vehicle prices, and receding subsidies. The average price of 95 gasoline rose from 8.44 on February 18th to 9.41 CNY per liter on April 1st, recording the highest gasoline prices in China, as

Variable attributes	Variable	Vehicle type					
		PHVs			PEVs		
		Coefficient	Std. error	*P*-value	Coefficient	Std. error	*P*-value
Vehicle attributes	vehicle prices	-0.392***	0.046	0.000	-0.392***	0.046	0.000
	charging time	0.001	0.002	0.703	0.001	0.002	0.703
	recharge mileage	0.001***	0.000	0.000	0.001***	0.000	0.000
Environment attributes	oil prices	1.036***	0.051	0.000	1.874***	0.063	0.000
	purchase subsidy	0.135***	0.040	0.001	0.148***	0.048	0.002
	charging convenience	0.255*	0.140	0.069	0.396**	0.175	0.024
Individual characteristics	female	-0.044	0.118	0.708	0.074	0.143	0.604
	more than 30 yeaes old	-0.127	0.123	0.302	-0.041	0.149	0.782
	married	-0.188	0.155	0.225	-0.290	0.191	0.129
	bachelor's degree	1.056***	0.276	0.000	1.457***	0.350	0.000
	above	0.896**	0.346	0.010	0.840*	0.442	0.057
	monthly income	0.001	0.000	0.588	0.001	0.000	0.598
	license	-0.004	0.315	0.988	0.284	0.540	0.874
	technical staff	-0.022	0.129	0.866	0.037	0.1569	0.814
	new energy vehicles	0.918***	0.129	0.000	1.132***	0.156	0.000
	no vehicle	0.680***	0.220	0.002	0.828***	0.274	0.003
	income drops due to pandemic	-0.049	0.128	0.697	0.070	0.157	0.653
	income rises due to pandemic	-0.016	0.327	0.960	0.865**	0.371	0.020
	planning to buy or change a car after a year	-1.152	0.118	0.198	-0.141	0.144	0.327
	planning to buy a plug-in hybrid vehicle	1.190***	0.195	0.000	1.175***	0.256	0.000
	planning to buy a pure electric vehicle	0.828***	0.205	0.000	2.656***	0.265	0.000
	vehicle travel frequency drops	-0.261**	0.128	0.041	-0.237	0.157	0.130
Model fit	Wald chi2(41) =1103.73	Log likelihood = -2290.127			Prob > chi2= 0.0000		

Note: *** $P < 0.01$, ** $P < 0.05$, * $P < 0.1$

shown in Figure 6. We discussed the comprehensive effect of rising gasoline and PEV prices on vehicle purchase intention based on the fluctuations of China's 95 gasoline prices.

Figure 6. China's 95 gasoline fluctuation before and during the war (Source: Constructed by authors)

6.1 Travel behavior

Based on Study 1, we discussed the impact of record-high gasoline prices on vehicle travel frequency in different groups (fuel vehicle owners, new energy vehicle owners, and hybrid vehicle owners). For fuel vehicle owners, there was a significant correlation between record-high gasoline prices and consumers' travel frequency, reducing their vehicle usage. The result was consistent with prior work that car-owners consumers drive less with rising gasoline prices (Du and Lin, 2017). However, the travel frequency of new energy vehicle owners had no significant difference before and during record-high gasoline prices. Gender did not significantly affect vehicle trip frequency before the record-high gasoline prices. During the record-high gasoline prices, females' vehicle travel frequency was significantly less than males. Females were more affected by record-high gasoline prices and decreased vehicle travel frequency than males. We divided respondents into high-income and low-income groups using the 7,000 CNY, which was the average monthly income of the Chinese in 2020. Consumers with a low income below 7,000 CNY were more likely to reduce their vehicle travel frequency.

;

6.2 Vehicle purchase intention

Study 2 showed that compared with the FVs gasoline prices positively affected consumers' PEVs purchase intention while PEV prices significantly negatively impacted. The average price of 95 gasoline rose from 8.44 on February 18th to 9.27 on March 18th and 9.41 CNY per liter on April 1st. Meanwhile, with the rising gasoline prices, the sale prices of PEVs rose between 6,000 and 30,000 CNY in March 2022 (Jiao and Li, 2022; Peng, 2022). Therefore, we increased the PEV prices by 10,000, 20,000, and 30,000 CNY to explore the impact of the high rise in both gasoline and vehicle prices on Table 6 Changes in the selection probability of each group the consumers' vehicle purchase intention quantitatively based on the results of Study 2. Economic conditions also affected consumers' perceptions of gasoline and vehicle prices. Thus the ratio of gasoline and vehicle prices to the consumer's monthly income was adopted for marginal effect analysis. Vehicle types may also influence consumers' purchase intention of PEVs. We subdivided the respondents into fuel vehicle owners, new energy vehicle owners, and car-free individuals.

6.2.1 Changes in selection probability with the rising gasoline and vehicle prices

China's 95 gasoline prices rose from 8.44 on February 18th to 9.41 CNY per liter on April 1st. With the rising prices of PEVs, the selection probability changes for FVs, PHVs, and PEVs of the three respondent groups are shown in Table 6.

As shown in Table 6, the selection probability for FVs and PEVs in different groups would reduce significantly with the gasoline and PHV prices increasing by 0.97 CNY per liter and 30,000 CNY. Conversely, respondents were more likely to choose the PHVs with the rising gasoline and PEV prices. In particular, the increasing gasoline and PEV prices significantly impacted car-free individuals, and the probability of choosing PHVs increased by 3.4%. In other words, a high rise in both gasoline and PEV prices urged car-free individuals to be more inclined to purchase PHVs.

6.2.2 Offset mechanism of three groups with vehicle or gasoline prices

The increase in PEV prices had the greatest impact on the selection of PEVs for new energy vehicle owners when the 95 gasoline price is 8.44 CNY per liter. The corresponding increase in gasoline prices for three groups maintaining the selection

probability of PEVs is shown in Table 7. We had the following discussion on the premise that the PEV prices would increase by 30,000 CNY. When the 95 gasoline prices rose by 1.12 and 1.21 CNY per liter, there was no significant change in the intention of fuel vehicle owners and new energy vehicle owners to purchase PEVs. The intention of car-free individuals purchasing PEVs did not change significantly when the gasoline price rose from 8.44 to 9.76 CNY per liter.

Gasoline prices rose from 8.44 CNY per liter on February 18th to 9.27 CNY per liter on March 18th and further to 9.41 CNY per liter on April 1st, 2022. The maximum increase in PEV prices was shown in Table 8 to keep the consumers' PEV purchase intention from falling significantly.

We discussed the following on the premise that 95 gasoline prices have risen from 8.44 to 9.41 CNY per liter. The willingness of fuel owners to purchase PEVs would be offset when the PEV prices increase by more than 27,000 CNY. When the PEV prices exceeded 25,000 CNY, the high prices of PEVs would offset the willingness of new energy vehicle owners to purchase PEVs. Besides, the intention of car-free individuals to purchase PEVs would be offset when the PEV prices increased by more than 22,000 CNY.

In conclusion, we considered the comprehensive effect of gasoline and vehicle prices on the consumers' PEV purchase intention with different vehicle types. As shown in Figure 7, the results of this research provided a more hierarchical theoretical reference for promoting the development of the new energy vehicle market.

7. Conclusion and Policy Implications

Our study focused on record-high gasoline prices across China from February 18th to April 1st, 2022. We used the data collected through the uniform experimental design conducted by Sojump in China. A total of 3450 observations from 575 respondents were deemed usable for the analysis. The study could be divided into two

Vehicle price increase/ CNY	Fuel vehicle owners/%			New energy vehicle owners/%			Car-free individuals /%		
	FVs	PHVs	PEVs	FVs	PHVs	PEVs	FVs	PHVs	PEVs
+10000	-3.50	+1.40	+2.10	-2.40	+0.90	+1.50	-3.70	+1.70	+2.00
+20000	-3.10	+2.30	+0.80	-2.20	+2.00	+0.20	-3.40	+2.60	+0.80
+30000	-2.70	+3.20	-0.50	-1.90	+3.00	-1.10	-3.00	+3.40	-0.40

Table 7 Increase of 95 gasoline prices by groups under the change of PEV prices

Vehicle price increase/ 10000 CNY	Gasoline price increase CNY/liter					
	Fuel vehicle owners	*p*	New energy vehicle owners	*p*	The car-free individuals	*p*
+10000	8.44—>8.78	0.738	8.44—>8.82	0.885	8.44—>8.86	0.950
+20000	8.44—>9.16	0.984	8.44—>9.23	0.975	8.44—>9.31	0.950
+30000	8.44—>9.56	0.852	8.44—>9.65	0.954	8.44—>9.76	0.992

Table 8 The maximum increase in PEV prices by groups under the change in 95 gasoline prices

Gasoline price increase CNY/liter	New energy vehicle price increase/ CNY					
	Fuel vehicle owners	*p*	New energy vehicle owners	*p*	Car-free individuals	*p*
8.44—>9.27	+23000	0.999	+21000	0.987	+19000	0.990
8.44—>9.41	+27000	0.995	+25000	0.990	+22000	0.997

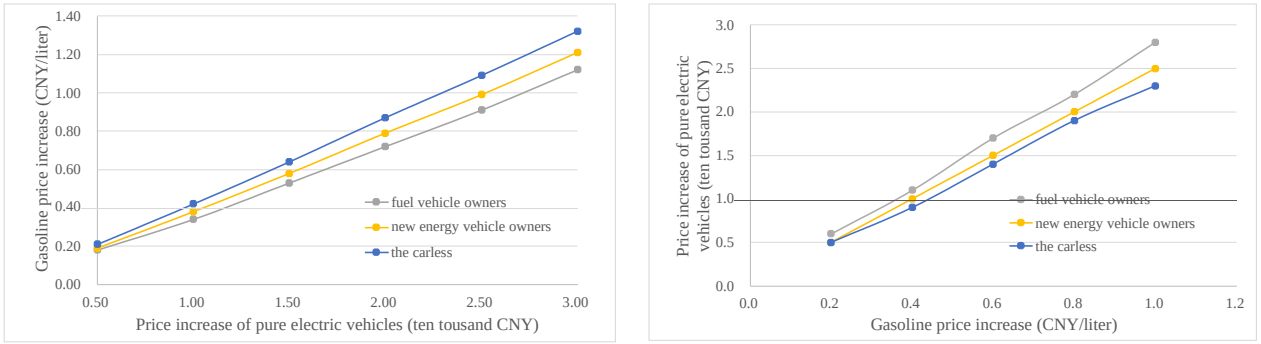

(a) 95 gasoline prices offset changes in PEV prices (b) PEV prices offset changes in 95 gasoline prices

Figure 7. The offsetting mechanism of PEV prices and 95 gasoline prices for each group (Source: Constructed by authors)

parts: how the record-high gasoline prices affected consumers' travel behavior and vehicle purchase intention. In addition, we discussed the comprehensive effect of rising 95 gasoline and PEV prices on consumers' PEV purchase intention with different demographic characteristics. The following observations were obtained:

The sharp rising gasoline prices had a significantly negative effect on the travel frequency of fuel vehicle owners. Furthermore, female and low-income consumers' vehicle travel frequency significantly decreased during the record-high gasoline prices, which differed from the results before the rising. For the vehicle purchase intention, the results showed that the consumers' travel behavior affected by record-high gasoline prices was also a significant factor that may impact the vehicle purchase intention, and vehicle prices had a significant negative impact on the consumers' vehicle purchase preferences.

Therefore, we discussed the combined effect of rising 95 gasoline and PEV prices on consumers' vehicle purchase intention based on the increase in gasoline and vehicle prices in real-life situations. The results suggested that the record-high gasoline prices could offset the negative impact of the increase in the PEV prices on consumers' vehicle purchase intention. For fuel vehicle owners, if the maximum increase in PEV prices were below 27,000 CNY, they would still incline to purchase PEV, accompanied by China's gasoline prices rising from 8.44 on February 18th to 9.41 CNY per liter on April 1st, 2022. For car-free individuals and new energy vehicle owners, the model result displayed that the increase in PEV prices is 22,000 and 25,000 CNY, which would offset the impact of rising gasoline prices.

The evolution of climate effects has shown that we should consider reducing environmental pollution as much as possible. Promoting new energy vehicles has significantly contributed to energy conservation and emission reduction. The policy implications are mainly aimed at the

government and automobile enterprises, focusing on improving consumers' new energy vehicle purchase intention and travel quality, as shown in Figure 8.

Firstly, the results showed that charging convenience significantly impacted consumers' purchase intention of new energy vehicles while charging time did not. Automobile enterprises should pay more attention to charging convenience compared with the charging time of new energy vehicles to improve the purchase intention and the market share at the present stage. The government could invest more resources to define standards for charging piles in public places and subsidize the construction cost of private charging piles. Meanwhile, the sales price of pure electric vehicles has risen inevitably due to the shortage of raw materials and the decline of subsidies. Fuel vehicle owners are the least sensitive to increasing pure electric vehicle prices in the context of rising gasoline prices. Fuel vehicles also dominated the automobile market, with a share of nearly 85 percent in 2021 (China Association of Automobile Manufacturers, 2022; Tencent News, 2022). In our scenario, we suggest that automobile enterprises focus on fuel vehicle owners' purchase intention when adjusting pricing, not more than 27,000 CNY. Moreover, the government could give different vehicle purchase subsidies to the three groups in a targeted manner, such as subsidies for car-free individuals should be greater than new energy vehicle owners.

The fuel tax still has much room for improvement in China compared to other countries with similar economic conditions (Tan et al., 2019). It is suggested that the government could influence consumers' intention to choose new energy vehicles by adjusting the fuel tax. The finding of Study 2 showed that the introduction of a fuel tax is one of the effective measures to increase consumers' purchase intention for new energy vehicles and achieve carbon-neutral in response to rising vehicle prices and subsidy withdrawal in China. Finally, rising gasoline prices would prompt consumers to reduce the travel frequency of fuel vehicles, which meant the usage of other travel modes would increase. Therefore, alternative travel modes should be convenient and comfortable to guarantee consumers' travel quality and protect the environment. For example, the departure frequency of public transport could increase to a certain extent during periods of high gasoline prices.

Although the study has some interesting findings, it also has limitations that need to be acknowledged and concerned. Firstly, we used the online survey to collect data from Sojump, not including consumers who do not use the Internet, which is not nationally representative. For example, our sample overrepresented young-aged, middle-aged, and well-educated groups, possibly due to the skewed of Sojump's participant pool. Future studies should extend the field of investigation to offline consumers, expand the sample size and overcome the sample selection bias to the greatest extent. Another limitation is that the dependent variable in our study is consumers' vehicle purchase intention, not behavior. Although behavioral intentions are closely related to behavior, the results of studies that use behavior as the dependent variable will be more satisfactory (Tan & Teo, 2000). Subsequent studies may use purchase behavior as a dependent variable to examine vehicle purchases. Finally, consumers' purchase intention of new energy vehicles is not only affected by gasoline and vehicle prices, but other factors such as cruising range and infrastructure construction may also affect the probability of consumers purchasing a new energy vehicle. Future research could consider consumers' purchase intention of new energy vehicles under the combined effect of other relevant factors to improve the rationality of the study.

References

Akhtar, N., Nadeem Akhtar, M., Usman, M., Ali, M., Iqbal Siddiqi, U., 2020. COVID-19 restrictions and consumers' psychological reactance toward offline shopping freedom restoration. The Service Industries Journal 40 (13-14), 891–913. https://doi.org/10.1080/02642069.2020.1790535

Ali, Y., Haque, Md.M., Zheng, Z., Bliemer, M.C.J., 2021. Stop or go decisions at the onset of yellow light in a connected environment: A hybrid approach of decision tree and panel mixed logit model. Analytic Methods in Accident Research 31, 100165.

https://doi.org/10.1016/j.amar.2021.100165

Antonakakis, N., Gupta, R., Kollias, C., Papadamou, S., 2017. Geopolitical risks and the oil-stock nexus over 1899–2016. Finance Research Letters 23, 165–173. https://doi.org/10.1016/j.frl.2017.07.017

Autohome, 2022. URL https://www.autohome.com.cn/ (accessed 5.6.22).

Badi, H.B., 1998. Panel Data Methods, Handbook of Applied Economic Statistics. CRC Press.

Bliemer, M.C.J., Rose, J.M., 2010. Construction of experimental designs for mixed logit models allowing for correlation across choice observations. Transportation Research Part B: Methodological 44 (6), 720–734.

Bowerman, B.L., 2017. Business statistics in practice: using modeling, data, and analytics, Eighth edition. McGraw-Hill Education.

Burke, P.J., Nishitateno, S., 2013. Gasoline prices, gasoline consumption, and new-vehicle fuel economy: Evidence for a large sample of countries. Energy Economics 36, 363–370. https://doi.org/10.1016/j.eneco.2012.09.008

Chen, F., Chen, S., Ma, X., 2018. Analysis of hourly crash likelihood using unbalanced panel data mixed logit model and real-time driving environmental big data. Journal of Safety Research 65, 153–159. https://doi.org/10.1016/j.jsr.2018.02.010

China Association of Automobile Manufacturers, 2022. Economic operation of the automotive industry in 2021. URL http://en.caam.org.cn/

China Development Network, 2022. China's new energy vehicle sales in 2021. URL http://www.chinadevelopment.com.cn/fgw/2022/01/1762872.shtml (accessed 4.3.22).

China Economic Net, 2022. Is the continuous rise of oil prices interfering with the market in a short-term outbreak or a long-term positive? URL http://auto.china.com.cn/view/qcq/20220321/716785.shtm l (accessed 5.5.22).

Chu, S., Chen, H., 2019. Impact of consumers' corporate social responsibility-related activities in social media on brand attitude, electronic word-of-mouth intention, and purchase intention: A study of Chinese consumer behavior. Journal of Consumer Behaviour 18 (6), 453–462. https://doi.org/10.1002/cb.1784

Cooray, K., 2010. Generalized Gumbel distribution. Journal of Applied Statistics 37(1), 171–179. https://doi.org/10.1080/02664760802698995

Dimitropoulos, A., Rietveld, P., van Ommeren, J.N., 2013. Consumer valuation of changes in driving range: A meta-analysis. Transportation Research Part A: Policy and Practice 55, 27–45. https://doi.org/10.1016/j.tra.2013.08.001

Du, Z., Lin, B., 2017. How oil price changes affect car use and purchase decisions? Survey evidence from Chinese cities. Energy Policy111, 68–74. https://doi.org/10.1016/j.enpol.2017.09.017

Egbue, O., Long, S., 2012. Barriers to widespread adoption of electric vehicles: An analysis of consumer attitudes and perceptions. Energy Policy 48, 717–729. https://doi.org/10.1016/j.enpol.2012.06.009

Fang, K., 2004. Theory, Method and Application of Uniform Experimental Design - A Historical Review. Journal of Applied Statistics and Management 23 (3), 69–80. https://doi.org/10.13860/j.cnki.sltj.2004.03.016

G., Xie, F., Gong, S., Pan, H., 2019. The role of cultural values in green purchasing intention: Empirical evidence from Chinese consumers. International journal of consumer studies 43 (3), 315–326.

General Office of the State Council, 2020. Notice of the General Office of the State Council on Printing and Distributing the New Energy Vehicle Industry Development Plan (2021-2035). URL http://www.gov.cn/zhengce/content/2020-11/02/content_5 556716.htm (accessed 4.3.22).

Gnedenko, B., 1943. Sur La Distribution Limite Du TermeMaximum D'Une Serie Aleatoire. The Annals of Mathematics 44, 423. https://doi.org/10.2307/1968974

Grigolon, A., Kemperman, A., Timmermans, H., 2013. Facet-based analysis of vacation planning processes: a binary mixed logit panel model. Journal of Travel Research 52, 192–201.

Goetzke, F., Vance, C., 2021. An increasing gasoline price elasticity in the United States? Energy Economics 95, 104982. https://doi.org/10.1016/j.eneco.2020.104982

Hajivassiliou, V.A., 2000. Some practical issues in maximum simulated likelihood, in: Mariano, R., Schuermann, T., Weeks, M.J. (Eds.), Simulation-Based Inference in Econometrics. Cambridge University Press, pp. 71–99.

https://doi.org/10.1016/j.energy.2021.122501
https://doi.org/10.1016/j.trb.2009.12.004
https://doi.org/10.1111/ijcs.12513
https://doi.org/10.1177/0047287512459107

Hu, L., Wei, W., Yang, J., Jiang, H., 2011. Impact of high gasoline price on resident travel behavior. Journal of Railway Science and Engineering 8 (4), 90–94.

Jenkinson, A.F., 1955. The frequency distribution of the annual maximum (or minimum) values of meteorological elements. Q.J Royal Met. Soc. 81, 158–171. https://doi.org/10.1002/qj.49708134804

Jiao, Y., Li, M., 2022. Lithium price surge and lack of core interwoven within the year new energy vehicles to meet the fourth round of price increases. zqrbbaoxian B02.

Jing, P., Cai, Y., Sun, H., Wang, W., Wang, B., Ming, B., 2022. Can high oil prices promote consumers to purchase new energy vehicles? Journal of Transportation Engineering and Information 1–29. https://doi.org/10.19961/j.cnki.1672-4747.2022.05.021

Jing, P., Juan, Z., Jia, L., 2012. Modeling and Sensitivity Analysis of Travel Choice Based on Uniform Design and SP Survey. Prediction 31, 75–80.

Jreige, M., Abou-Zeid, M., Kaysi, I., 2021. Consumer preferences for hybrid and electric vehicles and deployment of the charging infrastructure: A case study of Lebanon. Case Studies on Transport Policy 9 (2), 466–476. https://doi.org/10.1016/j.cstp.2021.02.002

Keller, G., 2022. Statistics for management and conomics., 7th ed. Cengage Learning

Khoo, H.L., Ong, G.P., Khoo, W.C., 2012. Short-term impact analysis of fuel price policy change on travel demand in Malaysian cities. Transportation Planning and Technology 35 (7), 715–736. https://doi.org/10.1080/03081060.2012.710039

Lee, H., Lovellette, G., 2011. Will Electric Cars Transform the U.S. Vehicle Market? http://dx.doi.org/10.2139/ssrn.1927351

Li, J., Nian, V., Jiao, J., 2022. Diffusion and benefits evaluation of electric vehicles under policy interventions based on a multiagent system dynamics model. Applied Energy 309, 118430. https://doi.org/10.1016/j.apenergy.2021.118430

Li, S., Wang, Q., Liu, L., 2022. Continuous price increases are still difficult to buy new energy vehicles to wait for two or three months. Shanghai Securities News 005.

Liu, L., Liu, S., Wu, L., 2023. New energy vehicle sales forecast based on discrete time grey power model. Chinese Journal of Management Science.

https://doi.org/10.16381/j.cnki.issn1003-207x.2021.2567

Ma, Y., 2020. The portation of the dependence of China' s oil on foreign countries was 73%. URL https://new.qq.com/rain/a/20210307A02BLY00 (accessed 7.3.22).

Measures for the Administration of Petroleum Prices.

Ministry of Finance, 2019. Notice of the four departments on further improving the financial subsidy policy for the promotion and application of new energy vehicles. URL http://www.gov.cn/zhengce/zhengceku/2019-10/14/conten

Ministry of Finance, 2020. Notice on further improving the financial subsidy policy for the promotion and application of new energy vehicles. URL http://www.gov.cn/zhengce/zhengceku/2020-12/31/conten t_5575906.htm (accessed 5.2.22).

Ministry of Finance, 2022. Notice on the promotion and application of financial subsidy policies for new energy vehicles in 2022. URL http://www.gov.cn/zhengce/zhengceku/2021-12/31/conten t_5665857.htm (accessed 5.2.22).

Monge, M., Cristóbal, E., 2021. Terrorism and the behavior of oil production and prices in OPEC. Resources Policy 74, 102321.

Selmi, R., Bouoiyour, J., Miftah, A., 2020. Oil price jumps and the uncertainty of oil supplies in a geopolitical perspective: The role of OPEC's spare capacity. International Economics 164, 18–35. https://doi.org/10.1016/j.inteco.2020.06.004

Shafiei, E., Thorkelsson, H., Ásgeirsson, E.I., Davidsdottir, B., Raberto, M., Stefansson, H., 2012. An agent-based modeling approach to predict the evolution of market share of electric vehicles: A case study from Iceland. Technological Forecasting and Social Change 79 (9), 1638–1653. https://doi.org/10.1016/j.techfore.2012.05.011 Sheng,

Sierzchula, W., Bakker, S., Maat, K., van Wee, B., 2014. The influence of financial incentives and other socio-economic factors on electric vehicle adoption. Energy Policy 68, 183–194. https://doi.org/10.1016/j.enpol.2014.01.043

Sina, 2022. Oil prices are rising, and new energy vehicles will usher in explosive growth? URL https://finance.sina.com.cn/chanjing/cyxw/2022-03-17/do c-imcwiwss6612312.shtml (accessed 5.5.22).

Song, Y., Chen, B., Hou, N., Yang, Y., 2022. Terrorist attacks and oil prices: A time-varying causal relationship analysis. Energy 246, 123340.https://doi.org/10.1016/j.energy.2022.123340

Stock, J.H., Watson, M.W., 2003. Introduction to Econometrics, 4th Edition. Boston: Addison Wesley.

t_5439544.htm (accessed 5.2.22).

Tan, J., Xiao, J., Zhou, X., 2019. Market equilibrium

Xu, P., 2022. Why do the prices of new energy vehicles increase? PEOPLE's DAILY OVERSEAS EDITION 011.

Yang, O., Sivey, P.M., Scott, A., 2016. Preschool Children's Demand for Sugar Sweetened Beverages: Evidence from Stated-Preference Panel Data. SSRN Journal. https://doi.org/10.2139/ssrn.2822070

https://doi.org/10.1016/j.resourpol.2021.102321

National Bureau of Statistics, 2021. Communiqué of the seventh National Population Census.

National Development and Reform Commission, 2016.

Organization of the Petroleum Exporting Countries, 2023. International crude oil prices (dollars/barrel). URL https://www.opec.org/basket/basketDayArchives.xml (accessed 4.4.22).

Ozgur, O., Aydin, L., Karagol, E.T., Ozbugday, F.C., 2021. The fuel price pass-through in Turkey: The case study of motor fuel price subsidy system. Energy 226, 120399. https://doi.org/10.1016/j.energy.2021.120399

Peng, T., 2022. The price rise has made the whole industrial chain face a big challenge. Business China 354 (05), 50–54.

Qi, H., Xia, J., Wang, G., Jia, N., He, Z., 2021. A Behavioral Intention to Use Model of Autonomous Vehicle Ride-hailing Incorporating Traveler Habit and Altruistic Preference. Journal of Transportation Engineering and Information 19 (02), 1–10.

Qian, L., Soopramanien, D., 2011. Heterogeneous consumer preferences for alternative fuel cars in China. Transportation Research Part D: Transport and Environment 16 (8), 607–613.

and welfare effects of a fuel tax in China: The impact of consumers' response through driving patterns. Journal of Environmental Economics and Management 93, 20–43. https://doi.org/10.1016/j.jeem.2018.10.006

Tencent News, 2022. China's vehicle sales structure in 2021. URLhttps://new.qq.com/omn/20220129/20220129A02I6Z 00 (accessed 4.20.22).

Wang, J., Han, Y., Zhao, J., 2013. Analysis and model of travel choice behavior with influence of fuel prices. Journal Transportation Systems Engineering and Information Technology 13 (4),171–175. https://doi.org/10.16097/j.cnki.1009-6744.2013.04.030

Wang, K.-H., Su, C.-W., Xiao, Y., Liu, L., 2022. Is the oil price a barometer of China's automobile market? From a wavelet-based quantile-on-quantile regression perspective. Energy 240, 122501.

Wang, Z., Wang, C., Hao, Y., 2013. Influencing factors of private purchasing intentions of new energy vehicles in China. Journal of Renewable and Sustainable Energy 5, 063133. https://doi.org/10.1063/1.4850516

Wilcoxon, F., 1945. Individual Comparisons by Ranking Methods. International Biometric Society 1, 80–83. https://doi.org/10.2307/3001968

Woolson, R.F., 2007. Wilcoxon signed-rank test. Wiley encyclopedia of clinical trials 1–3. https://doi.org/10.1002/9780471462422.eoct979

Yiche, 2022. URL https://www.yiche.com/ (accessed 4.2.22)

Yu, L., 2022. Cost transmission superposition strong demand for China's new energy vehicle volume and price rise. Shanghai Securities News 005.

Zhao, L.-X., Miao, Q., 2012. The impact of rising gasoline prices on private car use in Beijing. Financial Theory and Practice 33 (05), 117–119.

Huiqian Sun
Master student, Master of Engineering (Traffic and Transportation Engineering)
Research Interests:
Travel behavior; sustainability

Peng Jing
Professor (Traffic and Transportation Engineering)
Research Interests:
Traffic simulation;
Travel behavior analysis;
Intelligent transportation systems

BaiHui Wang
Master student, Master of Engineering (Traffic and Transportation Engineering)
Research Interests:
Autonomous driving acceptance

YunHao Cai
Master student, Master of Engineering (Traffic and Transportation Engineering)
Research Interests:
Travel behavior analysis;
Human factors engineering for autonomous driving

Jie Ye
Master student, Master of Engineering (Traffic and Transportation Engineering)
Research Interests:
Travel behavior analysis;
Quality of life in older adults

Bichen Wang
Master student, Master of Engineering (Traffic and Transportation Engineering)
Research Interests:
Travel behavior analysis;
Social Media Data Mining

Predicting Electricity Consumption of An Office Space in Chiang Mai by Using Machine Learning Methods

Nichakarn Morakote[1*], Worawut Kongwee[2] , Witsarut Achariyaviriya[3] , Damrongsak Rinchumphu[4]

[1]Graduate student, Department of Civil Engineering, Faculty of Engineering, Chiang Mai University, Thailand
[2] Research Assistant, City Research and Development Center, Faculty of Engineering, Chiang Mai University, Thailand
[3] Lecturer, Department of Electrical Engineering, Faculty of Engineering, Chiang Mai University, Thailand
[4] Lecturer, Department of Civil Engineering, Faculty of Engineering, Chiang Mai University, Thailand
*E-mail: nichakarn_mo@cmu.ac.th

Abstract: The heightened greenhouse effect caused by human activities is contributing to global warming, presenting considerable challenges for the climate and ecosystems of our planet. Shifting to Chiang Mai in northern Thailand, this city experiences diverse weather patterns throughout the year, impacting daily life and influencing the energy requirements of commercial buildings and office spaces. Given Chiang Mai's emergence as a growing employment hub, these spaces consume a notable amount of electrical power. To tackle this issue, our research collected weather conditions by using sensors composed of air quality modules. The electricity consumption data was detected from air conditioners, lighting, and outlets. Four machine learning approaches, including Extreme Gradient Boosting (XGB), Random Forest (RF), Multilayer Perceptron (MLP), and Support Vector Regression (SVR) were used to predict and comprehend electricity usage within office spaces in Chiang Mai. The results show that the Extreme Gradient Boosting model performed effectively with the gathered data. The potential of a development framework for effective modeling in areas can be characterized by similar environmental conditions.

Keywords: Machine Learning, Electricity Consumption, Office Space, Chiang Mai, Extreme Gradient Boosting

1. Introduction

In a period marked by heightened energy demands and an escalating focus on ecological sustainability, the energy consumption trend per capita was raised rapidly (Wang, Su, Li, & Ponce, 2019). The growing awareness of environmental concerns has prompted more deliberate actions to decrease energy consumption. This attempt has resulted in the initiation and implementation of various green building construction projects (Zhao, McCoy, & Du, 2016). Incorporating efficient energy storage solutions and supplementary backup systems to guarantee an adequate energy supply is important but the execution of backup systems is accompanied by related expenses (Jacob, Das, Abraham, Banerjee, & Ghosh, 2017).

Thailand is a tropical country where the influence of ambient temperature on room energy usage is pivotal, particularly given the widespread reliance on cooling systems for indoor comfort (De Cian & Sue Wing, 2019). Hot climates extended usage periods lead to heightened energy consumption during peak daytime hours (Ma, Si, Li, Yan, & Zhu, 2015).

Employing energy prediction models is an opportunity to optimize resource management

effectively (Zeyu & Srinivasan, 2015). Organizations can allocate resources, including electricity, by accurately forecasting energy demand based on various environmental parameters like temperature, humidity, and occupancy levels. Combining predictions of energy generation with demand allows for the implementation of energy-saving measures. This research project seeks to create an energy consumption prediction model for a small-sized office room in Chiang Mai, Thailand, as a representative case study of a tropical climate environment. The study provides valuable insights into the distinct energy consumption characteristics and challenges associated with regions characterized by high temperatures and humidity using machine learning techniques. The study aims to contribute to the development of an effective modeling framework applicable to areas with similar environmental conditions.

2. Methods

The office room used as the case study is located on the 8th floor of a building in the Faculty of Engineering, Chiang Mai University in Chiang Mai Province, Thailand.

The research progress started with hardware development, sensors were designed to detect the weather conditions, equipment, and occupants. Afterward, data collection and validation involved the information recorded by these sensors and was stored in a database. In the third part, model evaluation, machine learning models were trained using the accumulated data. Finally, the most effective model was determined.

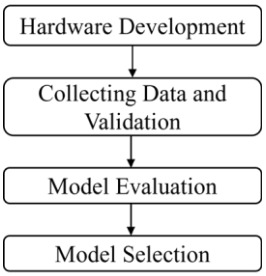

Fig 1. Research Methodology

- *Hardware Development*

NodeMCU, air quality modules detected PM 2.5, temperature, and humidity were set as weather condition sensors. These sensors were placed in two locations: within and outside the room. Air conditioning, lighting, and outlet were collected energy consumption using sensors by setting up NodeMCU which was linked with energy meter modules. In terms of occupants, a camera was installed in the room, transmitting images to a computer. Eventually, object detection was employed to count the number of individuals in the room.

- *Collecting Data and Validation*

Sensors monitored indoor and outdoor humidity, temperature, and PM 2.5. Power consumption sensors detected air conditioning, lighting, and outlets, along with the status of the lighting switch (on/off). A camera captured images for occupant counting, and data from each sensor was collected every minute before being stored in a database.

- *Model Evaluation and Selection*

This research utilized four widely recognized machine learning algorithms: Extreme Gradient Boosting (XGB), Random Forest (RF), Multilayer Perceptron (MLP) – a form of artificial neural network (ANN), and Support Vector Regression (SVR) for modeling purposes. Training of these models involved the use of collected data along with additional features derived from inherent data relationships. In order to objectively assess the performance of the estimation model in this study, evaluation metrics such as the Coefficient of Determination (R-squared or R^2) and Average Error (as a percentage) were employed. This can be expressed as follows:

$$RR^2 = 1 - \frac{\sum(yy_{ii} - \hat{y}_{ii})^2}{\sum(yy_{ii} - \bar{y})^2} \quad (1)$$

$$\text{Average Error} = \frac{1}{nn}\sum \left| \frac{yy_{ii} - \hat{y}_{ii}}{yy_{ii}} \right| \times 100 \quad (2)$$

Typically, superior model performance is indicated by a higher R^2 value and a lower average error, signifying a decreased differential between the predicted and actual outputs.

3. Results and Discussion

- *Collected Data Criteria*

The chosen set of input data (features) for the machine learning models consists of lighting switches, occupants, indoor humidity, indoor temperature, indoor PM 2.5, outdoor humidity, outdoor temperature, and outdoor PM 2.5, with power consumption serving as the target variable. Table 1 displays the values, mean values, and standard deviation (SD) of both input and output variables. It is important to highlight that all data obtained from the experiment was utilized for ML processing.

Table 1 Statistical details of the data

Feature	Unit	Range	Mean	SD
Lighting switches	On (1) / Off (0)	0.00,1.00	2.9093	0.4542
Occupants	-	0.00,5.00	0.1549	0.4802
Indoor humidity	%	46.40,80.30	66.1614	9.4973
Indoor Temperature	Celsius	23.70-32.60	27.807	2.2068
Indoor p.m. 2.5	µg/m³	1.00,49.00	6.0488	2.7536
Outdoor humidity	%	31.00,82.00	67.1959	13.1374
Outdoor Temperature	Celsius	23.80,43.00	2.9787	4.2717
Outdoor p.m. 2.5	µg/m³	6.00,42.00	21.3593	7.7948

- *Machine Learning Performances*

In this research, cross-validation, a method involving the division of available data into multiple folds or subsets, allocated 70 percent for training data and 30 percent for testing data. The machine learning approaches employed comprised Random Forest, Support Vector Regression, Multi-Layer Perceptron, and Extreme Gradient Boosting, respectively. The four model approaches were trained using features derived from the dataset, and their performances are presented in Table 2.

Table 2 The evaluated performance of the machine learning algorithms

ML Algorithm	R^2	Average Error
RF	0.93	10.00
SVR	0.80	84.50
XGB	0.96	7.96
MLP	0.91	20.85

Consequently, Extreme Gradient Boosting was selected to enhance the predictive model due to its superior R-squared (R^2) and the lowest average error. Subsequently, the XGB model was employed for predicting the room's electrical power. Figure 3 displayed a slight delay in the graph, primarily attributed to the temperature undergoing changes at a more gradual pace compared to the electrical power.

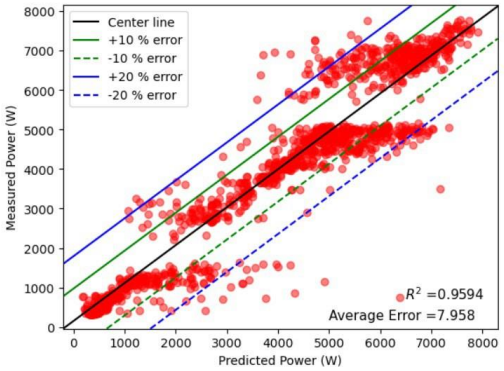

Fig 2. Q-Q plot using XGB

The machine learning evaluations indicated that the Extreme Gradient Boosting model exhibited the most favorable outcomes. Nevertheless, Figure 2 revealed that the predicted values did not consistently align precisely with the center line. The model encountered challenges in handling value ranging from 1500 Watts to 2000 Watts and from 5000 Watts to 6000 Watts. Notably, there was an error ranging from -10% to -20% in the interval between 4000 Watts and 5000 Watts, and an error ranging from +10% to +20% in the range between 6000 Watts and 7000 Watts. The outcomes of the predicted values are illustrated in Figure 3.

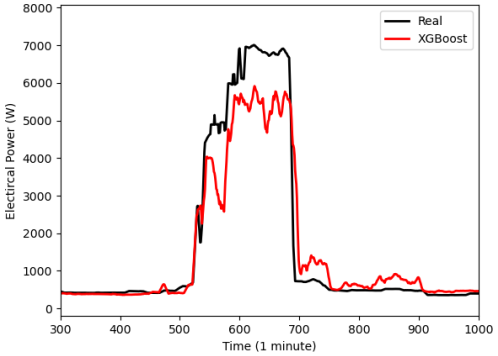

Fig 3. The prediction of electrical power using XGB

4. Conclusions

From the study of predicting electricity consumption of office space in Chiang Mai by using Machine Learning methods, the Extreme Gradient Boosting (XGB) model could provide the best results with a value of the highest R^2 equal to 0.96 and the lowest average error equal to 7.96. However, when using the XGB model to forecast electrical power and plotting the graph every minute, a comparison between the actual measured power and the predicted values revealed errors in the range of electrical power between 4000 and 7000 Watts, ranging from -20 to +20%. This discrepancy highlights certain challenges in the research, suggesting a need for cautious fine-tuning of the model until the results closely align with the center line for accurate predictions. Moreover, the variations in values over time exert a noteworthy influence on the model. Consequently, it is recommended to incorporate time-series machine learning techniques in the development of energy prediction models.

References

[1] De Cian, E., & Sue Wing, I. (2019). Global Energy Consumption in a Warming Climate. Environmental and Resource Economics, 72(2), 365-410.

[2] Jacob, A. S., Das, J., Abraham, A. P., Banerjee, R., & Ghosh, P. C. (2017). Cost and Energy Analysis of PV Battery Grid Backup System for a Residential Load in Urban India. Energy Procedia, 118, 88-94.

[3] Ma, H., Si, F., Li, L., Yan, W., & Zhu, K. (2015). Effects of ambient temperature and crosswind on thermo-flow performance of the tower under energy balance of the indirect dry cooling system. Applied Thermal Engineering, 78, 90-100.

[4] Zeyu, W., & Srinivasan, R. S. (2015, 6-9 Dec. 2015). A review of artificial intelligence based building energy prediction with a focus on ensemble prediction models. Paper presented at the 2015 Winter Simulation Conference (WSC).

[5] Zhao, D., McCoy, A., & Du, J. (2016). An Empirical Study on the Energy Consumption in Residential Buildings after Adopting Green Building Standards. Procedia Engineering, 145, 766-773.

Nichakarn Morakote

Graduate student
Department of Civil Engineering
Faculty of Engineering,
Chiang Mai University,
Thailand

Worawut Kongwee

Research Assistant,
City Research and Development Center,
Faculty of Engineering,
Chiang Mai University,
Thailand

Witsarut Achariyaviriya
Ph.D.

Lecturer,
Department of Electrical Engineering,
Faculty of Engineering,
Chiang Mai University,
Thailand

Damrongsak Rinchumphu,
Ph.D.

Associate Professor,
Department of Civil Engineering,
Faculty of Engineering,
Chiang Mai University,
Thailand

Optimizing Phycocyanin Production in *Spirulina* Using Blue and White LEDs

Obaid Bhat[1,2], Yuwalee Unpaprom[2,3], Maria Onyemowo[1,2], Rameshprabu Ramaraj[1,2*]

[1]School of Renewable Energy, Maejo University, Chiang Mai, 50290, Thailand
[2]Sustainable Resources and Sustainable Engineering Research Lab, Maejo University, Chiang Mai, 50290, Thailand
[3]Program in Biotechnology, Faculty of Science, Maejo University, Chiang Mai 50290, Thailand
**Corresponding author, e-mail: rrameshprabu@gmail.com ; rameshprabu@gmail.com*

Abstract: Humans have extensively harnessed *Spirulina platensis* due to its high nutritional value, potential medical applications, and valuable pigments it contains. One such valuable pigment, phycocyanin (PC), can be extracted from *Spirulina platensis*. The lighting conditions play a crucial role in the production of PC. In this study, two different types of light, blue and white, were employed to cultivate *S. platensis* using a light-emitting diode (LED) as a light source. During the cultivation period, a light-dark cycle of 12 hours each (12:12) was maintained. This research optimized the growth of this algae strain at a moderate pH level of 9, light intensities of 1500 lux, and a temperature range of 28 ± 2°C. The comparative analysis of the results reveals that blue light effectively increases the proportion of PC within the biomass, although the overall biomass production is lower compared to cultivation under white light. The highest concentration of phycocyanin, at 0.0266 mg/ml, was achieved when using a blue light-emitting diode, while a phycocyanin concentration of 0.022 mg/ml was recorded under white light-emitting diode conditions. The highest optical density of 0.315 was recorded for white light and an optical density of 0.259 for blue clearing, showing decreased biomass production with blue light. The study finds that blue light boosts phycocyanin levels in *Spirulina platensis* but reduces biomass growth compared to white light, which yields more biomass with less pigment concentration. This has implications for tailoring *Spirulina* cultivation based on desired outputs.
Keywords: Phycocyanin, LEDs, *Spirulina*, Optical density.

1. Introduction

The production of natural resources like food and energy is at risk by a growing global population, the effects of global warming, and the depletion of fossil fuels [1]. Cultivating microalgae and cyanobacteria is an alternative approach to solving these issues. These microbes help mitigate atmospheric CO2 and may reduce the effects of global warming [2]. Certain species yield significant concentrations of polyunsaturated fatty acids and essential amino acids. Furthermore, several microalgal species, including cyanobacteria, have been shown to possess phycocyanin, a photosynthetic pigment with established nutraceutical qualities that can be added to food to support health promotion [3, 4]. Furthermore, it is possible to extract the biomass's carbohydrates and lipids from microalgae and cyanobacteria and then turn them into biofuels like bioethanol and biodiesel [5].

Phycocyanin (PC) is a blue pigment that absorbs light and is found in both the eukaryote algae species, Rhodophyta, Cryptophyte, and cyanobacteria. Many cyanobacteria get their blue color from PC, which is also the reason these cyanobacteria are also referred to as blue-green algae. PC possesses antioxidant qualities, is highly fluorescent, and is soluble in water. Numerous applications in food and cosmetics, biotechnology, diagnostics, and medicine make use of PC and related phycobiliproteins [6]. The FDA authorized PC, which is derived from *Spirulina*, as a food coloring in August 2013. A Future Market Insights analysis estimates that by 2028, the global market would be worth over US$ 224 million [4]. Western European nations are the biggest users of phycocyanin (33%), with the food industry accounting for 80% of its utilization. However, the degree of purity of phycobiliproteins has a significant impact on their market pricing. For instance, the cost of one milligrams of highly purified molecular markers labelled with antibodies of different fluorescent compounds can reach up to $1500 USD [3]. However, the high expense of manufacture, extensive extraction, and especially purification which is still difficult and costly has restricted the commercial usage of PC.

During the process of photosynthesis, PC, an auxiliary pigment of chlorophyll, provides light energy while reflecting blue and absorbing red and orange light. PC has been utilized for many years as a fluorescent reagent, natural edible pigment, cosmetic, and medication [7]. Chlorophyll a, auxiliary phycobiliprotein pigments, phycocyanin

(PC), allophycocyanin (AP), and phycoerythrin (PE) are all found in the photosynthetic apparatus of cyanobacteria [5]. They are made up of one or more chromophores, or bilins, along with an apo-protein. Phycobiliproteins are specialist pigments found on antennas that collect light. They combine to create larger protein complexes known as phycobilisomes (PBSs), which are made up of staked rods of phycocyanin and an allophycocyanin core, frequently in conjunction with phycoerythrin. PBSs shift their energy to photosystem II (PSII), neutralizing PSI's increased ability to absorb light because of its higher chlorophyll concentration [7].

One of the most important factors in the growth of microalgae and cyanobacteria is light, that the pigments use to absorb energy and carry out the process of photosynthesis [8]. The majority of large-scale cultivations rely on solar light as their energy source. However, artificial light is more frequently employed in cultivations for the high added value bio compounds production, phycocyanin and essential fatty acids, because it allows for the effective and standardized handling of photosynthetic photon flux density and produces high productivities [9]. The most popular artificial energy source utilized in microalgae cultivation is fluorescent lighting. Light-emitting diodes, or LEDs, are regarded as an affordable and environmentally responsible energy source [8]. The primary benefits of LEDs are as follows: (1) high conversion efficiency of power; (2) low energy consumption; (3) less mass and volume of material; (4) long-lasting and non-polluting; (5) reduced heat dissipation; and (6) single wavelength [10]. A number of studies have recently reported using LEDs as a light source in the cultivation of cyanobacteria and microalgae. The biomass productivity in the *Nannochloropsis sp*. and *Botryococcus braunii* cultivations was enhanced by the blue and red LEDs, respectively [11]. When blue LEDs were utilized as an energy source in the cultivations of *Tetraselmis* sp.

2. Materials and methods

2.1 Material and Methods

Microorganism

The sample, which was collected from the Department of Fisheries at Maejo University (18°.51" 49°.70" N, 99°.10" 40.06" E), contained Spirulina platensis. The strain was subculture and grown at 28 °C utilizing a natural light source every two weeks.

2.2 Nutrients utilized in microalgae culture medium

To prepare the Spirulina culture medium, the following components were added to regular tap water: $NaNO_2$, $MgSO_4$, NaCl, $NaHCO_3$, and N:P: K.

2.3 Chemical analysis

Every day, the absorbance of the two samples was measured at 560 nm using a spectroscopic instrument model DV 8000 to determine their optical density. Every day at noon, the optical density was measured. Additionally, the pH and temperature of the samples were checked every day. A pH meter (APERA PH700) was used to measure the sample's pH, and a UNI-T UT333S was used to monitor its temperature. To determine dry weight, wet biomass was weighed and dried in a hot air oven SHEL LAB (1390 FX) for 12 hours at 50°C.

2.4 Acclimatization

Spirulina normally thrives in alkaline, humid climates with sea water as its native habitat. Thailand experiences tropical weather, with summertime highs of up to 40°C and colder months of up to 15°C. Therefore, by modifying the climatic conditions in accordance with the ideal growing parameters for Spirulina in indoor lab conditions, Spirulina cultivation was successfully completed at Maejo University, Thailand.

2.5 Cultural conditions

Spirulina was subculture for the inoculum in a plastic clear cylinder-shaped bag (inner diameter of 50 mm, height of 1500 mm) with 1000 mL of the liquid medium. An air bubble system was used to aerate the plastic bag and maintain a constant temperature of 28 ± 2 °C in a well-lit environment. Aeration is necessary to meet the CO_2 requirements of Spirulina; the bubble system was used to maintain the growth medium's constant CO_2 requirements. Furthermore, using the predicted amount of nutrient ($NaHCO_3$) in the growth medium helps to maintain the right CO_2 content for the duration of the experiment. Furthermore, the bubble system's agitation aids in continuous exposure to light and reliable nutrient circulation. The initial optical density (OD) of the culture medium was 0.06. The Spirulina was cultivated until the optical density reached a range of 0.5 to 0.6. For the experiment, 5 liters of tap water were used in glass bottle. Nutrients were added to the water and thoroughly mixed. The culture was started with an optical density (OD560) of approximately 0.060. This process was repeated in two replicates, each of which was grown under different light sources for a duration of 14 days. Each glass bottle was exposed to additional light-emitting diodes with different wavelengths, maintaining a 12-hour light and 12-hour dark cycle. Figure 1 shows the experimental setup for the research.

2.6 *Phycocyanin extraction and analysis*

Traditional (Soxhlet) extraction: this method employed 95% solvent and was done in a Soxhlet extractor. The extraction process lasted four hours, with a temperature of 50°C and a biomass to solvent ratio of 15 gr biomass/ 250 ml solvent.

Ultrasound assisted extraction

About 15 grams of biomass and 250 ml of 95% ethanol were combined. After that, the biomass was sonicated for 30 minutes at 50° C at frequencies of 28 and 42 KHz in an ultrasonic bath powered by 200 W.

Spectrophotometer analysis was used to determine the concentration of phycocyanin, the concentration of phycocyanin is defined as

PC= (OD620-0.474 OD 652)/5.34

Where OD615 is the optical density of the sample at 615 nm, and OD652 is the optical density of sample at 652 nm.

Figure 1 White and Blue LEDs used for the experimental research for study of Phycocyanin content in Spirulina

3. Results and discussion

3.1. Effect of light wavelength on cell growth

The photobioreactor surface was illuminated with light at a level of 2500 lux, while cyanobacteria *Spirulina platensis* were cultivated using a variety of light sources, including a White and blue light-emitting diodes. The experiment utilizing white LEDs in an integral light photoperiod showed significantly higher ($p < 0.05$) biomass concentration compared to the control experiment, which employed blue light. The observed result was approximately twice as much as the blue LEDs. The highest optical density of 0.239 was recorded with white light source. The optical density of culture grown under white light source showed continues growth in biomass till day 14 of cultivation without any visible lag and stationary phase Similarly, high concentrations of *Spirulina* biomass were achieved when white LEDs when employed as an energy source in the cultivations [4]. Reason for the higher biomass production can be that the primary photosynthetic pigments in cyanobacteria, chlorophyll a (absorbing energy at wavelengths between 430 and 680 nm) and phycobiliproteins (absorbing energy at wavelengths between 550 and 620 nm), play a crucial role in this process [12]. White LEDs have a wide pigment light absorption spectrum (400-700 nm). This can result in enhanced energy utilization, leading to higher biomass production by the cells, as evidenced by the results obtained for *Spirulina sp*. In all LED experiments, biomass concentration, productivity, and maximum specific growth rate were significantly higher ($p < 0.05$) compared to the blue LED experiment with only white light. Therefore, extended exposure times to LED light favored the growth of microalgal cells. The wavelengths emitted by the fluorescence light spectrum have lower photosynthetic activity for certain microalgae and cyanobacteria species [13]. Conversely, LEDs emit specific wavelength bands that can enhance the energetic utilization by these microorganisms, leading to greater photosynthetic activity in the cells [14]. Culture utilizing white LEDs as an energy source with integral light photoperiod exhibited significantly higher biomass concentrations compared to the partial light photoperiod. However, there were no significant differences ($p > 0.05$) in biomass productivity and specific growth rate between cultures with blue with integral light photoperiod and those with the partial light photoperiod. No physiological adaptation phase was observed in any of the evaluated LED conditions, as indicated in Figure 2. The use of white LEDs with (12L: 12D photoperiod resulted in more pronounced cell growth compared to blue light-emitting diode conditions. *Spirulina* might have utilized more energy from this wavelength range, leading to the continuation of the cell growth exponential phase. In contrast, the blue LED experiments tended towards the stationary phase within 11 days of culture. The pH of the cultures varied from 8.5 to 10, maintaining ideal conditions for cyanobacteria cell growth, such as *Spirulina*. Highest optical density of 0.239 (OD) was

recorded for white LED and an optical density of 0.211 (OD) was recorded for blue LED. From the growth curve it can be seen that for first 5 days of cultivation the growth in both the cultures is same but after day 6 it clearly visible that growth of culture under white LEDs has better optical density and it also recorded in the total biomass recorded.

Figure 2 Growth curve of *Spirulina* under different light source

our research illuminated the distinct influence of white and blue LED wavelengths on cyanobacterial biomass growth. White LEDs exhibited a superior impact on biomass proliferation compared to blue LEDs, suggesting the significance of light spectrum in enhancing cyanobacterial growth. This finding underscores the potential of tailored LED lighting to optimize biomass production in cyanobacteria cultivation, offering promising avenues for efficient and controlled growth strategies in diverse applications.

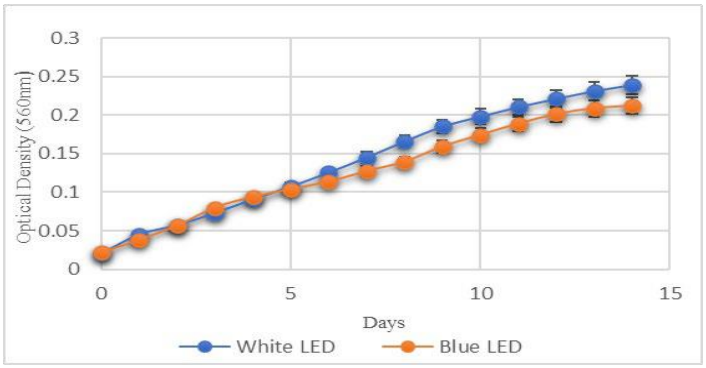

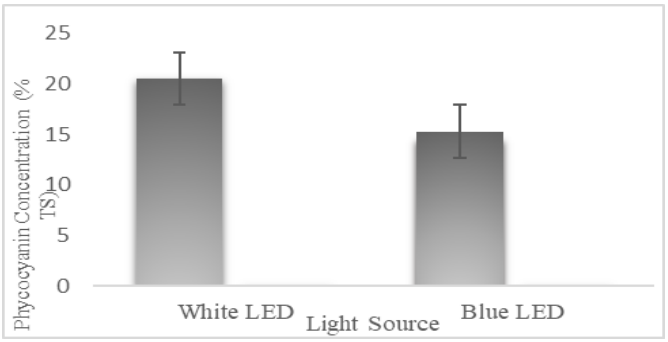

Figure 3 Total average Phycocyanin concentration in *Spirulina* biomass under different light sources

3.2 Phycocyanin

The application of LEDs as an energy source for *Spirulina* cultivation stimulated the production of phycocyanin by the cells. In almost all experiments, the concentration of this pigment at the end of the cultivations was significantly higher ($p < 0.05$) than in the natural light. LEDs emit specific wavelengths that may, in some cases, hinder the energy absorption by chlorophyll molecules in microalgae and cyanobacteria cells. Consequently, there may be an increased production of other pigments, such as phycocyanin, to enhance energy efficiency uptake. Phycocyanin molecules are responsible for absorbing energy in the visible light spectrum that is poorly utilized by chlorophyll, transferring the energy to the photosynthetic reaction center for use by chlorophyll a [15]. With photoperiod (12L: 12D) and white LEDs, the experiment yielded the highest phycocyanin concentration. The phycocyanin concentration was higher with white light source. Phycocyanin is photosensitive to light [16]. Therefore, a drop in chromophore proteins may occur from high light intensity, which would lower the quantity of phycobilisomes in each cell. This pigment breakdown in the *Spirulina* cells may have been brought on by constant LED culture illumination, which would have reduced the pigment's concentration in the final biomass. Figure 3 illustrates the impact of light with different wavelengths on the phycocyanin content and productivity of *Spirulina*. The biomass cultured under White LED lighting exhibited the highest phycocyanin content, reaching 20.31 ± 0.51%. In contrast, the culture with blue LED lighting showed the lowest phycocyanin content in the cells, measuring 17.54 ± 0.09%. Phycocyanin calculated on different days of cultivation is reported in (Table 2). In the investigation of the impact of light spectral quality on pigment accumulation in *Arthrospira platensis* biomass, it was observed that the highest concentration of phycocyanin (16.71%) was achieved with the use of a red LED (660 nm). Conversely, the utilization of blue light (450 nm) resulted in the lower concentration of phycocyanin in Arthrospira platensis biomass even lower than white light [17]. When examining the effects of red, white, blue, yellow, and green LEDs, it was found that the culture employing white and red light had the greatest phycocyanin content 15.2% TS [18]. (Table 1) gives detail effect of various light sources on

phycocyanin production in various cyanobacteria.

To get bioproducts from microalgae and cyanobacteria cultures, the primary obstacle is to combine high yields of the desired component with biomass. High biomass productivities can be obtained under different optimum growing conditions than those for high phycocyanin productivities. Nonetheless, the current investigation reveals that both LED experiment demonstrated higher phycocyanin and biomass productivities concurrently, yielding outcomes that were much better than the experiment done by some other researchers in natural light or that solely employed fluorescent light.

our investigation highlighted the profound impact of white and blue LED wavelengths on the production of phycocyanin pigment in *Spirulina*. The distinct response observed in phycocyanin synthesis under different LED spectra emphasizes the significance of light quality in manipulating pigment yield. These findings provide valuable insights into optimizing pigment-specific cultivation strategies using tailored LED lighting, offering a pathway to harness the full potential of Spirulina for specialized pigment production in various industries.

Table 1 Effect of different light sources on phycocyanin production in cyanobacteria.

Light Source	**Effect on Phycocyanin**	**Reference**
Green LEDs	2.7-time better phycocyanin concentration was obtained as compared to red control light source	[19]
White and Red LEDs	Highest Phycocyanin content 17.61± 0.51 and 15.78 ± 0.26 was reported with red and white LEDs	[20]
Blue Light	Phycocyanin increased up to 13.2 % ± 1.96 of dry weight at day.	[21]
White Light	With mild light intensity and white light, increased phycocyanin production of 11.94 ng/mg took place	[22]

Table 2 Phycocyanin calculation for different light source

Days	**White LEDs**	**Blue LEDs**
Phycocyanin Content Day 1	0.015 mg/ml	0.014 mg/ml
Phycocyanin Content Day 4	0.022 mg/ml	0.019 mg/ml
Phycocyanin Content Day 8	0.026 m/ml	0.023 mg/ml
Phycocyanin Content Day 12	0.031mg /ml	0.025 mg/ml
Phycocyanin Content Day14	0.035 mg/ml	0.028 mg/ml

4. Conclusion

This research has significantly contributed to our understanding of how different types of lighting impact the

production of a vital pigment called phycocyanin in *Spirulina* culture. Phycocyanin holds immense value due to its various applications in medicine, pharmaceuticals, and economics. This study revealed an intriguing relationship between the type of light used and the resulting growth of *Spirulina* biomass and the concentration of phycocyanin.

The LEDs employed in the experiment showcased varying efficiencies in stimulating phycocyanin production. The higher yield observed with white LEDs, reaching 20.31± 0.51% in phycocyanin content, suggests that the cells absorbed the broader spectrum of white light through chlorophyll. Conversely, blue LEDs, with their narrower wavelength range (450-495 nm), led to an intermediate level of biomass production, as evidenced by the optical density readings.

The optical density recorded under white LEDs (0.239) compared to blue LEDs (0.211) highlighted this difference in biomass production between the light types. This insight strongly advocates for a strategic use of different LEDs to harness Spirulina's potential for increased phycocyanin content in its biomass. This research paves the way for further exploration into optimizing Spirulina cultivation techniques and pigment production, with implications for various industries and scientific fields.

Conflicts of Interest The authors declare no conflict of interest.

References

[1] Alghanmi, H. (2023). Effects of various light intensities on phycocyanin composition of cyanobacterium limnospira fusiformis (voronichin) nowicka-krawczyk, mühlsteinová & hauer. *Malaysian Journal of Science*, 1-6.

[2] Atta, M., Idris, A., Bukhari, A., & Wahidin, S. (2013). Intensity of blue LED light: a potential stimulus for biomass and lipid content in fresh water microalgae Chlorella vulgaris. *Bioresource technology*, *148*, 373-378.

[3] Baba, Masato, Fumie Kikuta, Iwane Suzuki, Makoto M. Watanabe, and Yoshihiro Shiraiwa. "Wavelength specificity of growth, photosynthesis, and hydrocarbon production in the oil-producing green alga Botryococcus braunii." *Bioresource technology* 109 (2012): 266-270.

[4] Bhat, O., Unpaprom, Y., & Ramaraj, R. (2023). Spirulina Cultivation Under Different light-emitting Diodes for Boosting Biomass and Protein Production. *Molecular Biotechnology*, 1-9.

[5] Bhat, O., Unpaprom, Y., & Ramaraj, R. (2023). Spirulina Cultivation Under Different light-emitting Diodes for Boosting Biomass and Protein Production. *Molecular Biotechnology*, 1-9.

[6] Blanken, W., Cuaresma, M., Wijffels, R. H., & Janssen, M. (2013). Cultivation of microalgae on artificial light comes at a cost. *Algal Research*, *2*(4), 333-340.

[7] Carvalho, A. P., Silva, S. O., Baptista, J. M., & Malcata, F. X. (2011). Light requirements in microalgal photobioreactors: an overview of biophotonic aspects. *Applied microbiology and biotechnology*, *89*, 1275-1288.

[8] Carvalho, A. P., Silva, S. O., Baptista, J. M., & Malcata, F. X. (2011). Light requirements in microalgal photobioreactors: an overview of biophotonic aspects. *Applied microbiology and biotechnology*, *89*, 1275-1288.

[9] CDuarte, J. H., de Morais, E. G., Radmann, E. M., & Costa, J. A. V. (2017). Biological CO2 mitigation from coal power plant by Chlorella fusca and Spirulina sp. *Bioresource technology*, *234*, 472-475.

[10] Chen, H. B., Wu, J. Y., Wang, C. F., Fu, C. C., Shieh, C. J., Chen, C. I., ... & Liu, Y. C. (2010). Modeling on chlorophyll a and phycocyanin production by *Spirulina platensis* under various light-emitting diodes. *Biochemical Engineering Journal*, *53*(1), 52-56.

[11] da Fontoura Prates, D., Radmann, E. M., Duarte, J. H., de Morais, M. G., & Costa, J. A. V. (2018). *Spirulina* cultivated under different light emitting diodes: Enhanced cell growth and phycocyanin production. *Bioresource technology*, *256*, 38-43.

[12] Eriksen, N. T. (2008). Production of phycocyanin—a pigment with applications in biology, biotechnology, foods and medicine. *Applied microbiology and biotechnology*, *80*, 1-14.

[13] Hemlata, & Fatma, T. (2009). Screening of cyanobacteria for phycobiliproteins and effect of different environmental stress on its yield. *Bulletin of environmental contamination and toxicology*, *83*, 509-515.

[14] Jespersen, L., Strømdahl, L. D., Olsen, K., & Skibsted, L. H. (2005). Heat and light stability of three natural blue colorants for use in confectionery and beverages. *European Food Research and Technology*, *220*, 261-266.

[15] Lee, N. K., Oh, H. M., Kim, H. S., & Ahn, C. Y. (2017). Higher production of C-phycocyanin by nitrogen-free (diazotrophic) cultivation of Nostoc sp. NK and simplified extraction by dark-cold shock. *Bioresource Technology*, *227*, 164-170.

[16] Lima, G.M.; Teixeira, P.C.; Teixeira, C.M.; Filócomo, D.; Lage, C.L. Influence of spectral light quality on the pigment concentrations and biomass productivity of *Arthrospira platensis*. *Algal Res*. 2018, 31, 157–166.

[17] Schulze, P. S., Barreira, L. A., Pereira, H. G., Perales, J. A., & Varela, J. C. (2014). Light emitting diodes (LEDs) applied to microalgal production. *Trends in biotechnology*, *32*(8), 422-430.

[18] Sekar, S., & Chandramohan, M. (2008). Phycobiliproteins as a commodity: trends in applied research, patents and commercialization. *Journal of Applied Phycology*, *20*, 113-136.

[19] Szwarc, D., & Zieliński, M. (2018, October). Effect of Lighting on the Intensification of Phycocyanin Production in a Culture of *Arthrospira platensis*. In *Proceedings* (Vol. 2, No. 20, p. 1305). MDPI.

[20] Wang, H., Ji, C., Bi, S., Zhou, P., Chen, L., & Liu, T. (2014). Joint production of biodiesel and bioethanol from filamentous oleaginous microalgae Tribonema sp. *Bioresource technology*, *172*, 169-173.

[21] Wishkerman, A., & Wishkerman, E. (2017). Application note: A novel low-cost open-source LED system for microalgae cultivation. *Computers and Electronics in Agriculture*, *132*, 56-62.

[22] Zittelli, G. C., Mugnai, G., Milia, M., Cicchi, B., Benavides, A. S., Angioni, A., ... & Torzillo, G. (2022). Effects of blue, orange and white lights on growth, chlorophyll fluorescence, and phycocyanin production of *Arthrospira platensis* cultures. *Algal Research*, *61*, 102583.

Mr. Obaid Bhat
Ph.D. of Engineering (Renewable Energy Engineering).
Research Interests: Bioenergy, biomass analysis and Renewable Energy.

Dr. Yuwalee Unpaprom
Assistant Professor
Research Interests: Plant biotechnology, Plant physiology and biochemistry, and sustainable fuels/ bioenergy.

Assoc. Prof. Dr. Rameshprabu Ramaraj, MSc., MPhil., MEng., PhD
Associate Professor
Research Interests: Biofuels, Energy Engineering, Algae Biotechnology, and Fermentation Technology.

Ms. Maria Onyemowo.
Masters of Engineering (Renewable Energy)
Research Interests: DSSC, Pigment extraction and Solar Energy

Web application for Assessing the energy potential from agricultural residue on the agricultural crop database in Ping Khong, Chiang Dao, Chiang Mai Thailand

Surachart Sirichouangchote[1], Thongchai Maneechukate[2*], Sarawut Polvongsri[3], Chawaroj Jaisin[4]

[1]School of Renewable Energy, Maejo University
* Corresponding author, E-mail: thongchaimeajo@gmail.com

Abstract: This research has presented a web application for assessing the energy potential from agricultural residues such that the agricultural crop database in 2022 at Ping Khong Municipality, Chiang Dao, Chiang Mai Thailand. The web application development is based on the Laravel Framework and PHP web framework following the Model Views Controller (MVC) architecture. This framework to claimed low complex, allowing the integration of additional tools as needed, facilitating ease of use. The information in a database is utilized by the proposed web application via the APIs Which Axios are based on javascript The data format of the system therefore uses asynchronous operation. The system can operate on multiple tasks simultaneously without waiting for the completion of the preceding task. This furthermore is simply more a high-security, ensuring security against Cross-Site Request Forgery (CSRF) attacks. The collection for the proposed web application includes agricultural areas and production quantity, serving as information for evaluating the energy potential from agricultural residues. The energy potential assessment employs equations from the Department of Alternative Energy Development and Efficiency. This paper findings indicate that, after analyzing the energy potential from agricultural residues with energy potential more over we show experiments from crops such as rice, corn, mango wood branches, and longan wood branches, the ton of oil equivalent values are as follows: 376.87 TJ for rice, 648.95 TJ for corn, 45.71 TJ for mango wood branches, and 51.98 TJ for longan wood branches.

Keywords: web application, energy potential, agricultural residues

1. Introduction

Thailand's final energy consumption reached 3 6 , 7 9 5 ktoe, with a growth rate of 3 .0 percent from the corresponding period in 2012. The final energy consumption increased by 3.5 percent, comprising 3,312 ktoe of coal (9 percent), and the highest consumption was from refined oil at 17,476 ktoe (47.5 percent). Renewable energy usage accounted for 3 , 9 0 1 ktoe (1 0 . 6 percent), increasing by 1.7 percent, while traditional renewable energy decreased by 4 .4 percent, with a consumption of 1,332 ktoe (3 .6 percent) [1]. Due to the environmental impact of fossil fuels, such as greenhouse gas emissions contributing to global warming and pollution, utilizing appropriate and efficient methods to manage agricultural residues for bioenergy production can significantly reduce global energy-related emissions. This approach is effective in improving environmental conditions and contributes to substantial carbon dioxide reduction [2]. Energy derived from biomass is a sustainable source obtained from agricultural residues, forests, and households, processed into low-cost, environmentally friendly heat energy [3] . In recent years, there has been significant development in web applications for assessing bioenergy potential, focusing on bioenergy potential assessments. IRENA's global online tools aid in comprehensive regional assessments, facilitating easy data exploration. These tools source data directly from users, combining source, technology, and end-use information [4] . Geographical information is crucial in bioenergy potential assessments, incorporating spatial and characteristic data in the analysis process. Researchers have developed GIS tools, integrating geographical and characteristic data

using a data layer to help developers and investors manage sustainability risks and assess the efficiency of bioenergy utilization in all European Union member countries. To enhance preparedness for various risks, Geographic Information System (GIS) tools are employed for assessing bioenergy potential and quantities. A web portal designed for bioenergy potential assessment lacks in-depth links to local agricultural information, resulting in incomplete data coverage in some aspects. The BIORAISE application is a web-based tool providing detailed information about agricultural and forest biomass resources, considering the location of biomass producers and the costs of biomass collection and transportation. The National Renewable Energy Laboratory's web portal, developed by the U.S. Department of Energy, includes the BioPower and BioFuels Atlas, enabling comparative analysis of bioenergy, agricultural residues, biofuel potential, bioenergy distribution, and biomass data dissemination. These tools, however, lack interconnectivity, making them challenging to use.

The study of various literature reviews reveals that the Axios JavaScript Library technology has not yet been utilized in conjunction with web application development, despite its advantages. The tool excels in multitasking without waiting for the completion of preceding tasks, offering high security against Cross-Site Request Forgery (CSRF) attacks. This has led to its adoption in the development of a web application for assessing the energy potential from agricultural residues using the agricultural crop database in 2022 at Ping Khong Municipality, Chiang Dao, Chiang Mai, Thailand. For data acquisition, the system will gather information directly from users by specifying details such as agricultural area and production quantity. This data will be utilized for assessing the energy potential from agricultural residues in the Ping Khong Municipality area. Subsequently, the collected data will undergo processing within the backend system, where it will be analyzed and used to predict the quantity of agricultural residues. The processed information will then be sent to the frontend for user interaction, displaying the results on the screen.

The primary focus of this application is to support local farmers by providing tools for evaluating the energy potential of agricultural residues. The aim is to guide farmers in decision-making regarding the selection of suitable technologies for efficient bioenergy production, thereby minimizing negative environmental impacts. This approach assists farmers in making informed decisions about adopting technologies that align with the bioenergy potential of agricultural residues.

2. Methods

The research methodology for evaluating the energy potential from agricultural residues through a smart application involves several detailed steps. The web application design is divided into two main components: the user interface (UI) and the processing component, as illustrated in Figure 1. The user interface component has been developed using a combination of Laravel (PHP web application framework), HTML, Javascript, and the Bootstrap 5 toolkit (Front-end Framework). Additionally, Axios is employed to enhance the interface functionality, as depicted in Figure 2. To ensure easy access to various data, seamless data retrieval, transmission, and database interaction, the application utilizes an Application Programming Interface (API) as a central intermediary. This API acts as a communication channel between different components of the software, fostering effective communication between the application and the database [5].

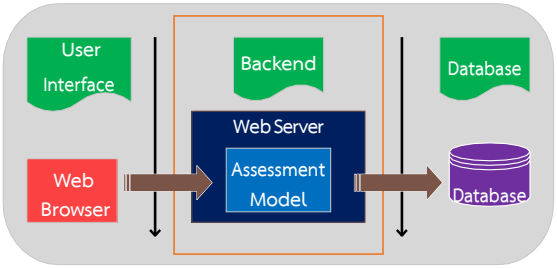

Figure 1. System Architecture.

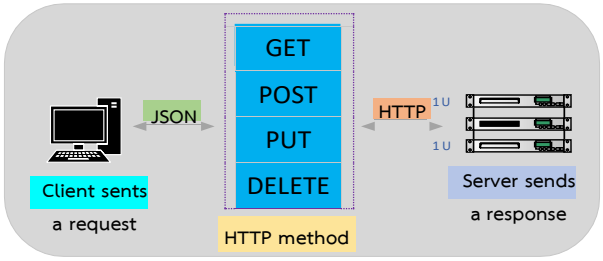

Figure 2. Work flow of API.

The processing component for evaluating the energy potential from agricultural residues in the spatial context utilizes agricultural crop data in the Ping Khong Subdistrict, Chiang Dao District, Chiang Mai Province, for the year 2022. The data is sourced from the agricultural plant database in the region, as shown in Table 1 . Additionally, factors considered for the assessment are based on criteria provided by the Department of Alternative Energy Development and Efficiency (DEDE) [6].

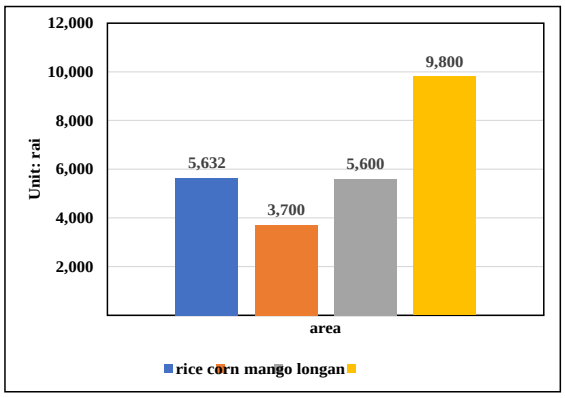

Figure 3. The agricultural crop database in 2022 at Ping Khong Municipality, Chiang Dao, Chiang Mai Thailand.

In the evaluation of biomass potential, key variables play a crucial role in determining the viability and quantity of biomass available. Two significant variables associated with assessing biomass potential are the Residue to Product Ratio (RPR) and the Surplus Availability Factor (SAF) [7].

The Residue to Product Ratio (RPR) is calculated using Equation 1 , providing a method to assess the proportion of agricultural residues concerning the total product yield [8].

$$CR = A \times Y \times RPR \qquad (1)$$

When CR denotes the quantity of agricultural residues, A signifies the cultivated area, Y represents the yield, and RPR stands for the Residue to Product Ratio. The value of RPR is contingent upon the type of biomass in each specific area.

TABLE 1 Table Showing Calorific Values of Biomass and Residue to Product Ratio.

	plant	product	residue	RPR
1	rice	599	husk	0.21
			straw	0.49
2	corn	866	stems	0.24
			cob	0.82
3	mango	1000	wood	0.43
4	longan	919	wood	0.31

The evaluation of the SAF, representing the proportion of biomass remaining unused or unutilized after meeting existing demands, can be determined using Equation 2

$$AR = CR \times SAF \qquad (2)$$

When AR Represents the Remaining Biomass After Utilization, and SAF Represents the Percentage of Unused Biomass.

TABLE 2 Table Showing Calorific Values and Percentage of Unused Biomass After Various Uses.

	plant	residue	heating value (MJ/kg)	SAF
1	rice	husk	13.52	0
		straw	12.33	27.70
2	corn	stalk	9.83	53.10
		cob	9.62	
3	mango	wood	18.98	0
4	longan	wood	17.35	0

The evaluation of the potential quantity of biomass materials can be conducted using Equation 3

$$BQ = A \times Y \times CR \times AR \quad (3)$$

When BQ Represents the Biomass Quantity Potential (in kg), A Represents the Cultivated Area (in rai), Y Represents the Yield (in kg per rai), B Represents the Ratio of Biomass Material to Yield, and C Represents the Proportion of Unused Biomass

The evaluation of energy potential can be considered through Equation 4

$$EQ = BQ \times HV \qquad (4)$$

When HV Represents the Calorific Value of Biomass Material (MJ/kg) The outcomes of energy potential assessments differ based on the diversity of biomass types present in each specific area. The obtained calorific value, which represents the heat content of biomass material, exhibits variations according to the characteristics and quantities of the specific biomass in that particular region.

The gathered variables for assessing biomass potential were utilized in the development of a system. This system incorporates a frontend interface for overviewing and displaying the results of biomass potential within the Ping Khong Municipality area. The biomass potential data is derived from calculations performed by the backend system, where Axios API serves as the intermediary for data requests and responses. These requests are sent to the backend system, developed using the Laravel framework, facilitating the retrieval of data from the database for computation. The data then undergoes a calculation process using a set of developed code to assess biomass potential. Upon completion of the calculations, the backend system responds with the computed data to the frontend, which initiated the request via Axios API. Subsequently, the received data is displayed on the interface.

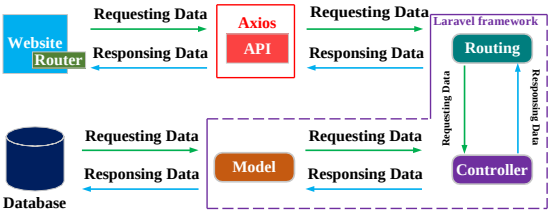

Figure 4. Overview of Web application.

In the calculation procedure for assessing the energy potential from biomass in the Ping Khong Municipality area, various detailed steps are involved, as illustrated in Figure 5.

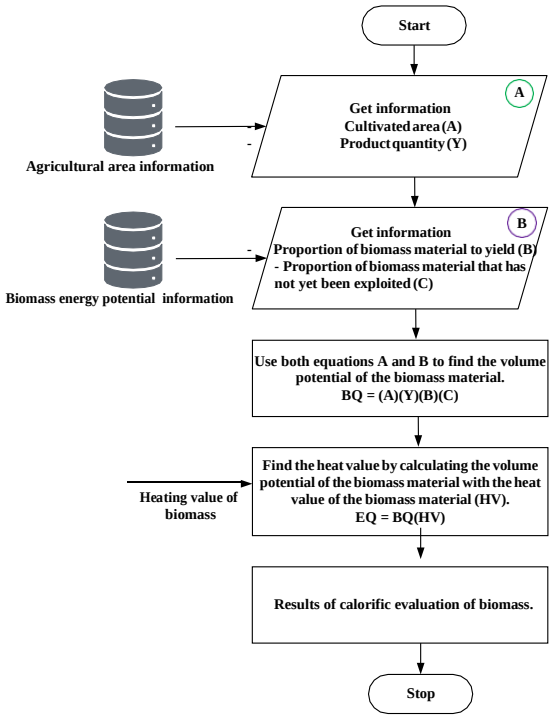

Figure 5. The flow diagram of the evaluate.

3. Results and Discussion

3.1 Energy potential from biomass

According to the assessment of energy potential from agricultural residues in the Ping Khong sub-district, it was found that corn exhibits the highest energy potential, estimated at 648.95 TJ. Following this, rice is calculated to have an energy potential of 376.87 TJ, followed by longan wood branches at 51.98 TJ, and finally, mango wood branches at 45.71 TJ. The overall energy potential is summarized at 1,123.52 TJ.

- Energy potential from rice

The energy potential assessment data for rice residue reveals that Ban Pang Makong has the highest potential, with 185.27 TJ for straw and 3.14 TJ for husk. On the other hand, Ban Pa Tueng Ngam demonstrates the lowest potential, with 47.36 TJ for straw and 0.80 TJ for husk, show in Figure 6.

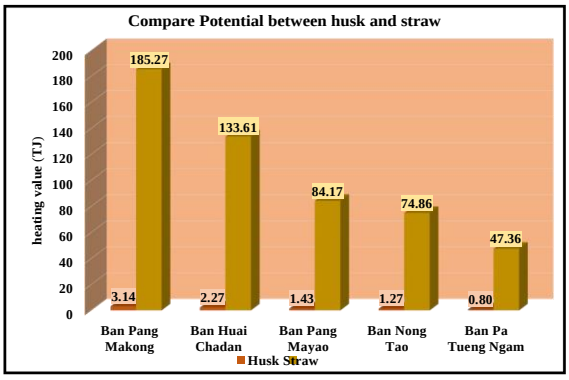

Figure 6. Energy potential between husk and straw.

- Energy potential from corn

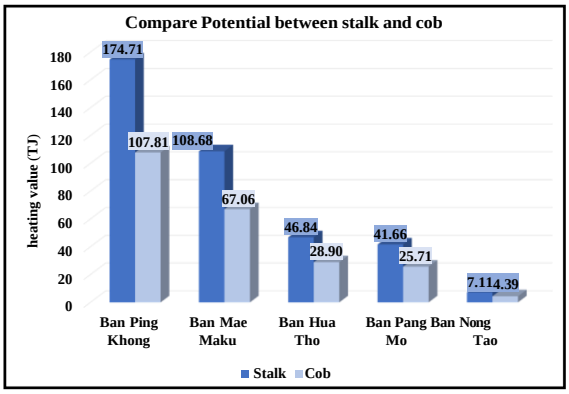

Figure 7. Energy potential between stalk and cob.

From Figure 7, it is evident that Ban Ping Khong has the largest cultivation area, resulting in the highest potential for energy from corn residue. The quantities are notably high, with 174.71 TJ for stalk and 107.81 TJ for cob. Following closely is Ban Mae Maku, with 108.68 TJ for straw and 67.06 TJ for husk. It can be observed that the energy potential from corn residue is highest in Ban Ping Khong, making it suitable for conversion into energy for utilization in the area.

- Energy potential from mango

The results of the assessment on the energy potential of mango wood branches residue reveal that there are three villages with closely comparable potentials, namely Ban Hua Tho with 3.68 TJ, Ban Pang Mo with 3.44 TJ, and Ban Nong Tao with 3.29 TJ. Among these, Ban Ping Phong exhibits the highest potential at 17.80 TJ, while Ban Nong Tao has the lowest potential at 3.29 TJ, show in Figure 8.

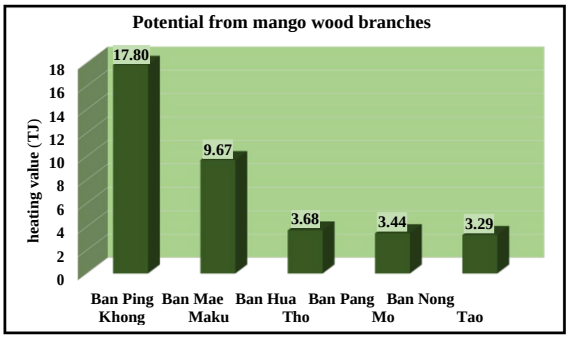

Figure 8. Energy potential for mango wood branches.

- Energy potential from longan

The energy potential assessment data for longan wood branches residue reveals that Ban Mae Maku and Ban Hua Tho exhibit a moderate level of potential. Ban Mae Maku has a potential of 7.84 TJ, while Ban Hua Tho has a potential of 7.13 TJ, show in Figure 9.

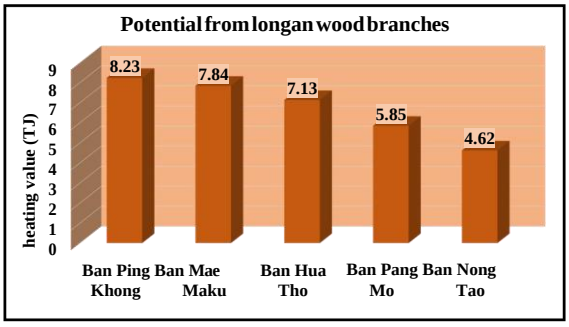

Figure 9. Energy potential for longan wood branches.

3.2 Display screen

- Overview energy potential in Ping Khong Municipality show in Figure 10 and Figure 11 – 13 show the energy potential categorized by each type.
- Display Calculate the composition of agricultural waste show in Figure 14. The explanation of the process is as follows.

  Step 1: Choose the crop from the list that you want to calculate.

  Step 2 : Specify the agricultural production quantity (kilograms) and the cultivation area (rai).

  Step 3: Click the search button.

  Step 4: After the search is complete, the results of the energy potential calculation for the selected crop will appear on the screen. The information

will include the biomass residue of the crop, crop type, production yield (kilograms), cultivation area (rai), heat value (MJ/kg), and energy value (MJ). This will help determine the energy potential from the remaining material in the deep cultivation area.

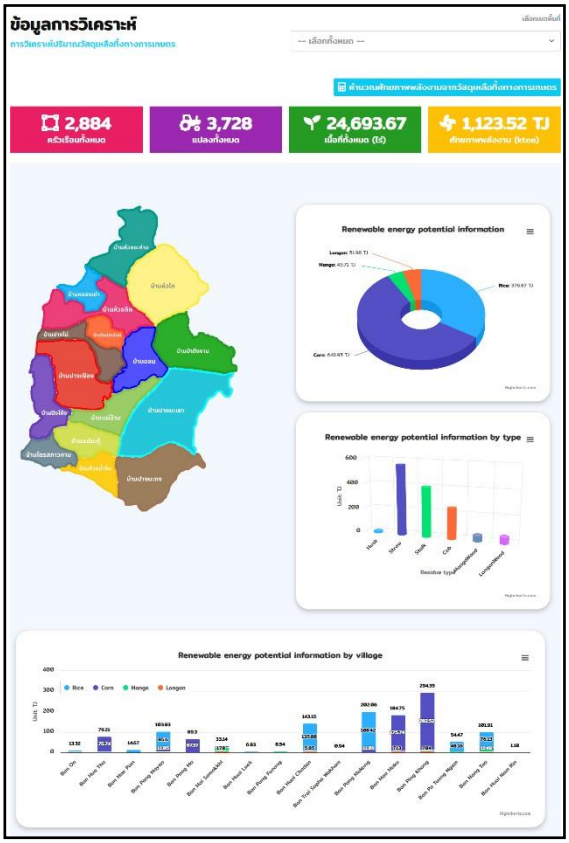

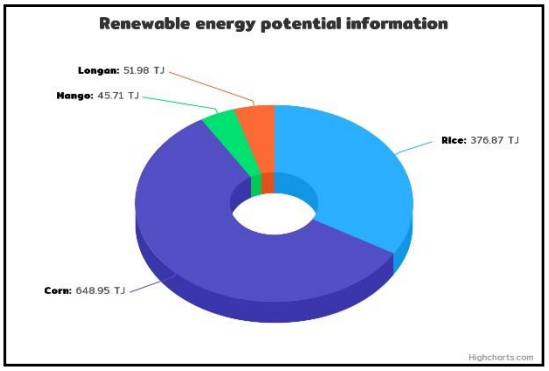

Fig. 11 Renewable energy potential information.

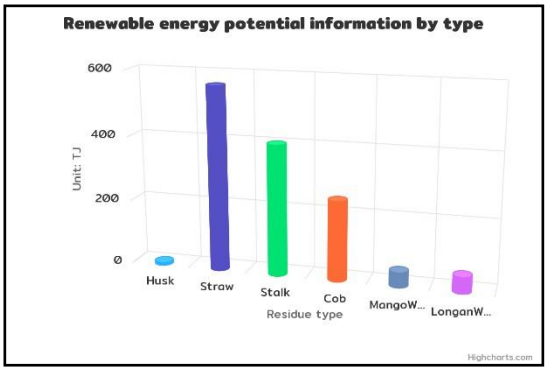

Figure 12. Renewable energy potential information by type.

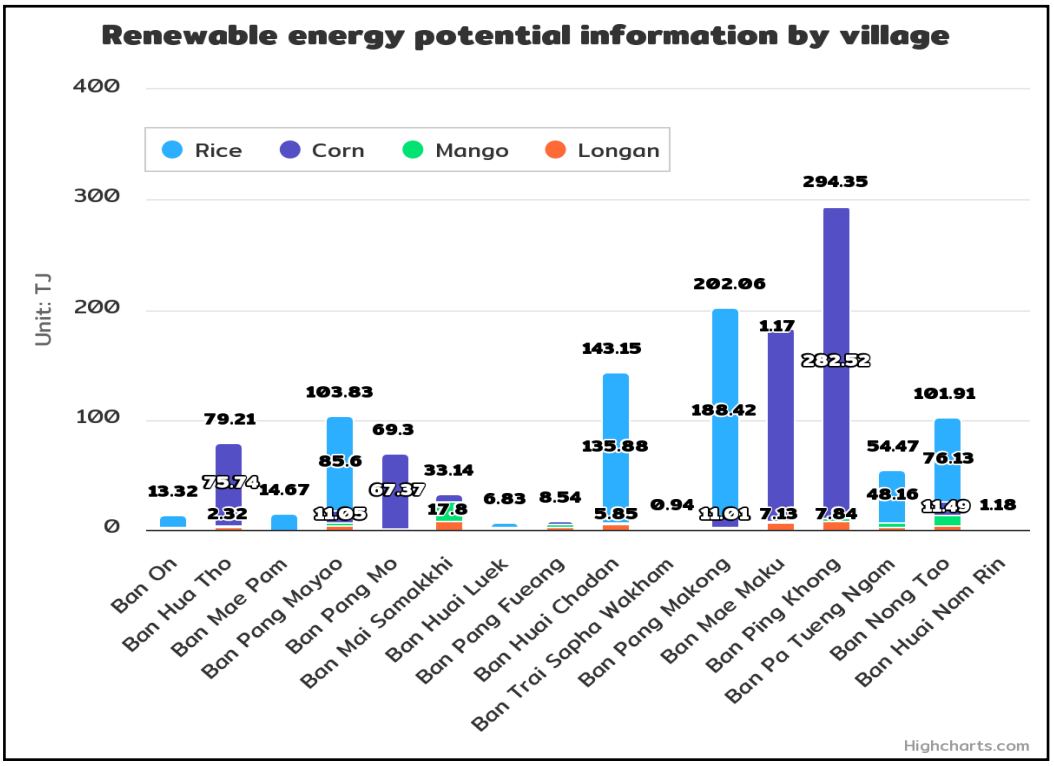

Figure 13. Renewable energy potential information by village.

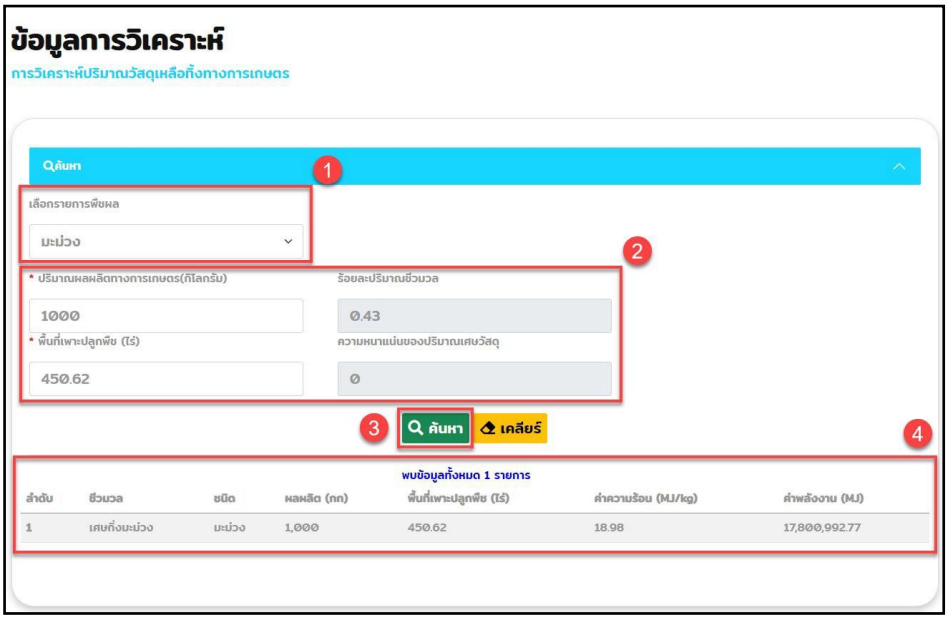

Figure 14. Display Calculate the composition of agricultural waste.

4. Conclusions

In this research, a web application has been adapted for the purpose of assessing the energy potential from agricultural residues in the municipal sub-district of Ping Khong. This adaptation aims to address air pollution issues stemming from burning practices. The overall energy potential in the area is estimated at 1,123.52 TJ. The energy potential from corn is the highest, totaling 648.95 TJ, followed by rice at 376.87 TJ, longan wood branches at 51.98 TJ, and mango wood branches at 45.71 TJ. It is evident that corn residue holds the highest energy potential in the region, making it suitable for undergoing processing into a thermal energy form for local community use.

5. Acknowledgment

This research received support from the School of Renewable Energy at Maejo

University, Chiang Mai, Thailand. We extend our gratitude to the school for providing laboratory facilities and scholarships. Special thanks are given for the scholarship awarded in the project aimed at producing and developing graduates in renewable energy for ASEAN countries, specifically for the graduate students in the year 2022.

References

[1] Department of Alternative Energy Development and Efficiency, 2023.

[2] Charfeddine, L., Kahia, M., (2019). Impact of renewable energy consumption and financial development on CO2 emissions and economic growth in the MENA region: a panel vector autoregressive (PVAR) analysis. *Renew. Energy*, *139*, 198–213. https://doi.org/10.1016/j.renene.2019.01.010.

[2] Weidner, T., Yang, A., (2020). The potential of urban agriculture in combination with organic waste valorization: Assessment of resource flows and emissions for two European cities. *Journal of Cleaner Production*, *244*(20), 118490. https://doi.org/10.1016/j.jclepro.2019.118490.

[3] Brahushi F., Alikaj M., Abeshi P., Draeck M., Geylan O., Hyso H. (2020). Assessment of biomass potential as bio-energy source from fruit trees and grapes in Albania. *Bulgarian Journal of Agricultural Science*, *26*(6), 1143–115.

[4] Tauro, R., Rangel, R., Suarez, R., Caballero, J., Anaya-Merchant, C., Salinas-Melgoza, M., Guzman, H., Ghilardi, A. (2021). An integrated user-friendly web-based spatial platform for bioenergy planning. *Biomass and Bioenergy*, *145*, 105939. doi:https://doi.org/10.1016/j.biombioe.2020.105939.

[5] E. Daga, L. Panziera, C. Pedrinaci. (2015 A BASILar Approach for Building Web APIs on top of SPARQL Endpoints. *Proceedings of the Third Workshop on Services and Applications over Linked APIs and Data (Maleshkova, Maria; Verborgh, Ruben and Stadtmüller, Steffen eds.)*, *1359*, pp. 22–32. http://ceur-ws.org/Vol-1359/paper4.pdf.

[6] Pattana S., Wiratkasem K. (2013, September). The analysis of biomass potential in Thailand. *The Fifth International Conference on Science, Technology and Innovation for Sustainable Well-Being (STISWB V)*. Luang Prabang, Lao.

[7] Assoc. Prof. Dr. Sawitree Karivat (2010). Complete research report, project, review and comparative analysis of research results in evaluating the potential of biomass energy sources. Graduate School of Energy and Environment King Mongkut's University of Technology Thonburi.

[8] Rodriguez Caceres K., Blanco Patino F., Araque Duarte J., Kafarov V., (2016). Assessment of the energy potential of agricultural residues in non-interconnected zones of colombia: case study of chocó and putumayo. Chemical Engineering Transactions, 50, 349-354. https://doi.org/10.3303/CET1650059.

Mr. Surachart Sirichouangchote
Master student, Master of Engineering (Renewable Energy Engineering).
Research Interests:
Biomass, and Web application.

Dr. Thongchai Maneechukate, PhD
Assistant Professor.
Research Interests:
Electrical Engineering, Control System Engineering and Smart Farm.

Dr. Sarawut Polvongsri, PhD
Assistant Professor.
Research Interests:
Solar thermal cooling and heating, Energy conservation and Energy Economic.

Dr. Chawaroj Jaisin, PhD
Associate Professor.
Research Interests:
Embedded technology, Postharvest technology and Energy conservation.

The 29th Tri-U International Joint Seminar and Symposium
Maejo University, Chiang Mai, Thailand, 21–24, December 2023

Influence of vegetation on rain garden for stormwater quality improvement

Chamaiporn Nantakham[1], Prattakorn Sittisom[1*]

[1]Department of Environmental Engineering, Faculty of Engineering, Chiang Mai University, Thailand
*E-mail: prattakorn.s@cmu.ac.th

Abstract: A major concern in water quality problem is eutrophication which is caused by the nutrients, namely nitrogen and phosphorus. Recent studies have reported efficiency of nitrogen and phosphorus removal from stormwater runoff using rain garden or bioretention. The objective of this study is to examine and evaluate the efficiency of rain garden in nitrogen and phosphorus removal by using local plant, Ruellia tuberosa, in lab-scale reactors and estimate for future design to be used in the rain garden. Ruellia tuberosa was considered for its ability to remove pollutants and for survivability. Ruellia tuberosa used in this study showed a significant TSS, TN removal and slightly TP removal ability compared to soil. The effects of nutrients on aquatic organisms and eutrophication can be mitigated by improving the soil media with Ruellia tuberosa in the bioretention cells such as raingarden. This could be applied in the real world where stormwater runoff can be treated before entering river or stream therefore cutting the need for future restoration.

Keywords: *Ruellia tuberosa*, Rain Garden, Stormwater Runoff

1. Introduction

Rain gardens are being increasingly adopted in different parts of the world as strategies to manage stormwater pollution and to help mitigate the deleterious effects of climate change and urbanization [1,2]. Stormwater biofiltration systems (also known as bioretention, biofilters, rain gardens) comprise one example of a popular GI measure that has found application in a range of urban settings. Biofilters consist of a vegetated basin or trench, filled with an engineered media and often equipped with an underlying saturated zone. Their numerous bio-ecological benefits have been documented [3]. Stormwater biofilters effectuate treatment through a range of bio-physico-chemical processes. Pollutant treatment effectiveness, therefore, varies depending on the surrounding climate; for instance, lower pollutant removal has been recorded in cold climates due to reduced biotic activity because of lower temperatures [4] while specific design considerations (incl. proper plant selection) are required in semi-arid climates to sustain plant health and treatment performance due to the negative impact of drying on treatment performance [5]. While studies have investigated the performance of stormwater biofilters in different climatic regions [6-8], few have specifically investigated the effect of type of plant species [5].

Plants form a key design component of these systems, not only in their role in enhancing biodiversity and the natural beauty of the urban landscape but also in their contribution to improved biofilter treatment performance [9]. Plants help facilitate treatment both directly through biotic uptake and indirectly by influencing the soil porosity and microbial communities responsible for pollutant degradation [10]. For example, the presence and/or type of plant species employed in stormwater biofilters have been reported to benefit removal of nitrogen (TN), fecal indicator organisms (E. coli) and to a lesser extent phosphorus (TP) [11].

This study aims to address the investigating the response of local plant species, namely *Ruellia tuberosa* in nutrient removal under tropical weather conditions. The interactive relationships between plant root characteristics, system infiltration capacity and pollutant removal are additionally explored to inform processes. This study offers practical recommendations for the selection of plant species for designing rain gardens.

2. Materials and methods

2.1. Experimental design and procedure

This study examines the effect of a plant species, namely, *Ruellia tuberosa* (RT) and a non-vegetated control. *Ruellia tuberosa* is a Thai native species that recommended for its effective performance from Department of Highways. This research focuses on investigating the treatment performance of *Ruellia tuberosa*.

The reactors were set up in an outdoor area (Figure 1). The reactors were constructed from 60 cm width, 180 cm length and 100 cm height steel frame, with a transparent acrylic plate allowing for media observation. Reactors were filled with different layers of media (from top to bottom: 40 cm of washed sand, 10 cm of fine sand and 30 cm of gravel aggregates). A permanent saturated layer of 40 cm was created by raising the outlet pipe; this comprised part of the filter media, the gravel drainage, and the transition layer (Figure 1). Plants, sourced from local nurseries, were planted (8 plants). Following an initial plant establishment phase, columns were watered with 200 L of synthetic stormwater.

The frequency of stormwater application was designed to match the average occurrence of storm events based upon rainfall data from Chiang Mai Province, and the dose volume (200 L) was determined using the same rainfall data. This was based on a monthly average effective rainfall of 200 mm/month of rainy season in Chiang Mai and using a biofilter sized to 4% of its contributing catchment.

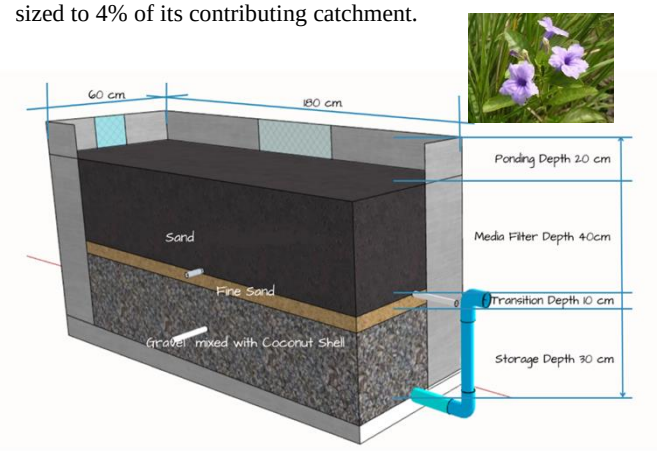

Figure 1 Reactor column (with and without plants use the same design, plant names *Ruellia tuberosa*)

2.2. Synthetic runoff

Synthetic runoff was introduced to the rain garden systems during the experiment. Bentonite was added to tap water as Total Dissolved Solid (TSS); Disodium phosphate and Glycine were used to imitate Total Phosphorus (TP) and Total Nitrogen (TN).

2.3. Data analysis

Concentrations of all pollutants below the detection limit were taken as the detection limit for analysis. Removal efficiency of TSS, TN and TP were calculated as the percentage of the difference between inflow and outflow concentrations divided by the inflow concentration.

3. Results and discussion

3.1. Pollutant leaching process

The concentrations in the outflow TSS, TN, and TP of each reactor during the experiment are presented in Figure 2-4. The outflow TSS from reactor without plant was lower than 1.0 mg/L and TSS from reactor with plant was lower than 1.0 mg/L as well. There was no significant difference in the emission of TSS between reactors with different structures.

As the run time increased, the outflow TN from each reactor decreased gradually. The outflow TN from without and with plant were lower than 3.40 mg/L and 3.0 mg/L, respectively. These results indicate that the reactor with the plant had slightly better nitrogen leaching control performance. This was partly attributed to the change in system structure. Specifically, the extension of hydraulic retention time was beneficial to denitrification, which was consistent with the nitrogen control performance observed in previous studies, in which nitrogen removal was enhanced by providing a saturated zone [12].

The outflow TP from each reactor decreased gradually, eventually stabilizing. The outflow TN from without and with plant were both lower than 0.1 mg/L. The phosphorus leaching from each reactor may be attributed to phosphorus release from the media [13,14]. The performance of TP leaching mainly depends on media type [15]. Hence, the relatively higher phosphorus leaching from the reactor may have been related to the larger media volume.

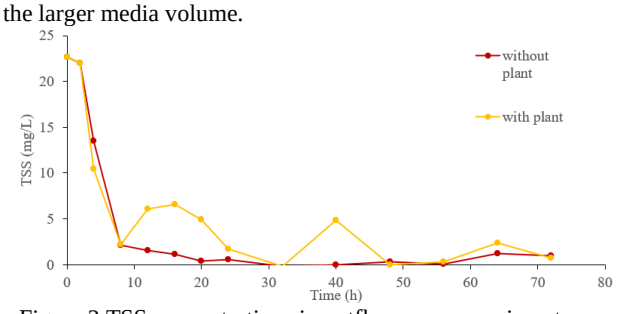

Figure 2 TSS concentrations in outflow over experiment run times.

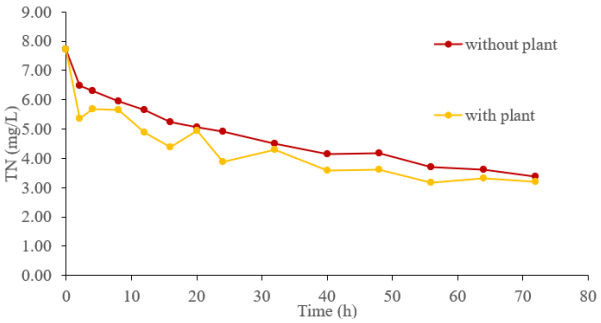

Figure 3 TN concentrations in outflow over experiment run times.

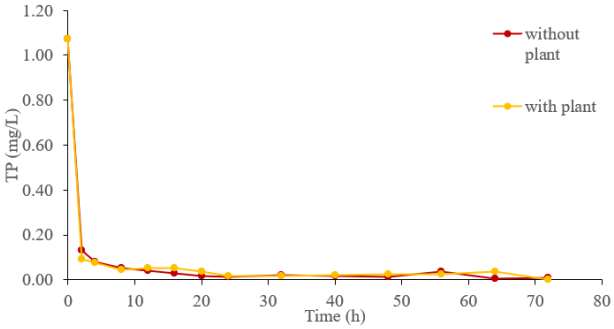

Figure 4 TP concentrations in outflow over experiment run times.

3.2. Nutrient removal from Synthetic runoff

The percent removal plots of outflow pollutant concentrations for each reactor during the synthetic runoff experimental stage (TSS, TN, and TP) are shown in Figure 5 - 7.

Figure 5 shows outflow TSS. The inflow TSS was set at 22.7 mg/L. The outflow TSS levels from without and with the plant reactor were not significantly different from the synthetic runoff experimental stage. The outflow TSS from reactor without plant ranged from 22.7 to 1.0 mg/L and from reactor with plant ranged from 22.7 to 0.8 mg/L. The rain garden better controlled TSS in runoff, which was confirmed by the high removal efficiency for total suspended solids (TSS) by rain garden reported in previous studies [16,17].

Figure 6 shows outflow TN. The inflow TN was set at 7.7 mg/L. The outflow TN levels from without and with the plant reactor were slightly different from the synthetic runoff experimental stage. The outflow TN from reactor without plant ranged from 7.7 to 3.4 mg/L and from reactor with plant ranged from 7.7 to 3.0 mg/L. Reactor can improve TN removal. Both reactors provided saturated zones to strengthen denitrification and extended the hydraulic retention time to improve nitrogen removal efficiency [18]. When the reactor received runoff, during the wetting period, dissolved organic N and NH^{+}_{4} were adsorbed by media, plant root. Particulate organic N was removed through filtration. Subsequently, during the drying period, nitrogen species were transformed into nitrate by ammonification and nitrification. Denitrification may occur in anoxic conditions as well as in subsequent wetting periods [18]. In addition, because of the structure of the reactor the hydraulic retention time, in-flow paths, and anoxic conditions are all strengthened to some extent. The level of

carbon from media, stormwater inflow, and root and microbial turnover in the media was sufficient to allow denitrification [18].

Figure 7 shows outflow TP. The inflow TP was set at 1.0 mg/L. The outflow TP levels from without and with the plant reactor were almost completely removed from the synthetic runoff experimental stage. The rain garden mainly removed P through adsorption and precipitation, and only a small part of the P was utilized by plants and microbes [19]. Particulate phosphorus was managed with particulate matter, which was effectively removed through precipitation and filtration in the rain garden. Rain gardens were shown to have high removal efficiency for phosphorus in runoff in previous studies [17,19].

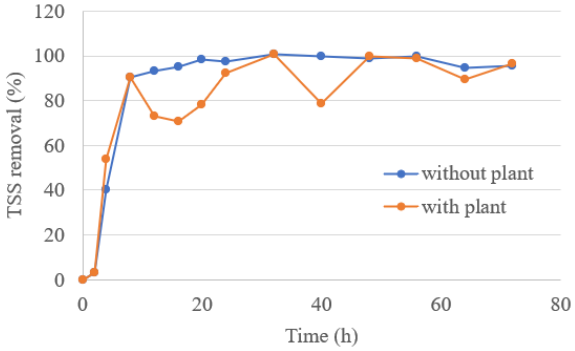

Figure 5 TSS removal efficiency

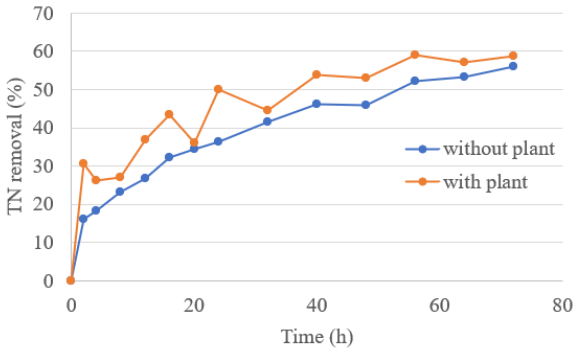

Figure 6 TN removal efficiency

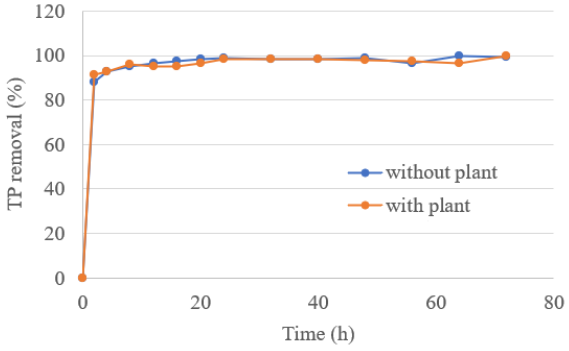

Figure 7 TP removal efficiency

4. Conclusions

Pollutants removal from synthetic runoff by without and with plant rain garden, which were proposed in this study, was assessed through a laboratory-scale experiment. The main findings were as follows:

During the synthetic runoff experimental stage, the TSS and TP removal efficiencies of the without and with plant rain garden clearly improved, increasing to 100%. And TN removal efficiencies of the without and with plant rain garden clearly improved, increasing to 56% and 59%, respectively. Both without and with plant rain garden can effectively improve TSS and TP removal from precipitation and filtration mechanism. TN can be absorbed effectively by plant uptake.

Results from this study could be useful to stormwater managers who are utilizing rain garden basins to improve the water quality of stormwater runoff in a similar tropical climate setting.

References

[1] Charlesworth, S.M., 2010. A review of the adaptation and mitigation of global climate change using sustainable drainage in cities. J. Water Clim. Change 1 (3), 165 – 180.

[2] Li, C., Peng, C., Chiang, P.-C., Cai, Y., Wang, X., Yang, Z., 2019. Mechanisms and applications of green infrastructure practices for stormwater control: A review. J. Hydrol. 568, 626 – 637.

[3] Zhang, K., Chui, T.F.M., 2019. Linking hydrological and bioecological benefits of green infrastructures across spatial scales – A literature review. Sci. Total Environ. 646, 1219 – 1231.

[4] Kratky, H., Li, Z., Chen, Y., Wang, C., Li, X., Yu, T., 2017. A critical literature review of bioretention research for stormwater management in cold climate and future research recommendations. Front. Environ. Sci. Eng. 11 (4), 16.

[5] Houdeshel, C.D., Hultine, K.R., Johnson, N.C., Pomeroy, C.A., 2015. Evaluation of three vegetation treatments in bioretention gardens in a semi-arid climate. Landscape Urban Plann. 135, 62 – 72.

[6] Blecken, G.-T., Zinger, Y., Deleti ´ c, A., Fletcher, T.D., Hedstr ¨ om, A., Viklander, M., 2010. Laboratory study on stormwater biofiltration: Nutrient and sediment removal in cold temperatures. J. Hydrol. 394 (3-4), 507 – 514.

[7] Mahmoud, A., Alam, T., Yeasir A. Rahman, M., Sanchez, A., Guerrero, J., Jones, K.D., 2019. Evaluation of field-scale stormwater bioretention structure flow and pollutant load reductions in a semi-arid coastal climate. Ecol. Eng. X 142, 100007. https://doi.org/10.1016/j.ecoena.2019.100007.

[8] Roseen, R.M., Ballestero, T.P., Houle, J.J., Avellaneda, P., Briggs, J., Fowler, G., Wildey, R., 2009. Seasonal performance variations for storm-water management systems in cold climate conditions. J. Environ. Eng. 135 (3), 128 – 137.

[9] Payne, E.G.I., Hatt, B.E., Deletic, A., Dobbie, M.F., McCarthy, D.T., Chandrasena, G.I., 2015. Adoption Guidelines for Stormwater Biofilter Systems (Version 2). Cooperative Research Centre for Water Sensitive Cities, Melbourne, Australia.

[10] Payne, E.G.I., Fletcher, T.D., Cook, P.L.M., Deletic, A., Hatt, B.E., 2014a. Processes and drivers of nitrogen removal in stormwater biofiltration. Crit. Rev. Environ.

Sci. Technol. 44 (7), 796 – 846.
[11] Muerdter, C.P., Wong, C.K., LeFevre, G.H., 2018. Emerging investigator series: The role of vegetation in bioretention for stormwater treatment in the built environment: Pollutant removal, hydrologic function, and ancillary benefits. Environ. Sci. Water Res. Technol. 4 (5), 592 – 612.
[12] Lucas W.C., Greenway M., 2010. Nitrogen retention in bioretention mesocosms with outlet controls. In: Proceedings of the World Environmental and Water Resources Congress 2010, Providence, Rhode Island, USA, 16 – 20 May, pp 3038 – 3047
[13] O ' Neill S.W., Davis A.P., 2012. Water treatment residual as a bioretention amendment for phosphorus. II: long-term column studies. J Environ Eng 138:328 – 336
[14] Li J., Davis A.P., 2016. A unified look at phosphorus treatment using bioretention. Water Res 90:141 – 155
[15] Jay J.G., Brown S.L., Kurtz K., Grothkopp F., 2017. Predictors of phosphorus leaching from bioretention soil media. J Environ Qual 46(5): 1098 – 1105
[16] Hatt B.E., Fletcher T.D., Deletic A., 2009. Pollutant removal performance of field-scale stormwater biofiltration systems. Water Sci Technol 59: 1567 – 1576
[17] Goh H.W., Zakaria N.A., Lau T.L., Foo K.Y., Chang C.K., Leow C.S., 2017. Mesocosm study of enhanced bioretention media in treating nutrient rich stormwater for mixed development area. Urban Water J 14: 134 – 142
[18] Zinger Y., Blecken G.T., Fletcher T.D., Viklander M., Deleti ć A., 2013. Optimising nitrogen removal in existing stormwater biofilters: benefits and tradeoffs of a retrofitted saturated zone. Ecol Eng 51:75 – 82
[19] Liu J., Davis A.P., 2014. Phosphorus speciation and treatment using enhanced phosphorus removal bioretention. Environ Sci Technol 48: 607 – 614

Chamaiporn Nantakham

Master Student, Master of Engineering (Environmental Engineering)

Research Interests: Water Treatment, Stormwater Runoff Improvement, Rain Garden

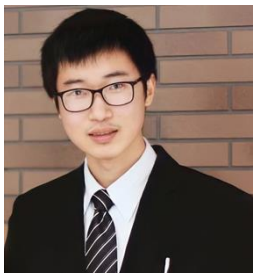

Dr. Prattakorn Sittisom

Lecturer

Research Interests: Water Treatment, Membrane Filtration Technology

The 29th Tri-U International Joint Seminar and Symposium
Maejo University, Chiang Mai, Thailand, 21–24, December 2023

Green Culture, Environmental Information Disclosure Quality and Financing Constraints: A Textual Analysis Based on Corporate Social Responsibility Reports

Yaosheng Liang[1]

[1] *School of Business, Guangxi University, Nanning 530004, China*

Abstract: In the era of ecological sustainability, embracing a green development mindset is crucial for the long-term success of businesses. With the rise of machine learning and text analysis methods for mining unstructured data, green culture, as the top-level design in corporate governance, determines the behavior patterns, operational strategies, and fulfillment of social responsibilities by companies. This study, based on the agency theory, utilizes unbalanced panel data from listed companies between 2010 and 2021. By employing Python for web scraping of textual content from corporate social responsibility reports, it constructs indicators to measure green culture and empirically examines its relationship with financing constraints through text analysis and machine learning techniques. The results indicate that green culture alleviates financing constraints. The quality of environmental information disclosure mediates the relationship between green culture and financing constraints. Heterogeneity tests reveal that the inhibitory effect of green culture on financing constraints is significant only for state-owned enterprises, heavily polluting industries, and companies located in eastern regions. Ultimately, this study enriches the research on factors influencing financing constraints from the perspective of cultural informal institutions. Moreover, it provides empirical evidence for enhancing green culture development and broadening the horizons of corporate culture.

Keywords: Green culture, Financing constraints, Environmental information disclosure quality, Mediating effect.

1. Introduction

Financing constraints are a global business challenge(Elshaarawy and Ezzat, 2023). China's emphasis on green development aligns with its macroeconomic policies, yet Chinese enterprises face hindrances in securing funding for green initiatives. This necessitates an expedited focus on enhancing green development.

Green culture is centered on green values and image(Abbas and Dogan, 2022). Cultivating green culture may entail costs, both internally in regulating values throughout the organization and externally through image promotion and information disclosure. However, it is essential to determine if fostering green culture yields returns.

New Institutional Economics theory highlights the profound influence of informal institutions like culture on economic operations in nations like China, where formal institutional frameworks are gradually improving. Recent research explores the impact of culture on corporate behavior and economic outcomes. While prior studies have examined how various cultures affect corporate governance, financing, and economic results, limited research exists on the economic implications of green culture in China.

Key questions emerge: Can green culture act as an effective governance mechanism, improving internal management and external resource acquisition to address financing difficulties? Can external investors discern positive signals conveyed by enhanced green images and environmental information disclosure in China's underdeveloped financial markets? Will robust environmental information disclosure, driven by green culture, reduce capital costs? These academic inquiries require prompt investigation.

2. Theory and hypotheses

2.1 Green culture and Financing constraints

Eco-Civilization Construction extends beyond the "human and nature" relationship, embracing "human and human, human and society." Enterprises, as crucial participants, shape their culture, reflecting agreements between them and employees and alignment with societal stakeholders. Cognitive behavior theory highlights corporate culture as an intermediary in coordinating emotions and actions, while intersubjectivity theory emphasizes multi-stakeholder interaction in culture building. Green culture alignment signifies not just ecological responsibility but consensus and collaboration among diverse stakeholders—employees, creditors, suppliers, investors, analysts, consumers, and government—in pursuing sustainable green development.

Responsibility and Feedback Perspective: Green culture enhances corporate social responsibility and value creation by influencing executive team collaboration. It represents ethical norms, reducing moral hazards, and embodying corporate integrity and collaborative governance ideals. This fosters trust in relationships with suppliers, customers, and the entire supply chain. Executives, under green principles, prioritize interactions with external stakeholders, emphasizing ecological benefits alongside economic gains, shaping a holistic sense of responsibility values. This enhances competitiveness and attracts green investors, reducing adverse selection and moral risks. Building a green culture also enhances corporate reputation, conveying a positive future trend, attracting more investor attention and support.

Regulatory and Supportive Bodies Perspective: Corporate green culture shapes strategic decisions and business objectives, making it easier to gain recognition from environmental authorities and non-social environmental subsidies. In China's socialist market economy, institutional support is crucial for green economy development. Governments focus on environmental protection and green growth, providing fiscal subsidies and tax incentives to promote green development. Financial institutions adapt financing policies, offering green credit to support corporate green initiatives. Green culture symbolizes social responsibility and compliance with the national green sustainable development concept, providing access to significant financing sources.

Identity Subjects Perspective: As a cultural value, green culture influences employee behavior cognitively, fostering shared understanding and values alignment. It strengthens company identification, as personal property is an extension of self-concept. Employee shareholding positively impacts corporate identification by signaling to investors and supplementing cash flow, alleviating financing constraints.

Hypothesis 1: A higher level of green culture in a company correlates with reduced financing constraints, indicating green culture's potential in easing financing constraints for enterprises.

2.2 Mediating effect of Environmental information disclosure

Resource Theory Perspective: Green culture, arising from daily operations, is a unique asset shaping corporate decision-making. A strong green culture increases consideration of environmental protection in daily operations. Such firms are more willing to proactively disclose environmental information, fostering a green corporate atmosphere and signaling eco-friendliness to society.

Reputation Theory Perspective: A robust green culture builds a positive corporate image and social reputation. Companies with strong reputations attract support from stakeholders with varying capital. Green culture signifies a commitment to ecological norms, enhancing industry reputation. Investors favor reputable companies. Corporate social responsibility reduces default risk, encourages transparency, and lowers financing costs.

Agency Theory Perspective: Shareholders entrust investments to management, but their interests may not align. Management sometimes neglects environmental and social responsibility. Strengthened internal governance, focusing on social responsibility and environmental protection, is vital for sustainability. Information asymmetry hinders understanding, but green culture promotes fair environmental information disclosure.

Environmental Information Disclosure: Communicating economic environmental information to stakeholders aids financing decisions. Environmental disclosure promotes governance, regulation compliance, and social reputation, reducing financing constraints.

Signal Transmission Theory Perspective: Green culture shapes business strategy, emphasizing long-term environmental disclosure. Stricter regulations and investor focus lead to institutional investor scrutiny. High-quality disclosure reduces risks, assures cash flows, and attracts investor interest. Companies with high environmental risks must enhance disclosure quality to mitigate financing constraints.

Hypothesis 2: Environmental information disclosure mediates the relationship between green culture and financing constraints. Green culture improves disclosure quality, easing financing constraints.

3. Materials and research methods

3.1 Models

In this paper, to test H1, whether green culture significantly impacts financing constraints while avoiding the "false regression" phenomenon, this study further controls for time and industry fixed effects, constructing the following econometric regression model:

$$sa_{i,t} = \alpha_0 + \alpha_1 ln\_green_{i,t} + \alpha_2 Controls_{i,t} + \sum Symbol / Year / IndustryFe + \varepsilon_{i,t} \quad (1)$$

To validate H2, this study follows the mediation analysis three-step method.It supplements with the following econometric regression models:

$$edi_{i,t} = \alpha_0 + \alpha_1 ln\_green_{i,t} + \alpha_2 Controls_{i,t} + \sum Symbol / Year / IndustryFe + \varepsilon_{i,t} \quad (2)$$

$$sa_{i,t} = \alpha_0 + \alpha_1 ln\_green_{i,t} + \alpha_2 edi_{i,t} + \alpha_3 Controls_{i,t} + \sum Symbol / Year / IndustryFe + \varepsilon_{i,t} \quad (3)$$

Where Controls represent control variables, α_0 denotes the intercept term, α_1 represents the regression coefficient, and $\varepsilon_{i,t}$ signifies the error term.

3.2 Definition of variables

(1) Explained variables

Following the practices of Zhang and Wang et al.(2023), the SA index is used to measure corporate financing constraints due to the strong exogeneity of two variables: firm size and years since listing. The SA index is calculated based on the formula from the research by Ju Xiaosheng et al., as follows:

$$SA = -0.737 \times lnSize + 0.043 \times lnSize^2 - 0.040 \times Age$$

Where: lnSize represents the natural logarithm of total assets of the company. Age represents the years since the company's initial public offering (IPO).

The results obtained from the above formula are all negative values. Therefore, the absolute value of SA is taken as the index, where a larger SA value indicates a higher degree of financing constraints faced by the company.

(2) Explanatory variables

The explanatory variable is "green culture" (ln_green), measured using a methodology inspired by Zhang and Shi et al.(2019)., Baier and Berninger et al.(2020).

The measurement process for "green culture" (ln_green) involves several steps:

First, keywords related to green culture are chosen from corporate social responsibility reports, following Zhang et al.'s guidelines.

Python programming is employed to scrape social responsibility reports from publicly-listed companies on CNINFO (China Stock Market & Accounting Research). These reports are then batch-downloaded in PDF format and converted into TXT files. This step includes rigorous data filtering to eliminate unreadable or corrupted PDF documents.

Subsequently, a set of seed keywords is established to capture green values, principles, and mission statements, aligning with the concept of green culture.

To quantify green culture, the Continuous Bag-of-Words Model (CBOW) from Word2Vec is applied to Chinese text data extracted from Management Discussion and Analysis (MD&A) reports. This model constructs word vectors for predicting similar words within the context of a target word. The resulting value is transformed logarithmically, where a higher value indicates a stronger presence of green culture. As shown in Table 1. The larger the value of this indicator, the higher the level of green culture within the company.

Table 1: Keyword Table for Green Culture

Seed Word	Vocabulary of "Green Culture"
Green Ecology	Environmental Governance
	Beautiful Countryside
	Ecological Construction
	Ecological Civilization
	Ecological Environment
	Green Living
	Green Development
	Green Production
	Green Engineering
	Green Environmental Protection
	Ecological Balance
	Biodiversity

Harmonious Coexistence	Human and Nature
	Species Diversity
	Environmentally Friendly
	Coexisting in Beauty
	Natural Resources
Stakeholders	Shareholders
	Creditors
	Business Partners
Social Responsibility	The Public
	Social Interests
	Credibility
	Corporate Citizenship
Energy Conservation and Emission Reduction	Low Energy Consumption
	Green and Clean
	Zero Emissions
	Clean Production
	Efficiency and Intensity
	Pollution Reduction
	Energy Production
	Energy Storage
	Low Energy Consumption
Circular Economy	Comprehensive Utilization
	Circular Regeneration
	Resource Conservation
	Sustainable Development
Low Carbon Operation	Low Carbon
	Carbon Reduction
	Carbon Reduction
	Carbon Neutrality
	Low Carbon Economy
	Low Carbon Operation
Green Development	Green Investment
	Green Financing
	Pollution Prevention and Control
	Comprehensive Improvement
	Sustainable
	High-Quality Development

（3）Mediation variables

Drawing on the studies by Lin and Huang et al. (2021), this research adopts a "content analysis" approach. It selects four dimensions, namely environmental liabilities, environmental management disclosure, environmental regulations and certification disclosure, and environmental disclosure medium, to construct an Environmental Disclosure Index for assessing the quality of environmental information disclosure.

（4）Other variables

Following the empirical research on corporate financing constraints by Zhang and Wang et al. (2023), and the studies on environmental information disclosure quality by Lin and Huang et al. (2021), this study considers the characteristics of China's relational society to enhance robustness and mitigate the impact of omitted variables.

In terms of corporate performance and financial conditions, control variables include company size (size), company age (fnage), leverage ratio (lev), return on assets (roa), profitability (loss), revenue growth rate (gro), total asset turnover (turnover), free cash flow (fcf), fixed asset intensity (ppe), intangible asset intensity (intangible), earnings per share (eps), current ratio (cr).

Regarding corporate governance aspects, control variables encompass the first major shareholder's ownership percentage (co), board size (dn), supervisor board size (sn), management ownership percentage (mshare), institutional investor ownership percentage (inshare), state ownership percentage (coshare), executive compensation (salary), CEO duality (chairman_ceo), auditor type (big4), political ties (pc), and property rights nature (pr).

At the regional economic level, the marketization level of the region (market) is considered, alongside industry dummy variables (ind) and yearly dummy variables (year).

3.3 Samples and data

This study utilizes a sample of publicly listed manufacturing companies on the Shanghai and Shenzhen stock exchanges in China from 2010 to 2021. ST, *ST, and companies listed on the Beijing Stock Exchange are excluded from the sample. Additionally, companies with missing data sources are removed, resulting in a dataset comprising 640 listed enterprises and 4,876 observations.

The primary data sources for this study are collected from the CNRDS data platform, CSMAR database, China provincial marketization index database, and web scraping. Both structured and unstructured data are processed using Stata 17 and Python. To mitigate the influence of extreme values, a winsorization technique is applied to continuous variables at the 1st and 99th percentiles.

4. Empirical test and result analysis

4.1 Analysis of regression results

Firstly, the inflation factor coefficient is 1.43, indicating the absence of severe multicollinearity. Through the Hausman test and p-values, Models (1) and (2) should use a fixed effects model. Table 2 below shows the panel regression results.

From the regression results of Model (1), it can be observed that, without including control variables, the regression coefficient of green culture is -0.004<0 at the 1% significance level. After fully controlling for relevant variables, the regression coefficient of green culture is -0.004<0 at the 5% significance level. This suggests a significant negative correlation between green culture and financing constraints, indicating that green culture significantly mitigates financing constraints, confirming Hypothesis 1.

To test whether the quality of environmental information disclosure mediates the relationship between green culture and financing constraints, Model (2) results indicate that the regression coefficient of green culture is 0.028>0 at the 1% significance level, indicating a significant positive correlation between green culture and the quality of environmental information disclosure. At the same time, it is found that the regression coefficient of green culture is -0.004<0 at the 5% significance level, and the regression coefficient of environmental information disclosure quality is -0.018<0 at the 1% significance level. This suggests a significant negative

correlation between the quality of environmental information disclosure and financing constraints and that it mediates the relationship between green culture and financing constraints, confirming Hypothesis 2.

The results indicate that green culture is a core competitive advantage in helping companies mitigate financing constraints. Firstly, green culture promotes cooperation among the executive team, enhances social responsibility, and the ability to create value. Secondly, green culture enhances the competitiveness of the company and attracts green investors. Thirdly, green culture receives policy support and government subsidies and is recognized by financial institutions. Finally, green culture influences employee behavior, creating consensus and identification among employees with the company, thereby alleviating financing constraints. Companies with a strong green culture are more likely to realize the importance of environmental protection and are more likely to engage in substantive disclosure to showcase their environmental actions and achievements. On the one hand, this can increase the company's transparency and credibility, and on the other hand, it can enhance the company's sense of social responsibility and public image, attracting more attention and recognition from investors, further reducing financing constraints.

Table 2: Model regression results

	(1)		(2)	
variables	sa	sa	edi	sa
ln_green	-0.004**	-0.004**	0.028***	-0.004**
	(-2.22)	(-2.33)	-6.56	(-2.03)
edi				-0.018***
				(-2.81)
size		-0.060***	0.004	-0.059***
		(-20.97)	-0.61	(-20.96)
fnage		-0.112	0.116	-0.11
		(-0.00)	0	(-0.00)
lev		0.059***	-0.056**	0.058***
		-6.13	(-2.40)	-6.03
roa		0.132***	-0.146**	0.129***
		-5.49	(-2.48)	-5.38
loss		-0.006*	-0.009	-0.006*
		(-1.78)	(-1.20)	(-1.83)
gro		0.001	0.005**	0.001
		-0.84	-1.98	-0.93
turnover		0.002	-0.016*	0.002
		-0.64	(-1.86)	-0.56
fcf		0.008*	0.002	0.008*
		-1.65	-0.19	-1.66
ppe		-0.042***	-0.02	-0.042***
		(-3.96)	(-0.76)	(-4.00)
intangible		-0.128***	0.054	-0.127***
		(-4.09)	-0.71	(-4.06)
eps		-0.008***	0.007*	-0.008***
		(-4.36)	-1.67	(-4.28)
cr		-0.002***	0	-0.002***
		(-5.48)	(-0.70)	(-5.52)
co		-0.019	-0.021	-0.019
		(-1.36)	(-0.62)	(-1.39)
indep		0.051**	-0.025	0.051**
		-2.47	(-0.50)	-2.45
dn		0.003***	0	0.003***
		-3.59	(-0.11)	-3.59
sn		-0.008***	0.007*	-0.008***
		(-5.38)	-1.9	(-5.30)
mshare		-0.105***	0.039	-0.105***
		(-10.29)	-1.58	(-10.22)
inshare		-0.018***	-0.02	-0.018***
		(-2.68)	(-1.21)	(-2.73)
coshare		0.042***	-0.007	0.041***
		-5.96	(-0.44)	-5.95
salary		-0.001	0.019***	-0.001
		(-0.44)	-3.58	(-0.28)
chairman_ceo		0.002	-0.016**	0.002
		-0.78	(-2.52)	-0.67
big4		0.005	0.029**	0.006
		-0.85	-1.99	-0.94
pc		-0.006	0.015	-0.006
		(-1.10)	-1.11	(-1.05)
pr		-0.020***	-0.001	-0.020***
		(-3.22)	(-0.08)	(-3.23)
market		-0.004**	0.005	-0.004**
		(-2.42)	-1.24	(-2.37)
Sample Size	4692	4692	4692	4692
Goodness of Fit	0.974	0.978	0.739	0.978
Corporate Fixed Effects	-	control	control	control
Time Fixed Effects	-	control	control	control
Industry Fixed Effects	-	control	control	control

4.2 Heterogeneity Analysis

Through heterogeneity analysis of two dimensions, internal characteristics of companies and external environmental factors, we delve deeper into the state of corporate development. Within the realm of internal characteristics, the focus is on exploring the heterogeneity in property rights and environmental attributes. In contrast, when considering the external environment, attention is directed towards regional heterogeneity.

The empirical results, as presented in Table 3 below, reveal that in columns (1), (3), and (5), green culture exhibits significant negative correlations at the 1%, 10%, and 1% significance levels, respectively. The regression coefficients are -0.008<0, -0.003<0, and -0.007<0, demonstrating a notable negative relationship between green culture and the variables being examined. Conversely, in all other scenarios, the correlations do not display statistical significance

4.3 Robustness test

In this paper, different methods were used to check the robustness: (1) Propensity Score Matching (PSM): In the first step, the study uses PSM to minimize the potential bias arising from self-selection in the sample. The results consistently show that the negative association between green culture and financing constraints remains strong and reliable, reinforcing the study's main findings;(2) Substitution of Explanatory Variable: we reevaluated green culture using content analysis on official websites, with significant results;(3) Addressing Management Tone Manipulation;(4) Industry-year parallel trend interactive fixed effects are introduced to consider industry-specific and time-related effects.

.

Table 3: Heterogeneity Analysis Regression Results

	Property Rights Heterogeneity		Environmental Attributes Heterogeneity		Regional Heterogeneity		
sa	(1)State-Owned Enterprises	(2)Non-State-Owned Enterprises	(3)Heavy Pollution	(4)Non-Heavy Pollution	(5)Eastern Region	(6)Central Region	(7)Western Region
ln_green	-0.008***	0.004	-0.003*	-0.004	-0.007***	0.005	-0.001
	(-3.77)	-1.29	(-1.65)	(-1.57)	(-3.27)	-1.54	(-0.34)
Control Variables	control	control	control	control	control	control	control
Sample Size	2687	1993	2207	2478	3020	874	797
Goodness of Fit	0.979	0.981	0.983	0.974	0.98	0.984	0.97
Corporate Fixed Effects	control	control	control	control	control	control	control
Time Fixed Effects	control	control	control	control	control	control	control
Industry Fixed Effects	control	control	control	control	control	control	control

(2)Heterogeneity analysis reveals that state-owned enterprises prioritize internal control systems and green culture development compared to non-state-owned enterprises. Consequently, state-owned enterprises have richer green culture, enhancing their capabilities and competitiveness for sustainable development. External investors exhibit greater interest in green culture development among heavily polluting companies, while non-polluting companies may have easier access to financing. For heavily polluting companies, green culture development highlights their sense of social responsibility, elevating their recognition and image in society, thus alleviating financing constraints. Furthermore, heavily polluting companies need to establish comprehensive green environmental management systems to enhance their management and sustainability, thus gaining more financing opportunities. Developed markets in the eastern region significantly alleviate financing constraints through the promotion of green culture.

In summary, this study expands the economic consequences of green culture, enriches its impact on financing constraints, and provides empirical evidence for the mechanisms of green culture's influence on financing constraints.

. Conclusion

This paper empirically examines the relationship between green culture and financing constraints in Chinese manufacturing companies listed on the Shanghai and Shenzhen stock exchanges from 2010 to 2021. Drawing on agency theory and various principles from management, resource-based theory, reputation theory, and new institutional economics, we employ text analysis and machine learning methods to investigate this relationship.

Our findings reveal the following:

(1)The green culture index constructed from corporate social responsibility report text reflects the overall level of a company's green culture. Green culture helps alleviate financing constraints. We validate that corporate green culture, formed as a set of values over long-term operations, explicitly defines future development visions and missions, acts as the "words" motivating management to disclose environmental information to society effectively ("actions"), and subsequently lowers the company's cost of capital ("reporting").

References

Abbas, J. and E. Dogan (2022). "The impacts of organizational green culture and corporate social responsibility on employees' responsible behaviour towards the society." Environmental Science and Pollution Research 29 (40): 60024-60034.

Baier, P. and M. Berninger, et al. (2020). "Environmental, social and governance reporting in annual reports: A textual analysis." Financial Markets, Institutions & Instruments 29 (3): 93-118.

Elshaarawy, R. and R. A. Ezzat (2023). "Global value chains, financial constraints, and innovation." Small Business Economics 61 (1): 223-257.

Lin, Y. and R. Huang, et al. (2021). "Air pollution and environmental information disclosure: An empirical study based on heavy polluting industries." Journal of Cleaner Production 278: 124313.

Zhang, D. and C. Wang, et al. (2023). "How Does Firm ESG Performance Impact Financial Constraints? An Experimental Exploration of the COVID-19 Pandemic." The European Journal of Development Research 35 (1): 219-239.

Zhang, C., & Shi, Y. (2019). "Green Culture, Environmental Performance, and Corporate Environmental Performance Disclosure." Journal of Finance and Economics, 06, 83-93.

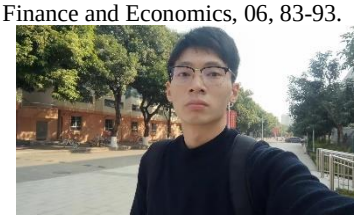

Mr. Yaosheng Liang
Master student,
Master of Business Administration (Accounting).
Research Interests:
Environmental Accounting.

Ultra-sensitive molecularly imprinted fluorescent sensor based on zeolitic imidazolate framework-8 with a novel assembling strategy using Mg, N co-doped graphene quantum dots for sulfadiazine detection

Shuqi Li [1], Qin Ming [1], Wenming Yang [2], Wanzhen Xu [1],*

[1] School of the Environment and Safety Engineering, Jiangsu University, Zhenjiang 212013, China
[2] School of materials Science and Engineering, Jiangsu University, Zhenjiang 212013, China

Abstract: The overuse of antibiotics has led to environmental pollution and has had a significant impact on human health, garnering high levels of attention from the scientific research community. This report investigates the development of an ultra-sensitive fluorescent sensor constructed from molecularly imprinted polymers (MIPs), metal-organic frameworks (MOFs), and Mg, N co-doped graphene quantum dots (Mg, N-GQDs) for the detection of sulfadiazine (SDZ) in environmental samples. The response signal quantum dots were synthesized via a hydrothermal reaction of citric acid with Mg(OH)2 and ethylenediamine. Subsequently, the MIPs were fabricated using a sol-gel method at room temperature on the MOFs, which possess imprinted sites tailored to the size and shape of the target SDZ molecule, thus enabling specific recognition and leading to the fluorescence quenching of the quantum dots. The sensor exhibited exceptional selectivity and a rapid response time of 4 minutes, likely due to the incorporation of MOFs which increase the number of effective sites significantly. Under optimized conditions, the fluorescence quenching rate of the quantum dots demonstrated a strong linear correlation with SDZ concentrations ranging from 0 to 80 μM, and the detection limit was determined to be 16 nM. The relative standard deviation was less than 0.44%, and the recovery rate of SDZ in real sample analyses ranged from 97.5 to 101.3%. In conclusion, the sensor developed in this study is highly feasible and holds potential value for the detection of SDZ in environmental matrices, offering a practical and straightforward approach for the rapid and sensitive detection of antibiotic drugs in complex samples.

Keywords: Fluorescent sensor,Molecularly imprinting,Mg,N co-doped graphene quantum dots,Sulfa-diazine detection

1. Introduction

The rapid development of our society, the current envirSulfadiazine (SDZ) is a common sulfonamides antibacterial drug in clinical practice at present[1]. Because of its good stability and low cost, it can not only be used as a broad-spectrum antibacterial agent, but also be widely used in animal husbandry and aquatic product aquaculture[2,3]. Because of its chronic toxicity, it has posed a serious threat to human beings and ecosystems. Therefore, it is very important to detect sulfonamides in the environment sensitively. At present, a variety of methods have been developed for detection, such as high-performance liquid chromatography[4], electrochemical method[5–7], etc.[8], but the equipments involved in these methods are expensive, and the pretreatment is complex, which is not suitable for low-cost, rapid and sensitive detection. Therefore, it is necessary to develop an easy to prepare, low-cost and efficient method for the detection of sulfadiazine.

In recent years, it has been reported that quantum dots[9], which are low toxicity, easy to prepare, and stable semiconductor nanomaterials[10–12], are used as response signals to detect targets, namely, fluorescence analysis methods. For example, Tang et al. reported that a novel fluorescence adapter sensor based on mesoporous silica nanoparticles was used to selectively detect sulfadiazine in edible tissues[13]. In addition, the fluorescence properties of quantum dots can be changed by surface passivation and heteroatom doping among which heteroatom doping is more effective[14]. For example, a highly luminescent nitrogen doped carbon quantum dots (N-CQDs) developed by Qi et al. is used to detect hypochlorite ions by fluorescence quenching[15]. However, the sensitivity of these methods is poor, so it is very important to establish a fast and sensitive identification method.

Molecular imprinting technology (MIT) is a molecular recognition technology formed by simulating antigen and antibody[16,17], which is widely used in chromatographic separation, sensor and other fields[18–20]. Molecularly imprinted polymers (MIPs) were prepared by copolymerization of functional monomers, cross-linking agents and template molecules under the induction of initiators, and then the template molecules were eluted to obtain imprinted holes that were similar in shape and size to the target and could specifically recognize the template molecules. However, direct imprinting of quantum dots will easily cause aggregation of quantum dots, which will lead to fluorescence quenching and affect the detection result. Therefore, it can be combined with porous materials to solve the agglomeration problem.

Metal-organic frameworks (MOFs) are a kind of crystalline porous materials with periodic network structure formed by self-assembly of inorganic metal centers (metal ions or metal clusters) and bridged organic ligands[21,22]. Because of their large specific surface area[23], controllable porosity, good thermal stability and other advantages[24], they are widely used in catalysis[25], sensing[26–28] and other fields. For example, Chen et al. reported a ratiometric fluorescence sensor based on MOFs and quantum dots for detection of ascorbic acid[29]. A dual emission ratio fluorescent capillary imprinting sensor based on a MOF developed by Tang et al. is sensitive to L-tyrosine[30]. Therefore, quantum dots, molecular imprinting technology and MOFs materials can be combined to prepare a sensor that can quickly and sensitively detect sulfadiazine in real samples. On the basis of the above, this work makes use of the synergistic effect of Mg and N to make the Mg, N co-doped graphene quantum dots that exhibit excellent optical properties. Then the polymer was prepared by combining MOFs (ZIF-8) and molecular imprinting technology to detect SDZ in the environment

2. Experimental

2.1. Reagents and apparatus

Citric acid (CA), Sodium hydroxide (NaOH), 2-Methylimidazole (2-Hmin), methanol, acetic acid, magnesium dihydroxide ($Mg(OH)_2$), sulfadiazine (SDZ), sulfamethoxazole (SMX), sulfamethazine (SM_2), sulfamerazine (SMZ) and Acrylamide (AM) were purchased from Aladdin company. Zinc acetate dihydrate ($Zn(Ac)_2{\cdot}2H_2O$), ethylenediamine (EDA), Sodium dihydrogen phosphate (NaH_2PO_4), Disodium phosphate (Na_2HPO_4), hydrochloric acid (HCl), Tetraethyl orthosilicate (TEOS) and aqueous

ammonia ($NH_3 \cdot H_2O$) were purchased from Sinopharm Company (Shanghai China). The distilled water was provided by the laboratory of Jiangsu University. The milk was purchased from the supermarket of Jiangsu University and the lake water was from Jiangsu University. Phosphate buffer solution (PBS) was prepared of NaH_2PO_4 and Na_2HPO_4 together.

The morphology and structure of the synthesized samples were characterized by scanning electron microscope (SEM, JSM-7800) and Transmission Electron Microscope (TEM, JEM-2100). The infrared spectrum from 4000cm^{-1} to 500cm^{-1} was measured by Fourier Transform Infrared Spectrometer (FT-IR, Nexus-470). The crystal surface and crystal form were obtained by X-Ray diffractometer (D8 ADVANCE). The absorption spectrum was tested by ultraviolet spectrophotometer (UV-Vis, UV-2600). The synthesized samples were analyzed and tested by X-ray photoelectron spectroscopy (Escalab 250XI). Nitrogen adsorption desorption (BET) experiment was carried through surface area and porosity analyzer (TriStarII2030, Micromeritics Instrument Co., Ltd, Shanghai, China.) A series of fluorescence related test results were obtained by fluorescence spectrophotometer (Lumina).

2.2. Synthesis of Mg, N-GQDs

First, 2 g of CA was weighed and dissolved in 10 mL of distilled water, 1 g of Mg $(OH)_2$ and 1mL of EDA are added under stirring conditions, and ultrasonic mixing is performed. Then transfer the solution to a polytetrafluoroethylene stainless steel reactor and react at 200 ℃ for 10 h. Finally, the quantum dots obtained from the reaction were further purified by microporous membrane with pore size of 0.22 μm, which were named Mg, N-GQDs.

2.3. Synthesis of ZIF-8

ZIF-8 was synthesized according to previous reports in the literature with some modifications[31]. In brief, 1 mmol of Zn $(Ac)_2 \cdot 2H_2O$ and 4 mmol of 2-Hmin were dissolved in 80 mL and 100 mL of methanol respectively, and the zinc salt solution was poured into the imidazole solution under stirring conditions. Mixed them completely by ultrasonic, and then stirred for 2 h at 50 ℃. The reaction solution was centrifuged at 8500 rpm for 5 min, washed it with methanol at several times, and finally dried it in an oven at 60 ℃ to obtain ZIF-8 powder.

2.4. Synthesis of MIPs and NIPs

In this work, the fluorescent imprinted sensor was synthesized by sol-gel method as shown in Scheme.1. First, 1mL of Mg, N-GQDs and 50 mg of ZIF-8 were transferred to a flask and ultrasonic dispersed in 40 mL of ethanol, then 100 μL of TEOS and 100 μL of ammonia were added into the flask and reacted with magnetic stirring for 30 min to obtain precursor solution. Secondly, 0.2 mmol of SDZ and 200 μL of APTES were added to the precursor solution, and the mixture was stirred at room temperature for 12 h. The solution after reaction was centrifuged at 8000 rpm for 5 min, and washed alternately with ethanol and water for several times. Finally, the template molecule SDZ was eluted with methanol/acetic acid (v/v=9:1) until the SDZ in the eluent could hardly be detected by UV-vis, and the product was dried at 60 ℃ to obtain MIPs. The preparation method of NIPs is similar to MIPs, except that the template molecule SDZ is not added.

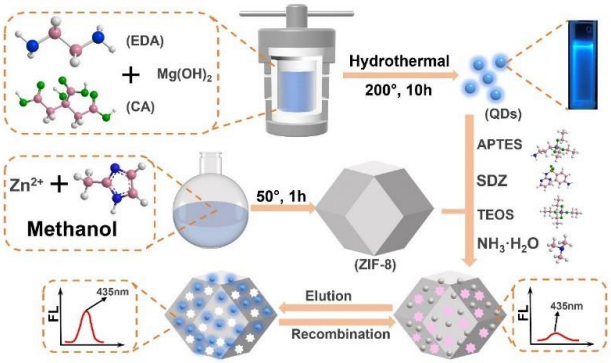

Scheme. 1. Synthesis process of SiO_2@GQDs@MIPs and its mechanism of identifying SDZ.

2.5. Fluorescence detection

All fluorescence intensity tests in this work were carried out on fluorescence spectrophotometer (Lumina) under the following conditions: the excitation wavelength of 360 nm, excitation/emission slit widths of 10 nm, the spectrum test range of 380-650 nm and photomultiplier tube voltage of 700 V. The MIPs powder was dispersed in 5 mL PBS (pH=7, 0.2 mM), then added appropriate amount of SDZ solution to abtain the fluorescence quenching spectrum. Some structural analogs of SDZ, such as sulfamethoxazole (SMX), sulfamethazine free acid (SM_2) sulfamethazine (SMZ), and some ions, such as Mg^{2+}, Ca^{2+}, Na^{+}, Fe^{2+}, were added to perform selective comparative experiments with SDZ.

2.6. Actual water sample detection

The practicability of MIPs was evaluated by testing the tap water and lake water from the laboratory of Jiangsu University. The water sample was filtered with 0.22 μM filter membrane for pretreatment, and then the recovery rate of SDZ was detected by spiked recovery method. Then, different concentrations of SDZ solution and actual sample solution were added to the test tube, and the volume was fixed to 5mL with phosphate buffer solution (PBS). Three parallel experiments were performed for each sample.

3. Results and discussion

3.1. Characterization of MIPs

The morphologies of ZIF-8 and MIPs were characterized in detail by SEM and TEM. It can be seen from Fig. 1a that ZIF-8 exhibits a rhombic dodecahedron structure with a diameter of about 800 nm and a smooth surface. ZIF-8 in Fig. 1b shows a hexagonal shape with uniform distribution, and the size is about 800 nm, which is consistent with the result in Fig. 1a. As shown in Fig. 1c, the size of MIPs is about 1000 nm, and the surface of ZIF-8 is covered with an imprint layer of about 200 nm. The rough surface is due to the existence of imprinted cavities. Compared with the TEM image of ZIF-8, the surface of MIPs in Fig. 1d is obviously coated with an imprinted layer

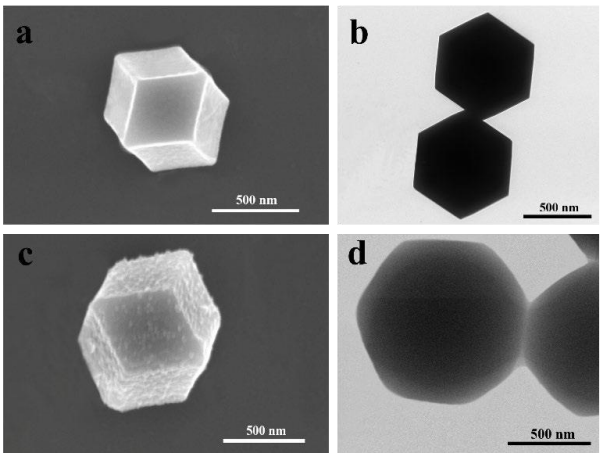

Fig. 1. (a). TEM image of SiO_2. (b). TEM image of SiO_2@GQDs@MIPs. (c). SEM image of SiO_2. (d). SEM image

of SiO_2@GQDs@MIPs.
of about 200 nm, which indicates the successful synthesis of the imprinted polymer.
In order to verify the crystal structure of the nanocomposites, the crystal structures of ZIF-8 and MIPs were analyzed by XRD, and the results are shown in Fig. 2. It can be seen that the diffraction peaks displayed by ZIF-8 are almost identical with the simulated results of ZIF-8, indicating the successful synthesis of ZIF-8. The diffraction peak of MIPs is quite different from that of ZIF-8, and a wide characteristic amorphous silica diffraction peak (2θ=23°) can be observed, indicating that the crystallinity changes after polymerization and the imprinting layer is likely to disrupt the order in the MOF.

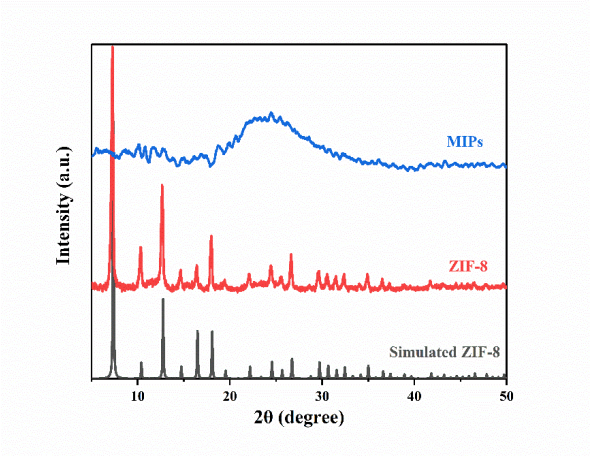

Fig. 2. (a). XRD patterns of ZIF-8 and MIPs.
In order to understand the possible role of chemical bonds in ZIF-8 and MIPs, they were tested by FT-IR. As shown in Fig. 3a, the peak at 422 cm^{-1} is typical Zn-N stretching vibration, 1421 cm^{-1} and 994 cm^{-1} are stretching vibration and plane bending vibration of imidazole ring respectively. In addition, 952 cm^{-1}, 757 cm^{-1} and 691cm^{-1} can be attributed to bending vibration of olefin, 1309 cm^{-1} can be attributed to C-N stretching vibration of imidazole ring, and 1177 cm^{-1} and 1147 cm^{-1} may be caused by in-plane bending of ring. All above can prove that 2-Hmin and Zn^{2+} have an effect and ZIF-8 has been successfully synthesized. At 3440 cm^{-1} and 1610 cm^{-1} are stretching and stretching vibrations of O-H respectively, 457 cm^{-1} and 790 cm^{-1} are attributed to stretching vibration of Si-O, and the peak at 1076 cm^{-1} is attributed to characteristic stretching vibration of Si-O-Si. In addition, the new peak at 1301 cm^{-1} in the figure is the characteristic peak of SDZ, which disappears after MIPs elution, and the MIPs after elution have

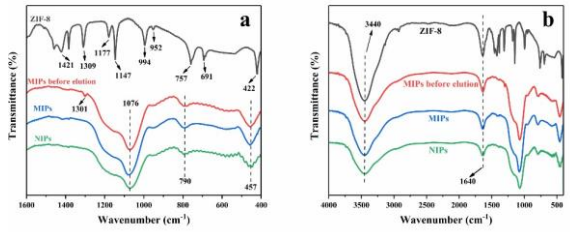

Fig. 3. (a). The fluorescence intensity of SiO_2@GQDs@MIPs with different concentrations from 0.5 g/L to 3.0 g/L (blue line) and the fluorescence quenching amounts of SiO_2@GQDs@MIPs with different concentrations exposed to SDZ (red line). (b). Fluorescence intensity of SiO_2@GQDs@MIPs in 80 min. (c). Fluorescence intensity of SiO_2@GQDs@MIPs exposed to SDZ in 60 min. (d). Effect of pH on fluorescence intensity of SiO_2@GQDs@MIPs before and after exposed to SDZ.
similar peaks to NIPs, indicating that the target SDZ has been successfully eluted (Fig. 3b). All above can prove the successful synthesis of ZIF-8 and MIPs.

3.2. Optimization of Reaction Conditions

If the concentration of fluorescent substance is too high, the detection sensitivity will be reduced, while if it is too low, the linear range of detection will be narrow. Therefore, we discussed the fluorescence changes of MIPs with different concentrations (0.2-2.4 g/L) before and after adding SDZ, as shown in Fig. 4a. Considering the fluorescence intensity and detection sensitivity, we finally chose 2 g/L MIPs as the optimal concentration for the subsequent whole fluorescence test.
It is well known that stability is an important parameter for evaluating the fluorescence sensors. In this work, fluorescence changes of MIPs were tested for 10 times continuously at room temperature within 60 min (Fig. 4b) and the results show that the fluorescence intensity of MIPs is well maintained. It can be considered that the material can be stable for a long period of time, which indicates that MIPs have excellent stability.
In order to study the optimal response time of MIPs to SDZ, as shown in Fig. 4c, the fluorescence intensity of MIPs solution after added SDZ solution was tested for 11 times within 10 min. F_0 is the fluorescence intensity of MIPs without SDZ, and F is the fluorescence intensity of MIPs after adding SDZ. As can be seen from the figure that the ratio of fluorescence intensity F_0/F keeps rising in the first 4 min, that is, the amount of fluorescence intensity quenching keeps increasing, while it almost remains unchanged after 4 min. The fluorescence intensity changes of MIPs before and after adding SDZ at different pH (3-12) were compared in Fig. 4d. Among them, the red line is the fluorescence intensity before adding the target SDZ. It can be seen from the figure that the fluorescence intensity rises first and then decreases with the increase of pH and reaches the maximum value when pH=7, while the blue line is the ratio of the fluorescence intensity after adding SDZ. The larger F_0/F is, the greater the amount of fluorescence quenching is. Combined with the above conclusions, it can be concluded that the optimal pH is 7, that is, the pH of all phosphate buffer solutions in subsequently tests is 7.

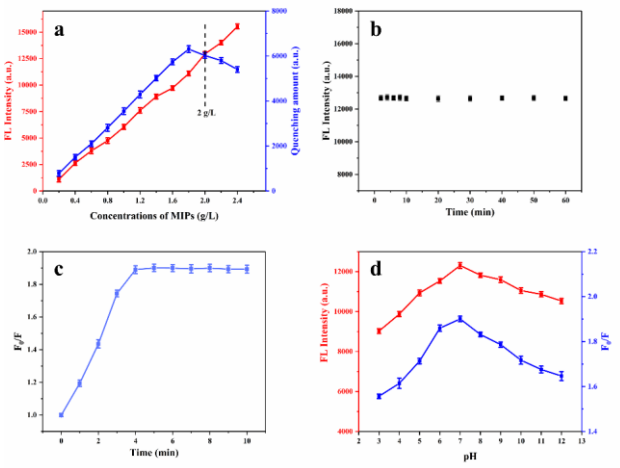

Fig. 4. (a) Fluorescence spectra of SiO_2@GQDs@MIPs and (b) SiO_2@GQDs@NIPs exposed to different concentrations of SDZ from 0 μM to 35 μM. (c). Linear relationship between SiO_2@GQDs@MIPs and SDZ with same concentrations range. (d). Linear relationship between SiO_2@GQDs@NIPs and SDZ with same concentrations range.

3.3. Performance analysis of MIPs and NIPs

After the condition optimization test, the fluorescence performance of MIPs and NIPs was tested under the above optimized conditions. As shown in Fig. 5a and 5c, the fluorescence intensity of MIPs and NIPs decreases with the increase of SDZ concentration, but the fluorescence quenching degree of MIPs is far greater than that of NIPs under the same concentration of SDZ. This is because MIPs have imprinted holes similar in shape and size to the target SDZ on the surface, so MIPs are more responsive to SDZ. In addition, Fig. 5b and 5d show that the fluorescence quenching degree within the concentration range of 0-100 μM shows a good linear relationship with the SDZ concentration. The linear relationship equation of MIPs is $F_0/F-1=0.02232$ [C] -0.01512, $R^2=0.99375$, while the linear fitting equation of NIPs was $F_0/F-1=0.00246$ [C]+0.00955, $R^2=0.99635$. The limit of detection (LOD) was calculated to be 16 nM. The above results indicate that the MIPs synthesized in this work can be effectively used to detect SDZ.

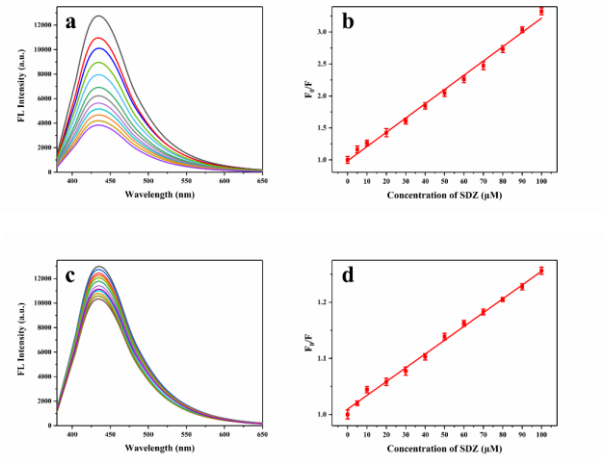

Fig. 5. (a). Selectivity of SiO_2@GQDs@MIPs and SiO_2@GQDs@NIPs to SDZ, SM_2, SMX, SMZ. (b). Selectivity of SiO_2@GQDs@MIPs and SiO_2@GQDs@NIPs to SDZ and other ions.

3.4. Selectivity of MIPs and NIPs

To evaluate the specific recognition ability of the imprinted sensor to SDZ, the fluorescence responses of MIPs and NIPs to SDZ in the presence of different interfering substances were investigated. As shown in Fig. 6a, analogues of SDZ such as SMX, SM_2 and SMZ are selected for comparative experiments. As can be seen from the figure, compared with SDZ, MIPs show less response to these analogues and little change in fluorescence intensity before and after, which indicated that MIPs can specifically identify SDZ. In order to further study the response ability of the sensor to SDZ under complex environmental conditions, Fig. 6b selects Mg^{2+}, Ca^{2+}, Na^+, NH_4^+, Fe^{2+}, K^+, Zn^{2+}, ClO^-, Cl^- and SDZ for comparative experiments and the data shows that the above ions will hardly affect the recognition ability of MIPs to SDZ. The above results can show that MIPs have the best fluorescence quenching effect on SDZ, while NIPs have similar and insignificant responses to SDZ, analogues and ions, which is due to that MIPs have imprinted holes with similar structure and size to SDZ, while NIPs do not. Therefore, this sensor can specifically identify SDZ in complex environments.

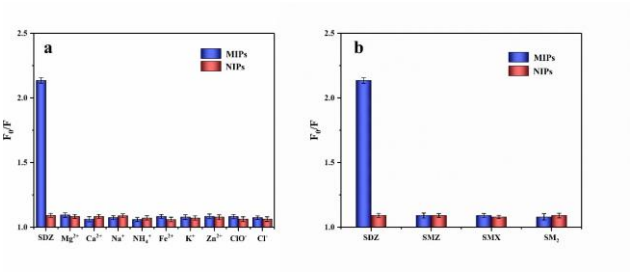

Fig. 6. (a). Selectivity of MIPs and NIPs to SDZ, SM_2, SMX, SMZ. (b). Selectivity of MIPs and NIPs to SDZ and other ions.

3.5. Real samples analysis

In order to prove the practicability of the sensor, the practical detection of the actual water sample is carried out. Here, laboratory tap water and studio tap water were taken as real samples, and the samples were first filtered with 0.22 μm filter membrane. We used the standard adding recovery experiment to detect the above samples. The test was repeated three times at each concentration and the recovery rate and re lative standard deviation (RSD) were calculated. In conclusion, the sensor provides a feasible and reliable sensitive detection method for detecting SDZ in actual samples.

4. Conclusion

The innovative fluorescent molecularly imprinted sensor developed in this study hinges on the integration of Mg, N co-doped graphene quantum dots (Mg, N-GQDs) as the fluorescence signal source, with metal-organic frameworks (MOFs) serving as the supporting matrix, and molecular imprinting technology to ensure specificity towards sulfadiazine (SDZ). Detailed morphological, elemental, and optical analyses have substantiated the successful synthesis of the sensor material. Fluorescence assays have demonstrated the material's exceptional specificity, rapid detection capability, and a notably low detection limit (LOD) of 16 nM. The sensor's efficacy is further evidenced by the satisfactory recovery rates and relative standard deviations obtained from the analysis of real environmental samples, confirming its applicability for the accurate detection of SDZ. Consequently, the ZIF-8@Mg, N-GQDs@MIPs sensor presents a significant advancement for the practical monitoring and detection of SDZ in environmental matrices, showcasing its potential for future applications in the field.

5.Acknowledgments

This work was financially supported by the National Natural Science Foundation of China (No. 32072297), Jiangsu Collaborative Innovation Center of Technology and Material of Water Treatment.

References

[1] X. Zou, T. Zhou, J. Mao, X. Wu, *Chem. Eng. J.* 2014, **257**, 36.
[2] Y. Feng, D. Wu, Y. Deng, T. Zhang, K. Shih, *Environ. Sci. Technol.* 2016, **50**, 3119.
[3] X. Liu, Y. Liu, S. Lu, W. Guo, B. Xi, *Chem. Eng. J.* 2018, **350**, 131.
[4] E. Alipanahpour Dil, M. Ghaedi, F. Mehrabi,; L. Tayebi, *Talanta* 2021, **232**, 122449.
[5] Z. Bitew, M. Amare, *Electrochem. commun.* 2020, **121**, 106863.
[6] B. Z. Liu, Y. R. Ma, F. Zhou, Q. Wang, G. Q. Liu, *Int. J. Electrochem. Sci.* 2020, **15**, 9590.
[7] X. P. Hong, Y. Zhu, Y. Z. Zhang, *J. Zhejiang Univ. Sci. B* 2012, **13**, 503.
[8] X. Q. Chen, X. Y. Luan, N. W. Wang, N. Z. P. Zhou, X. N. Ni, Y. F. Cao, G. S. Zhang, Y. F. Lai, W. M. Yang, *J. Sep. Sci.* 2018, **41**, 4394.

[9] S. Ansari, S. Masoum, *Talanta* 2021, **223**, 121411.
[10] H. J. Zhang, Y. L. Chen, M. J. Liang, L. F. Xu, S. D. Qi, H. L. Chen, X. G. Chen, *Anal. Chem.* 2014, **86**, 9846.
[11] L. B. Li, B. Yu, T. Y. You, *Biosens. Bioelectron.* 2015, **74**, 263.
[12] S. Chen, X. Hai, X. W. Chen, J. H. Wang, *Anal. Chem.* 2014, **86**, 6689.
[13] J. M. Tang, Q. M. Kou, X. Y. Chen, Y. R. Wang, L. L. Yang, X. Wen, X. L. Zheng, X. L. Yan, T. Le, T. *Arab. J. Chem.* 2022, **15**, 104067.
[14] V. K. Sagar, S. Dey, S. Bhattacharya, P. Lesani, Y. Ramaswamy, G. Singh, H. Zreiqat, P. B. Bisht, *J. Photochem. Photobiol. A Chem.* 2022, **423**, 113618.
[15] F. Li, C. J. Liu, J. Yang, Z. Wang, W. G. Liu, F. Tian, *RSC Adv.* 2014, **4**, 3201.
[16] M. Arabi, A. Ostovan, J. H. Li, X. Y. Wang, Z. Y. Zhang, J. Choo, L. X. Chen, *Adv. Mater.* 2021, **33**.
[17] R. R. Xing, Z. C. Guo, H. F. Lu, Q. Zhang, Z. Liu, *Sci. Bull.* 2021, **27**, 678.
[18] M. L. Yola, T. Eren, N. Atar, *Sensors Actuators, B Chem.* 2015, **210**, 149.
[19] M. Mehmandoust, N. Erk, C. Karaman, O. Karaman, *Chemosphere* 2022, **291**, 132807.
[20] M. P. Shirani, B. Rezaei, A. A. Ensafi, M. Ramezani, *Food Chem.* 2021, **339**, 127920.
[21] X. X. Xuan, M. J. Wang, M. Zhang, Y. V. Kaneti, X. T. Xu, X. Sun, Y. Yamauchi, *J. CO_2 Util.* 2022, **57**, 101883.
[22] C. Y. Xiong, J. Huang, H. Liu, M. M. Chen, W. Wen, X. H. Zhang, S. F. Wang, *Talanta* 2022, **249**, 123602.
[23] B. Qiu, Y. L. Wang, J. J. Chen, Y. Chen, S. Q. Fan, Z. H. Mai, J. Y. Liu, K. Bai, L. Deng, Z. Y. Xiao, *J. Memb. Sci.* 2022, **644**, 120183.
[24] Y. J. Du, J. Gao, H. J. Liu, L. Y. Zhou, L. Ma, Y. He,; Z. H. Huang, Y. J. Jiang, *Nano Res.* 2018, **11,** 4380.
[25] F. Gao, X. L. Tu, Y. F. Yu, Y. S. Gao, J. Zou, *Nanotechnology*, 2022, **33**.
[26] F. K. Arabbani, D. Vasu, S. Sakthinathan, T. W. Chiu, M. C. Liu, *Electroanalysis* 2022, **1**.
[27] S. M. Pirot, K. M. Omer, *Microchem. J.* 2022, **182**, 107921.
[28] J. L. Fu, S. Zhou, P. F. Zhao, X. D. Wu, S. S. Tang, S. Chen, Z. X. Yang, Z. H. Zhang, *Biosens. Bioelectron.* 2022, **198,** 113848.
[29] L. Chen, L. M. Zheng, F. Q. Wang, S. M. Yi, D. H. Liu, X. Z. Huang, R. Chen, H. He, *Opt. Mater. (Amst).* 2021, **121**, 111622.
[30] S. S. Tang, P. F. Zhao, X. D. Wu, Y.Chen, K. L. Tang, S. Zhou, J. L. Fu, H. B. Lei, Z. X. Yang, Z. H. Zhang, *Sensors Actuators B Chem.* 2022, **367**, 132058.
[31] W. Wang, C. Deng, S. Xie, Y. Li, W. Zhang, H. Sheng, C. Chen, J. Zhao, *J. Am. Chem. Soc.* 2021, **143**, 2984.

Ms. Shuqi Li
Undergraduate (Environment Engineering).
Research Interests:
Fluorescence sensors, molecular imprinted materials

Dr. Wanzhen Xu
Professor
Research Interests:
Intelligent environmental protection functional materials, fluorescence sensors, electrochemical sensors, solar cell materials/devices.

Dr.Wenming Yang
Associate Professor
Research Interests:
Molecular imprinted materials, conjugated polymer materials, two-dimensional material design, fluorescence sensors, electrochemical sensors, microfluidic chips, flexible microelectronic devices

A Review of Thermal and Energy Performance of Microalgae Photobioreactor Façade

Napassawan Khammayom[1]*, Chatchawan Chaichana[1]

[1] Department of Mechanical Engineering, Faculty of Engineering, Chiang Mai University, Chiang Mai, Thailand
**Corresponding author, E-mail: Napassawan.k@cmu.ac.th*

Abstract: Microalgae show significant potential in decreasing the CO_2 emissions associated with buildings throughout their life cycle by both enhancing energy efficiency and actively capturing CO_2. The use of microalgae photobioreactor façade as integral building components provides several advantages, such as serving as an efficient insulation system. This work reviews the state-of-the-art knowledge on microalgae photobioreactor facades, provide a survey of the current research of this innovative system. This article also provides an overview of the thermal performance of different microalgae photobioreactor façades. Some significant recommendations for future work will also be discussed in terms of environmental sustainability and thermal behavior of microalgae photobioreactor façades.

Keywords: Microalgae, Photobioreactor, Building façade, CO_2 fixation

1. Introduction

Buildings accounted for 19% of energy-related greenhouse gas (GHG) emissions and 32% of the total globally final energy usage in 2010 [1]. In order to reduce global warming, countries around the world joined the Paris Agreement with the aim to achieve the climate neutral by the middle of century. Many countries and regions have set "Net zero" climate protection targets and stated that they will make every effort to achieve carbon emission and sink balance within the next 10-50 years [2].

Microalgae have ability to capture and utilize CO_2. Microalgae cultivation has high potential to produce carbon-neutral energy and recycle of environmental pollutants without competing with agriculture for land and fresh water [3]. Microalgae can use sunlight and CO_2 through photosynthesis with much faster growth rate and have 10-50 times greater carbon fixation capacity than that terrestrial plants [4].

Recently, many researchers have been focusing on the use of microalgae photobioreactor façade as integral building components. This could significantly decrease the energy demand and reduce heat entering the building. Therefore, the purpose of this article are to (1) review the current research on microalgae photobioreactor façades, (2) thermal behavior of microalgae photobioreactor façades and (3) CO_2 fixation by microalgae cultivation.

2. Microalgae photobioreactor façades

Generally, there are two systems for microalgae cultivation: open ponds and closed-loop bioreactors. Closed-loop bioreactors can be categorized as flat-plate and tubular bioreactors. Additionally, closed systems have shown many advantages, such as reducing the risk of contamination, increasing biomass production, providing sterilization for cultivation and maintenance, and demonstrating the ability to resist climate change. Nowadays, microalgae photobioreactor facades have been introduced and utilized as a part of building design to create a healthier indoor environment, reduce heat entering buildings, and enhance overall energy efficiency.

Thus, the novelty of the design and optimization of photobioreactors will be presented in this section. The summary of the literature on microalgae photo bioreactor façades is given in Table 1.

Table 1 Summary of the literature review on microalgae photobioreactor façades

References	PBRS* type	Major findings	Schematic panel design
Kim [5]	Vertical Flat-panel	• The U-factor of the flat-plate microalgae facade is similar to that of a low-e coated insulated glass unit (IGU). • To achieve the required insulation value and thermal comfort in the vision zone, a two-layered acrylic paneling is necessary. • Vision zone can light the perimeter zone of interior space without using any artificial lighting.	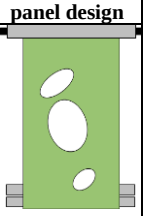
Lakenbrink [6]	Vertical Flat-panel	• PBRs energy-generated per m^2 Biomass production 15g TS/m^2/day (900 kg/year) • Energy production in biomass 345 kJ/m^2/day • Biogas production from biomass 10.20 L methane/m^2/day	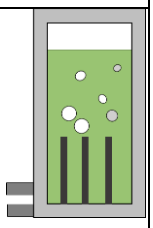

Elokaly & Keeling [7]	Vertical tubular	• Increasing in microalgae culture density leads to reducing penetration of light and internal luminance. • The relation between culture density and shading efficiency is weak.	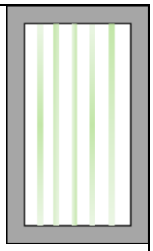
Pagliolico et al. [8]	Circular cubicles	• The amount of daylight was greater when using Venetian blinds on glazing, leading to a reduction in energy demands for lighting.	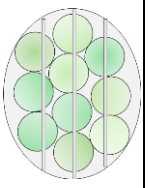

* PBRS = Photobioreactor

Table 1 shows the previous studies. Further investigation is required to record the influence of microalgae facade design based on PBRs (Photobioreactor) on its functionality. For example, it is essential to examine the effects of design elements like cavity depth and height, openings, and window-wall ratio on the thermal and natural ventilation performance of these facades. The effect of environmental factors such as solar radiation, wind direction and speed also need further investigation.

3. Thermal behavior of microalgae photobioreactor façades

Microalgae photobioreactor façades can fulfill the thermal requirements of buildings by serving as adaptable shading, thermal insulators, solar collectors, and so on [9]. Microalgae façades can provide thermal insulation and help thermal comfort in the building [10]. The study of Sarda and Vicente [11] revealed that integrating microalgae photobioreactor to buildings enhances its energy-saving potential for two primary reasons. Firstly, the photosynthesis process in algae reduces temperature by absorbing solar energy and providing parasol effects and facade shadings. Secondly, the water medium in microalgae enhances the acoustic and thermal insulation capabilities of the façade. In another study, Umdu et al. [12] conducted experiment and evaluated the overall heat transfer coefficient (U-value) of various photobioreactors with variations in reservoir, air layer and thickness. They found that all parameters had significantly effect on U-value with air layer thickness had the greatest effect. They suggested that incorporating closed microalgae photobioreactors into the building façades offers substantial benefits, such as efficient insulation and adaptive shading. In another study, Kim [13] conducted experimental and simulation studies by constructing a prototype with two vision and alga zones. Based on the thermography-based thermal testing, this study demonstrated that U-value of the flat-plate microalgae facade is comparable to a low-e coated insulated glass unit (IGU)

Another noteworthy concern is the interaction of this system with users. One of the key challenges in energy-efficient systems is addressing users' requirements for daylight, especially as solar radiation is controlled for energy conservation. It is worthwhile to explore the integration of innovative and energy-efficient facades with these user needs. Developing a user-friendly algae system that offers visual connection and adaptive shading, considering factors like culture density and user preferences, could help achieve the system's goal of regulating thermal load while meeting the occupants' needs.

4. CO_2 fixation by microalgae

It is generally known that plants, microalgae and so on are typically used for the biological sequestration. Normally, plants can reduce carbon emissions by 3-6%. However, under appropriate conditions, microalgae, including cyanobacteria and green algae, have the potential to be 50 times more efficient [14]. Yahya et al. [15] evaluated the potential of microalgae as biological carbon fixers. The results of this study establish the feasibility of using microalgae as a biological agent for carbon fixation, offering a potential avenue for sustainable coal-fired power generation through the reduction of CO_2 emissions. In another study, Dasan et al. [16] enhanced the efficiency of carbon dioxide fixation in *Chlorella vulgaris*. The experimental outcomes revealed that microalgae, when cultivated under optimized conditions, achieved the highest biomass productivity (0.83–0.86 g/L/day) compared to the control conditions. Ding and colleagues [17] discovered that employing native microalgae species is an effective strategy for mitigating effluents in palm oil mills and reducing CO_2 emissions from industrial discharges.

Microalgae use solar energy directly for carbon dioxide fixation, generating oxygen and secondary metabolites. This represents a typical example of carbon sequestration organisms [18]. This process is commonly known as photosynthesis, encompassing primary reactions, electron transfer, photophosphorylation, and carbon assimilation, which includes CO_2 fixation and the formation of sugars. Microalgae biomass, possessing valuable components such as lipids, proteins, and polysaccharides, holds significant application potential as raw materials for biofuel, biochemicals, food, medicine, and various industries. Microalgae species and environmental circumstances influence photosynthesis and carbon sequestration efficiency, which is beneficial to further effective utilization of microalgae [19].

5. Conclusions

The photobioreactor system includes living microorganisms. Future research should focus on selecting the best strain of microalgae based on the geographical situation and study their shading effect, biomass production efficiency and thermal buffer potential as well as estimation of PBRs u for each strain. In addition to the previously mentioned suggestions, it is crucial to emphasize the importance of thoroughly examining the thermal potential of algae photo-reactive façades. This involves the indispensable task of optimizing the thermal parameters specified as variables in algae façade design. The optimization of these factors is essential for achieving increased energy efficiency when implementing this system, consequently boosting its popularity as an innovative solution for high-performance architecture.

References

[1] Edenhofer, O. (2014). IPCC WG3 AR5 summary for policymakers. *IPCC, Potsdam, Germany*.

[2] Xu, P., Li, J., Qian, J., Wang, B., Liu, J., Xu, R., ... & Zhou, W. (2023). Recent advances in CO2 fixation by microalgae and its potential contribution to carbon neutrality. *Chemosphere*, 137987.

[3] Umdu, E. S., Kahraman, İ., Yildirim, N., & Bilir, L. (2018). Optimization of microalgae panel bioreactor thermal transmission property for building façade applications. *Energy and Buildings*, *175*, 113-120.

[4] Vuppaladadiyam, A. K., Yao, J. G., Florin, N., George, A., Wang, X., Labeeuw, L., ... & Zhao, M. (2018). Impact of flue gas compounds on microalgae and mechanisms for carbon assimilation and utilization. *ChemSusChem*, *11*(2), 334-355.

[5] Kim, K. H. (2013). Beyond green: growing algae facade. In *ARCC Conference Repository*.

[6] H. Lakenbrink, Smart Mater. House. BQI., in: International Building Exhibition, 2013, p. 1e22. Hamburg, https://www.iba-hamburg.de/fileadmin/Mediathek/Whitepaper/130716_White_Paper_BIQ_en.pdf.

[7] Elnokaly, A., & Keeling, I. (2016). An empirical study investigating the impact of micro-algal technologies and their application within intelligent building fabrics. *Procedia-Social and Behavioral Sciences*, *216*, 712-723.

[8] Pagliolico, S. L., Verso, V. R. L., Bosco, F., Mollea, C., & La Forgia, C. (2017). A novel photo-bioreactor application for microalgae production as a shading system in buildings. *Energy Procedia*, *111*, 151-160.

[9] Casini, M. (2016). *Smart buildings: Advanced materials and nanotechnology to improve energy-efficiency and environmental performance*. Woodhead Publishing.

[10] Öncel, S. Ş., Köse, A., & Öncel, D. Ş. (2016). Façade integrated photobioreactors for building energy efficiency. In *Start-Up Creation* (pp. 237-299). Woodhead Publishing.

[11] Pacheco Torgal, F., Buratti, C., Kalaiselvam, S., Granqvist, C. G., & Ivanov, V. (2016). Nano and biotech based materials for energy building efficiency.

[12] Umdu, E. S., Kahraman, İ., Yildirim, N., & Bilir, L. (2018). Optimization of microalgae panel bioreactor thermal transmission property for building façade applications. *Energy and Buildings*, *175*, 113-120.

[13] Kim, K. H. (2013, July). A feasibility study of an algae façade system. In *Proceedings of international conference on sustainable building Asia (SB13)* (pp. 8-10).

[14] Rossi, F., Olguín, E. J., Diels, L., & De Philippis, R. (2015). Microbial fixation of CO2 in water bodies and in drylands to combat climate change, soil loss and desertification. *New biotechnology*, *32*(1), 109-120.

[15] Yahya, L., Harun, R., & Abdullah, L. C. (2020). Screening of native microalgae species for carbon fixation at the vicinity of Malaysian coal-fired power plant. *Scientific reports*, *10*(1), 22355.

[16] Dasan, Y. K., Lam, M. K., Yusup, S., Lim, J. W., Show, P. L., Tan, I. S., & Lee, K. T. (2020). Cultivation of Chlorella vulgaris using sequential-flow bubble column photobioreactor: A stress-inducing strategy for lipid accumulation and carbon dioxide fixation. *Journal of CO2 Utilization*, *41*, 101226.

[17] Ding, G. T., Yasin, N. H. M., Takriff, M. S., Kamarudin, K. F., Salihon, J., Yaakob, Z., & Hakimi, N. I. N. M. (2020). Phycoremediation of palm oil mill effluent (POME) and CO2 fixation by locally isolated microalgae: Chlorella sorokiniana UKM2, Coelastrella sp. UKM4 and Chlorella pyrenoidosa UKM7. *Journal of Water Process Engineering*, *35*, 101202.

[18] da Rosa, G. M., de Morais, M. G., & Costa, J. A. V. (2018). Green alga cultivation with monoethanolamine: Evaluation of CO2 fixation and macromolecule production. *Bioresource technology*, *261*, 206-212.

[19] uang, Z., Zhang, J., Pan, M., Hao, Y., Hu, R., Xiao, W., ... & Lyu, T. (2022). Valorisation of microalgae residues after lipid extraction: Pyrolysis characteristics for biofuel production. Biochemical Engineering Journal, 179, 108330.

Investigation of the effects of soil and biochar in a rain garden on stormwater contaminant removal

Natthapon Muangmaya[1], Prattakorn Sittisom[1*]

[1]Department of Environmental Engineering, Faculty of Engineering, Chiang Mai University, Thailand
**Corresponding author, E-mail: prattakorn.s@cmu.ac.th*

Abstract: Stormwater runoff from urban areas often contains a variety of elements and compounds in different forms and concentration that may pose risks to biota in receiving aquatic systems. Total Suspended Solid (TSS), Total Nitrogen (TN) and Total Phosphorus (TP) are of particular concern in Stormwater runoff due to their availability to aquatic organisms in the environment. The ability of commercially available biochar to remove pollutants of concern through reactor treatments was assessed in this study. Biochar was considered for its ability to remove pollutants compared to soil. The biochar used in this study showed a significant TSS, TN removal and slightly TP removal ability compared to soil. The effects of nutrients on aquatic organisms and eutrophication can be mitigated by improving the soil media with biochar in the bioretention cells such as raingarden. This could be applied in the real world where stormwater runoff can be treated before entering river or stream therefore cutting the need for future restoration.

Keywords: Biochar, Rain Garden, Stormwater Runoff

1. Introduction

In recent years, the rapid urbanization process has brought many serious problems while driving economic development. Urban water problems are particularly prominent, which are mainly in terms of flooding, non-point source pollution, and destruction of the natural hydrological cycle [1]. Low impact development (LID) is a new stormwater management strategy for urban water environment protection and sustainable development that is widely recognized in the world. In the LID systems, the bioretention facilities have good effects on runoff pollution control, runoff volume regulation and flood discharge reduction [2,3]. As an efficient and economical technical measure necessary for LID systems, bioretention technology plays an important role [4,5].

Biochar is an excellent soil conditioner, which can improve the sustainability of soil fertility. The discovery has attracted the attention of researchers around the world, and many have begun to explore the potential value of biochar [6]. In recent years, a lot of studies have emerged that combine biochar as a filler modifier with bioretention systems. The modified bioretention facilities have improved water holding capacity and infiltration performance to varying degrees, as well as pollutant adsorption capacity and microbial activity and community diversity in the filler. It also can effectively reduce the load of pollutants such as total suspended solids, total nitrogen (TN), total phosphorus (TP), heavy metals and organic carbon in rainwater runoff [7,8].

At present, there is a lack of relevant research on the preparation method of rain garden facilities in tropical countries. At the same time, there are few studies on parameters optimization combining the results of field monitoring and simulation to improve the operation effects of rain garden technology. Based on these considerations, this study aims: (i) to develop efficient biochar improved fillers by selecting suitable biochar ratio in rain garden.

2. Materials and methods

2.1. Experimental design and procedure

This study examines the effect of biochar, namely, and non-biochar control. Biochar is made from bamboo that was recommended for its effective performance from many studies. This research focuses on investigating the treatment performance of biochar mixed media.

The reactors were set up in an outdoor area (Figure 1). The reactors were constructed from 60 cm width, 180 cm length and 100 cm height steel frame, with a transparent acrylic plate allowing for media observation. Reactors were filled with different layers of media (from top to bottom: 40 cm of washed sand, 10 cm of fine sand and 30 cm of gravel aggregates). A permanent saturated layer of 40 cm was created by raising the outlet pipe; this comprised part of the filter media, the gravel drainage, and the transition layer (Figure 1). Biochar was purchased from a local store. And 5% (by mass) biochar was use on this study. Following an initial experimental phase, columns were watered with 200 L of synthetic stormwater.

The frequency of stormwater application was designed to match the average occurrence of storm events based upon rainfall data from Chiang Mai Province, and the dose volume (200 L) was determined using the same rainfall data. This was based on a monthly average effective rainfall of 200 mm/month of rainy season in Chiang Mai and using a biofilter sized to 4% of its contributing catchment.

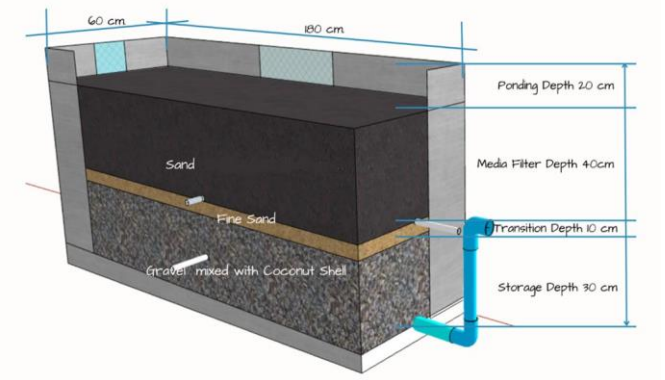

Figure 1 Reactor column (with and without biochars use the same design)

2.2. Synthetic runoff

Synthetic runoff was introduced to the rain garden systems during the experiment. Bentonite was added to tap water as Total Dissolved Solid (TSS); Disodium phosphate and Glycine were used to imitate Total Phosphorus (TP) and Total Nitrogen (TN).

2.3. Data analysis

Concentrations of all pollutants below the detection limit were taken as the detection limit for analysis. Removal efficiency of TSS, TN and TP were calculated as the percentage of the difference between inflow and outflow concentrations divided by the inflow concentration.

3. Results and discussion

3.1. Pollutant leaching process

The concentrations in the outflow TSS, TN, and TP of each reactor during the experiment are presented in Figure 2-4. The outflow TSS from reactor without biochar was lower than 1.00 mg/L and TSS from reactor with biochar was lower than 1.00 mg/L as well. There was no significant difference in the emission of TSS between reactors with different structures.

As the run time increased, the outflow TN from each reactor decreased gradually. The outflow TN from without and with biochar were lower than 3.40 mg/L and 4.40 mg/L, respectively. These results indicate that the reactor without the biochar had slightly better nitrogen leaching control performance. This was partly attributed to the change in system structure. Specifically, the extension of hydraulic retention time was beneficial to denitrification, which was consistent with the nitrogen control performance observed in previous studies, in which nitrogen removal was enhanced by providing a saturated zone [9].

The outflow TP from each reactor decreased gradually, eventually stabilizing. The outflow TN from without and with biochar were both lower than 0.10 mg/L. The phosphorus leaching from each reactor may be attributed to phosphorus release from the media [10,11]. The performance of TP leaching mainly depends on media type [12]. Hence, the relatively higher phosphorus leaching from the reactor may have been related to the larger media volume.

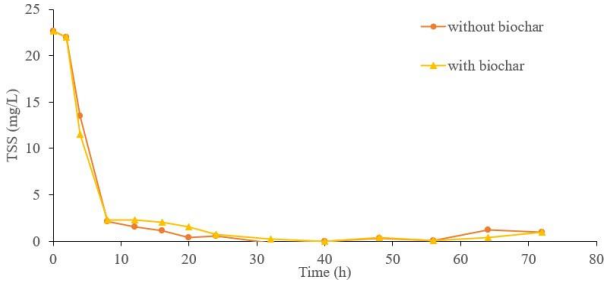

Figure 2 TSS concentrations in outflow over experiment

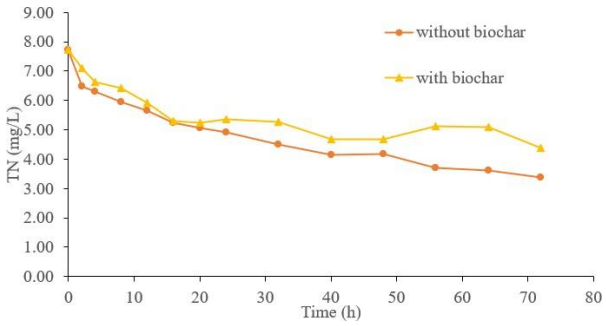

Figure 3 TN concentrations in outflow over experiment run times.

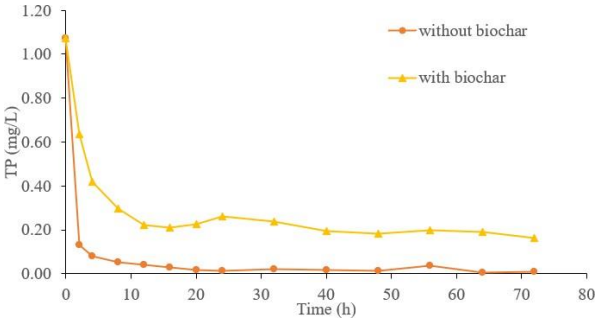

Figure 4 TP concentrations in outflow over experiment run times.

3.2. Nutrient removal from Synthetic runoff

The percent removal plots of outflow pollutant concentrations for each tractor during the synthetic runoff experimental stage (TSS, TN, and TP) are shown in Figure 5 - 7.

Figure 5 shows outflow TSS. The inflow TSS was set at 22.7 mg/L. The outflow TSS levels from without and with the biochar reactor were not significantly different from the synthetic runoff experimental stage. The outflow TSS from reactor without biochar ranged from 22.7 to 1.0 mg/L and from reactor with biochar ranged from 22.7 to 1.0 mg/L as well after 72 h. The rain garden better controlled TSS in runoff, which was confirmed by the high removal efficiency for total suspended solids (TSS) by rain garden reported in other previous studies [13,14].

Figure 6 shows outflow TN. The inflow TN was set at 7.7 mg/L. The outflow TN levels from without and with the biochar reactor were slightly different from the synthetic runoff experimental stage. The outflow TN from reactor without biochar ranged from 7.7 to 3.40 mg/L and from reactor with biochar ranged from 7.7 to 4.40 mg/L. Reactor can improve TN removal. But, in this experiment, 5% biochar did not show the TN removal more effectively than the control reactor. However, both reactors provided saturated zones to strengthen denitrification and extended the hydraulic retention time to improve nitrogen removal efficiency [18]. When the reactor received runoff, during the wetting period, dissolved organic N and NH^+_4 were absorbed by media, biochar root. Particulate organic N was removed through filtration. Subsequently, during the drying period, nitrogen species were transformed into nitrate by ammonification and nitrification. Denitrification may occur in anoxic conditions as well as in subsequent wetting periods [18]. In addition, because of the structure of the reactor the hydraulic retention time, in-flow paths, and anoxic conditions are all strengthened to some extent. The level of carbon from media, stormwater inflow, and root and microbial turnover in the media was sufficient to allow denitrification [15].

Figure 7 shows outflow TP. The inflow TP was set at 1.0 mg/L. The outflow TP levels from without the biochar reactor was almost completely removed from the synthetic runoff experimental stage. But TN level from with biochar reactor was found at 0.17 mg/L after 72 h. The rain garden mainly removed P through adsorption and precipitation, and only a small part of the P was utilized by microbe [16]. Particulate phosphorus was managed with particulate matter, which was effectively removed through precipitation and filtration in the rain garden. Rain gardens were shown to have high removal efficiency for phosphorus in runoff in other previous studies [14,16].

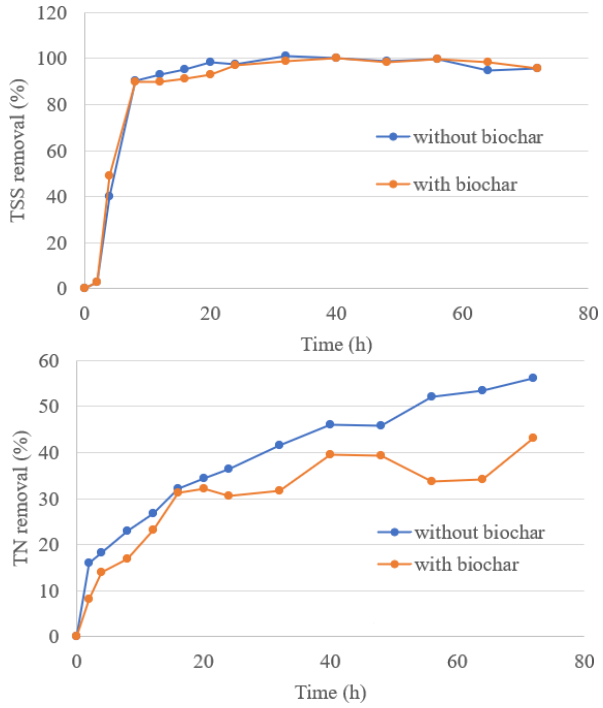

Figure 6 TN removal efficiency

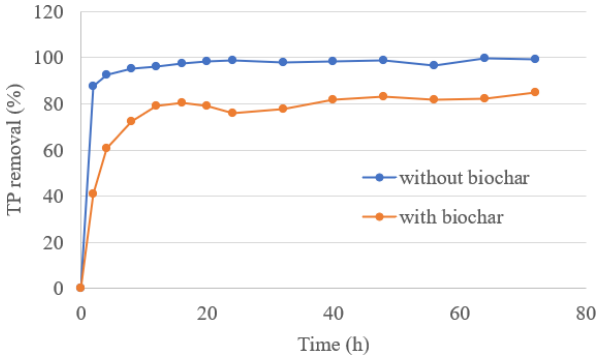

Figure 7 TP removal efficiency

4. Conclusions

Pollutants removal from synthetic runoff by without and with biochar rain garden, which were proposed in this study, was assessed through a laboratory-scale experiment. The main findings were as follows:

During the synthetic runoff experimental stage, the TSS efficiencies of the without and with biochar rain garden clearly improved, increasing to 100%. TN and TP removal efficiencies of the without biochar rain garden clearly improved, increasing to 56% and 100%, respectively. But TN and TP removal efficiencies of the with biochar rain garden increasing to 43% and 85%, respectively. These results indicated that reactor with 5% by mass biochar in this experiment did not perform the adsorption ability as it should. The critical concern must be biochar porosity and crush size. Therefore, recommendations for future study, biochar percentage, porosity, crush size and retention time will be focused for better stormwater quality improvement.

Results from this study could be useful to stormwater managers who are utilizing rain garden basins to improve the water quality of stormwater runoff in a similar tropical climate setting

References

[1] Q.T. Zuo, Water science issues in sponge city construction, Water Resour. Prot., 32 (2016) 21–26.

[2] M.B. de Macedo, C.A.F. do Lago, E.M. Mendiondo, Stormwater volume reduction and water quality improvement by bioretention: potentials and challenges for water security in a subtropical catchment, Arch. Pharm. Res., 4 (2018) 1–14.

[3] H. Yang, W.A. Dick, E.L. Mccoy, P.L. Phelan, P.S. Grewal, Field evaluation of a new biphasic rain garden for stormwater flow management and pollutant removal, Ecol. Eng., 54 (2013) 22–31.

[4] B. Ding, F. Rezanezhad, B. Gharedaghloo, P.V. Cappellen, E. Passeport, Bioretention cells under cold climate conditions: effects of freezing and thawing on water infiltration, soil structure, and nutrient removal, Sci. Total Environ., 649 (2019) 749–759.

[5] S. Ishaq, K. Hewage, S. Farooq, R. Sadiq, State of provincial regulations and guidelines to promote low impact development (LID) alternatives across Canada: content analysis and comparative assessment, J. Environ. Manage., 235 (2019) 389–402.

[6] D.A. Beck, G.R. Johnson, G.A. Spolek, Amending greenroof soil with biochar to affect runoff water quantity and quality, Environ. Pollut., 159 (2011) 2111–2118.

[7] K. Lu, X. Yang, G. Gielen, N. Bolan, Y.S. Ok, N.K. Niazi, S. Xu, G.D. Yuan, X. Chen, X.K. Zhang, D. Liu, Z.L. Song, X.Y. Liu, H.L. Wang, Effect of bamboo and rice straw biochars on the mobility and redistribution of heavy metals (Cd, Cu, Pb and Zn) in contaminated soil, J. Environ. Manage., 186 (2016) 285–292.

[8] N. Xu, G.C. Tan, H.Y. Wang, X.P. Gai, Effect of biochar additions to soil on nitrogen leaching, microbial biomass and bacterial community structure, Eur. J. Soil Biol., 74 (2016) 1–8.

[9] Lucas W.C., Greenway M., 2010. Nitrogen retention in bioretention mesocosms with outlet controls. In: Proceedings of the World Environmental and Water Resources Congress 2010, Providence, Rhode Island, USA, 16 – 20 May, pp 3038 – 3047

[10] O ' Neill S.W., Davis A.P., 2012. Water treatment residual as a bioretention amendment for phosphorus. II: long-term column studies. J Environ Eng 138:328 – 336

[11] Li J., Davis A.P., 2016. A unified look at phosphorus treatment using bioretention. Water Res 90:141 – 155

[12] Jay J.G., Brown S.L., Kurtz K., Grothkopp F.,2017. Predictors of phosphorus leaching from bioretention soil media. J Environ Qual 46(5): 1098 – 1105

[13] Hatt B.E., Fletcher T.D., Deletic A., 2009. Pollutant removal performance of field-scale stormwater biofiltration systems. Water Sci Technol 59: 1567 – 1576

[14] Goh H.W., Zakaria N.A., Lau T.L., Foo K.Y., Chang C.K., Leow C.S., 2017. Mesocosm study of enhanced

bioretention media in treating nutrient rich stormwater for mixed development area. Urban Water J 14: 134 – 142

[15] Zinger Y., Blecken G.T., Fletcher T.D., Viklander M., Deleti ć A., 2013. Optimising nitrogen removal in existing stormwater biofilters: benefits and tradeoffs of a retrofitted saturated zone. Ecol Eng 51:75 – 82

[16] Liu J., Davis A.P., 2014. Phosphorus speciation and treatment using enhanced phosphorus removal bioretention. Environ Sci Technol 48: 607 – 614

Natthapon Muangmaya
Master Student, Master of Engineering (Environmental Engineering)
Research Interests: Water Treatment, Biochar Improvement, Rain Garden

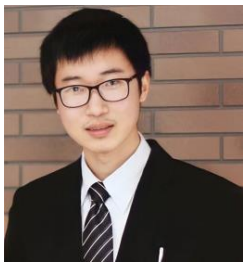

Dr. Prattakorn Sittisom
Lecturer
Research Interests: Water Treatment, Membrane Filtration Technology

The Role of Local Government on Tai Young Culture in Pasang District, Lamphun, Thailand

Non Naprathansuk[1*], Jirapong Chaichawwong[2], and Suriyajaras Techatunminasakul[3]

[1] School of Administrative Studies, Maejo University, Chiang Mai, Thailand
[2] School of Administrative Studies, Maejo University, Chiang Mai, Thailand
[3]School of Administrative Studies, Maejo University, Chiang Mai, Thailand

*Corresponding author, E-mail: nonnaprathansuk@hotmail.com

Abstract: This article aims to study the role of local government on Tai Yong culture in Moungnoy municipality, Pasang district, Lamphun province. This article employed a documentary study. The primary information will be collected on Moungnoy municipality administrative documents, and the secondary data will be collected on related documents. To achieve the studies of this article, the study focusses on identity theory, and public administration theory. The result of the study shows that Moungnoy municipality plays the main role to promote Tai Young Culture for tourism rather than intensively preserve to be a way of life in their community. Policies, budgeting, long term planning focus on developing community to more effectively for modern lifestyles and infrastructure.

Keywords: Local government, Tai Young culture, Pasang District.

1. Introduction

The local administrative has been founded in rural Thailand as the main organization of local management. They are a bureaucratic body where they work in principle the same as a small size autonomous government office. However, the local administrative function can comprehensively as structure, budgeting, authority, and operation which are a body of local administrative. From the local administrative point of view the structure which is services to local community or rural area spread around Thailand must be studied seriously according to autonomy and decentralization that changed the act of Thai bureaucracy in new paradigm of Thai administrative.

Thus, the decentralization released the identity of local community around Thailand which was nation identity hide, repress, and detain their identity since Thailand became a nation. The discourse of Thai nation no longer is a homogenous but became a diversity of ethnic groups over Thai nation. From this point, it seems localization became a main role that impact to nation. Decentralization empowers local government where community elect their own people who administrative and govern themselves. Therefore, we cannot avoid studying from a local government perspective where it is the richest sources of information and data to study a reflection on their community.

Meanwhile, the interaction between globalization and localization seems very aggressive since the technology of internet became a common word. Many local communities' struggles from westernization with came from U.S.A. for an example music, dresses, foods, and way of life such as pop-culture, rap-culture. Even though from the Eastern side like Korea (K-pop) and Japan (J-pop) as well. This phenomenon strongly impacts to their identity that is many local communities cannot stand against American culture K-culture, or J-culture.

The discourse or pitfall from globalization created a primary discourse that hegemony to many nation-states around the world where towards to the smallest units in nation-state. It encloses, represses, and transforms local culture to western culture, K-culture, and J-culture. This discourse creates a phenomenon in present day, not only globalization but also decentralization created a phenomenon of localization which seems to be an anti-globalization. It made many communities try to review their knowledge and cultures which protest the outsider culture that came with capitalism and brought another procedure of making a colony that assimilate with way of life. As well as Moungnoy municipality, Pasang district, Lamphun province. Therefore, how does the role of local government shapes Tai Yong culture is the main question for the study. This article consists of four parts. The first part is an introduction; the second part is identity and public administration theory; the third part is Tai-Young culture in Moungnoy municipality; the fourth part is a conclusion.

2. Identity and public administration theory

According to Desrochers (2008) defined Identity theory as a micro-sociological theory, which links self-attitudes, or identities, to the role

relationships and role-related behavior of individuals. Identity theorists argue that the self consists of a collection of identities, each of which is based on occupying a particular role.

However, some scholars argued that a tendency to follow their own preconceptions of identity, following the frameworks listed above, rather than considering the mechanisms by which the concept is crystallized as reality.

In this environment, some analysts, such as Brubaker and Cooper (2000) have suggested doing away with the concept completely. Others as Gay and Hall (2012) have sought to introduce alternative concepts to capture the dynamic and fluid qualities of human social self-expression for example, suggests treating identity as a process, to consider the reality of diverse and ever-changing social experience.

Some scholars have introduced the idea of identification, whereby identity is perceived as made up of different components that are 'identified' and interpreted by individuals. The construction of an individual sense of self is achieved by personal choices regarding who and what to associate with. Such approaches are liberating in their recognition of the role of the individual in social interaction and the construction of identity. Therefore, in this study, identity means social group identity that has a common ways of like such as language, ritual, and national origin.

On the other hand, public administration theory administration can be broadly described as the development, implementation and study of branches of government policy. The pursuit of the public good by enhancing civil society, ensuring a well-run, fair, and effective public service are some of the goals of the field.

Dubois and Fattore (2009) pointed out that public administration is also an academic field. In comparison with related fields such as political science, public administration is relatively new, having emerged in the 19th century. Multidisciplinary in character, it draws on theories and concepts from political science, economics, sociology, administrative law, behavioral science, management, and a range of related fields. The goals of the field of public administration are related to the democratic values of improving equality, justice, security, efficiency, effectiveness of public services usually in a non-profit, non-taxable venue; business administration, on the other hand, is primarily concerned with taxable profit.

United Nations (2000) pointed out that public administration should be a key element in the web of governance institutions, sometimes influencing other institutions, and sometimes being influenced by them. Within this complex network, the capacity, productivity, and accountability of public administration may depend upon the strengthening of extra administrative institutions.

Therefore, in this study public administration is concerned on the implementation of government policies also including some responsibility for determining the policies and programs of governments. Specifically, it is the planning, organizing, directing, coordinating, and controlling of government operations.

3. Tai-Young culture in Moungnoy municipality

Yong or Tai Yong is one of Tai Lue ethnic who origin lives in and Xishuangbanna in Yunnan County southern of China. In Xishuangbanna, the climate and lands destitute to cultivation also Haw clan invade in their territory and turn them to starveling. Therefore, Yong people relocated to the south around Kong basin and Salawin basin in ChiangTung province Shan state Burma where desolate and wide flat land which enriches for agriculture. Moreover, in this area has some clan who speak Tai-Laos language which make them feel like a sibling not only in Shan state but also in north-east of Kong basin also in Chaopraya basin in Thailand as well.

Malasam (2017) explainted that Yong people often immigrate to Lan na in history since Mangrai dynasty. The war between Lan na and another city around Chiang San made people moved around and Yong people as well. They moved down to Lan na in many reasons such as married between clan which made a politics alliance, trading relation, religions and belief, and war that gathered people to relocation from Prachao Kawaila policy as "collected vegetable in basket gathered people in town" which noted in the evidence in the great immigrated Yong history in Lamphun province in 2 times.

The first one of the great immigrated in 1805-1812 Prachao Kawaila had a policy to rehabilitated Lamphun where was almost unoccupied city because Burma army gathered people from Lamphun to relocated in Angwa city also Lamphun people moved out to another safe places from the war. From rehabilitated Lamphun policy, not only to gathered people to be reinforcement for Chiang Mai but also Lamphun is a nearest city where he commanded easier. Second, the great immigrated in 1813- 1852 in 1852 had been gathered people from Yong once again in

Chiang Tung war 2 rd.

Although the second great immigrated did not located where they were settled in Lamphun, but we can assume from their villages and spread around and settled with other communities in Lamphun also around another province such as Chiang Rai, Lam Pang, and Chiang Mai. However, the Yong population is higher than other provinces in another word, approximate 80 percents from population in Lamphun.

Sripasang (1993) pointed out that Tai Yong people have a unique culture is language Yong's language translated from another languages which is close to Lan Na. Yong's language has not compound words which is compound with vowel. If the words are necessary, it will use another vowel such as vowel "A" take place from vowel "EAU". However, this unique culture in present day is fading because of Yong people do not confidence in themselves for using Yong language for communication. Because of inferiority complex which cannot pronounce compound words with vowel.

Malasam (2017) emphasized that Yong people who immigrated to Lamphun always settled along the river or river basin for agriculture and food supply such as Kwang shore, Ping shore, and Mae Nam Ta shore.

Moreover, Moungnoy community is compound of 8 communities. First communities are Ban Rai most people in Ban Rai were immigrated from KwangThung and Xishuangbanna in southern China. Thao Supamit, Thao Sanmahayot, and Thao Sanpanya were leaders to settle and named was Ban Rai Lung in 1799 and had 50 households. Now a day, the population in this community was increased about 711 peoples: male 331 and female 380 from 212 households. In this area has 571 Rai where are 455 Rai for agriculture, 111 Rai for living, 5 Rai for another.

Figure1: Moungnoy Communities (http://www.moungnoy.com/map.html)

Also, Charoenmuang (1996) expressed that from the phenomenon in history that Yong people relocated and immigrated to Lamphun since 1805. It is a significant impact to Lamphun social and culture development which was adjusted to another local ethnic groups. However, Yong people was a majority group in Lamphun approximately 80 percents hence, the perception of their culture remain by conservative their culture for identify themselves from another ethnic groups in Lan Na.

Yong people had been relocated to Lamphun not only brought social structure system but also thinking system, belief, value, culture, and worship. Especially, the perception of Yong traditional has been brought as well like in the earlier period that Yong people relocated to Lamphun. They made a village and named as Yong original city such as Ban Pa Moung, Ban Huay Yang in Pratupa area or Ban Viang Yong, Ban Vang Hai, Ban Srimoungyu, and Ban Lhuy in Ving Yong district.

Moreover, Yong people immigrated to Lamphun province. They brought old belief to Lamphun society such as Hor Tewabhud in Hou Kaow temple. Malasm (1996) pointed out that Hor Tewabhud in Hou Kaow temple was a Holy Spirit and belief for Yong community which first immigrated to Lamphun, it is a symbol of protection for them when they build a new villages in the new place.

Moo	**Villages name**	**Houses**	**Population**		
			Male	**Female**	**Total**
1	Ban Rai	258	325	357	682
2	Ban Sam	332	385	408	793
3	Sapoong	263	284	360	644
4	Moungnoy	129	180	189	369
5	Ban Pa Tan	232	298	287	585
6	Ban Ta Kon Moung	139	207	224	431
7	Ban Rainoi	133	179	186	365
8	Sapoong Luang	250	319	373	692
Total		**1,736**	**2,177**	**2,384**	**4,561**

Table 1: Population and household in Moungnoy municipality area (Moungnoy municipality, 2023)

Moreover, mostly their occupation is agricultural. Longans are mostly grown in Pa Sang,

Li and Ban Hong; garlic is mostly grown in Li, Pa Sang and Ban Hong; shallots are grown in Ban Hong, Li and Pa Sang; vegetables are grown in the Mueang and Ban Hong Districts. Lamphun is a major vegetable producing area in the north. Part of the products are supplied to food processing factories and the rest are sold in Chiang Mai, Lampang, Bangkok, Nakhon Sawan, etc. and the labor is from local areas in Moungnoy municipality and nearby as well.

For religion, Tai Yong people had same culture in Tai reu-Tai Yown in Sip Song Pan na which was culture transferred. Hence, their culture is almost the same, especially religion and belief. They believed in Buddhism as Terawart denomination or Yong denomination. Hence, in Moungnoy municipality area most of population are Buddhism. It has many temples in this area.

On the other hand, according to Moungnoy municipality report (2022) Moungnoy municipality was transformed from sanitation district to municipality according to sanitation regulation all over Thailand from the government gazette number 116 article 9 ก . On 24 February 1999. It was activated on 25 May 1999. Their vision is considering the municipality's weaknesses, strengths, opportunities, and limitations. Therefore, the vision of the municipality has been defined in terms of wording. that rhyme as follows.

“Muang Noi Subdistrict Municipality It's a nice community to live in. The environmental landscape is good, people are educated and economically advanced. People have a good quality of life. Participate in management.” Also, their mission has 5 main points which are as follows.

1. Improving and developing public utilities and utilities to meet standards and be sufficient to meet the needs of the people. to support future urban expansion and the local economy
2. Develop the potential of people and communities to be strong and able to be self-reliant.
3. Promote and support the development of the education and public health systems. as well as preserving and developing the beautiful arts, culture, and local wisdom.
4. Improve and develop management systems by allowing people to participate in decision making. To provide citizens with a good quality of life, stability and safety in life and property.
5. Increase efficiency in environmental management to create a good environment. including the development of tourist attractions for sustainable development.

Moreover, the strategies and developments plan in Moungnoy Municipality has 5 categories to develop community in Moungnoy area as follow:

Strategies	Develop Plan
1.Infrastructure	• Construction and maintenance sidewalk, over pass and wastewater pipeline • Upgrade traffic communication • Develop water supply for households. • Construction and development infrastructure system
2.Economic	• Develop and promote occupation to gain more income. • Reduce cost production
3.Education Social and Culture	• Upgrade school building and education quality • Make alternative information and news. • Promoting culture religion and local identity
4.Health Care	• Protection and promotion community health care service • Develop health care system. • Promoting recreation and welfare
5. Political and Management	• Promoting civil society and democracy with local government • Improvement and development efficiency management • Improvement operation equipment management • Improvement local fiscal system • Protection and alleviation public hazard
6.Environment and Natural resource management	• Create conscious in environment and natural resource management. • Restoration assuages protection and management in environment and natural resource

Table 2: (continued) The strategies and developments plan in Moungnoy Municipality (Moungnoy municipality, 2023)

In their strategic plan 2022-2023 on social and culture, the municipality tries to promote religious

activities, restoring, continuing, preserving, and disseminating Arts, culture, customs and traditions and local wisdom by created 10 projects and budget in total are 530,000 Baht. As wee seen, in their strategic annual plan, Tai Yong identity still a small agenda to mayor and municipality concerned.

Therefore, Moungnoy Municipality constructs Yong culture identity by using the old historical constructions such as temples, pagodas, and cultures. However, they did not review Yong culture to become a way of life but just using for promoting their identity for tourism more than local people realize and important conscious. Moreover, their mixed between local Tai culture and Yong culture rather than conservative and review Yong culture seriously also according to their budgeting, it demonstrates that their concern in infrastructure for modern economy rather than sustain economic by based on culture and identity. Thus, they manage Yong culture which blended with Local Tai culture therefore, the result for Yong identity has been transformed to "Tai-Yong culture". Whereas, both original cultures no longer exist anymore.

4. Conclusion

Therefore, as the result of the study shows that Moungnoy municipality plays the main role to promote Tai Young Culture for tourism rather than intensively preserve to be a way of life in their community. Policies, mission, vision, budgeting, and long-term planning focus on developing community to more effectively for modern lifestyles and infrastructure.

References

[1] Brubaker, R. &. (2000). Beyond "Identit. *Theory and Society*, 1-47.
[2] Charoenmuang T. (2011). *Kon Muang: Modern Lanna History (1774-2009).* Chiang Mai: Chiang Mai Urban Development Institute.
[3] Department of economic and social affairs division for public economics and publicadministration. (2000, September 20). *Public Administration and Development.* Retrieved from United Nation: https://publicadministration.un.org/publications/content/PDFs/E-Library%20Archives/2000%20Publications%20in%20Public%20Administration%20and%20Development%20%281989-2000%29.pdf
[4] Desrochers, S. J. (2004). Identity Theory. *Organization Management Journal*, 61-69.
[5] Dubois, H. F., & Fattore, G. (2009). Definitions and Typologies in Public Administration Research: The Case of Decentralization. *International Journal of Public Administration.*, 704-727.
[6] Gay, S. H. (2012). *Questions of Cultural Identity.* London: SAGE Publications Ltd.
[7] Malasam, S. (2017). *Local history The Yong people move the land: The movement and settlement of the Yong people in Lamphun (1805-1902).* bangkok: Toyota Thailand Foundation.
[8] municipality, M. (2023, October 10). *Operational plan for fiscal year 2023.* Retrieved from moungnoy.go.th: http://www.moungnoy.go.th/system_files/178/273949b266be54d9e7b528ab77ba7428.pdf
[9] Sripasang, W. (1993). *Khon Yong Ban Lao Du: History, life and living conditions. Belief and identity.* Chiang Mai: Chiang Mai University.

Dr. Non Naprathansuk
Assistant Professor
Research Interests: Thai Politics, Asia pacific Studies, and Southeast Asia Studies.

Mr. Jirapong Chaichawwong
Lecturer
Research Interests: International Relations, Peace Studies, and Asian Studies.

Dr. Suriyajaras Techatunminasakul
Assistant professor
Research Interests: Local Administration, Local Budgeting, and Social enterprise.

The 29th Tri-U International Joint Seminar and Symposium
Maejo University, Chiang Mai, Thailand, 21–24, December 2023

Current mode DC power load sharing circuit for agriculture

Phiromporn Sathapanasiri[1], Thongchai Maneechukate[1*], Chawaroj Jaisin[1], Parin Kongkraphan[1]
[1]School of Renewable Energy, Meajo University, Chiang Mai, Thailand
**E-mail: pirom_s@windowslive.com*

Abstract: This paper introduces a direct current electrical load-sharing circuit designed for agricultural settings, integrating both solar energy production and grid-based power supply. The primary focus of the circuit design is to efficiently harness energy from photovoltaic sources and distribute it among power loads. The load-sharing circuit operates continuously, facilitating a seamless transition between power sources. Its components include a condition control switch circuit, boost/buck converter circuit and a three-phase bridge rectifier circuit. The circuit's operation is governed by three distinct conditions: $P_{PV} \geq P_{load}$, $P_{PV} < P_{load}$ and $P_{load} = P_G$. Where, the electrical power supplied to the load is in the form of a current variable, while the voltage corresponds to the voltage coordinates of the load. Testing was conducted at load capacities of 75 W and 150 W, with a load voltage rating of 24 V. It was observed that the circuit could harvest a minimum of 6 watts of electrical power from the photovoltaic (PV) source and effectively share power between both supply sources. The presented circuit is capable of performing exceptionally well while satisfying all specified conditions.

Keywords: Current mode, Energy management, Load sharing

1. Introduction

Thailand participated in the 21st Conference of the Parties (COP21) under the United Nations Framework Convention on Climate Change (UNFCCC). The nation committed to reducing greenhouse gas emissions by 20-25% in the year 2030, thereby transitioning towards the adoption of renewable energy sources. Consequently, Thailand adjusted its Alternative Energy Development Plan (AEDP) from the year 2015 to 2018 by increasing the share of renewable energy by an additional 30% from the original plan. This adjustment aimed to achieve a proportion of 34.25% of the country's total electricity consumption in the year 2080 [1,2]. As a result, the Thai government formulated policies to promote renewable energy adoption across all sectors, particularly focusing on the industrial and agricultural sectors. Within these sectors, there has been a significant increase in the production and distribution of direct current electrical appliances, ranging from small to large-scale devices, to meet the evolving demands of consumers.

In the agricultural sector, crop production encompasses a spectrum ranging from small-scale to large-scale entrepreneurs, including community-based enterprises. Smart agricultural technology has been integrated to enhance the efficiency of agricultural crop production. Presently, there is a noticeable trend where technology predominantly involves a shift from alternating current (AC) electrical equipment to an increasing use of direct current (DC) equipment. This transition is prevalent in medium to large-sized agricultural operations, necessitating the utilization of such DC-powered equipment in line with the scale of production. Consequently, the costs associated with electricity usage have escalated due to the use of DC-powered equipment. Given that the equipment employed in crop production operates on DC electricity, the most widely chosen alternative among agricultural practitioners to mitigate production costs is harnessing renewable energy from solar power systems. Thailand's substantial solar energy potential (4-5 kWh/m^2) has prompted the production of electricity from solar energy through the use of PV. This electricity is converted into DC and channeled through a DC-DC converter, responsible for voltage regulation to ensure stable output by employing automatic algorithms for voltage control. The voltage output depends on the input power and the specific characteristics of the load. Generally, DC-DC converters are classified into two types: isolated and non-isolated converters. Isolated converters employ high-frequency transformers suitable for high-voltage applications, capable of adjusting positive or negative values; a feature not available in non-isolated converters. Non-isolated converters, known as boost-buck converters, offer the advantages of smaller size, cost-effectiveness, and widespread usage [3,4,5].

The research investigates the utilization of solar cells in conjunction with an alternating current power supply and its conversion into direct current electricity for loads. Several studies have explored different control techniques in this regard: Mohamed et al. studied the operation of a DC-DC converter using proportional-integral (PI) and fuzzy logic control. Through MATLAB simulations, they compared PI and fuzzy logic control, concluding that fuzzy logic control exhibited better response and efficiency [6]. Ndiaye et al. examined the implementation of PID control for predicting and regulating load sharing among multiple sources [7]. Jaisin et al. researched a hybrid load system between direct current and alternating current for small-scale agricultural loads, utilizing Time Division Multiplexing technique to allocate time slots for the direct current load using fuzzy logic control. This method enhanced system efficiency by over 90% [8]. Ostrerov and Umminger studied LTC4370, an IC facilitating power sharing between two power sources using PWM signals to control the operation of the MOSFET. When the main power source dropped by 5% in voltage, it shared the load equally at a 50% per 50% ratio with the secondary source [9]. Chattopadhyay and Das presented control of a DC-DC converter using digital signal processing to control the switching induced current of the buck converter in current mode control, enhancing frequency control effectiveness in high switching [10]. Li and Lee developed a new model for constant ON-time control of the converter using a duty factor. This method was applied to current-mode control [11].

Based on the research findings, it was discovered that when the voltage drops below 5%, power sharing occurs at a 5 0 % per 5 0 % ratio between two power sources, preventing the complete harvesting of electricity from the primary source. Additionally, most research related to current mode techniques focuses on control methodologies used specifically for boost-buck converters. This research

aims to investigate the energy harvesting from PV., which serve as the primary power source across all ranges from low power to high power. It utilizes current mode techniques for energy sharing.

2. Methods

The aim of this research is to harvest electrical energy in the form of electrical power from solar power supplies, which are the main source of electricity. This involves controlling a shared load using a current mode technique based on Kirchhoff's current law. This law states that the total electric current entering any node in an electrical circuit is equal to the total electric current leaving that node. The principle applied is that every voltage source will provide the same constant voltage, as illustrated in figure 1. Suppose there are two power sources, both supplying a constant voltage (V_{DC}). Consequently, the voltage supplied to the input of the load will be V_{DC}.

$$V_{DC} = V_{PV} = V_G \quad (1)$$

The electrical current supplied to the load's input can be calculated by utilizing Equation 2.

$$I_{total} = I_{PV} + I_G \quad (2)$$

When considering the electrical voltage levels, the power delivered to the load can be calculated using the following formula:

$$P_{load} = V_{DC} I_{total} \quad (3)$$

Substitute equation 2 into equation 3 to get.

$$P_{load} = V_{DC}(I_{PV} + I_G) \quad (4)$$

According to Equation 4, it's evident that the electrical power supplied to the load is sourced from two power sources, indicating load sharing in the current mode. Additionally, with the direct current voltage consistently set at 24 volts, the electrical power of the load in this current mode of load sharing can be calculated using Equation 5.

$$P_{load} = 24(I_{PV} + I_G) \quad (5)$$

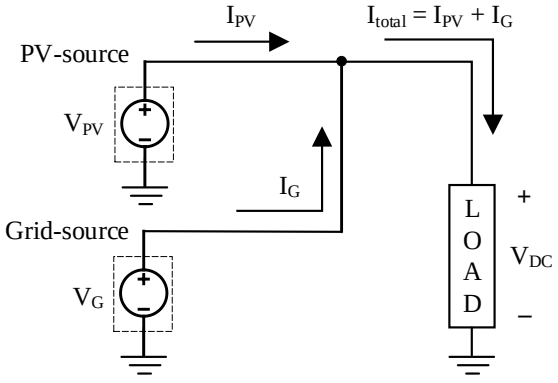

Figure 1. Conceptualizing a current mode load sharing circuit.

In order to maintain the voltage level in the circuit, a boost-buck converter device is necessary. Each device operates as follows: The boost converter circuit is utilized for converting the output voltage to a value greater than the input voltage fed into the circuit. The operation of the Boost converter is divided into two-time intervals: continuous conduction mode and discontinuous conduction mode, as depicted in Figure 2 .

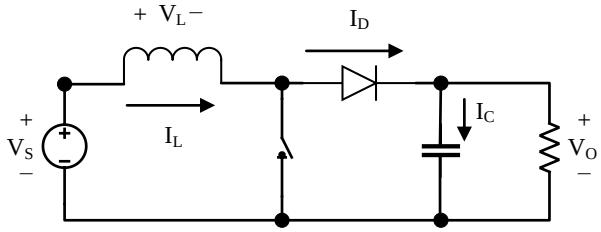

Figure 2. Boost converter circuit.

The operation occurs in continuous conduction mode, where the DC flows from the power source through the conductor via the switch, simultaneously, the diode is reverse biased, preventing the conduction of current. The voltage across the conductor (V_L) will be equal to the voltage of the power source (V_S) according to Kirchhoff's Voltage Law as expressed in Equation 5.

$$V_L = V_S = L\frac{dI_L}{dt} \quad (5)$$

Where I_L denotes the electric current passing through the conductor. When discontinuous conduction mode, the electrical current in the inductor cannot change instantaneously. The diode will be forward biased to allow current to flow, enabling a continuous flow of electrical current through the inductor. Assuming the output voltage (V_O) remains constant, according to the law of conservation of energy, the equation for the voltage across the diode will be as follows.

$$V_L = V_S - V_o \quad (6)$$

A buck converter circuit is an electrical circuit that converts direct current voltage into direct current, typically reducing the output voltage to a level lower than the input. This circuit can operate in two modes: continuous conduction mode and discontinuous conduction mode.

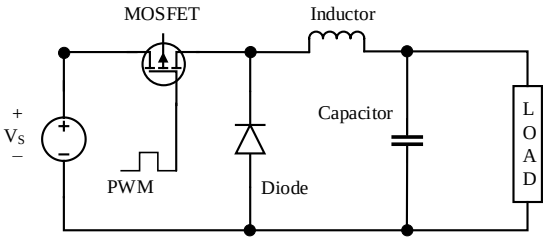

Figure 3. Buck converter circuit.

In continuous conduction mode, current flows from the power supply through a switch, traverses an inductor, and reaches the load. In this process, a segment of this current passes through a capacitor, as represented by Equation 7. Furthermore, Equation 8 allows for the determination of the change in current during the continuous conduction period ($\Delta i_{L,on}$).

$$V_L = V_S - V_o \quad (7)$$

$$\Delta i_{L,on} = \left[\frac{V_S - V_o}{L}\right] DT \quad (8)$$

Where D represents the Duty Cycle, T represents the time period and L represents the inductor.

During discontinuous conduction mode, when the

switch cannot conduct current, the diode will be forward biased. The current from the output terminal can continuously flow through the inductor. This relationship is expressed by Equation 9, enabling the determination of the current variation during the discontinuous conduction period ($\Delta i_{L,off}$), as outlined in Equation 10.

$$V_L = -V_o \tag{9}$$

$$\Delta i_{L,off} = \frac{-V_o}{L}(1-D)T \tag{10}$$

Current mode DC power load sharing circuit diagram

The circuit presented in this article consists of two sources of electrical voltage: PV and Grid. The control circuit section comprises a switching control circuit, and the voltage stability control will be implemented using a Boost-Buck converter. As for the output circuit section utilizes a 3 Phase Bridge Rectifier
Circuit, illustrated in Figure 4.

The operating conditions of the current mode DC power load sharing circuit proposed.

The system is designed to operate primarily using solar energy. Control condition changes will rely on a reference voltage as a criterion for altering the control conditions. The energy management control will consist of a total of three conditions.

Condition 1: When the PV generate electricity equal to or greater than the load demand, all the generated electrical power will be sent for use. This can be expressed by Equation 11.

$$P_{PV} \geq P_{load} \tag{11}$$

In this scenario, the switching control circuit will manage the electronic switch, SW1, to allow the electrical power from the PV system to pass through SW1 and enter the buck converter. This process ensures that the output voltage remains constant at the level required by the load. Subsequently, the power will enter the circuit of the 3-Phase Bridge Rectifier Circuit and be supplied to the load. Therefore, the electrical current of the load can be obtained from

$$I_{PV} = I_{PV(buck)} \tag{12}$$

$$I_{load} = I_{PV(buck)} \tag{13}$$

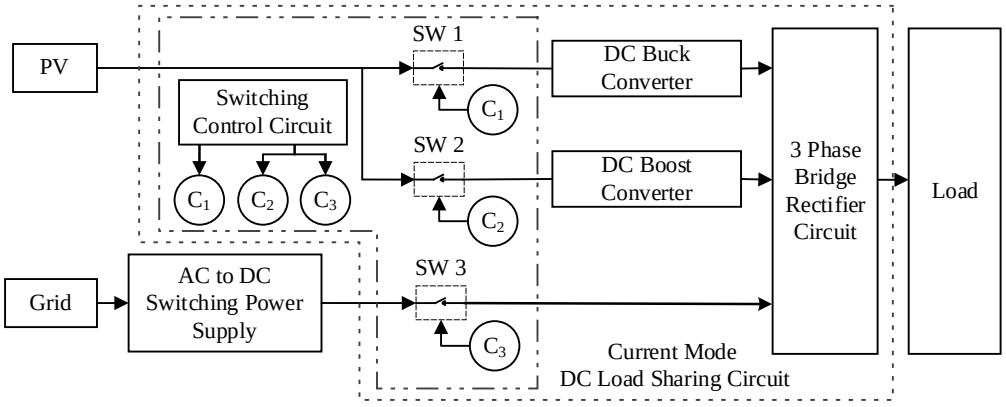

Figure 4. Current Mode DC Power Load Sharing circuit diagram

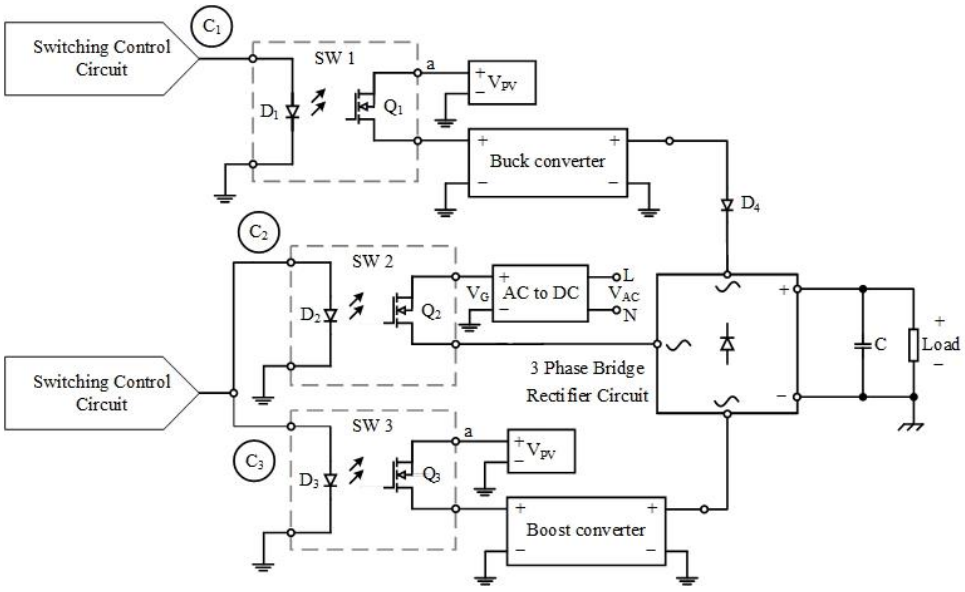

Figure 5. Current mode DC power load sharing circuit

Condition 2 : When the PV generate produces less electricity than the demand, all the generated electrical power will be provided to the load. Moreover, the deficient electrical power will be shared, coming from the state grid system, to supply the required power to the load. This condition can be represented by Equation 1 4 for the condition and Equation 1 5 for the total load power.

$$P_{PV} < P_{load} \quad (14)$$

$$P_{load} = P_{PV} + P_G \quad (15)$$

In this condition, electronic switches SW2 and SW3 operate to allow the electrical power from the PV system to flow through SW3 into the boost converter. This action stabilizes the output voltage to meet the required load demands. Moreover, for the grid, the AC electrical voltage is converted into DC voltage (AC-DC converter) that matches the voltage required by the load. Subsequently, the electrical power enters the
3-Phase Bridge Rectifier Circuit and is supplied to the load. Therefore, the electrical current of the load can be obtained from

$$I_{PV} = I_{PV(boost)} \quad (16)$$

$$I_{total} = I_{PV(boost)} + I_G \quad (17)$$

Condition 3: When the PV system is unable to produce electricity, the system will operate using electrical power solely from the grid, as defined by Equation 18.

$$P_{load} = P_G \quad (18)$$

In this condition, the electronic switch will operate similarly to Condition 2. Additionally, the electrical power from the grid will be converted into DC electricity using an AC-DC converter. It will then enter the 3- Phase- Bridge Rectifier Circuit and be supplied to the load. Thus, the electrical current of the load can be derived from equation 18 and depicted in the current mode DC power load sharing circuit as shown in Figure 5.

$$I_{total} = I_G \quad (19)$$

Testing the operation of the Current Mode DC Power Load Sharing circuit.

Given that the system voltage and the load working voltage are specified at 24 volts in a direct current. The PV system is simulated using a DC power supply rated at 64 volts and 6 amps, supplying power to light bulbs sized at 75 watts and 150 watts, respectively. The switching control circuit operates using a 24 V, derived from the load's operating voltage, as a voltage reference for controlling the operations according to conditions stipulated by equations 11, 14, and 18.

3. Results and Discussion

The Current Mode DC Power Load Sharing circuit's operation will be tested with load sizes of 75 and 150 watts, respectively. The voltage will be supplied from the PV system using a DC power supply rated at 64 volts and 6 amps, which will also be set as the reference voltage value for the PV. The voltage supply will gradually increase from 0 to 64 volts.

Case with a load of 75 W.

Testing at a 75 W load from Figure 6(a) during period shows an insufficiency in power generation from the PV system to fulfill the load's requirements. Consequently, the grid supplies power to the load, as indicated by condition 3. When the reference voltage of the PV is 12 V in range B, it is found that the control circuit will connect the PV by supplying power from the PV through a boost converter to increase the voltage to 24 V to be supplied to the load. The PV will supply power **Case with a load of 75 W.**

Testing at a 75 W load from Figure 6(a) during period shows an insufficiency in power generation from the PV system to fulfill the load's requirements. Consequently, the grid supplies power to the load, as indicated by condition 3. When the reference voltage of the PV is 12 V in range B, it is found that the control circuit will connect the PV by supplying power from the PV through a boost converter to increase the voltage to 24 V to be supplied to the load. The PV will supply power

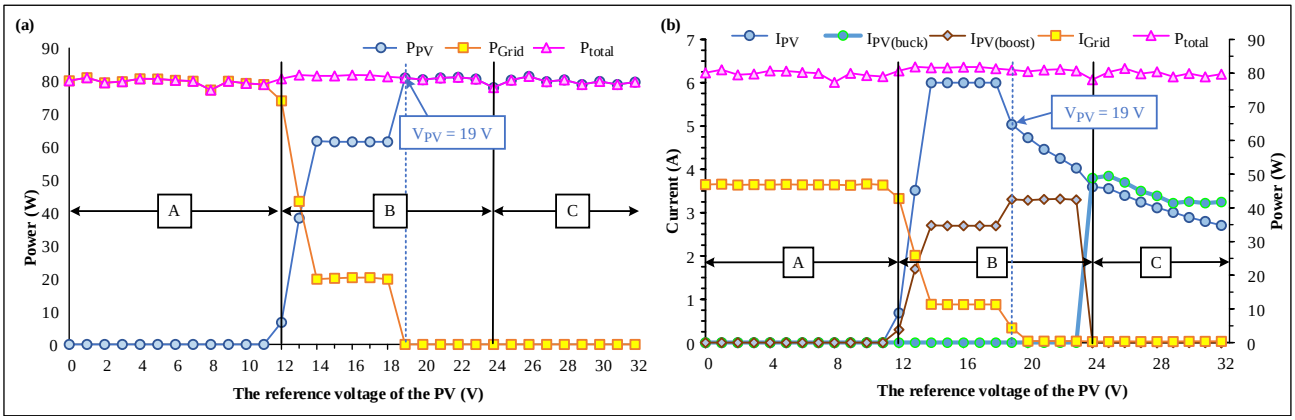

Figure 6. (a) The electrical power from the PV and the Grid supplied to the load is 75 W and (b) The electrical current and the total electrical power supplied to the load amounting to 75 W.

which will also be set as the reference voltage value for the PV. The voltage supply will gradually increase from 0 to 64 volts.

From Figure 6(b) within range B, which is related to range B in Figure 6(a), it is observed that the current flowing into the load is shared between the PV system and the Grid, demonstrating the characteristic behavior of current mode load sharing. The electrical power output to the load is dependent on the current of the source, as determined by the conditions outlined in criterion 2. The power allocated to the load is contingent upon the behavior of the power generated by the PV system, which dictates the power sharing.

When considering the PV's reference voltage, while the voltage at 19 volts, the electrical current output from the PV stands at 5 amps. This signifies that, at this moment, the PV possesses a power output of 95 watts, which is sufficient to adequately supply the load. Consequently, the circuit designed and presented does not sharing power with the Grid. Therefore, this operation aligns with criterion 2. Subsequently, as the PV's reference electrical voltage increases up to 24 volts, the control circuit sends a signal to activate the electronic switch SW1. The circuit operation directs the power from the PV system to the buck converter. If the voltage output from the PV system exceeds 24 volts, the buck converter regulates the output voltage to a constant 24 volts. Consequently, the PV system supplies power exclusively to the load from a single source, conforming to condition 1. This operational behavior of the circuit is illustrated in Figure 6(a) during period C.

Case with a load of 150 W.

However, in range B, where the PV's reference voltage ranges between 24-27V, it's noted that the circuit experiences an approximate power dissipation of 6W. Consequently, this causes the electrical power generated by the PV to be insufficient to meet the 150W load demand. Despite the load requirement, during this voltage range, the circuit continues to engage in power sharing between both sources continuously until reaching the 27V mark. Therefore, the electronic switch control circuit does not send control signals to switch SW1 to alter the control conditions according to the condition $P_{PV} \geq P_{load}$

The operation of the circuit in range C, in Figures 7(a) and 7(b), where the reference voltage of the PV is from 28 V onwards, demonstrates that the power generated by the PV system is sufficient to meet the load's requirements. Consequently, the circuit operates according to condition 1. where the power supply will exclusively deliver electrical power from the PV to the load

4. Conclusions

From testing at load sizes of 75 W and 150 W, it was found that the operation of the designed and presented circuit can work according to the designed conditions in all respects. and can share electrical power with the load very well Including the ability to harvest electricity from PV even under conditions of low power production by the PV. The circuit is capable of commencing the power harvest from the PV, supplying power to the load starting from 6 W onwards, and can sharing power in conjunction with the Grid. In addition, this circuit is capable of initiating power harvesting to supply the load from as low as 6 W onwards. Additionally, it can also supply electrical power in conjunction with the grid. The circuit operates based on three conditions: First, when the PV generates sufficient electrical power to meet the load's demand. Second, when the power supplied by the PV is insufficient, the circuit immediately transitions to a state where the PV supplies power concurrently with the Grid. Lastly, the third condition dictates that the grid provides electrical power exclusively when the PV generates less than 6 W of power. The conducted experiments reveal that the presented circuit operates as a current mode DC power load sharing circuit. Additionally, it is observed that there is a power loss of 6 watts within the circuit.

5. Acknowledge

This article has been funded by research grants from Maejo University's Disciple Scholarship and the School of Renewable Energy at Maejo University, Chiang Mai, Thailand, specifically in the laboratory facilities and through a scholarship. We would like to express our gratitude for the scholarship provided for the project aimed at cultivating and developing graduate students in renewable energy across ASEAN countries for the year 2022.

References

[1] Annual Report 2018 Department of Alternative Energy Development and Efficiency. Ministry of Energy, Thailand, Bangkok (2018)

[2] Department of Alternative Energy Development and Efficiency: Thailand PV Status Report 2020. Ministry of Energy, Thailand, Bangkok (2020)

[3] Duong, M. Q., Nguyen, H. H., Nguyen, T. H. D., Nguyen, T. T., & Sava, G. N. (2017, March). Effect of component design on the DC/DC power converters dynamics. In 2017 10th International Symposium on Advanced Topics in Electrical Engineering (ATEE) (pp. 617-620). IEEE.

[4] Sick, F., & Erge, T. (Eds.). (1996). Photovoltaics in buildings: a design handbook for architects and engineers. Earthscan.

[5] Abouchabana, N., Haddadi, M., Rabhi, A., Grasso, A. D., & Tina, G. M. (2021). Power efficiency improvement of a boost converter using a coupled inductor with a fuzzy logic controller: application to a photovoltaic system. Applied Sciences, 11(3), 980.

[6] Mohamed, H. A., Khattab, H. A., Mobarka, A., & Morsy, G. A. (2016, December). Design, control and performance analysis of DC-DC boost converter for stand-alone PV system. In 2016 Eighteenth International Middle East Power Systems Conference (MEPCON) (pp. 101-106). IEEE.

[7] Ndiaye, M. F., Guérin, F., Lefebvre, D., & Ndiaye, P. A. (2015). Model Predictive Control and Generalized Adaptative PID for Load Sharing In Systems of Multiple Sources of Energy. IJARCCE, 4, 307-312.

[8] Jaisin, C., Intaniwet, A., Nilkhoa, T., Maneechukate, T., Mongkon, S., Kongkraphan, P., & Polvongsri, S. (2019). A prototype of a low-cost solar-grid utility hybrid load sharing system for agricultural DC loads. International Journal of Energy and Environmental Engineering, 10, 137-145.

[9] Ostrerov. V., Umminger, C. (2016). Easy Balanced Load Sharing for Three or Four

Supplies, Even with Unequal Supply Voltages. https://www.analog.com/en/technical-articles/easy-balanced-load-sharing-for-three-or-four-supplies.html.
[10] Chattopadhyay, S., & Das, S. (2006). A digital current-mode control technique for DC–DC converters. IEEE Transactions on Power Electronics, 21(6), 1718-1726.
[11] Tan, C. W., Green, T. C., & Hernandez-Aramburo, C. A. (2007, September). A current-mode controlled maximum power point tracking converter for building integrated photovoltaics. In 2007 European Conference on Power Electronics and Applications (pp. 1-10). IEEE.

Phiromporn Sathapanasiri
Master student, Master of Engineering (Renewable Energy Engineering).
Research Interests:
Smart Farm,
Renewable Energy

Dr. Thongchai Maneechukate
PhD Assistant Professor.
Research Interests:
Electrical Engineering,
Control System,
Engineering,
Smart Farm.

Dr. Chawaroj Jaisin, PhD
Associate Professor.
Research Interests:
Embedded technology,
Postharvest technology,
Energy conservation.

Dr. Parin Khongkrapan
Assistant Professor
Research Interests:
Plasma technology,
Drying technology,
Machine design,
Energy

Vibration Character Monitoring of Submerged Hollow Fiber Membrane in AnMBR by using Accelerometer

Prattakorn Sittisom[1*], Tomoaki Itayama[2]

[1]Department of Environmental Engineering, Faculty of Engineering, Chiang Mai University, Thailand
[2]Graduate School of Engineering, Nagasaki University, Japan
**Corresponding author, E-mail: prattakorn.s@cmu.ac.th*

Abstract: The research of anaerobic wastewater treatment has received much interest in recent years because of its low energy and nutrient requirements, low sludge generation, and capacity to produce methane. But membrane fouling is a significant operational challenge for the AnMBR method. In this study, vibration character of hollow fiber membrane (HFM) bundles, we conducted the experiment using a lab-scale AnMBR system. To develop Accelerometer (ACM) which can help to understand the vibration characteristic under the close system of AnMBR. When vibration in the lab-scale experimental condition can be understood, the better arrangement of membrane module in AnMBR system can be designed, fouling can be reduced effectively and extend maintenance operation. The experimental set-up for measuring the vibration of the hollow fiber membrane (HFM) module was set to a lab-scale AnMBR with the looseness of the module varied, 0%, 1%, 2% and 3%. The acceleration was measured under constant aeration conditions (20 l/min). The results showed stronger vibration before fouling than after fouling. And at different looseness, smaller looseness showed stronger vibration respectively. Moreover, Z-axis showed stronger vibration than X-axis. This study suggests that the ACM is a suitable option to measure the membrane vibration in a lab-scale AnMBR. Therefore, ACM should be recommended to be used as a cheap and effective option for designing on a practical scale.

Keywords: Hollow Fiber Membrane, Vibration, Accelerometer, Anaerobic MBR, Membrane Fouling

1. Introduction

The research of anaerobic wastewater treatment has received much interest in recent years because of a growing concern about sustainability in wastewater management [1]. Because of its low energy and nutrient requirements, low sludge generation, and capacity to produce methane, the anaerobic membrane bioreactor (AnMBR) has the potential to be a more sustainable wastewater treatment technology than traditional methods [2,3].

Despite these benefits, membrane fouling is a significant operational challenge for the AnMBR method, and it has been thoroughly investigated for both aerobic and anaerobic MBR [4,5]. Permeating flux and membrane lifespan are decreased because of fouling. When compared to aerobic MBRs, anMBRs reach a higher biomass concentration, affecting rheology and thus reactor hydraulics and pumping [6,7]. The technical improvement of AnMBRs has been based on membrane fouling during their growth. As a result of this aim, several techniques for continuously preventing the accumulation of scale and solids cake on the membrane surface, which causes membrane fouling and a significant reduction in filtration capability, have been developed. Therefore, numerous studies have been conducted to monitor and minimize membrane fouling.

To maintain the filtration potential of membrane, bubbling is widely used [8]. The flow on the membrane surface caused by rising bubbles will suppress the concentration polarization layer of solid suspensions and membrane foulants around the membrane, which limits the filtration rate [9]. Furthermore, rising bubbles were directly linked to membrane vibration, which influences membrane fouling prevention [10]. The membrane vibration was assumed to be caused by the surface turbulent flow of bubbles and the direct collision of bubbles with the membrane. The stress sensor was effective in measuring the fluctuating shear stress and the laser displacement sensor was successful in measuring the fluctuating motion of the flat sheet membrane [11]. A high-speed camera was used to test the vibration of hollow fiber membranes in a model MBR chamber made of transparent plastic (HSC). The results of the study were then used to enhance the membrane module's design. Therefore, controlling membrane vibration in an MBR is very useful for designing a membrane module or device that effectively suppresses membrane fouling [12].

However, it is complicated to measure the membrane vibration in a practical MBR using such optical methods as HSC because of the high turbidity of sludge suspension in an MBR chamber. For this purpose, we developed the measurement method using an accelerometer (ACM). It was succeeded to measure membrane vibration using the ACM attached to an HFM. In the experiment to clarify the effect on the vibration of a single string HFM with the different looseness, the comparison between ACM measurement and HSC measurement was performed. Then we used the turbulence flow generated by the submerged pump to cause the membrane vibration. It presented the complete identical results for both measurement methods that the root mean square of the acceleration of the membrane vibration decreased as the looseness increased [12].

In this study, vibration character of hollow fiber membrane (HFM) bundles, we conducted the experiment using a practical scale MBR and lab-scale AnMBR system. The vibration was measured using accelerometers (ACMs) attached on the middle position on a string of a membrane in AnMBR to analyze the vibration character in each looseness in the membrane module, then the effect of the bubbling strength (air sparge rate) for the vibration character was measured, because there has been no research to clarify these characters though the basic vibration characters must be important to design the new membrane module in MBR and AnMBR system.

2. Materials and methods

2.1. Experimental set-up of Anaerobic MBR system

The experimental set-up for measuring the vibration of the hollow fiber membrane (HFM) module is illustrated in Figure 1. A PVDF HFM of 0.4 μm nominal pore diameter, 2.8 mm fiber diameter (Mitsubishi Chemical Co. Ltd., JAPAN) was set to a lab-scale AnMBR. A membrane module was crafted from 90 HFMs with 60 cm. length. The ACM was attached on the HFM in the middle of the crafted membrane module in the Anaerobic MBR (AnMBR). The acceleration was measured under constant aeration conditions (20 l/min). The distance

between the upper end point of HFM and the lower endpoint was able to be adjusted between 60cm to 58.2cm (=D_{frame}) in length using a screw mechanism. When each HFM of looseness of 0%, 1%, 2%, and 3% was set, the actual length of HFM was kept to 60.0cm (=L_{HFM}). The looseness is defined as follows.

$$\text{Looseness (\%)} = \frac{L_{HFM} - D_{frame}}{L_{HFM}} * 100 \ldots (1)$$

, where L_{HFM} is the length of HFM, D_{frame} is the distance between the upper and lower fixed points on the frame.

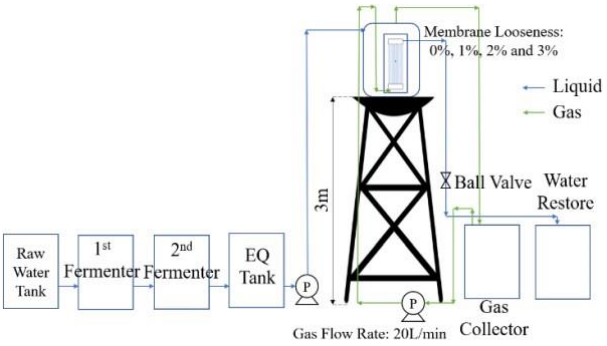

Figure 1 Anaerobic MBR system

Accelerometer (ACM) KXP84 (Kinonix, Inc., USA) of 0.049 g in weight, the size of 5mm x 5mm x 1.2mm (thickness) can measure the acceleration values for the three directions (X, Y, Z), as shown in Figure 2.

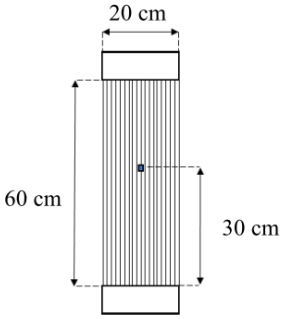

Figure 2 Crafted membrane module

2.2. Measurement of the membrane motion by an accelerometer (ACM)

An accelerometer KXP84 (Kinonix, Inc., USA) with a weight of 0.049 g, the size of 5mm x 5mm x 1.2 mm (thickness) was used for the membrane motion measurement. The ACM measured the acceleration for the three directions (x, y, z), as shown in Figure 3.

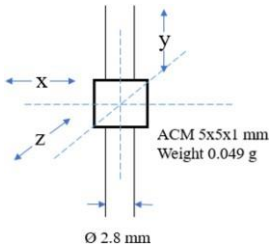

Figure 3 KXP 84-2050 chip and reference axis

The ACM was attached on HFM surface at 30cm below from the top end of the HFM with UV resin of 0.1 g. The X, Y and Z directions of the ACM for the sensing was defined as shown Figure 3. The ACM transmitted the acceleration data converted to each analog voltage of 660 mV/G. Polyurethane coated copper wires (0.06 mm diameter, 450 mm length) were connected to the ACM including three data lines, a positive power supply (6 V), ground and the logic line for data acquisition enable. The 6 wires were passed through inside the hollow fiber membrane. The total weight of the 6 wires was 0.08 g. Thus, the total weight of the assembled ACM was 0.229 g. It was attached on the HFM of 2.03 g weight. The accelerometer data line for X-direction was connected to data logger of 12bit ADC (DS1M12), where each data line from the ACM was also connected to the ground through a capacitance of 0.033μF according to the company's instruction manual for the high-frequency noise reduction. The time interval for data collection of the data logger was set with 0.00100 seconds period for 60 seconds, where the time interval was tested by the same wave generator as the calibration of the HSC. The measurement was repeated three times for each experimental condition.

Before the experiment for HFM vibration measurement, the response of the ACM was tested in different frequency from 0 to 500 Hz by vertical and horizontal vibration testing machine (LABTONE, Labtone Test Equipment, Co., Ltd.) at Nagasaki Industrial Technology Center.

2.3. Data processing

The average was subtracted from each acceleration time series data (mean centering). Then Butterworth band stop filter (6th order) was applied to remove electric noise 60Hz and its harmonic frequency in software package "dplR". The width of the stop frequency region was designed as 4 Hz.

The probability density function (PDF) of acceleration was estimated for all data points of three repeating measurement data using the function "density" in the software R. Root mean square (RMS) value of acceleration time series a(k) as an indicator of the strength of the random vibration corresponds to the standard deviation (SD) of the estimated probability density function as shown in the following equation (2).

$$RMS = SD = \sqrt{\frac{1}{N}\sum_{k=0}^{N-1}(a(k) - < a(k) >)^2} \quad \ldots(2)$$

Where < a(k)> is the mean value.

In order to analyze the acceleration data with finite measurement time T in frequency domain, Discrete Fourier transformation (DFT) defined by equation (2) was applied for each time series [13] . The DFT was calculated by "fft" command with the hamming window in the package "Signal (ver . 0 . 6 - 7)" in the R . Then the power spectrum density was calculated by use of the following equation (3) [13] .

$$Fa(f:T) = \sum_{k=0}^{N-1} a(k) e^{-i2\pi lk/N} \Delta t : f = \frac{k}{T}, T = N\Delta t \quad \ldots(3)$$

Then the power spectrum densities for three repeating measurements were averaged to one power spectrum density. The averaged power spectrum density was smoothed by using "ksmooth" function in the R to present distinct peaks in the spectrum. Furthermore, to test the numerical error of the FFT calculation and the power spectrum density calculation, Parseval' s identity was tested between the frequency domain data and the original time - domain data [13]. Both calculation results for sinusoidal time - series test data matched in all seven

digits.

3. Results and discussion

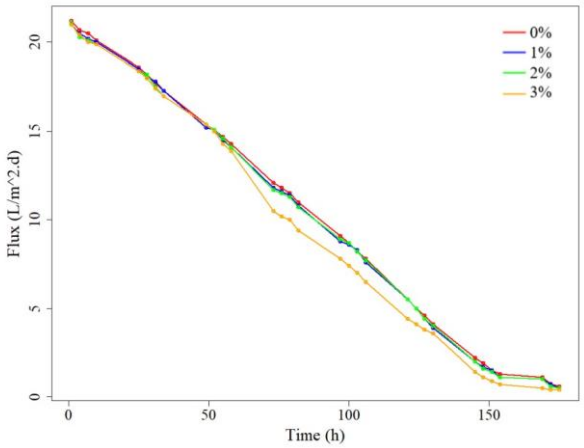

Figure 4 Flux Declining Rate

In this experiment, we investigated the flux declining rate of AnMBR with different looseness of HFM. The filtration process was conducted by using gravity-driven method (syphon). The crafted membrane module was vibrated by bubbling mechanism from gas re-circulation diffuser. The results showed that flux of a 3%-looseness HFM module decreased significantly, in Figure4, which fouling formation occurred on the HFM surface and the vibration performance from bubbling mechanism could not reduce fouling at the 3%-looseness well.

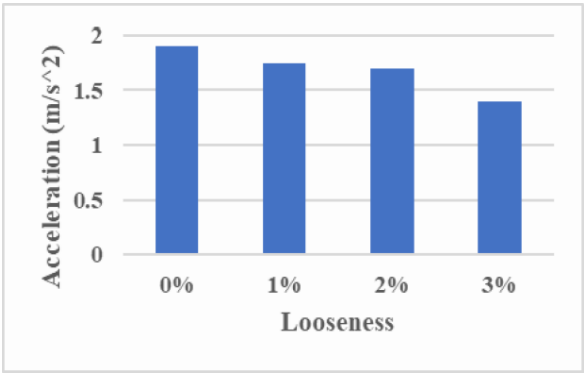

Figure 5 Standard deviation of acceleration on X-axis at different looseness

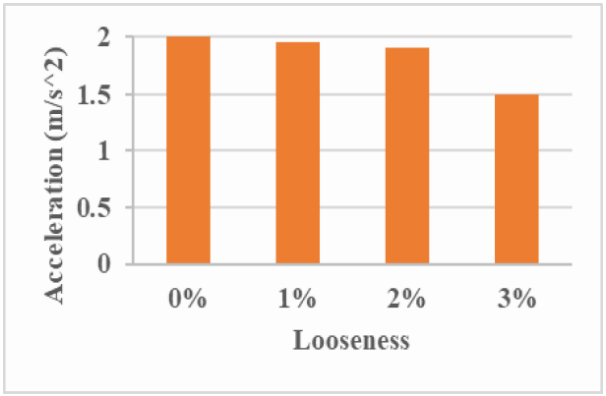

Figure 6 Standard deviation of acceleration on Z-axis at different looseness

ACM was used to measure vibration from the crafted membrane module in anaerobic tank. Figure 5 and Figure 6 showed standard deviation of acceleration on X-axis and Z-axis respectively. The experiment was also conducted under different looseness, from 0%, 1%, 2% and 3%. The results showed stronger vibration on Z-axis than X-axis. It could be indicated that looseness of HFM effected directly to HFM vibration. And the results also clearly showed in Fig.7 that membrane bundle affected for the vibration direction comparison between X and Z-axis.

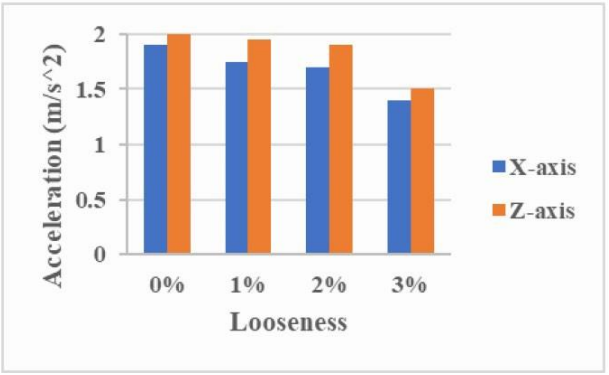

Figure 7 Standard deviation of acceleration on X and Z-axis at different looseness

4. Conclusions

This study succeeded in measuring the vibration of a hollow fiber membrane using an ACM and suggest that the ACM is a suitable option to measure the membrane vibration in a lab-scale AnMBR system with high turbidity. Therefore, vibration measurement in practical situations, ACM should be recommended to be used. It would be a cheap and effective option for designing in the commercial market.

References

[1] Robles, A., Ruano, M.V., Ribes, J., Ferrer, J., 2012. Sub-critical long-term operation of industrial scale hollow-fibre membranes in a submerged anaerobic MBR (HF-SAnMBR) system. Separation and Purification Technology 100, 88–96.

[2] Donga, Q., Parker, W., Dagnewb, M., 2016. Long term performance of membranes in an anaerobic membrane bioreactor treating municipal wastewater. Chemosphere 144, 249–256

[3] Ho, J., Sung, S., 2010. Methanogenic activities in anaerobic membrane bioreactors (AnMBR) treating synthetic municipal wastewater. Bioresource Technology 101, 2191–2196.

[4] Choo, K.H., Lee, C.H., 1996. Membrane fouling mechanisms in the membrane-coupled anaerobic bioreactor. Water Research 30, 1771–1780.

[5] Li, T., Law, A.W.K., Cetin, M. and Fane, A.G. 2013. Fouling control of submerged hollow fibre membranes by vibrations. Journal of Membrane Science 427, 230-239.

[6] Sainbayar, A., Kim, J.S., Jung, W.J., Lee, Y.S., Lee, C.H., 2001. Application of surface modified polypropylene membranes to an anaerobic membrane bioreactor. Environmental Technology 22, 1035–1042.

[7] Nagaoka, H., Ueda, S., Miya, A., 1996. Influence of bacterial extracellular polymers on the membrane separation activated sludge process. Water Science and Technology 34, 165–172.

[8] Bellara S.R., Cui Z.F., Pepper D.S., 1996. Gas sparging to enhance permeate flux in ultrafiltration using hollow

fiber membranes. Journal of Membrane Science 121(2): 175.
[9] Cabassud C., Laborie S., Laine J.M., 1997. How slug flow can improve ultrafiltration flux in organic hollow fibres. Journal of Membrane Science 128(1): 93.
[10] Cheng T.W., Yeh H.M., Gau C.T., 1998. Enhancement of permeate flux by gas slugs for crossflow ultrafiltration in tubular membrane module. Journal of Membrane Science 33 (15): 2295.
[11] Sakai S., Nagaoka H., Inoue M., 2014. Measurement of vibration patterns of flat-sheet membrane module induced by aeration using laser displacement meters in MBRs, Journal of Environmental Engineering Research 70(7): pp. III 165-173
[12] Sittisom P., Itayama T., 2020, Analysis on a vibration character of hollow fiber membrane for MBR using a high-speed camera and an accelerometer. Journal of Faculty of Engineering, Chiang Mai University Vol.27(1).
[13] Brigham E . O . , 1988 . The Fast Fourier Transform and Its Application . Englewood Cliffs, New Jersey .

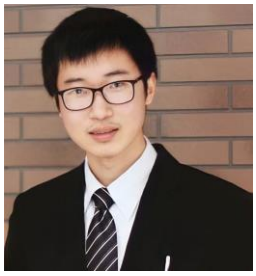

Dr. Prattakorn Sittisom
Lecturer
Research Interests:
Water Treatment, Membrane Filtration Technology

Dr. Tomoaki Itayama
Professor
Research Interests:
Bioinformatics, Water and Wastewater Treatment, Environmental Biology

The potential of biogas production from wastewater of shredded pork processing with pig manure sludge inoculum

Puwadon Chumpoochai[1], Rotjapun Nirunsin[1*], Kittikorn Sasujit[1], Jutaporn Chanathaworn[1]

School of Renewable Energy, Maejo University, Chiang Mai, Thailand

[*]Corresponding author, E-mail: puwadon37904@gmail.com

Abstract: Thai small and medium enterprises (SMEs) are growing up fastly in 2023 especially food processing. Shredded pork is one major product that provide to various market and shop. However, in shredded pork processing, the large amount of wastewater is released. This study aims to study biochemical methane potential (BMP test) of wastewater from shredded pork processing (WSPP) by using pig manure (PM) as inoculum. The BMP test with substrate / inoculum (S:I) ratios of 1:1, 1:2, and 2:1 g VS added were conducted using 1000 mL glass bottles and maintained at a controlled temperature of 35±2 °C in a batch reactor setup. The results showed the accumulative biogas yields were 476.59, 362.97, and 391.07 N ml/g VS added, respectively. The methane content was 83.60. %, 46.47%, and 46.13%, respectively. The ratio of WSPP with PM at 1:1 was the optimized condition in this research. In addition, WSPP had biogas production potential because it had a high percent of methane component in all conditions and needed to be applied on a pilot scale.

Keywords: Biogas production, Biochemical methane potential, Pig manure, Wastewater from shredded pork processing

1. Introduction

The import and export of goods are increasing in Thailand's industrial sector. Export performance is very important for the development of the country, including creating innovations for products or creating added value for products in this industry [1, 2], particularly in part of food processing. Especially within the realm of medium-sized and small enterprises (SMEs) are growing and are interested, especially in shredded pork processing (WSPP) shown in Figure 1.

Figure 1. Shredded pork processing industry in the SME group

One of the major problems concerns that shredded pork processing had a lot of wastewaters that had chemical oxygen demand in the range of 80,000-140,000 mg/L. The components of wastewater from WSPP consisted of blood, fat, and protein [3]. So, entrepreneurs must be concerned and plan about the solution for wastewater treatment because the Pollution Control Department limits the Chemical Oxygen Demand (COD) [4] value of wastewater does not exceed 120 mg/L before being released back into the environment. Biogas technology is one of the best technologies to use for wastewater treatment on an industrial scale.

Biogas can reduce the pollution potential in wastewater by reducing the oxygen levels required by the organic matter via anaerobic digestion which converts organic waste into gaseous energy. Biogas generally consists of methane (50–75%), carbon dioxide (25–50%), and lesser quantities of nitrogen (2–8%) [5], and methane is the major component to provide heat applications such as LPG. Biogas is usually produced from wastewater, sludge, agricultural waste, and other organic wastes [6,7]. This work aimed to study the efficiency of micro-organisms in treating oil/fat and COD. This research studied Organic Loading Rates at 0.05 0.11 0.17 and 0.22 kg.COD/m^3d Experiments were conducted as a batch process from wastewater analysis removal of COD were 0.05-0.17 kg. COD/m3d. The trials could remove the COD up to 90 % [8]. Musa et al. [9] aimed to study the Wastewater Treatment from Cracker Industry by Biogas Production Process, using a 20 L gas fermentation tank.

Hydraulic retention time (HRT) took 21 days to operate and the duration between 0 - 24 days. The treatments were investigated, including the single-phase, two-phase, and single-phase(mediated). The results showed single-phase. Therapeutic efficacy of pH, COD, TSS and TP were 49.47%, 24.15%, 71.86% and 72.13% respectively. The efficacy of the two-phase was 51.19%, 64.62%, 69.77%, and 77.95% respectively. The efficacy of single-phase (mediated) were 54.03%, 57.88%, 72.55% and 78.89% respectively. From the experiment single-phase (mediated), expanding to a wider size is the most suitable course of action. Therefore, this study aims to study the biochemical methane potential (BMP test) of wastewater from shredded pork processing (WSPP) by using pig manure (PM) as inoculum.

2. Materials and methods

2.1 Substrates and Inoculum

The waste sample was collected from the Shredded pork processing plant (SPP), Lampang Province, using wastewater from the shredded pork processing. Lampang Province, Thailand uses wastewater from shredded pork processing. As shown in Figure 2(a). and pig manure samples were collected from the biogas treatment system. As shown in Figure 2(b).

(a) (b)

Figure 2. (a) wastewater from shredded pork processing (WSPP) and (b) pig manure (PM)

2.2 Experimental set-up

Biomethane potential (BMP) was the standard method by standard VDI 4630 [9]. by using wastewater from shredded pork processing as substrate and pig manure was used as inoculum. The experiment was divided into three conditions. The conditions of SPP to PM were 1:1, 1:2, and 2:1. The bottle working volume was 400 mL. The temperature system was at mesophilic of 35 ± 2 and the pH was valued at between 6.8 and 7.2. The inoculum was digested in an anaerobic digestion time of 7 days [10] The biogas production from WSPP with an anaerobic was tested in triplicate (Figure 3). The BMP tests were conducted was performed for 33 days. At the end a study of Fundamental analysis factors. This includes the measurement of chemical oxygen demand (COD), total solids (TS), volatile solids (VS), volatile fatty acids (VFA), alkalinity, and pH [11]. The analysis was conducted using a gas composition measuring instrument (GFM-406 series: Gas Data, United Kingdom).

Figure 3. System setting of BMP test.

3. Results and Discussion

3.1. Sample Characterization of Wastewater and Inoculum

Sample characterization of wastewater and the inoculum is important for biogas production, especially when processing shredded pork and using pig dung as a leavening agent. This is an illustration of how one could offer such characterization: The chemical oxygen demand, or COD value, is a crucial measure of the amount of organic matter in wastewater [7, 8].

Table 1. The characteristics of biogas production from wastewater from shredded pork processing (WSPP) and pig manure (PM)

Parameters	WSPP	PM
COD (mg/L)	148,376.70	71,895.90
Total Solid (mg/L)s	60.04	55.83
Volatile Solid (mg/L)	14.84	7.19
TS/VS ratio	0.94	1.79
AVF/ALK	4.24	0.73
pH	6.58	7.38

When comparing WSPP to PM, the COD value is much greater, indicating a higher level of organic content. The proportion of volatile solids to total solids [9]. Similar ratios for WSPP and PM indicate a similar amount of organic matter in the overall solid composition.

The ratio of alkalinity to volatile fatty acids. This is a crucial component in keeping anaerobic digestion processes stable. The greater VFA/ALK value of WSPP may suggest higher Characteristics of wastewater generated during the wastewater from shredded pork processing and pig manure leavening agent Shown in Table 1 Ratio of WSPP and PM, COD value 148,376.70 71,895.90 mg/L, VS/TS ratio is 60.04 and 55.83, respectively, VFA/ALK value is 4.23±0.06, 2.43±0.02, and pH value is 6.58 and 7.38, respectively.

3.2 Daily Biogas Production and Methane Content

Biogas production from WSPP and PM in the ratios of 1:1, 1:2, and 2:1 are shown in Figure 4. The experiment took 33 days to terminate. The results of this experiment showed that the cumulative biogas production rate in each ratio during the first 10 days was 92.00, 98.33, and 96.67 N ml./g respectively. Each ratio resulted to be like each gas production rate. The 1:1 ratio indicated the slowest gas production in the first period due to the proportion between wastewater and leavening agent. When compared to other ratios, the solids of 1:1 ratio in this substance were consistent, resulting in a biogas production of up to 127.05 N ml/g. However, the decomposition of organic compounds was a lengthy process due to the TS value of 19,183.733 mg/L.

In consequence of this, the pace at which methanogen was broken down was greatly slowed down. Due to the fact that it has a limited number of carbohydrates and a high proportion of fat and protein, it is designed in order to generate the highest amount of biogas and methane [11]. This is because of the composition of the material. This was distinct from the 1:2 ratio which had the inoculum ratio more than the wastewater. This result was produced from a cumulative biogas production of 72.39 N ml/g compared to an additional TS value of 15,213.81 mg/L. On the other hand, the 2:1 ratio had a higher proportion of wastewater. The inoculant yielded a total biogas production of 79.77 N ml/g a TS value of 14,081.92 mg/L. There was an observable similarity in the total biogas output. Consequently, 1:1 ratio was different from the others.

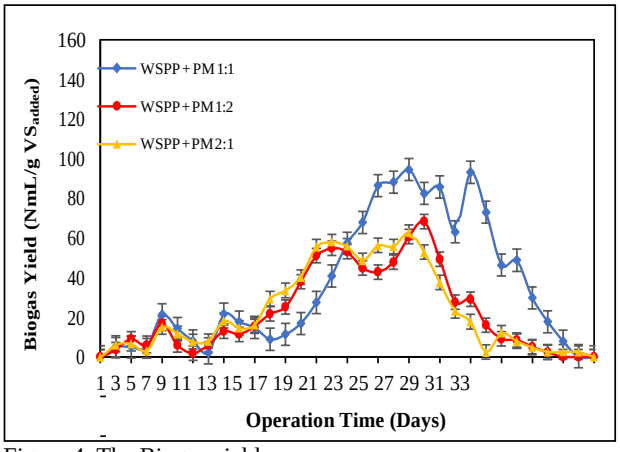

Figure 4. The Biogas yield

Figure 5. showed the results of the cumulative biogas average of the wastewater which had been fermented with pig manure in the ratio of 1:1, 1:2 and 2:1. The highest biogas production values in the ratios 1:1, 1:2, and 2:1 were 1,181.23 ml., 793.30 ml., and 909.85 ml., respectively. During day 11 to day 23, 1:1 ratio took longer decomposition time than the other 2 ratios. Therefore, 1:1 is indicated as the highest biogas

production. After the mentioned processes, the biogas production was terminated. The %TS Removal of each ratio was 53.45±5.4%, 54.62±1.1%, and 54.30±3.2% respectively. The results for %VS Removal were 1.34±0.9, 0.94±0.2, and 0.90±0.34, respectively. The pH value of each ratio was in the range of 5.51-7.28. In comparison to the values of the other two ratios, this particular ratio had the lowest value of the three compared to the other two. Even though the 1:1 ratio was shown to have the lowest pH value, it was also demonstrated to have the highest potential for the production of biogas [13]. There is a possibility that methanogen bacteria could have an initial pH value concentration that has a significant impact on the anaerobic digestion system. This is because the concentration of the pH value affects [14] the solubility of degradable components and the effectiveness of biogas production during fermentation [15].

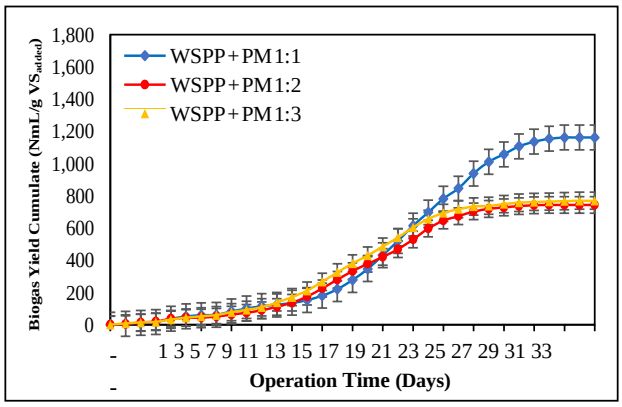

Figure 5. Cumulative biogas yield

In Figure 6. the CH_4, production capacity of all experiments was shown at the ratios of 1:1, 1:2, and 2:1, resulting in the highest daily methane production of the 3 rates, which were 83.60%., 46.47%, and 46.13%, respectively, the accumulated methane amounts are 657.57, 431.57, and 466.78 NmL/gVS added, respectively and was shown in Figure 7. As a result, the potential capacities of the methane production volumes in each of the three ratios are equivalent to one another. The presence of methane gas, on the other hand, is more obvious when the ratio approaches one to one. That the rate of methane generation will eventually increase, regardless of the ratio, is something that is anticipated to happen. The production of methane is at its maximum during the peak period, after which it begins to decrease until it eventually reaches a stable level [14].

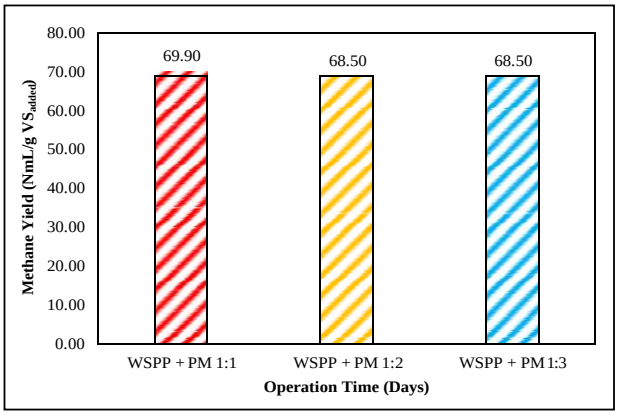

Figure 6. Methane Yield

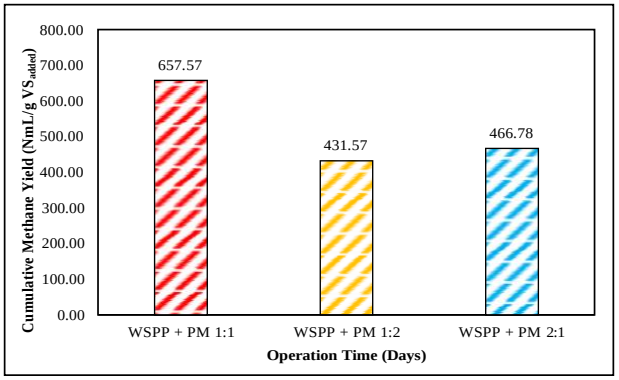

Figure 7. Cumulative Methane Yield

4. Conclusions

The study centered on the treatment of wastewater generated by Shredded Pork Processing (WSPP) using anaerobic digestion. The substrate's COD was measured to be 148,376.70 mg/L. A noteworthy observation was discovered when this wastewater was co-fermented with pig dung in equal proportions. The particular ratio enabled the production of a notably high total biogas output, reaching 127.05 ml. In addition, the combination of equal parts of these substances led to the generation of methane gas with a remarkable concentration of 69.90%. In addition, the method successfully removed 53.45±5.4 mg/L of total solids and 1.34±0.2 mg/l of volatile solids. To summarize, the results of this experiment show potential for being able to expand and apply the findings to larger-scale operations in the transformation business. The effectiveness of the 1:1 co-fermentation ratio in increasing biogas output, specifically methane concentration, highlights its suitability for industrial use. This study establishes a basis for further investigations into enhancing the efficiency of wastewater treatment and the generation of biogas on a broader scope.

5. ACKNOWLEDGEMENTS

This research is supported by scholarship for manufacture and develop graduate potential at graduate level of School of Renewable Energy and scholarship from Maejo University alumni at Maejo University. Thank you to advisor and co-advisers for their comments to improve the paper. And thank you to everyone in the fuel lab, friends, and family for their support.

References

[1] Chummee, P. (2022). The Structural RelationshipAnalysis between Innovation and Export Performance of Food Industries, Thailand. Turkish Journal of Computer and Mathematics Education (TURCOMAT), 13(1), 108-112.

[2] Chummee, P. (2022). A confirmatory factor analysis of domestic market environment affecting to export decision of food industries in Thailand. *Journal of Positive School Psychology*, *6*(3), 9606-9609.

[3] Otero, A., Mendoza, M., Carreras, R., & Fernandez, B. (2021). Biogas production from slaughterhouse waste: Effect of blood content and fat saponification. Waste Management, 133, 119-126.

[4] Orellana, G., del Mar Darder, M., & Quílez-Alburquerque, J. (2023). Luminescence-Based Sensors for Water Quality Analysis.

[5] Van Tran, G., Ramaraj, R., Balakrishnan, D., Nadda, A. K., & Unpaprom, Y. (2022). Simultaneous carbon dioxide reduction and methane generation in biogas for rural household use via anaerobic digestion of wetland

grass with cow dung. Fuel, 317, 123487.
[6] Nikiema, M., Barsan, N., Maiga, Y., Somda, M. K., Mosnegutu, E., Ouattara, C. A., ... & Ouattara, A. S. (2022). Optimization of Biogas production from sewage sludge: impact of combination with bovine dung and leachate from municipal organic waste. Sustainability, 14(8), 4380.
[7] Nong, H. T. T., Unpaprom, Y., Whangchai, K., & Ramaraj, R. (2022). Sustainable valorization of water primrose with cow dung for enhanced biogas production. Biomass Conversion and Biorefinery, 12, 1647-1655.
[8] Sumada, K., Damayanti, C. S., & Lina, T. (2022). Wastewater treatment of shrimp crackers industry using aerobic biological by contact-stabilization technology. Nusantara Science and Technology Proceedings, 152-161.
[9] Musa, M. A., & Idrus, S. (2020). Effect of hydraulic retention time on the treatment of real cattle slaughterhouse wastewater and biogas production from HUASB reactor. Water, 12(2), 490.
[10] American Public Health Association (APHA), (2005). Standard Methods for the Examination of Water and Wastewater. Washington DC: American Public Health Association.
[11] Rakić, N., Šušteršič, V., Gordić, D., Jovičić, N., Bošković, G., & Bogdanović, I. (2023). Characteristics of biogas production and synergistic effect of primary sludge and food waste co-digestion. BioEnergy Research, 1-14.
[12] Xue, S., Zhao, N., Song, J., & Wang, X. (2019). Interactive effects of chemical composition of food waste during anaerobic co-digestion under thermophilic temperature. Sustainability, 11(10), 2933.
[13] Ali, S., Hua, B., Huang, J. J., Droste, R. L., Zhou, Q., Zhao, W., & Chen, L. (2019). Effect of different initial low pH conditions on biogas production, composition, and shift in the aceticlastic methanogenic population. Bioresource technology, 289, 121579.
[14] Wannapokin, A., Ramaraj, R., Whangchai, K., & Unpaprom, Y. (2018). Potential improvement of biogas production from fallen teak leaves with co-digestion of microalgae. 3 Biotech, 8, 1-18.
[15] Sabarikirishwaran, P., Shen, M. Y., Ramaraj, R., Unpaprom, Y., Wu, H. C., & Chu, C. Y. (2023). Feasibility and optimizing assessments on biogas and biomethane productions from E. coli fermenter effluent. Biomass and Bioenergy, 173, 106783.
[16] Bien, J. B., Malina, G., Bien, J. D., & Wolny, L. (2004). Enhancing anaerobic fermentation of sewage sludge for increasing biogas generation. Journal of Environmental Science and Health, Part A, 39(4), 939-949.
[17] Linyi, C., Yujie, Q., Buqing, C., Chenglong, W., Shaohong, Z., Renglu, C., ... & Zhiju, L. (2020). Enhancing degradation and biogas production during anaerobic digestion of food waste using alkali pretreatment. Environmental Research, 188, 109743.

	Mr.Puwadon Chumpoochai Master student, Master of Engineering (Renewable Energy Engineering). **Research Interests:** Biogas, and Wastewater treatment.
	Dr. Rotjapun Nirunsin, B.Ed.,ME.d.,Ph.D. Assistant Professor Renewable Energy Engineering **Research Interests:** Plant biotechnology, (Community and Industrial Scale),Biodiesel technology, Energy Engineering
	Dr. Kittikorn Sasujit, B. Eng M. Eng Ph.D. Assistant Professor **Research Interests:**Biomass conversion technology and Renewable Energy technology,Anaerbic fermentation for biogas production from dung and biomass.
	Dr. Jutaporn Chanathaworn, B.sc M.sc PhD. Associate Professor **Research Interests:** Renewable Energy, Biomass conversion technology (Briquette fuel, Biofuel Biomass Stove), Catalyst for energy production.

Thailand Soft power: A Case Study on food policy

Non Naprathansuk[1*], Sudarat Sirichokphon[2], and Wirawan Chaysukkasam[3]

[1] School of Administrative Studies, Maejo University, Chiang Mai, Thailand
[2] School of Administrative Studies, Maejo University, Chiang Mai, Thailand
[3]School of Administrative Studies, Maejo University, Chiang Mai, Thailand
*Corresponding author, E-mail: nonnaprathansuk@hotmail.com

Abstract: This article aims to study Thailand soft power policy on food policy. This article uses policy soft power theory and cycles model as a framework for study. Documentaries from official government and present government policy are primary sources, also related documents and research are secondary sources. The result of the study shows that after Covid-19 Thailand needs to boost economy growth and soft power is one of the best tools for quick win and long-term economy growth. Therefore, at a present Thai's government heavily relied on soft power and strongly drive food policy for promote and stimulate Thai economy especially on food and tourist industry.

Keywords: Thailand, Soft power, Food policy

1. Introduction

Thailand's economy, heavily reliant on tourism and foreign investment, was badly hit by the COVID-19 pandemic. It only recovered to pre-pandemic levels of growth earlier this year, trailing regional counterparts. A series of "quick win" economic stimulus measures has already been announced by the new cabinet, showing a rare sense of official urgency. These measures include cuts in electricity rates and diesel taxes, a three-year debt moratorium for agricultural loans and a temporary scrapping of visa requirements for tourists from China and Kazakhstan (Adulwattana, 2023).

Under his campaign for tourists' attraction, his cabinet has ordered the appointment of Strategic Committee on Soft Power to determine the strategy on Soft Power of Thailand which is prime Minister is the chairman of this committee and Ms. Praethongthan Shinawatra is the vice-chairman. Along with Mr. Pansak Winyarat as advisor and Dr. Suraphong Suebwonglee as director.

Thus, the Thailand Creative Content Agency (THACCA) was appointed. It is an agency with complete authority to support every soft power industry. Also, unlock laws, break down barriers, support funding expands exports through foreign policy including managing a budget that is sufficient to carry out the duties of building the entire ecosystem. To create the Thai's soft power industry to grow exponentially.

Moreover, Thai food is a magnet for foreigners. This is evident from the ranking articles of various websites, including TasteAtlas, which ranked Khao Soi No. 1 of the best soups in the world in The 50 Best Soup and Panang Tid Curry, the best food in the world, and The Best Traditional Dishes In The World. In 2022, Reader's Digest 2022 ranked Pad Thai 6th out of the top 50 foreign foods popular with US residents, green curry ranked 3rd on the UK population's list of the 10 Most Popular International. Cuisines In The UK, Massaman Curry that CNN Travel (2022) lists as the best food in the world in The World's 50 Best Foods, the Most Popular Ethnic Foods from Around the World article of Discovery Lifestyle (2021) stating that Thai food It's a popular dish in the world for its blend of flavors, and Thailand's Le Du took the #1 spot on Asia's 50 Best Restaurants list in 2023 (Gateway, 2023).

Therefore, this article raises a question that how does Thailand soft power policy on food aspect? To answer this question, this article has four parts which are first part is introduction, second part is soft power theory, third part is public policy theory, fourth part is conclusion.

2. Soft power theory

Joseph S. Nye, Jr., who introduces the soft power concept, has described it as the power to convince others to be willing to do as demanded, with a gentle approach, rather than to coerce.

Nye (2005) proposed the term soft power to refer to the power that makes other countries willing to comply with our demands (co-opt). Without needing to be forced or any exchange. In other words, the ability to make other people satisfied is consistent with our desires, leading to acceptance. This is different from the use of influence, which is hard power, including military power. economic power, etc. The use of soft power is including culture and political values or having

an outstanding foreign policy. Therefore, using soft power is an extremely effective diplomatic tool and an important diplomatic policy tool.

Nye (2005) also explained the differences between soft power and hard power. Hard power is power that comes from Force or intimidation (threat) using a hard stick such as military power that is used as a tool for persuasion (inducement) or using a carrot or a tangible benefit, which is different from soft power that comes from the force of attraction in creating popularity and acceptance by the quiet (acquiescence). Nye also divided the requirements of soft power is divided into three factors: culture, values, and foreign policy (foreign policy).

The study of soft power can also develop and define indicators that are more in-depth and easier to use in studies. Steven B. Rothman (2011) has extended the concept of soft power to be more in-depth. By adding to the mechanism of soft power, that is procedures for control and use of Policy makers for example, set the agenda and frame that is a useful analytical variable to understand international relations and to make policy recommendations.

Also, Cetin and Yavuzaslan (2016) studied soft power to be able to measure and compare results obtained in other countries. There are several soft power indicators. It is large and based on Diplomatic relations, such as foreign aid Leading national products Traveling to different places without a visa environmental surveillance government indicator such as human resources, freedom, social violence, government responsibility, the death penalty, and cultural indicators such as tourism.

Moreover, Alan Chong (2007) described soft power models that show shades of soft power and varying spectrum of intensity. It is shown in the picture as follows.

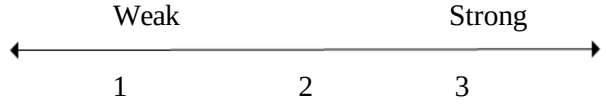

1.Elite and academic debates
2.Regimes and policy networks
3. Cultural imperialism

Figure 1: Alan Chong's level of intensity spectrum of soft power use (2007)

Therefore, soft power is the ability to make others ‘want’ and ‘accept’ what you want to. Most importantly it is the ability to attract the desire of others ‘willingly’ without any perceived coercion, as it is human nature to respond more positively and openly to something when one does not feel they are being forced or pressured. This is why soft power is not merely cultural propagation as many people understand it to be. Soft power is much more than just a simple strategy for exporting culture, it is a metric for the effectiveness of social and economic policies that represent a country's strengths and potential advantages of the country to other countries.

Meanwhile, Thailand is ranked 35th out of 120 countries around the world, with 40.2 points, which is an increase from 38.7 points in 2021.In Asia, Thailand is ranked 6th, following China, Japan, South Korea, Singapore, and India. Out of the 7 main soft power indicators, Thailand has a high score in Business and Trade, Culture and Heritage, and People and Values (creative economy review, 2023)

This reflects our strengths as having a clear cultural cost. But the Thai government must support the mechanisms for independence and not obstruct the extension of culture. This reflects our strengths, which include a distinct cultural cost. However, the government must promote autonomous mechanisms rather than obstruct cultural expansion.

Moreover, Food is one of the industries that play a greater role in supporting the tourism industry. Thailand ranks 15th in food exports in the world because Thailand has an advantage in raw materials for domestic agricultural products. related to Thai food both raw materials such as seasonings Including ready-to-cook food at 4,589 million US dollars (approximately 161,100 million baht), accounting for 11.5% of all Thai food exports. From 2011-2022, the export value of products in this group has an average growth rate of 5.8. % per year (Gateway, 2023).

Therefore, without a doubt, the food business will stimulate Thai’s economy along with tourism. The food business in many dimension from the seasoning business company, food production, local restaurant, Thai restaurant business abroad, and travel business especially the quality tourism business in the group of food tourism (Foods Tourism or Gastronomy Tourism) which will benefit from the number of foreign tourists in this group that tend to grow due to the behavior of modern tourists who want to learn about food culture. Thai’s food as a soft power will be a great opportunity for Thai people and it will help Thailand’s economy will recover from the Covid-19 pandemic.

3. Public policy theory

The concept of public policy came from western academics especially in the United States. In fact, the concept of public policy has been around for thousands of years, but the study of it as a science in public administration has only come about recently.

Dye (2002) defined public policy as: Public policy is the activities that a government chooses to do or not to do.

All so, Kaplan and Lasswell (1970) defined public policy as a plan of values and operations. In the same way, Birkland (2011) gave the meaning of an order of a government doing something, such as a law, regulation, regulation, decision, order, or a combination of the foregoing. As well as Hogwood & Gunn (1984) defined it as A policy is an expression of the objectives or goals of a government's activities in a particular matter that describes the process for achieving the stated objectives. While, Cairney (2012) has given a broad meaning that Policy can refer to objectives, decisions, or results.

Moreover, Laswell originally outlined the policy cycle in 1956, which at the time had seven stages. Since then, the stages within the cycle have evolved. Jann and Wegrich (2007) propose that the five "generally accepted" steps of the policy cycle are:

1. Agenda setting is the first stage, involves identifying a problem that requires government intervention and proposing it as an issue to the public.

2. Policy formulation is the government has identified the problems it would like to address; it needs to decide how it will address them.

3. The decision-making process is not an exclusively rational exploration of alternatives. It is a bargaining process by those with interests in the problem with the decision-making levels of government to advance those interests.

4. Implementation is after decided on, the proposed actions to solve the policy problem need to be implemented.

5. Evaluation is to evaluate the policy so that we will know whether we solved the policy problem or not.

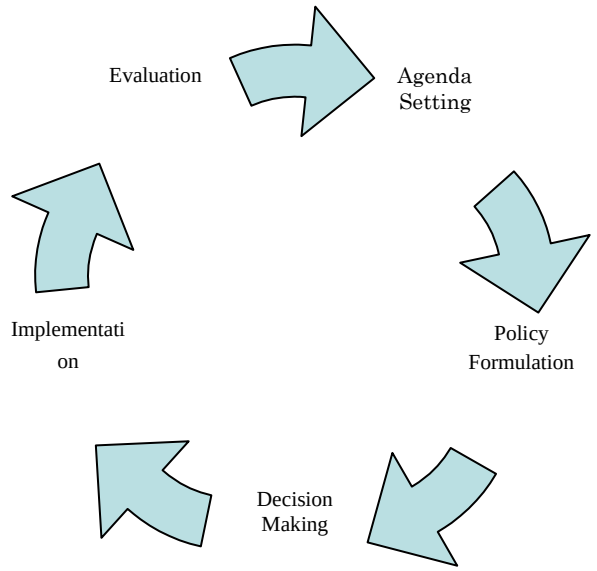

Figure 2: Policy Cycle (adapted from Jann and Wegrich, 2007)

Therefore, we could say that public policy is a generally consists of the set of actions plans, laws, and behaviors adopted by a government. Concern with the new governance draws attention to the extent to which these actions are often performed now by agents of the state rather than directly by the state.

In case of Thailand, Thailand's economy, heavily reliant on tourism and foreign investment, was badly hit by the COVID-19 pandemic. It only recovered to pre-pandemic levels of growth earlier this year, trailing regional counterparts. To achieve the government's ambitious target, Thailand needs new growth engines (Adulwattana, 2023). Thus, the policy to stimulate Thai's economy, the government must launch and implement the policy instantly and intensively.

Hence, Thai government has launched a strategy to harness the nation's "soft power" with the aim of generating an annual revenue of approximately 4 trillion THB (nearly 113 million USD) within the next four years. A core component of this initiative is the creation of the Thailand Creative Content Agency (THACCA); launch the "One Family One Soft Power" (OFOS) project (Vietnam, 2023)

Thailand Creative Content Agency (THACCA) is an agency with complete authority to support every soft power industry, whether it be the liberation of freedom. Unlock laws, break down barriers, support funding Expand exports through foreign policy Including managing a budget that is sufficient to carry out the duties of building the entire ecosystem. To create the Thai soft power

industry to grow exponentially. Thailand Creative Content Agency (THACCA) will focus on 11 targeted creative 11 distinct creative sectors including food, sports, festivals, tourism, music, books, movies, games, arts, design, and fashion.

According to a policy cycle model, at the first stage the agenda setting is a pinpoint to Thailand's economy needs to recovery from the Covid-19. Then, the second stage is policy formulation at this stage the government launches the "One Family One Soft Power" (OFOS) project which is to find the potential of every family member At least one person per family comes to promote, train, and cultivate potential. To create 20 million highly skilled workers.

The third stage is decision-making, at this point the government was appointed the Thailand Creative Content Agency (THACCA). It is an agency with complete authority to support every soft power industry under the ministry of culture.

The policy will be implemented as follows: survey and collect information on potential cultural capital. To bring further development in 10 creative industries and pushing for the policy of 1 family, 1 soft power, surveying and developing cultural workers to have high skills Supports market needs.

Manage cultural spaces and networks from the community, village, sub-district, district, and province levels to develop the potential to be a creative space and cultural power. Also, raise the level of traditional cultural events to be internationally accepted. Also, promote national traditional festivals and other cultural festivals to be landmarks for tourists around the world, amend laws to be modern and promote creativity and use technology and innovation to further the important cultural works and traditions of the nation to maintain their value (Thai Post, 2023)

For the final stage, the evaluation, this stage must be watched due to the process of implementation.

4. Conclusion

After Covid-19 Thailand needs to boost economy growth and soft power is one of the best tools for quick win and long-term economy growth. Therefore, at a present Thai's government heavily relied on soft power and strongly drive food policy for promote and stimulate Thai economy especially on food and tourist industry. The policy of soft power drive by Thailand Creative Content Agency (THACCA) was appointed under the ministry of culture. As a policy cycle analysis, the policy is on the implementation stage that deploy the action plans.

References

[1] Retrieved from Asia.nikkei.com: https://asia.nikkei.com/Opinion/Time-for-Thailand-s-new-government-to-match-rhetoric-with-reform

[2] Birkland, T. A. (2011). *An introduction to the policy process: theories, concept, and model.* New York: Routledge.

[3] Cairney, P. (2012). *Understanding Public Policy.* New York: Palgrave and Macmilan.

[4] Cetin, K. Y. (2016). *Soft Power Concept and Soft Power Indexes.* Switzerland: Springer.

[5] Chong, A. (2007). *Foreign Policy in Global Information Space: Actualizing Soft Power.* New York: Palgrave Macmilan .

[6] Creative economy review. (2023, October 20). *Soft Power: The Driving Force of Creative Economy*. Retrieved from Creative economy review: https://www.cea.or.th/en/single-softpower/cea-soft-power

[7] Gateway, S. (2023, April 18). *Soft Power Thai food helps drive the economy*. Retrieved from SUN GATEWAY: https://amazingthaiproperty.com/en/37040/

[8] Gunn, B. W. (1984). *Policy Analysis for the Real World.* New York: Oxford.

[9] Jann W. & Wegrich, K. (2007). Theories of the Policy Cycle. In &. M. F., *Handbook of Public Policy Analysis* (pp. 43-59). New York: Routledge.

[10] Kaplan, H. D. (1970). *Power and Society.* New Haven, CT: New Haven, CT: Yale University.

[11] Nye Joseph S. (2005). *soft power: The means to success in world politics.* New York: Public Affairs.

[12] Thai Post. (2023, October 3). *Sermsak highlights 10 policies to move Thai Soft Power*. Retrieved from ThaiPost: https://www.thaipost.net/news-update/459499/

[13] Vietnam. (2023, November 14). *Thailand launches 'Soft Power' Strategy to Boost Economy*. Retrieved from Vietnam: https://en.vietnamplus.vn/thailand-launches-soft-power-strategy-to-boost-economy/270972.vnp

Dr. Non Naprathansuk
Assistant Professor
Research Interests: Thai Politics, Asia pacific Studies, and Southeast Asia Studies.

Ms. Sudarat Sirichokphon
Undergraduate Student
Research Interests: Thai politics, Public Policy

Ms.Wirawan Chaysukkasam
Undergraduate Student
Research Interests: Thai politics, Public Policy

Metabolite profiling reveals the metabolic features of the progenies resulting from the low phytic acid rice (*Oryza sativa* L.) mutant

Chenguang Zhou, Jiyong Shi, Xiaobo Zou*

School of Food and Biological Engineering, Jiangsu University, Zhenjiang 212013, China
*E-mail: zou_xiaobo@ujs.edu.cn

Abstract: The *low phytic acid* (*lpa*) rice mutant *Os-lpa*-XS110-2, exhibiting *OsMRP5* mutation-induced metabolic features (i.e. decreased levels of phytic acid and raffinose, and increased levels of amino acids and biogenic amine GABA), was crossed with two commercial rice cultivars. The inferior field emergence rate of the *lpa* mutant was significantly improved upon cross-breeding. The GC/MS-based metabolomics was utilized to investigate the impact of cross-breeding on the metabolite profiles of the resulting progeny rice grains. Multivariate and univariate analyses showed that in spite of the predominant influence of crossing parent on the metabolite profiles of the progenies, the *OsMRP5* mutation-induced metabolite signature, was stably expressed in the *lpa* mutant progenies over generations. The *OsMRP5 lpa* rice mutant seeds might be considered valuable genetic resources to develop rice grains with favorable metabolic traits.

Keywords: *low phytic acid* rice mutant, metabolomics, cross-breeding, *MRP* mutation

1. Introduction

Phosphorus is a macronutrient essential for plant growth and development. In legume seeds and cereal grains, phytic acid (PA) represents the major storage form of phosphorus (P) up to 85% (Raboy, 2009). However, due to the insufficient secretion of phytases essential for PA hydrolysis in the digestive tract, PA-P is generally unavailable to humans and nonruminant animals. Furthermore, strongly negatively charged PA in the digestive tract could chelate cations (e.g., Ca^{2+}, Fe^{2+} and Zn^{2+}) to reduce bioavailability of these minerals (Bohn, Meyer, & Rasmussen, 2008). In addition to being considered an antinutrient, the undigested phytate excreted from animal wastes contributes to phosphorus pollution and groundwater eutrophication (Kumar, Singh, Sangwan, & Gill, 2015). To minimize these negative effects of PA, many *low phytic acid* (*lpa*) mutant crops have been generated via physical and chemical mutagenesis (Raboy, 2009).

The *lpa* mutants are grouped into different types based on the affected functions of PA metabolism, and a high proportion of these *lpa* mutants have been shown to carry mutated genes coding for multi-drug resistance-associated proteins (MRPs) which are responsible for PA transport from the cytosol to the storage location vacuole (Sparvoli & Cominelli, 2015). Various MRP *lpa* mutant lines have been successfully isolated and characterized in a wide range of major crops, such as maize, rice, wheat, barley, soybean and common bean (Colombo, Paolo, Cominelli, Sparvoli, Nielsen, & Pilu, 2020; Sparvoli et al., 2015). This type of *lpa* mutants has gained more attention compared with other mutation types, since it exhibits the most significant reductions of PA contents up to 90%, and a consequent expected increase in free cations (Dong, Echigo, Raboy, & Saneoka, 2020).

Rice (*Oryza sativa* L.) is the staple food for over half the world's population, thus the development of *lpa* rice mutants is of great importance, especially for those populations in less developed regions suffering from mineral deficiencies. In the previous study, we developed a number of MRP *lpa* rice mutants with the PA reduction ranging from 23% to 90% (Liu, Xu, Ren, Fu, Wu, & Shu, 2007; Xu et al., 2009). The subsequent metabolomics analysis revealed that the defects in *OsMRP5* gene of *lpa* rice mutant *Os-lpa*-XS110-2 resulted not only in a pronounced PA reduction, but also in remarkable metabolic changes compared with the corresponding wild-type XS110, e.g., reduced levels of *myo*-inositol, fructose, and raffinose, as well as increased contents of organic acids, amino acids and health-promoting compound γ-aminobutyric acid (GABA) (Tan, Zhou, Goßner, Li, Engel, & Shu, 2019).

Unfortunately, *lpa* mutant crops often exhibit poor agronomic performance, and therefore, cross and selection breeding of *Os-lpa*-XS110-2 mutant with elite commercial cultivars have been performed to minimize these undesired pleiotropic effects. Target analysis in our previous studies has demonstrated that the *lpa* trait of the *lpa* mutant progenies was consistently expressed over generations (Zhou, Tan, Gossner, Li, Shu, & Engel, 2019). However, the information regarding the impact of such crossing steps on the agronomic performance of the crossbred progenies is lacking. In addition, it remains unclear whether the mutation-induced metabolic changes in the progenitor *lpa* mutant *Os-lpa*-XS110-2 could still be observed in the crossbred progenies.

In the present study, the agronomic traits of the crossbred progenies were evaluated. In addition, all the generated rice samples were subjected to our previously established GC/MS-based metabolite profiling approach for rice grains (Zhou, Tan, Gossner, Li, Shu, & Engel, 2018). The objectives of this study were (i) to investigate the impact of cross-breeding on the agronomic performance of the *lpa* rice mutants, (ii) to explore the impact of crossing parent on the metabolite profiles of the progenies, and (iii) to assess the stability of the *OsMRP5* mutation-induced metabolic changes in the crossbred progenies over generations.

2. Materials and Methods

2.1 Chemicals

Reference standards were purchased from Sigma-Aldrich (Steinheim, Germany), Roth (Karlsruhe, Germany), VWR International (Darmstadt, Germany), and Fluka (Buchs, Switzerland). All other chemicals and reagents were supplied by Sinopharm Chemical Reagent (Shanghai, China).

2.2 Development of Sample Materials

The progenitor *lpa* rice mutant *Os-lpa*-XS110-2 was obtained from the conventional cultivar XS110 via γ-rays irradiation followed by NaN_3 treatment. Two elite commercial cultivars JX081 and JH218 were selected as the crossing parents to produce the progenies of the crosses *Os-lpa*-XS110-2 × JX081 and *Os-lpa*-XS110-2 × JH218 (Figure 1). In brief, F_2 seeds of each cross were bulk-harvested and grown into F_2 plants. For each cross, two hundred F_2 plants were genotyped into homozygous wild-type, homozygous *lpa* mutant and heterozygous progenies by the high-resolution melting (HRM) curve analysis (Figures S2 and S3). Owing to the segregation for other agronomic traits (e.g. plant height, flowering time and fertility), five F_2 plants of the homozygous wild-type, five of the homozygous *lpa* mutant and ten of the heterozygous progenies were chosen based on the similarity of flowering time, and the corresponding F_3 seed were collected. The harvested homozygous F_3 seeds were carefully

stored for the subsequent cultivation, and the segregating F_3 seeds were grown and genotyped according to the same approach performed in F_2 plants. Similar breeding and genotyping procedures were conducted until F_5. The harvested homozygous wild-type and *lpa* mutant seeds from F_2 to F_5 plants, as well as the original wild-type XS110, the progenitor *lpa* mutant *Os-lpa*-XS110-2, and the crossing parents JX081 and JH218, were all grown in 2013 at the same field trial in Jiaxing to eliminate the impact of the growing

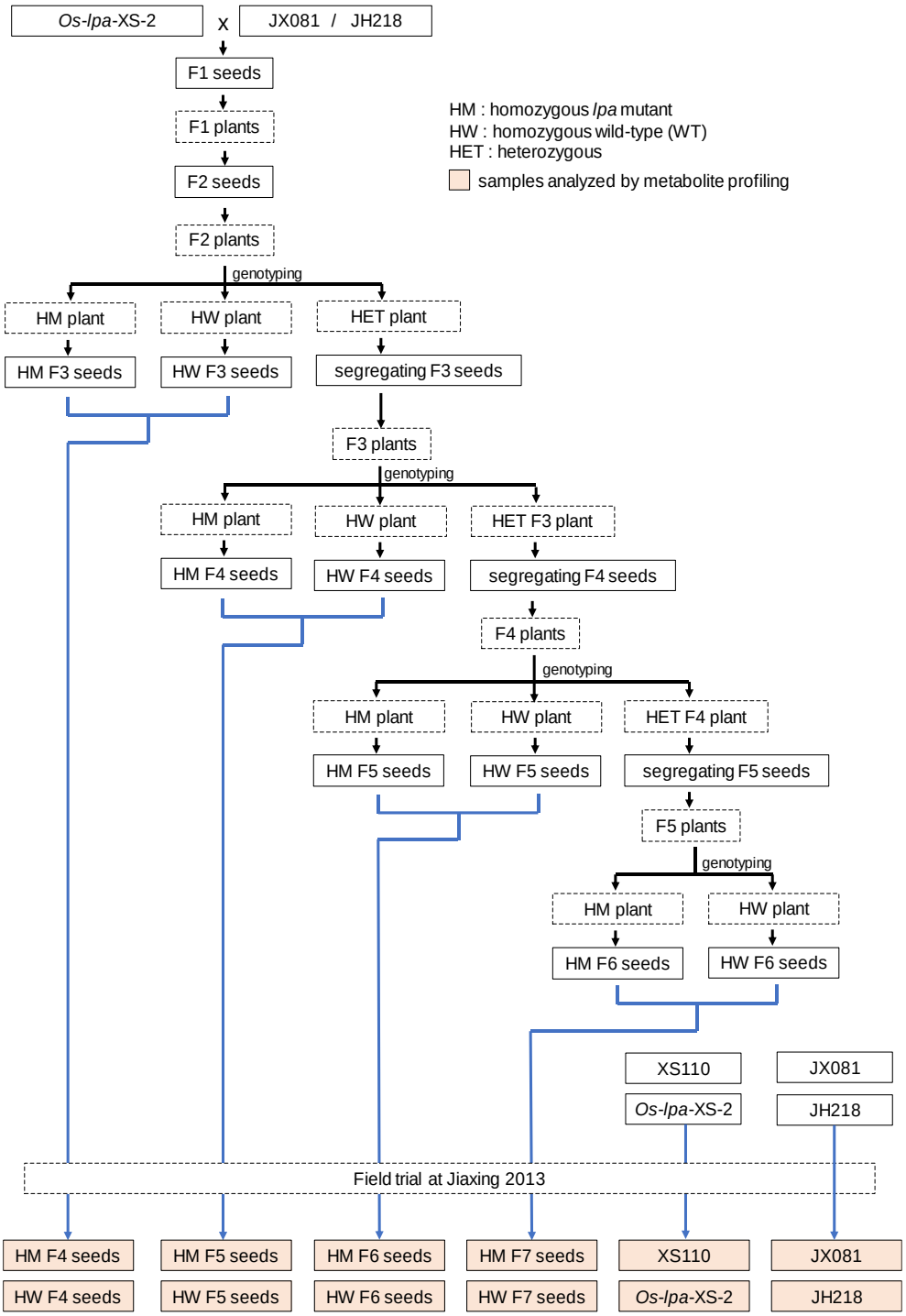

Figure 1. Flowchart of the cross-breeding steps in generating rice sample materials.

environment on the metabolite profiles of sample materials (Figure S1).

For each cross and each generation rice seed samples from 4-5 plants of each genotype were pooled. The harvested rice seeds were husked and ground by a cyclone mill with a 500-μm sieve. The collected rice flour was freeze-dried for 48 h and stored in low-density polyethylene bottles at − 20 °C until analysis.

2.3 Genotyping of Crossbred Progenies

Genomic DNA was extracted from leaf tissues following a previously described Cetyltrimethylammonium Bromide (CTAB) method (Liu et al., 2007), and was further adjusted to about 25 ng/μL by Nano-drop 2000 Spectrophotometer (Thermo Scientific, Wilmington, USA). The PCR primers were designed according to the genome sequence of the rice cultivar Nipponbare (Gramene release 34b, http://www.gramene.org/) using Primer Premier 5 software. For HRM analysis, the amplified fragments should be <400 bp. Therefore, the forward primer (5'-GTCGCCGGTGATCCATTT-3') and the reverse primer (5'-ATTGTGCCAGGAGGGAAGC-3') were used to amplify the fragment with the size of 234 bp containing the mutation site.

PCRs were performed in 10-μL volume with 25 ng of genomic DNA, 5 μL 2× Master Mix (2× PCR buffer, 4 mM $MgCl_2$, 0.4 mM dNTPs, 50 units/mL *Taq* DNA polymerase), 0.2 μL of each 10 μM primer and 1 μL of 10 × LCGreen Plus+ (BioFire, Salt Lake City, USA), covered with one drop of mineral oil to prevent solution evaporation. The employed PCR program was as follow: 5 min at 94 °C, followed by 40 cycles of 30 s at 94 °C, 30 s at 55°C and 30 s at 72 °C with a final extension at 72 °C for 8 min.

Following PCR, the plates were transferred to Lightscanner (Idaho Technology Inc., Salt Lake City, USA) and subjected to HRM analysis according to our previously developed method (Tan et al., 2013). In brief, the temperature was ramped up from 55 to 95 °C at 0.1 °C per second. After the normalization and temperature shifting of the melting curves in accordance with the Lightscanner Operator's Manual, the data were analyzed by the coupled software CALL IT™ 2.0.

2.4 Assessment of Agronomic Traits

The evaluation of agronomic performance was conducted for *Os-lpa*-XS110-2, the crossing parents JX081 and JH218, and the homozygous wild-type and *lpa* mutant progenies (F_7) of the two crosses. Thousand-grain weight was assessed as the grain weight per plant divided by the number of grains multiplied by 1,000. The seed setting ratio (%) was expressed as the number of filled grains per plant divided by the total number of florets on the plant. For the field emergence rate test, clean seeds were soaked in distilled water for 48 h and germinated at 35 °C for 3 days. Both the germinated and not germinated rice seeds were sown in seedling beds. The field emergence rate (%) was calculated after 10 days as the number of seedlings divided by the number of the sown seeds.

2.5 Metabolomics Analysis

Preparation of Internal Standards (IS) Solutions. The IS solutions of tetracosane (IS solution I), 5*α*-cholestane-3*β*-ol (IS solution II), phenyl-*β*-D-glucopyranoside (IS solution III), and 4-chloro-L-phenylalanine (IS solution IV) were prepared as previously described (Zhou et al., 2018).

Sample Preparation. The low-molecular-weight metabolites in rice flour were extracted and fractionated according to the methodology established in our previous studies (Zhou et al., 2018). In brief, three aliquots (600 mg) of rice

flour were weighted into cartridges (3 mL volume) connected to a vacuum manifold. The non-polar and polar constituents were consecutively extracted by dichloromethane (4 mL) and by a mixture of methanol and deionized water (80 + 20, v/v, 10 mL), respectively. After the addition of 100 µL of IS solutions I and II, the non-polar extract was subjected to rotatory evaporation for to remove extraction solvent. Then the lipophilic extract was trans-esterified with sodium methylate at room temperature for 90 min, followed by solid phase extraction into fraction I containing fatty acid methyl esters (FAMEs) and hydrocarbons, and fraction II containing free fatty acids (FFAs), fatty alcohols and phytosterols.

The polar extract was evaporated to dryness and redissolved in 300 µL of pyridine. The silylation of the polar section was performed with 100 µL of trimethylsilyl-imidazole at 70 °C for 30 min. Fraction III (sugars and sugar alcohols) was obtained via selective hydrolysis of the silylated derivatives. In addition, another 4 mL of the polar extract was treated with oximation (300 µL of hydroxylamine hydrochloride at 70 °C for 30 min), silylation (50 µL of N-methyl-N-(trimethylsilyl) trifluoroacetamide at 70 °C for 20 min) and selective hydrolysis to generate fraction IV, which contains amino acids, organic acids, and amines.

GC-MS Analysis. The obtained four fractions were analyzed on a TraceGC Ultra (Thermo Fisher Scientific, Austin, USA) gas chromatography (GC) system coupled with a flame ionization detector and an ISQ mass spectrometer, in accordance with the previously described conditions (Zhou et al., 2018). Metabolites were identified in light of the mass spectra and the retention times of reference substances, as well as of the data from the NIST08 mass spectra library and the literature. The concentrations of the identified metabolites in fractions I-IV were expressed in relative peak intensity, which was calculated as the peak intensity of the metabolite divided by the peak intensity of the corresponding internal standard and then multiplied by 100.

Quality Control (QC). A QC sample was prepared by pooling the same amount (3 g) of all the investigated rice seeds flour in this study. The QC sample was regularly inserted into the analytical sequence of the actual samples to monitor the reproducibility of the analytical method and check the potential contaminations in the laboratory.

2.6 Data processing and statistical analysis

Acquisition and integration of the total ion chromatograms were performed in Xcalibur-2.1 (Thermo Fisher Scientific), and the peaks exhibiting less than 1 % of peak height relative to the corresponding internal standards were discarded as the noise signals. The generated data matrix files were subjected to Chrom*pare* (Frenzel, Miller, & Engel, 2003) for standardization and alignment. Log-transformation and pareto-scaling were applied as the pretreatment of the metabolomics data.

The resulting data were imported into XLSTAT (version 19.5, Addinsoft, Paris, France) for principal component analysis (PCA) and the construction of the heat map. Orthogonal-partial-least squares-discriminant analysis (OPLS-DA) was conducted by Workflow4Metabolomics. The quality of the model was described by the R^2 and Q^2 values, and validation was performed by 10-fold cross-validation and 1000 permutation tests.

Comparisons of the metabolite levels were performed using Student's *t*-test and ANOVA with Tukey's post hoc test when metabolite profiling data were normally distributed and homoscedastic; otherwise, the non-parametric univariate analyses Mann-Whitney test and the Kruskal-Wallis test with Dunn's post hoc test were applied. The metabolic pathway was constructed on the basis of Kyoto

Encyclopedia of Genes and Genomes (KEGG) database.

3. Results

3.2 Impact of crossing parent on the metabolite profiles of the cross-bred progenies

In the present study, the harvested rice samples at the same filed trial, including the original wild-type XS110, the progenitor *lpa* mutant *Os-lpa*-XS-2, the crossing parents JX081 and JH218, as well as the homozygous wild-type and *lpa* mutant progenies of generations F_4 to F_7 from the two crosses, were all subjected to our previously established fractionation and metabolite profiling approach (Zhou et al., 2018). The analytical procedure resulted in four fractions comprising FAMEs and hydrocarbons (fraction I), FFAs, fatty alcohols and phytosterols in (fraction II), sugars and sugar alcohols (fraction III), and amino acids, organic acids, and amines (fraction IV) (Figure 2).

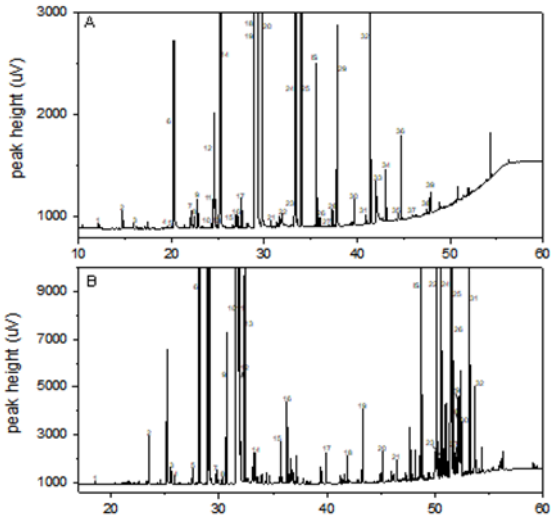

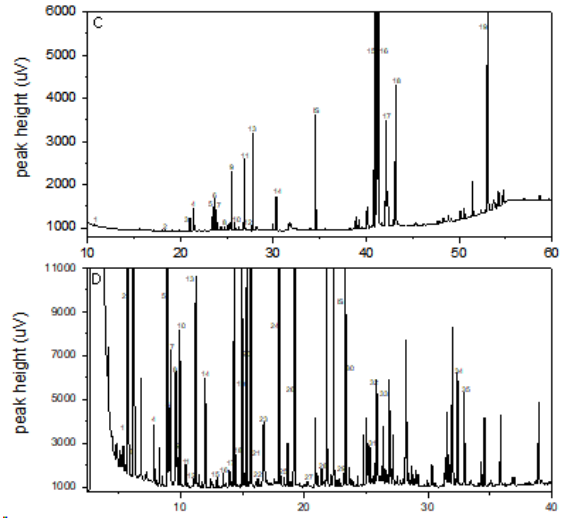

Figure 2. Exemplary GC chromatograms of fraction I (A), fraction II (B), fraction III (C) and fraction IV (D) of QC rice seeds.

As shown in the PCA score plot (Figure 3A), the rice sample JX081 was clearly separated from JH218, suggesting distinct metabolite profiles of the two crossing parents. In addition, the resulting progenies from each cross clustered closely to their crossing parents JX081 and JH218, respectively. As a result, remarkable discrimination between the progenies from the two crosses was observed in the score plot along PC1, regardless of genotype and generation variation. Within each clustering, a mild segregation between the homozygous wild-type and *lpa* mutant progenies was presented. This result indicated that the metabolite profiles of the crossbred progenies were mainly characterized by the crossing parents.

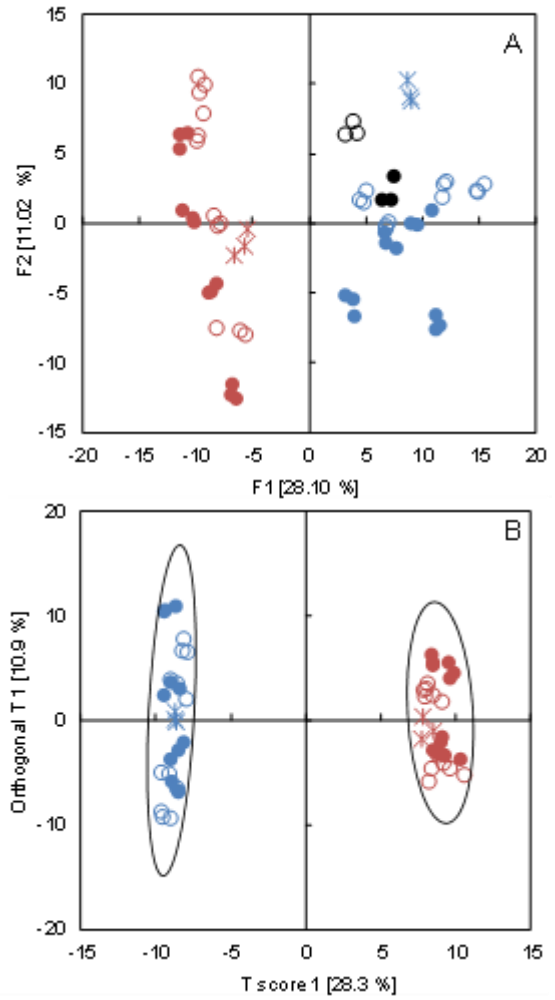

Figure 3. PCA score plot (A) and OPLS-DA score plot (B) of metabolite profiling data of combined fractions I-IV of rice samples.

In order to determine the metabolites contributing to this discrimination, the supervised multivariate analysis OPLS-DA was performed. The resulting score plot exhibited a distinct separation between the generated progenies from the two crosses along the predictive component (Figure 3B). The high values of R^2 (0.97) and Q^2 (0.96), as well as the results of permutation tests (n = 1000), suggested the validity and robustness of the OPLS-DA model without overfitting (Figure 4). Based on the cutoff (VIP >1.5 and Benjamini–Hochberg $p < 0.05$) for the selection of the discriminating metabolites, 43 metabolites were identified as the contributors to the differentiation of the cross-bred progenies depending on cross in the OPLS-DA model. It can be seen that these metabolites varied in different classes, such as FAMEs, FFAs, phytosterols, sugars, organic acids, and amino acids. For each class, several representative compounds were depicted in boxplots (Figure 4). Interestingly, the crossing parent JX081 and the corresponding progenies exhibited more abundant FAMEs and FFAs, while the other crossing parent JH218 and its progenies were rich in hydrophilic constituents such as sugars, organic acids and amino acids.

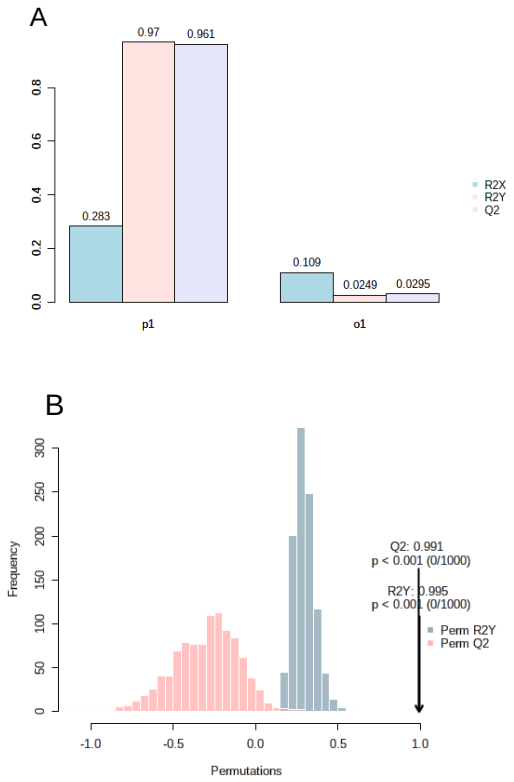

Figures 4. Parameters and permutation tests (n = 1000) of the OPLS-DA model.

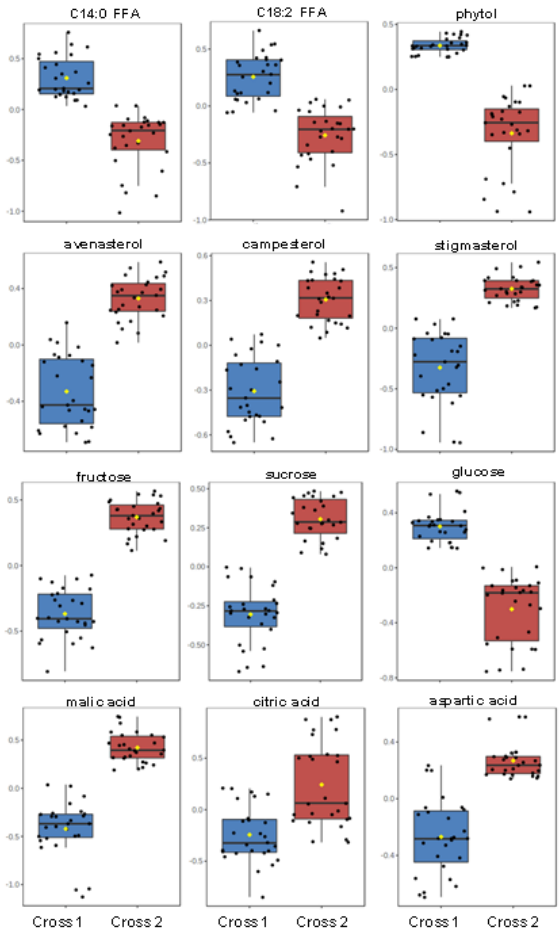

Figure 5. Boxplots of representative metabolites contributing to the OPLS-DA differentiation of progenies from Cross 1 Os-lpa-XS-2×JX081 (blue) and Cross 2 Os-lpa-XS-2×JH218 (red).

3.3 Multivariate analysis of the metabolite profiling data for each cross

Considering the predominant impact of crossing parent on the metabolite profiles of the progenies, the following multivariate analysis was conducted for each cross separately, to investigate the mutation effect on the metabolite profiles of the generated progenies.

For the cross *Os-lpa*-XS-2×JX081, the PCA core score plot of the metabolite profiling data of combined fractions I-IV is shown in Figure 6A. There was a clear separation between the original wild-type XS110 and the corresponding *lpa* mutant *Os-lpa*-XS-2, indicating the metabolic changes induced by the *OsMRP5* mutation in *Os-lpa*-XS-2. For the crossbred progenies, in addition to the similar

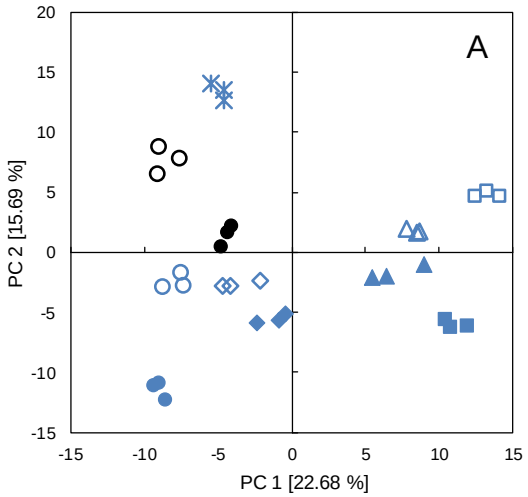

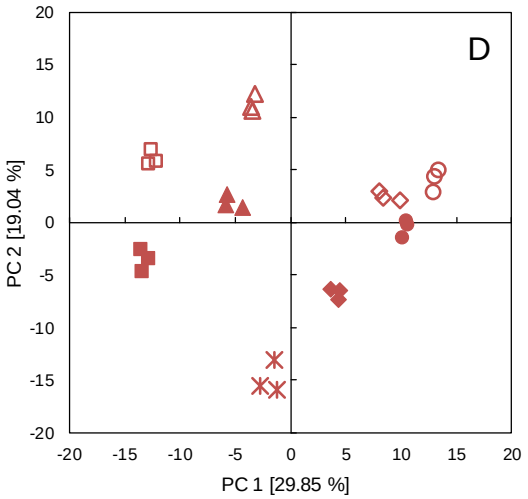

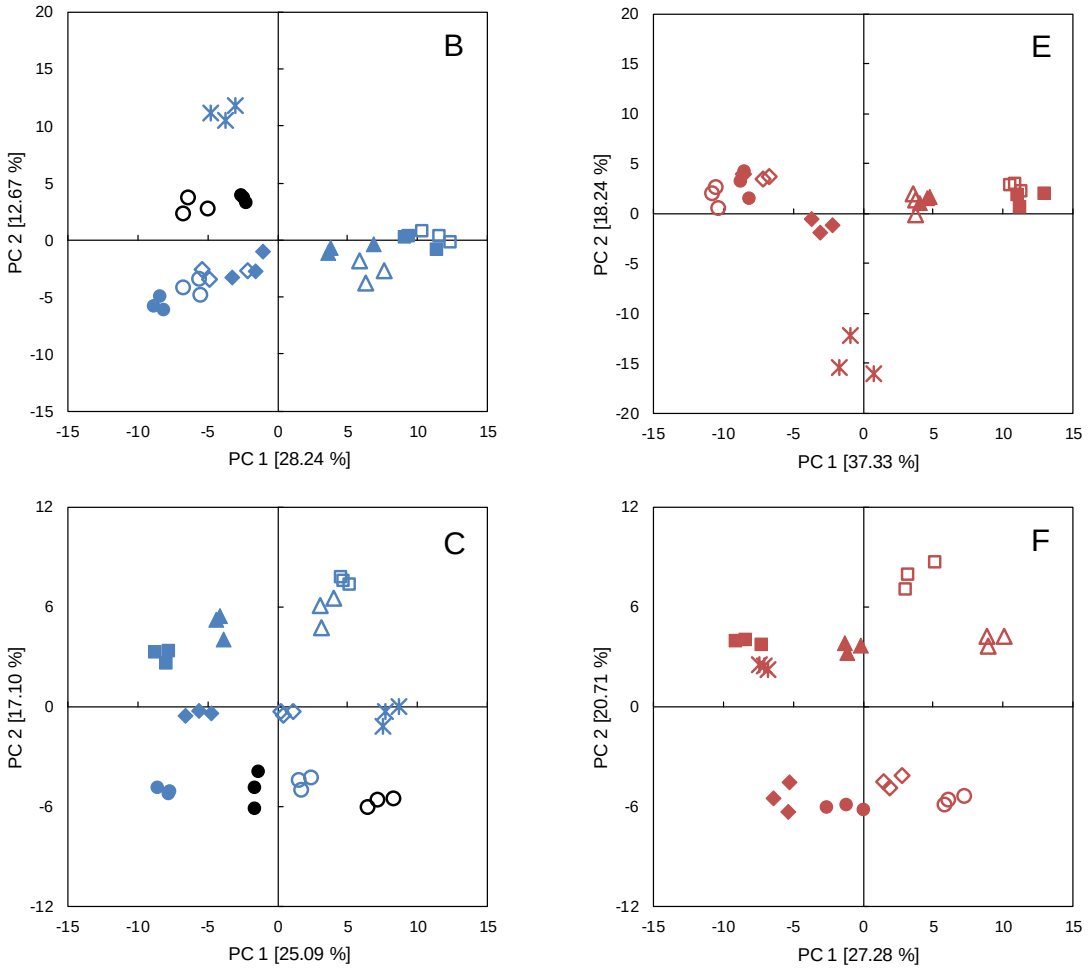

Figure 6. PCA score plots of metabolite profiling data of combined fractions I–IV (A and D), lipophilic fractions I-II (B and E) and polar fractions III-IV (C and F) of rice samples from the crosses Os-lpa-XS-2×JX081 (A-C) and Os-lpa-XS-2×JH218 (D-F). Parental lines (black): original wild-type XS110 (solid circles) and progenitor lpa mutant Os-lpa-XS-2 (open circles); crossing parent JX081 (blue asterisks) and JH218 (red asterisks); crossbred progenies of homozygous wild-type (solid) and homozygous lpa mutants (open) of generations F4 (circles), F5 (diamonds), F6 (triangles), and F7 (squares).

separations between the homozygous wild-type and the homozygous *lpa* mutant progenies for each generation, a distinct metabolic shift with ascending generations (F_4 to F_7) was observed along PC1 (Figure 3A).

To further elucidate these differentiations in light of genotype and of generation, the PCA of the lipophilic fractions I-II and the polar fractions (III-IV) were performed, respectively. In the score plot of the lipophilic fractions (Figure 3B), there was a similar metabolic shift for the crossbred progenies from F_4 to F_7, whereas no separation was observed between the wild-type and the corresponding *lpa* mutant. This demonstrated that the non-polar metabolites are the dominant contributors to the metabolic variations depending on generation in the crossbred progenies. In contrast, the PCA score plot of the polar fractions III-IV (Figure 6C) revealed a pronounced differentiation between the original wild-type XS110 and the progenitor

lpa mutant *Os-lpa*-XS-2, and this differentiation was consistently presented between the homozygous wild-type and *lpa* mutant progenies for each generation.

The parallel multivariate analyses were conducted for the other cross *Os-lpa*-XS-2×JH281, and the PCA score plots were shown in Figure 6D-F. Interestingly, for the combined fractions I-IV, the discriminations of the rice samples in light of genotype (wild-type *vs.* *lpa* mutant) and of generation (early to late) presented in the cross *Os-lpa*-XS-2×JH281 (Figure 6D) were similar to that observed in *Os-lpa*-XS-2×JX081 (Figure 6A). These findings suggest that on the one hand, the cross-breeding resulted in a metabolic shift of lipophilic constituents among crossbred progenies with ascending generations for both crosses; on the other hand, the metabolic changes in the polar fractions induced by the *OsMRP5* mutation in the progenitor *lpa* mutant *Os-lpa*-XS-2 were not affected by the cross-breeding step, and was consistently expressed in the homozygous *lpa* mutant progenies from generations F_4 to F_7, independent from the employed commercial crossing parents and from the generation variations.

3.4 Metabolic variations among progenies upon cross-breeding

The individual metabolites contributing to the metabolic shift in the lipophilic fractions for both crosses (Figure 6B and 6E) were selected via corresponding loading plots (Figure 7), and the dynamic changes of these metabolites were expressed by heat map. As shown in Figure 8A, for the crossbred progenies of *Os-lpa*-XS-2×JX081, a broad spectrum of non-polar metabolites, e.g., FAMEs, FFAs, fatty alcohols, and phytosterols, all displayed increased levels from F_4 to F_7 both for the homozygous wild-type and *lpa* mutant progenies.

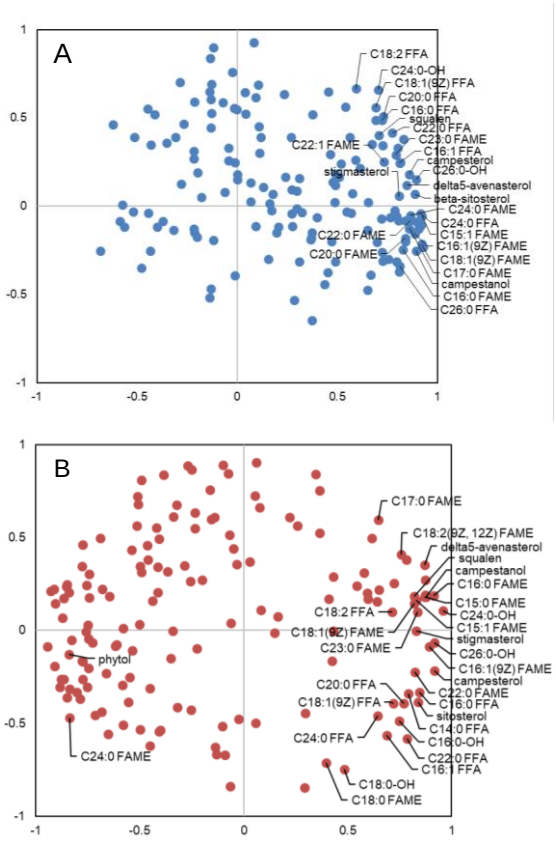

Figure 7. PCA loading plots of metabolite profiling data of the lipophilic fractions of the rice samples from the cross Os-lpa-XS-2×JX081 (A) and Os-lpa-XS-2×JH2181 (B).

Heat map analysis of the other cross *Os-lpa*-XS-2×JH218 showed that apart from a few exceptions (i.e. C24:0 FAME and phytol), the concentrations of a considerable amount of non-polar metabolites in the crossbred

progenies were also increased along ascending

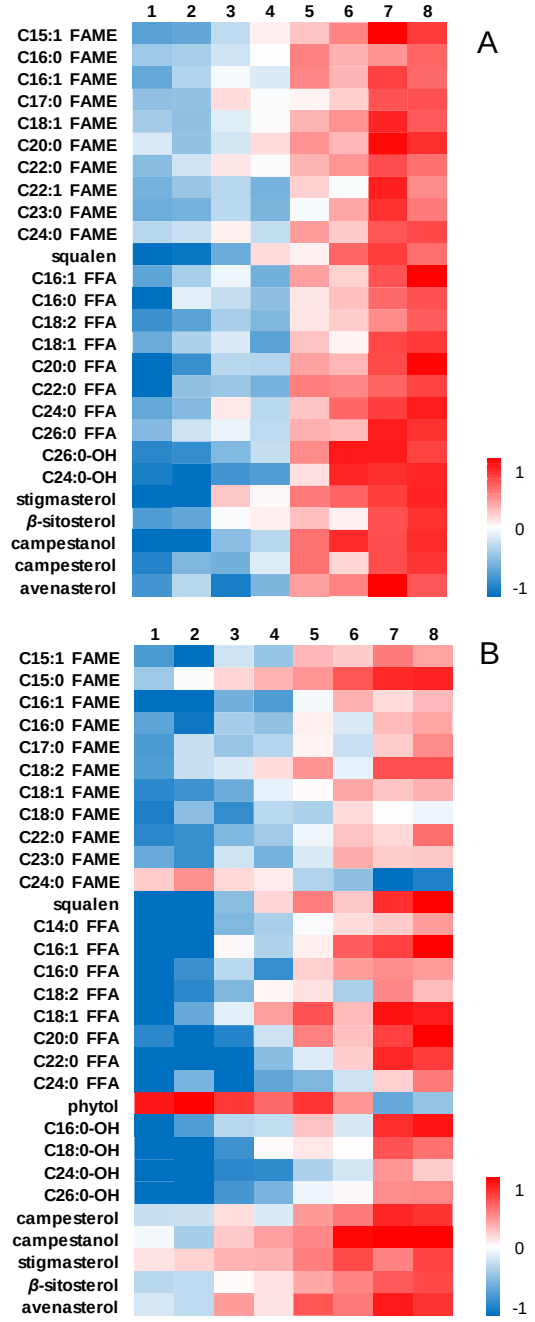

Figure 8. Heat map of the metabolites responsible for the metabolic shift along ascending generations among progenies from the cross Os-lpa-XS-2×JX081 (A) and Os-lpa-XS-2×JH218 (B). Lanes 1 to 8: homozygous wild-type and lpa mutant progenies of generations F4 to F7, respectively.

generations (Figure 8B). It is noteworthy that most of the discriminant metabolites, such as FAMEs (e.g., C16:0, C18:1 and C18:0), FFAs (e.g., C16:0, C18:1 and C20:0), fatty alcohol (e.g., C24:0 and C26:0) and phytosterols (campesterol and *β*-sitosterol), contributing to the metabolic shift among progenies for the two crosses are in good agreement.

3.5 Metabolic differentiation between homozygous wild-type and *lpa* mutant progenies

In addition to the metabolic variations depending on generation, there were also consistent differentiations between the homozygous wild-type and the homozygous *lpa* mutant progenies of each generation for both crosses. In order to determine the metabolites mostly contributing to the separation in light of genotype, the corresponding PCA loading plots were utilized, and peak-by-peak comparisons were performed by *Chrompare* (Frenzel et al., 2003). The discriminating metabolites were mapped in a simplified pathway referring to the KEGG database and were quantitated based on their relative peak intensities (i.e., metabolite peak intensity/ internal standard peak intensity × 100).

As shown in Figure 9, the *OsMRP5* mutation-induced metabolic features in *Os-lpa*-XS-2 were characterized not only by the significantly decreased level of phytic acid, but also by the metabolic changes in several metabolites that are involved in the biosynthetic pathway of phytic acid. A number of sugars and sugar alcohols, e.g., *myo*-inositol, mannitol, fructose, maltose and raffinose, all exhibited decreased levels in *Os-lpa*-XS-2 mutant compared with the corresponding wild-type XS110, while the contents of sorbitol and trehalose were increased. The similar metabolic features were also presented in the homozygous *lpa* mutant progenies compared with the corresponding homozygous wild-type progenies from

generations F_4 to F_7. For the other cross *Os-lpa*-XS-2×JH218, KEGG-based pathway analysis revealed that despite the variations in absolute concentrations of the

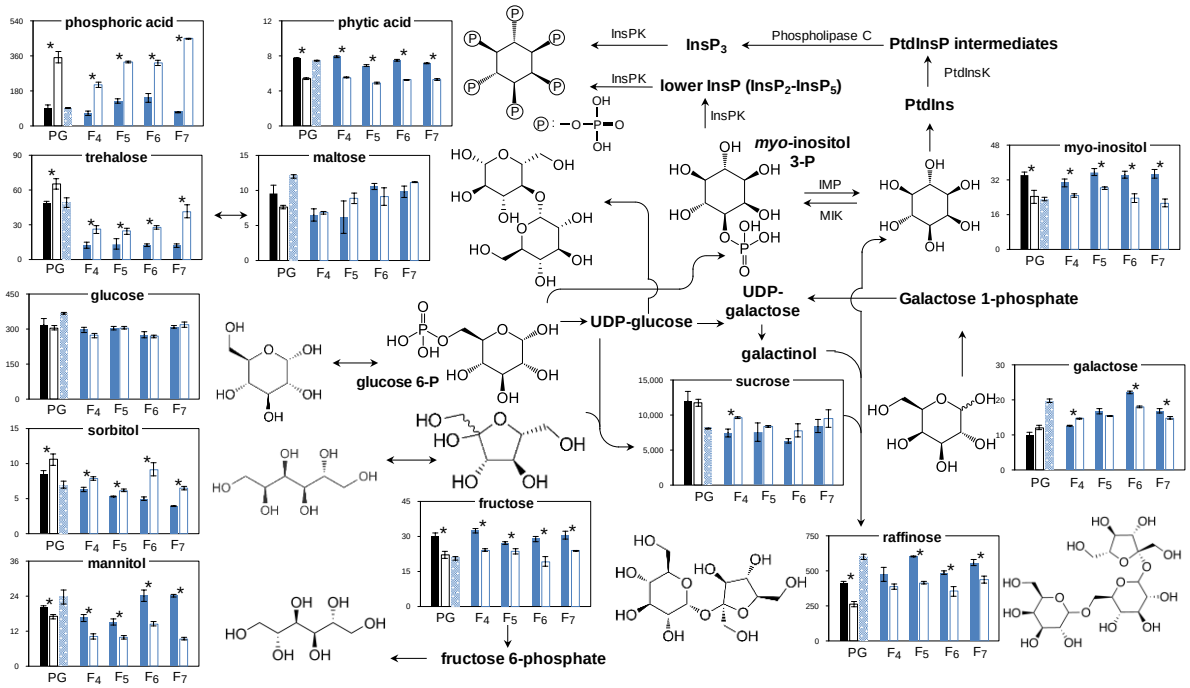

Figure 9. Simplified biosynthetic pathways of the metabolites involved in phytic acid, sugar, and sugar alcohol metabolism. The bars are presented in the following order: parental generation (PG) of original wild-type XS110 (solid bar in black), Os-lpa-XS-2 (open bar in black) and JX081 (partly filled in blue); cross-bred progenies of homozygous wild-type (solid bar in blue) and lpa mutants (open bar in blue) from the cross Os-lpa-XS-2×JX081.

mapped metabolites, the mutation-induced metabolite signature in the homozygous *lpa* mutant progenies of each generation, i.e., decreased levels of *myo*-inositol, mannitol, fructose, maltose and raffinose, and the increased levels of sorbitol and trehalose, were very comparable to those observed in the cross *Os-lpa*-XS-2×JX081. These results demonstrated that the *OsMRP5* mutation-induced metabolite signature in the progenitor *lpa* mutant *Os-lpa*-XS-2 was not compromised upon cross-breeding, and was stably expressed in the crossbred *lpa* mutant progenies over generations, independent from cultivar of the crossing parent.

OsMRP5 mutation also led to increased levels of a number of organic acids (e.g., malic acid and threonic acid), amino acids (e.g., glycine, leucine, methionine, serine and proline), and biogenic amine GABA in *Os-lpa*-XS-2 compared with XS110. Similarly, independent from the levels of metabolites in the commercial crossing parents, these *OsMRP5* mutation-induced metabolic changes were not affected upon cross-breeding step, and in most cases, were consistently observed in the homozygous *lpa* mutant progenies from generations F_4 to F_7 for the both crosses *Os-lpa*-XS-2×JX081 and *Os-lpa*-XS-2×JH218.

4. Discussion

Lpa mutations are often accompanied by some adverse pleiotropic effects, especially on agronomic performance, such as reduced field emergence rate, decreased seed viability and low grain yield, thus limiting the interest of breeders (Pilu, Landoni, Cassani, Doria, & Nielsen, 2005). In the present study, *OsMRP5*

mutation resulted in an almost 50% reduction in field emergence rate of *Os-lpa*-XS-2 compared with the corresponding wild-type XS110, and such drastic drops were also observed in maize (Pilu et al., 2005) and soybean (Hulke, Fehr, & Welke, 2004) *lpa* mutants carrying MRP mutations. During seed development, the oxidation of Fe^{2+} to Fe^{3+} in the cell environment is considered a source of reactive oxygen species (ROS) detrimental to seed viability (Hobo, Iwabuchi, & Ogawa, 2005). Due to the ability to chelate Fe^{2+}, phytic acid is supposed to provide protection against oxidative stress during seed germination and seedling growth. Therefore, the paucity of phytic acid content induced by *lpa* mutations would result in more free or weakly bound iron cations and in consequent high level of toxic ROS, further increasing the oxidative stress on seed viability (Doria et al., 2009).

A possible approach to defending plant cells from ROS consists in scavenging these toxic free radicals by introducing molecules endowed with antioxidant properties. Thus, aiming at increasing the agronomic performance of the *lpa* mutants, it might be a practical way to employ classical breeding strategy introgress the ability to synthesize and mainly concentrated in the germ, and the perturbation of phytic acid biosynthesis are expected to have more adverse impacts on the yielding of the crop (Colombo et al., 2020; Doria et al., 2009).

The integrated PCA analysis consisting of rice samples from both crosses was conducted to evaluate the impact of crossing parent on the metabolite profiles of the generated progenies. As shown in Figure 1A, the crossbred progenies were grouped into two clusterings in light of the crossing parents rather than of the mutation types, and only a slight differentiation was observed between the wild-type and *lpa* mutant progenies within each clustering. The discriminant metabolites

accumulate more natural antioxidants, such as carotenoids and polyphenols in grains (Colombo et al., 2020). It is worthy to note that after cross-breeding of progenitor *lpa* mutant *Os-lpa*-XS-2 with commercial cultivar JX081, the field emergence rate of the homozygous *lpa* mutant progenies increased significantly from 42.7% to 78.5% (Table 1). A recent study on soybean also reported that two lines of *lpa* progeny obtained via backcrossing exhibited improved filed emergences that were comparable to the high-yielding cultivars with no germination issues (Boehm, Walker, Bhandari, Kopsell, & Pantalone, 2017). These results suggest that conventional cross and selection breeding could be employed to improve the field emergence rate of the MRP *lpa* mutants.

In contrast to the considerable reduction of grain weight in the previously developed maize mutant *lpa241-1* (Pilu et al., 2005), no significant decreases of 1000-grain weight and seed setting ration were observed in *Os-lpa*-XS-2. This might be due to the different distributions of the phytic acid deposits, since 90% of phytic acid in rice seed are located in the aleurone, while for maize kernel they are

covered a wide range of lipophilic and hydrophilic rice constituents, e.g., FAMEs, FFAs, fatty alcohols, phytosterols, sugars, organic acids, and amino acids. Interestingly, the univariate analyses showed that in most cases, the differential ratios in the contents of the discriminating metabolites between the two crossing parents were very comparable to that between the *lpa* progenies from the two crosses (Table S3). These results indicate that crossing parent has a more significant impact on the metabolite profiles of the progenies than the *OsMRP5* mutation effect.

On the contrary, our previous studies found that for the *lpa* progenies carrying the *OsSULTR3;3* mutation target, their metabolic

features were driven mainly by the mutation effects instead of by the crossing parents (Zhou, Tan, Goßner, Li, Shu, & Engel, 2019). This discrepancy might be attributed to the differences in the complexity of the mechanisms underlying the *lpa* mutations. The *OsMRP5* mutation may affect the transport and storage of phytic acid into the vacuole (Sparvoli & Cominelli, 2014), and this complexity is definitely increased for the disruption of the putative sulfate transporter gene *OsSULTR3;3*, which is thought to play a role in the cross-talk between sulfate and phosphate homeostasis and signaling (Zhao et al., 2016). Taking this scenario into account, the metabolite profiles of the *OsMRP5 lpa*

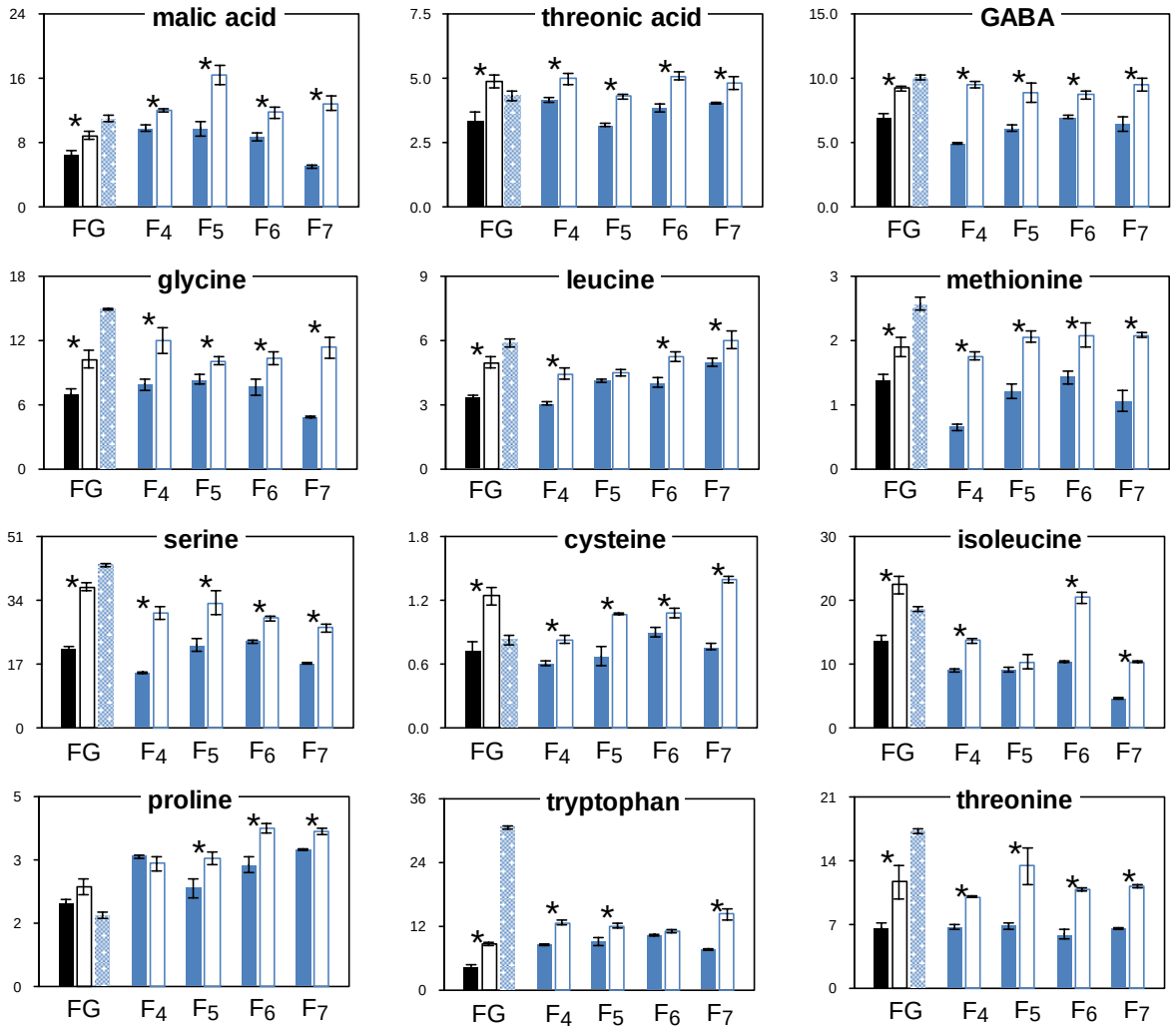

Figure 10. Metabolites in fraction IV responsible for the discrimination between the wild-type and the corresponding lpa mutants. The bars are presented in the following order: parental generation (PG) of original wild-type XS110 (solid bar in black), Os-lpa-XS-2 (open bar in black) and JX081 (partly filled in blue); cross-bred progenies of homozygous wild-type (solid bar in blue) and lpa mutants (open bar in blue) from the cross Os-lpa-XS-2×JX081.

mutant progenies are expected to be more susceptible to the variable factors such as crossing parent, growing condition and temperature. This hypothesis is also supported by the results from a recent study on the variations of phytic acid contents in response to different mutation types and growing conditions (C. G. Zhou et al., 2019).

The metabolite profiling of the progenitor *lpa* mutant revealed that in addition to the significantly decreased content of phytic acid, *Os-lpa*-XS-2 was characterized by reduced levels of sugars and sugar alcohols such as *myo*-inositol, mannitol, fructose, and raffinose. Similar results were also observed in the MRP *lpa* mutant lines of maize (Doria et al., 2009), soybean (Shi et al., 2007), and common bean (Panzeri et al., 2011). As the precursor of phytic acid, *myo*-inositol and its derivatives (raffinose-type oligosaccharides and galactose) have been reported to be involved in the synthesis of some important metabolites such as polyols and phosphoinositides (Sparvoli et al., 2014). Investigation on *PvMRP1* of common bean, orthologous to *OsMRP5* of rice, revealed that the MRP *lpa* mutation was shown to significantly inhibit the expression of the *PvIMP* genes coding for the key enzyme *myo*-inositol monophosphates (IPM) (Panzeri et al., 2011), which is responsible for the conversion of *myo*-inositol 1-P into *myo*-inositol. As a result, the contents of *myo*-inositol, galactose and raffinose were all decreased.

On the contrary, the previously developed *lpa* rice mutant *Os-lpa*-XS-1, carrying the *myo*-inositol kinase (*OsMIK*) mutated gene, was shown to exhibit increased levels of *myo*-inositol, galactose and raffinose (Tan et al., 2019). The *OsMIK* mutation is expected to disrupt the conversion of *myo*-inositol into *myo*-inositol-3phosphate (Figure 5), and as a result, the contents of *myo*-inositol and its derivatives galactose and raffinose were increased. As one of the predominant form of raffinose family oligosaccharides (RFOs), raffinose in grains is considered an antinutrient owing to its flatulence-inducing effects, and molecular-assisted breeding has been employed by Hagely et al. (Hagely, Jo, Kim, Hudson, & Bilyeu, 2020) and Redekar et al. (Redekar, Glover, Biyashev, Ha, Raboy, & Maroof, 2020) to improve the nutritional profiles of soybeans with low-RFOs/low-phytate/normal-sucrose phenotype. In this regard, the *OsMRP5* mutation-induced reduction of raffinose content in *Os-lpa*-XS-2 is also favorable.

Plant responses to abiotic stress include various modifications in metabolism (Batista-Silva et al., 2019). Chun et al. reported higher levels of sugars, amino acids and intermediary metabolites accumulated in *Arabidopsis* root in response to salt stress (Chun et al., 2019). Metabolomics study also revealed the changed levels of metabolite biomarkers (e.g., glycerolipids, glutaric acid, pheophorbide A and abscisic acid) in hop (*Humulus lupulus* L.) plants under drought stress (Morcol, Wysocki, Sankaran, Matthews, & Kennelly, 2020). Generally, the contents of free amino acids increase considerably, which are attributed to the up-regulated synthesis rates, the proteolysis of some highly abundant proteins or the restricted consumption for secondary metabolites production (Batista-Silva et al., 2019; Wen, Zhang, Feng, Duan, Ma, & Zhang, 2020). In the present study, the *Os-lpa*-XS-2 was expected to be suffering from the oxidative stress, since the reduced accumulation of phytic acid resulted in more free iron cations, further contributing to the enhanced levels of ROS. As a result, a similar process in the metabolic changes was observed in *Os-lpa*-XS-2, i.e., the increased contents of a broad spectrum of amino acids such as glycine, leucine, methionine, serine, cysteine and proline, as well as the well-

known plant oxidative stress biomarker GABA (Figure 5). Such similar metabolic changes were also observed in our previously developed *lpa* rice mutant *Os-lpa*-MH86-1 compared to the corresponding wild-type MH86. The mutation of a 1-bp deletion in the putative sulfate transporter gene *OsSULTR3;3* was shown to affect the expressions of several genes involved in sulfate and phosphate homeostasis and/or signaling. Consequently, the *Os-lpa*-MH86-1 mutant exhibited a metabolic profile similar to that observed in plants subjected to sulfate deficiency, and the levels of a broad spectrum of sugars, amino acids and GABA were increased (Zhao et al., 2016).

The observed metabolic changes in the progenitor *lpa* mutant *Os-lpa*-XS-2, namely the decreased levels in some sugars and sugar alcohols, as well as the increased levels of organic acids, amino acids and biogenic amine, are characterized as the *OsMRP5* mutation-induced metabolite signature. To assess the stability of this metabolite signature in the *lpa* mutant after cross-breeding, the resulting homozygous wild-type and *lpa* mutant progenies from the crosses *Os-lpa*-XS-2×JX081 and *Os-lpa*-XS-2×JH218 were also subjected to the metabolite profiling, respectively. Multivariate and univariate statistical analyses showed that the mutation-induced metabolic differentiations in polar fractions between the wild-type and the *lpa* mutants were not affected by the cross-breeding step. Additionally, these metabolic features, especially the improved nutritional properties (i.e., reduced levels of phytic acid and RFOs, and increased contents of essential amino acids and renowned health-promoting compound GABA), were all consistently expressed in the homozygous *lpa* mutant progenies from generations F_4 to F_7 for both crosses, independent from the generation variations in lipophilic profiles and from the cultivars of the employed crossing parent (Figures 5, S11, S12, and S13). This key result suggests that the *OsMRP5* gene can be considered a promising target to develop *lpa* mutant progenies with improved field emergence rate via cross and selection breeding.

5. Conclusions

In summary, the results in the present study are valuable from a breeder's standpoint. They show a practical way to improve the inferior filed emergence rate of *OsMRP5 lpa* mutants via cross and selection breeding. The elaborated metabolite profiling data demonstrate that in spite of the predominant impact of crossing parent on the metabolite profiles of the progenies, the *OsMRP5* mutation-induced metabolite signature, especially improved nutritional-relevant properties, was not compromised upon cross-breeding and was stably expressed in the *lpa* mutant progenies over generations. The *OsMRP5 lpa* mutants might be considered valuable genetic resources for commercial breeding programs in developing rice cultivars with favorable metabolic traits. Further investigations on other *OsMRP5* mutant crops such as soybean and maize could be conducted to substantiate the usefulness of this type of mutants.

References

References are needed to all citations and arranged by alphabetical order using author-date system.

[1] Batista-Silva, W., Heinemann, B., Rugen, N., Nunes-Nesi, A., Araujo, W. L., Braun, H. P., & Hildebrandt, T. M. (2019). The role of amino acid metabolism during abiotic stress release. *Plant Cell and Environment*, *42*(5), 1630-1644

[2] Boehm, J. D., Walker, F. R., Bhandari, H. S., Kopsell, D., & Pantalone, V. R. (2017). Seed inorganic phosphorus stability and agronomic performance of two low-phytate soybean lines evaluated across six southeastern US environments. *Crop Science*, *57*(5), 2555-2563.

[3] Bohn, L., Meyer, A. S., & Rasmussen, S. K. (2008). Phytate: impact on environment and human nutrition. A challenge for molecular breeding. *Journal of Zhejiang University-Science B*, *9*(3), 165-191.

[4] Chun, H. J., Baek, D., Cho, H. M., Jung, H. S., Jeong, M. S., Jung, W. H., . . . Kim, M. C. (2019). Metabolic adjustment of arabidopsis root suspension cells during adaptation to salt stress and mitotic stress memory. *Plant and Cell Physiology, 60*(3), 612-625.

[5] Colombo, F., Paolo, D., Cominelli, E., Sparvoli, F., Nielsen, E., & Pilu, R. (2020). MRP transporters andlow phytic acidmutants in major crops: main pleiotropic effects and future perspectives. *Frontiers in Plant Science, 11*.

[6] Dong, Q., Echigo, K., Raboy, V., & Saneoka, H. (2020). Seedling growth, physiological characteristics, nitrogen fixation, and root and nodule phytase and phosphatase activity of a low-phytate soybean line. *Plant Physiology and Biochemistry, 149*, 225-232.

[7] Doria, E., Galleschi, L., Calucci, L., Pinzino, C., Pilu, R., Cassani, E., & Nielsen, E. (2009). Phytic acid prevents oxidative stress in seeds: evidence from a maize (Zea mays L.) low phytic acid mutant. *Journal of Experimental Botany, 60*(3), 967-978

[8] Frenzel, T., Miller, A., & Engel, K. H. (2003). A methodology for automated comparative analysis of metabolite profiling data. *European Food Research and Technology, 216*(4), 335-342.

[9] Hagely, K. B., Jo, H., Kim, J. H., Hudson, K. A., & Bilyeu, K. (2020). Molecular-assisted breeding for improved carbohydrate profiles in soybean seed. *Theoretical and Applied Genetics, 133*(4), 1189-1200.

[10] Hobo, T., Iwabuchi, M., & Ogawa, K. (2005). Role of reactive oxygen species generated during the germination of Arabidopsis seeds. *Plant and Cell Physiology, 46*, S81-S81.

[11] Hulke, B. S., Fehr, W. R., & Welke, G. A. (2004). Agronomic and seed characteristics of soybean with reduced phytate and palmitate. *Crop Science, 44*(6), 2027-2031.

[12] Kumar, V., Singh, D., Sangwan, P., & Gill, P. K. (2015). Management of environmental phosphorus pollution using phytases: current challenges and future prospects. In G. Kaushik (Ed.), *Applied Environmental Biotechnology: Present Scenario and Future Trends* (pp. 97-114). New Delhi: Springer India.

[13] Liu, Q. L., Xu, X. H., Ren, X. L., Fu, H. W., Wu, D. X., & Shu, Q. Y. (2007). Generation and characterization of *low phytic acid* germplasm in rice (*Oryza sativa* L.). *Theoretical and Applied Genetics, 114*(5), 803-814.

[14] Morcol, T. B., Wysocki, K., Sankaran, R. P., Matthews, P. D., & Kennelly, E. J. (2020). UPLC-QTof-MSE metabolomics reveals changes in leaf primary and secondary metabolism of hop (*Humulus lupulus L.*) plants under drought stress. *Journal of Agricultural and Food Chemistry, 68*(49), 14698-14708.

[15] Panzeri, D., Cassani, E., Doria, E., Tagliabue, G., Forti, L., Campion, B., . . . Sparvoli, F. (2011). A defective ABC transporter of the MRP family, responsible for the bean lpa1 mutation, affects the regulation of the phytic acid pathway, reduces seed myo-inositol and alters ABA sensitivity. *New Phytologist, 191*(1), 70-83.

[16] Pilu, R., Landoni, M., Cassani, E., Doria, E., & Nielsen, E. (2005). The maize lpa241 mutation causes a remarkable variability of expression and some pleiotropic effects. *Crop Science, 45*(5), 2096-2105.

[17] Raboy, V. (2009). Approaches and challenges to engineering seed phytate and total phosphorus. *Plant Science, 177*(4), 281-296.

[18] Redekar, N. R., Glover, N. M., Biyashev, R. M., Ha, B. K., Raboy, V., & Maroof, M. A. S. (2020). Genetic interactions regulating seed phytate and oligosaccharides in soybean (Glycine max L.). *PloS One, 15*(6).

[19] Shi, J. R., Wang, H. Y., Schellin, K., Li, B. L., Faller, M., Stoop, J. M., . . . Glassman, K. (2007). Embryo-specific silencing of a transporter reduces phytic acid content of maize and soybean seeds. *Nature Biotechnology, 25*(8), 930-937.

[20] Sparvoli, F., & Cominelli, E. (2014). Phytate Transport by MRPs. In M. Geisler (Ed.), *Plant ABC Transporters* (pp. 19-38). Cham: Springer International Publishing.

[21] Sparvoli, F., & Cominelli, E. (2015). Seed biofortification and phytic acid reduction: a conflict of interest for the plant? *Plants, 4*(4), 728-755.

[22] Tan, Y., Zhou, C., Goßner, S., Li, Y., Engel, K.-H., & Shu, Q. (2019). Phytic acid contents and metabolite profiles of progenies from crossing low phytic acid *OsMIK* and *OsMRP5* rice (Oryza sativa L.) mutants. *Journal of Agricultural and Food Chemistry, 67*(42), 11805-11814.

[23] Tan, Y. Y., Fu, H. W., Zhao, H. J., Lu, S., Fu, J. J., Li, Y. F., . . . Shu, Q. Y. (2013). Functional molecular markers and high-resolution melting curve analysis of *low phytic acid* mutations for marker-assisted selection in rice. *Molecular Breeding, 31*(3), 517-528.

[24] Wen, C., Zhang, J. X., Feng, Y. Q., Duan, Y. Q., Ma, H. L., & Zhang, H. H. (2020). Purification and identification of novel antioxidant peptides from watermelon seed protein hydrolysates and their cytoprotective effects on H2O2-induced oxidative stress. *Food Chemistry, 327*.

[25] Xu, X. H., Zhao, H. J., Liu, Q. L., Frank, T., Engel, K. H., An, G. H., & Shu, Q. Y. (2009). Mutations of the multi-drug resistance-associated protein ABC transporter gene 5 result in reduction of phytic acid in rice seeds. *Theoretical and Applied Genetics, 119*(1), 75-83.

[26] Zhao, H., Frank, T., Tan, Y., Zhou, C., Jabnoune, M., Arpat, A. B., . . . Shu, Q. (2016). Disruption of *OsSULTR3;3* reduces phytate and phosphorus concentrations and alters the metabolite profile in rice grains. *New Phytologist, 211*(3), 926-939.

[27] Zhao, H. J., Liu, Q. L., Fu, H. W., Xu, X. H., Wu, D. X., & Shu, Q. Y. (2008). Effect of non-lethal *low phytic acid* mutations on grain yield and seed viability in rice. *Field Crops Research, 108*(3), 206-211.

[28] Zhou, C., Tan, Y., Goßner, S., Li, Y., Shu, Q., & Engel, K.-H. (2019). Impact of crossing parent and environment on the metabolite profiles of progenies generated from a low phytic acid rice (*Oryza sativa L.*) mutant. *Journal of Agricultural and Food Chemistry, 67*(8), 2396-2407.

[29] Zhou, C. G., Tan, Y. Y., Gossner, S., Li, Y. F., Shu, Q. Y., & Engel, K. H. (2018). Stability of the metabolite signature resulting from the *OsSULTR3;3* mutation in *low phytic acid* rice (*Oryza sativa* L.) seeds upon cross-breeding. *Journal of Agricultural and Food Chemistry, 66*(35), 9366-9376.

[30] Zhou, C. G., Tan, Y. Y., Gossner, S., Li, Y. F., Shu, Q. Y., & Engel, K. H. (2019). Impact of cross-breeding of *low phytic acid* rice (*Oryza sativa* L.) mutants with commercial cultivars on the phytic acid contents. *European Food Research and Technology, 245*(3), 707-716.

Authors profile

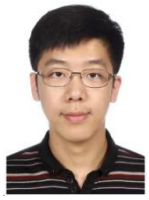

Assoc. Prof. Dr. Chenguang Zhou
Born on 1990
Majoring in agricultural food quality and safety inspection and intelligent processing

Prof. Dr. Jiyong Shi
Born on 1984
Majoring in agricultural food quality and safety inspection and intelligent processing

Prof. Dr. Xiaobo Zou
Born on 1974
Majoring in agricultural food quality and safety inspection and intelligent processing

Bio-based materials from and back to agriculture, and beyond

Jun Liu[1*], Jianzhong Sun[1], Qianqian Wang[1], Huan Liu[1], Hua Shang[1]

[1] *Biofuels Institute, School of Emergency Management, School of Environment and Safety Engineering, Jiangsu University, Zhenjiang 212013, China*
**E-mail: junliu115142@hotmail.com*

Abstract: Environmental pollution and resource waste resulting from the disposal of agricultural and forestry biomass waste have become a global issue. The search for effective methods of solid waste treatment and disposal is progressing worldwide. Consequently, finding ways to recycle and utilize these biomass wastes in high-value applications presents a significant challenge for both academia and industry. This work provides a comprehensive overview of the current advancements in recycling and reutilization of biomass waste, with a particular focus on the development of biomass-based materials using agricultural biomass waste and their potential applications in the agricultural and biomedical fields. This work also highlights the challenges and future prospects of bio-based materials derived from agriculture, emphasizing their return to agriculture and beyond. We anticipate that this research will contribute to the understanding and promotion of recycling and reutilization of biomass waste, offering promising solutions for the sustainable development of agricultural engineering.

Keywords: Biomass waste, Bio-based materials, Nanocellulose, Biomedical applications.

1. Introduction

The global issue of solid waste disposal has led to environmental pollution and resource waste. Treatment and disposal methods for solid waste are being explored globally. In China, both urban and rural areas generate approximately 6.3 billion tons of organic waste annually, including agricultural and forestry residues, household garbage, domestic sludge, livestock and poultry waste, fruit and vegetable residues, and industrial organic residue waste liquid. Forestry residues account for 160 million tons, while agricultural residues account for 980 million tons. If not managed properly, this solid waste has the potential to cause significant environmental pollution and resource wastage [1].

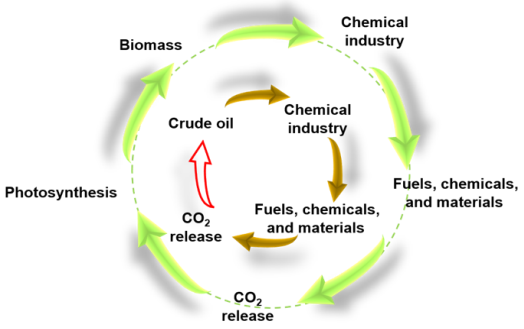

Figure 1. Production cycles comparison of products derived from fossil fuel and biomass

Biomass waste shares similar chemical compositions with traditional biomass raw materials and has the advantages of high abundance, renewability, and biodegradability. This makes it a promising candidate for incorporation into the biorefinery industry, either as a supplement or a replacement for the traditional fossil fuel refinery industry (Figure 1). At present, agricultural and forestry waste biomass is primarily used for feed, fertilizer, and matrix. However, these products have weak market competitiveness and low added value. Therefore, there is a significant challenge in achieving resource and high-value utilization of these wastes in both academia and industry. This work summarizes the current advances in recycling and reutilization of biomass waste, with a focus on the development of biomass-based materials using agricultural biomass waste or application exploration in the agricultural field. The challenges and future perspectives of bio-based materials from agriculture, back to agriculture, and beyond are proposed at the end of this work. We hope that this work will provide valuable insights into the recycling and reutilization of biomass waste with high-added value, serving as a promising solution to the sustainable development of agricultural engineering.

2. Recent progress of bio-based materials prepared from agricultural sources and applied in agricultural engineering

In recent years, aligning with sustainable development goals of society, economy, and environment, many countries have prioritized the research and application of new bio-based materials in agricultural production. Bio-based materials have a natural and significant interrelationship with agricultural production, promoting comprehensive development and utilization of agricultural resources, and supporting green, efficient, and intelligent modern agriculture. New bio-based materials such as biochar materials, bio-nano materials, biodegradable plastics, and bio-based 3D printing materials have gained increasing attention in academic research and agricultural applications both domestically and internationally [2]. Further industrialization of these bio-based materials is expected to drive technological innovation in agricultural production, fostering a new pattern of modern agricultural production by promoting development in planting, breeding, biomass waste collection and processing, and ecological restoration.

2.1. Preparation and application of biochar

Biochar is a stable, carbon-rich solid substance produced by pyrolysis of biomass under oxygen-limited or anaerobic conditions. Its high carbon content, rich pore structure, and strong adsorption capacity make it a promising material for improving soil quality, increasing crop yield, and environmental governance. Recent research focuses on developing functional materials by selecting biomass raw materials, optimizing pyrolysis temperature and reaction time, and other process conditions. By reducing pyrolysis temperature, constructing biochar/fertilizer composite materials, and surface modification, biochar can be endowed with special functions to improve soil fertility and crop yield [3]. Additionally, modified biochar can be developed for water, soil, and other agricultural environmental governance to achieve efficient adsorption, rapid repair, and sustainable recycling (Figure 2) [4]. However, there is still a lack of standardized guidance, systematic research results on the environmental application of biochar and environmental risk assessment, and production equipment and technologies suitable for large-scale and low-cost preparation of biochar. We

believe that the development of suitable functional biochar, the quantitative determination of the optimal application ratio of biochar, and breakthroughs in biochar green, low-cost, and large-scale production technologies are the key to promoting large-scale, diversified, and efficient biochar in agricultural production.

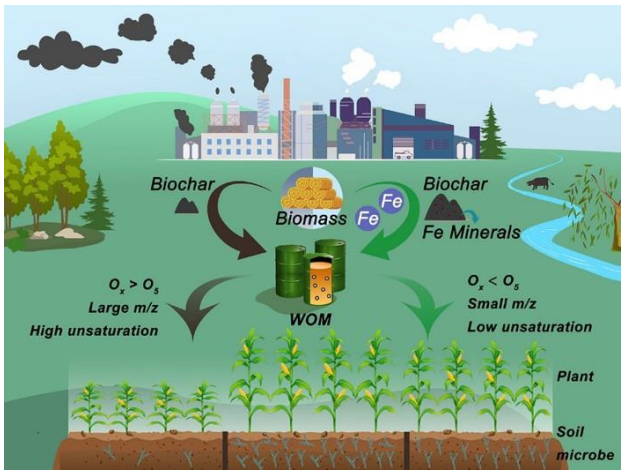

Figure 2. Biochar preparation and application in agriculture.

Adapted from Shang et al. Sci. Total Environ. (2021)[4].

2.2 Preparation and application of nanocellulose

Since the early 21st century, researchers have been exploring agricultural nanotechnology and innovating its application in various fields of agricultural production. New nano-materials, such as nanocellulose, exhibit unique characteristics of environmental friendliness, biosafety, and controllable functions that other materials cannot match [5]. Nanocellulose can be prepared from various agricultural waste biomass raw materials, such as straw, bagasse, and rice husk, through green processes. However, the complex raw material components, numerous impurities, and difficult purification present challenges in the preparation of nanocellulose from agricultural waste biomass [6, 7].

Nanocellulose has a high aspect ratio and can be used to enhance biodegradable agricultural mulch films and other new agricultural chemicals, e.g., new pesticides, feed, nano slow-release fertilizers, and soil water retaining agents. Efficient utilization and sustainable development of agricultural resources based on nanocellulose materials are expected to control the agricultural biomass-waste pollution from the source and improve the quality and efficiency of agricultural product production. However, high production costs remain a challenge to the industrial application of nanocellulose in agricultural products. Therefore, the development of agricultural waste biomass-based nanocellulose with high quality for application in high value-added fields, such as biomedicine or pharmacy, could be one solution to make up for the high production cost (Figure 3) [8-11]. Using low-cost agricultural waste biomass as raw materials to prepare full-component nanofibers that meet agricultural production applications is expected to be a solution to this challenge.

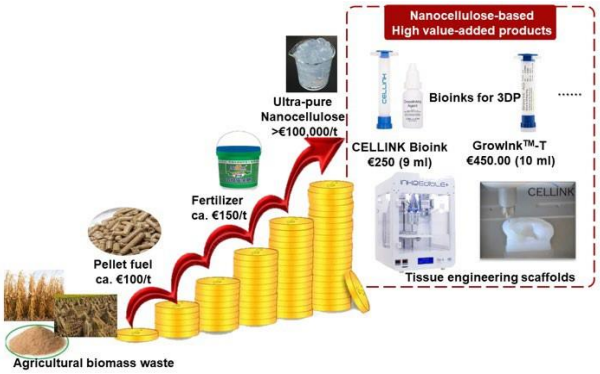

Figure 3. Development of ultra-pure nanocellulose from agricultural biomass waste towards high value-added application

2.3 Preparation and application of biodegradable plastics

The concept and technical products of bio-based, environmentally degradable plastics originated in Europe and the United States in the 1990s. Bio-based degradable agricultural mulch has gained global attention from governments, enterprises, and research institutions due to the significant contribution of film mulching technology to crop yield (increasing yield by 20%-30%) and enriching the fertility of the soil microenvironment after biodegradation (Figure 4) [12-14]. China is the world's largest user and coverage of agricultural mulch, with an annual area of major crops nearly reaching 300 million acres (coverage rate of about 13%). Mulching technology has played a vital role in ensuring China's food security and adequate supply of vegetables, contributing to the safe supply of agricultural products in the country. However, although biodegradable mulch is expected to replace traditional mulch in the future, its large-scale promotion still faces technical and application challenges, such as high impurities in the raw material of agricultural biomass waste, low saccharification and fermentation conversion efficiency, degradation controllability, and reducing industrial production and application costs.

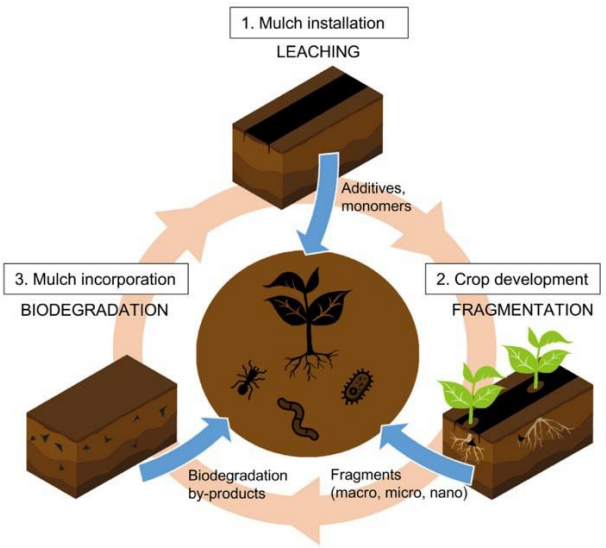

Figure 4. Biodegradable agricultural mulching in agriculture. Adapted from Hadaly et al. Sci. Total Environ. (2021)[13].

2.4 Preparation and application of bio-based 3D printing materials

3D printing, or additive manufacturing, is a rapid

prototyping technology that builds and reproduces materials layer by layer based on a digital 3D model. The development of 3D printing technology relies on the innovation of printing materials. In agricultural production, the preparation and application of new bio-based 3D printing materials focus on two aspects: developing 3D printing raw materials from agricultural biomass waste towards high-value applications in other fields (Figure 3) [2, 15]; and using 3D printing technology to customize the production of special facilities or functional materials for bio-based agricultural production. For instance, 3D printing of drip irrigation core valves, water pump paddles, and hydroponic substrate trays using bio-based PLA, PBAT, PHA, etc. [16, 17]. A key research trend is to separate and extract biopolymers from agricultural waste, or process with all components of agricultural waste, to develop 3D printing feedstocks and functional materials that meet the requirements of different 3D printing technologies. Currently, the research and application fields of 3D printing intelligent manufacturing technology based on new bio-based materials are increasing in agricultural production. These include not only the construction of agricultural equipment and accessory parts, but also multiple application directions in agricultural biological engineering.

3. Challenges and outlook of bio-based materials prepared from agricultural sources and applied in agricultural engineering

Despite the increasing innovation and development of bio-based materials from agricultural resources and for agricultural production applications that have been demonstrated in recent decades in China, the industrialization of related products started relatively late and is unbalanced, leading to relatively few applications in the agricultural field and weak international competitiveness. Currently, China faces a few challenges in the formulation and planning of national policies, the platform construction of basic research and infrastructure, personnel training, and the industrial application of agricultural engineering and interdisciplinary development. To address these challenges, we need to focus on building high-end research teams and research platforms, promoting interdisciplinary research, accelerating the establishment of a collaborative pilot test sharing platform, transforming basic research into real industrial productivity, improving mechanical properties and degradation properties, and reducing costs to meet market demand for "bio-based zero-carbon" new materials (Figure 5).

To further strengthen our research and development of new bio-based materials, we are supposed to focus on forward-looking research and strategic layout, improve supporting policies and operating mechanisms, and establish product R&D centers and promotion platforms. In terms of key technologies, we may focus on the development of agricultural biomass-based carbon materials, environmentally degradable materials, and nanomaterials. We should also promote the development of 3D printing intelligent manufacturing technology based on agricultural resources and for agricultural applications, promoting the green and low-cost agricultural production and environmental protection. It is important to cultivate and support a forward-looking and exploratory academic research, build a high-level interdisciplinary research platform, improve the overall research and application level, and support the industrial development foundation and the layout of the whole industrial chain for the application of bio-based materials in the agricultural field.

In addition, it is of importance to strengthen basic research and field layout, make breakthroughs in key technologies, and realize industrial applications through technology demonstrations. The basic research of bio-based materials and their application in agricultural production in China is still lagging behind, and breakthroughs are needed in key technical fields to gain independent intellectual property rights for products. To strengthen basic research and field layout, policy recommendations include systematically carrying out basic theory and applied technology research on the core parameters of the biochar preparation process and the structure, properties, and application characteristics of the material. It is also important to focus on the complex characteristics of agricultural waste biomass raw materials, systematically carry out basic theoretical research on the mechanism of agricultural waste biomass components affecting the structure, properties, and application characteristics of nanocellulose. Besides, it is necessary to address technical challenges and product defects in the current process of converting agricultural waste biomass into environmentally degradable plastics, and to promote low-cost production and multi-field applications of bio-based degradable plastics. Finally, it is worth to develop 3D printing materials based on agricultural production waste biomass and its potential high-value product application. The interfacial compatibility between components in composite 3D printing of agricultural facilities and equipment made of biomass and degradable plastics, printing adaptability, and basic and applied research on printing structure functionality are essential to help the development of green and smart agricultural production (Figure 5).

Regarding the research platform layout and hardware facilities construction, there is a need to deepen system reform and increase the construction of interdisciplinary disciplines such as new agriculture and materials. Suggestions include increasing the establishment of new majors in related research fields, developing a national platform for the research and industrial application of bio-based materials, providing more learning and exchange opportunities for relevant experts, establishing an agricultural science and technology innovation consortium or a new research and development institution, accelerating the construction of a national bio-based material industry science and technology innovation center, and carrying out scientific and technological support actions for rural revitalization. Additionally, it is important to strengthen social service such as science popularization, establish a professional service system, and cultivate high-tech farmers.

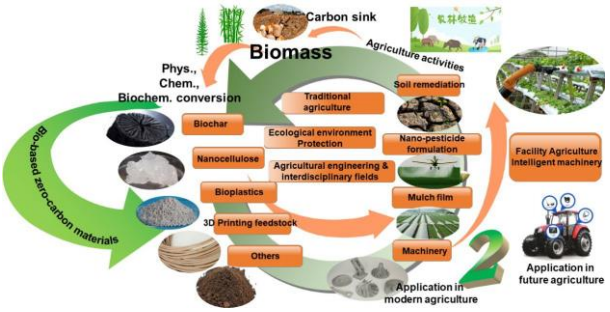

Figure 5. Roadmap for development of bio-based materials from and back to agriculture, and beyond

4. Conclusions

The industrialization of new bio-based materials must align with the country's major development strategies, such as the "rural revitalization" strategy and "green and low-carbon" goals, while achieving economic benefits, production costs, and product value. To achieve this, relevant policies should be formulated, and the core technology system and industrial chain system for the transformation and production of new

green bio-based materials should be improved and built. It is important to break through the bottleneck of core process technology for low-cost production and realize the large-scale production and integration of bio-based material series products. In the field of agricultural engineering, new green bio-based materials have unique advantages and irreplaceable application value in a wide range of fields, and we need to plan the pace of industrialization of new bio-based materials at the national level and promote their large-scale application and promotion in various fields of agricultural production.

References

[1] Chen, D.M.-C., et al., The world's growing municipal solid waste: trends and impacts. Environmental Research Letters, 2020. 15(7).
[2] Liu, J., et al., Current advances and future perspectives of 3D printing natural-derived biopolymers. Carbohydrate Polymers, 2019. 207: p. 297-316.
[3] Amalina, F., et al., Biochar production techniques utilizing biomass waste-derived materials and environmental applications – A review. Journal of Hazardous Materials Advances, 2022. 7.
[4] Shang, H., et al., Heating temperature dependence of molecular characteristics and biological response for biomass pyrolysis volatile-derived water-dissolved organic matter. Science of The Total Environment, 2021. 757.
[5] Klemm, D., et al., Nanocelluloses: a new family of nature-based materials. Angew Chem Int Ed Engl, 2011. 50(24): p. 5438-66.
[6] Liu, J., S. Willför, and A. Mihranyan, On importance of impurities, potential leachables and extractables in algal nanocellulose for biomedical use. Carbohydrate Polymers, 2017. 172: p. 11-19.
[7] Liu, J., et al., Potentially Immunogenic Contaminants in Wood-Based and Bacterial Nanocellulose: Assessment of Endotoxin and (1,3)-β-d-Glucan Levels. Biomacromolecules, 2017. 19(1): p. 150-157.
[8] Yu, S., et al., Nanocellulose from various biomass wastes: Its preparation and potential usages towards the high value-added products. Environmental Science and Ecotechnology, 2021. 5.
[9] Liu, J., et al., Development of nanocellulose scaffolds with tunable structures to support 3D cell culture. Carbohydrate Polymers, 2016. 148: p. 259-271.
[10] Biranje, S., et al., Development of Cellulose Nanofibril/Casein-Based 3D Composite Hemostasis Scaffold for Potential Wound-Healing Application. ACS Applied Materials & Interfaces 2022. 14: p. 1792-3808.
[11] Biranje, S.S., et al., Cellulose nanofibril/polylysine-based 3D composite antibacterial scaffold for wound healing applications. Cellulose, 2023. 30(8): p. 5289-5306.
[12] Menossi, M., et al., Current and emerging biodegradable mulch films based on polysaccharide bio-composites. A review. Agronomy for Sustainable Development, 2021. 41(4).
[13] Serrano-Ruiz, H., L. Martin-Closas, and A.M. Pelacho, Biodegradable plastic mulches: Impact on the agricultural biotic environment. Science of The Total Environment, 2021. 750.
[14] Mahmoud, N.A., et al., Impacts of Biodegradable Plastic on the Environment, in Handbook of Biodegradable Materials. 2022. p. 1-27.
[15] Wang, Q., et al., 3D printing with cellulose materials. Cellulose, 2018. 25(8): p. 4275-4301.
[16] Wang, Q., et al., Cellulose Nanofibrils Filled Poly(Lactic Acid) Biocomposite Filament for FDM 3D Printing. Molecules, 2020. 25(10).
[17] Zhu, Q., et al., Emissions from the fused filament fabrication 3D printing with lignocellulose/polylactic acid filament. BioResources, 2020. 15(4): p. 7560-7572.

Prof. Dr. Jun Liu
Professor
Research Interests:
Biopolymers, Bio-based materials, Environmental Functional Materials

Prof. Dr. Jianzhong Sun
Professor
Research Interests:
Biofuels, Energy Engineering, Biotechnology,
3D printing

Prof. Dr. Huan Liu
Professor
Research Interests:
Cellulose Chemistry, Nanocellulose,
Self-assembly

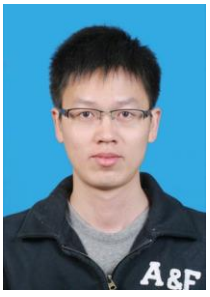

Assoc. Prof. Dr. Qianqian Wang
Associate Professor
Research Interests:
Pulp and Paper Nanocellulose,
Environmental functional materials

Dr. Hua Shang
Assistant Professor
Research Interests:
Biofuels,
Biomass,
Biochar

Reasons and Ripples of China's Population Decline

Tianhong Yang

Guangxi University, No. 100 Daxue Road, Nanning, 530000, P.R. China e-mail:1576202077@qq.com

Abstract: In 2022, census showed that China's population registered its fist negative growth for the past 61 years. And the yearly number of births has been going down since 2016. This demographic trend may come across as shocking because China is flourishing in economy, culture, technology and many other aspects and has rolled out a three-child policy. But, that is what's going on in this country. The similar situation has happened or is also happening to countries like Japan, South Korea, and Russia. By digging into the fall of China's population and its ripple effect through literature study and a survey, this paper finds that the contradiction between people's increasing expectation for their future generations and their economic strength is the major contributing factor. The ripple effect of this phenomenon is "consumption downgrade" across the nation.

Key words: China, population, demographic trend

1. Introduction

1.1 Background

While China is presenting itself on the international arena as a strong power with ever-growing economic prosperity, political clout, and technological advancements, its demographic statistics seem to show the opposite. The birth rate has started dropping since 2016 and was finally be outrun by the death rate in 2022, which led to a record-breaking population decline after 60 consecutive years of positive growth.

Before we go any further into this subject, we should have a look at some statistics and figures.

For starters, we need to be clear of the economic development pace of China since its founding in 1949.

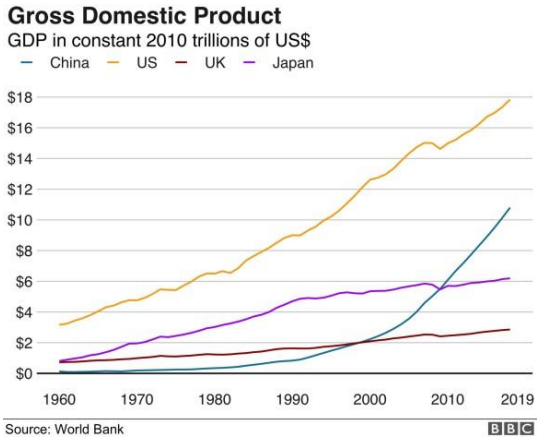

Fig 1 GDP Growth Trend from 1960 to 2019 in China

The lie chart in Fig 1 from World Bank shows GDP growth of four big economic powers, China, US, UK and Japan to make a comparison. From the chart, we can see that China's economy has been developing with great momentum since the 1980s when China started its reform and opening-up. In the beginning of the 21st century, China acceded to WTO and thereby its GDP started to grow at a surprisingly rapid pace. In 2011, China's economy jumped to the second place globally. While China's GDP is lower than that of US, China comes on top when it comes to the growth rate defined by the slope.

Now, let's dig into the demographic changes of China during this period.

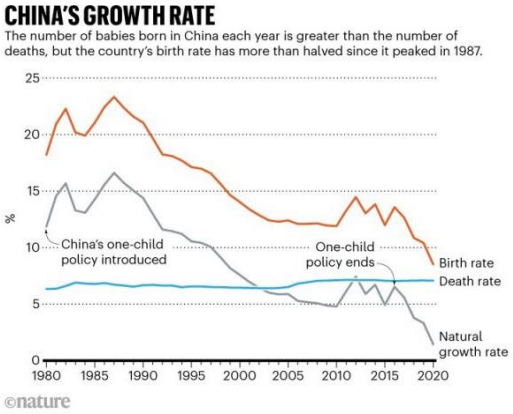

Fig 2 Population Growth Rate Trend from 1980 to 2020 in China

Considering China's economic boom, it's natural to assume that the population growth will follow that trend. Yet statistics show the opposite. It's understandable that the first birth rate drop started in the 1980s since China rolled out the one-child policy in the late 1970s whereas it seems unnatural that the birth rate kept dwindling and has even been slumping since 2016 when the government ended the one-child policy and encouraged people to have two babies, not to mention that the three-child policy has been carried out since 2021.

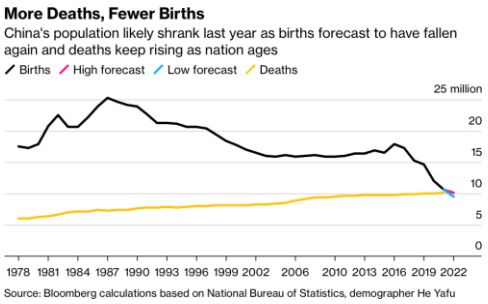

Fig 3 Number of Newborns and Deaths from 1978 to 2022 in China

In this line chart which put the birth rate and the death rate together, 2022 was the year when the death rate exceeded the birth rate for the first time, a phenomenon also know as population decline. In 2022, China's population was down by approximately 850,000. The downward trend is projected to continue this year since the birth rate is even lower than 2022.

China current demographic situation reminds people of what has happened to Japan and South Korea, another two economic powers in Asia, a continent where most countries are underdeveloped.

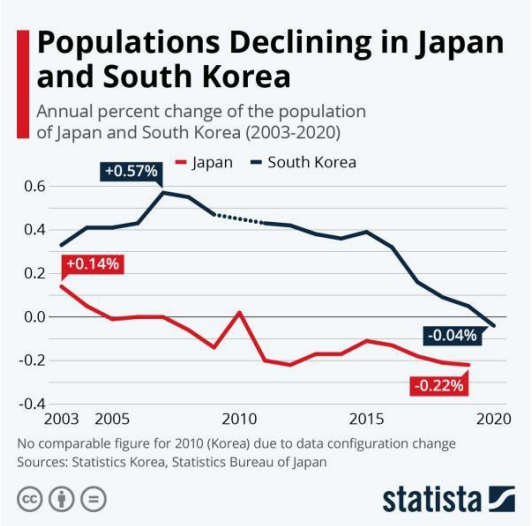

Fig 4 Populations Declining in ROK and Japan from 2003 to 2020

From Fig 4, it's not hard to tell that Japan's population has clocked up continuous declines since as early as 2008 except for an unexpected increase in 2009. South Korea, one of the few developed countries in Asia, its depopulation appeared in 2021 when its GDP per capita was twice that of China.

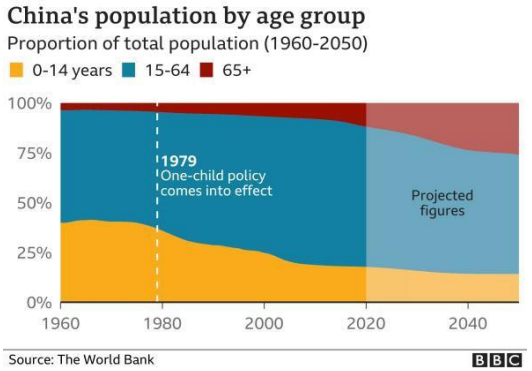

Fig 5 China Population Structure Changes from 1960 to 2040

The chart in Fig 5 reveals a more daunting fact, namely, population aging, as the population structure has clocked up an ever-increasing share of elders for years running, which has become more conspicuous since the 2010s and has hit Japan way ahead of China.

1.2 Meaning of this Essay

This essay will explore the reasons of the drastically dropping population and dig into its ripple effects in various aspects. And in the end, I will offer some inputs in how to approach this issue based on my survey and my reflections.

It goes without saying that at the heart of China's population growth dilemma is fertility rate, or fertility desire, to be more specific.

Yet, to be fair, the reality is far more complicated with a myriad of factors to be taken into consideration, such as ideological progress, feminism, gender antagonism, social advancement, economic downturn, unemployment, individualism, environment inclusiveness, etc.

This essay will sift out the major factors and discuss to what extent they contribute to China's population decline and how we make of and respond to it.

2. Methods

The whole essay is finished based on literature research complemented with a

questionnaire, data from official organizations or websites, and reasoning.

The questionnaire aims to carry out a survey on the fertility willingness of people divided by gender, locality, and income rungs. The respondents are aged from 18 to 40, most from 18 to 25. Therefore, the results can reflect the though of youngsters nowadays. It will probe into the factors that bother people when it comes to matrimony and procreation.

I will combine data released by official websites and previous papers in major journals to guarantee the authenticity and reliability of this essay.

3. Results and Discussions

3.1 Marriage and Divorce

Unlike their elder generations, young people nowadays don't see marriage as a necessary thing or consider divorce a shame, thus leading to a higher divorce rate and an ever-decreasing marriage rate.

According to a report issued by the Ministry of Civil Affairs, the marriage rate of China has fallen to 4.8‰ after straight declines from 9.9‰ in 2009 while the divorce rate went up to 3.1‰ in 2020 from 0.96‰ in 2000. The drop of divorce rate only came to a halt after the proposal of a cool-off period before an divorce officially went into effect in 2021.

And by the traditional values of most Chinese families, it is improper to have babies when one is not in a marriage, which results in a shocking number of abortions in the wake of premarital pregnancy.

Statistics released by National Bureau of Statistics of China reveals that 2022 saw some 9.75 million abortions in this country while the number of births was merely around 9.5 million. More pitifully, more than half abortions happened to young women aged below 25.

However, conventions are just partly responsible for the abortions or the dwindling birth rate of China. About 76% of the respondents of my questionnaire choose not to have kids as shown in the chart below. Most of the respondents age from 18 to 30.

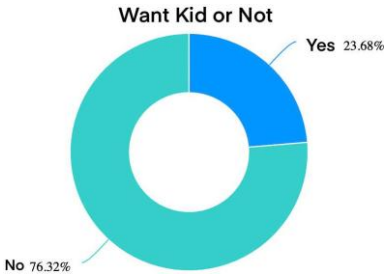

Fig 6 Young People's Willingness of Having Kids

3.2 Contributing Factors to People's Unwillingness of Having Babies

Today, since young people refuse to be defined by traditional conventions, they will not just get married at a proper age and have kids as their parents expect from them. Yet the reasons for not having kids vary from person to person.

Now I will conduct an analysis by combining the results of my questionnaire, phenomenon in real life, and official statistics.

The following pie chart shows the proportions of people who incline not to have babies for different reasons.

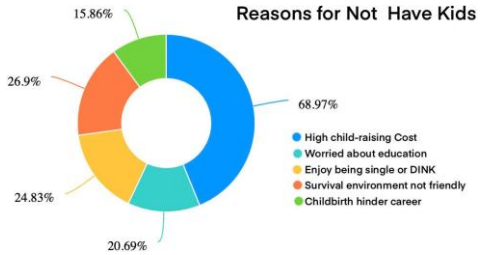

Fig 7 Reasons for Not Having Kids

3.2.1 High Cost of Raising A Child

The cost of raising a child has always been a concern in the spotlight. A report issued by YuWa Population Research shows that in China, the average cost of raising a child till she or he graduates from college is around 627,000 yuan, 6.9 times the country's per capita GDP, which double that of Germany and triple that of France, making China a country of the highest cost of raising, second only to South Korea. Even if one starts working at 18, it still costs their parents 485,000 yuan to bring them up to this age.

In my questionnaire, the results say that in general, 68.97% of the respondents tend to have no kids because of the high cost of raising a child.

To raise a child well means you have to guarantee their basic needs, invest in education, and do everything possible to make sure they have a promising future.

In China, the primary cost for raising a child lies in the purchase of house, which is closely connected to medical, educational, and transportation resources. However, China's skyrocketing housing prices can be intimidating.

Let's take Beijing for example. From 2012 to 2020, Beijing's housing prices quadrupled while its average salary only doubled from 36,000 yuan to 75,000 yuan. Do the math and you will find that 40-year average salary equals to the total price of a 90-sqaure-meter house in the suburb region. In other words, an ordinary couple, without family support, must spend all their 20-year salary on buying a house, which is impossible considering their basis living needs. Things are the same in the small cities, just not so harsh.

In other words, though the national economy is moving forward, the young people now are facing greater difficulties in buying houses.

The second largest child-raising expenditure is education. Since Chinese society become highly competitive thanks to its rapid development, Chinese children can't lag behind since their birth. Therefore, just like out of herd behavior, almost all parents choose to do everything possible to offer their children educational resources as best as they do, such as buying district houses, vying for quotas into the best local schools from kindergarten to 12th grade, signing up for extracurricular, and hiring well-educated tutors. This long process costs a large amount of time, energy, and money.

To sum up, no matter one stays in metropolises or small towns, most people are facing the same dilemma where their income cannot support a decent that they desires, not to mention with children.

3.2.2 Preference for Single Life and DINK

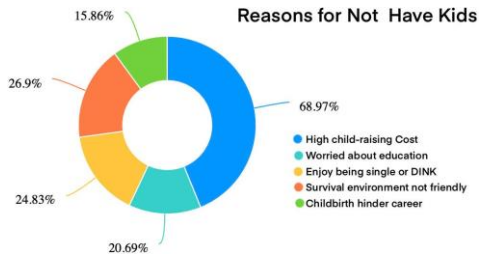

Fig 8 Reasons for Not Having Kids

Approximately one quarter of the respondents prefer single life or DINK compared to a family life with children.

The old Chinese philosophy of "raise children against aging" seems to be not persuasive for Chinese young people today. Statistics will tell us the truth.

According to the Seventh National Population Census of China conducted in 2020, the average size of a family household wa 2.62 persons then, which suggested that many households are DINK, namely, a married couple with no children. Also, in accord with a study aimed to assess the fertility intentions of young people in China, the number of DINKs in China has exceeded 600,000, that is to say, each one out of ten women may choose DINK.

Moreover, Yearbook 2022 issued by National bureau of Statistics of China showed that as of 2021, there were some 239 million single young people above 15, accounting for 14.6% of the total population.

The trend can be attributed to a more functional society in elder care and a more developed lonely economy.

3.2.3 Impact of Having Children on Career

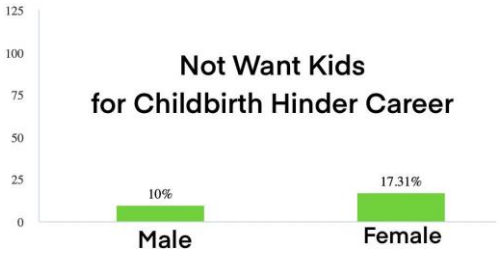

Fig 9 Not Have Kids for Better Career Development Divided by Gender

When we compare the choices of female and male respondents, it's clear that females have more misgivings about the impact of having children on their career development.

Naturally, women are more involved in the process of having a baby, from duration of pregnancy to child birth, from breast feeding to daily care, which leads to enterprises' preference for male candidates in recruitment, not to mention the risk of being dismissed when a women gets pregnant.

Report of Women's Career 2023 in China issued by YuWa Population Research shows as of 2022, only 13.8% of board directors in China's enterprises business world are female. In others words, women are under-represented among senior officials in the business world.

In current cutting-throat world, having children or being pregnant will render a

woman much less competitive than her male counterpart in the working place. And as women are getting better-educated, they incline to rely on themselves and thus have a better control of their life. Therefore, a child will only come as a hindrance or burden instead of joy or hope.

3.3 Ripple of Population Decline

The population decline didn't come without consequences, especially the negative ones. All these factors lead to an undesired sweeping phenomenon - "consumption downgrade" among the young people on individual level.

Since the population decline is resulted from a decreasing birth rate, China's demographic dividend has been gradually shifting to a demographic deficit, demonstrated in total population, unfavorable demographic structure (an aging society), gender imbalance, and insufficient human capital. Consequently, the labor market and the overall economy is registering a stagnant sign, where youngsters are having a hard time landing jobs with a decent salary and enough leisure time.

The consumption downgrade is reflected in various industries.

First, young people are more cautious about buying houses, resulting in a downturn in the real estate market.

For example, according to China's National Bureau of Statistics, in October of 2023, the selling prices of houses in first-tier cities of Beijing, Guangzhou, and Shanghai fell by 0.4%, 0.7%, and 0.5% that last month. Things are the same for second-tier and third-tier cities. The investment in real estate development dropped by 9.11% in the first three quarters of 2023, sales area by 7.5% and newly constructed area by 23.4%. What's more, Fitch Ratings issued an report that projected approximately a 5% decrease of housing sales in 2024.

Second, young people are paying more attention to cost-effectiveness and utility in their consumption behavior.

That explains why Mixuebingcheng, a national chain brand that sells low-priced fresh ice cream and tea and Luckin Coffee, a Chinese coffee brand that sells comparatively cheap coffee drinks are gaining great popularity among the young.

Another example is "Special Forces-style Tourism", which refers to a new trend among young people to visit as many attractions and try as much delicious food as possible while spending the least amount of time and money.

Having realized a lower purchasing power of the money they earn, young people are doing everything possible to make every penny count.

4. Conclusions

Combining the questionnaire results and statistics from authoritative institutions, the author has two findings.

First, the major contributing factors to China's population decline are a high child-raising cost, the change of young people's attitude towards marriage, and impact of childbirth on women's career development.

Second, the ripple effect in wake of the population decline is "consumption downgrade" among the young people in a wide range of aspect.

This paper still has some shortcoming due to insufficient samples and a lack of field survey. Demographic changes have a bearing the national interests in many ways, thus it deserves to be delved into. We still have more work to do in this regard.

References

[1] Kim, H.W., Kim, S.Y. Gender differences in willingness for childbirth, fertility knowledge, and value of motherhood or fatherhood and their associations among college students in South Korea, 2021. Arch Public Health 81, 110 (2023).

[2] Feng Wang, China's Population Destiny: The Looming Crisis, BROOKINGS, 2021.

[3] Riley, Nancy E. "China's population: new trends and challenges." (2004).

[4] 乔晓春.从"七普"数据看中国人口发展、变化和现状[J].人口与发展,2021,27(04):74-88.

[5] 王广州.新中国 70 年:人口年龄结构变化

与老龄 化发 展趋 势 [J]. 中国人口科学,2019(03):2-15+126.
[6] 张鹏,施美程.从人口红利到人口负债：新发展阶段人口转型问题研究[J]. 江淮论坛 ,2021(06):20-27+82.DOI:10.16064/j.cnki.c n34-1003/g0.2021.06.003.
[7] 茆长宝,穆光宗.国际视野下的中国人口少子化[J].文化纵横,2018(04):16.
[8] Beijing's average income changes over the past decade: https://baijiahao.baidu.com/s?id=1745314755788910379&wfr=spider&for=pc
[9] Data of child-raising cost and women's career status: http://yuwa.org.cn
[10] Beijing's housing prices changes over the past decade: https://zhuanlan.zhihu.com/p/221809466
[11] Data of housing prices drop: https://www.stats.gov.cn
[12] Yearbook 2022: https://www.stats.gov.cn/sj/ndsj/2021/indexeh.htm

Mr. Tianhong Yang
Master student, Master of Interpreting (E-C).
Research Interests: Translation and interpreting.

A method of seedling conveying and picking for automatic transplanter

Yao Mengjiao[1], Hu Jianping[1*], Wang Lianghui[1], Yue Rencai[1], Liu Wei[1]

[1] College of Agricultural Engineering, Jiangsu University, Zhenjiang, China
**Corresponding author, E-mail: hujp@ujs.edu.cn*

Abstract: In view of the complexity of the seedling tray conveying positioning device of the existing automatic transplanter with problems of high injury rate, low accuracy of the conveying positioning, taking other seedlings when picking the designated seedlings and the complex motion trajectory of the seedling conveying and picking. To solve these problems, a row of spaced seedling picking claws and supporting seedling tray conveying method were designed to efficiently pick seedlings at intervals without dragging out or damaging other seedlings in the seedling tray, simplifying the mechanical structure and movement. The device combined transversally conveying seedling trays and longitudinally moving to pick seedlings to enable the continuous action. The 72-hole seedling trays were used for seedling tray conveying positioning and seedlings picking. The results showed that the faster the motor pulse frequency, the larger the positioning deviation hence the coefficient of variation. The max deviation was 1.2 mm at a motor pulse frequency of 800 Hz, which was still within the range. The success rate of seedling positioning was 100% with different transmission speeds, and the average rate of picking seedlings successfully was 97.75%, meeting the requirement of accurate picking. The results in this paper provide technical support for the efficient cooperation of seedling tray conveying and seedling picking for automatic transplanter

Keywords: Automatic transplanter, Seedlings, Conveying, Picking, Deviation.

1. Introduction

In China, the annual planting area of vegetables is kept at more than 23.33 million hectares, and the annual yield of the vegetables is more than 800 million tons. Vegetable production provides a primary income for farmers (Xin et al., 2022). In terms of the planting area and yield of the vegetables, China produces and consumes the most vegetables in the world. However, the level of mechanization of the national vegetable industry, especially during planting and harvesting, is still quite low when compared with European countries (Cui et al., 2020; Yu et al.,2014). Currently, most transplanters in the market are semi-automatic, and the seedlings need to be manually divided and fed, and then planted by the semi-automatic transplanters. It still cannot liberate human labor and fail to solve the problem of domestic labor shortage (Chen et al., 2005). Developing full-automatic transplanters is beneficial to solve the problem of artificial planting labor intensity, low production efficiency which is widely considered at home and abroad is the main trend and direction of crop seedling transplanting mechanization development (Han., 2014).

Seedling tray conveying and seedling picking are two key parts which need to be coordinated of the full-automatic transplanter different from the semi-automatic transplanter (Wang et al., 2021). Foreign automatic machines are more automatic (Rahul et al., 2019; Frasconi et al., 2019), including Europe, the United States and Japan. Flying Shuttle company in Netherlands (Davood et al., 2020) produced PC21 automatic transplanter combining machinery and electricity and controlling all the actions one by one, so the structure is huge and complex. (Khadatkar et al., 2018) produced a TEA XP404N tea socket tray transplanter in the United States adopted a folding transport platform, which fully saves space while is relatively complex in structure. PF2R automatic transplanter produced by Yama in Japan (Sun., 2019) was fully automated by the mechanism and transmission pair, the path of the picking seedlings was realized by hard limit on the mechanical surface, which had low accuracy and poor adaptability. Especially, automatic transplanters of these countries are used with the special seedling tray which does not match the domestic seedling tray and cannot be used directly in china (Yang et al., 2018).

For conforming to the common seedling tray in China, the researchers have had preliminary results, while due to the complex technology of automatic seedling tray conveying and seedling picking, the research in China is still in the laboratory stage (Song et al., 2016; Xue et al., 2013). The existing relevant technologies are mainly divided into three categories, which are mobile tray-fixed claws, fixed tray-mobile claws and mobile tray-mobile claws (Wang., 2022). Most researchers adopt the way of mobile tray-fixed claws. (Zhou et al., 2015) designed an automatic transplanter which used two stepper motors to control the horizontal and longitudinal movement of the conveying device. The manipulator was fixed, and the mechanical connecting rod was coordinated to picking the seedlings at fixed points. A seedling picking device of a transplanter (Qiu et al., 2012) that was fixed and it provided the seedlings with transverse and longitudinal movement of the seedling tray conveying device, the bearings and ratchet mechanism were used for seedling tray positioning and this method was complicated and with errors. Both of them used a single claw to pick seedlings which had low efficiency. A new machine which conveyed the seedling tray with transverse and longitudinal motion was designed (Hu et al., 2018), the seedling picking device was fixed and pick seedlings in rows, which greatly improved the efficiency of the machine. The automatic conveying device of transplanter (Yang et al., 2013) placed the seedling tray vertically and located the seedling tray with the positioning sensor, the device tops out a whole row of the seedlings for transportation which is different from others. Some researchers adopt the way of fixed tray-mobile claws, the whole row of seedling picking device which drove the whole row of claws with the liner module to move in the longitudinal and vertical direction (Li et al., 2019). The seedling tray of an adjustable seedling throwing device is stationary, and the manipulator driven by horizontal and vertical transmission components was used to take and throw seedlings in rows (Tian et al., 2023), while a disk changing mechanism was still needed for continuous working. Few researchers adopt the way of mobile tray-mobile claws, the transplanter for pot seedling (Han et al., 2016) conveyed the rows of target seedlings with motor driving, the motor drove the liner module to control the picking claws with lateral displacement, it has high efficiency while the structure is complex.

These methods have advantages and disadvantages, however, duo to the low efficiency of single picking claw (Ma et al., 2019; Wei et al., 2016), the method of whole tray picking has gradually become a major research direction. Most transplanters are mainly controlled by mechanical

transmission, some of them use electrical control for seedling tray conveying and seedling picking (Wang et al., 2019; Zhou et al., 2018), electro-hydraulic control system is a major research direction. In the development of the automatic transplanters, it is of great significance to increase the efficiency of the machine by improving the method of seedling tray conveying and seedling picking.

Our team has done relevant research in this aspect, a system designed can perform position compensation by a slight increase button and a slight decrease button (Fei., 2019), thus eliminating positioning errors of the seedling trays. Nevertheless, when the system was in use, manual calibration was still needed, multiple complex buttons were adopted, and the problem that other seedlings in the seedling tray were likely to be dragged out or damaged within a return stroke of horizontally extracted seedlings was not taken into consideration. A device and method disclosed for automatically extracting and dropping seedlings for a transplanter (Yang et al., 2018; Liu., 2020). The device could extract seedlings in a row without an interval. In spite of that, the device had seedling distribution parts spaced by a larger distance and performed seedling dropping after seedling picking claws were dispersed. As a result, the action and complexity of the seedling picking claws were increased. A system for extracting seedlings in a row at intervals and dropping the seedlings in turn of a potted seedling transplanter (Luo et al., 2020). The seedlings in a column can be all extracted at intervals for two times. However, the device was singly driven by an air cylinder, resulting in poor stability. Furthermore, the device needed six seedling picking claws and a rotary type seedling distribution mechanism, resulting in structural complexity of the transplanter.

To solve the problem of taking and injuring the remaining seedlings during the process of picking seedlings back and forth, a special control method of seedling conveying was adopted to pick seedlings in row and intervals. In addition, to simplify the operation steps and improved the operation efficiency, a special control method of picking seedlings was used to complete the performance of picking seedlings through the straight and back movement of fixed-point positioning. This paper stated with four sections, firstly introduced the context, issue relevance and objective, then recommend the structure of the device, the methods of control system and the experiments, afterward analyzed data and discussed why did the results, finally concluded this paper and pointed out what can be studied more.

2. Materials and methods

2.1. Structure of the seedling tray conveying device and seedling picking device

2.1.1 Seedling tray conveying device

Seedling tray conveying device is a vital part of an automatic transplanter for conveying continuously and positioning precisely. In this paper, it was mainly composed of one stepper motor (86BYGGH450B), one motor driver (DP-504), 12 push rods, 2 drive chains (08B), 2 photoelectric sensors and one bench, and driving shaft, driving wheel, conveying chain, driven shaft, driven wheel, tensioning device (Fig.1). There were two parallel conveying chains installed on both sides of the platform, and fixed push rods with equal intervals were connected between them. The tray could be stuck on the push rod by an inverted V clearance. The stepper motor was used to transfer the power to the driving shaft through the drive chain, then the driving wheel drove the conveying chain for translational movements which push the rods forward and convey the seedling tray towards the position of the picking claw. The photoelectric sensors were used to sense whether the seedling tray was in place. The tensioning device was used to keep the conveying chain tensioned and ensure the conveying accuracy.

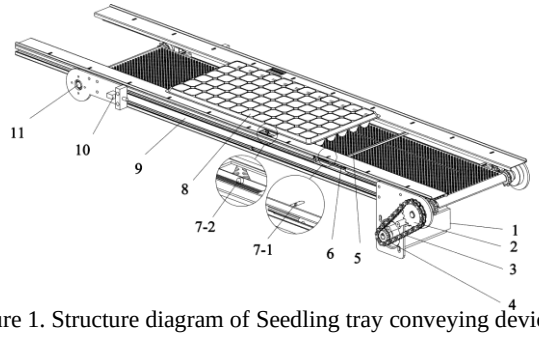

Figure 1. Structure diagram of Seedling tray conveying device
1. Stepper motor 2. Driving wheel 3. Drive chain 4. Driven wheel 5. Conveying chain 6. Push rod 7-1. Sensor 1 7-2. Sensor 2 8. 72-hole seedling tray 9. Frame 10. Tensioning device 11. Driven shaft

The stepper motor conveyed the seedling tray forward from the starting position, so that the front of the seedling tray could be induced by sensor 1 (7-1), the push rod continued to push the seedling tray forward, so that the closet rod to the front of the seedling tray can be induced by sensor 2 (7-2). According to the two position values induced and the structural parameters of the conveying device, the system could accurately calculate the displacement that could convey the seedling tray to the seedling-picking position (Yao et al., 2023).

The length, width and height of the 72 holes seedling tray are 540, 280 and 45mm respectively. It has 12 lines and 7 columns and the center distance is 42.3mm, the upper caliber is 40mm×40mm, the down caliber is 20mm×20mm.

As is shown in Fig.2, the seedling tray matching the automatic transplanter is 72 holes (12×6) which center distance is d. To ensure the push rod can be accurately stuck into the inverted V-shaped gap of the seedling tray, the distance S between two push rods have to be an integral multiple of d which is S=n×d. S is also the integral multiple of chain pitch P because the push rods are connected with the chain which is S=m×P. The center distance of 72 holes tray is d=42.3mm, 08B chain was used in this device which the chain pitch is P=12.7mm, so the common multiples of d and P was taken as the distance between two push rods which was n=3, m=10, S=127mm. The stuck position of the rods was lower than the height of the hole which can match the arrangement of seedling tray according to the trapezoidal size of the hole. In the picture, D is the diameter of dividing circle of wheel.

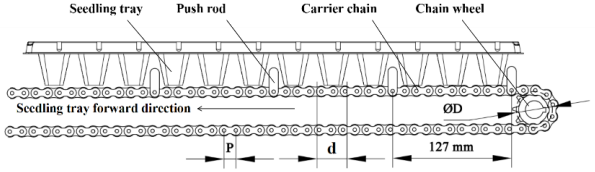

Figure 2. Dimensions of seedling tray and seedling tray conveying device

2.1.3 Seedling picking device

The automatic seedling picking device is significant to picking and throwing the seedlings and especially cooperates with the seedling tray conveying device. This part with bidirectional motion in rows has the function of picking the seedlings from trays and throwing the seedlings to the guiding tubes for planting. The device was mainly composed of one steeper motor (86BYGGH450B), one motor driver (DP-504), 2 picking claws assembly, drive chain, lifting cylinder, telescopic

cylinder, linear slide rail and one zero sensor (Fig.3). The picking claws assemblies were installed on the horizontal straight slide rail which can be driven by stepper motor to realize picking seedlings when merged and throwing seedlings when dispersed.

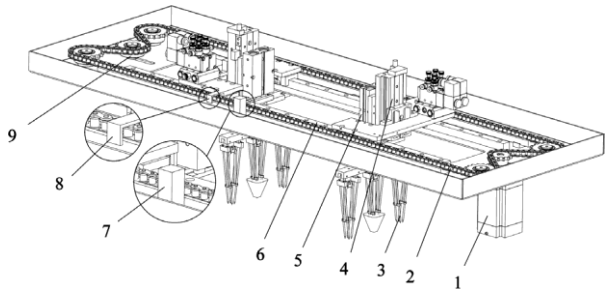

Figure 3. Structure diagram of Seedling picking device
1. Stepper motor 2. Drive chain 3. Picking claws assembly 4. Lifting cylinder 5. Telescopic cylinder 6. Linear slide rail 7. Zero sensor 8. Sensor trigger device 9. Tensioning device

In order to prevent picking seedlings with adjacent holes, the distance of the picking claws was two grid holes, so as to realize the whole row of spacing picking with 3 seedlings one time. The motor drives chain with two picking claws assemblies on both sides was used to take the seedlings at the same time, so it could take 6 seedlings at a time.

2.1.3 Coordination of seedling tray conveying and seedling picking

After finishing picking, the seedling tray conveying device had transported to ensure the holes with seedlings were conveyed to the picking position. Therefore, it was very significant for the seedling conveying device and seedling picking device to coordinate. As is shown in Fig.4, the seedling conveying device transmitted the tray transversely and the seedling picking device drove the claws longitudinally.

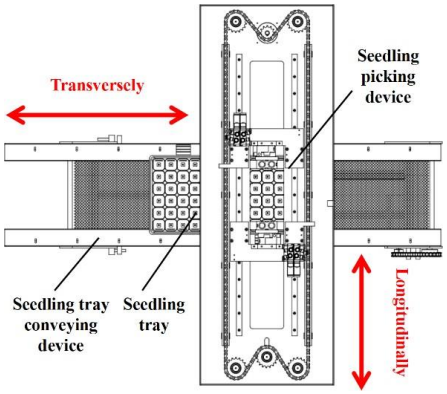

Figure 4. Schematic diagram of two devices

In order to prevent the claws moving with other seedlings which were not target seedlings, it was designed to take the outside of the seedling tray. From the longitudinal direction of the seedling picking, the both outside of the tray were the first column, and inside were the second and the third successively which is shown in Fig.5a. From the transverse direction of the seedling conveying, the picking claws were the first, the second and the third successively which is shown in Fig.5b. The picking position was where the middle of the first line aligns with the third picking claw. As the Fig.6 shown, the claws were picking the seedlings in the first column, the picking claws assemblies merged above the tray to take the seedlings, and then reversed above the guiding tubes to throwing the seedlings, after picking all the seedlings in the first column, the assemblies moved to the second column to do the round-trip motion.

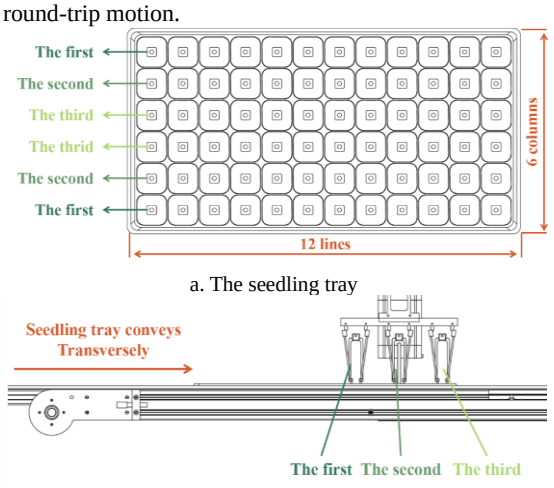

a. The seedling tray

b. The picking claws

Figure 5. Description of the seedling tray and picking claws

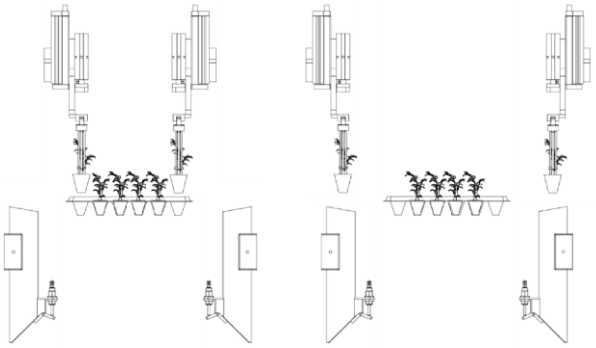

a. Picking the seedlings b. Throwing the seedlings

Figure 6. Operation diagram of seedling picking and throwing

The steps of the seedlings conveying and picking were as follows: When the seedling tray was conveyed to the picking position, the two picking claw assemblies moved to the first column to pick 6 seedlings as Fig.7a. Then the device transmitted a distance of one line more to supply new seedlings, after throwing the seedlings for planting, the picking claw assemblies moved back to the first column to pick another 6 seedlings as Fig.7b. So, the half seedlings of the first column had been picked, the seedling conveying device had to transmit a distance of 5 lines more, after the seedlings picking and throwing, the tray was conveyed one line more so that the first column was picked all. The seedling tray was reversed to the initial picking position, the picking claws assemblies moved longitudinally to the second column, so as to pick the seedlings with the seedling tray conveying device transmit one line, five lines and one line. The third columns were as the follows.

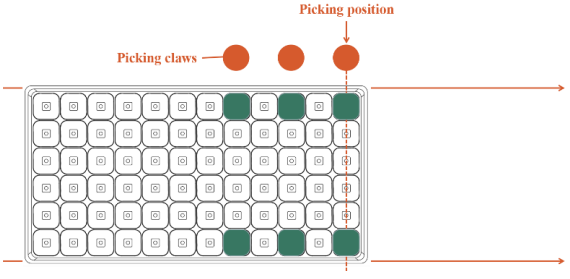

a. Picking the first time in the first column

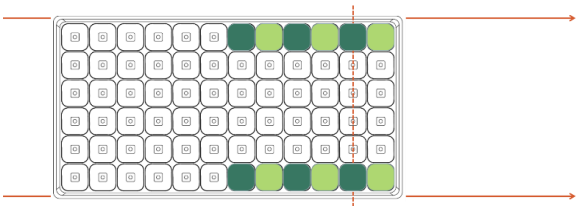

b. Picking the second time in the first column

Figure 7. Steps of the seedlings conveying and picking

2.2 Design of the control system

2.2.1 Control system hardware

The control system of seedling tray conveying and seedling picking is shown in Fig.8, which was mainly divided into signal input module, control processing module, driver execution module and power module. In the seedling tray conveying part, there were 2 photoelectric sensors, 1 stepper motor and 1 motor driver used to induct the information of the seedling tray. And 1 photoelectric sensor, 4 electromagnetic sensors for cylinders, 1 stepper motor and 1 motor driver were needed in the seedling picking part, the photoelectric sensor was for sensing the zero point where was the middle of the device, the electromagnetic sensors were fixed on the cylinders to detect the position of the piston in the cylinders. The cylinders were used to control the picking claws assembly to move down and stretch the seedling needles which driven by solenoid valves. The system was powered by the accumulator.

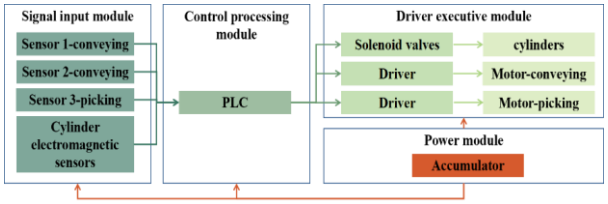

Figure 8. The control system of seedling tray conveying and seedling picking

Selecting the components was very significant, among them the controller is the most vital which is satisfied for calculation and distribution of inputs and outputs. As is shown in Table 1, the selected PLC must have 6 inputs and 6 outputs, the XD5-24T3 model was selected.

Table 1 PLC I/O table

Input		Output	
X0	Photoelectric sensor 1 for conveying	Y0	Pulse of seedling conveying motor
X1	Photoelectric sensor 2 for conveying	Y1	Pulse of seedling picking motor
X2	Zero point of seedling picking part	Y2	Direction of seedling conveying motor
X3	Upper limit of seedling picking	Y3	Direction of seedling picking motor
X4	Lower limit of seedling picking	Y4	Cylinder 1 for seedling picking
X5	Middle position of seedling picking	Y5	Cylinder 2 for seedling picking

2.2.2 Control system software

The software flowchart of this control system is shown in Fig.9. It is mainly composed of two parts which are seedling tray conveying and seedings picking.

When it starts the picking time N1 is 0 which will add 1 until finish picking 6 seedlings and the picking column N2 is 1 initially that means the picking claws will pick the outside 2 columns first which named the first, and when the first column is picked over, it will move to the second column to pick other seedlings. One column has 12 seedlings, the picking claws can take 3 seedlings one side per time, so the picking time per column is 4 when the N1 will be clear to 0. The seedlings tray has 6 columns total and 3 columns per side so that the whole tray is picked over when the N2 is 3 and it is needed to convey a new seedling tray.

The method of seedling tray conveying is introduced before and after the first or the third picking time, the conveying device has to transmit one line more to supply new seedlings. After the second picking time, the device has to convey five lines more, and after the forth picking time, it has to reverse to the initial position and the picking time is return to 0 and recounts with another column.

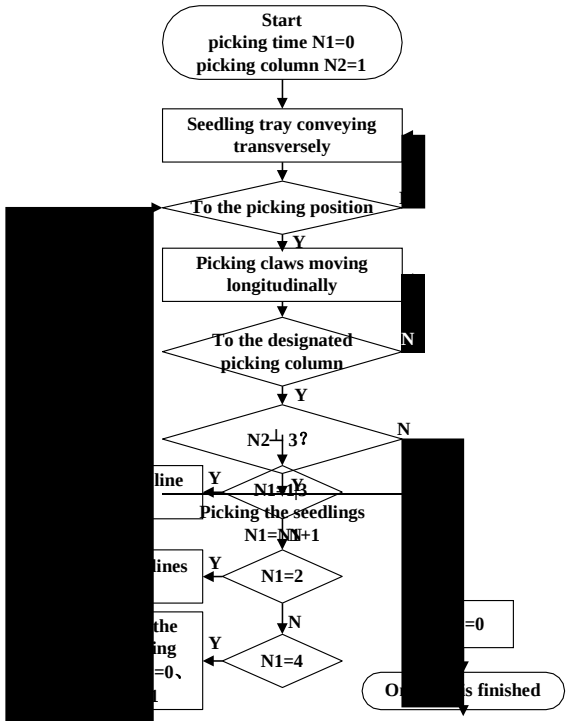

Fig ware flowchart of this control system

2.3 Experiments

2.3.1 Test of influencing factors of accuracy of seedling tray conveying

The orthogonal test was used to verify what is the most important factor for seedling tray conveying. Steel rule and marker pen were used to measure the displacement of seedling tray. Speed, the starting frequency and the acceleration time of the stepper motor are three adjustable parameters for motor performance, so taking them as the orthogonal test factors, the influencing relationships between the three factors were detected. Three levels were selected, in which the speed was designed as 200mm/s, 300mm/s, 400mm/s; The starting

frequency was set as 3000, 4000, 5000; Acceleration time was 1s, 2s, and record the displacement of the seedling tray. According to the selected level, the orthogonal test of three factors was carried out. The table of orthogonal test factors is shown in Table 2.

Table 2 Orthogonal test factors

Level	Speed (mm/s)	Starting frequency	Acceleration time (s)
1	A1(200)	B1(3000)	C1(1)
2	A2(300)	B2(4000)	C2(2)
3	A3(400)	B3(5000)	

2.3.2 Test of prototype

To test the accuracy of seedling convey positioning and picking, an automatic transplanter with this device, steel rule and marker pen were used, the equipment is shown in Fig.10. The seedling tray conveying device is in the middle of the whole machine and located in the middle of the two seedling claw assemblies and two guiding tubes.

Figure 10. Automatic transplanting machine prototype

The seedling tray used in the experiment was standard 72 holes, Pepper seedlings (Jing Line No. 1) cultivated in the seedling house were used for seedlings, the seedling age was 40~50 days and the pepper seedlings had grown to two leaves or three leaves one core, and the seedling height was 150~180 mm. The test site is located in Shiyezhou Test Base, Zhenjiang, China.

The marker pen was used to mark at the picking position, when seedling tray was transmitted on the seedling tray conveying device, marking the arriving position and using steel rule to measure the distance to the picking position. Recording the distance of each forward and backward of the seedling tray and the moving times. The accuracy of conveying positioning of seedling tray was measured by positioning deviation *D*, that was the deviation between the actual stopping position and the theoretical picking position. There were 10 seedling trays used in this experiment, we record 5 data of one tray and take the average value respectively at the motor pulse frequency of 600, 700, 800Hz.

3. Results and Discussion

3.1 Test of influencing factors of accuracy of seedling tray conveying

From the results of the orthogonal test, the response surface diagram of the three factors are shown in Fig.11.

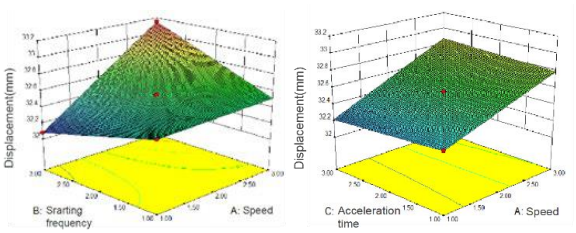

Fig.11 Response surface diagram of the three factors

From the Fig.11, the influence of stepper motor speed to the distance was more significant than that of starting frequency when the motor speed changed from 1s to 3s as the acceleration time increases. The displacement increased with the speed of the stepper motor increasing and also was the starting frequency, while the increasing speed of that was lower than speed. The effect of stepper motor speed to the distance was more significant than that of acceleration time when the motor speed changed from 1s to 3s as the acceleration time increases. The displacement increased with the speed of the stepper motor increasing, while the trend of displacement was relatively flat with the increase of acceleration time. It can be seen that the most influential factor is the speed of stepper motor.

3.2 Test of prototype

After processing, the deviation of the seedling tray conveying positioning is shown in Fig.12.

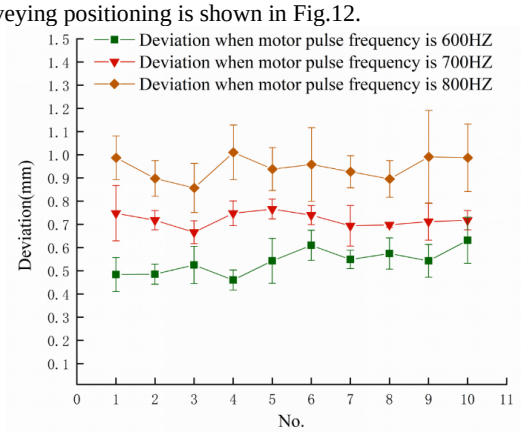

Fig.12 The deviation of the seedling tray conveying positioning

When motor pulse frequency was 600 Hz, the range of the deviation was from 0.4 mm to 0.7 mm and the error bars had the similar length. When motor pulse frequency was 700 Hz, the range of the deviation was from 0.6 mm to 0.9mm, which was higher than 600 Hz. The length error bars varied greatly and the longest was nearly 0.2. When motor pulse frequency was 800 Hz, the range was the highest and from 0.8 mm to 1.2 mm, the errors were maximum. From the picture, it can be seen that the faster the seedling tray conveying, the larger the positioning errors and the coefficient of variation.

The deviation is positively correlated with the speed of the motor, and the error bars of each speed are variable, that is because the parameter of different seedling trays vary a lot in their weights, thickness and edge length, and the errors of each speed are random.

Table 2 Rate of picking successfully

No.	Data				Index
	Seedling trays	Times of moving	Numbers of seedling	Numbers of picking successfully	Rate of picking successfully
1	10	50	720	713	99.03%
2	10	50	720	708	98.33%
3	10	50	720	698	96.94%

4	10	50	720	701	97.36%
5	10	50	720	699	97.08%
Average				603.8	97.75%

As the table shown, each group of 10 seedling trays had the same time of moving forward or backward of 80. There was no tying or interruption during the experiment that means the seedling conveying position was accurate, and in the Fig.14, the max deviation was 1.2 mm which still within the allowance error range of the mechanical structure. So, the positioning accuracy was 100%. While there were 720 seedlings in total, and the average of success rate of picking seedlings was 97.75%, the lowest rate was 96.94%. The success rate of picking seedlings only indirectly validates the positioning accuracy of the seedling tray.

Combined with the rate of picking successfully and the positioning accuracy of the seedlings tray conveying, there were some seedlings in the designated position while not be picked well. This omissive seedlings might be caused by the failure of picking out from the tray which due to poor root-ness of the seedling tray, or the removal of the seedlings due to mechanical vibration during the movement of the claws.

4. Conclusions

In this paper, a transverse conveying device of seedling tray and a longitudinal picking device of seedling were designed. The precise positioning could be achieved by motor driving. The special control method of seedling conveying was adopted to pick seedlings in row and intervals, which effectively solved the problem of taking and injuring the remaining seedlings during the process of picking seedlings back and forth. In addition, the special control method of picking seedlings was used to complete the performance of picking seedlings through the straight and back movement of fixed-point positioning, which simplified the operation steps and improved the operation efficiency.

Taking the speed, the starting frequency and the acceleration time of the stepper motor as the three factors of the orthogonal experiment, it was verified that the motor speed had the greatest influence on the operation of the device. Therefore, the prototype experiment was carried out under different conveying speed, and the positioning error of the seedling tray with this device and methods was smaller than 1.2 mm. The success rate of seedling tray positioning was 100%, while the average rate of seedling picking successfully was 97.75% which was affected by the poor root of the seedlings.

The efficiency of the automatic transplanters was affected by the quality of the seedlings, directly decreased the accuracy of seedling picking, so a detect device can be added before seedling throwing, or focus on seedling cultivation before using the transplanting machines

References

[1] Xin Z.L., Cui Y.J., Yang X.W, et al., 2022. Current situation of global vegetable industry and development path of vegetable breeding in China [J/OL]. Molecular plant Breeding, 1-26.

[2] Cui Z.C., Guan C.S., Yang Y.T., et al., 2020. Research status of vegetable mechanized transplanting technology and equipment [J]. Chinese Journal of Agricultural Mechanization, 41(3), 85-92.

[3] Yu X.X., Zhao Y., Chen B.C., et al., 2014. Development Status and Prospect of Transplanting Machinery [J]. Transactions of the Chinese Society for Agricultural Machinery, 45(8), 44-53.

[4] Chen F., Chen Y.C., Wang W.X., 2015. Current situation and development trend of dryland transplanter [J]. Agricultural Mechanization Research, 24-26. (in Chinese)

[5] Han C.J., 2014. Design and experimental study on automatic Feeding System of Pothole Seedling Transplanter [D]. Nanjing Agricultural University.

[6] Wang N., Ren L., Li J.Q., et al., 2021. Hole tray seedlings transplanting machine automatic seedling technology research status and prospect [J]. Journal of Chinese agricultural mechanization, 59-66

[7] Rahul K, Raheman H, Paradkar V. Design and development of a 5R 2DOF parallel robot arm for 72 handling paper pot seedlings in a vegetable transplanter[J]. Computers and Electronics In Agriculture, 2019,166(C):105014-105014.

[8] Frasconi C, Martelloni L, Raffaelli M, et al. A field vegetable transplanter for use in both tilled and no-till soils[J]. TRANSACTIONS OF THE ASABE,2019,6(2):593-602.

[9] Davood Mohammad Zamani, et al. Development and evaluation of a vegetable transplanter[J]. International Journal of Technical Research and Applications, e-ISSN:2320-8163.

[10] Khadatkar A,Mathur SM,Gaikwad BB.Automation in transplanting: a smart way of vegetable cultivation[J].CURRENT SCIENCE,2018,115(10):1884-1892.

[11] Yang Ma PF2R automatic vegetable Transplanter [J]. Modern Agricultural Machinery, 2019.

[12] Sun N., 2018. Structural Performance, Adjustment, Inspection and Maintenance of Toyang PF455S Hand transplanter [J]. Agricultural Machinery Use and Maintenance, 37.

[13] Song Y.j., Hu J., 2016. Current situation and development trend of dry land transplantation technology in China [J]. Agricultural Machinery, 102-104+106. (in Chinese)

[14] Xue D.Q., Hou S.L., Zhang J.X., 2013. Research progress and development trend of dry land transplantation machinery in Our country [J]. Journal of Chinese Agricultural Mechanization, 34(5):8-11. (in Chinese)

[15] Wang N., 2021. Hole tray seedlings transplanting machine take cast blade control system design and test [D]. Xinjiang shihezi university, DOI: 10.27332 /, dcnki. Gshzu. 2021.000571.

[16] Zhou Y., Sun L., 2015. Design of control system of automatic transplanting machine based on PLC in dry land [J]. Modern Agricultural Science and Technology, 199-200.

[17] Qiu L.G., Yu G.H., 2012. Design and experiment of Vegetable Pot Seedling Conveying Device in Automatic Transplanting machine [J]. Journal of Zhejiang University of Science and Technology, 29(05):683-687+692.

[18] Hu J.P., Chang H., Yang L.H., et al., 2018. Design and experiment of Control System for whole row and interval seeding of Automatic Transplanter [J]. Transactions of the Chinese Society for Agricultural Machinery, 49(06):78-84.

[19] Yang C.H., Fang Z.X., Yang X.J., 2013. Automatic Conveying Device of Vegetable Pot Seedling Transplanting Machine Based on PLC [J]. Transactions of the Chinese Society for Agricultural Machinery, 44(S1):19-23+18.

[20] Li S.F., Lian G.D., Ma X.X, et al., 2019. Design and experiment of the control system of whole row taking and sending seedlings in Transplanter [J]. Chinese Journal of Agricultural Mechanization, 40(12):136-143.

[21] Tian S.B., Xie T., Wang H.J., et al., 2023. Adjustable

feeding seedling device design and test [J/OL]. South China agricultural university press, 1-12 [20230331].

[22] Han L.H., Mao H.P., Hu J.P., 2016, Design and experiment of Automatic Transplanting Machine for greenhouse Hole Plate [J]. Transactions of the Chinese Society for Agricultural Machinery, 47(11): 59-67.

[23] Wei X.H., Bao S., Liu X.K., et al., 2016. Design and Transplanting Experiment of Motion Coordination Control System of Automatic Transplanter with hole Disc [J]. Transactions of the Chinese Society for Agricultural Machinery, 47 (12) :1-7+52.

[24] Ma R., Cao W.B., Ren L., et al., 2019. The design and research of the whole row hole Plate seedling transplanting machine taking and sending device [J]. Agricultural Mechanization Research, 41(04): 85-90. (in Chinese)

[25] Wang J., Zhang H.Y., Jin X., et al., 2019. Design and experiment of Pot Holding Force Detection System for Automatic Pot Transplanting Machine [J]. Chinese Journal of Agricultural Machinery, 50(05):79-87.

[26] Zhou M.F., Xu J.J., Tong J.H., et al.,2018. Design and experiment of integrated Automatic Transplanting mechanism for flower pot-tray plantings [J]. Transactions of the Chinese Society of Agricultural Engineering, 34(20):44-51.

[27] Fei W.Z., 2019. Design and experiment of Control System for Automatic Vegetable pot-plate Transplanting Machine [D]. Jiangsu University.

[28] Yang Q.Z., Xu L., Shi X.Y., et al. 2018. Design of seedlings separation device with reciprocating movement seedling cups and its controlling system of the full-automatic plug seedling transplanter[J]. Computers and Electronics in Agriculture, 147:131-145.

[29] Yang L.H., 2018. Design and experiment of Control System for whole row and interval seeding of Automatic Transplanter [J]. Transactions of the Chinese Society for Agricultural Machinery, 49(6):78-84.

[30] Liu Y.J., 2020. Research on Design and Key Technology of Hanging Automatic Transplanting Machine [D]. Jiangsu University.

[31] Yao M.J., Hu J.P., Liu W., 2023. Positioning control method for the seedling tray of automatic transplanters based on interval analysis[J]. Transactions of the Chinese Society of Agricultural Engineering (Transactions of the CSAE), 2023, 39(4): 27-36.

Characteristics and properties of emulsion-based film coating from chitosan incorporated with carnauba wax

Arthit Dankathok[1], Chanathit Khadsri[2] and, Theeraphol Senphan[3]*
[1]*Program in Food Science and Technology, Faculty of Engineering and Agro-Industry, Maejo University, Chiang Mai, 50290, Thailand*
*E-mail: theeraphol_s@mju.ac.th

Abstract: Plastic pollution harms the environment, generating difficult-to-dispose-of waste. Currently, natural, and edible laminating films are popular alternatives, reducing respiration rates and extending preservation for fruits and vegetables. This research aims to investigate the characteristics and properties of emulsion-based edible film coatings made from chitosan incorporated with carnauba wax at varying concentrations of 0%, 25%, and 50%. The results revealed that the chitosan film incorporated with carnauba wax 50%, exhibited the greatest thickness. Nonetheless, as the concentration of carnauba wax increased in the film, both tensile strength (TS) and elastic modulus (EM) of the chitosan films declined. No significant difference in elongation at break values was observed across all film treatments. Specifically, the chitosan film incorporating 50% carnauba wax demonstrated higher lightness values (L*) and yellowness values (b*) compared to the chitosan film with 25% carnauba wax and control film sample. Therefore, the resulting edible film coating solution can be applied to coat and preserve the quality of fruits and vegetables.

Keywords: Carnauba wax, Chitosan, Edible coating. Emulsion-based film

1. Introduction

In contemporary times, there has been a noticeable surge in consumer demand for packaging, leading to a corresponding increase in the demand for packaging materials, including recycled options. This upswing in demand has, unfortunately, resulted in the accumulation of substantial amounts of plastic in the environment. Simultaneously, heightened consumer concerns regarding food safety have catalyzed the development of biodegradable films. These films, often composed of recyclable synthetic polymers, have gained acceptance due to their cost-effectiveness. Consequently, there is a growing trend towards incorporating natural materials like polysaccharides, proteins, and fats from the biopolymer group into edible films and coatings, aligning with international standards and environmental sustainability [1].

Edible coating refers to a thin layer of edible material applied as a coating on food products. This can take the form of either a solid sheet or a liquid coating achieved by immersing the product in a solution of edible materials. The practice of fruit coating has emerged as an effective means to reduce post-harvest losses and extend the shelf life of produce. The coatings used serve to replace the natural wax layer lost during harvesting or cleaning, closing openings to reduce water loss and gas exchange, thereby preserving fruit quality. Moreover, these coatings enhance the visual appeal of fruits, providing a glossy shine and preventing germ-related damage, particularly on peeled fruits. Edible coatings, as an alternative, have proven valuable in extending the shelf life of cut fruits like pineapples [2]. Pre-cut pineapples typically have a short shelf life due to increased susceptibility to damage during peeling and cutting. Edible coatings mitigate these issues by slowing down respiration rate, inhibiting polyphenol oxidase enzyme activity, and reducing microbial growth, resulting in enhanced shelf life [3]. The development of an edible coating film

specifically designed for freshly cut fruits aims to characteristics and properties of emulsion-based film coating from chitosan incorporated with carnauba wax at different concentration.

2. Materials and methods

2.1 Preparation of emulsion-based film from chitosan

The chitosan film solution was prepared by adapting the method outlined by Afifah, Ratnawati & Darmajana [4]. In this process, 1.5% (w/v) chitosan powder was dissolved in 1% (w/v) lactic acid, resulting in a clear-colored solution. Carnauba wax, incorporated into the solution at concentrations of 0%, 25%, and 30% (w/v) relative to the Tween 80 sample weight, enhanced the film's properties. Specifically, at a concentration of 25% (w/v) of the carnauba wax volume, and glycerol at 30% (w/v) of the sample weight, were added to the film solution. The mixture was stirred until a uniform consistency was achieved, as outlined in Table 1. Subsequently, 15 ml of the resulting solution was carefully poured onto a 9 cm diameter plastic agar plate to form a film. The film was subjected to airflow from a fan at room temperature for 48 hours, followed by incubation in a desiccant jar saturated with magnesium nitrate (maintaining a relative humidity of 50%). Afterward, the films were stored at 25 degrees Celsius for an additional 48 hours in a temperature-controlled cabinet. The resulting films were then systematically analyzed to assess their physical and mechanical properties.

Table 1. Formulas of emulsion-based film coating from chitosan incorporated with carnauba wax.

Carnauba wax (%)	Tween 80 (%)	Glycerol (%)
0	25	30
25	25	30
30	25	30

2.1.1 Analysis of film Thickness.

The thickness of t emulsion-based film from chitosan was gauged using a micrometer (Mitutoyo, Model ID- C112PM, Serial No.00320, Mitutoyo Corp., Japan). Random measurements were taken at five distinct areas on three separate regions of the edible film sheet, with the resultant values being averaged.

2.1.2 Analysis of tensile strength (Ts)

The tensile strength of the chitosan edible coating film samples was ascertained using a Universal Testing Machine (Lloyd Instrument, Hampshire, UK) with a load cell capacity of 100 newtons. Film samples, sized at 2×5 cm², were clamped using a 3 cm long clamp, and the compression head speed was set to 30 mm/min.

2.1.3 Analysis of elastic modulus (EM)

To determine the elastic modulus of the chitosan edible coating film samples, a Universal Testing Machine with a 100 Newton load cell was employed. Similar to the tensile strength test, film samples (2×5 cm²) were clamped with a 3 cm long clamp, and the compression head speed was set to 30 mm/min.

2.1.4 Analysis of elongation at break (EAB)

The film's elongation at break was measured by applying a constant pulling speed to the chitosan edible coating film samples. During the test, tension force changes were recorded as the film stretched, encountering resistance that was measured in kilograms (kg) or newtons (N). The film was pulled until it reached the breaking point, with the maximum resistance reflecting the measured force generated.

2.1.5 Analysis of color

Color values of the samples were determined using a colorimeter, reported as L* (brightness), a* (red/green), and b* (yellow/blue). Additionally, contrast (ΔE*) was measured, following the methodology of Robles-Sánchez et al [5].

2.1.6 Statical analysis

The experiments were carried out in triplicate. The data underwent analysis of variance (ANOVA), and mean comparisons were conducted using Duncan's multiple range test. The T-test was utilized for conducting pairwise comparisons. The analysis was conducted utilizing the SPSS software package (SPSS for Windows, SPSS Inc., Chicago, IL, USA).

3. Results and Discussion

3.1 Film Thickness

The thickness values obtained from the experimental measurements, as presented in Table 2, revealed a notable increase in film thickness when incorporating carnauba wax. Specifically, the film with 50% carnauba wax exhibited the maximum thickness at 0.05 mm, while the minimum thickness of 0.04 mm was observed in the absence of carnauba wax (0% concentration). Based on the experimental findings regarding the analysis of edible coating film thickness, it was observed that Carnauba wax, glycerol, and Tween 80 had a uniform impact on augmenting film thickness when applied to 15 ml plastic plates across all samples. This phenomenon may be attributed to the formation of an emulsion film, influenced by various factors such as film expansion, structural alterations within the film, shifts in the pattern of capture, and a potential loss of bonding properties between bonds. Additionally, factors including experimental controls, the formation of air bubbles within the film, tolerance in sample solution filling in the plate, and the flatness of the sample storage area might contribute to this effect [6].

Table 2. Film thickness of emulsion-based film coating from chitosan incorporated with different concentration of carnauba wax.

Carnauba wax		
0%	25%	50%
0.04±0.002*[a]**	0.05±0.002[a]	0.05±0.001[a]

*Mean ±SD (n=3)
**Different letter in the same column indicate significant different ($p<0.05$)

3.2 Tensile Strength (Ts)

The investigation into the tensile strength of films filled with various concentrations of carnauba wax, as detailed i n Table 3 , demonstrated an 8 . 17 MPa decrease in resistance for the chitosan film with 50% carnauba wax, in comparison to the sample without carnauba wax (0% concentration).

Table 3. Tensile strength of emulsion-based film coating from chitosan incorporated with different concentration of carnauba wax.

carnauba wax		
0%	25%	50%
10.04±3.83*[aαα]	8.83±1.70[b]	8.17±2.33[b]

*Mean ±SD (n=3)
**Different letter in the same column indicate significant different ($p<0.05$)

3.3 Elastic Modulus (EM)

Examining the flexibility of the films, as outlined in Table 4, revealed that the chitosan film with 0% carnauba wax exhibited the highest elasticity at 71.82 MPa, while the lowest value of 63.66 MPa was noted for the chitosan film with 50% carnauba wax.

Table 4. Elastic modulus of emulsion-based film coating from chitosan incorporated with different concentration of carnauba wax.

carnauba wax		
0%	25%	50%
71.82±6.10*[a]**	68.61±9.11[a]	63.66±8.27[a]

*Mean ±SD (n=3)

**Different letter in the same column indicate significant different ($p<0.05$)

3.4 Elongation at Break (EAB)

Analyzing the breaking points of films at various carnauba wax concentrations, as presented in Table 5, indicated no significant differences among the three concentrations of chitosan. Furthermore, the examination of mechanical properties, including tensile strength (Ts), elastic modulus (EM), and film elongation at break (EAB), indicated that when Chitosan was combined with Carnauba wax, the Ts, EM, and EAB values did not exhibit significant differences. This consistency may be attributed to the inherent ability of chitosan to break down fat, as noted in previous studies [7].

Table 5. Elongation at break (EAB) of emulsion-based film coating from chitosan incorporated with different concentration of carnauba wax.

carnauba wax		
0%	25%	50%
0.11±0.001*[a**]	0.11±0.004[a]	0.11±0.01[a]

*Mean ±SD (n=3)

**Different letter in the same column indicate significant different ($p<0.05$)

3.5 Color Value

Results from the assessment of the film's color values, as displayed in Table 7, highlighted that the L* value, indicative of film clarity, reached its highest at 17.57 for the film using chitosan with 50% carnauba wax. Furthermore, the a* and b* values, representing red and yellow colors, respectively, peaked for the chitosan film with 25% carnauba wax at -0.11 and 2.66, respectively (Fig). Acceptance, especially in the context of edible coatings on fruits and vegetables, it is crucial for the applied coating to be clear and minimally impact the natural color of the fruit. Analysis of prototype films incorporating chitosan with Carnauba wax concentrations of 0%, 25%, and 50% revealed that as more Carnauba wax was added, the film became clearer. This clarity is attributed to the reflective and shiny properties of Carnauba wax, which effectively enhances light reflection. Considering the paramount importance of color in consumer decision-making. Lastly, a surface mechanical property of the films demonstrated that Chitosan films, when filled with Carnauba wax at concentrations of 25% and 50%, exhibited almost no significant structural changes. This stability is attributed to the fat-breaking properties of chitosan, as elucidated in previous research [8].

Table 6. Color values of emulsion-based film coating from chitosan incorporated with different concentration of carnauba wax.

Color value		
L*	a*	b*
7.026±0.82*[c**]	-1.13±0.09[b]	0.76±0.23[b]
15.20±0.59[b]	-1.48±0.10[a]	2.66±1.17[a]
17.57±0.71[a]	-1.45±0.04[a]	2.55±1.69[a]

*Mean ±SD (n=3)

**Different letter in the same column indicate significant different ($p<0.05$)

Fig. 1 Physical appearance of emulsion-based film coating from chitosan incorporated with different concentration of carnauba wax.

4. Conclusions

This research explores the development of emulsion-based edible film coatings using chitosan and carnauba wax at varying concentrations (0%, 25%, and 50%). The study finds that while the 50% carnauba wax concentration yields the greatest film thickness, higher concentrations lead to decreased tensile strength and elastic modulus. Despite these

mechanical property changes, elongation at break remains consistent across all treatments. Notably, the film incorporating 50% carnauba wax exhibits higher lightness and yellowness values. Overall, the findings suggest that the developed edible film coating, particularly with 50% carnauba wax, has potential applications for preserving fruits and vegetables, offering an environmentally friendly alternative to traditional plastic packaging.

References

[1] Bhargava, N., Sharanagat, V. S., Mor, R. S., & Kumar, K. (2020). Active and intelligent biodegradable packaging films using food and food waste- derived bioactive compounds: A review. *Trends in Food Science & Technology*, *105*, 385-401.

[2] Prakash, A., Baskaran, R., & Vadivel, V. (2020). Citral nanoemulsion incorporated edible coating to extend the shelf life of fresh cut pineapples. Lwt, 118, 108851.

[3]] Yong, H., & Liu, J . (2021). Active packaging films and edible coatings based on polyphenol-rich propolis extract: A review. Comprehensive Reviews in Food Science and Food Safety, 20(2), 2106-2145.

[4] Afifah, N., Ratnawati, L., & Darmajana, D. A. (2019, April). Evaluation of plasticizer addition in composite edible coating on quality of fresh-cut mangoes during storage. In IOP Conference Series: Earth and Environmental Science (Vol. 251, p. 012029). IOP Publishing.

[5] Robles-Sánchez, R. M., Rojas-Graü, M. A., Odriozola-Serrano, I., González-Aguilar, G., & Martin-Belloso, O. (2013). Influence of alginate-based edible coating as carrier of antibrowning agents on bioactive compounds and antioxidant activity in fresh-cut Kent mangoes. LWT-Food Science and Technology, 50(1), 240-246.

[6] M. Ekrami, Z. Emam-Djomeh, Water vapor perm Ekrami, M., & Emam-Djomeh, Z. (2014). Water vapor permeability, optical and mechanical properties of salep-based edible film. Journal of Food Processing and preservation, 38(4), 1812-1820.

[7] Fahrullah, F., Radiati, L. E., Purwadi, P., & Rosyidi, D. (2020). The effect of different plasticizers on the characteristics of whey composite edible film. *Jurnal Ilmu dan Teknologi Hasil Ternak (JITEK)*, *15*(1), 31-37.

[8] Tafa, K. D., Satheesh, N., & Abera, W. (2023). Mechanical properties of tef starch based edible films: Development and process optimization. Heliyon, 9(2) 1-8.

Mr. Arthit Dankathok
Master student,
Research Interests: Food Processing, edible film, Plant extract

Mr. Chanathit Khadsri
Research Interests: Food Processing, edible film

Dr. Theeraphol Sanphan
Assistant Professor
Research Interests: Food Processing, Value added product from Utilization

Agricultural product marketing strategy driven by digital and intelligent marketing concepts：a case study of Zi Chang New Farmers Association

Wei Zhang[1*], Prayong Kusirisin [1], Jirachai Yomkerd [2], Sutthikarn Khong-khai[3]

[1]International College, Maejo University, Chiang Mai, Thailand
[2]International Colleges, Maejo University, Chiang Mai, Thailand
[3] International College, Maejo University, Chiang Mai, Thailand
**Corresponding author, E-mail: 309544920@qq.com*

Abstract: With the development of the economy and the improvement of people's living standards, as well as the advent of the digital and intelligent era, how agriculture, as the basic industry of the national economy, adapts to the new era has attracted more and more attention. At the same time, as market competition intensifies and consumers' requirements for agricultural products increase, agricultural enterprises need to continuously improve their competitiveness, adapt to market changes, and meet consumer needs. Therefore, studying the business strategies and market trends of agricultural enterprises is of great significance for promoting the development of agricultural enterprises and protecting the interests of consumers. This research takes agricultural associations as the research object, and explores issues such as the digital transformation of agricultural enterprises, market competition strategies, brand awareness, and the quality and safety of agricultural products through methods such as questionnaire surveys and quantitative analysis. Through research, it was found that the application of digital technology can improve the efficiency and quality of agricultural production and enhance the competitiveness of agricultural enterprises.

Keywords: Digitalization, intelligent marketing concepts, marketing strategy, New Farmers Association

1. Introduction

1.1 China's Rural Revitalization Policy

In the context of my country's rapid social and economic development, the gap between urban and rural areas has become increasingly prominent, and rural areas are facing multiple problems and challenges. In order to achieve the goal of comprehensively building a modern socialist country, rural revitalization has been established as a key strategy for the next stage of development in our country. In recent years, rural land has been rationally planned and utilized, and agricultural production efficiency and farmers' quality of life have improved. As the state continues to increase its investment in rural areas, rural infrastructure construction and public service levels have also been significantly enhanced. Despite this, there are still some problems and shortcomings in rural areas, such as the gap between urban and rural areas is still large, farmers' income and quality of life are relatively low, and rural areas are weak in adapting to the new era of digitalization and intelligence, and manufacturers and sellers have failed to Keep up with the times in time. However, the widespread application of smart technology in the current digital era has brought new opportunities for the sales of agricultural products. The application of digital intelligent marketing concepts can not only improve sales

efficiency and reduce costs, but also enhance consumer experience. This study takes the Zi Chang New Farmers Association as an example to deeply explore the application and significance of digital intelligent marketing concepts in agricultural product sales, with a view to injecting new vitality into rural development.

1.2 Zi Chang City and New Farmers Association

Zi Chang City is located in northern Shaanxi and has rich agricultural resources and high-quality agricultural products. Its main products are apples and potatoes. Thanks to the abundant sunshine and climatic conditions with large temperature differences between day and night, the fruit in this region is of high quality. However, with the development of the market economy and the increase in demand for healthy food, the traditional agricultural product sales model has shown shortcomings in efficiency and quality, which has brought certain pressure to local farmers. To this end, as the economic consultant of the Zi Chang New Farmers Association, I am working with the association to explore how to use digital and intelligent marketing strategies to improve the sales efficiency and quality of agricultural products, thereby increasing farmers' income. I hope that through this research, we can find practical solutions for the marketing of local agricultural products, which is where I think this research is of far-reaching significance.

2. Methods

2.1 The 3W Golden Circle model

The 3W Golden Circle is a commonly used model for thinking and analyzing problems, consisting of three questions: Why, What and How. This model was originally proposed by marketing guru Simon Sinek, who believed that the most successful leaders and organizations in the world think and act in the order of these three questions.

The definition of the 3W golden circle model can be summarized as: a framework used to guide thinking and analysis of problems. Through the three core questions of Why, What and How, the essence of the problem is deeply explored, the purpose and method of the research are clarified, and a better understanding of the problem is obtained. A convincing conclusion. This model can help people better understand problems and find the best path to solve them.

2.2 Application of 3w golden circle model in this study

We apply the 3w golden circle model to analyze the new professional farmers association in Zi Chang City and give relevant suggestions.

Why: The root and purpose of the research problem

First, we use Why in the 3W Golden Circle to explain the root and purpose of the research problem. Zi Chang New Farmers Association faces the challenges and opportunities of digital marketing. How to evaluate its digital marketing strategy, digitalization, intelligence level and agricultural product sales is the focus of our research. Our aim is to provide targeted improvements to the association's marketing strategy through in-depth research and analysis, thereby increasing sales and competitiveness.

What: Specific research objects and questions

Next, we use What in the 3W Golden Circle to clarify specific research objects and questions. Our research object is the New Farmers Association of Zi Chang City. Specific research questions include evaluating its digital marketing strategy, digitalization, intelligence

level and the current situation and problems of agricultural product sales, as well as the impact of digital marketing strategy and digitalization and intelligence on agricultural product sales.

How: methods and paths to solve problems

Finally, we use the How in the 3W Golden Circle to explain the methods and paths to solve the problem. In order to evaluate the digital marketing strategy, digitalization, intelligence level and agricultural product sales of Zi Chang New Farmers Association, we will use methods such as questionnaires, interviews and data analysis. By collecting and processing relevant data, we will conduct an in-depth analysis of digital marketing strategies and the impact of digitalization and intelligence on agricultural product sales, thereby providing improvement suggestions for the association's marketing strategies.

2.2 Meaning of 3w golden circle model variables

Based on the 3w golden circle model, this study focuses on various factors of digital intelligent marketing strategies and combines them with the actual local conditions. According to the characteristics of this study, various variables are given, and each statistical indicator is given different specific meanings, as shown in

3. Results and Discussion

3.1: Digital and intelligent marketing strategies can improve the sales volume and efficiency of agricultural products .**Table 3.1**

Hypothesis H1 posits that the implementation of digital and intelligent marketing strategies can significantly enhance the sales volume and efficiency of agricultural products. The statistical analysis conducted supports the assertion that various factors within the realm of digitalization and marketing strategies exert a notable influence on the sales volume and efficiency of agricultural products.

The regression analysis reveals compelling insights into the relationship between specific factors and the targeted outcomes. Notably, the non-standardized coefficients present significant associations. The coefficient for Digital Marketing Strategy (DMS) stands at 0.326, implying that for every unit increase in the implementation or effectiveness of digital marketing strategies, there is a corresponding increase of 0.326 units in the sales volume and efficiency of agricultural products. Similarly, Brand Awareness Enhancement exhibits a coefficient of 0.307, suggesting that improvements in brand visibility through intelligent marketing positively correlate with increased sales volume and efficiency.

The statistically significant t-values and p-values (all exhibiting 0.000*** significance levels) for DMS and Brand Awareness Enhancement further reinforce the validity of the relationships identified. These low p-values affirm the strength and reliability of the associations between the variables, bolstering the hypothesis that a well-executed digital and intelligent marketing strategy significantly impacts the sales volume and efficiency of agricultural products.

Moreover, the VIF (Variance Inflation Factor) values below the threshold indicate a lack of multicollinearity among the predictor variables. This absence of multicollinearity strengthens the credibility of the individual effects of digital marketing strategies and brand enhancement on sales volume and efficiency within the agricultural domain.

The model's R^2 value, specifically 0.512, denotes the proportion of variance in sales volume and efficiency that can be explained by the included variables. This suggests that over 51% of the variability in sales volume and efficiency of agricultural products is accounted for by Digital Marketing Strategy and Brand Awareness Enhancement, signifying their substantial impact on these outcomes.

Table 2.1: *Specific meanings of variables*

Index	Meaning
Digital Marketing Strategy (DMS)	Digital marketing strategy refers to various digital sales strategies adopted in the sales process of agricultural products, including Search engine marketing, (SEM),Social Media Marketing (SMM) , Content Marketing (CM), Video Marketing (VM)
Digitalization and Intelligent Technology (DI)	Digital intelligent technology refers to various technical means that may be used in all aspects of agricultural production, circulation and sales, including Artificial intelligence, Intelligent agricultural production, Big data analysis, Intelligent sales and customer service
Degree of Digitalization and Intelligence Implementation (DDI)	Degree of Digitalization and Intelligence Implementation (DDI) refers to the degree of use of digital intelligent means in the production, circulation and sales of agricultural products.
Sales volume of agricultural products (SAP)	Agricultural Product Sales Volume (SAP) refers to the impact of digital and intelligent means on agricultural product market sales, including income and costs, market competition, and agricultural product prices.
Brand Awareness Enhancement (BA)	Brand Awareness Enhancement (BA) refers to the impact of digital and intelligent means on the brand value of agricultural products, including brand image, brand communication, and brand reputation.
Agricultural Production Quality (APQ)	Agricultural Production Quality (APQ) refers to the impact of digital and intelligent means on the quality of agricultural products, including consumer evaluation of agricultural products, agricultural output and production efficiency, and the development of green agriculture.

Results of 3.1 regression analysis

variable	Non-standardized Coefficient	t-value	P-value	VIF	R^2	F-value
Constant	0.804	0.215	3.736	0.000***	-	0.512
Digital Marketing Strategy (DMS)	0.326	0.064	5.099	0.000***	1.921	
Agricultural Production Quality	0.161	0.063	2.555	0.011**	1.676	
Brand Awareness Enhancement	0.307	0.06	5.114	0.000***	1.643	

Note: *p<0.05. **p<0.01. ***p<0.001

These findings affirm Hypothesis H1, underscoring the pivotal role of digital and intelligent marketing strategies in augmenting the sales volume and efficiency of agricultural products. The positive and statistically significant coefficients, coupled with the low p-values and absence of multicollinearity, substantiate the notion that strategic implementation of digital marketing initiatives and heightened brand visibility through intelligent strategies contribute significantly to the increased sales volume and efficiency observed within the agricultural sector. Therefore, these results advocate for a strategic emphasis on digital and intelligent marketing approaches to optimize agricultural product sales volume and efficiency.

3.2: Digitalization and intelligent technology can improve the production of agricultural enterprises and the quality of agricultural products Table 3.2

Results of 3.2 regression analysis

Variable	**Non-standardized Coefficient**	**t-value**	**P-value**	**VIF**	**R^2**	**F-value**
Constant	0.763	0.222	3.444	0.001***	-	0.497
Digital Intelligent Technology (DI)	0.28	0.063	4.418	0.000***	1.762	
Agricultural Production Quality	0.209	0.061	3.407	0.001***	1.537	
Brand Awareness Enhancement	0.314	0.062	5.103	0.000***	1.684	

Note: *p<0.05. **p<0.01. ***p<0.001

Hypothesis H2 asserts that digitalization and intelligent technology interventions have the potential to enhance both the production processes of agricultural enterprises and the overall quality of agricultural products. The statistical analysis conducted in alignment with this hypothesis offers valuable insights into the relationship between digitalization, technological integration, and the improvement

of agricultural productivity and product quality.

The regression analysis presents a series of key findings that underscore the significance of digital and intelligent technology in agricultural contexts. Notably, the non-standardized coefficients provide indications of the strength and direction of these associations. The coefficient for Digital Intelligent Technology (DI) stands at 0.28, implying that with each unit increase in the implementation or effectiveness of intelligent technology, there's an associated increase of 0.28 units in agricultural production and quality.

The statistical significance is underscored by the t-values and p-values associated with the variables. All variables—DI, Agricultural Production Quality, and Brand Awareness Enhancement—display significantly low p-values of 0.000***, affirming the robustness and reliability of their effects on the targeted outcomes. This statistical significance supports the notion that digitalization, intelligent technology, and brand enhancement significantly influence the improvement of agricultural production and product quality.

Moreover, the VIF (Variance Inflation Factor) values for these variables remain within acceptable limits, suggesting a lack of multicollinearity, which further substantiates the individual impacts of digitalization and intelligent technology on agricultural production and product quality.

The R^2 value, representing the proportion of variance in agricultural production quality and enterprise productivity explained by the included variables, stands at 0.497. This indicates that approximately 49.7% of the variability in agricultural production and quality can be attributed to Digital Intelligent Technology, Agricultural Production Quality, and Brand Awareness Enhancement. Such a substantial percentage suggests the considerable influence these factors wield over the improvement of agricultural processes and product caliber.

In conclusion, the findings corroborate Hypothesis H2, illustrating the pivotal role that digitalization and intelligent technology play in elevating agricultural production and product quality. The positive coefficients, coupled with the statistical significance and absence of multicollinearity, affirm the significance of these technological interventions in enhancing agricultural enterprises' production capabilities and the overall quality of their products. Hence, the results advocate for strategic emphasis on digital and intelligent technology integration within agricultural practices to optimize productivity and elevate the standards of agricultural products.

3.3: The strengthening of digital and intelligent implementation will enhance the brand recognition of agricultural products in Zi Chang City.

Table 3.3

Results of 3.3 regression analysis

Variable	Non-standardized Coefficient	t-value	P-value	VIF	R^2	F-value
Constant	0.855	0.222	3.856	0.000***	-	0.482
Implementation Level of Digital Intelligence (DDI)	0.253	0.07	3.621	0.000***	2.067	
Agricultural Production Quality	0.227	0.062	3.65	0.000***	1.528	
Brand Awareness Enhancement	0.303	0.067	4.529	0.000***	1.927	

Note: *p<0.05. **p<0.01. ***p<0.001

Hypothesis H3 posits that the reinforcement and advancement of digital and intelligent implementation strategies will lead to a notable enhancement in brand recognition for agricultural products within Zi Chang City. To delve into the implications of this hypothesis, a statistical analysis was conducted to explore the relationship between the implementation of digital intelligence, brand recognition, and its impact on agricultural product branding within this specific geographic context.

The regression analysis offers substantive insights into the relationship between digital and intelligent implementation levels and brand recognition within the agricultural domain. The non-standardized coefficients serve as indicators of the magnitude and direction of these relationships. Specifically, the coefficient for the Implementation Level of Digital Intelligence (DDI) stands at 0.253. This suggests that with each incremental improvement or reinforcement in digital and intelligent implementation strategies, there's a corresponding increase of 0.253 units in brand recognition for agricultural products in Zi Chang City.

The statistical significance of these relationships is evidenced by the associated t-values and p-values. All variables—IDI, Agricultural Production Quality, and Brand Awareness Enhancement—display notably low p-values of 0.000***, indicating a robust and significant influence on brand recognition. This statistical significance substantiates the claim that the strengthening of digital and intelligent implementation significantly contributes to enhancing brand recognition for agricultural products in Zi Chang City.

Additionally, the VIF (Variance Inflation Factor) values for these variables remain within acceptable limits, suggesting an absence of multicollinearity, which further reinforces the individual impact of digital and intelligent implementation on brand recognition.

The R^2 value, representing the proportion of variance in brand recognition explained by the included variables, stands at 0.482. This implies that approximately 48.2% of the variability in brand recognition among

agricultural products in Zi Chang City can be attributed to the Implementation Level of Digital Intelligence, Agricultural Production Quality, and Brand Awareness Enhancement. This substantial percentage underscores the considerable influence of these factors on elevating brand recognition within the agricultural sector.

In summary, the findings strongly support Hypothesis H3, demonstrating that an escalated focus on digital and intelligent implementation strategies significantly contributes to bolstering brand recognition for agricultural products in Zi Chang City. The positive coefficients, coupled with the statistical significance and absence of multicollinearity, underscore the pivotal role of digital and intelligent implementation in amplifying brand visibility and recognition. Thus, these results advocate for strategic investment and advancement in digital and intelligent technologies within agricultural practices to augment brand recognition and competitiveness within Zi Chang City's agricultural sector.

4. Conclusions

The empirical findings obtained from the study provide comprehensive insights into the intricate relationship between digital marketing strategies, digitalization, intelligence, and their impact on the sales volume of agricultural products within the Zi Chang New Farmers Association. Addressing the research questions posed in this study, the analysis sheds light on pivotal aspects crucial for enhancing marketing strategies and increasing sales volumes within the agricultural domain.

Firstly, the evaluation of digital marketing strategy, digitalization, and intelligence levels reveals their significant influence on agricultural product sales volumes. The statistical analysis uncovered a substantial relationship between these variables and sales volume. Specifically, the Implementation Level of Digital Intelligence (DDI) demonstrated a positive and significant association with sales volume, emphasizing the instrumental role of digital intelligence in augmenting sales within the association.

The investigation into the specific impact of digital marketing strategies on agricultural product sales volume provided further elucidation. The results showcased a noteworthy correlation between certain digital marketing strategies and increased sales volumes. Notably, strategies focused on brand awareness enhancement exhibited a significant positive influence on sales volume. This underscores the importance of employing targeted digital marketing initiatives aimed at amplifying brand visibility to drive higher sales figures for agricultural products.

Moreover, the analysis delineated how the adoption of digitalization and intelligence positively affects sales volume for agricultural products. The findings highlighted that an increased emphasis on digitalization and intelligence correlates with augmented sales volumes. This underscores the pivotal role of leveraging digital technologies and intelligence-driven approaches in enhancing the marketing landscape and subsequently boosting sales performance within the Zi Chang New Farmers Association.

Drawing practical recommendations from these empirical results becomes imperative to fortify marketing strategies and amplify sales volumes for the association. Emphasizing the implementation of comprehensive digital marketing strategies, including those focusing on brand recognition enhancement, emerges as a pivotal recommendation. Strengthening efforts in digital intelligence and technology adoption within agricultural practices stands out as a critical avenue for enhancing sales volume.

In conclusion, the empirical evidence from this study underscores the pivotal role of digitalization, intelligent implementation,

and targeted digital marketing strategies in elevating sales volumes for agricultural products within the Zi Chang New Farmers Association. Leveraging these insights, the association can formulate and implement tailored strategies to optimize their digital presence, enhance brand recognition, and ultimately drive higher sales volumes within the agricultural domain.

References

[1] Research Report on the Digitalization of China's Agricultural Production in 2021 (https://zhuanlan.zhihu.com/p/426960848)

[2] Liu Miao, （2023）Exploration on the Internet Marketing Strategy of Agricultural Products in Shaanxi Province under the Background of Rural

Revitalization, Source: Shanxi Agricultural Economics, Issue 2, 163-165,

[3] Mayire Tursun, (2023)Discussion on the Optimization of Xinjiang Agricultural Products Network Marketing Model Under the Background of Rural Revitalization, Source "BUSINESS OBSERVATION" Issue 20, 74-76,80,

[4]Cai Rui, （2023）analysis of the application of new media platforms in online marketing of agricultural products, Source: China Food Issue 2,, 100-102

[5] Chui, M., Lohse, G., & Roberts, J. (2015). Smart Machines: Flipping the Classroom for Learning and Teaching in the Digital Age. Education Digitized.

[6]Digital Marketing: The Future of the Internet, （2020）report by PwC.

[7] Dave Chaffey and Fiona Ellis-Chadwick. (2022).Digital Marketing: Strategy, Implementation and Practice (7th Edition).Publisher: Tsinghua University Press

[8]Food and Agricultural Policy Research Institute. (2021). Agricultural Marketing: An International Perspective. Food and Agricultural Policy Research Institute.

[9]Gao Jia, （2023）Dilemmas and breakthrough strategies of online marketing of agricultural products from the perspective of "Internet +" Source "Shanghai Business" Issue 2, 56-58

[10]Guan Rongxia, （2023） Discussion on Internet Marketing Issues and Strategies of Agricultural Products in the E-Commerce Environment, Source: "Marketing management review " Issue 3, 149-151

Wei Zhang
Lecturer, Master student, Master of Business Administration (Digital Economy and Management Innovation)
Research Interests:
Digitalize and Enterprise Strategy.

Current Status and Solutions of Energy and Environmental Problems

Yao Feng

Guangxi University, No. 100 Daxue East Road, Nanning, 530000, P.R. China
E-mail: 2114402028@st.gxu.edu.cn

Abstract: Energy and environmental issues have always been significant challenges for humanity. In an era of industrial expansion and urban development, the relentless increase in energy demand exacerbates environmental problems and highlights the urgent need for sustainable solutions. Despite their different circumstances and challenges, China, Japan, and Thailand share common energy and environmental problems. With their unique energy and environmental circumstances, exploring innovative approaches and fostering international cooperation to address these pressing global concerns becomes crucial. This article addresses the energy and environmental issues these countries face and provides insights into their key problems in the energy and environmental sectors. Additionally, it proposes effective solutions that can serve as valuable references for global efforts toward energy and environmental sustainability.

Keywords: Energy, Environment, Pollution, Solutions.

1. Introduction

As a crucial cornerstone for the development of nations and human society, energy serves as a fundamental guarantee for economic prosperity, national security, and the overall health of the lives of citizens. Human reliance on energy permeates various aspects of life, encompassing essential daily needs such as lighting, heating, and cooking; the functioning of factory equipment and transportation systems vital for economic growth and industrial operations; laboratory facilities, computers, and communication technologies essential for scientific and technological innovation; modernized transportation and communication infrastructure contributing to the improvement of living standards; mechanized irrigation in agriculture and food production; and even playing a pivotal role in ensuring social stability and national security[4].

The advent of energy has ushered in both convenience and development, fundamentally altering lifestyles and significantly improving life quality. However, this transformation has also led to a worsening of environmental issues to a certain extent. Meeting energy demands coincides with waste and pollutant production during resource extraction, energy production, and consumption. Using fossil fuels has notably contributed to substantial greenhouse gas emissions, exerting a considerable impact on climate dynamics. Moreover, energy extraction and production activities commonly result in environmental concerns such as land degradation, wastage of water resources, and biodiversity loss. There is a growing recognition that despite energy being the driving force behind modern societal progress, its development and utilization necessitate environmental conservation and sustainability considerations. Therefore, it becomes crucial to profoundly acknowledge the pressing nature of environmental issues while

striving for advancements in energy development and societal progress. Taking proactive measures to seek sustainable energy solutions is imperative to foster a harmonious coexistence between humanity and the environment.

This study aims to comprehensively examine the significance of energy in human life and the necessity of its development for society. The study will delve deeply into exploring the impact of different energy sources on the environment, investigating the close relationship between environmental issues and sustainable development, and extensively researching strategies to address energy and environmental challenges. By analyzing existing data and research findings, this study intends to provide a comprehensive understanding and profound insights into the relationship between energy and the environment. This endeavor will assist scholars who focus on specific domains of study in broadening their perspectives, enabling them to develop a more holistic comprehension of the overall energy and environmental issues.

2. Overviews of Energy Supply

The escalating consumption and growing demand for energy indicate that energy will emerge as one of the principal future challenges globally [5]. With the increasing demand for energy by humans, energy will have to face two primary issues: the gradual depletion of non-renewable energy sources and the arising from environmental concerns associated with energy consumption, such as the emission of greenhouse gases. Therefore, this section conducts a comprehensive analysis and comparison of global energy consumption, categorizing energy into two major classifications: non-renewable and renewable sources. Within this context, our focus is particularly directed towards an in-depth investigation and analysis of the energy supply and consumption scenarios in China, Thailand, and Japan. Through a comparative study of these countries' energy sources and consumption patterns, we aim to gain a better understanding of both the disparities and similarities in their energy landscapes. This endeavor is poised to offer valuable insights and references for formulating future sustainable and efficient energy policies.

2.1 Total Energy Consumption

Although humanity has become aware of the environmental issues associated with energy consumption, the energy demand continues to grow. The primary energy consumption in 2022 increased by 1.1% compared to 2021, showing a 2.8% rise from the levels observed in 2019 before the onset of the COVID-19 pandemic. [3]。Figure 1 illustrates the global total energy consumption since 2000 and the proportionate consumption of various energy sources.

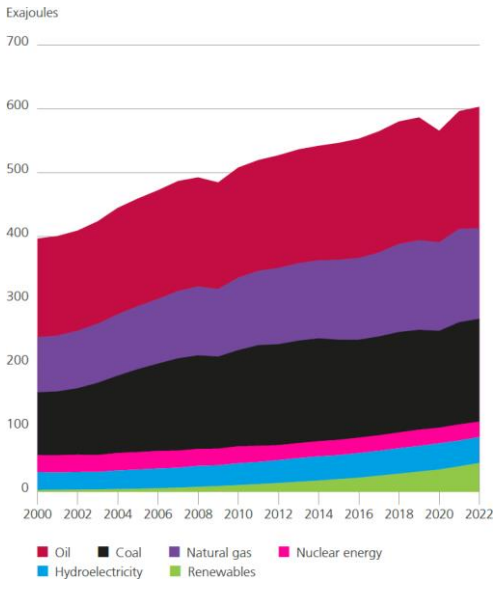

Fig 1. The total energy consumption and the consumption levels of different energy sources [3]. Note: 1 Exajoules = 1×10^{18}J

Fig.1 shows that the overall energy consumption continues to increase, except for the circumstances around 2020 (influenced mainly by COVID-19). Simultaneously, among various energy sources, coal, oil, and natural gas remain the primary sources, accounting for the vast majority of energy supply. Concurrently, the proportion of nuclear and hydrogen energy

Table 1

Primary energy Consumption (1×10^{18} J)[3].

Regions	2012	2013	2014	2015	2016	2017	2018	2019	2020	2021	2022
World	527.96	537.19	542.87	547.39	553.98	565.60	581.05	587.39	566.49	597.41	604.04
Asia	213.72	219.05	225.17	229.17	232.54	240.67	250.82	258.98	257.78	271.84	277.60
China	117.45	121.87	125.03	126.49	127.00	131.94	138.30	144.74	149.45	157.94	159.39
Japan	19.99	19.84	19.34	19.07	18.82	19.05	18.95	18.51	17.15	17.94	17.84
Thailand	4.68	4.71	4.86	4.98	5.08	5.17	5.33	5.34	4.97	5.01	5.06

consumption has remained relatively stable since 2000. However, in recent years, there has been a noticeable increase in the proportion of renewable energy sources in overall energy consumption.

Table 1 illustrates the primary energy consumption worldwide, including Asia and the three countries of China, Japan, and Thailand. Over the past decade, there has been a gradual awareness of the environmental issues stemming from primary energy consumption. However, overall energy consumption has continued to rise annually, with a notable deviation in 2020 due to the impact of COVID-19. Similar patterns in primary energy consumption are observed in Asia and globally.

As a populous nation, China accounts for over half of Asia's primary energy consumption and has seen a consistent annual increase in consumption. In contrast, Japan's primary energy consumption presents a slightly different trend. There was a decline in consumption in 2016, followed by a short-term increase in 2017. However, starting from 2018, there has been a consecutive annual decrease, making Japan one of the few countries with a negative growth trend in primary energy consumption over the past decade. Thailand's primary energy consumption has remained relatively stable, with a minor increase over the past ten years.

2.2 Different Energy Consumption

From the perspective of overall energy consumption, human energy demand continues to increase annually. However, with the continuous development and utilization of new clean energy sources, coupled with the ongoing enhancement of new energy technologies, the usage patterns of energy types remain an area worthy of in-depth research and observation [3].

Table 2

Different energy consumptions (1×10^{18} J) and their proportions in total energy consumption (%).

Regions	Types	Oil	Natural gas	Coal	Nuclear energy	Hydroelectricity	Renewable energy	Total
World	consumption	190.69	141.89	161.47	24.13	40.68	45.18	604.04

Asia	proportion	31.57	23.49	26.73	3.99	6.73	7.47	277.59
	consumption	69.61	32.65	130.50	6.65	17.94	20.24	
China	proportion	25.08	11.76	47.01	2.40	6.46	7.29	159.39
	consumption	28.16	13.53	88.41	3.76	12.23	13.30	
Japan	proportion	17.67	8.49	55.47	2.36	7.67	8.34	17.85
	consumption	6.61	3.62	4.92	0.47	0.70	1.53	
Thailand	proportion	36.97	20.28	27.56	2.63	3.92	8.57	5.07
	consumption	2.39	1.60	0.71	-	0.06	0.31	
	proportion	47.14	31.56	14.00	-	1.18	6.11	

Table 2 displays the energy consumption statistics for various sources, including world, Asia, China, Japan, and Thailand in 2022. The data reveals that traditional primary energy sources—coal, oil, and natural gas—continue to occupy a significant share. Among these, oil is the most consumed energy source, representing 31.57% of the total energy consumption. Japan and Thailand rely heavily on oil, accounting for 36.97% and 47.14% of their overall energy consumption. China predominantly relies on coal as its energy source, comprising 55.47% of its total energy consumption, and this influences Asia, where coal contributes 47.01% to the total energy consumption in the region.

In the realm of clean energy, the consumption and proportion of renewable energy sources are more pronounced in the world, Asia, and the countries of China, Japan, and Thailand. Renewable energy accounts for 7.47% of global usage, with Asia slightly lower at 7.29%. However, both Japan and China surpass the global and Asian averages, standing at 8.57% and 8.34%, respectively. In contrast, Thailand's utilization of renewable energy, at 6.11% of total energy consumption, slightly trails behind the global and Asian standards. The global consumption of hydroelectric power ranks second, following renewable energy sources, accounting for 6.73% of energy consumption worldwide. In Asia, the share of hydropower consumption is slightly lower at 6.46%. Notably, China utilizes hydroelectric power at a rate of 7.67% in its energy structure, surpassing global and Asian averages. Japan and Thailand have lower shares of hydroelectric power consumption at 3.92% and 1.18%, respectively. Additionally, nuclear power consumption constitutes the smallest share of the energy mix, with global consumption at 3.99%, Asia at 2.40%, and China and Japan at 2.36% and 2.63%, respectively. Despite the efficiency of nuclear power, its relatively low representation in the global energy mix may be due to associated risks.

3. Environmental Implications of Energy

3.1 Overall Environmental Impact

The above discussions reveal a continual rise in human energy demand annually, fostering extensive reliance on primary energy sources and aggravating prevalent environmental concerns. The waste from energy extraction, production, and consumption processes contributes to varying degrees of pollution in the atmosphere, water bodies, and soil, impacting biodiversity. Notably, the combustion of fossil fuels emits substantial greenhouse gases, significantly shaping global climatic patterns. Therefore, while benefiting from the convenience of energy

resources, humanity must actively address environmental conservation and sustainable development.

Environmental pollution encompasses various domains, including major environmental accidents incidents, water and marine pollution, radioactive substances, solid waste, air pollution, ozone layer depletion, and global warming. Table 3 delineates crucial directives of the European Union concerning environmental aspects related to water, air, and land.

Table 3

Significant EU environmental directives in water, air and land environments [1].

Environment	Directive name
Water	Surface water for drinking
	Sampling surface water for drinking
	Drinking water quality
	Quality of freshwater supporting fish
	Shellfish waters
	Bathing waters
	Dangerous substances in water
	Groundwater
	Urban wastewater
	Nitrates from agricultural sources
Air	Smokes in air
	Sulphur dioxide in air
	Lead in air
	Large combustion plants
	Existing municipal incineration plants
	New municipal incineration plants
	Asbestos in air
	Sulphur content of gas oil
	Lead in petrol
	Emissions from petrol engines
	Air quality standards for NO2
	Emissions from diesel engines
Land	Protection of soil when sludge is applied

The European Union has outlined specific plans concerning conventional primary energy source emissions. These noteworthy pollutants and their respective standards are detailed in Table 4.

Table 4

EU criteria pollutant standards in the ambient air environment [1].

Pollutant	EU limit
CO	30 mg m^{-2};1h
NO_2	200 μg m^{-2}; 1h
O_3	235 μg m^{-2}; 1h
SO_2	250 – 350 μg m^{-2}; 24h
	80 – 120 μg m^{-2}; annual
PM_{10}	250 $^{-2}$; 24h
	80μg m^{-2}; annual
$SO_2 + PM_{10}$	100 – 150 μg m^{-2}; 24h
	40 – 60 μg m^{-2}; annual
Pb	2 μg m^{-2}; annual
Total suspended particulate (TSP)	260 μg m^{-2}; 24h
HC	160 μg m^{-2}; 3h

As this paper primarily delves into environmental pollution caused by energy consumption, the ensuing discussion will focus on analyzing the waste generated from primary energy consumption, particularly greenhouse gases.

3.2 Emission of Greenhouse Gas

There has been a growing acknowledgment of the severity of environmental issues, notably the concerns related to temperature escalation due to greenhouse gas emissions. The 21st Conference of the Parties (COP21) convened in Paris in 2015 to address global warming. It established a target to restrict the global temperature rise to below 2°C above pre-industrial levels, aiming ideally for 1.5°C. Regrettably, as preparations for COP28 were underway, the United Nations Environment Programme released the "2023 Emissions Gap

Report," revealing less-than-optimistic data. The report indicates that it will be challenging to limit the temperature rise to 1.5℃ by 2030, and achieving the goal of restricting the temperature increase to 2℃ will also present challenges. The report mentions that countries must implement more robust emission reduction measures than those outlined in the Paris Agreement; otherwise, global warming could reach 2.5℃ to 2.9℃ by 2030[2]. Fig. 2 depicts the emissions of various greenhouse gases since 1990.

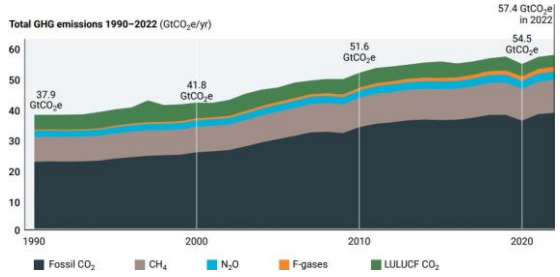

Fig .2 Total net anthropogenic GHG emissions,1990-2022

The graph clearly illustrates the continuous increase in greenhouse gas emissions over the years. Among these emissions, CO_2 from fossil fuels remains predominant, underscoring the urgency of addressing greenhouse gases generated from energy consumption. Additionally, emissions of CH_4 and F-gases are on the rise, while N_2O emissions remain relatively stable with a slow growth rate, and there is a decreasing trend in LULUCF CO_2 emissions.

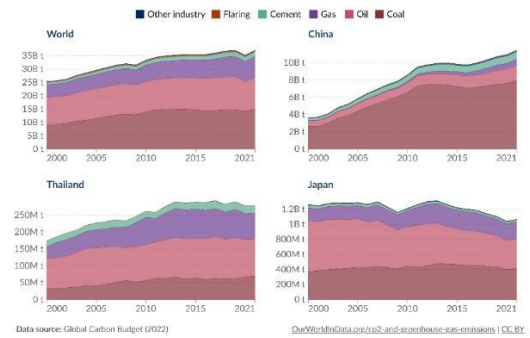

Fig .3 CO_2 emissions by fuel or industry type

Fig. 3 illustrates the CO_2 emissions from different sources in the world, China, Japan, and Thailand. Coal, oil, and natural gas are the major contributors to CO_2 emissions. Similarly, in China, CO_2 emissions predominantly stem from coal combustion, in line with the earlier conclusion that coal is China's primary energy source. The graph indicates a deceleration in global CO2 emission growth, with a similar trend observed in Thailand. Japan has effectively controlled CO2 emissions, showing an overall declining trend. In contrast, China's CO_2 emissions continue to grow significantly, signaling the need for more significant efforts to control CO_2 emissions.

4. Results and Discussion

Energy is the primary impetus for societal advancement, powering various facets of global economic, technological, and social progress. However, the escalating demand for energy across nations has led to a concurrent increase in greenhouse gas emissions, exacerbating environmental concerns. This paper endeavors to comprehensively amalgamate existing scientific methodologies and innovative techniques. It delves into an in-depth analysis to propose a multifaceted set of solutions addressing the challenges of burgeoning energy consumption and its resultant environmental impacts.

Initially, the focus should be on fundamentally reducing dependence on fossil fuels and progressively enhancing the utilization of renewable energy sources, including solar, wind, hydro, and biomass energies, aiming to diminish the emission of greenhouse gases. Using clean energy sources contributes to reducing environmental pollution. However, it's crucial to note certain limitations. These include

application constraints: for instance, solar and wind energy are heavily influenced by weather conditions. In adverse weather, their stability may not match traditional energy sources. For example, nuclear power plants pose certain risks under extreme environmental conditions. Additionally, many clean energy technologies are still evolving, resulting in higher costs in the initial stages of development and implementation. Next, for irreplaceable energy sources, enhancing energy efficiency is crucial. This can be achieved by employing more efficient technologies and equipment to minimize energy waste and unnecessary consumption, reducing overall energy usage and lowering greenhouse gas emissions. The methods aimed at enhancing energy conversion rates also encounter several challenges. These include the demand for more advanced technologies, which may lead to higher costs. Additionally, the stability and reliability of new technologies require a period of validation during their operational phase.

Third, the behavior of emitting pollutants could be exploited, for example, in the case of straw burning, where the heat energy generated can be utilized. Although this behavior leads to the emission of pollutants, the collection of thermal energy can reduce the energy consumption of using conventional energy sources to generate heat. At the same time, gas emissions should be treated and utilized, such as carbon capture and storage technology. This technology captures greenhouse gases such as carbon dioxide and stores them underground or in other containers, reducing the amount of these gases released into the atmosphere.

In addition, there are auxiliary methods, such as forest protection and ecosystem restoration. By safeguarding and re-vegetating, especially forests, carbon dioxide can be absorbed, contributing to the reduction of greenhouse gas concentrations. Although this approach is relatively less efficient, it is a fundamental method to decrease CO2 levels. Implementing policies and regulations can promote the use of green energy and reduce fossil fuel consumption. Simultaneously, raising public awareness and encouraging individuals and organizations to adopt more environmentally friendly lifestyles and practices are crucial. Establishing comprehensive institutions is essential. Developed nations have relatively comprehensive statistics and data on various pollutants, while data collection in developing countries is somewhat limited. This disparity makes it challenging to comprehensively understand environmental data in these countries and provide targeted solutions to the issues.

The issues related to energy and the environment are not confined to any single nation but are a shared concern for all of humanity, impacting every life on Earth. Scientific methodologies primarily aid in understanding and utilizing natural laws. As humans, it's crucial to recognize our insignificance in the grand scheme of nature and learn to harmonize with it rather than exploit it opportunistically. Therefore, we should approach nature humbly and work toward sustainable practices, respecting and preserving our natural resources to ensure a balanced and mutually beneficial coexistence between humanity and the environment.

References

[1] A.M. Omer, Energy, environment and sustainable development, 12 (2008) 2265-2300.

[2] Emissions Gap Report 2023: Broken Record – Temperatures hit new highs, yet world fails to cut emissions (again), 2023.
[3] Energy Institute, Statistical Review of World Energy, Energy Institute London, UK, 2023.
[4] H. Saulat, M.M. Khan, M. Aslam, M. Chawla, S. Rafiq, F. Zafar, M.M. Khan, A. Bokhari, F. Jamil, A.W. Bhutto, A.A. Bazmi, Wind speed pattern data and wind energy potential in Pakistan: current status, challenging platforms and innovative prospects, Environ Sci Pollut Res Int 28 (2021) 34051-34073.
[5] M.M. Rafique, S. Rehman, National energy scenario of Pakistan – Current status, future alternatives, and institutional infrastructure: An overview, Renewable and Sustainable Energy Reviews 69 (2017) 156-167.

Ms. Yao Feng
doctoral student
Harbin, Heilongjiang Province, China
Majoring in Mineral flotation separation, and mining wastewater treatment

Environmental Education and Public Awareness

Liu Chengxin[1], Su Xiujuan[2] *,

[1] Faculty of Resources, Environment and Materials, Guangxi University, Nanning, China
[2] Faculty of Resources, Environment and Materials, Guangxi University, Nanning, China
**Corresponding author, E-mail: 2267635105@qq.com*

Abstract: This paper discusses the importance and influence factors of environmental education on public awareness of environmental protection, and the roles and strategies of government, enterprises and individuals in promoting environmental education and public awareness. Emphasize the key role of environmental education in raising public awareness of environmental protection and promoting sustainable development. The government should formulate clear environmental education policies, enterprises should promote green production and consumption, and individuals should participate in environmental protection actions and social dissemination of environmental protection concepts. With the joint efforts of the whole society, we are confident that we can build a more environmentally friendly and sustainable future.

Keywords: Environmental Education, Public Awareness, Government, Enterprise, Individual

1. Introduction

Environmental issues have become a global challenge, involving various aspects such as climate change, ecosystem collapse, and water scarcity. These issues not only threaten human health and livelihoods but also have a serious impact on the ecological balance of the Earth. With the development of technology and the increase in human activities, the complexity and urgency of environmental issues are becoming increasingly prominent. Therefore, understanding and enhancing the public's awareness and concern for environmental issues are crucial [1,2].

Research over the past few decades has shown that environmental education is an effective way to raise public awareness of environmental protection. It involves not only school education but also government and corporate publicity campaigns, community initiatives, and media channels. However, how to better implement environmental education and its specific effects on the public at different levels and backgrounds still require in-depth research [5].

This paper aims to comprehensively explore the impact mechanisms of environmental education on public awareness and analyze its practical applications at the government, corporate, and individual levels. Through a summary of existing research and practices, we will propose strategies to improve and strengthen environmental education to more effectively promote the formation of a positive environmental attitude and behavior among the public [8].

2. Environmental Education

In a broad sense, environmental education refers to an educational and practical process centered around the relationship between humans and the environment. It aims to enhance the awareness and capabilities of individuals regarding the natural environment by educating them about environmental issues. In a narrow sense, environmental education specifically involves students as the main recipients of education. Throughout the educational process, students acquire background knowledge related to the environment, fostering practical activities that develop their environmental psychology, environmental awareness, and environmentally responsible behaviors. Environmental education is a systematic, interdisciplinary educational process aimed at cultivating individuals' awareness, understanding, and respect for the environment, prompting them to adopt proactive environmental behaviors. Its goal is to cultivate citizens with environmental awareness and a concept of sustainable development, enabling them to understand the essence of environmental issues, participate in environmental practices, and pursue environmentally friendly lifestyles in their daily lives.

The significance of environmental education lies not only in providing environmental knowledge but also in inspiring public environmental awareness, fostering environmental values, and guiding individuals toward adopting sustainable lifestyles. Through environmental education, individuals can better understand the interrelationship between humanity and nature, recognize the impact of their behavior on the environment, and gradually become environmentally responsible citizens.

Research indicates that, through systematic environmental education, individuals are more likely to transform their environmental behavior into long-term habits. This transformation not only positively influences the quality of individuals' lives but also has a profound impact on the overall sustainable development of society.

The impact of environmental education on public awareness is evident in several aspects. Firstly, it enhances the public's level of awareness of environmental issues, enabling them to better understand urgent problems such as climate change and biodiversity loss. Secondly, environmental education contributes to shaping the public's understanding of sustainable development, encouraging them to make more environmentally friendly choices in their lives and careers. Most importantly, through environmental education, the public is more likely to engage in environmental activities, thereby facilitating actual environmental actions [9].

3. Factors of Influencing Environmental Education

3.1. Individual Factors

Knowledge: The extent to which individuals are aware of environmental issues directly relates to the formation of their environmental consciousness. Possessing systematic environmental knowledge helps individuals better understand the impact of human activities on the environment, thereby inspiring a positive environmental attitude.

Values: Individual values profoundly impact their environmental behavior. Values such as an emphasis on sustainable development and respect for natural ecosystems can guide individuals toward adopting environmentally friendly actions. Attitude: An individual's attitude toward environmental behavior is a crucial factor in shaping their actual actions. A positive environmental attitude implies a greater willingness to participate in environmental activities, support environmental policies, and promote the diffusion of environmental consciousness [10].

3.2 Social Factors

Culture: Cultural background has a profound influence on the formation of environmental concepts. Some societal values and traditional customs may align with environmental protection, while others may pose obstacles to environmental consciousness.

Education Level: There is a positive correlation between education level and environmental awareness. Individuals with a good education are more likely to understand the complexity of environmental issues, making them more inclined to take environmental action.

Media: Social media plays an increasingly important role in disseminating environmental information and shaping public awareness. Through social media platforms, environmental information can spread widely, shaping collective environmental perspectives.

3.3 Environmental Factors

Natural Disasters: Individuals who experience natural disasters are more likely to develop an awareness of environmental vulnerability, leading to a deeper environmental consciousness.

Environmental Quality: Individuals residing in relatively clean, healthy environments may be more likely to overlook environmental issues. Conversely, individuals living in areas with severe environmental pollution are more likely to pay attention to and participate in environmental actions.

These factors are interconnected, collectively shaping individuals' awareness and attitudes toward the environment. A thorough understanding of these factors contributes to the development of more targeted environmental education strategies [15].

4. Three Different Roles of Government Departments

4.1 Role of Government Departments

The government plays a crucial role in environmental education. By formulating clear environmental education policies, the government can provide direction for schools, communities, and businesses, ensuring the comprehensiveness and consistency of environmental education. Policy formulation should include the integration of environmental curricula, updating of teaching materials, and clear definition of education standards. The government should also encourage and support research to assess and enhance the effectiveness of environmental education [11].

The government needs to integrate various environmental education resources, including financial support, professional talent, and educational facilities. By establishing collaborations with schools, NGOs, and industry institutions, the government can better leverage the benefits of resources. This collaboration can promote knowledge sharing, the development of innovative environmental education methods, and broader community involvement [16].

Government departments should be responsible for organizing and supervising various environmental education activities. This includes activities within and outside schools, community initiatives, and public awareness campaigns. The government can establish dedicated environmental education institutions to monitor and evaluate the effectiveness of various educational activities, ensuring they align with the government's overall objectives. Additionally, the government should establish an assessment mechanism to track public participation levels in environmental education and improvements in public awareness of environmental issues.

Clearly defining and effectively executing these roles will contribute to ensuring the long-term sustainable development of environmental education, thereby cultivating more citizens with environmental awareness and initiative [13].

4.2 Role of Businesses

Businesses can enhance employees' environmental awareness through internal training and educational activities. This includes training on the company's sustainable development goals, resource efficiency, and how individuals impact the environment in their work. Through internal communication and training, businesses can instill a sense of environmental responsibility in employees, encouraging them to prioritize environmental issues in their work [3].

Businesses can adopt more environmentally friendly technologies and materials in product design and manufacturing processes to reduce their negative impact on the environment. Promoting green production not only helps lower the company's environmental footprint but also meets the growing demand from environmentally conscious consumers. Businesses can guide consumers toward green consumption by labeling environmental information on product packaging and introducing environmentally friendly product lines [4].

Businesses should recognize their importance in the community and take on social responsibility. By conducting environmental education activities in the community, businesses can disseminate environmental concepts and raise awareness among community residents. Additionally, businesses can participate in community environmental projects, such as clean-up activities and green initiatives, to fulfill social responsibilities through practical actions. This helps build a positive image for the business and enhances its social identity within the community [7].

Implementing these roles not only contributes to environmental protection but also enhances the competitiveness of businesses. More and more consumers and investors favor businesses that prioritize environmental sustainability and social responsibility.

4.3 Role of Individual

The individual's role in environmental issues begins with the learning of environmental knowledge. By participating in environmental courses, reading relevant literature, and staying informed through reliable news channels, individuals can develop a profound understanding of environmental issues. This knowledge acquisition helps spark an individual's interest in environmental issues and forms values aligned with sustainable development [6].

The personal responsibility for the environment is reflected in various aspects of daily life. This includes conserving energy, reducing waste generation, and choosing environmentally friendly products. By taking these practical environmental actions, individuals can directly minimize their negative impact on the environment, fostering a sustainable lifestyle. Additionally, by sharing experiences of these actions, individuals can influence their surrounding communities 14].

Individuals can contribute to environmental efforts by participating in various environmental activities such as tree planting, garbage cleanups, and environmental lectures. This not only benefits the environment but also spreads environmental ideas through social channels. Through social media, family, friends, and other avenues, individuals can share their environmental actions and perspectives, creating a positive feedback loop within society.

Individual environmental behaviors not only have a positive impact on the environment but can also amplify this influence through social networks, inspiring more people to participate in environmental activities [12].

5. Conclusion

Through a comprehensive study of environmental education, the following conclusions can be drawn:

⑴. Critical Role of Environmental Education: Environmental Education plays a crucial role in cultivating public environmental awareness and promoting sustainable development. By learning environmental knowledge, fostering environmental values, and taking environmental actions, individuals can become advocates and practitioners of sustainable development.

⑵. Crucial Importance of Collaboration: The success of environmental education relies not only on schools and educational institutions but also on the active participation of government, businesses, and individuals. Collaboration from various sectors ensures comprehensive support for environmental education, forming a societal consensus on environmental protection.

⑶. Interdisciplinary Integration as a Future Trend: With the increasing complexity of environmental issues, interdisciplinary integration is essential for the future development of environmental education. Integrating knowledge from sciences, social sciences, humanities, and more into teaching helps students develop a comprehensive understanding and problem-solving abilities for Environmental Issues.

References

[1] Buckler C, Creech H. Shaping the future we want: UN Decade of Education for Sustainable Development; final report[M]. Unesco, 2014.
[2] Carson, R. (1962). Silent Spring. Houghton Mifflin.
[3] Elkington J, Rowlands I H. Cannibals with forks: The triple bottom line of 21st century business[J]. Alternatives Journal, 1999, 25(4): 42.
[4] Hart S L, Milstein M B. Creating sustainable value[J]. Academy of Management Perspectives, 2003, 17(2): 56-67.
[5] Hungerford H R, Volk T L. Changing learner behavior through environmental education[J]. The journal of environmental education, 1990, 21(3): 8-21.
[6] Hines J M, Hungerford H R, Tomera A N. Analysis and synthesis of research on responsible environmental behavior: A meta-analysis[J]. The Journal of environmental education, 1987, 18(2): 1-8.
[7] Jenkins H. Small business champions for corporate social responsibility[J]. Journal of business ethics, 2006, 67: 241-256.
[8] Louise Chawla (1998) Significant Life Experiences Revisited: A Review of Research on Sources of Environmental Sensitivity, The Journal of Environmental Education, 29:3, 11-21, DOI: 10.1080/00958969809599114
[9] Rickinson, M., et al. (2004). A Review of Research on Outdoor Learning. National Foundation for Educational Research and King's College London.
[10] Schultz P W. The structure of environmental concern: Concern for self, other people, and the biosphere[J]. Journal of environmental psychology, 2001, 21(4): 327-339.
[11] Social responses to large technical systems: Control or anticipation[M]. Springer Science & Business Media, 2012.
[12] Steg L, Dreijerink L, Abrahamse W. Factors influencing the acceptability of energy policies: A test of VBN theory[J]. Journal of environmental psychology, 2005, 25(4): 415-425.
[13] Sterling S R, Orr D. Sustainable education: Re-visioning learning and change[M]. Totnes: Green Books for the Schumacher Society, 2001.
[14] Stern P C, Dietz T, Kalof L. Value orientations, gender, and environmental concern[J]. Environment and behavior, 1993, 25(5): 322-348.
[15] Stren P C. Toward a coherent theory of environmentally significant behaviour[J]. Journal of Social Issues, 2000, 56(3): 407-424.
[16] Tilbury D, Wortman D. Engaging people in sustainability[M]. IUCN, 2004.

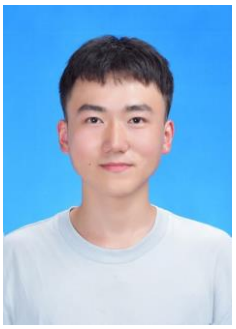

Mr. LIU CHENGXIN
Master student, Master of Environmental Engineering
Research Interests:
Wastewater treatment.

Dr. SU XIUJUAN
Associate Professor
Research Interests:
Microwave Metallurgy Technology and Theory, Harmless and Resourceful Utilization Technology and Theory of Tailings, Bio-flotation, Development of Biomass Carbon Materials, and Treatment of Heavy Metal Wastewater.

Experimental Study on High Pressure Sealing Performance of Water-filled Impedance Tube

Yiming Peng1*,Yifeng Fu11

1School of Automobile and Traffic Engineering, Jiangsu University,China
**E-mail: 1721179144@qq.com*

Abstract: Water acoustic tube is an important underwater acoustic material testing device, but most of the underwater acoustic tube can only meet the test under normal pressure, the test under high pressure environment is still facing some challenges, especially high pressure sealing is the research difficulty.This paper designed the high pressure seal of the acoustic tube, including the installation seal of the hydrophone of the tube, the sealing of the top sample and the bottom end of the underwater transducer section, using the design method of casing and O-ring respectively, which not only improves the sealing of the acoustic tube under high pressure, and ensures the fast and convenient installation of the hydrophone and sample. The hydrostatic pressure test shows that the designed water acoustic tube can stably maintain the pressure of 3.1 MPa without pressure relief and water leakage. The high-pressure underwater acoustic test shows that the test results of the underwater acoustic tube at 1.5 MPa pressure have good stability. This study provides the test basis for the design and improvement of hydraulic acoustic tube.

Keywords: High pressure,Sealing,Test study,Water acoustic tube

1. Introduction

Underwater acoustic material is to improve the underwater ship stealth and survival ability, because underwater acoustic materials long service in Marine environment, corrosion, high pressure, Marine attachments harsh environment coupling action put forward higher requirements for underwater acoustic materials, especially the deep sea of underwater acoustic testing put forward serious challenges. At present, the underwater acoustic materials are mainly tested by the underwater acoustic pipe, pressure tank, acoustic acoustic pool or free field method, among which the underwater acoustic pipe is suitable for small sample measurement, convenient to operate and high cost performance, and has been more widely used. The commonly used methods of water acoustic tube include transfer function method and acoustic pulse method. The basic principle is to generate one-dimensional plane wave in a rigid tube, and calculate the sound absorption coefficient of the material by testing the complex reflection coefficient and transmission coefficient of the sample in the case of vertical incident. At present, most studies of underwater acoustic tube only focus on underwater acoustic material testing, underwater acoustic tube design and new test methods, while there are few studies on high-pressure underwater acoustic tube. Air acoustic pipes are also mature testing equipment, but they hardly focus on high-pressure testing.[1]

In fact, as the depth increases in the ocean, the water pressure increases,and the submarine usually works depth of more than 300 meters, the corresponding water pressure of 3 MPa. In order to simulate the test environment of the deep sea, the underwater acoustic pipe must be designed with high pressure sealing. The sealing connection of the water acoustic pipe mainly exists in the installation part of the hydrophone and the upper and lower end flange interface, especially the installation part of the hydrophone. During the test process, the hydrophone needs to be disassembled and installed frequently, so it is necessary to take into account the firm and long time of the seal, as well as the convenience of disassembly. The O-ring is a commonly used sealing device, but is generally suitable for end surfaces. The hydrophone in the traditional water acoustic pipe is sealed through the O-ring, but it is difficult to ensure the sealing under high pressure, and there will be water leakage and pressure relief. For the sealing of the upper and lower flanges, the pressure head in part of the acoustic pipe equipment adopts the wood type head and the sealing ring. However, this design is not lasting, long time extrusion it is easy to lead to the sealing decline, and even the phenomenon of water leakage. There are many articles on the design and new test methods, but the problem of high pressure sealing. Therefore, it is necessary to design the high pressure seal of the high pressure water acoustic pipe and study the sealing performance test. In this paper, the author adopts the casing sealing design for the installation seal of the hydrophone of the pipe wall hydrophone, adopts the O-ring design method for the installation section of the sample section at the top of the acoustic pipe and the underwater transducer section at the bottom end, and verifies the sealing of the acoustic tube under the pressure of 3.1 MPa, and the acoustic test performance of the acoustic pipe under 1.5 MPa.[2]

2.Test device design

In order to realize underwater acoustic testing and high pressure environment simulation, the underwater acoustic pipe includes pipe system, tube system, pressure system, underwater acoustic source system, test system and auxiliary system. The pipe body system includes high pressure sealing design, and the schematic diagram of the underwater acoustic pipe design is shown below.

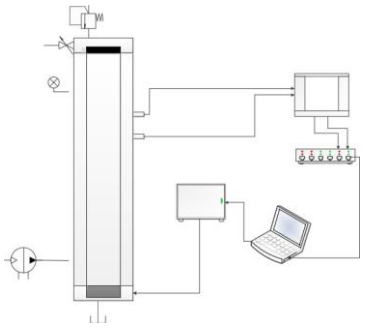

Fig.1. Schematic diagram of the test platform principle

2.1 Pipe body design

The impedance tubes are usually stainless steel and shall be straight and uniform in section (diameter or cross size within ± 0.2%) with rigid, smooth, non-porous walls with no holes or seams in the test section (except for hydrophone position). The wall thickness should be large enough that it does not vibrate by sound signals and no vibration resonance in the operating frequency range. For metal walls containing air, for circular tubes, Which recommended the thickness to be about 5% of the diameter. For aqueous metal walls, an

increased thickness is required. According to the relevant literature, and GB / T 143692011.The ratio of the thickness to the inner radius is not less than 1. In this design, the inner diameter is 120mm, so the thickness is not less than 60mm, so the outer diameter is selected as 250mm. Thus, the upper cutoff frequency f of the acoustic tube test can be determinedu ：

$$fu= 1.84cw/2a \quad (1)$$

Among cw ,it's the speed of sound in water, and it has a cut-off frequency of about 7000 Hz.[3]

The length of the tube is from the lower cutoff frequency fl Decision, for the transfer function method fl limited by the accuracy of the signal processing equipment, and avoiding the occurrence of non-plane wave propagation, the plane wave forms between the sound source and the sample, and the hydrophone measurement point should be in the plane wave field. For the pulse method, the acoustic tube must be long enough to accommodate that part of the standing wave required for the measurement, meaning that its length must contain at least one and two more desirable sound pressure minima. To ensure that at least two minima can be observed in the tube, the length shall meet Equation (2).

Where is the length of the tube, and p is the internal diameter of the tube. In this study, the works of China Shipbuilding Industry Corporation 702 Research Institute and Shanghai Jiao Tong University are taken as a reference, The lower cut-off frequency is 1000 Hz, and the length of the calculated tube is 1.2 m.[4]

2.2 High-pressure seal design

Two hydrophones need to be installed on the tube body as sensors, a sample fixture needs to be installed at the upper end, and an underwater transducer at the lower end as the sound source. The effect is as shown in Figure 2. The test pressure range of this design is 0-2 MPa and the pressure retention time is 1 hour, so these installation components require high pressure sealing design.[5]

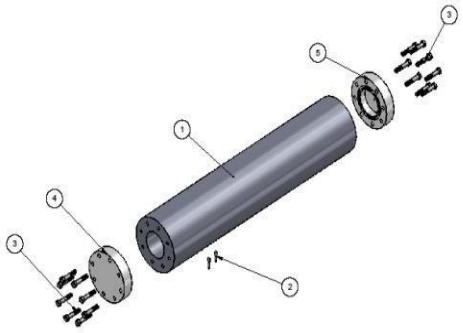

① Pipe body; ② hydrophone ; ③ bolt; ④ sample fixation end ; ⑤ sound source end

Fig .2. Diagram of the water filled impedance tube .

The installation and sealing design of the hydrophone is shown in Figure 3.The installation and sealing of the hydrophone is composed of sealing pipe and casing. The outer ring of the hydrophone itself includes a sealing ring, which ensures the sealing between the two by cooperating with the sealing pipe. Then, through the cooperation between the casing and the sealing pipe, the hydrophone is installed on the wall of the water acoustic pipe. The casing is locked, and the gap between the sealing pipe and the casing can be completely eliminated through the tightening thread. Compared with the simple O-ring seal, this design does not have the hidden danger of pressure relief and water leakage, and has the advantages of convenient and quick installation and disassembly.

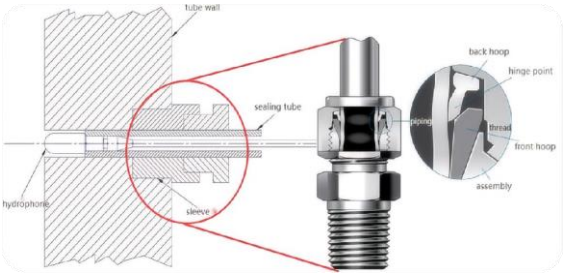

Fig.3.Schematic diagram of hydrophone tube wall installation and sleeve seal

The bottom and the top of the flange large contact, so they can be sealed through the O-ring, in order to meet the requirements of the design pressure, according to the standard. In this case, the O-ring specification is inner diameter 133.35 mm and outer diameter 146.05 mm, pair cover depth of 5.74 mm and 9.65 mm width, flange with O-ring in field test as shown in Figure 4.

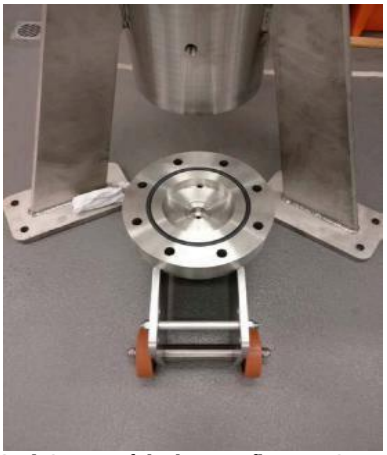

Figure 4. Seal O-ring of the bottom flange 1.3

Other subsystem design hydrostatic pressure can be generated by electric pump or manual pump foreasy control of this test platform. The connecting line should be able to balance the upper and lower hydrostatic pressure of the sample, otherwise the sample position will change and hinder the test results. Several stop valves must be provided for easy control.

The goal of the underwater acoustic pipe developed in this project is a wide frequency range. In order to meet the design requirements, it is necessary to select a suitable underwater sound source system. In order to generate sound source signal, signal generator, underwater transducer and power amplifier are required, realizing signal input by MATLAB homemade programming in this design.[6]

The sound pressure in the acoustic tube is the measured physical quantity of the test platform. The sensor used is the underwater acoustic phone, and the sound pressure signal received by the hydrophone is converted into the electrical signal, entered into the acquisition system by cable, and analyzed. The measurement system includes computer, data acquisition card, hydrophone, amplifier, signal source and power supply.

In order to realize all the functions of the acoustic tube, also need other auxiliary system, such as operating stand, water supply and drainage facilities, water used in the acoustic pipe for ultra-pure water after purification, the main purpose is to reduce the micro bubbles of the water of the influence of the test results, can also reduce the scale sediment caused by the use of tap water, and reduce the bubbles caused by often change water.[7]

3.Application of the test device

3.1. Test protocol

The test device is shown in Figure 4. In order to verify the high pressure sealing performance, hydrostatic pressure test and high pressure underwater acoustic test are designed. Three pressures were selected for hydrostatic pressure test, namely 3.15 MPa, 2.1 MPa and 1.5 MPa respectively, of which 2.1 MPa is the designed maximum working pressure ; 3.15 MPa is the maximum working pressure of 1.5 times as the maximum pressure; 1.5 MPa is the maximum pressure of the underwater transducer, which is the actual maximum working pressure of the water acoustic pipe. First, the inside of the water acoustic pipe is filled with super clean water through the manual pressure pump, and the bubbles mixed in the water injection process are eliminated for 24 hours before the hydrostatic pressure test begins. Increase the internal pressure of the water acoustic pipe to 3.15 MPa, record the pressure value displayed by the pressure meter every 10 minutes, and record the pressure value after 1 hour. Because the test operation of underwater sound absorption materials can be basically completed within 1 hour, the one-hour hydrostatic pressure test can fully meet the real test needs. Observe the overall condition of the water acoustic pipe during the recording process, and pay special attention to whether there is water leakage at each sealing seam. Thereafter, the hydrostatic pressure of 2.1 MPa and 1.5 MPa was performed, following the same procedure, and the test results were recorded.[8]

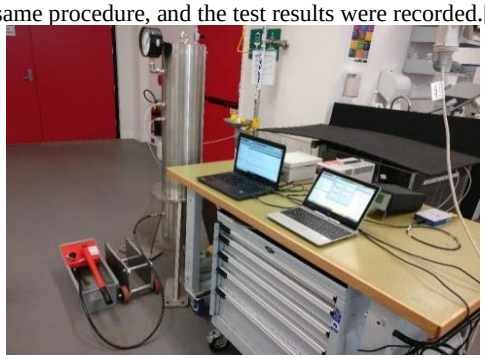

Fig. 4. Field test device of water acoustic pipe

The high-pressure underwater acoustic test object is an underwater sound absorption material sample, and the sound absorption performance of the test sample changes at 0 MPa and 1.5 MPa. The underwater sound absorption material is a nanocomposite made by the laboratory. The tested sample diameter is 120 mm and the frequency range is 1500 Hz to 7000 Hz, which has good sound absorption performance at atmospheric pressure. The test method is the transfer function method. The two points are selected in the acoustic pipe, and the sound pressure is obtained from the position coordinates. Even if the transfer function and the reflection coefficient , and the suction of the sample are obtained.

The acoustic coefficient α is :

$$\alpha = 1 - |r|2 \quad (2)$$

3.2 Test results and analysis

The results of the hydrostatic pressure test are shown in Figure 5. In the three tests of different hydrostatic pressure, the hydroacoustic pipe pressure could remain stable without any obvious pressure drop. When the initial hydrostatic pressure test was 3.15 MPa, the pressure drop was 0.01 MPa after 10 minutes and 30 minutes respectively, and the pressure remained unchanged in other times. For the test pressure of 2.1 MPa, the pressure drop of 0.01 MPa occurred at 10 minutes and 40 minutes, which means that the high pressure is more prone to the pressure drop. When the test pressure was 1.5 MPa, only one pressure drop of 0.01 MPa was observed at 20 min. During the whole pressure test process, there was no water leakage in the gap of each interface.[9]

According to the relevant literature, when the test pressure is 15 min and the pressure drop does not exceed 0.03 MPa, the pressure drop test is qualified, so that the underwater acoustic pipe can meet the requirements of high pressure underwater acoustic test [15]. The reason for the slight decrease in hydrostatic pressure may be the precipitation of partially dissolved microbubbles under high pressure and the infiltration of some gaps in the tube into less water under high pressure. The hydrophone and the top flange can still maintain the same good sealing effect after repeated disassembly.

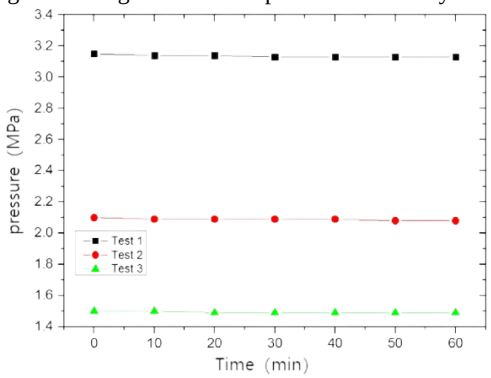

Fig. 5. Hydrostatic pressure change curve

The test results of underwater sound absorption material are shown inFigure 6. The material has good sound absorption performance under high pressure. Only the sound absorption coefficient of low frequency band 1500 Hz to 1800Hz is lower than 0.8, the sound absorption coefficient of high frequency band 4500 Hz to 7000 Hz is higher than 0.9, and the overall average sound absorption coefficient is close to 0.9. [10]When the material is under the hydrostatic pressure of 1.5 MPa, the underwater acoustic pipe still measures the stable and accurate underwater sound absorption coefficient of the sample, which can prove that the internal pressure of the underwater acoustic pipeunder high pressure is stable, and the internal sound field is also very stable, which fully meets the test requirements of underwater acoustics.[11] Compared with the underwater sound absorption coefficient at atmospheric pressure, the sound absorption performance of the sample is significantly reduced. The lowest sound absorption coefficient to 0.40, significantly lower than the lowest 0.76, even 1.5 MPa high pressure under the highest coefficient is only 0.68, also for the lowest coefficient under pressure, the average absorption coefficient down to 0.53, compared with 0.9 gap, this test also proved from the side of high pressure on underwater sound absorption material has obvious influence[16]. therefore,The design of underwater sound absorption materials must consider the influence of high pressure, and the high pressure underwater sound absorption performance must also be tested.[12,13

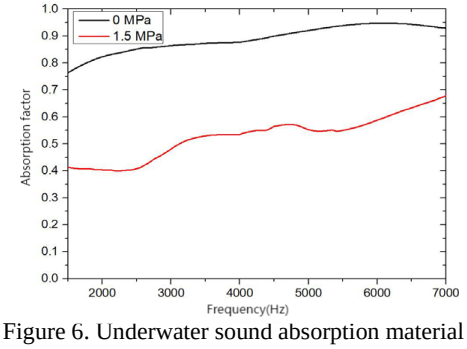

Figure 6. Underwater sound absorption material

4. Conclusions

A sealing device of high-pressure hydraulic acoustic pipe

is developed, in which the hydrophone realizes the sealing function through the sealing pipe and the casing, and the upper and lower flanges are sealed through the O-ring, and the feasibility of the designed sealing device is proved through the test. The hydrostatic high pressure test shows that the water acoustic pipe can maintain 3. 1MP a, with no water leakage, and the pressure can also be kept stable for a long time. The high-pressure underwater acoustic test shows that the average sound absorption coefficient of the underwater sound absorption material drops from 0.9 at atmospheric pressure to about 0.5 at 1.5 MPa, which is in line with the experimental law and further shows that the underwater acoustic pipe can meet the test of the high-pressure underwater sound absorption material. This device provides a test basis for the design improvement of the packer cylinder, a verification channel for the theoretical design model, and a test means for the evaluation of the sealing performance of the packer cylinder. It has important guiding significance for the selection of the packer cylinder model, the sealing performance test and test verification.[14]

References

[1] GB/T 14369-2011, Acoustics-Measurement methods of insertion loss, echo reduction and sound absorption coefficient for underwater acoustical material[S].
[2] ISO,10534-2, 1998 Acoustics-Determination of sound absorption coefficient and impedance in impedance tubes-Part 2: Transfer-function method.
[3] LI S, SHEN J X, TANG H Q, et al. Measurement for low-frequency properties of underwater acoustic materials in a standing wave tube[J]. Acta Metrologica Sinica, 2003, 24(3): 221-224.
[4] DAI Y, YANG J H, HOU H, et al. The absorption coefficient measurement of the underwater material in water tube with the wide-band pulse method[J]. Acta Acoustica, 2017, 42(4): 476-484.
[5] YAO G C, DAI Y, MA X M, et al. Design and realization of sound absorption coefficient test system based on transfer function method[J]. Instrument Technique and Sensor, 2022,478(11):55-59.
[6] ZHU P L, HUANG X C. Key anechoic technology of submarines-design of acoustic coatin
[7] WANG Q Q, MA G L, ZHENG G Y, et al. Test and analysis of dynamic sealing performance of large size O-shaped nitrile rubber ring[J]. Lubrication Engineering,2022,47(2):116- 121.
[8] WILSON P S, RONALD A, WILLIAM M C. An improved water-filled impedance tube[J]. The Journal of the Acoustical Society ofAmerica, 2003,113(6): 3245-3252.
[9]WANG Y. The Noise Elimination design in fan-tube and the research of water-tube experimentation[D]. Beijing: Beihang University, 2005.
[10] GUO F, WEN T Z, HUANG Y J, et al. Experimental study on high temperature and high pressure sealing performance of packer rubber[J]. Lubrication Engineering, 2020, 45(7): 23-27.
[11] FU Y F, JEOFFREY F, PAN K Q, et al. Underwater sound absorption properties of carbon nanotube composites with steel plate backing. Applied Acoustics,2021, 107668.
[12] SUN L, HONG H. Measurement of sound absorption by underwater acoustic material using pulse-separation method[J]. Applied Acoustics, 2014, 85: 106- 110.
[13]WANG Q H. The basic study on water acoustic absorption polymer materials[D]. Changsha: National University of Deference Technology, 2009.
[14] LI Y, XU F, LIN Z S, et al. Electrically and thermally conductive underwater acoustically absorptive graphene / rubber composites for multifunctional applications[J]. Nanoscale 9.38 (2017): 14476- 14485.
[15] ZHANG H L, ZHONG G R, ZHU Z W. Hydrostatic pressure test technology for deep-sea equipment[J]. Naval Architecture and Ocean Engineering, 2019, 35(05):14- 19.
[16] FU Y F, WANG H M, CAO P. Thin shell structure enhanced nano composite coating for deep-sea high pressure sound absorption[J]. China Mechanical Engineering, 2022, 33(12): 1444- 1451.

Innovation Agricultural Museum of the Maejo University

Chokanan Wanitlertthanasarn [1], Punsak Pakdee [1], and Tanwutta Thaisuntad [1*]

[1] *Faculty of Architecture and Environmental Design, Maejo University, Chiang Mai, Thailand*
**Corresponding author, E-mail: Tanwutta1@gmail.com*

Abstract:
The "Agricultural Innovation Museum" project of the Maejo University is designed to be a center of information and knowledge about agricultural innovation of Maejo University. It contributes public opportunity to access the knowledge and innovation from a base of physical, biological, cultural and local wisdom resources. The museum is designed on national development process to agriculture, food and health sectors. Goals of architectural design intend to identity and uniqueness of Maejo University agriculture where harmony with the local context. The method of concept design is inspired by the rice seeds which is a prominent symbol of farmers, representing the Maejo University's leadership in agriculture study. The museum contributes the Universal Design and appropriate energy to the public users. Important results of the project are participation in design by stakeholders at all levels. To conclude with the goal of developing Maejo University to become a "University of Life", the process intends to be Organic University, Green University, and Eco University attribution.

Keywords: agriculture museum, rice seed, Maejo University, Organic University, Green University, Eco University

1. Introduction

1.1 Background

Her Royal Highness Princess Maha Chakri Sirindhorn permission granted Maejo University hosting an academic conference and exhibition according to the Plant Genetic Conservation Project (PGCP) on 23 March 2021. Therefore, the "Agricultural Innovation Museum" project of Maejo University is designed to be a continuous and sustainable extension of such activities. It is a center of information and distribution of knowledge regarding agricultural innovation of Maejo University to the community and providing knowledge to the public. Innovation of the museum contents are based on physical, biological, cultural and local wisdom resources which enhancing national development to the agriculture, food and health sectors.

1.2 Brief literature

1.2.1 Analysis of the project area

The concepts of "Museum Cultural District" [5] have been summarized as conditions for selecting an area. Case study of the Maejo University's Agricultural Innovation Museum is preparing, learning, and developing education toward the 21 st century, i t is considered in principles as follows:

-Network externalities Number of concerned networks are highly guaranteed for success. Museum density in a limited space can creates cultural connections with other museums. The limited space allows people to connect with the stories and cultures of the area. The density of this museum can attract more visitors and tourists to the area than standing alone for a district.

- Consumption externalities of cultural connections Cultural concern always connects to awareness of the public. It is causing an increase in various public services and utilities in some ways. Impact of activities that involve many people can be measured by the start of a group of people entering a museum. This causes some trends for other groups of people to come and do the same. While a neighborhood succeeds in making a

large number of people interested in a museum, it is creating affect to the critical mass in positive supporting influx of visitor and tourist outcomes.

-Externalities of time temporary exhibition A museum i s consisting of permanent and t emporary exhibition. Temporary exhibitions are difficult for tourists to visit all different topics through the year. Planning and exhibition design should consider outstanding contents for available highlights for a limited time.

- Economies of scale and scope Identify an appropriate size of the museum district will result in cost savings. Save costs according to the principle of "economies of scale" to become practical policy to each museum.

1.2.2 Concept design for an agricultural museum

Agricultural Innovation Museum has a mission to focus on being a source of learning and disseminate agricultural, food and health innovations based on physical, biological and intellectual resources, showing the identity of agriculture in the northern region. Building on the knowledge base of the university, the Plant Genetic Conservation Project (PGCP), and network partners. With the philosophy of knowledge, practice, results, build on, and be sustainable, leading to " Less, Enough, Beautiful." concept.

Learning museum networking is a tool for lifelong learning for all. It is a place that promotes equality creating and individual opportunities to develop potential and values. Feelings and attitudes are also encouraging lifelong education. [3]

1.2.3 Participation in design

The design process will focus on designing to meet the needs of different groups of users. (User-Centered Design). It has a method to measure user satisfaction (User Experience) together with the participatory design process. (Participatory Design), which is important in creating long-term user satisfaction [4]

Participatory design process (Participatory Design) will help bridge the gap between designers and users. There are 3 conditions to use as following; 1) the physical characteristics of the user that affect the shape, size, and material functionality 2) the psychology of response, such as attitude and positive feelings towards use 3) culture and traditions which is a design reaches and understands the context of use in that area [1]

Attending to the opinions and needs of stakeholders is important. Outstanding steps of the user-centered design process will focus on the needs and satisfaction users as the main goal. Through discussion and understanding of the needs and observing user reactions are also included. [6]

1.3 Goals

1. To respond the Plant Genetic Conservation Project (PGCP) under the royal initiative of Her Royal Highness Princess Maha Chakri Sirindhorn
2. To contribute knowledge of the PGCP and Maejo University to the public
3. To design Maejo University's Agricultural Innovation Museum archhitecture that represents identity of Maejo University

Fig 1 Location of the design project

1.4 Scopes.

The project area is17,600 square Meters (11 Rais) situates in the Maejo University, Chiang Mai Campus. 1001 and 1367 Rd. from the Chiang Mai city.

2. Methods

2.1 Problem analysis Design limitations

According to location analysis, the project is located in the lower right corner of the campus that lack of main circulation then functional accessibility must be considered to the site. Therefore, additional entry and exit gates have been added to facilitate access to the project. The project site situates oriented along the southwest and northeast axis. The design orientation is needed to plan layout in protectional utilization from high temperature of the east, south, and west side from the sun path of the day and seasons.

Project location is a linkable area to the Organic Agriculture Learning Center where demonstrations rice farming and gardens. The museum design needs to consider the use of space linking activities. Finding the outstanding identity of the Maejo University in agriculture is a main concept creating under the practical budget and time frame**.**

2.2 Detailed information

Architectural design intends to express identity, agriculture uniqueness, and harmony with context of the Maejo University district. The design concept is inspired by the rice seeds which is a prominent symbol of Thai farmers. Products of the rice farming are not only consumed domestic but also exported as international products from Thailand to the world market.

The r ice seeds and farming also represent continuously prosperity and fertile ears of rice growing. This is a circular cycle through the design of the architectural form which represents the Maejo University's agricultural leadership. Enhancing public space of the museum in term of the Universal Design to facilitate all people and energy saver.

2.1 Concept, participation, and requirement process

-To define the concept and identity symbol to the museum by agreement of designer team, PGCP committee, and university members.

-To participate with the stakeholders such as local community, university's officers, PGCP committee, alumni society, and students

-To summarize functional requirements Bill of Quantities (BOQ), feasibility, and sum budget of the project

2.2 Primary design process

-To make preliminary sketch design which inspired from the "rice seeds" in various forms and styles for selective development. Including with layout, plan, and interior are created as a first draft of idea.

- To discuss and select some of initiative plans and ideas developing to the secondary design process.

2.3 Secondary design process

- To develop selected plans and styles for more functional details, feasibility, and basic materials.

-To design and develop functional details in construction such as infrastructure, water and electric system, circulation and parking lots, including Universal Design for public users.

-To design final model of the project presenting overview perspectives for stakeholders consideration.

-To present final model to the executive committee, there are the Maejo Natural Agriculture Museum's board, consultants, PGCP, the Golden Jubilee Museum of Agriculture Office (Public Organization), and the National Scient Museum Organization.

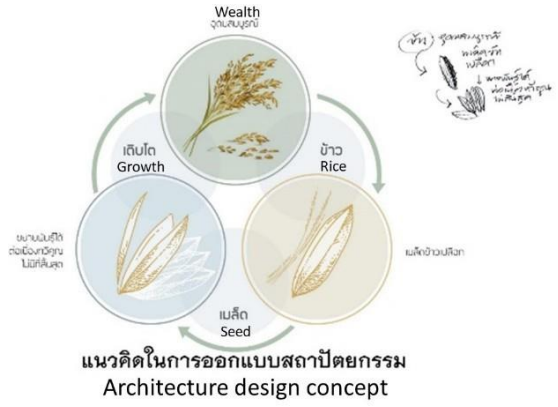

Fig 2. Architecture design concept

3. Results and Discussion

3.1 Concept, participation, and requirement process

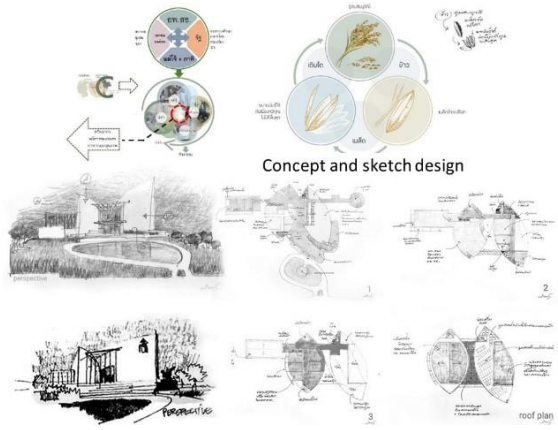

Fig 3. Concept and primary design process

This process contributes application of concepts in designing various parts of the project, such as designing building shapes, interior, landscape design, decoration, and building materials.

3.2 Primary design process

Fig 4. Primary design process

3.3 Secondary design process

This process designs plans for consideration, such as area plans, floor plans, cross-sectional plans, side plans, perspectives, and site plans overlaying for presentation.

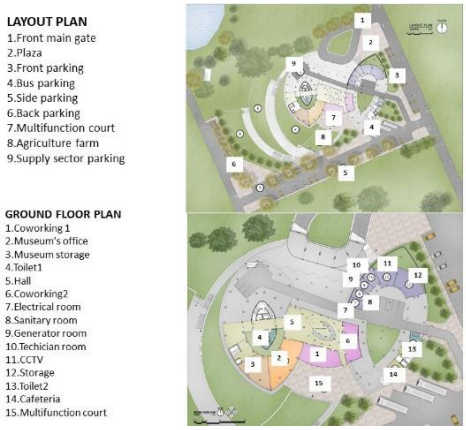

Fig 5. Secondary design process: Layout and floor plan design

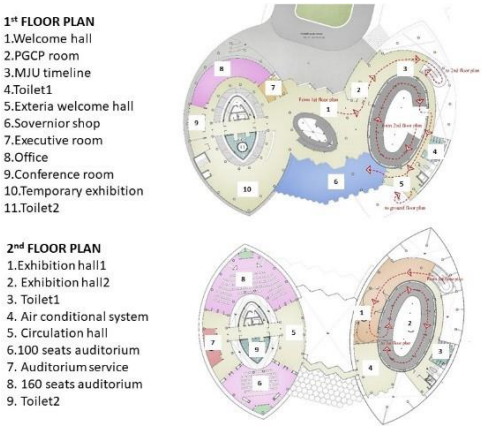

Fig 6. Secondary design process: Floor plan design

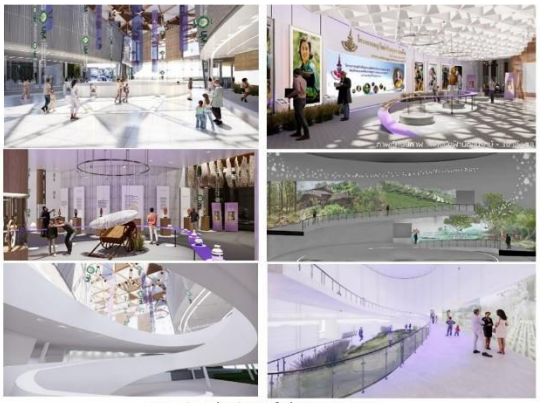

Fig 7. Secondary design process: interior design

Fig 8. Secondary design process: exterior design

Fig 9. Secondary design persppective1-2 of the museum

Fig 10. Secondary design process: overview perspective design

4. Conclusions

4.1 Aim or objective

Agricultural Innovation Museum of the Maejo University is a "Life Museum" or a living museum where encourages physical arrangements for facilitate learning. Enhancing future skills, knowledge and abilities for the 21st century to visitor and student. Particularly, the museum encourages young visitor to proceed lifelong learning and visionary skill for future entrepreneurship and labor market in agricultural movements.

Benefits of the design

-The project responds to the royal initiative under the Plant Genetic Conservation Project (PGCP) under the royal initiative of Her Royal Highness Princess Maha Chakri Sirindhorn

- The project is the center for contribute knowledge of the PGCP and Maejo University to the public

- The project creates value for the Maejo University's Agricultural Innovation Museum project where enhances identity of the university roles to the national perspective

4.2 Problems, limitations and solutions

Creating museum spaces or organizing exhibitions are intended to provide roles of the PGCP and the Maejo University to the country.

The project required more participation with involved professional groups in both reginal and national sectors to achieve highest utilization of space, personnel, resources, knowledge and learning resources for the future. Agricultural Innovation Museum of the Maejo University has a mission to be a learning center and cultivate agriculture, food, and health innovations based on physical, biological, and intellectual resources in a conceptual framework of "Noi Por Ngam" (Less-Enough-Beautiful) Aiming at creating knowledge, understanding and the learning process of agricultural innovation in the form of exhibition and media learning experience. Systematic analytical thinking is emphasis on practical teaching and revision to the 21st century entrepreneurship. There are short courses created toward creativity, continues, expands, develops, and creates awareness to the next generation of national agriculture growth. The national resource, cultural heritage, and local wisdom in cultivation are designed to sustainability in conservation.

5. References

[1] Gould, J. D. and Lewis, C.(1985). "Designing for usability: Key principles and what designers think". Communications of the ACM. 28 (3). 300-311.

[2] Jean Piaget. (1896). *The origins of intelligence in children*. New York: W.W. Norton & Company.

[3] J Kaewphichit. (2016). A study of the learning process in museums. to enhance learning throughout life. Journal of Human Resource and Organizational Development Faculty of Human Resource Development National Institute of Development Administration.

[4] Turan, S. Ö., et al. (2016). User evaluation of the urban park design implementation with participatory approach process. Procedia Social and Behavioral Sciences. 216, 306 – 315.

[5] Walter Santagata. (2002). *Cultural districts, property rights, and sustainable economic growth.* University Library of Munich, Germany.

[6] Zeisel, J. (2006). Inquiry by Design : Environment / Behavior / Neuroscience in Architecture, Interior, Landscapes and Planning. New York: Norton & Company.

Dr. Chokanan Wanitlertthanasarn
Lecturer/Dean
Born on 2 February 1973
Majoring in Architecture Design

Punsak Pakdee
Assistant Professor
Born on 27 January1978
Majoring in Architecture Design

Dr.TanwuttaThaisuntad
Assistant Professor
Born on 22 March 1977
Majoring in Architectural Heritage Management and Tourism

Assessment of the energy potential of residue materials from pineapple cultivation in the northern region of Thailand

Supamas Thaweesuk[1*], Tanate Chaichana[1], Kittikorn Sasujit[2], Pakamon Pintana[2]

School of Renewable Energy, Maejo University, Chiang Mai, Thailand
*Corresponding author, E-mail: ningsupamasthaweesuk@gmail.com

Abstract: The research investigates the energy potential of pineapple leaf residues using cold compression and cassava starch as a binder. The study involved analyzing the energy potential of leaves and carbonizing them at 350 °C to produce briquettes in 90:10, 80:20, and 70:30 ratios. In this process, briquettes were meticulously produced in varying ratios. The findings reveal significant heat values, with raw pineapple leaves exhibiting a heat value of 18.92 MJ/kg, while the engineered briquettes demonstrated a substantially higher heat value of 31.92 MJ/kg. The study further delved into the properties of the briquettes, noting key metrics such as moisture content at 20.01%, volatile matter at 45.79%, fixed carbon at 42.82%, and ash content at 8.08%. Elemental analysis provided further insights, revealing a composition of hydrogen (4.12%), oxygen (23.79%), carbon (62.59%), and nitrogen (1.83%). The study emphasized temperature's crucial role in altering the physical and chemical properties of the briquettes. It estimated the energy potential of pineapple residues in the northern region at 84.76 ktoe. This research contributes to sustainable energy sources by utilizing pineapple cultivation waste, offering insights into effective briquette production, and highlighting the region's substantial energy potential.

Keywords: Carbonizing process, Charcoal, Energy Potential, Pineapple leaves

1. Introduction

In the pursuit of sustainable energy solutions and environmental conservation, the exploration of alternative and renewable energy sources has become increasingly imperative. While the agricultural sector often stands as an overlooked reservoir of untapped resources, this thesis seeks to address this oversight by conducting a comprehensive assessment of the energy potential inherent in residue materials generated from pineapple cultivation in the northern region of Thailand. Specifically, the focus of this study extends to the utilization of these residues for charcoal production, a valuable avenue for sustainable energy [1-5].

Thailand, renowned for its agricultural prowess, has witnessed a significant surge in pineapple farming, particularly in the northern region [6]. As the pineapple industry thrives, it concurrently generates substantial volumes of residue materials, including leaves, stems, and peels, often considered as waste [7 - 8]. However, these byproducts contain intrinsic energy content that, if harnessed efficiently, could serve as a valuable source for renewable energy production, especially in the form of charcoal [9].

The northern region of Thailand, characterized by its fertile agricultural landscapes and vibrant pineapple cultivation, serves as the epicenter for this study. By delving into the specific composition of pineapple residue materials and employing advanced analytical techniques, this research aims to quantify their energy content and assess the feasibility of converting them into charcoal. The exploration of viable technologies such as pyrolysis, a process involving the thermal decomposition of organic materials, will be integral to understanding the most efficient and sustainable methods for charcoal production from pineapple residue [10-12].

Furthermore, this study will evaluate the environmental implications of harnessing energy from pineapple residue for charcoal production, taking into consideration factors such as reduced greenhouse gas emissions and other environmental benefits associated with charcoal as a renewable energy source. Additionally, an economic analysis will be conducted to assess the viability of implementing such bioenergy initiatives in the context of the local pineapple industry, specifically focusing on the economic feasibility of charcoal production [13].

In summary, this thesis aspires to shed light on the largely untapped energy potential embedded in the residue materials of pineapple cultivation in the northern region of Thailand, with a specialized focus on their suitability for charcoal production Through a multidimensional exploration encompassing technical, environmental, and economic perspectives, the findings of this research endeavor to provide valuable insights for policymakers, agricultural stakeholders, and energy enthusiasts alike, contributing to the sustainable development of the region and beyond [14-15].

2. Methods

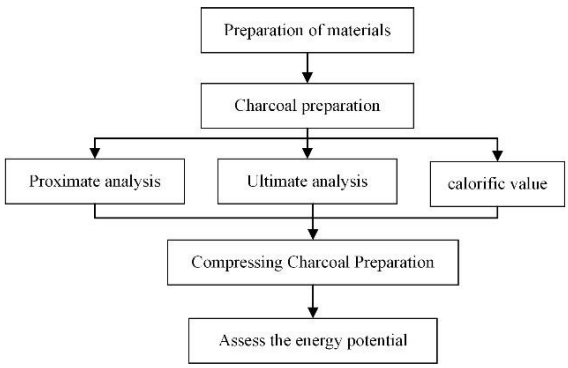

Figure 1. Experimental Procedure.

2.1 Preparation of materials

Study focused specifically on the cultivation of pineapples as raw materials for input into the factory.

2.2 Charcoal preparation

The material preparation in this research is associated with residue materials from the pineapple cultivation process, which were sourced from a plantation located in Ban Doo, Mueang District, Chiang Rai Province, Thailand. The primary material comprises pineapple leaves remaining after agricultural processes.

The initial stage of charcoal preparation involves reducing the moisture content of pineapple leaves through sun-drying for a period of one week. This step is conducted to acquire essential data for proximate analysis, ult imate analysis, and calorific value assessments.

2.3Compressing Charcoal Preparation

The dried pineapple leaves, after reducing moisture content, undergo the carbonization process using a 50 L-sized kiln at a temperature of 350°C for 2 hours. The charcoal is then pulverized into fine particles and filtered through a 150 μm sieve for approximate analysis, ultimate analysis, and calorific value assessment.

2.4 Production of bio-briquette

Each adhesive was mixed with carbonized in a briquette mold until homogeneous. The percentage composition of each adhesive and the carbonized charcoal were respectively 10 and 90%, which makes the composition of sludge, pineapple peels, and adhesives in the ratios of (90:10), (80:20), (70:30), respectively. Afterward, the thoroughly blended mixture was compacted to form a rectangular bio-briquette using a manual briquette press with a dimension of 5 cm x 5 cm x 7 cm. The resulting briquettes were dried for 1–2 days under sunlight to reduce the water content

2.5 Proximate analysis

2.5.1 Moisture content test

The moisture experiment begins by weighing the Porcelain Crucible. The Porcelain Crucible is heated at a temperature of 105 °C for 1 h. The Porcelain Crucible is then placed in a Dessicator Porcelain Plate. The weight is recorded before and after heating.

$$M = \frac{(m_3 - m_1)}{(m_2 - m_1)} \times 100$$

Where
M = Percentage of the moisture content as analyzed.
m_1 = The mass in gm of the empty crucible plus lid.
m_2 = The mass in gm of the dish plus lid plus sample before drying.
m_3 = The mass in gm of the dish plus lid plus sample after drying.

2.4.2 Ash content test

The ash experiment begins by weighing a 1 g sample in a porcelain crucible. Place the sample in a ceramic crucible and heat it in a furnace at a temperature of 500 °C for 1 hour. Then, increase the temperature by an additional 200 °C and continue heating for another 2 hours. Remove the porcelain crucible from the furnace and place it on a porcelain plate in a desiccator. Record the weight before and after heating.

$$A = \frac{(m_3 - m_1)}{(m_2 - m_1)} \times 100$$

Where
A = Percentage of the ash content as analyzed.
m_1 = The mass in gm of the empty dish.
m_2 = The mass in gm of the dish plus sample before heating.
m_3 = The mass in gm of the dish plus sample after heating

2.4.3 Volatile matters test

The volatile experiment by weighing a 1 g sample in a porcelain crucible. Close the lid tightly and put it into the furnace at a temperature of 950 °C. Leave the sample in the furnace for 7 minutes. Remove the porcelain crucible from the furnace and place it in a Dessicator Porcelain Plate. Record the weight before and after the evaporation process.

$$VM = \frac{(m_3 - m_1)}{(m_2 - m_1)} \times 100 - M$$

Where
VM = Percentage of the volatile matters content as analyzed.
m_1 = The mass in gm of the empty crucible and lid.
m_2 = The mass in gm of the crucible and lid plus sample before heating.
m_3 = The mass in gm of the crucible and lid plus content after heating.

2.4.4 Fixed carbon calculation

In general, fixed carbon is a solid carbon in solid biomass fuels, which stays in the char after pyrolysis and devolatilization processes. It was calculated as shown in the empirical equation

$$\%FC = 100(\%M + \%A + \%VM)$$

2.6 Ultimate analysis

2.6.1 Carbon element C

The following correlation, Equation, in terms of fixed carbon FC, volatile matters VM, and ash content A was used to compute the carbon element (C) composition in weight percent

$$C = 0.635(FC) + 0.460(VM) - 0.095(A)$$

2.6.2 Hydrogen element H

The following correlation, Equation, in terms of fixed carbon FC, volatile matters VM, and ash content A was used to computing the hydrogen element (H) composition in weight percent

$$H = 0.059(FC) + 0.060(VM) + 0.010(A)$$

2.6.3 Oxygen element O

The following correlation, Equation, in terms of fixed carbon FC, volatile matters VM, and ash content A was used to computing the oxygen element (O) composition in weight percent

$$O = 0.340(FC) + 0.469(VM) - 0.023(A)$$

2.7 Physical properties analysis

2.7.1 Density measurement.

The density of the briquettes was calculated from the mass-to-volume ratio of the briquette sample, which was influenced by applied pressure on briquette making. A rectangular-shaped container of 112 cm^3 was used for determination. The measurement was done referring to SNI 1973:2016 about the Density Measurement Method. The calculation of density was defined by using Equation.

$$D = \frac{m}{v}$$

2.7.2 Compressive strength.

Compressive strength testing is often employed to assess the ability of a briquette to withstand crushing loads. This test is conducted using a Universal Testing Machine, which measures the maximum crushing stress that the briquette can endure before breaking.

2.8 Calorific value

The calorific value is determined by conducting a combustion test using a bomb calorimeter. The fundamental principle of the bomb calorimeter is to combust a sample material in a closed container filled with oxygen. Then, the heat of combustion is measured at a constant volume. The calorific value has an impact on the quality of the briquette. Increasing this value improves the quality of the briquette. Additionally, the type of adhesive also affects the calorific value. Increasing the amount of adhesive decreases the calorific value because the moisture in the binder can reduce the carbon content, leading to a decrease in calorific value.

3. Results and Discussion

Table 1. Analysis results proximate analysis

Parameter	Charcoal
Moisture content (%)	20.21
Ash content (%)	8.08
Volatile Matter (%)	45.79
Fixed Carbon (%)	42.82

Using charcoal as an energy source, it is advisable to choose one with a high Fixed Carbon content and low Moisture content. On the other hand, if it is intended for use as a raw material in production or for burning purposes, attention should be given to the Ash Content value.

Table 2. Analysis results ultimate analysis

Parameter	Charcoal
H (%)	4.12
O (%)	23.79
C (%)	62.59
N (%)	1.83

The high carbon content indicates the ability to provide energy when burned. The high oxygen content, mostly derived from water or other sources with oxygen, can impact combustion and efficiency in energy production. The moderate hydrogen content can affect resilience. The low nitrogen content, while not significant, may still have an impact on combustion efficiency.

Table 3. Analysis results calorific value

Parameter	Charcoal
Calorific value (MJ/kg)	31.92

It seems like you've provided information about the pyrolysis of biochar and its effects on the elemental composition, specifically carbon (C), oxygen (O), hydrogen (H), and nitrogen (N). The text mentions that at higher pyrolysis temperatures, there is a significant decrease in oxygen and hydrogen content, which can be attributed to various chemical processes such as the breaking down of weak alkyl-aryl ether bonds, dehydration, and the release of gases like CO, CO_2, and H_2 as syngas.

The increased nitrogen content in biochars compared to the original feedstock (PPR) is suggested to be a result of pyro-compound formation during pyrolysis, leading to the incorporation of nitrogen into the heterocyclic structure of biochar. Additionally, the text notes that nitrogen content in biochar is more influenced by the type of feedstock used rather than the specific pyrolysis conditions.

Overall, this information provides insights into the chemical changes occurring during the pyrolysis process and how they impact the elemental composition of biochar. If you have specific questions or if there's anything specific would like to know or discuss further

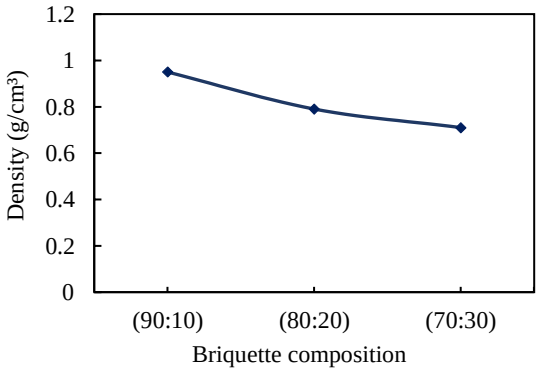

Figure 2. Effect of adhesives and briquette composition on density.

The graph illustrates the proportions of charcoal and cassava starch in the production of briquettes, along with the corresponding density of the briquettes. The characteristics are as follows (90: 10) Proportion: 90% charcoal, 10% cassava starch Briquette Density: 0.95, (80: 20) Proportion: 80% charcoal, 20% cassava starch Briquette Density: 0.79, (70: 30) Proportion: 70% charcoal, 30% cassava starch Briquette Density: 0.71, From this data, i t can be observed that an increase in the proportion of cassava starch in the composition of the briquettes results in a decrease in density. This may have implications for the quality and efficiency of the briquettes in practical use.

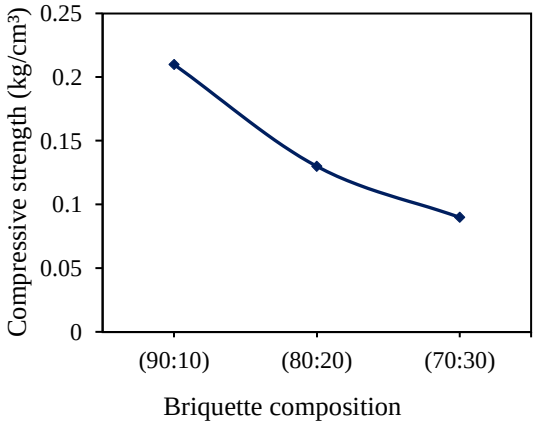

Figure 3. Effect of adhesives and briquette composition on compressive strength

The addition of sludge increased the compressive strength so that briquettes were more consistent and compact. The highest compressive strength (0.2151 kg/cm^3) was obtained by a briquette composition of 90:10 with tapioca starch adhesive. This adhesive was very good for producing higher compressive strength than cow dung and rejected papaya because tapioca adhesive had a denser particle arrangement [31]. The least value of compressive strength (0.04071 kg/cm^3) was obtained by briquettes composition of 70:30 with cow dung adhesive. This was due to the raw material used being biomass waste. Briquette from biomass tends to crack and break easily because of its less dense texture.

4. Conclusions

The study found that good quality briquette characteristics were produced from 0% sludge, 90% pineapple peel, and 10% starch as a proportion. This composition had the following properties: 20.01% moisture content, 8.08% ash content, 45.79% volatile matter, 42.82% fixed carbon, and 31.92 MJ/kg calorific value. Composition of 4.12% hydrogen, 23.79% oxygen, 62.59% carbon, 1.83% nitrogen. Additionally, briquette with starch as the adhesive had better physical properties compared to adhesive from rejected papaya and cow dung.

References

[1] Alhwayzee, Mohammed, et al. “Evaluation of Solid Biomass Fuel for Some Iraqi Agricultural Wastes Using Proximate and Ultimate Analyses.” *IOP Conference Series*, vol. 671, no. 1, 1 Jan. 2020, pp. 012006–012006.

[2] Ismi Khairunnissa Ariani, et al. “Production of Bio-Briquettes from Pineapple Peels and Sewage Sludge as an Alternative Renewable Energy.” *IOP Conference Series*, vol. 1201, no. 1, 1 June 2023, pp. 012014–012014.

[3] Mohanty, A. K., et al. “Sustainable Bio-Composites from Renewable Resources: Opportunities and Challenges in the Green Materials World.” *Journal of Polymers and the Environment*, vol. 10, no. 1/2, 2002, pp. 19–26.

[4] Song, Shuhui, et al. “Properties of Biochar Obtained from Tropical Crop Wastes under Different Pyrolysis Temperatures and Its Application on Acidic Soil.” *Properties of Biochar Obtained from Tropical Crop Wastes under Different Pyrolysis Temperatures and Its Application on Acidic Soil*, vol. 13, no. 3, 20 Mar. 2023, pp. 921–921.

[5] Srisophon, Mewadee, et al. “Characterization of Thermal Distribution in 50-Liter Biochar Kiln at Different Heating Times.” *IOP Conference Series: Earth and Environmental Science*, vol. 463, 7 Apr. 2020, p. 012079.

[6] Upadhyay, Atul, et al. “Utilization of Pineapple Waste: A Review.” *Journal of Food Science and Technology Nepal*, vol. 6, 29 June 2013, pp. 10–18.

[7] Faizah S I and Husaeni U A 2018 *Int. J. Energy Econ. Policy* 8 313–21

[8] Drozyner P, Rajmer W, Starowicz P, Klasa A and Skibniewska K A 2013 *Technical Sci.* 16 211– 20
[9] Yerizam M, Zaman M, Jauhari T, Yuli N, Setiawan R and Affrilla U 2021 *Proceedings of the 4th Forum in Research, Science, and Technology (FIRST-T1-T2-2020)* 7 57–61
[10] Haryana A 2018 Pengembangan Pemanfaatan Biomassa sebagai Energi Terbarukan untuk Mencapai Bauran Energi Nasional yang Optimal *Ministry of National Development Planning* 1 55–65
[11] Sharukh Khan; Vivek Paliwal, Vikrant Vikram Pandey V K 2015 *Int. Adv. Res. J. Sci. Eng. Technol.* 2 197–205
[12] Ifa L, Yani S, Nurjannah N, Sabara Z, Yuliana Y, Kusuma H S and Mahfud M 2019 *Ecol. Environ. Conserv.* 25 S125–31
[13] Benti N E, Gurmesa G S, Argaw T, Aneseyee A B, Gunta S, Kassahun G B, Aga G S and Asfaw A A 2021 *Biotechnol. Biofuels* 14 1–24
[14] Perea-Moreno M A, Samerón-Manzano E and Perea-Moreno A J 2019 *Sustainability (Switzerland)* 11 863
[15] Chaudhary V, Kumar V and Singh K 2019 *J. Pharmacogn. Phytochem.* 8 4642–52
[10] Huang Y L, Chow C J and Fang Y J 2011 *J. Food Drug Anal.* 19 4

Ms. Supamas Thaweesuk
Master student, Master of Engineering (Renewable Energy Engineering).
Research Interests:
Biomass

Dr. Tanate Chaichana
Assistant Professor
Research Interests:
Energytechnology, Energy, Renewable energy

Dr. Kittikorn Sasujit
Assistant Professor
Research Interests:
Energy technology, Energy, Renewable energy

Dr.Pakamon Pintana
Lecturer
Research Interests:
Energy technology, Energy, Renewable energy

Self-cleaning Integrative Aerogel for Stable Solar-assisted Desalination

Yufei Gu[1], Lei Miao[2*] Zhixia Li[1*]

[1]School of Chemistry and Chemical Engineering, Guangxi University, 530004, Nanning, China
[2]School of Physical Science and Technology, Guangxi University, 530004, Nanning, China
*E-mail: miaolei@gxu.edu.cn and zhixiali@gxu.edu.cn

Abstract: The solar-assisted desalination generator (SADG) shows great potential for solving water scarcity problems. However, salt precipitation and accumulation is still a challenge for SADG, which slows down solar steam generation performance of evaporator during operation. Here, a facile integrative evaporator featuring stable and high evaporation performance breaks this bottleneck. By using a rational design in which amorphous carbon particles are evenly composited within the porous chitosan aerogel, the evaporator not only integrates excellent light absorption, heat management, and water transportation abilities but also endows a large vapor escape space. Upon desalination, salt concentration ingredients between carbon particles and chitosan membranes can be quickly balanced by water transport in interconnected chitosan chains, and thus salt precipitation on the evaporator surface would be avoided. Compared to other salt-rejection evaporators, the integrative evaporator can operate in 3.5 wt% brine for 60 days without salt precipitation and exhibits a stable evaporation rate (1.70 kg m^{-2} h^{-1}), indicating its potential for practical applications in seawater desalination and the harvest of clean drinking water.

Keywords: solar assisted desalination generator, solar steam generation, integrative evaporator, salt-rejection

1. Introduction

Water scarcity has been cited as one of the most rigorous global problems for human. To solve the issue, man demands fresh water from the sea Reverse osmosis has been industrialized as a recognized desalination technology, however, the huge construction and maintenance costs make the technology difficult to popularize. In recent years, solar steam generation as a new emerging solar-assisted desalination technology, it has a great potential to solve water and energy shortages due to high photothermal conversion efficiency, low-cost, and sustainability [1, 2]. Typical configuration for a solar steam generator (SSG) is efficient light absorber which converts incident sunlight to heat energy and heats water to generate vapor, while bulk water is pumped continuously by a transport layer. However, in a long-term solar-assisted desalination process, the fast gas-liquid exchange at the air-liquid interface of the absorber layer leads to a significant increase in the local saline concentration [3]. When the salt concentration at the surface of SSG is up to saturate, the salts will preferential precipitate and accumulate at the interface, resulting in dramatical desalination performance degradation. Moreover, for a long-term desalination, the stability of materials needs to be rigorously tested, which involves not only the stable of SSG itself, but also the chemical stability of photothermal materials. Because desalination is operated under a high humidity and high salinity condition, wet atmosphere corrosion is inevitable when SSG consists of metal matrix, and if possible, materials harmful to the environment should be avoided [4]. Thus, SSG with high regeneration ability, stability and environmental-friendly in desalination is a new tendency [5].

Currently, the solar assisted desalination generator (SADG) reported can be divided into three types. The cleanable SADG consists of

photothermal materials and polymer film, which exhibits high reusable ability due to its flexible and stable structure [6-11]. For this SADG, the addition of salt removal process would decrease the efficiency of solar assisted desalination and increase the operating costs. The reversible SADG consists of solar absorber and functional layer, in which the functional layer is hydrophilic material (such as cotton, melamine sponge and polyvinyl alcohol gel) [12-26]. During long-term solar desalination, the functional layer can transport water to the absorber for vaporing, and reduce the heat conduction from the absorber to bulk water, as well as maintain the dynamic salt concentration level below the salt saturation in the system. However, the salt adjustment capacity of functional layer is weak. The evaporation rate still decreases in long-term solar desalination because the fast gas-liquid exchange at surface of the absorber layer makes it achieve salt saturation easily. To be sure, salt at the surface of the SADG will dissolve spontaneously in hours without solar illumination, which partially meet the practical sustainable demand of solar desalination.

The self - regeneration SADG can desalinate seawater without salt precipitation for a long time and keep a steady evaporation rate, which is based on the optimization and improvement of the internal structure of the reversible SADG. Hu and co-workers reported a salt-rejecting SADG that demonstrated the immobilization of graphene-based material on hydrophobic polytetrafluoroethylene (PTFE) membrane surface for water desalination [27]. In this system, SADG is placed at the bottom of a transparent sealed chamber containing salt water, and the vapor escapes from the bottom PTFE membrane without salt precipitation in a long-term solar desalination. However, this system has a low evaporation efficiency (49%) under one-sun irradiation (1 kW m^{-2}) because solar absorber directly heats bulk seawater, resulting in low heat utilization of the system. Zhu and co-workers reported a flexible and salt resistant Janus absorber that demonstrated stable water output (1.3 kg m^{-2} h^{-1}, over 16 days) under one-sun, with a solar efficiency of 72% [28]. Meanwhile, Chen and co-workers reported a Janus evaporator with low tortuosity and demonstrated a stable evaporation rate (1.24 kg m^{-2} h^{-1}) during continuous solar desalination tests (100 hours) in 3.5 wt% NaCl solution under one-sun [29]. The asymmetric wettability designing of Janus evaporator enables the hydrophobic layer out of the water for heat localization and the hydrophilic layer in the water for continuous water pumping. However, the efficiency was much lower than the typical reported evaporation performance (over 80%) of interfacial solar evaporation. Hu and co-workers reported an artificial channel-array wood based SADG, which can rapidly exchange the salt with the bulk solution, enabling real-time self-regeneration of the evaporator with stable evaporation efficiency (~75%) at wide concentration range salt solution (0 to 20 wt% NaCl) under one-sun irradiation [30]. However, the millimeter-sized drilled channels occupy the large area ratio of wood based SADG (~ 20% of the total insulation area) resulting in the increased heat loss to the bulk solution and mediocre evaporation performance comparing the reported SSG. Hence, to achieve long-term efficient evaporation performance of SADG, there is still a long way to go. The advanced structure design for self-regeneration, high heat utilization efficiency, together with fast vapor escaping are comprehensive solutions.

Here, based on our previous work on mimetic transpiration system (MTS) and frozen photothermal aerogel technology [31], an integrative self-regeneration chitosan based photothermal aerogel for long-term solar-assisted desalination is exhibited in Figure 1. Three-dimensional (3D) honeycombed chitosan (CS) based aerogel was prepared using phase transition freeze- drying method, where amorphous carbon powders (pomelo peel carbonization powders, named as PPCPs) were evenly distributed on porous CS backbone. During solar desalination, the aerogel as

photothermal layer was placed on MTS device, in which the air-laid paper as water pathway supplied water for aerogel, wrapping with expandable polyethylene (EPE) foam to restrict the heat conduction from aerogel to bulk water. Thanks to unique porous structure and super hydrophilic, integrative CS based aerogel exhibits self-heat management, continuous water supply, large vapor escape space, and long-term salt resistant abilities. Moreover, owing to PPCPs homogeneous intersperse on the hydrophilic CS membrane, the inducing transient salinity difference of fast-exchange solar driven-vapor on every PPCPs can be quickly balanced by CS skeleton. Therefore, the integrative CS based aerogel performs stable and efficient evaporation performance (efficiency greater than 90%), and superior salt resistance even in high concentration brine (up to 10 wt%), which has broad application prospects in long-term solar desalination and industrial wastewater treatment.

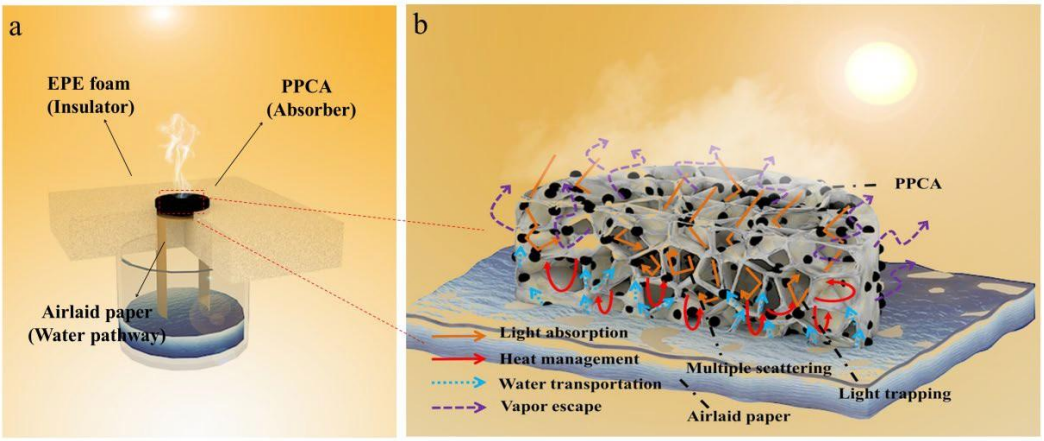

Figure 1. Schematic diagram of (a) MTS device and (b) PPCA under solar-assisted desalination experiment.

2. Methods

2.1. Preparation of $PPCP_x$

Pomelo peel (recycled from fruit shop in Guilin) was suffered simple cleaning treatment, and then was dried in oven (DHG-9075A Qixin Scientific Instrument Co. LTD Shanghai) at 80 ° C. Next, the drying pomelo peel was carbonized in a vacuum tube furnace (OTF-1200X, Kejing Materials Technology Co., Ltd. Hefei) under nitrogen atmosphere with a flow rate of 20 sccm, by adjusting different carbonization temperature for 300, 500, 700, and 900 ºC, respectively. Final, each carbonized product was grinded and sieved through a stainless-steel sieve of 120, 300, and 500 meshes to fabricate different pomelo peel carbonization powder ($PPCP_x$, *x* can be 3, 5, 7, and 9, which refers to different carbonization temperature).

2.2. Preparation of $PPCA_y$

Each 0.1 g $PPCP_x$ with the size of 500 mesh was dispersed in 6 mL CS solution, and then, freeze drying by a lyophilizer (ALPHA 2-4 LSC, CHRIST, Germany) to fabricate $PPCA_y$ (*y* can be 3, 5, 7, and 9, which refers to different carbonization temperature).

Preparation of PPCA5-Z: Each 0.1 g PPCP5 with the different sizes (120, 300, 500 mesh) was dispersed in 6 mL CS solution, and then, freeze drying by a lyophilizer to fabricate PPCA5-*Z* (*Z* can be 120, 300, 500).

2.3. Characterization

The pyrolysis process of raw PP was investigated by thermogravimetric analysis and differential thermal analysis device (TGA-DTA, SDT Q600, TA Instruments, USA), with ramp 5 ºC min^{-1} to 900 ° C, in nitrogen atmosphere. The morphology and structure of raw PP, $PPCP_x$, and $PPCA_y$ samples were investigated by a scanning electron microscope (SEM, S- 4800, Hitachi, Japan). X- ray diffraction (XRD, D8-ADVANCE, Bruker, Germany) with Cu Kα radiation was conducted on phase analysis. The chemical component of

materials was comprehensive analysis by Raman spectroscopy (LabRAM HR, Horiba, French) with objective X 50, grating 1800 gr nm^{-1}, laser 532 nm, Fourier transform infrared spectrometer (FTIR, Nicolet IS10, Thermo Fisher, USA) with a KBr disc in the range of 400-4000 cm^{-1}, X-ray photoelectron spectroscopy (XPS, ESCALAB 250Xi, Thermo Fisher, USA) with an Al K-alpha anode emitter as the excitation source. The absorptance spectrum of each sample was transformed from its diffuse reflectance spectral and transmittance spectral, which measured from 2500 to 250 nm via a UV-Vis-NIR spectrometer (V-570, JASCO, Japan) equipped with an integrating sphere. The infrared reflectance spectral of materials were measured by a FTIR spectrometer (Nicolet IS10, Thermo Fisher, USA) connecting an IntegratIRTM mid-infrared integrating sphere with Mercury-Cadmium-Telluride (MCT) detector (PIKE). The macropore parameter of $PPCA_y$ was measured by mercury porosimetry (AutoPore IV 9500, Micrometritics, USA). Thermal conductivity of $PPCA_y$ was measured by thermal conductivity instrument (TCi, C-therm, Canada). Zeta potentials of materials were investigated by laser particle analyzer (MS2000, Malvern, UK).

2.4. SSG experiment

The whole process of the experiment was conducted at an ambient temperature of 25 ± 2 °C and a relative humidity of 48 ± 2%. The pretreatment $PPCA_y$ sample was loaded on homemade MTS to conduct experiment. X xenon lamp (CEL-S500/350, ZJJY, Beijing) with an AM1.5 optical filter was used as the light source. A piece of Fresnel lens with 20 cm focal length was applied to enhance incident light. During SSG experiment, light intensity of 1 kW m^{-2} was calibrated by an optical power densitometer (843-R, Newport, USA) with a thermopile sensor (919P-010-16, Newport, USA). The mass change of sample was recording by a high-precision electric balance (ATX224, Shimadzu, Japan) for 60 min at constant condition. The surface temperature distribution of $PPCA_y$ was captured by an infrared camera (E60, FLIR, USA). The temperature of vapor was measured by a thermal sensor probe (BD-PT100-3022A).

In long-term SADG experiments, brine of different concentrations (3.5, 7, 10, 13, 17 and 20 wt%) was prepared by dissolving NaCl in water in each proportion. During laboratory solar wastewater treatment, $MnSO_4 \cdot H_2O$, $Fe(NO_3)_3 \cdot 9H_2O$, $(CH_3COO)_2Ni \cdot 4H_2O$, $CuCl_2 \cdot 2H_2O$, $(CH_3COO)_2Pb$ were selected as model heavy metal ion (Mn^{2+}, Fe^{3+}, Ni^{2+}, Cu^{2+}, Pb^{2+}) contamination to evaluate SSG water treatment performance. The concentration of the heavy metal in the production fresh water was measured by inductively coupled plasma atomic emission spectroscopy (ICP-AES, Optima 8000, PerkinElmer, Waltham, MA, USA). Moreover, NaCl, $MgCl_2$, KCl, and $CaCl_2$ were selected for simulated desalination experiment, the production water was measured by ICP-AES for evaluating water quality.

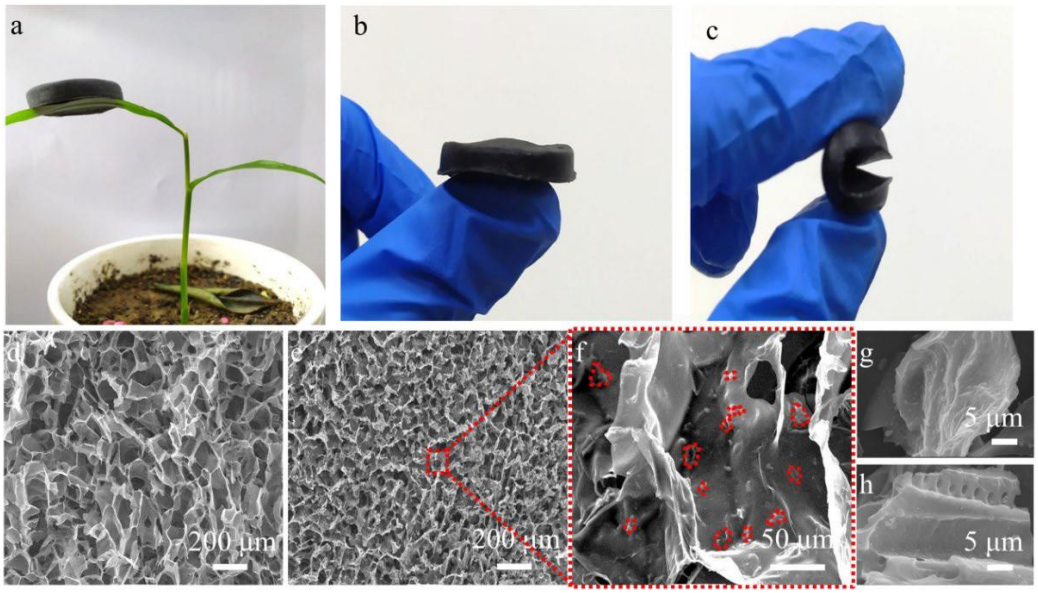

Figure 2. (a) Photograph of PPCA loading on plant. (b, c) Diagrams of wet aerogel under external loading. (d) Image of chitosan aerogel. (e, f) images of PPCA. (g, h) images of PPCP.

3. Results and Discussion

3.1. Structure design and characterization of integrative CS based aerogel

For SADG, the structure stability is the precondition of long- term desalination. Amorphous carbon has broad-band light absorption and chemical stability, which can be fabricated by biomass carbonization in low-cost way. CS is a biocompatibility material and can be extracted from crustaceans. The integrative SADG consists of PPCPs and CS aerogel (denoted as PPCA) that can be readily prepared by assembling the PPCPs with CS solution and directly freeze-drying. As a proof of concept, PPCPs can be stably loaded on CS chains by electrostatic adsorption (Table S1). Based on our previous work, the structure and pore size of aerogel can flexibly be controlled by adjusting frozen preferential direction and temperature [31]. Here, a 3D honeycomb-like porous PPCA is fabricated by a lyophilizer with circular frozen system, which promotes the growth of ice crystals from outside to inside along the radial direction and then removes the ice template by sublimation. The porous structure of PPCA results in ultralight performance and can stand on the green shoots of ginger (Figure 2a). Moreover, after alkali treatment to remove redundant acetate ion, the aerogel has excellent resilient ability under wetting conditions. The PPCA not only can easy be bent, but also can quickly recover when contacts water, even if after suffering extremely extruded by external forces (Figure 2a, b), which ensures that it can operate normally under harsh conditions. As Figure 2d-f shown, the PPCPs uniformly loading on CS pore wall has good compatibility with CS and the original structure of the CS aerogel is preserved. The surface of PPCPs is folds and tubular (Figure 2g, h), which is benefit to light absorption.

The chemical compositions of PPCA were conducted on Raman spectra, Fourier transform infrared spectroscopy and X-ray photoelectron spectroscopy technology to comprehensive analyze (Figure S1), which demonstrated the PPCA contains plenty of hydrophilic groups (hydroxyl, carboxyl, and amino group) [32-35], and these hydrophilic groups play key roles in water transportation as well as structure springback. Furthermore, the pore character and thermal management ability of PPCA were shown in Figure S2 and Table S2. The PPCA has low thermal conductivity (~0.035 W m^{-1} k^{-1}) and high porosity (~94%), which is benefit to heat management and vapor escape while solar assisted desalination is operated.

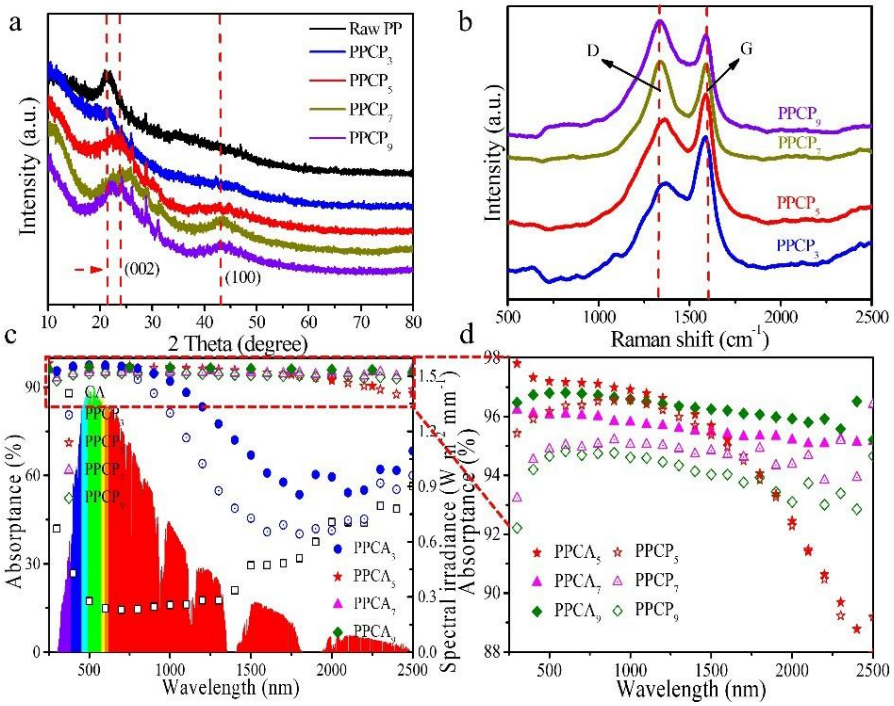

Figure 3. (a) XRD spectral of raw PP and $PPCP_x$. (b) Raman spectral of $PPCP_x$. (c, d) Absorptance spectral of chitosan aerogel (CA), $PPCP_x$ and $PPCA_y$ at the range of 250-2500 nm.

3.2. Material and solar absorption optimization

The thermal decomposition process of raw pomelo peel can be separated from three stages by thermogravimetric analysis and derivative thermogravimetry device. As shown in Figure S3, the first stage of raw pomelo peel's weight loss is 9.3% from 30 to 197°C, it can be ascribed to the removal of bound water molecule and some volatile organic compounds decomposition. The second stage is the temperature range from 197 to 305°C, the weight loss of pomelo peel is 17.4%, which involves undecomposed organic compounds and hemicellulose. The last stage involves hemicellulose, cellulose, and lignin decomposition at the temperature range from 305 to 900 °C [36].

To investigate the relationship of light absorption performance with disorder of amorphous carbon, the PPCPs with different carbonization temperatures were characterized. In Figure 3a, XRD spectra of different PPCP samples shows that the characteristic peak width of (002) lattice plane increased with the increase of pyrolysis temperature. Moreover, when the pyrolysis temperature reaches more than 700 °C, another characteristic broad peak appears at the (100) lattice plane [37]. The appearance of broadened graphite diffraction peak and new diffraction peak indicates that PPCPs are amorphous carbon structure, which is the result of the structure fracture of graphite carbon during pyrolysis. The characteristic peaks of stretching vibration of homonuclear diatomics in PPCP samples were detected by Raman spectroscopy. As shown in Figure 3b, there are two characteristic peaks located around 1343 and 1587 cm^{-1}, which are related to the D and G bands, respectively. As for PPCP samples, the intensity of D band increased, indicating the carbon-based lattice defects increased while t he pyrolysis temperature rising. As shown in Figure 3c, d, PPCA samples have extensive full-spectrum absorption at the range of 250-2500 nm, which demonstrates that CS has a good compatibility with PPCPs. Moreover, compared with PPCP samples, the light absorption of all PPCA samples were increased due to the unique porous structure of aerogel have light multiple-scattering and light traps enhancement effects. $PPCA_3$ has several absorption attenuation peaks at the near infrared region, which is due

to partially undecomposed organic functional groups remains in $PPCP_3$. The $PPCA_5$ has the best light absorption performance of 96% at full-spectrum (The absorptance calculation process of sample was shown in Supporting Information).

3.3. Solar steam generation optimization experiment

Based on the excellent optical properties, superhydrophilicity and good thermal management ability of PPCA samples, it is a good candidate material for solar photothermal conversion. In this work, PPCA samples were loaded on MTS device to conduct solar steam generation experiment (Figure 1a). Basically, the PPCA sample was embedded in the EPE foam as planar system. As shown in Figure S4a, when the illumination time reached 10 minutes, the mass loss rate of each sample tended to be stable, indicating that aerogels had fast photothermal conversion abilities. The evaporation rate (0.91 kg m^{-2} h^{-1}) of CA is faster than pure water (0.6 kg m^{-2} h^{-1}). As for the planar system, the PPCA5 has evaporation rate of 1.57 kg m^{-2} h^{-1} and evaporation efficiency of 97.1% (Figure S4a), which is better than conventional planar SSG [2, 6, 8, 10]. The MTS has heat utilization efficiency of 90%. It demonstrated that the PPCA-MTS has excellent solar steam generation performance. More detail information of photothermal conversion efficiency and thermal utilization of PPCA samples and MTS were discussed in calculation section in Supporting Information.

Moreover, in the MTS, when PPCA samples are placed on EPE foam as open system (Figure S4b), the mass loss rates of each sample are faster compared with the planar system under the same experimental conditions. It is attributed to the unique open 3D honeycomb structure of the integrated aerogel that provides more steam escape channels than the planar system. The $PPCA_5$ sample with open system has the best evaporation rate of 1.78 kg m^{-2} h^{-1}, which breaks the limit rate (1.47 kg m^{-2} h^{-1}) of the interface system [15, 38, 39]. The increased evaporation rate of open system can be attributed to its good heat management ability and the additional energy gain form ambient environment, which increased the vapor production [38-40]. The evaporation rate of $PPCA_5$ can be further improved by rational designing system structure, each $PPCA_5$ as a building block unit can be simply accumulated to enlarge lateral area. As the lateral areas of $PPCA_5$ increased (Figure S5), it realizes the utilization of the environmental energy [38]. Specifically, the enhancing solar steam generation performance of 2.04 kg m^{-2} h^{-1} was obtained.

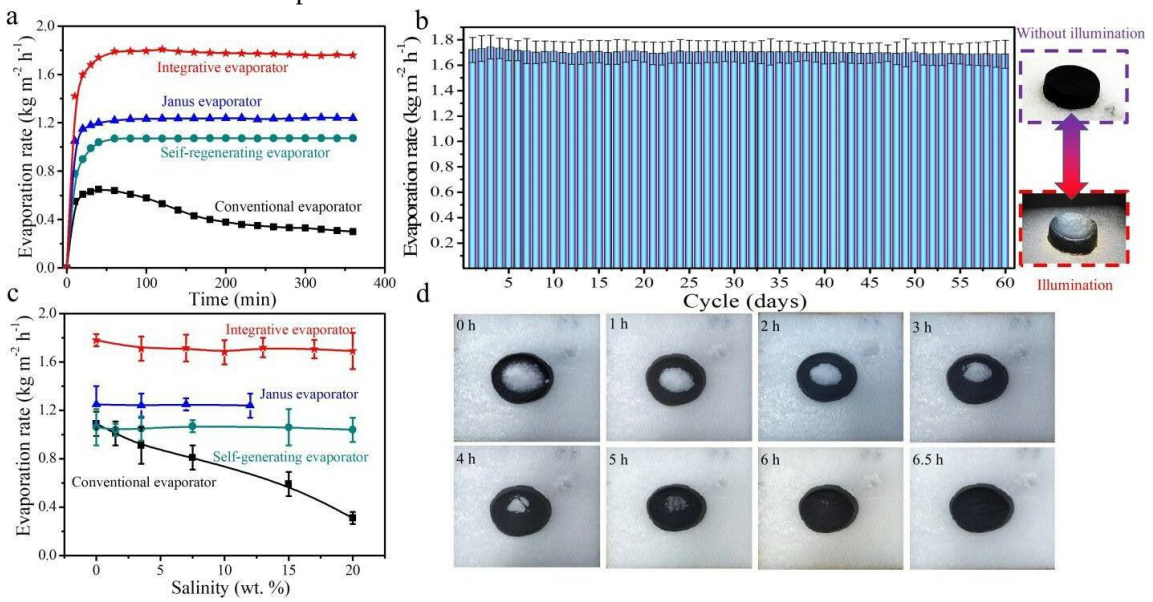

Figure 4. (a) Comparison of long-term solar-assisted desalination performance between integrative

evaporator and other evaporators in 3.5 wt% brine. (b) The evaporation rate of integrative evaporator during a static-continuous illumination experiment in 3.5 wt% bine for 60 days. (c) Comparison of the evaporation capacity of integrative evaporator and other evaporators with different concentrations of brine. (d) Self-cleaning experiment of an integrated evaporator in 3.5 wt% brine.

3.4. Long-term solar-assisted desalination experiment

To evaluate the solar-assisted desalination performance of integrative aerogel, we carefully studied the long-term evaporation rate of the PPCA $_5$ open system (Integrative evaporator) with one unit on the MTS device in 3.5 wt% NaCl (average salinity of seawater). As shown Figure 4a, the integrative evaporator fast reached its highest evaporation rate after 1 h under 1 kW m^{-2} solar irradiation. And the integrative evaporator has stable evaporation performance (1.70 kg m^{-2} h^{-1}) in the sequence 6 h test, which is much higher than Janus evaporator and self-regenerating evaporator [29,30]. Moreover, there was no visible salt on the surface of evaporator. The stable solar-assisted desalination performance of integrative evaporator was evaluated from a static-continuous illumination experiment by soaking the aerogel in 3.5 wt% NaCl solution for 60 days (Figure 4b). The evaporator was installed on MTS to conduct solar-assisted desalination, which was continuously irradiated for 6 h twice daily. During the experimental interval, the sample was still kept in 3.5 wt% NaCl solution. The evaporator showed a stable evaporation rate of ~ 1.70 kg m^{-2} h^{-1} under one-sun and without structure deterioration last for 60 days. It demonstrates that the integrative evaporator has excellent cycle ability in solar-assisted desalination. The stability and evaporation performance of integrative evaporator was also compared to current work in Table S7.

The solar-assisted desalination properties of integrative evaporator were evaluated by in a series of NaCl solutions with different concentrations ranging from 0 to 20 wt%. As shown in Figure 4c, the evaporation rates of the integrative aerogel are higher than Janus evaporator and self-regenerating evaporator in all the concentrations tests. Moreover, we carefully conducted long-term solar-assisted desalination experiments of the integrative evaporator with different concentration salt solutions to investigate the stability of steam performance, which demonstrated that the integrative evaporator has stable evaporation performance of salt concentration solutions ranging from 0 to 10 wt%. When the salt concentration is more than 10 wt%, the performance of integrative aerogel is gradually decreased. The time of salt precipitation is corresponding t o the change point of evaporation rate, which is used to evaluate salt tolerance ability of the integrative evaporator to different salt concentration solutions. As shown in Figure S6, the integrated evaporator has no salt precipitation under the salinity condition of 3.5 wt %, even continuous illumination lasts to 12 h. Under conditions of 10 wt % and 20 wt %, the salt precipitation of integrative evaporator occurred at 8.2 h and 1.9 h, respectively. It's proved that the integrative evaporator performs well in saline solution of 1-10 wt%.

The salt tolerance mechanism of integrative evaporator is similar to mangrove forest. The cell of mangrove forest has high osmotic pressure that allows it to survive near the sea. As for integrative evaporator (Figure S7), the interconnected CS chain is superhydrophilic and can quickly absorb water and reserve it. The PPCP evenly distributes on the CS chains. When the integrative evaporator is conducted on desalination experiment, the rapid gas-liquid exchange induces local salt concentration increase on the PPCP. It achieves real-time salt exchange between PPCP and CS chains under the competition of evaporation and temperature difference driving force, as a result, the locally salinity gradient of the evaporator can be quickly balanced. Specifically, the spatial distribution of photothermal material on aerogel skeleton has a great influence on the evaporation performance and stability of evaporator, which was demonstrated by seawater desalination

experiments with inhomogeneous aerogels (Figure S8). Based on the real-time salt exchange, the integrative evaporator exhibits highly efficient evaporation performance for seawater. CS chains play the key role of water supply as well as balancing the salt concentration in the evaporator, which extends the time to reach the saturation concentration of salt for the evaporator. However, when the concentration of brine treated by the integrated evaporator exceeds 10 wt%, this efficient and stable desalination performance will be weakened. Compared with natural seawater, the shrink of controllable real- time salt exchange ability of CS chains in high-concentration brine makes the evaporator reach salt saturation earlier at high-speed evaporation rate under solar- assisted desalination experiment (Figure S9). Moreover, the 1 g NaCl crystal was placed on the top of the integrated evaporator. As shown in Figure 4d, after 6.5 h natural evaporation, the salt at the surface of evaporator was disappeared, which demonstrated that the integrative evaporator has extremely salt tolerance and self-cleanable abilities in seawater.

For investigating mineral elements content in the collected condensate water, the simulated desalination performance of integrated evaporator was tested. The result shows that the mineral elements of the collected water are much lower than the World Health Organization (WHO) and the US Environmental Protection Agency (EPA) standards for drinkable water (Figure 5a) [41]. Furthermore, to demonstrate treatment ability of the multiple pollution water, a simulated industrial wastewater experiment of the integrative evaporator was also conducted. After the treatment (Figure 5b), all of the concentrations of the heavy metal ions are below of the government standard for the heavy metal ions in the drinking water (GB5749-2006) [8].

As a proof-of-concept, the PPCA5 as the building block was placed on the self-made MTS container to consist of 2 × 2 matrix SSG, which was placed in a polymethyl methacrylate (PMMA) organic glass condensation collector (Figure 5c). The 3.5 wt% brine at the bottom of the container was used as the simulated seawater and the condensed vapor during the outdoor experiment would be collected in a bottle. The experiment was carried out from 10:00 to 16:00 under natural sunlight with a solar flux of about 0.56 kW m^{-2}. The average evaporation rate of the SADG with $PPCA_5$ was calculated to 0.96 kg m^{-2} h^{-1} (Figure 5d), which is much higher than that of the blank SADG under the same illumination condition. The SADG with $PPCA_5$ shows a capacity to produce about 11.52 kg m^{-2} d^{-1} of drinkable water under long-term desalination with natural sunlight. It opens a promising path for sustainable, low-cost and high-performance seawater desalination.

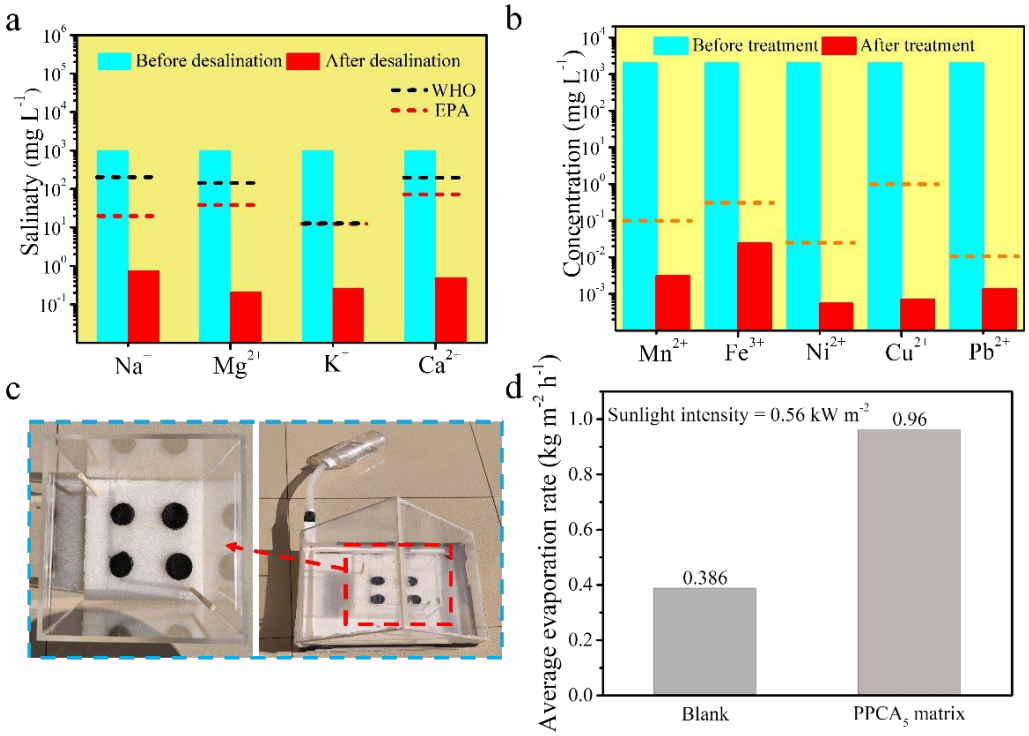

Figure 5. (a) The salinities of different mineral elements before and after desalination by integrative evaporator. (b) The concentrations of different heavy metal ions before and after water treatment by integrative evaporator. (c) Photograph of self-made outdoor desalination device. (d) Average evaporation rate of blank and $PPCA_5$ matrix generator.

4. Conclusions

An integrated evaporator with high absorption, thermal management, water transportation and salt tolerance abilities is prepared through structural and material optimization. The evaporator consists of renewable amorphous carbon and CS chains, which is environmental-friendly and structure stable for long-term solar desalination. The advanced structural design endows the evaporator with integrative properties, enabling long-term desalination in 3.5 wt% NaCl solution under one-sun with greater than 90% efficiency, which is better than the reported evaporators. Moreover, owing to the real-time salt exchange between PPCP and CS chains of the evaporator, which can perform stable steam generation without salt precipitation even in highly brine water (up to 10 wt%). The integrated evaporator exhibits excellent solar-assisted desalination performance, high salt tolerance of integrative evaporator in brine water, and superior heavy metal removal ability, indicating a promising prospect for solar-assisted desalination and other industrial wastewater treatment.

References

[1] J. Zhou, Y. Gu, P. Liu, P. Wang, L. Miao, J. Liu, A. Wei, X. Mu, J. Li, J. Zhu, Adv. Funct. Mater. 2019, 29, 1903255.
[2] B. Hou, D. Kong, J. Qian, Y. Yu, Z. Cui, X. Liu, J. Wang, T. Mei, J. Li, X. Wang, Carbon 2018, 140, 488.
[3] N. Shahidzadeh-Bonn, S. Rafai, D. Bonn, G. Wegdam, Langmuir 2008, 24, 8599.
[4] C. Mu, Y. Song, K. Deng, S. Lin, Y. Bi, F. Scarpa, D. Crouse, Adv. Sustain. Syst. 2017, 1, 1700064.
[5] X. Hu, J. Zhu, Adv. Funct. Mater. 2019, 30, 1907234.
[6] Y. Jin, J. Chang, Y. Shi, L. Shi, S. Hong, P. Wang, J. Mater. Chem. A 2018, 6, 7942.
[7] M. Chen, Y. Wu, W. Song, Y. Mo, X. Lin, Q. He, B. Guo, Nanoscale 2018, 10, 6186.
[8] Z. Deng, P. Liu, J. Zhou, L. Miao, Y. Peng, H. Su, P. Wang, X. Wang, W. Cao, F. Jiang, L. Sun, S. Tanemura, Sol. RRL 2018, 2, 1800073.

[9] Y. Wa ng, C . Wa ng, X . S ong, S . K . Megarajan, H. Jiang, J. Mater. Chem. A 2018, 6, 963.
[10] P. Liu, L. Miao, Z. Deng, J. Zhou, H. Su, L. Sun, S. Tanemura, W. Cao, F. Jiang, L. Zhao, Mater. Today Energy 2018, 8, 166.
[11] M. Kim, K. Yang, Y. S. Kim, J. C. Won, P. Kang, Y. H. Kim, B. G. Kim, Carbon 2020, 164, 349.
[12] Y. Chang, Z. Wang, Y. Shi, X. Ma, L. Ma, Y. Zhang, J. Zhan, J. Mater. Chem. A 2018, 6, 10939.
[13] Q. Chen, Z. Pei, Y. Xu, Z. Li, Y. Yang, Y. Wei, Y. Ji, Chem. Sci. 2018, 9, 623.
[14] L. Cui, P. Zhang, Y. Xiao, Y. Liang, H. Liang, Z. Cheng, L. Qu, Adv. Mater. 2018, 30, e1706805.
[15] Z. Deng, L. Miao, P. Liu, J. Zhou, P. Wang, Y. Gu, X. Wang, H. Cai, L. Sun, S. Tanemura, Nano Energy 2019, 55, 368.
[16] P. Liu, L. Miao, Z. Deng, J. Zhou, Y. Gu, S. Chen, H. Cai, L. Sun, S. Tanemura, Appl. Energ. 2019, 241, 652.
[17] X. Lin, J. Chen, Z. Yuan, M. Yang, G. Chen, D. Yu, M. Zhang, W. Hong, X. Chen, J. Mater. Chem. A 2018, 6, 4642.
[18] Z. Guo, G. Wang, X. Ming, T. Mei, J. Wang, J. Li, J. Qian, X. Wang, ACS Appl. Mater. Inter. 2018, 10, 24583.
[19] G. Ni, S. H. Zandavi, S. M. Javid, S. V. Boriskina, T. A. Cooper, G. Chen, Energ. Environ. Sci. 2018, 11, 1510.
[20] J. Zeng, Q. Wang, Y. Shi, P. Liu, R. Chen, Adv. Energy Mater. 2019, 9, 1900552.
[21] C. Liu, C. Cai, X. Zhao, ACS Sustain. Chem. Eng. 2020, 8, 1548.
[22] N. Hu, Y. J. Xu, Z. T. Liu, M. Liu, X. Y. Shao, J. Wang, Carbohyd. Polym. 2020, 243, 8.
[23] X. X. Guo, H. Gao, S. Y. Wang, L. F. Yin, Y. R. Dai, Desalination 2020, 488, 9.
[24] L. Li, T. Hu, A. Li, J. Zhang, ACS Appl. Mater. Inter. 2020, 12, 32143.
[25] X. Mu, Y. Gu, P. Wang, J. Shi, A. Wei, Y. Tian, J. Zhou, Y. Chen, J. Zhang, Z. Sun, J. Liu, B. Peng, L. Miao, Sol. RRL 2020, 4, 2000341.
[26] Q. Zhang, L. Li, B. Jiang, H. Zhang, N. He, S. Yang, D. Tang, Y. Song, ACS Appl. Mater. Inter. 2020, 12, 28179.
[27] L. Huang, J. Pei, H. Jiang, X. Hu, Desalination 2018, 442, 1.
[28] W. Xu, X. Hu, S. Zhuang, Y. Wang, X. Li, L. Zhou, S. Zhu, J. Zhu, Adv. Energy Mater. 2018, 8, 1702884 .
[29] R. Hu, J. Zhang, Y. Kuang, K. Wang, X. Cai, Z. Fang, W. Huang, G. Chen, Z. Wang, J. Mater. Chem. A 2019, 7, 15333.
[30] Y. Kuang, C. Chen, S. He, E. M. Hitz, Y. Wang, W. Gan, R. Mi, L. Hu, Adv. Mater. 2019, 31, e1900498.
[31] Y. Gu, X. Mu, P. Wang, X. Wang, J. Liu, J. Shi, A. Wei, Y. Tian, G. Zhu, H. Xu, J. Zhou, L. Miao, Nano Energy 2020, 74, 104857.
[32] R. Yu, Y. Shi, D. Yang, Y. Liu, J. Qu, Z.-Z. Yu, ACS Appl. Mater. Inter. 2017, 9, 21809.
[33] W. Lu, X. Qin, S. Liu, G. Chang, Y. Zhang, Y. Luo, A. M. Asiri, A. O. Al-Youbi, X. Sun, Anal. Chem. 2012, 84, 5351.
[34] M. Kasaai, Carbohyd. Polym. 2008, 71, 497.
[35] A. Zajac, J. Hanuza, M. Wandas, L. Dyminska, Spectrochim. Acta A Mol. Biomol. Spectrosc. 2015, 134, 114.
[36] Y. Wu, L. Cha, Y. Fan, P. Fang, Z. Ming, H. Sha, Water Air Soil Poll. 2017, 228, 405.
[37] L. Zhu, Y. Wang, Y. Wang, L. You, X. Shen, S. Li, Micropor. Mesopor. Mat. 2017, 241, 285.
[38] X. Li, J. Li, J. Lu, N. Xu, C. Chen, X. Min, B. Zhu, H. Li, L. Zhou, S. Zhu, T. Zhang, J. Zhu, Joule 2018, 2, 1331.
[39] K. Li, T. H. Chang, Z. Li, H. Yang, F. Fu, T. Li, J. S. Ho, P. Y. Chen, Adv. Energy Mater. 2019, 9, 1901687.
[40] J. Li, M. Du, G. Lv, L. Zhou, X. Li, L. Bertoluzzi, C. Liu, S. Zhu, J. Zhu, Adv. Mater. 2018, 30, e1805159.
[41] Y. Wang, C. Wang, X. Song, M. Huang, S. K. Megarajan, S. F. Shaukat, H. Jiang, J. Mater. Chem. A 2018, 6, 9874.

Yufei Gu is a Ph.D. candidate in Guangxi University. His main research interests are the preparation of biomass aerogels and carbon-based composites and their application in solar steam power generation, as well as the preparation of solid acid catalysts, and the high-value conversion of waste plastics and biomass resources.

Lei Miao received her PhD degree from Nagoya Institute of Technology, Japan. She is currently a professor at Guangxi University. Her current research focuses on thermoelectric and solar thermal conversion materials: synthesis, mechanisms and applications.

Zhixia Li received her PhD degree from Tohoku University, Japan. She is currently a professor at Guangxi University. Her current research focus contains the synthesis and modification of solid acid catalysts, composite polymer materials and applied research on solid waste disposal and high value conversion of oil and biomass resources.

Sustainability evaluation of broiler waste management practices in Thailand using AHP analysis

Senaka Bandara[1], Chatchawan Chaichana[2,3*], Nitthinan Borirak[3]

[1]Master's Degree Program in Energy Engineering, Department of Mechanical Engineering, Faculty of Engineering, Chiang Mai University, Chiang Mai 50200, Thailand
[2]Renewable Energy and Energy Conservation Laboratory, Department of Mechanical Engineering, Faculty of Engineering, Chiang Mai University, Chiang Mai 50200, Thailand
[3]Department of Mechanical Engineering, Faculty of Engineering, Chiang Mai University, Chiang Mai 50200, Thailand
*E-mail: c.chaichana@eng.cmu.ac.th

Abstract: In addressing the pressing concern of sustainable broiler waste management in Thailand, a leading global broiler meat producer and exporter, this study meticulously evaluates the viability of distinct waste management methodologies- direct land application, composting, and gasification. Employing an Analytic Hierarchy Process (AHP) analysis, the study examines environmental, economic, technical, and social main criteria along with 15 sub-criteria. Climate change is identified as the sub-criterion with the highest priority ranking (0.2272), closely followed by water use (0.1324). The study highlights gasification as the most preferred option at 52.6%, succeeded by composting at 24.8%, and direct land application at 22.6%. A thorough analysis underscores the outstanding performance of gasification in environmental and social aspects, while direct land application showcases economic effectiveness. Additionally, composting demonstrates a well-balanced performance across all four criteria. Innovatively introducing an AHP model for the first time in the domain of broiler waste management, the evaluation in this study provides policymakers with valuable insights for crafting sustainable long-term policies.

Keywords: AHP analysis, Broiler water management, Climate change, Sustainable agriculture.

1. Introduction

The broiler chicken industry, vital for global protein supply, is poised for significant growth amid rising demand for chicken meat. Thailand, ranking seventh in chicken meat production (3.425 MT) and fourth in exports (1.035 MT), exemplifies this trend. However, this expansion poses environmental challenges, particularly in broiler waste management. Broiler waste, a mix of bedding material and poultry manure, carries environmental risks if not handled properly.

Broiler waste management is complex, considering environmental, economic, technical, and social factors. Environmentally, it involves mitigating greenhouse gas emissions and preventing soil and water contamination [9]. Economic assessment includes analyzing capital and operational costs, along with potential income from energy production or byproduct sales. Technical analysis assesses reliability, feasibility, and scalability of solutions [5]. Social performance considers the impact on the community and workers.

Direct land application, composting, and gasification are prevalent broiler waste management techniques [7]. Direct land application fertilizes crops and reduces waste, composting transforms waste into stable fertilizer, and gasification converts waste into synthesis gas for energy production, and biochar for soil conditioning.

This paper utilizes multi-criteria decision analysis (MCDA) to select a sustainable broiler waste management technology for Thailand's

industry, evaluating environmental, economic, technical, and social performance among direct land application, composting, and gasification.

2. Methods

2.1 Analytic hierarchy process: a tool for multi-criteria decision making

Multi-Criteria Decision Analysis (MCDA) in Operations Research employs diverse methods, including the widely utilized Analytic Hierarchy Process (AHP) developed by Thomas L. Saaty in the 1970s [1]. AHP aids decision makers in breaking down complex problems into manageable criteria, sub-criteria, and alternatives, enabling comprehensive pairwise comparisons to determine rankings.

The AHP methodology involves key steps [10]: organizing the decision problem hierarchically, conducting pair-wise comparisons, determining maximum eigenvalue, consistency index (CI), consistency ratio (CR), and normalized eigenvector for each comparison matrix, and synthesizing judgments to create a priority ranking for alternatives. A consistency check mechanism ensures coherence, with a recommended CR below 0.10 to maintain reliability [1].

This study aims to identify the most sustainable broiler waste management technology for Thai broiler farms, considering environmental impact, economic viability, technical feasibility, and social acceptability. The AHP model was constructed through a comprehensive literature search, and a questionnaire was distributed for pairwise comparisons among experts. Super Decisions software facilitated constructing the hierarchy network and determining the optimal alternative based on expert feedback [1].

2.2 Criteria, sub-criteria selection

AHP systematically evaluates criteria and sub-criteria for waste management sustainability. Main criteria for broiler waste management were determined based on environmental, economic, technical, and social aspects. Previous AHP studies on livestock and waste management informed this selection [3,4,6,8]. Sustainability, as established through literature review and expert input, encompasses environmental friendliness, economic viability, technical feasibility, and social acceptability.

Sub-criteria selection involves relevance, measurability, and significance. Drawing from studies like Lijó et al. and Azahari et al., environmental sub-criteria include climate change, marine eutrophication, and terrestrial acidification. Economic sub-criteria comprise capital cost, operational cost, and potential revenue [2,6]. Technical sub-criteria encompass infrastructure, equipment, technical expertise, and process parameters. Social sub-criteria involve health and safety, public acceptance, and employment opportunities.

This study tailors sub-criteria selection to Thailand's broiler waste management context, ensuring a comprehensive and localized evaluation.

3. Results and Discussion

The assessment model demonstrates a distinct hierarchy in criteria importance for broiler waste management. Environmental considerations take the lead with a substantial weight of 0.53, closely followed by technical at 0.22, economic at 0.19, and social criteria at 0.06 as shown in Figure 1.

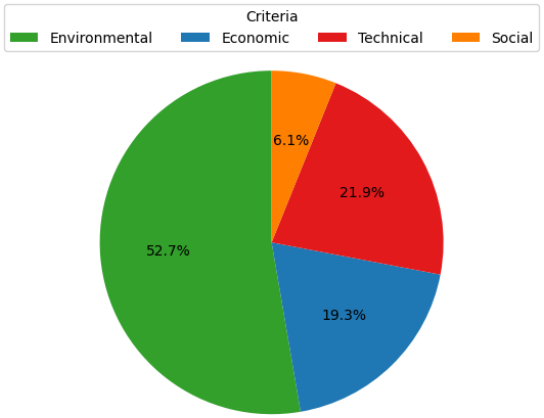

Figure 1. Priority rankings based on criteria

Within the sub-criteria, "Climate Change" commands the highest weight at 0.2272, signifying its paramount significance within the overarching environmental criterion. In

contrast, "Community Benefits" and "Public Acceptance" display the lowest weights at 0.0129 and 0.0147, respectively, indicating their relatively diminished impact within the social criterion. This discernible contrast underscores the unequal weighting of distinct aspects. Figure 2 illustrates the weight distribution of these sub-criteria. It highlights the pivotal role of climate change as a predominant concern in broiler waste management, while community benefits and public acceptance play more marginal roles in the assessment.

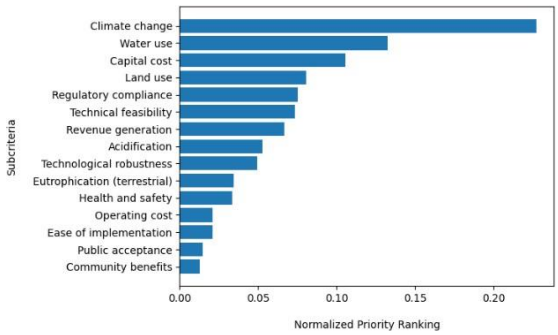

Figure 2. Normalized priority rankings of subcriteria

The assessment of broiler waste management methods reveals that gasification achieved the highest ranking at 0.526, signifying its superior performance. Composting closely follows with a ranking of 0.248, while direct land application secures the lowest ranking at 0.226. These results highlight the effectiveness of gasification as the most favorable method, showcasing its comprehensive performance across environmental, economic, technical, and social criteria in comparison to the other methods considered (Figure 3).

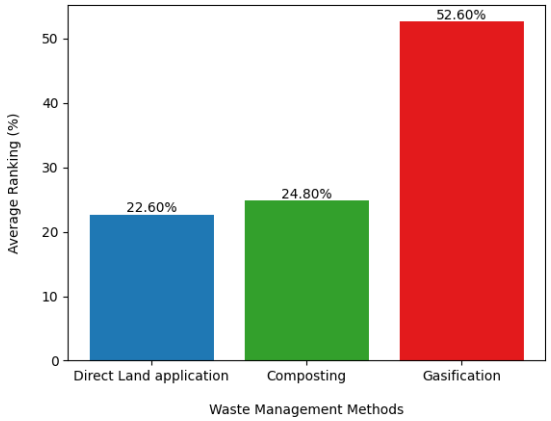

Figure 3. Average ranking of broiler waste management methods

The performance of each method with respect to each main criterion is visually depicted through a web chart in Figure 4. A thorough analysis underscores the outstanding performance of gasification in environmental and social aspects, while direct land application showcases economic effectiveness. Additionally, composting demonstrates a well-balanced performance across all four criteria.

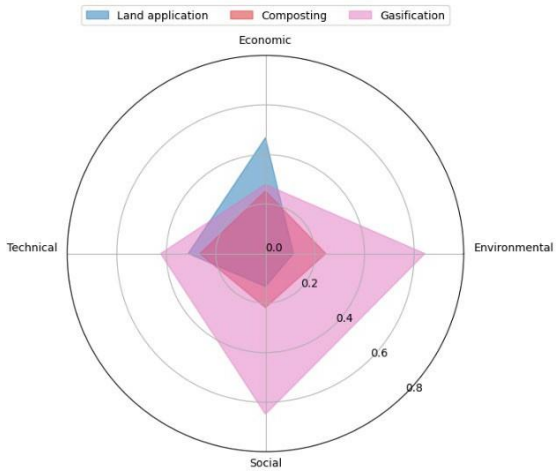

Figure 4. Broiler waste management: multi-criteria performance chart

4. Conclusions

In addressing the imperative of sustainable broiler waste management in Thailand, a key global producer and exporter of broiler meat, this study comprehensively evaluates three waste management methodologies: direct land application, composting, and gasification. Utilizing an Analytic Hierarchy Process (AHP) analysis, the research scrutinizes environmental, economic, technical, and social

criteria, encompassing 15 sub-criteria. Notably, climate change emerges as the highest priority sub-criterion (0.2272), closely followed by water use (0.1324).

The study identifies gasification as the optimal choice, commanding a preference rate of 52.6%, followed by composting at 24.8%, and direct land application at 22.6%. A nuanced analysis underscores gasification's outstanding performance in environmental and social aspects, while direct land application proves economically effective. Furthermore, composting demonstrates a well-balanced performance across all four criteria.

This research introduces an AHP model innovatively into the domain of broiler waste management, providing policymakers with invaluable insights for formulating sustainable, long-term strategies. The findings contribute to the discourse on effective waste management practices, offering a foundation for evidence-based decision-making in the agricultural sector.

References

[1] Amer, M., Daim, T.U. (2011). Selection of renewable energy technologies for a developing county: A case of Pakistan. Energy Sustain Dev [Internet]. 15(4):420–35.

[2] Azahari, S.N.S.S., Abas, M.A., Hussin, H., Nor, A.N.M., Wee, S.T., Fitriani, N., et al. (2021). Developing a Sustainable Solid Waste Management System Using Analytical Hierarchy Process (AHP) Method at Pondok Institutions in Kelantan. IOP Conf Ser Earth Environ Sci. 842(1).

[3] Boonkanit, P., Kantharos, S. (2016). An AHP for Prioritizing and Selecting Industrial Waste Management Method Case Study: Map Ta Phut Industrial Estate. Appl Mech Mater. 848(July):251–4.

[4] Gebrezgabher, S.A., Meuwissen, M.P.M., Oude Lansink, A.G.J.M. (2014). A multiple criteria decision making approach to manure management systems in the Netherlands. Eur J Oper Res [Internet]. 232(3):643–53.

[5] KannadhasanM., S., Lawrence, C., Kumar, V.R.S. (2017). Study on Disposal of Broiler Slaughter Waste Implying Eco-Friendly Waste Management..

[6] Lijó, L., Frison, N., Fatone, F., González-García, S., Feijoo, G., Moreira, M.T. (2018). Environmental and sustainability evaluation of livestock waste management practices in Cyprus. Sci Total Environ. 634:127–40.

[7] Manogaran, M.D., Shamsuddin, R., Mohd Yusoff, M.H., Lay, M., Siyal, A.A. (2022). A review on treatment processes of chicken manure. Clean Circ Bioeconomy [Internet]. 2(May):100013.

[8] Md Zaini, N.S., Basri, N.E.A., Md Zain, S., Saad, N.F.M. (2015). Selecting the best composting technology using analytical hierarchy process (AHP). J Teknol. 77(1):1–8.

[9] Modak, M., Chowdhury, E.H., Rahman, M.S., Sattar, M. (2019). Waste management practices and profitability analysis of poultry farming in Mymensingh district: A socioeconomic study. J Bangladesh Agric Univ.

[10] Saaty, T.L. (1980). The Analytic Hierarchy Process. McGrawhill, Juc New York.

Senaka Bandara

Sri Lanka, September 1991
Mechanical Engineering and Energy Engineering

Asst. Prof. Dr. Chatchawan Chaichana

Mechanical Engineering and Renewable Energy

Nitthinan Borirak

Mechanical Engineering and Energy Engineering

A Comprehensive Approach to Standard Time and Sustainable Waste Reduction in Granola Manufacturing for SMEs

Jidapa Chanjaroen[1,*], Korrakot Y. Tippayawong[1,2], Patcharida Dokbua[1] And Pittaya Tepma[1]

[1] Department of Industrial Engineering, Faculty of Engineering, Chiang Mai University
[2] Supply Chain and Engineering Management Research Unit, Chiang Mai University
*Corresponding author, E-mail: jidapa_ch@cmu.ac.th

Abstract: This research aims to study granola processing by repurposing raw materials from products with unattractive shapes. To enhance processing efficiency and address identified issues, such as a lack of standardized time limits and insufficient awareness among employees regarding each other's duties, were observed. The implementation of a granola processing timer was employed to establish a standard time for the process. As a result, the granola processing timer was used to determine the standard time for this process. There are 8 main steps and 22 sub-steps in the granola production process with 11 types of raw materials. This enables the calculation of the standard time for granola production to be 136.04 minutes per 20 boxes, and the standard time per production unit to be 6.80 minutes. In addition, the work instruction was developed to clarify employee duties, covering steps, personnel, raw materials, processes, and time details. The application of industrial engineering principles, emphasizing motion and time studies, aims to standardize procedures and enhance clarity in employee duties. Applying this principle to developing production processes for other whole grain food-related products in small and medium-sized enterprises (SMEs) could establish standardized workflows and guidelines for similar operations.

Keywords: Motion and Time Study, Standard Time, Responsible Consumption and Production, Cereal Grain Product.

1. Introduction

The company's case study is principally at developing the efficiency of granola production, with attempts to enhance the efficiency of processes for its products while simultaneously addressing sustainability issues within the production process [2-3]. Nevertheless, an examination of the current work process reveals a deficiency in standardization within production procedures, leading to disorder and the generation of non-standard output. The absence of standardized time for individual process steps contributes to workflow inefficiencies and the production of substandard products. Additionally, certain workings rely on the expertise of experienced workers without specific guidelines. Furthermore, the lack of a standardized job description results in worker uncertainty regarding their scope of responsibilities.

The objective of the case study is to propose standard time calculation in Industrial Engineering for granola products by integrating motion and time study theories [1]. In addition to creating work instruction for standard time throughout the entire production process. The determination of standard time for each production step will facilitate the development of an efficient work procedure manual and implementation of sustainable problem management including aligning production with the operational plan, enabling precise control over production timelines and adherence to schedules. [3]. The standardization of the production process is expected to reduce unhealthy conflicts and increase overall improvement in performance [9].

2. Methods

This study focuses on the granola production process within a selected company, exemplifying a case study. Therefore, the research investigated the Time Study technique and analyzed data obtained from the production process diagram supplied by the company [4]. of the production process. Initially, our investigation involved a comprehensive examination of information about the current granola production. For example, production process steps, the equipment utilized in production and raw materials. Subsequently, the research employed an approach to collect by direct time study technique, employing step-by-step timing spanning from the initial process to the final stage [6].

The Maytag method is employed to determine the optimal number rounds. Steps with durations under 2 minutes will be monitored and timed 10 rounds, while steps taking more than 2 minutes will be timed 5 rounds and Equation (1) outlines the method for calculating the normal time. Next, Equation (2) outlines the method for calculating the standard time [8].

Normal time = Selected time x Rating factor (1)

Standard time = Normal time x (1+ Allowance time) (2)

The result of standard time calculations is systematically implemented in the work instruction through the study and research of the work manual prototype, the objective is to ascertain the essential details required for the production process.

3. Results and Discussion

3.1 Current Production Process Analysis

Inquiries regarding challenges encountered during production work and the imperative for process enhancement were initiated, leading to the identification of solutions for production-related issues [6]. The absence of standard time and the lack of interconnected relationships among employees within the production line are evident. Consequently, employees continue to experience a lack of clarity regarding their collaborative working relationships. Currently, the granola production process has 8 main steps, 22 sub- steps, and 11 types of raw materials.

3.2 The computation of the standard time

The time study approach involves both the time and the rate of work for steps within a defined state. When studying or measuring time, it is imperative to ensure the accuracy and appropriateness of the chosen methodology [5]. Furthermore, the comparison between actual time and standardized time helps measure enabling the identification of inefficient time and facilitating the implementation of precautions in the production process [2].

The determination of standard time involves a comprehensive evaluation of normal time through meticulous calculations. Table 1 and Table 2 present the sample data utilized in establishing the standard time for Granola, focusing on the initial two steps. Additionally, Table 3 offers a summary of the standard time per unit for each step of the Granola production process. Consequently, the calculation of the standard time for granola production to be 136.04 minutes per 20 boxes, and the standard time per production unit to be 6.80 minutes. Figure 1 visually represents the standard time proportion of the granola production process form a pie chart.

Table 1. The Sample of Determine the Standard Time for Granola (1)

Step	Detail	Average Time (Min)	Rating Factor (RF)	Total RF (%)
1	Step 1.1	1.31	0.17	1.17
	Step 1.2	0.84	0.17	1.17
2	Step 2.1	12.71	0.09	1.09
	Step 2.2	10.00	0.09	1.09
	Step 2.3	20.00	0.09	1.09
	Step 2.4	33.65	0.07	1.07

Table 2. The Sample of Determine the Standard Time for Granola (2)

Detail	Normal Time (Min)	Total (1+A)	Standard Operation Time	Standard Waiting Time
Step 1.1	1.53	1.10	1.68	-
Step 1.2	0.98	1.10	1.08	-
Step 2.1	13.86	1.10	15.24	-
Step 2.2	10.90	1.10	0.00	11.00
Step 2.3	21.80	1.10	0.00	22.00
Step 2.4	36.01	1.10	0.00	37.02

Table 3. The Standard Time for Granola

Step	Detail	Standard Time (Min)
1	Step 1.1	0.08
	Step 1.2	0.05
2	Step 2.1	0.76
	Step 2.2 (Waiting)	11.00
	Step 2.3 (Waiting)	22.00
	Step 2.4 (Waiting)	37.00
3	Step 3.1	0.68
	Step 3.2	0.60
	Step 3.3	0.12
	Step 3.4	0.56
4	Step 4.1	0.85
	Step 4.2	0.43
	Step 4.3 (Waiting)	44.00
	Step 4.4 (Waiting)	66.00
5	Step 5.1	0.07
	Step 5.2	0.27
6	Step 6.1	0.16
7	Step 7.1	0.63
	Step 7.2	0.68
	Step 7.3	0.46
	Step 7.4	0.32
8	Step 8.1	0.06

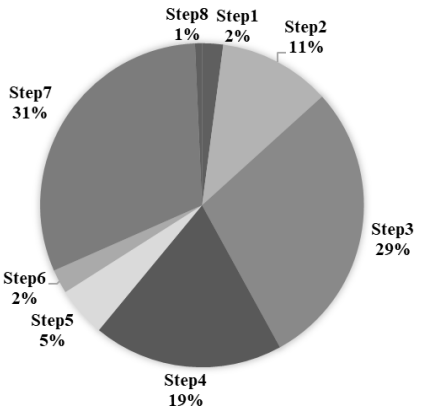

Fig1. the standard time proportion of the granola production process

3.3 Work Instruction

This work instruction provided comprehensive information on the raw materials utilized and the workforce involved in the production process. Additionally, it includes in-depth descriptions of work methods, accompanied by illustrative demonstrations of operations and time standards for all product components [7]. The work instruction was developed to clarify employee duties, covering steps, personnel, raw materials, processes, and time details. Figure 2 visually represents a sample of work instructions for the first step of the Granola.

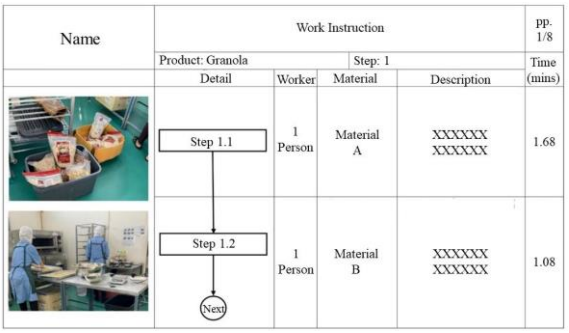

Fig2. The sample of work instruction for Granola

4. Conclusions

In conclusion, this study emphasizes the critical importance of standardization in manufacturing to arrange resources and labor. The application of motion and time study techniques, coupled with the integration of work instruction, the case study company demonstrated development in process efficiency and human resource management. Hence, Standardizing processes and procedures ensures a consistent and uniform approach to manufacturing. The outcomes of this research enhance the broader understanding of efficiency manufacturing management practices, shedding light on their profound influence on both organizational performance and sustainability.

References

[1] Caicedo Solano, N. E., García Llinás, G. A., & Montoya-Torres, J. R. (2020). Towards the integration of lean principles and optimization for agricultural production systems: a conceptual review proposition. *Journal of the Science of Food and Agriculture*, *100*(2), 453-464.

[2] Duran, C., Cetindere, A., Aksu, Y. E., Productivity improvement by work and time study technique for earth energy-glass manufacturing company, *Procedia Economics and Finance*, Vol. 26, 2015, pp. 109 – 113.

[3] Javaid, M., Haleem, A., Singh, R. P., Suman, R., & Gonzalez, E. S. (2022). Understanding the adoption of Industry 4.0 technologies in improving environmental sustainability. *Sustainable Operations and Computers*, *3*, 203-217.

[4] Kittichotsatsawat, Y., Tippayawong, K. Y., Conceptual Framework of Performance Improvement in Coffee Production Using Integrated Lean Technique, *11th Annual International Conference on Industrial Engineering and Operations Management Singapore*, 2021.

[5] Kunza, A., Zanka, M., Neschera, T., Wegenera, K., Virtual reality-based time and motion study with support for real walking, *49th CIRP Conference on Manufacturing Systems*, Vol.57, 2016, pp. 303 – 308.

[6] Mishan, N. N., & Tap, M. M. (2015). Increasing line efficiency by using time study and line balancing in a food manufacturing company. *Jurnal Mekanikal*.

[7] Muchtar, A. H., Maulidizen, A., & Winanto, S. (2022). Human Resources Management in Improving Company Performance. *International Journal of Education, Information Technology, and Others*, *5*(2), 317-329.

[8] Ralph M., Barnes, Motion and Time Study: Design and Measurement of Work, 7th Edition, *Wiley*, 1991.

[9] Realyvásquez-Vargas, A., Flor-Moltalvo, F. J., Blanco-Fernández, J., Sandoval-Quintanilla, J. D., Jiménez-Macías, E., & García-Alcaraz, J. L. (2019). Implementation of production process standardization—A case study of a publishing company from the SMEs Sector. *Processes*, *7*(10), 646.

Ms. Jidapa Chanjaoen
Master student
Major in Master degree of Industrial Engineering
Research Interests:
Logistics and Supply Chain Management, Renewable Energy

Dr. Korrakot Y. Tippayawong
Assistant Professor
Research Interests:
Financial Engineering, Logistics and Supply Chain Management, Performance Measurement

Ms. Patcharida Dokbua
Student
Major in Industrial Engineering

Mr. Pittaya Tepma
Student
Major in Industrial Engineering

Extraction of humic acid from Mae Moh leonardite for sustainable agriculture

Jaturong Kongwutthivech

Laboratory Section, Geology Department, Mae Moh Mine Planning and Administration Division, Electricity Generation Authority of Thailand. Lampang, 52220, Thailand ffiliation, Country (Times New Roman 10)
*E-mail: Jaturong.Kon@egat.co.th

Abstract: Humic acids are the large organic molecular soil conditioner which play the major role in agriculture improving process because their major functional groups are consisted of carboxylic, phenolic and hydroxyl functional groups which give highly ion exchange and hydrophilic properties. Fortunately, Leonardite, a natural organic material (NOM) that contains high amount of humic acid was commonly found in Mae Moh mine as by-products from mining process. According to International Humic Substance Society (IHSS) method, Humic acids can be extracted from leonardite by using base-acid treatment because humic acids can be converted to soluble form in basic condition and precipitated in acidic condition. In addition, variety of cation was significantly affected to %yield of humic acid extraction due to intermolecular interaction between dipole functional groups on humic acids and cation. Therefore, this research will focus about the effect of pH range in humic acids extraction process to yield highly percentage of humic acid from Mae Moh leonardite. Simultaneously, the effect of cation of alkali bases as sodium hydroxide (NaOH) and potassium hydroxide (KOH) was studied. The results showed that the best base-acid extraction condition by using NaOH is pH 14 at 1:20 extraction ratio to yield humic acid 24.93%. Moreover, the best base-acid extraction condition by using KOH is pH 14 at 1:10 extraction ratio to yield humic acid 33.38%.

Keywords: pH, humic acid, leonardite

1. Introduction

Mae Moh mine is the biggest lignite coal mine in Thailand which have authorized by Electricity Generating Authority of Thailand (EGAT). Our mission is providing the lignite coal which is the supply to generate electricity for Mae Moh Power plant. Fortunately, some layer between the coal seam, they found leonardite which is an important organic matter because it contained humin, humic acid and fulvic acid. Humic acid is a valuable plant biostimulant in agriculture and horticulture due to increasing plant growth, yield and resistivity (Canellas, et al., 2015; Calvo, et al., 2014). Especially, it improving the structural and physiological changes in roots and shoots relate to nutrient uptake and distribution (Zandonadi, et al., 2007; Mora, et al., 2014). Moreover, fulvic acid which is a humic acid derivatives (Volikov, et al., 2021; Aeschbacher, et al., 2012). It has a smaller molecule than humic acid but it has a highly antioxidant property cause to improving immunity and reducing inflammation (Vucskits, et al., 2010). According to Circular Economy (CE) policy in Thailand, EGAT would like to respond this policy by using zero waste strategies. Therefore, we planned to upgrade and added value of by product as leonardite by humic acid extraction. Following to International Humic Substance Society, (IHSS) method, Humic acid could be extracted from leonardite by using base-acid extraction procedure (Kuwatsuka, et al., 1992). Due to it solubility and structure, humic acid has a partial solubility in basic solution and it could be complexed with cation because it has many polar moieties for example carboxylic, phenolic and hydroxide (Harvey, et al., 1983; Cheshire, et al., 1967). The intermolecular interaction between the humic acid and cations is very important parameter for the extraction method (Piccolo, 2002). On the

other hand, pH level of the solution and extraction ratio could be affect to solubility of humic acid depended on the power of hydroxide ion in basic solution (Boguta, et al., 2019; Yates and von Wandruszka, 1999). Basic solution can be converted the hydrophobic humic acid to hydrophilic humic acid by deprotonation mechanism (Lan, et al., 2022).

Therefore, this work aimed to study the extraction process from Mae Moh leonardite which affected to %yield of humic acid due to the effect of pH and alkali metal in laboratory scale.

2. Methods

2.1 Chemical

Leonardite sample was collected from Mae Moh mine, Lampang, Thailand. The anhydrous sodium hydroxide (NaOH) and potassium hydroxide (KOH) were AR grade and the universal indicator (4 strips) purchased from Merck. Deionized water (Millipore Milli-Q system, resistivity: 18.2 MΩ at 25 °C) was used to prepare all solutions. The hydrochloric acid used for adjusted the pH of the solution, were AR grade and supplied by RCI Labscan. All of chemicals were used without further purification.

2.2 Preparation of reagent solution

2.2.1 NaOH 0.01 M (pH 12)

NaOH 0.4xx g. was dissolved in deionized water 200 mL and adjusted the volume in 1 L volumetric flask

2.2.2 NaOH 0.1 M (pH 13)

NaOH 4.0xx g. was dissolved in deionized water 200 mL and adjusted the volume in 1 L volumetric flask

2.2.3 NaOH 1 M (pH 14)

NaOH 40.xx g. was dissolved in deionized water 200 mL and adjusted the volume in 1 L volumetric flask

2.2.4 KOH 0.01 M (pH 12)

KOH 0.56xx g. was dissolved in deionized water 200 mL and adjusted the volume in 1 L volumetric flask

2.2.5 KOH 0.1 (pH 13)

KOH 5.6xx g. was dissolved in deionized water 200 mL and adjusted the volume in 1 L volumetric flask

2.2.6 KOH 1 M (pH 14)

KOH 56.xx g. was dissolved in deionized water 200 mL and adjusted the volume in 1 L volumetric flask

2.2.7 HCl 6 M

Conc. HCl 500 mL was dissolved in deionized water 200 mL and adjusted the volume in 1 L beaker

2.3 Experimental Setup.and Methodology

All Experiments were set up following these steps as shown in Figure 1. First of all, the 1 g of Leonardite sample was dissolved in 10 mL of 0.1 M NaOH into the beaker stirred 8 hr and measure pH value. Next, the sample solution was centrifuged at 2,000 rpm and collected the supernatant. After that, supernatant was adjusted to pH 1 by using 6 M HCl and humic acid was settling overnight. The solution was centrifuged 2,000 rpm and collected crude product. Dried the crude product in oven and weighted the dried sample. Calculated the %yield of humic acid.

Each experiment varied the pH condition before start including 12, 13 and 14. The pH was optimized by using 0.01 M, 0.1 M and 1 M NaOH solution, respectively. The extraction ratio between sample and solution was varied 1:10 and 1:20 ratio. Finally, the varieties of alkali metals were varied by using NaOH and KOH.

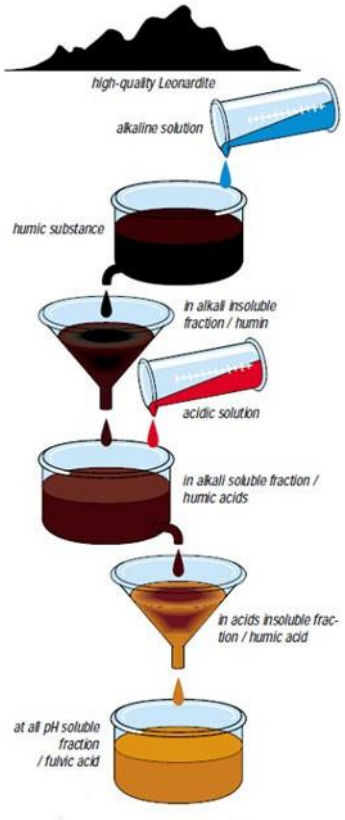

Figure 1. Schematic diagram for humic acid extraction from leonardite by using base-acid method.

3. Results and Discussion

3.1 The pH effect and extraction ratio by using NaOH

We performed the %yield of humic acid by using NaOH in Figure 2. The result showed that the range of %yield is 3% to 25%. The lowest %yield is 3.35% at 0.1 M NaOH in 1:10 extraction ratio and the highest %yield is 24.93% at 1 M NaOH in 1:20 extraction ratio. According to the IHSS method (Kuwatsuka, et al., 1992), humic acid was extracted from Mae Moh leonardite by using a 1:10 extraction ratio of 0.01 M NaOH. Firstly, leonardite was soaked in a basic solution which dissolved humic acid due to its water solubility and separated the others substances such as clay minerals, humin and rocks by using centrifuge. After that, we yield the humic acid by precipitating in an acidic solution. At extraction ratio 1:10 and pH 13, we noticed that this condition gives the lowest %yield of humic acid because of dissolution of some impurities (Ratanaprommanee, et al., 2017). Moreover, humic acid could be increased %yield when the volume of basic solution was increased. The amount of hydroxide ion is one of the important parameters in the extraction process to increase yield of humic acid because it could deprotonate the protons in basic condition. Therefore, the best condition for NaOH is pH 14 at 1:20 extraction ratio.

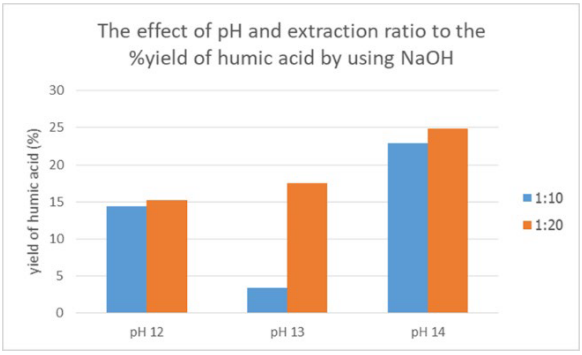

Figure 2. The pH effect and ratio to %yield of humic acid by using NaOH.

3.2 The alkali metals effect on %yield of humic acid at 1:20 extraction ratio

From the Figure 3, we would like to confirm the effect of alkali metals by using 1:20 as a study model and the result showed that the %yield of humic acid by using KOH is significantly higher than NaOH at the same ratio around 5%. Interestingly, the properties of metal ions could be affected by the extraction mechanism. The metal ions could be interacted with humic acid to stabilize the complex by using the intermolecular interaction as electrostatic force (Ai, et al., 2020). The strength of complexation between humic acid and metal ions could be considered by the strength of intermolecular interaction which depends on charge density, geometry and ion size (Boyd, et al., 1981). The stability between humic acid and K^+ ion is higher than Na^+ ion because the humic acid is a large dipole molecule which is easily attracted by a larger ion. Especially, the geometry of alkali metal ions is a sphere shape which could

be reduced the electrostatic repulsion between the molecules.

Finally, the best condition for humic acid extraction from Mae Moh leonardite is 1:20 extraction ratio at pH 14 to give the highest %yield at 33.38%

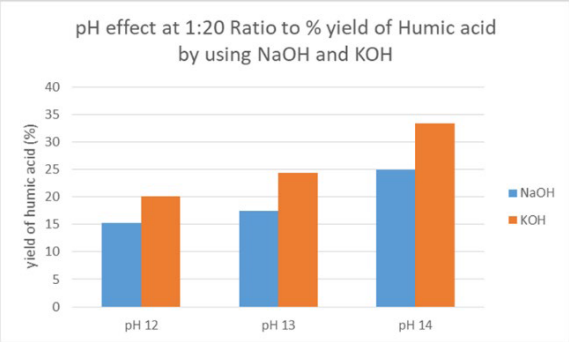

Figure 3. The pH effect to %yield of humic acid by using NaOH and KOH at 1:20 extraction ratio.

4. Conclusions

From the experiment, we concluded that pH value, extraction ratio and metal ions have significantly parameters because all of them can be effected to the efficiency for humic acid extraction by using base-acid method. The pH value and extraction ratio were directly proportional to the amount of hydroxide ion. Thus, the best condition for humic extraction by using NaOH is pH 14 at 1:20 extraction ratio to give 24.93%. Moreover, the stability of humic acid the properties of metal ions could be plays the important roles to stabilize the complex of humic acid. Finally, the best condition for humic acid extraction from Mae Moh leonardite to give the highest %yield by using KOH extraction is 1:20 extraction ratio at pH 14 to gives 33.38% in the laboratory scale.

References

Canellas L.P., Olivares F.L., Aguiar N.O., Jones D.L., Nebbioso A., Mazzei P. and Piccolo A., 2015. Humic and fulvic acids as biostimulants in horticulture. Scientia Horticulturae, 196, 15-27.

Calvo P., Nelson L. and Kloepper J.W., 2014. Agricultural uses of plant biostimulants. Plant and Soil, 383(1), 3-41.

Zandonadi D.B., Canellas L.P. and Façanha A.R., 2007. Indolacetic and humic acids induce lateral root development through a concerted plasmalemma and tonoplast H+ pumps activation. Planta, 225(6), 1583-1595.

Mora V., Bacaicoa E., Baigorri R., Zamarreño A.M. and García-Mina J.M., 2014. NO and IAA Key Regulators in the Shoot Growth Promoting Action of Humic Acid in Cucumis sativus L. Journal of Plant Growth Regulation, 33(2), 430-439.

Aeschbacher M., Graf C., Schwarzenbach R.P. and Sander M., 2012. Antioxidant Properties of Humic Substances. Environmental Science & Technology, 46(9), 4916-4925.

Vucskits A.V., Hullár I., Bersényi A., Andrásofszky E., Kulcsár M. and Szabó J., 2010. Effect of fulvic and humic acids on performance, immune response and thyroid function in rats. Journal of Animal Physiology and Animal Nutrition, 94(6), 721-728.

Kuwatsuka S., Watanabe A., Itoh K. and Arai S., 1992. Comparison of two methods of preparation of humic and fulvic acids, IHSS method and NAGOYA method. Soil Science and Plant Nutrition, 38(1), 23-30.

Harvey G.R., Boran D.A., Chesal L.A. and Tokar J.M., 1983. The structure of marine fulvic and humic acids. Marine Chemistry, 12(2), 119-132.

Cheshire M.V., Cranwell P.A., Falshaw C.P., Floyd A.J. and Haworth R.D., 1967. Humic acid—II: Structure of humic acids. Tetrahedron, 23(4), 1669-1682.

Boguta P., D'Orazio V., Senesi N., Sokołowska Z. and Szewczuk-Karpisz K., 2019. Insight into the interaction mechanism of iron ions with soil humic acids. The effect of the pH and chemical properties of humic acids. Journal of Environmental Management, 245, 367-374.

Yates L.M. and von Wandruszka R., 1999. Effects of pH and Metals on the Surface Tension of Aqueous Humic Materials. Soil

Science Society of America Journal, 63(6), 1645-1649.
Lan T., Wu P., Liu Z., Stroet M., Liao J., Chai Z., Mark A.E., Liu N. and Wang D., 2022. Understanding the Effect of pH on the Solubility and Aggregation Extent of Humic Acid in Solution by Combining Simulation and the Experiment. Environmental Science & Technology, 56(2), 917-927.
Ratanaprommanee C., Chinachanta K. and Chaiwan F., 2017. Chemical characterization of leonardite and its potential use as a soil conditioner for plant growth enhancement. Asia-Pacific Journal of Science and Technology, 22(4), APST-22-04-01 (10 pages).
Ai Y., Zhao C., Sun L., Wang X. and Liang L., 2020. Coagulation mechanisms of humic acid in metal ions solution under different pH conditions: A molecular dynamics simulation. Science of The Total Environment, 702, 135072.
Boyd S.A., Sommers L.E. and Nelson D.W., 1981. Copper(II) and Iron(III) Complexation by the Carboxylate Group of Humic Acid. Soil Science Society of America Journal, 45(6), 1241-1242.

Mr.Jaturong Kongwutthivech
Ph.D. Student, Agronomy
Research Interests:
Humic acid, Fulvic acid and Leonardite

Integrating Advanced Neural Networks and Computer Vision for Precision Classification of Palm Oil Fresh Fruit Bunches

Wahyu Nurkholis Hadi Syahputra[1,2*], Asst. Prof. Dr. Chatchawan Chaichana[1*]

[1]Doctoral Degree Student in Mechanical Engineering, Faculty of Engineering, Chiang Mai University, Chiang Mai 50200 Thailand
[2]Energy Technology and Environment Research Center, Department of Mechanical Engineering, Faculty of Engineering, Chiang Mai University, Chiang Mai 50200 Thailand
*E-mail: c.chaichana@eng.cmu.ac.th

Abstract: The misclassification of palm oil Fresh Fruit Bunches (FFB) hinders agricultural efficiency, prompting a need for advanced solutions. This study addresses the challenge by integrating neural networks and computer vision to surpass the limitations of manual classification. Traditional methods, prone to errors, impact FFB categorization based on ripeness and health. Embracing technology not only mitigates human errors but also accelerates and refines the classification process. The research utilizes the GoogleNet and AlexNet Convolutional Neural Network (CNN) on a dataset of 300 carefully curated FFB images. This dataset is strategically partitioned into 80% training, and 20% testing sets for robust model training, evaluation, and refinement. CNN learns intricate patterns, optimizing its performance in categorizing FFB attributes. Preliminary results indicate promising accuracy levels, showcasing the potential of GoogleNet and AlexNet CNN in effectively classifying palm oil FFB. This approach offers a transformative solution for automated, accurate FFB classification, revolutionizing palm oil plantation management. As the agricultural sector embraces technological advancements, the seamless integration of neural networks and computer vision emerges as a beacon of progress, enhancing the efficiency, sustainability, and overall productivity of the palm oil industry.

Keywords: Classification, Computer Vision, FFB Palm oil, Image processing, Machine Learning

1. Introduction

Oil palm (*Elaeis guineensis* Jacq.) stands as a prominent commodity not only in Indonesia but also in various Southeast Asian nations. The expansion of the palm oil industry in Indonesia has significantly contributed to economic growth and substantial employment opportunities (Makky, 2016). In 2021, the total expanse of oil palm plantations in Indonesia reached 14,663,600 hectares, with a noteworthy production output of 245.63 million tons in 2019. This production marked a substantial increase of 7.44 times compared to the figures recorded in 2015. Furthermore, Indonesia's palm oil exports amounted to 29.5 million tonnes in 2019, surpassing the 2015 export capacity of 27.7 million tonnes (Indonesia Statistic Agency, 2021). These statistics underscore the potential of palm oil as a crucial contributor to the country's economy through robust export activities. Being the primary producer of vegetable oil, palm oil undergoes various processing stages to yield products essential for cooking, industrial applications, biofuel (biodiesel), and even the health sector (Norhaizan et al., 2013). To enhance the overall quality of palm oil production, it becomes imperative to implement sustainable practices in oil palm cultivation. This encompasses addressing challenges related to plantation management, labor shortages, adopting improved crop varieties, and integrating mechanization into the cultivation processes (Murphy et al., 2021). Such initiatives are

crucial for ensuring the long-term viability and sustainability of the palm oil industry while concurrently addressing environmental and social concerns associated with its production.

In the realm of oil palm fruit processing for oil production, a substantial challenge revolves around accurately grading the maturity of oil palm fresh fruit bunches (FFBs). The prevailing approach involves manually gauging FFB maturity or counting loosened fruits per bunch. Unfortunately, this manual sorting method is time-consuming, labor-intensive, and prone to biases and errors, impacting growers' economic returns. Hence, there is a critical need for a reliable and swift sensing technique to accurately detect the maturity of oil palm FFBs (Shaarani et al., 2010). Historically, traditional methods of FFB classification through manual inspection have encountered issues like inconsistencies, errors, and increased labor costs. However, recent efforts have seen the rise of advanced technologies as potential solutions to enhance the precision and efficiency of FFB classification. Notably, the combination of Neural Networks and Computer Vision has shown promise in revolutionizing this aspect of the palm oil industry.

Neural Networks, particularly those employing deep learning architectures, have proven effective in understanding complex patterns and features within datasets. Simultaneously, Computer Vision techniques enable automated systems to interpret visual information, facilitating the automated recognition of important characteristics in FFBs. The collaborative use of these technologies presents a new and transformative approach to improve the accuracy of FFB classification in the palm oil industry, offering a more efficient and reliable alternative to traditional manual methods (Pamornnak et al., 2017).

This research endeavors to investigate the amalgamation of sophisticated Neural Networks and Computer Vision methodologies for the meticulous categorization of Palm Oil Fresh Fruit Bunches (FFBs). Through the utilization of advanced deep learning algorithms and image processing techniques, our objective is to formulate a robust system capable of accurately classifying FFBs according to parameters such as ripeness, quality, and other pertinent attributes. The proposed methodology holds significant promise in optimizing the harvesting process, mitigating reliance on manual labor, and, fundamentally, contributing to the sustainable and efficient production of palm oil.

2. Methods

This research follows a structured procedure involving image acquisition, labeling, preprocessing, image processing, and evaluation to explore the integration of AlexNet and GoogleNet algorithms for precise Palm Oil Fresh Fruit Bunches (FFBs) classification. The dataset is labeled systematically, and preprocessing techniques are applied for standardization and augmentation. AlexNet and GoogleNet, known for their distinct architectures, are then utilized for feature extraction.

Image Acquisition

The image acquisition process involves the use of a Samsung A10S mobile phone camera, equipped with a 13-megapixel resolution. This device is strategically employed for capturing visual data representing Palm Oil FFBs categorized into four distinct classes: Underripe, Ripe, Overripe, and Empty Bunch. The utilization of a mobile phone camera underscores the practicality and accessibility of the image collection approach, facilitating ease of data acquisition in diverse field conditions. To standardize the image format and size, all captured images are converted to the JPEG format. Furthermore, a resizing operation is performed on the images, ensuring a consistent size ratio of 1:1 (Putra et al., 2022). This standardization process enhances the uniformity of the dataset, contributing to the robustness and reliability of subsequent

machine l earning model t r a ining and evaluation.

Data Preparation

The initiation of the image processing phase involves the conversion of each image's resolution. Each image's resolution was reduced from 3024 × 3024 pixels to 224 × 224 pixels, a dimension commonly employed in prior studies for effectively encapsulating the salient characteristics of the original image. This resizing process is deemed necessary due to the impracticality of using high-resolution images for training purposes, as highlighted by previous works. The rationale behind this reduction lies in the fact that large-sized images with complex structures and abundant color information regarding image texture significantly impact the duration required for deep learning processes (Öztürk & Akdemir, 2018).

Data processing and analysis

The initial dataset consisted of 1,600 Fresh Fruit Bunches (FFB) images, distributed across four classes with 400 samples each. Each image underwent augmentation using TensorFlow/Keras preprocessing layers to enhance classification outcomes. This process involved modifications such as rotation, magnification, shift, shear, and alignment. The augmented dataset was then split, allocating 80% for training and 20% for testing purposes. This strategic division ensures a robust training regimen while maintaining a separate set for evaluating the model's performance. The data processing workflow is depicted in Fig. 1.

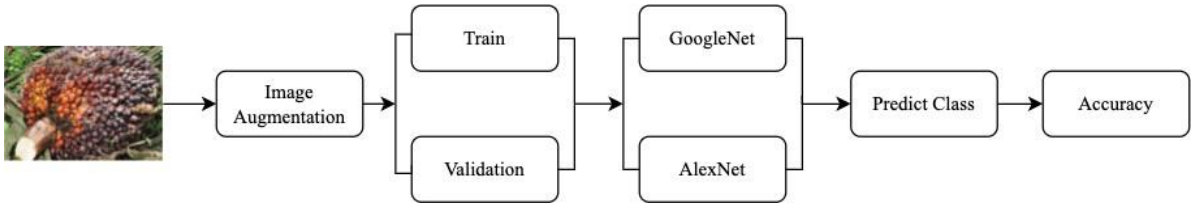

Figure 1. Data processing workflow

This research utilized AlexNet and GoogleNet architectures for image classification. AlexNet consists of five convolution layers, three max pooling layers, and three fully connected layers, with input images sized at 224 × 224 pixels. Various hyperparameters, including regularization, batch size, optimizer, dropout, and Adam, were integrated for binary classification. GoogleNet employs a stacked module approach, with this study utilizing a 22-layer deep convolutional network for image classification. GoogleNet's input images were also resized to 224 × 224 pixels.

3. Results and Discussion

Metrics and training setup

The efficacy and fine-tuning of Convolutional Neural Network (CNN) training pivot significantly on the judicious selection of critical parameters, including the learning rate and epoch. The epoch parameter, representing the number of complete passes the training dataset undergoes, emerges as a pivotal factor influencing accuracy and the model' s applicability in data validation. Noteworthy findings in this study underscored that a higher epoch value, particularly Epoch 100, yielded superior results compared to Epoch 50 and Epoch 75, showcasing the influence of this parameter on overall model performance (Fig. 2).

Moreover, it is paramount to acknowledge the nuanced impact of varying learning rates on the training process's temporal aspects. A discernible trend emerged, revealing that a reduction in the learning rate correlated inversely with the temporal requirements of the training procedure. This dynamic highlights a

delicate trade-off between achieving heightened precision and optimizing computational efficiency. The exploration of these parameters not only contributes to a more nuanced understanding of CNN training dynamics but also informs the optimal configuration for achieving superior accuracy while managing computational resources effectively.

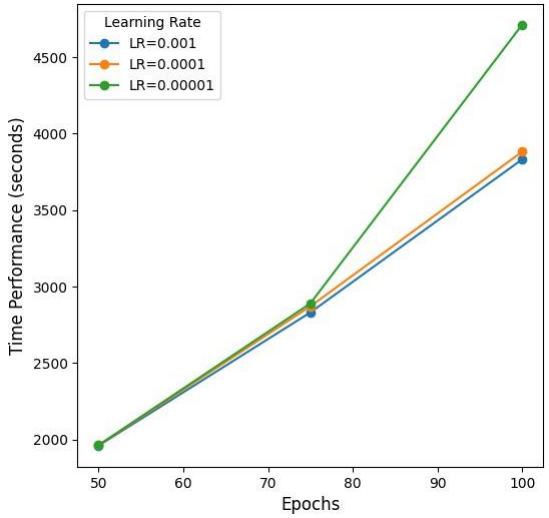

Fig 2. The time performance of different epochs with varying learning rates.

Comparison of Algorithm

In this investigation, Google Net and AlexNet architectures were integrated to conduct a comprehensive comparative analysis concerning the classification of Palm Oil using deep learning techniques. The study also systematically evaluated the model's performance under different architectural configurations, specifically considering epochs and learning rates. The selected values for these parameters were 100 epochs and a learning rate of 0.0001.

Table 1. Comparison of accuracy each algorithm

Algorithm	Accuracy (%)
GoogleNet	89.80
AlexNet	95.32

To validate t he performance of t he architectures, a crucial analysis was conducted using 10-fold cross-validation (CV). This method systematically divides the data into ten equal-sized subsets, allowing an unbiased evaluation. The study revealed that during the 10-fold CV process, AlexNet demonstrated the highest validation accuracy and the lowest loss, followed closely by GoogleNet (Fig. 3).

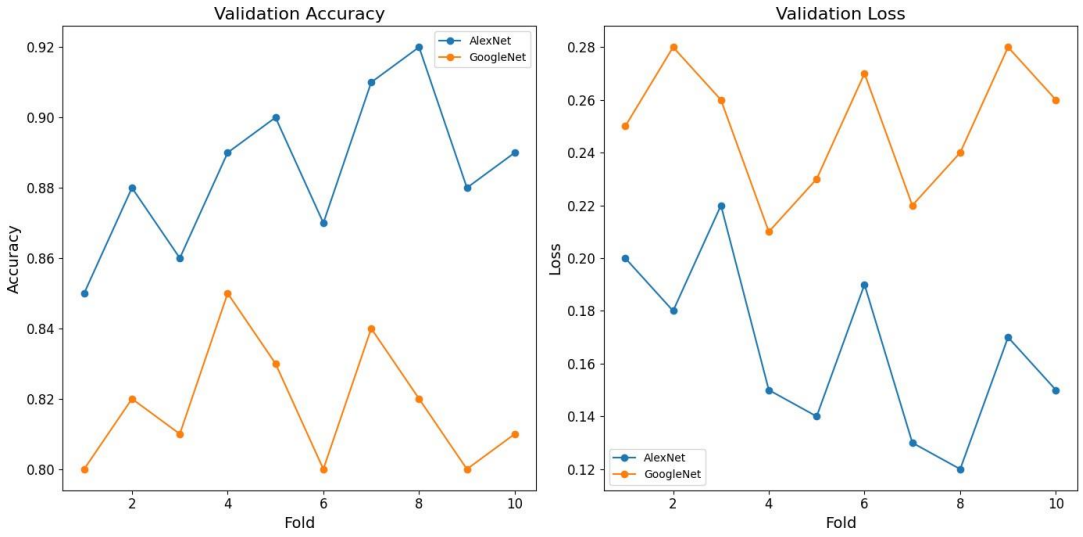

Fig. 3. The evaluations of architectural accuracy and validation loss.

4. Conclusions

The experimental outcomes reveal the best accuracy of Alex Net in comparison to GoogleNet when subjected to training with 100 epochs and a l earning r a t e of 0 .0001 . Specifically, AlexNet achieves a noteworthy accuracy of 95.32%, whereas GoogleNet registers a comparatively lower accuracy of

89.80%. This substantial variance in accuracy underscores the heightened efficacy of AlexNet within the specified training parameters, affirming its robust performance in the precise classification of Palm Oil Fresh Fruit Bunches. These findings substantiate the preferential consideration of AlexNet as an algorithmic choice for this specific application, offering consequential insights for the implementation of advanced neural network architectures in the realm of palm oil production.

References

Indonesia Statistic Agency. (2021). *Ekspor Kelapa Sawit Indonesia 2012-2021*. Badan Pusat Statistik.

Makky, M. (2016). A Portable Low-cost Non-destructive Ripeness Inspection for Oil Palm FFB. *Agriculture and Agricultural Science Procedia*, *9*, 230–240.

Murphy, D. J., Goggin, K., & Paterson, R. R. M. (2021). Oil palm in the 2020s and beyond: challenges and solutions. *CABI Agriculture and Bioscience*, *2*(1), 1–22.

Norhaizan, M. E., Hosseini, S., Gangadaran, S., Lee, S. T., Kapourchali, F. R., & Moghadasian, M. H. (2013). Palm oil: Features and applications. *Lipid Technology*, *25*(2), 39–42. https://doi.org/10.1002/lite.201300254

Öztürk, Ş., & Akdemir, B. (2018). Effects of Histopathological Image Pre-processing on Convolutional Neural Networks. *Procedia Computer Science*, *132*(Iccids), 396–403.

Pamornnak, B., Limsiroratana, S., Khaorapapong, T., Chongcheawchamnan, M., & Ruckelshausen, A. (2017). An automatic and rapid system for grading palm bunch using a Kinect camera. *Computers and Electronics in Agriculture*, *143*, 227–237.

Putra, B. T. W., Amirudin, R., & Marhaenanto, B. (2022). The Evaluation of Deep Learning Using Convolutional Neural Network (CNN) Approach for Identifying Arabica and Robusta Coffee Plants. *Journal of Biosystems Engineering*, *47*(2), 118–129.

Shaarani, S. M., Cárdenas-Blanco, A., Amin, M. H. G., Soon, N. G., & Hall, L. D. (2010). Monitoring development and ripeness of oil palm fruit (Elaeis guneensis) by MRI and bulk NMR. *International Journal of Agriculture and Biology*, *12*(1), 101 – 105.

Wahyu Nurkholis Hadi Syahputra

Indonesia, October 1997
Mechanical Engineering in Research field of Smart Agriculture

Asst. Prof. Dr. Chatchawan Chaichana

Mechanical Engineering and Renewable Energy Technology

The Environmental Governance on Dairy Cattle Breeding in Xinjiang Uygur Autonomous Region From the Perspective of Animal Welfare ——Based on the Field Research with Local Farms

Ziyan Leung[1*]

[1]*Guangxi University, The People's Republic of China*
**E-mail: lillianleung@foxmail.com*

Abstract: In the face of climate change, environmental governance in agriculture innovation receives tons of attention, while focusing on animal welfare is still a cause people need to fight for. Xinjiang Uygur Autonomous Region is famous for dairy cattle breeding which to some extent will create many issues including bacteria spreading, water contamination, and land acidity. How to find a balance between environmental governance and animal welfare is the key focus of this paper. This paper aims to contribute to the understanding of balance by drawing on case studies from Shihezi, Changji and Urumqi in Xinjiang. To compare the balance between environmental governance and animal welfare in three cities field research is conducted. With participant observation and qualitative interviews, it can be concluded that (1) manure processing and water management are the core issues of environmental governance on dairy cattle breeding. (2) big data system helps farmers understand more on dairy cattle so that animal welfare can be implemented. (3) environmental governance and big data system are the only mechanisms in real life. When combined with animal welfare and people's initiative, mechanisms can gain great outcomes. Thus, environmental governance and animal welfare are complementary with the help of a big data system, which can serve as the balance point between two aspects.

Keywords: Animal welfare, Big data system, Dairy cattle, Environmental governance.

1. Introduction

China has a large territory with livestock breeding as one of the main industries. With diverse provinces and autonomous regions, the Chinese Government implements different livestock breeding policies in different places by the landscape and soil conditions. The main livestock includes pigs, poultry, cattle and sheep. Under the guidance of Rural Revitalization from the Central Government, environmental governance becomes a key element in livestock breeding.

Among the provinces and regions that have great contributions to agriculture, Xinjiang Uygur Autonomous Region (hereinafter referred to as Xinjiang), Pearl in the Ancient Silk Road, is famous for its agriculture in China. Covering one-sixth of China's territory, Xinjiang is the largest region in China with the longest borderlines. Located in the northwestern part of China, the climate here is dry for most of the time. Thus, Xinjiang has realized 100% of the water irrigation implementation which is for water saving in the agriculture sector like farming and livestock breeding. Featured in Three Mountains and Two Basins, Xinjiang, in general, has three mountains including the Altai Mountains in the north, Kunlun Mountains in the south, and Tianshan Mountains in the middle as well as two basins, namely, Junggar Basin and Tarim Basin. Xinjiang has various geographical landscapes and different climates. With 4.3% of the habitable territory[12], the dominant landscape in Xinjiang is Gobi, snow-capped mountains, and glaciers. People live in the oasis which is also home to a rich cultural heritage and a diverse range of flora and fauna.

What is more, Xinjiang is known for its livestock breeding and high-quality agri-products. Natural pasture is a great place for sheep, cattle and pigs to live with freedom and happiness. According to the data from Xinjiang Government, the total output volume of the livestock industry amounts to 130.53 billion RMB this year. Pigs, cattle and sheep reached 59.856 million on hand and the poultry inventory is around 63.557 million, while the output of pigs, cattle and sheep is 44.314 million and poultry is 132.456 million[4]. Therefore, Xinjiang is an important livestock production base in China. Meat and milk products in Xinjiang are popular both in domestic and foreign markets.

Xinjiang Government shoulders the green mission from the Central Government and has completed poverty alleviation in the past two years. The main governance trend in China matches the global emergency, that is climate change. Chinese Government decided to have carbon peak by 2030 and carbon neutrality by 2060 to fully establish a green, low-carbon and circular economy[15]. Xinjiang's agriculture sector needs to improve its system to fulfill these tasks because livestock manure, sewage and odors from pastures have become one of the vital sources of ecological pollution. Based on respect to nature, environmental governance comprises living condition improvement, industry restructuring and adjustment, green products production, green lifestyle, green development mechanisms, and international cooperation on climate change and the green Belt and Road Initiative[8]. Xinjiang Government spares efforts in industry restructuring and adjustment as well as green products production, which are the definition of environmental governance in Xinjiang.

Several small farms and limited demonstration farms make Xinjiang's livestock breeding a mixture of extensive and intensive farming with extensive as the dominant style. The structure of Xinjiang's livestock breeding leads to many damages to the environment[9]. First of all, air pollution. Livestock breeding produces a large amount of malodorous gases, which contain a large amount of ammonia, sulfide, methane and other toxic and harmful elements, polluting the farm and the surrounding air as well as affecting the physical and mental health of farm workers. Second, water pollution. Farm sewage comprises pollutants with a high pollution load. Once the toxic components of livestock sewage enter the groundwater, it can reduce the dissolved oxygen of the groundwater, lead to eutrophication of the water and at the same time increase the toxic components in the water. What is worse, it will make the water black and smelly, resulting in permanent groundwater pollution. Third, health threats.

Pollutants in manure have pathogenic microorganisms, parasitic eggs, flies and mosquitoes, which will increase the number of pathogenic species in the environment, resulting in the spread of infectious diseases in humans and animals, especially in zoonotic diseases like brucellosis (hereinafter referred to as BRU). Fourth, land ecology destruction. If livestock sewage is used for irrigation, it will not only make the crops grow late or immature, resulting in yield reduction, and large-scale rotation, but also lead to clogging of soil pores seriously affecting the quality of the soil.[7]

Due to the Rural Revitalization Policy, universities and research institutes in Xinjiang have started to conduct experiments in intensive farming with big data system which is also known as smart farming. It originally starts with one farm. If successfully implemented, this system will be used on other different farms. When it comes to agriculture innovation, people usually talk about technology innovation in agriculture. However, technology is about system and coding. The real innovation is the concept of animal welfare within big data system. Animal welfare is a concept proposed initially in 1976 by Hughes, which refers to a state of complete mental and physical health, where the animal is in harmony with its environment[13]. It is not only about the health of the animals but also the living environment of the animals. Three years later, the Farm Animal Welfare Council was set up in response to Hughes' action[11]. 5 Freedoms are used to describe the rights of animals, that is, freedom from hunger and thirst, freedom from discomfort, freedom from pain, injury and disease, freedom from fear and distress, and freedom to express normal behavior. However, from the perspective of Chinese people, this term is a foreign term with political intent. Besides, ancient Chinese regarded animals as one of their belongings and assets. These two factors hinder the development of animal welfare in China. The Chinese Government chose to establish the Sub-Association of Animal Welfare in the China Veterinary Medical Association and China Association for the Promotion of International Agricultural Cooperation (CAPIAC) to gradually introduce animal welfare. The *Farm Animal Welfare Requirements-Dairy Cattle* was proved by CAPIAC in 2021[6], and *Laboratory Animals — General Code of Animal Welfare* was issued by the Sub-Association of Animal Welfare in 2022[3]. Thus, it is easy to conclude that animal welfare in China still needs more people to pay attention to.

2. Methods and Materials

2.1. Field Research

For this paper, a one-month field research is conducted in Xinjiang with in total of 4 farms. With the approval of local government and farm workers, the author can access farms in Urumqi, Shihezi, and Changji. 2 farms are in Urumqi, 1 in Shihezi, and 1 in Changji. Farms are chosen based on the development of smart farming and big data system as well as dairy cattle breeding. Because of the time limit and large territory in Xinjiang, only 3 cities in Xinjiang are visited for this research.

Both Participant Observation and Qualitative Interviews are used in this paper. Due to the written agreement made with workers, the farms and its workers will be anonymous to prevent identification. All farms will be coded with alphabets A, B, C and D and workers will be coded as A1, B1, C1, and D1, etc.. For workers participating in the interviews, only written notes are taken. The author got help from Xinjiang Agricultural University, Shihezi University and the Ministry of Agriculture and Rural Affairs in the Training Course on Modern Livestock Breeding and Processing Technology for Developing Countries. Therefore, the design of the interview and site visits are the outcome of the cooperation among the 3 sides.

2.2. Participant Observation and Qualitative Interviews

In terms of Participant Observation, the author is not only an observer but a participant. Discussions, small talks, daily work and employee training are both attended by the author. The whole day of one dairy cattle is observed by the author including sleeping, milking, exercise, rumination, eating, and socializing. Besides, the system operation room is also visited. Two evaluation tables of modern dairy farms are used in this part (See Evaluation Table 1 and Evaluation Table 2 below). The two evaluation tables offer the author some guidance in daily observation. Criteria are set according to the *Farm Animal Welfare Requirements-Dairy Cattle*, *Laboratory Animals — General Code of Animal Welfare* and *Evaluation of Modern Dairy Farming: Dairy Farm Classification and Evaluation*[5].

Smart Management of Dairy Cattle Farms
Evaluation Table 1
(1 Point for each and 10 points in total)

Farm Name:

No.	Requirement	Score
1.1	Use of Farm Informationization Management Platform Application	
1.2	Milking equipment with automatic measuring management and vacuum & pulsation monitoring systems	
1.3	Precise feeding system with the ability to monitor TMR production and feeding accuracy, and to record feed lists	
1.4	Dairy cattle oestrus monitoring system and intelligent wearable devices like pedometers, electronic ear tags and so on	
1.5	The cattle cottage, to be milked area, milking hall are equipped with sprinkler, fans which can meet the needs of cattle to prevent heat stroke, and be automatically adjusted.	
1.6	Cattle number identification system and use of automatic herd gates	
1.7	The milking equipment has automatic cleaning function and CIP data acquisition, which can monitor the water temperature, pH value and pressure during the process of cleaning pipelines and milk tanks to ensure that the cleaning program is carried out accurately.	
1.8	With monitoring facilities, covering at least the farm gate, veterinary medicine room, lactation cottage, milking parlor, laboratory, refrigeration room, feed processing workshop, feeding channel, loading plaza, with a retention period of not less than 15 days.	
1.9	With environmental monitoring system, including temperature, humidity, ammonia value, wind speed and other IoT terminals	
1.10	Warning system in detecting sick cattle, which is similar to an online system helping people to notice the abnormal behavior or body condition of dairy cattle	
Total		

Table 1. Smart Management of Dairy Cattle Farms Evaluation Table

Animal Welfare of Dairy Cattle Farms Evaluation Table 2 (1 Point for each and 6 points in total)		
Farm Name:		
No.	Requirement	Score
2.1	Provide dairy cattle with clean and sufficient drinking water, the quality of which meets the requirements of GB 5749.	
2.2	Provide dairy cattle with appropriate, high quality, adequate and consistent feeds	
2.3	Satisfying the socialization needs of dairy cattle and being able to express their nature	
2.4	Suitable living environment (temperature, light, air quality, etc.), comfortable resting area and facilities	
2.5	Measures are in place to safeguard the health of dairy cattle from disease and injury	
2.6	Guarantees dairy cattle no fear or sadness and reduces all types of stresses	
Total		

Table 2. Animal Welfare of Dairy Cattle Farms Evaluation Table

In terms of qualitative interviews, open-ended questions are created with animal welfare and environmental governance as orientation. Usually, the interviews are informal to avoid the anxiety of workers. Interviews are written by the author because recording devices may influence the worker's expression. Questions' orientations are as follows.

(1) Do you know anything about animal welfare?

(2) What do you think is the importance of animal welfare on this farm? Why?

(3) What efforts have been made to ensure animal welfare on the farm? Can you give some examples?

(4) How concerned are employees about animal welfare on the farm? What aspects do they consider to be important components of animal welfare?

(5) How do farm employees view environmental governance in farm operations? What measures do they think should be taken to improve environmental protection and sustainable development?

(6) Does the improvement of animal welfare on the farm have an impact on productivity and environmental governance? Do you think there is a balance among the three?

Although questions are not asked in order, the author will put the questions forward naturally in the small talks with workers. Only main points and perspectives are noted down. To better understand the workers, the author will add some footnotes when the workers mention something about Chinese beliefs and topics about Chinese culture.

2.3. Farm Contexts

Here are brief introductions about 4 farms. We used purposive sampling to select middle-scale dairies in Xinjiang (herd size >300 cattle) which are easier for farm entry approval. We first provide some basic farm context important to understanding the findings (information is accurate as of July 2023).

2.3.1. Farm A (herd size ~500; Holstein cattle, Simmental cattle, and Brown Cattle; ~20 workers)

Located in Urumqi, it is a farm run by a research institute at the University. Farm A was established in 2010 by the dean of the College of Animal Science with the purpose of research and commercial use. Dairy cattle can only take a walk indoors. A smart monitoring system is set for the management of the dairy cattle in body condition. The lactating cattle is milked three times per day and after the milking peak, it will switch to twice per day. Workers are only in charge of the manure processing and the sick cattle while other work is on the big data system. The manure of the dairy cattle will be cleaned once per day in the winter and twice per day in the summer. Most of the manure will be put under the sun and dried. Later they will be sent to the vegetable and fruit farms.

Figure 1. Lely Astronaut A5 in Farm A

2.3.2. Farm B (herd size ~700; Holstein cattle and Brown Cattle; ~30 workers)

Situated in Urumqi, Farm B is a state-owned enterprise farm. Dairy cattle has its own man-made playground and shower pool. Farm B is one of the suppliers of Xinjiang Yogurt so it is more commercial farm rather than a research one. A milking parlour is used for lactating cattle. This is quite a new farm, thus almost all facilities here are new including the milking parlour. Dairy cattle here must follow the schedule made by the farm owner. From breakfast to social activities, all the events are set on this farm. For better income, the lactating cattle will be milked 3 times per day until the end of their lactating period. The big data system is also implemented here with a 24/7 monitoring system and manure collection system as the core technology. The workers' duties are to check in detail the body condition of the dairy cattle to avoid mastitis and heat stress. The manure here will be collected every 2 days, which is mainly used in the playground and bedding after fermentation, sterilization, and drying process.

Figure 2. Milking Parlour in Farm B

2.3.3. Farm C (herd size ~400; Holstein cattle and Brown Cattle; ~10 workers)

Located in Shihezi, Farm C is quite a small and private farm. It is also a supplier for local yogurt production. The dairy cattle can enjoy natural pasture and playground, but the size of these two is relatively small because Shihezi is dominated by Gobi. It gains support from the university and at the same time, the dairy cattle is for both research and commercial use. Every day the workers will follow a certain schedule to lead the dairy cattle to specific activities including milking, playing, and self-

cleaning. The dairy cattle are lactated 3 times per day. Only a cloud system is set for monitoring the body condition of the dairy cattle via the chip within the cattle's body. No 24/7 monitors here because this farm is more traditional than modern. Only a semi-machinery manure scraper is used to clean the manure every day. After the collection of the manure, it will be sold and delivered to another factory.

Figure 3. Milkomax's Robomax in Farm C

2.3.4. Farm D (herd size ~700; Holstein cattle, Simmental cattle, and Brown Cattle; ~35 workers)

Situated in Changji, Farm D is a state-owned-enterprise farm with support from one vocational school. The dairy cattle can only enjoy indoor activity here. The workers use the smart farming system from the vocational school so that they can control the dairy cattle's diet menu, milking time, and body condition. This is a commercial farm with education and tourism features. Besides the workers, they also recruit interns from vocational school to cultivate vets for Changji and create a glass corridor for tourists. The lactating cattle is milked 3 times per day among which is at night. Manure of the cattle will be cleaned twice per day because this is not only a demonstration farm for local farmers but also a tourist spot for visitors. After collecting the manure, the untreated manure will be sold to other farmers to be fermented and used as natural fertilizer. On account of the vet interns here, the dairy cattle have a private vet and diet recipes and body condition are recorded via the ear tag by the big data system.

Figure 4. DeLaval Milking Machine in Farm D

3. Results and Discussion

3.1. City Gap in Farms: Technology Change Dairy Cattle Life and the Environment

Here are the scores obtained from two evaluation tables. Only the final scores are put in the table. Details of the score can be checked in the Appendix.

	Location	Smart Management (10 points in total)	Animal Welfare (6 points in total)	Total Score
Farm A	Urumqi	8.5	4.5	13.0
Farm B	Urumqi	8	5.5	13.5
Farm C	Shihezi	6.5	4.5	11.0
Farm D	Changji	8.5	5.5	14.0
Average	/	7.875	5	12.875

Table 3. Overall Scores for 4 Farms in Smart Management and Animal Welfare

According to the data, it can be concluded that different cities in Xinjiang offer a different smart system on farm. All the farms in research meet the basic requirements of a Smart Management system. Farm D in Changji gets the highest score while Farm C in Shihezi receives the lowest score. In terms of the animal welfare score, all farms value animal welfare with varied focus.

Due to different economic development among the three cities, farms' big data system are different. It is easy to find that with the university, college, or company support, farms can develop better and comprehensive system for dairy cattle. The monitoring system is the most basic facility and moreover, the ventilation system will protect the dairy cattle from heat stress. In terms of animal welfare, this is only a general score for one farm in this sector. The real animal welfare is shown in the details of the workers' daily work and the system. With different purposes for dairy cattle breeding, we can also notice that the score is different. If the dairy cattle is only for commercial use, the big data system is more precise and better developed because the farm owner wants to know the updated information from the cattle every time he/she opens the application. If the dairy cattle is for research and commercial use, the animal welfare score is not that high which might be the extra stress caused by human activities and the fear derived from experiments.

Environmental governance on the farm is also conducted and monitored by the big data system. We know that all the systems here are equipped with sensors for manure processing. The manure is cleaned either by the worker or by the scraper. Then it is laid under the sun to be dried or put together for fermentation. The manure will be delivered to different fruit and vegetable farms or used as the bedding materials for the dairy cattle again.

3.2. Perspective on Animal Welfare: Life or Money Matters?

Karma is mentioned very often. Below are 2 dialogues extracted from the note of the author.

Dialogue 1 with B5 (No. 5 Worker in Farm B)

Author: What you are saying is that the dairy cattle was a human being in its last life, but because of sin, it had to atone for its sins in this life, so it became a dairy cattle, right?

B5: Hmmm. You are too young to know this, kid. Ahhh, yes. Karma is the point. Because there are six great divisions in the wheel of karma[1], one of the divisions is the animal realm. If someone committed a crime in

and the human realm, as you go from the top, clockwise.

[1] The six segments are the God realm, the Demi-God realm, the Hungry Ghost realm, the Hell realm, the animal realm

a past life, he/she will be put into the animal realm in this life. So I do not think they deserve the welfare. They are supposed to live with other dairy cattle and used as a tool for us to earn money.
Author: Interesting. Are you a believer in Buddhism or Taoism?
B5: Kind of. I think I believe in the power of nature and karma. The Yuhuangdati (King of the Heaven) will surely handle the wheel of karma. We should just focus on our sins and do some good deeds so that in our next life we do not have to suffer so much.
B5: For the good deeds collection, I decided to treat dairy cattle nicely.

Dialogue 2 with D6 and C9 (a couple who works in different farms)

Author: What is the point for you to understand animal welfare?
D6: Dairy cattle are born to accumulate merits so that after her death maybe she can choose to be born as a human.
C9: You talk about this again. Yan, you still believe in the wheel of karma. As a worker here, you should just regard dairy cattle as an animal, not a sinner.
Author: Hmmm...

It can be noticed that *sin* and *crime* are used to describe dairy cattle. After interviewing workers, financial income is the driving force for workers to continue this career. To live a happy life is the ultimate goal of the worker.[10] Although dairy cattle might be a sinner in their last life, the workers choose to treat them well because, on the one hand, they can create financial income for them; on the other hand, workers want to be nice to creatures in nature to accumulate merits and values for next life.

This belief is quite common in people ranging between 30 years old to 60 years old, especially those with less education. Buddhism and Taoism are spread all around China. People can decide which belief to believe in. Due to the merits, workers still need to be well-behaved to live a better next life. But this is only one opinion on animal welfare, which is not the same as the official definition of animal welfare. Surprisingly, there is something in common between the academic definition of animal welfare and the workers' beliefs, that is, treating others well including animals. So from the perspective of religious belief, animal welfare has already been implanted into people's mindsets.

Some of the workers are from local universities and vocational schools. Though they do not believe in karma, they do maintain the idea that nature has huge power to have everything in control. Therefore, treating dairy cattle well is to show respect for nature. To some extent, farms can receive benefits in return, which are money and a great working as well as living environment.

3.3. Unfamiliar with the Definition

A WordCloud was generated from the dialogues between the author and workers on the farm. The word *benefit* is mentioned for more than 15 times ranking first in the WordCloud. Some interns also talk about *harmony* and *being environmentally friendly*. These words all reflect people's understanding of animal welfare.

Figure 5. Word cloud generated from the transcripts of the dialogues between the author and workers

From the WordCloud we know that workers link animal welfare and benefits together. Firstly, this might be shaped by the Chinese language system. Welfare (福利, pinyin: fú lì) in Chinese means the indirect benefit the company gives to the workers, such as paid holidays and festival coupons, which can make workers think of benefits when it comes to welfare. Welfare is used to describe things that workers receive and is not so commonly used on animals. Thus, when combining animal and welfare, people usually think about the benefit to the animals. Secondly, the definition is not well-known because the education and training of workers are more practical. When workers are hired on the farm, the only lectures the farm gives to the workers are about how to use the big data system and how to finish work in the appropriate time. No one will hire a professor to tell workers about animal welfare. Thirdly, at least from the WordCloud, we can see that some workers mention *environment* and *harmony*. It means that they understand animal welfare is an important element for humans and the environment.

We met some workers with positive feedback and understandings of animal welfare. From Dialogue 3 and 4, we notice that even though workers do not know the term *animal welfare*, they at least try to learn and express their thinking on it.

Dialogue 3

Author: Since you talk about the location of the farm and the benefit to dairy cattle, can you elaborate more on this connection?
A3: Sure. Everyone is happy then I am happy. So if my dairy cattle can live a happy life, I can also be in happiness. They are all my kids on the farm. Our farm is in the countryside of Urumqi with less pasture. Our location is not so good lah. (Sign) I used to visit my friend's farm. His farm is in Inner Mongolia. That is a really good farm. A good farm. The grass is fresh and the environment is so good. I cannot imagine how happy the dairy cattle would be if they were citizens of Inner Mongolia's pasture.
Author: Xinjiang is also a good place for them to live. Do not worry. They are happy.
A2: Hmmm...The most happy thing for dairy cattle is

that they can enjoy free medical treatment. Our big data system will detect all the abnormal behavior of the dairy cattle and if the system detects something unusual, it will report to us. We will call the barefoot vet here for medical treatment.
A3: Right! I saw Uncle Lou (the vet's name) once. He uses herbal medicine to dairy cattle. It looks very healthy. This is my first time to know dairy cattle can also eat Chinese herbal medicine.
Author: Really? This is also my first time to know!

Dialogue 4

Author: You say showing respect the nature is the best way for both humans and animals. Can you talk about this in more detail?
D10: I worked in a local school for more than 10 years. So I can kind of understand what you are just saying. Animal welfare is like the rights of animals. They, to some extent, are similar to human beings. So I think that in deeper meaning animal welfare is a part of the respect people show to nature. President Xi mentions the importance of green and sustainability. I think animal welfare is like environmental protection. We chose a good location for dairy cattle to live. And we also deal with their manure and sometimes their dead body. These are not only for their welfare but also for our welfare.

In these two dialogues, respect, benefit and the environment are mentioned over and over. For Chinese people, nature and environment are of great importance. Even if workers are not familiar with the concept of animal welfare, they try to use their encyclopedia knowledge to understand this term. Combining animal welfare and human welfare is a good way to elaborate this term. In Dialogue 3, A3 (No. 3 worker in Farm A) uses the word citizen to describe dairy cattle, showing that he with love and care regards dairy cattle as human beings. This is a common mindset among dairy cattle keepers. Usually, cattle keepers will take all cattle as one of the family members of their own. Though they raise the dairy cattle for money, cattle keepers still think taking good care of dairy cattle is their responsibility, which is very similar to the mindset of raising their own children. Though they do not have a clear definition of animal welfare, what they are doing now is part of animal welfare.

3.4. Manure Processing and Environmental Governance: Live a Good Life

Dialogue 5

D11: Sometimes visitors come here and are surprised that although the bedding of the dairy cattle is made of its manure, it is not as smelly as they think. We contribute efforts in managing the manure so that the manure can be used both in bedding and on arable land.
Author: Let them sleep in their manure? How come?
D10: We separated the solid and liquid in the manure. The solid one can be used in bedding. Although manure from dairy cattle has high water content, generally 80%-90%, and contains a large number of pathogenic microorganisms, parasite eggs and other harmful substances. It can be used as bedding after drying and harmless treatment.
Author: (Nodding) I see...

Manure is an asset on the farm with various ways to make good use of it. Dealing with manure is a big issue. Different farms have different ways of manure processing. A manure scraper is used to collect all the manure first. Besides, water is also needed to clean the cattle cottage. After cleaning, both manure and polluted water are kept for later use.

In Xinjiang, with dry weather, people often separate the solid and liquid in the manure. The solid one is dried under the sun and the liquid one is put to the harmless treatment system. The guiding principle of this process is the combination of animal husbandry and agricultural food planting. Manure is widely used in these two sectors to build sustainable agriculture in Xinjiang. As mentioned by D11 (No. 11 Worker in Farm D), manure can be put in the bedding for dairy cattle. Farms in Xinjiang use this method in manure processing because it can save the transportation fee in manure and at the same time it does not cost any extra expenditure to buy more materials in bedding.

For the environment, it is a sustainable way of manure processing with fewer chemicals going into the land.[1] Manure itself serves as a type of organic fertilizer for the land and other farmers, while the liquid manure being stored in the oxidation pond goes to farm cleaning or irrigation of the surrounding farmland after diluting and solid-liquid separation.

3.5. Big Data System on Dairy Cattle: Rational Data and Thorough Care

Almost all steps and events will be monitored and recorded by the farm's big data system, such as the diet menu, daily schedule for the dairy cattle, milking volume, milking frequency, and even the excretion frequency. According to the evaluation tables in the Appendix, we notice that none of the farms does a good job in environmental monitoring system, including temperature, humidity, ammonia value, wind speed, and so on.

The farms cooperate with local vets to ensure the dairy cattle can be treated when there is an emergency. These vets do not live on the farm with the name of barefoot vet in Xinjiang. The vet will first check the data from the system and then the workers will lead the vet to see the dairy cattle. Sometimes, data can only provide the background information of the dairy cattle, and the vet needs to check the cattle by himself/herself so that the vet can diagnose what happened to the cattle and which medicine should be applied to the cattle.

Data is rational stuff for workers to analyze the basic condition so that they might know what the cattle need and how the cattle feel. With this system, things can be within control on the premise of electricity.[14] If the whole farm is out of electricity, data cannot be collected so it might have some problems.

3.6. Relations: Animal Welfare in Environmental Governance

As is mentioned before, animal welfare is human welfare. One of the demonstrations of this opinion is that with better animal welfare, the farm can have higher productivity and a better living environment both for human beings and for animals.

Environmental governance is a motion and action proposed by human beings to create a green and sustainable society. Under the environmental governance, manure, polluted water and the smelly gas from the farm are to be handled.[2] To create a better place for dairy cattle, workers

here need to reply both on the big data system and talents from the university or colleges.

Environmental governance on the farm is required to consider the dairy cattle. Farms want to earn profit for sure but how to balance productivity, environmental protection and animal condition is a tough task for them to solve. From the interviews with more than 100 workers on the farm, it can be concluded that profits and environmental governance are all about animal welfare. By wisely using the smart farming system, workers can grasp the current situation of the farm knowing the updated body condition of the dairy cattle, the cleaning process of the manure and even the milking volume of one cattle per day. Workers desire to live a good life and at the same time dairy cattle's lives are in the hands of workers. Actions and responses are taken by workers according to the smart farming system, while animal welfare is protected by the workers with making profits as the driving force. As a consequence, the environment is well preserved and protected by the actions and responses of the workers.

4. Conclusions

Environmental governance is conducted by human beings. On the farm, one of the most important issues is manure and wastewater processing as well as cattle cottage cleaning. Through the big data system, the farm can be managed well on the premise of enough and sufficient electricity. With care and love for dairy cattle, the farm can gain benefits which can also be seen as human welfare. People always say technology changes the world. That is only part of the function of technology. The real thing that changes the world is the combination of animal welfare and technology. Only when environmental governance and big data system are filled with empathy, animal welfare and human welfare can be achieved comprehensively.

References

[1] 陈瑶 & 王树进.(2014).我国畜禽集约化养殖环境压力及国外环境治理的启示. *长江流域资源与环境*(06),862-868.

[2] 董存霞,姚娟,胡继然 & 李倩娜.(2022).农户参与生态环境治理行为研究——以新疆昌吉市为例. *中国农业资源与区划*.

[3] 科学技术部. (2022). '实验动物 福利通则/Laboratory animals—General code of animal welfare', 国家标准|GB/T 35892-2018. Available at: https://openstd.samr.gov.cn/bzgk/gb/newGbInfo?hcno=9BA619057D5C13103622A10FF4BA5D14 (Accessed: 01 December 2023).

[4] 新疆维吾尔自治区人民政府. (2023) '新疆维吾尔族概况', 新疆维吾尔自治区人民政府网. Available at: http://www.xinjiang.gov.cn/ (Accessed: 01 December 2023).

[5] 中国奶业协会 (2020). '现代奶牛场评价表', 中国奶业协会标准网. Available at: https://www.dac.org.cn (Accessed: 01 December 2023).

[6] 中国农业国际合作促进会. (2021). '农场动物福利要求 奶牛/Farm animal welfare requirements-dairy cattle', 全国团体标准信息平台. Available at: https://www.ttbz.org.cn/upload/file/20210813/6376445262277217633807764.pdf (Accessed: 01 December 2023).

[7] 中国农业农村部 .(2023).向绿而行 从畜禽粪污资源化利用开始. *中国畜牧业*(20),8.

[8] 中国政府. (2023a) '新时代的中国绿色发展', 中国政府网. Available at: https://www.gov.cn/zhengce/zhengcewenjianku/index.htm (Accessed: 01 December 2023).

[9] 中国生态环境部. (2002) '我国畜禽养殖业的环境问题与防治对策', 中华人民共和国生态环境部. Available at: https://www.mee.gov.cn/ (Accessed: 01 December 2023).

[10] Chen, M., & Weary, D. M. (2022). "Cattle Welfare Is Basically Human Welfare": Workers' Perceptions of 'Animal Welfare' on Two Dairies in China. *Frontiers in veterinary science*, 8, 808767. https://doi.org/10.3389/fvets.2021.808767

[11] Farm Animal Welfare Committee. (1979). 'Five Freedoms of Animal Welfare', Farm Animal Welfare Committee (FAWC). Available at: www.gov.uk (Accessed: 01 December 2023).

[12] Huang, H. and Wan, Y. (2023) 'Formation of an unprecedented yellow snow episode in Xinjiang on December 1, 2018', *Heliyon*, 9(8). doi:10.1016/j.heliyon.2023.e18857.

[13] Koknaroglu, H., & Akunal, T. (2013). Animal welfare: an animal science approach. *Meat science*, 95(4), 821–827. https://doi.org/10.1016/j.meatsci.2013.04.030

[14] Tuyttens, F. A. M., Molento, C. F. M., & Benaissa, S. (2022). Twelve Threats of Precision Livestock Farming (PLF) for Animal Welfare. *Frontiers in veterinary science*, 9, 889623. https://doi.org/10.3389/fvets.2022.889623

[15] Xinhua News. (2021) China maps path to Carbon Peak, neutrality under new development philosophy. Available at: https://english.www.gov.cn/policies/.html (Accessed: 01 December 2023).

Appendix

Evaluation Tables for Farm A

Smart Management of Dairy Cattle Farms
Evaluation Table 1
(1 Point for each and 10 points in total)

Farm Name: Farm A

No.	Requirement	Score
1.1	Use of Farm Informationization Management Platform Application	1
1.2	Milking equipment with automatic measuring management and vacuum & pulsation monitoring systems	1
1.3	Precise feeding system with the ability to monitor TMR production and feeding accuracy, and to record feed lists	1
1.4	Dairy cattle oestrus monitoring system and intelligent wearable devices like pedometers, electronic ear tags and so on	0.5
1.5	The cattle cottage, to be milked area, milking hall are equipped with sprinkler, fans which can meet the needs of cattle to prevent heat stroke, and be automatically adjusted.	1
1.6	Cattle number identification system and use of automatic herd gates	1
1.7	The milking equipment has automatic cleaning function and CIP data acquisition, which can monitor the water temperature, pH value and pressure during the process of cleaning pipelines and milk tanks to ensure that the cleaning program is carried out accurately.	1

1.8	With monitoring facilities, covering at least the farm gate, veterinary medicine room, lactation cottage, milking parlor, laboratory, refrigeration room, feed processing workshop, feeding channel, loading plaza, with a retention period of not less than 15 days.	1
1.9	With environmental monitoring system, including temperature, humidity, ammonia value, wind speed and other IoT terminals	0
1.10	Warning system in detecting sick cattle, which is similar to an online system helping people to notice the abnormal behavior or body condition of dairy cattle	1
Total		8.5

Animal Welfare of Dairy Cattle Farms
Evaluation Table 2 (1 Point for each and 6 points in total)
Farm Name: Farm A

No.	Requirement	Score
2.1	Provide dairy cattle with clean and sufficient drinking water, the quality of which meets the requirements of GB 5749.	1
2.2	Provide dairy cattle with appropriate, high quality, adequate and consistent feeds	1
2.3	Satisfying the socialization needs of dairy cattle and being able to express their nature	0.5
2.4	Suitable living environment (temperature, light, air quality, etc.), comfortable resting area and facilities	0.5
2.5	Measures are in place to safeguard the health of dairy cattle from disease and injury	1
2.6	Guarantees dairy cattle no fear or sadness and reduces all types of stresses	0.5
Total		4.5

Evaluation Tables for Farm B

Smart Management of Dairy Cattle Farms
Evaluation Table 1
(1 Point for each and 10 points in total)
Farm Name: Farm B

No.	Requirement	Score
1.1	Use of Farm Informationization Management Platform Application	1
1.2	Milking equipment with automatic measuring management and vacuum & pulsation monitoring systems	1
1.3	Precise feeding system with the ability to monitor TMR production and feeding accuracy, and to record feed lists	1
1.4	Dairy cattle oestrus monitoring system and intelligent wearable devices like pedometers, electronic ear tags and so on	0
1.5	The cattle cottage, to be milked area, milking hall are equipped with sprinkler, fans which can meet the needs of cattle to prevent heat stroke, and be automatically adjusted.	1
1.6	Cattle number identification system and use of automatic herd gates	1
1.7	The milking equipment has automatic cleaning function and CIP data acquisition, which can monitor the water temperature, pH value and pressure during the process of cleaning pipelines and milk tanks to ensure that the cleaning program is carried out accurately.	1
1.8	With monitoring facilities, covering at least the farm gate, veterinary medicine room, lactation cottage, milking parlor, laboratory, refrigeration room, feed processing workshop, feeding channel, loading plaza, with a retention period of not less than 15 days.	1
1.9	With environmental monitoring system, including temperature, humidity, ammonia value, wind speed and other IoT terminals	0
1.10	Warning system in detecting sick cattle, which is similar to an online system helping people to notice the abnormal behavior or body condition of dairy cattle	1
Total		8

Animal Welfare of Dairy Cattle Farms
Evaluation Table 2 (1 Point for each and 6 points in total)
Farm Name: Farm B

No.	Requirement	Score
2.1	Provide dairy cattle with clean and sufficient drinking water, the quality of which meets the requirements of GB 5749.	1
2.2	Provide dairy cattle with appropriate, high quality, adequate and consistent feeds	1
2.3	Satisfying the socialization needs of dairy cattle and being able to express their nature	1
2.4	Suitable living environment (temperature, light, air quality, etc.), comfortable resting area and facilities	1
2.5	Measures are in place to safeguard the health of dairy cattle from disease and injury	1
2.6	Guarantees dairy cattle no fear or sadness and reduces all types of stresses	0.5
Total		5.5

Evaluation Tables for Farm C

Smart Management of Dairy Cattle Farms
Evaluation Table 1 (1 Point for each and 10 points in total)
Farm Name: Farm C

No.	Requirement	Score
1.1	Use of Farm Informationization Management Platform Application	1
1.2	Milking equipment with automatic measuring management and vacuum & pulsation monitoring systems	1
1.3	Precise feeding system with the ability to monitor TMR production and feeding accuracy, and to record feed lists	1
1.4	Dairy cattle oestrus monitoring system and intelligent wearable devices like pedometers, electronic ear tags and so on	0.5
1.5	The cattle cottage, to be milked area, milking hall are equipped with sprinkler, fans which can meet the needs of cattle to prevent heat stroke, and be automatically adjusted.	0.5
1.6	Cattle number identification system and use of automatic herd gates	0.5
1.7	The milking equipment has automatic cleaning function and CIP data acquisition, which can monitor the water temperature, pH value and pressure during the process of cleaning pipelines and milk tanks to ensure that the cleaning program is carried out accurately.	0.5
1.8	With monitoring facilities, covering at least the farm gate, veterinary medicine room, lactation cottage, milking parlor, laboratory, refrigeration room, feed processing workshop, feeding channel, loading plaza, with a retention period of not less than 15 days.	0.5
1.9	With environmental monitoring system, including temperature, humidity, ammonia value, wind speed and other IoT terminals	0
1.10	Warning system in detecting sick cattle, which is similar to an online system helping people to notice the abnormal behavior or body condition of dairy cattle	1
Total		6.5

Animal Welfare of Dairy Cattle Farms
Evaluation Table 2 (1 Point for each and 6 points in total)
Farm Name: Farm C

No.	Requirement	Score
2.1	Provide dairy cattle with clean and sufficient drinking water, the quality of which meets the requirements of GB 5749.	1
2.2	Provide dairy cattle with appropriate, high	1

	quality, adequate and consistent feeds	
2.3	Satisfying the socialization needs of dairy cattle and being able to express their nature	0.5
2.4	Suitable living environment (temperature, light, air quality, etc.), comfortable resting area and facilities	0.5
2.5	Measures are in place to safeguard the health of dairy cattle from disease and injury	1
2.6	Guarantees dairy cattle no fear or sadness and reduces all types of stresses	0.5
Total		4.5

Evaluation Tables for Farm D

Smart Management of Dairy Cattle Farms
Evaluation Table 1 (1 Point for each and 10 points in total)

Farm Name: Farm D

No.	Requirement	Score
1.1	Use of Farm Informationization Management Platform Application	1
1.2	Milking equipment with automatic measuring management and vacuum & pulsation monitoring systems	1
1.3	Precise feeding system with the ability to monitor TMR production and feeding accuracy, and to record feed lists	1
1.4	Dairy cattle oestrus monitoring system and intelligent wearable devices like pedometers, electronic ear tags and so on	1
1.5	The cattle cottage, to be milked area, milking hall are equipped with sprinkler, fans which can meet the needs of cattle to prevent heat stroke, and be automatically adjusted.	1
1.6	Cattle number identification system and use of automatic herd gates	1
1.7	The milking equipment has automatic cleaning function and CIP data acquisition, which can monitor the water temperature, pH value and pressure during the process of cleaning pipelines and milk tanks to ensure that the cleaning program is carried out accurately.	1
1.8	With monitoring facilities, covering at least the farm gate, veterinary medicine room, lactation cottage, milking parlor, laboratory, refrigeration room, feed processing workshop, feeding channel, loading plaza, with a retention period of not less than 15 days.	0.5
1.9	With environmental monitoring system, including temperature, humidity, ammonia value, wind speed and other IoT terminals	0
1.10	Warning system in detecting sick cattle, which is similar to an online system helping people to notice the abnormal behavior or body condition of dairy cattle	1
Total		8.5

Animal Welfare of Dairy Cattle Farms
Evaluation Table 2 (1 Point for each and 6 points in total)

Farm Name: Farm D

No.	Requirement	Score
2.1	Provide dairy cattle with clean and sufficient drinking water, the quality of which meets the requirements of GB 5749.	1
2.2	Provide dairy cattle with appropriate, high quality, adequate and consistent feeds	1
2.3	Satisfying the socialization needs of dairy cattle and being able to express their nature	1
2.4	Suitable living environment (temperature, light, air quality, etc.), comfortable resting area and facilities	1
2.5	Measures are in place to safeguard the health of dairy cattle from disease and injury	1
2.6	Guarantees dairy cattle no fear or sadness and reduces all types of stresses	0.5
Total		5.5

Ms. Ziyan Leung
Master student, Master of Art in Translation and Interpretation
Research Interests:
China-ASEAN relations, animal welfare, and gender studies.

Climate-Related Disclosure Standards and China's Strategic Choices

Xiaoyun Li[1]

[1] *School of Business, Guangxi University, Nanning 530004, China*

Abstract: In recent years, climate change and its impact on economic and social life has become a rising topic in the international community. Since the adoption of the Paris Agreement at the United Nations Climate Conference in 2015, many organisations have established and developed a variety of disclosure standards and frameworks for sustainability reporting. However, the differences between reporting frameworks have led to poor comparability of financial information disclosed by companies. There is an urgent need for disclosure frameworks with uniformity, consistency and comparability around the world. 2021 saw the announcement of the establishment of the International Sustainability Standards Board (ISSB), which has now formally issued two international sustainability disclosure standards, including IFRS S2, which is an application of the sustainability disclosure requirements for financial reporting to climate-related information. Since the establishment of ISSB, China has actively participated in the development of the standards and contributed Chinese wisdom. In the face of climate change, President Xi Jinping has proposed a "dual-carbon" target. With reference to the new regulations on climate disclosure, China should take the lead and actively promote the development of sustainable disclosure standards, so that climate-related information disclosure can better serve the "dual-carbon" goal.

Keywords: accounting, climate disclosure, ISSB, Sustainability Disclosure Standards.

1. Introduction

"Climate issues affect human survival and the deep transformation of economic and social fields. The 17 sustainable development goals passed at the UN Sustainable Development Summit in 2015 reflect the international community's attention to climate issues[14]. D. Dragomir et al.'s research points out that how to slow down climate change through reducing greenhouse gas emissions is a core issue of concern for governments around the world[3], among which corporate greenhouse gas (GHG) emissions are one of the important factors leading to climate change[2]. Therefore, the UN Climate Conference held in Paris in 2015 passed the Paris Agreement. The United Nations Environment Programme releases the Emission Gap Report annually to assess whether the progress of greenhouse gas emissions reduction is sufficient to achieve the temperature control targets in the 21st century. However, the 2022 Emission Gap Report shows that there is still a significant gap between the greenhouse gas emissions reduction situation of countries worldwide and the goals set by the Paris Agreement[8]."

Climate change is an increasingly heated topic. At a time when the economy and society are deeply transitioning to a low-carbon economy, investors in the capital market and other stakeholders pay more and more attention to the disclosure of governance measures, risk management processes and business strategies for climate-related matters by enterprises, as well as the assessment of the impact of climate risks on their business models, financial conditions and operating results. And use this information as an important basis for decision-making. In 2019, Nick Anderson, a member of the International Accounting Board (IASB), published a paper explaining how to apply international Accounting standards (IFRS) to reflect emerging risks such as climate risk[1]. Subsequently, requirements related to climate change targets and disclosures were incorporated into sustainability standards.

Under the tireless efforts of governments and international organizations, the sustainable development of some typical reporting framework to form a system and is widely applied in practice, but the differences between different reporting framework led to the enterprise information disclosure not comparable to each other. The disclosure of information according to multiple frameworks not only increases the burden of editors, but also increases the confusion of users. It is increasingly urgent for the international community to resolve the confusion of different disclosure standards and realize the consistency and comparability of information disclosed by different frameworks[13]. The International Organization of Securities Commissions (IOSCO) issued a statement in 2021 stating that the world urgently needs a globally consistent, comparable and reliable set of sustainable disclosure guidelines[7]. In this context, the emergence of ISSB on the one hand should meet the user's dissatisfaction with the complicated disclosure framework system, on the other hand accord with the call to build a global uniform disclosure standards. Subsequently, the development of sustainable development disclosure standards entered a period of acceleration, with the promotion of international organizations such as the International Organization of Securities Commissions (IOSCO), the International Sustainable Development Standards Board (ISSB) announced the establishment of two international financial reporting sustainable disclosure standards in 2023. Two scholars, Huang Shizhong and Ye Fengying, pointed out that IFRS S2, one of the two standards, pays great attention to the emission and accounting of greenhouse gases by enterprises[8]. This is because greater transparency in the disclosure of climate-related risks can help governments better understand the sources of greenhouse gas emissions within their jurisdiction, and then formulate policies according to local conditions[4]. The early focus of the guidelines was on the risk of climate change, which was mainly affected by the following two factors: Climate change seriously threatened the survival and development of human beings, and became a risk that many countries and regions continued to pay attention to when exploring economic recovery in the post-pandemic period; In addition, the risks of climate change will be transmitted through the real economy to financial institutions such as banks, affecting the stability of the financial system.

Chinese scholars Hu Cheng and Fan Xingjian pointed out that the convergence of accounting standards changes constantly with the development of The Times. Historically, the concept of international convergence of accounting standards began in the late 1950s, which was an objective requirement of the process of economic integration and cross-border capital flow after World War II. The original convergence concept focused on accounting harmonization, i.e. reducing the differences between accounting principles in major capital markets. In the 1990s, the "harmonization view" was gradually replaced by the "convergence view", that is, the establishment of a set of high-quality accounting standards commonly used in

major international capital markets, in order to guide governments to adopt or converge their accounting standards with them[6][7]. The issue of accounting standards is not only related to the economic field, but also may rise to the political level, related to the recognition of market economy status of jurisdictions. Accounting standards are closely related to capital market, international trade, overseas listing of enterprises, attracting foreign capital, opening of accounting services and market expansion[16]. Therefore, the attitude of the world's major economies towards accounting internationalization will be adjusted according to the changes of their economic and political conditions. Some countries choose to fully adopt international norms, some countries give priority to national norms and international norms second, and some countries choose to adopt national norms in parallel with international norms. At present, economic globalization makes national accounting governance and global accounting governance show a high degree of mutual penetration. In this case, how to view the international convergence of accounting standards and make the right choice is related to the future development of Chinese accounting, which has great research significance.

2. A brief introduction of the guidelines

There are two published IFRS Sustainable Disclosure Standards (ISDS), namely IFRS Sustainable Disclosure Standard 1 - General Requirements for Sustainability-related Financial Information Disclosure (IFRS S1) and IFRS Sustainable Disclosure Standard 2 - Climate-Related Disclosure (IFRS S2). IFRS S1 aims to provide financial reporting users with information on the risks and opportunities associated with sustainable development.IFRS S2 is the application of the general requirements of information disclosure in the former to climate change issues. The subject of the report discloses information on climate-related risks and opportunities to stakeholders, and its core content is developed in terms of governance, strategy, risk management, indicators and objectives.

(1) Governance.IFRS S2 require subjects to disclose to climate related risks and opportunities for supervision and administration.

(2) Strategy.IFRS S1 requires an entity to disclose its management strategy related to sustainability and its impact on financial performance.IFRS S2 refines the general requirements for disclosure.

(3) Risk management.IFRS S1 requires entities to disclose their processes for managing sustainabilition-related risks and opportunities, while IFRS S2 imposes higher disclosure requirements by requiring entities to disclose scenario analyses of climate-related risks and opportunities.

(4) Indicators and targets.IFRS S1 request main body to provide relevant targets and indicators of sustainable development, IFRS S2 embodiment to these requirements, require the subject to disclose information can reflect the key factors that affect climate related risks and opportunities, as well as the risks and opportunities to disclose the potential effect of main body.

3. The situation facing China

In 2020, China proposed to complete the "dual carbon" goal of "carbon peak" by 2030 and "carbon neutral" by 2060.The production and operation activities of enterprises are the main sources of greenhouse gases, but most domestic enterprises lack the experience of disclosing greenhouse gas information, and have not established the management process of greenhouse gas.Overseas listed companies in China is facing severe challenges, including strict regulation and disclosure requirements.Economic development and the realization of the "double carbon" goal cannot be separated from the institutional arrangement. All walks of life call for the establishment of China's sustainable disclosure guidelines as soon as possible.Therefore, the establishment of disclosure criterion in our country must be put on the agenda.

The development of sustainability disclosure guidelines has been accelerating. The ISSB was established in 2021 and issued an exposure draft of the guidelines the following year.At the same time, the European Sustainability Reporting Standards (ESRS) working paper was released, and the United States also released an exposure draft of its proposal for climate-related disclosure.At this point, the international, the European Union and the United States are three pillars in the development of guidelines. Faced with such an international landscape, China needs to make a strategic choice.In this paper, China's strategy selection were discussed.

4. China's strategic choice

4.1. Analysis of adoption strategy

The fully adopted strategy refers to the direct application of ISDS translated into Chinese to the disclosure of information related to the sustainable development of Chinese enterprises. The advantages of this strategy are as follows: (1) It saves time and costs of compiling standards, and is completely consistent with ISDS, which can improve the horizontal comparability between the information disclosed by Chinese enterprises and the information disclosed in accordance with other new climate disclosure regulations, reduce the burden of editors and reduce the information use cost of financial report users. (2) China's overseas listed companies will be in a better position to deal with stricter regulatory measures for international investors.

However, it is impractical for China to fully adopt ISDS. Wang Jun, Vice Minister of Finance of China, pointed out in the five principles of convergence that "convergence does not equal equality"[9]. On the one hand, the single importance principle adopted by ISDS does not fully meet the information needs of our stakeholders. The information provided by ISDS for investors mainly includes the impact of risks and opportunities related to sustainable development on the business model and financial status of enterprises, while Chinese government agencies, as market supervisors, pay more attention to the impact of enterprises' production and operation activities on society and the environment. On the other hand, ISDS is impractical to be fully adopted in our country. Most companies in China lack the experience to disclose sustainability-related risks and opportunities, and do not have a management system for risk assessment and control.

4.2 Analysis of convergence strategy

The convergence strategy refers to the adjustment of the substantive provisions and disclosure requirements in ISDS to China's sustainable development disclosure standards in accordance with China's Legislation Law, and the exclusion of provisions not applicable to China's national conditions. The advantages of this strategy include the following two points: (1) it is consistent with China's accounting standards for business enterprises. The accounting standards of Chinese enterprises have adopted the international convergence strategy, and the financial information disclosure also adopts the convergence strategy, which can make China's financial report keep pace with the international on the whole. (2) Can accelerate the development process of sustainable disclosure standards in China. The ISSB has worked closely with the Climate Disclosure Guidelines Board in the development of the ISDS to ensure the professionalism and authority of the

guidelines. The convergence with ISDS greatly improves the efficiency of sustainable disclosure standards in China.

Similarly, convergence strategy also has defects: (1) Similar to the full adoption strategy, it is necessary to consider whether ISDS is operable in our country when adopting convergence policy. Most domestic enterprises lack experience in disclosing risks and opportunities related to sustainable development, including climate, and lack professional methodological guidance in assessing risks and opportunities. (2) ISDS may obscure the characteristics of China's institutional construction. ISDS in matters such as trade unions is more of a reflection of Western values and may not be universally applied in our country. China is unique in the environmental and social issues of enterprises, and the adoption of convergence strategy may cover up the Chinese characteristics.

4.3 Analysis of reference strategies

The reference strategy is based on the actual situation of our country, taking ISDS as a reference, and independently formulating sustainable disclosure standards suitable for our country's national conditions. The advantages of this strategy mainly include: (1) the initiative of the formulation and implementation of the standards is grasped in their own hands. The independent formulation of disclosure standards can avoid the passive state caused by following the pace of international standards, take the initiative in the formulation and implementation of standards in their own hands, respond to the problems in the implementation of standards in a timely manner, and optimize the effect of the implementation of standards. (2) Respond to the call of society to better serve the "double carbon" goal. The independent sustainable disclosure standards have responded to the call of all sectors of society for the basic system construction of sustainable information disclosure, and will become an important institutional arrangement for China to achieve the goal of "double carbon". (3) Improve the applicability of the standards and highlight Chinese characteristics. Based on the actual situation of our country, we can adjust or eliminate the provisions in ISDS that are not suitable for our national conditions to improve the applicability of the standard in our country. It can also combine China's unique economic construction practices, such as rural revitalization and comprehensive poverty alleviation, with sustainable development disclosure standards to reflect Chinese characteristics. (4) Improve the influence of China's sustainable related information disclosure. China's independent formulation of disclosure guidelines based on ISDS can provide reference for other countries, contribute Chinese wisdom, enhance China's influence in the formulation of international standards, and is expected to break the tripartitic pattern of the international community, the European Union and the United States, and strive for a place in the disclosure of sustainable information.

Similar to other strategies, the reference strategy also has some shortcomings, including: (1) The Chinese characteristics may lead to the low international comparability of the sustainable development-related information disclosed by Chinese enterprises. The development of sustainable disclosure standards by ourselves can fully demonstrate Chinese characteristics, but it will lead to the lack of comparability of relevant information disclosed in China with international counterparts, which is not conducive to attracting international capital for Chinese enterprises. (2) The high cost of setting standards. The popularization of sustainability-related information disclosure in China is low, and most domestic enterprises lack effective procedures to assess and manage sustainability-related risks and opportunities, as well as experience in disclosing sustainability-related information. The independent development of sustainable disclosure standards not only requires a lot of resources, but also the efficiency and quality of the development of standards are uncertain.

5. Conclusions

After analyzing the three strategies, this article believes that compared to the full adoption strategy and convergence strategy, the learning strategy should be the choice for China in the sustainable development information disclosure guidelines. First, the full adoption of International Financial Reporting Standards (IFRS) is not compatible with China's current development situation formed under its unique historical, cultural, political, and market environment[5][10]. Since the reform and opening up, China has achieved significant economic achievements, and under the influence of multiple factors such as historical culture, politics, and the market, China's accounting standards have gradually shown unique characteristics. To some extent, the full adoption of IFRS is not compatible with China's development situation under specific circumstances, which is manifested in the implementation and supervision of accounting standards.

Second, as the world's largest emerging economy, China has a key responsibility and mission in the international accounting governance[12][15]. At a time when the global economic governance framework is facing significant changes, China should adhere to rational choices, actively participate in the formulation of IFRS externally, and explore sustainable disclosure guidelines that conform to China's national conditions internally. This is the specific manifestation of the confidence in the socialist road with Chinese characteristics, theoretical confidence, institutional confidence, and cultural confidence in the internationalization process of accounting standards. By actively participating in international accounting governance, China not only contributes Chinese wisdom to the development of global accounting standards but also provides a reference for other emerging economies.

References

[1] Anderson, N. (2019). IFRS Standards and Climate-related Disclosures [R/OL]. Retrieved from www.ifrs.org.

[2] Busch, T. , Cho, C. H. , Hoepner, A. G. F. , Michelon, G. , & Rogelj, J. . Corporate greenhouse gas emissions' data and the urgent need for a science-led just transition: introduction to a thematic symposium. Journal of Business Ethics.

[3] Dragomir, V. , Dumitru, M. , & Perevoznic, F. M. . (2023). Carbon reduction and energy transition targets of the largest european companies: an empirical study based on institutional theory. Cleaner Production Letters.

[4] Walid Ben-Amar, Breeda Comyns, & Isabelle Martinez. (2022). The COVID-19 pandemic: Opportunity or challenge for climate change risk disclosure? Accounting, Auditing & Accountability Journal, 36(2), 649–676. Emerald Publishing Limited.

[5] Dao-Yang, G. , & Accounting, S. O. . (2013). On the global reform of the accounting system. Accounting and Economics Research..

[6] Hu Cheng & Fan Xingjian. (2022). The international convergence process of accounting standards from the American perspective and its implications for China.. Financial and Accounting Communication, (17), 153–158.

[7] Hu Cheng. (2021). International Convergence of Accounting Standards Paradox and China's Discourse Power Construction. Financial and Accounting Monthly,

(23), 76–80.
[8] Huang Shizhong & Ye Fengying. (2023). Greenhouse Gas Accounting and Reporting Standard System and Its Key Issues Analysis. Financial and Accounting Monthly, 44(2), 7–13.
[9] Li Yating & Li Yuhuan. (2019). Review of the Convergence of International Accounting Standards and its Enlightenment to China ——Take the EU,the US,Japan and Russia as Examples. Accounting Research(11), 6.
[10] Zong yan, L. , & Yu, Q. . (2019). Context cultures,translation strategies and learning efficiency of accounting standards: experimental evidence based on asbe and ifrs texts. Accounting Research.
[11] Li Zongyan, Wang Yihong, & Qu Xiaohui. (2021). The Institutional Logic of IFRS Global Diffusion: Empirical Evidence and China's Strategy. Accounting Research, (9), 3–23.
[12] Lu Jianqiao. (2020). IF R S Standards: Current Developments, Challenges and Future Trend. Accounting Research, (10), 3–12.
[13] Wang Pengcheng, Sun Mei, Huang Shizhong, & Ye Fengying. (2023). Analysis and Outlook of Two International Financial Reporting Sustainability Disclosure Standards. Financial and Accounting Monthly, 44(14), 3–13.
[14] Wu Yujun & Ju Fang. (2023). The evolution and outlook of the International Sustainability Disclosure Guidelines System - A review of the International Sustainability Disclosure Guidelines by the ISSB. Financial and Accounting Communication, (1), 144-152+164.
[15] Zhang Weiguo. (2021). One of the key factors affecting international accounting standards: Great Power Competition. Financial and Accounting Monthly, (2), 3–11.
[16] Zhu Yuanwu. (2022). International convergence of accounting and China's accounting countermeasures selection. Financial and Accounting Monthly, (24), 13–18.

Ms. Xiaoyun Li
Master student, Master of Business Administration (Accounting).
Research Interests:
Text features, and Corporate governance.

Low-carbon Optimization Operation Strategy for Multi-Energy System

Hongyu Zhu[1*], Dongdong Zhang[1,3], Thomas Wu[1,2,3]

[1]School of Electrical Engineering, Guangxi University, Nanning, China
[2]School of Computer, Electronics and Information, Guangxi University, Nanning, China
[3]State Key Laboratory of Featured Metal Materials and Life-cycle Safety of Composite Structures, Guangxi University, Nanning, China
*E-mail: hongyuzhu_cq@yeah.net

Abstract: To achieve carbon neutrality in the power and energy sector, this study explores the low-carbon optimization operation strategy of multi-energy system. Starting with a discussion of the low-carbon transformation of coal-fired power plants and the flexible operation characteristics of carbon capture system. Then, by implementing a multi-mode complementary demand response strategy under the coordination of diversified markets, the cooperativity between the carbon emission-reduction capability of the supplier and the energy-saving potential of the demander are tapped. Finally, the case study demonstrates that the effectiveness of the proposed method, which can improve system economy by about 20% and reduce carbon emissions by about 16%, thus achieving sustainable development of the multi-energy system, and boosting the growth of the carbon trading market.

Keywords: Multi-energy system, low-carbon technology, demand response, optimization operation.

1. Introduction

The formulation of the carbon neutrality target puts forward higher requirements for all sectors of society to take energy-conservation and emission-reduction (ECER) measures [1]. The power sector accounts for 43% of total carbon emissions, so it is of great significance to explore low-carbon technologies for power sector [2]. With the continuous application of coupling elements such as combined heat and power (CHP), the multi-energy system (MES) is more and more used in the power industry [3], making the low-carbon optimized operation of MES has become a hotspot in recent years.

Recently, scholars have explored the low-carbon operation characteristic of MES from multiple perspectives. On the one hand, the carbon is reduced through optimal energy management of the MES [4]. For example, a low-carbon economic operation model [5], a low-carbon flexible capability assessment method [6], and a low-carbon optimization planning method [7], have all improved the energy utilization efficiency of the MES. On the other hand, the zero-carbon MES is also promoted through the application of renewable energy sources (RES) [8].

Despite the increasing utilization of RES, most developing countries still rely on fossil fuels [9], making it important to explore low-carbon operation of the existing coal-fired power plants (CFPP). Scholars have carried out low-carbon transformation of CFPP mainly by carbon capture technology, proving that the flexible carbon capture power plant (CCPP) can increase the peak adjustment margin of CFPP [10]. Therefore, an optimization model for coordinating power generation and carbon capture is proposed in [11] to estimate the rotating reserve requirement for CCPP.

However, the above ECER methods at the energy supplier are far from enough to meet the requirements of zero-carbon MES. Thus, the user' ECER potential is explored. For one thing, users can reduce carbon emissions by adjusting their energy consumption structure, such as optimizing energy consumption structure by game method [12], or adopting smart energy management strategy [13], which can save energy by about 14%. For another, users began to pay for carbon emissions to promote ECER awareness, that is, the time-transfer characteristics of energy consumption under different carbon prices [14]. Moreover, the carbon cost combined with the demand response (DR) strategy will further drive low-carbon on the user side.

To summarize, in order to solve the problem of carbon emissions of MESs and enhance the energy saving potential of users, this study proposes an optimal operation strategy for MES with coordinated carbon reduction among multi-

stakeholders. Among them, a low-carbon transformation technology for traditional CFPP is implemented, which not only increase the peak shaving margin of MES, but also improves the consumption rate of RES. then, the diversified DR strategy is explored, which coordinated the electrical load DR based on TOU price and heat load DR based on layered carbon price, breaking through the singleness of DR mechanism.

2. Methods

2.1. Coordinated Carbon Reduction by Multi-Stakeholder

In this study, a low-carbon optimization strategy of multi-stakeholders coordinated carbon reduction for MES is formulated, as illustrated in Fig. 1. On the energy supply side, we have introduced carbon capture technology for low-carbon transformation of CFPP. The improved CCPP cooperates with CHP for flexible energy supply. On the user side, in order to improve ECER awareness, users actively participating in the DR under the dual role of power market and carbon trading market. In the operation process, different stakeholders realize coordinated operation through energy flow, information flow, capital flow carbon flow, thus promoting the low-carbon operation of MES.

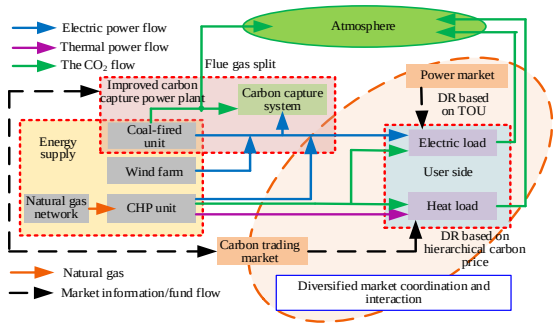

Fi. 1 Schematic diagram of diversified market operation in MES

2.2. Carbon Emission Trading Model in MES

The total carbon quota E_{Cquota} of coal-fired units and gas-fired units in supply side is:

$$E_{\mathrm{Cquota}}=\begin{pmatrix}P_{\mathrm{G}}(t)\cdot B_{\mathrm{G}}\cdot f_{\mathrm{l}}\cdot f_{\mathrm{f}}+\\(P_{\mathrm{CHPe}}(t)\cdot B_{\mathrm{CHPe}}+P_{\mathrm{CHPh}}(t)\cdot B_{\mathrm{CHPh}})\end{pmatrix} \quad (1)$$

where B_{G}, B_{CHPe} and B_{CHPh} are the carbon emission benchmarks for coal-fired units and gas-fired units, respectively. f_{l} is the correction coefficient of cooling mode.

To this end, the transaction model between supplier and the carbon market is as follows:

$$F_{\mathrm{trading}}(i,t)=c_{\mathrm{trading}}\left(E_{\mathrm{pf}}(i,t)+E_{\mathrm{CHP}}(i,t)-E_{\mathrm{Cquota}}(i,t)\right) \quad (2)$$

Then, this paper introduces a layered carbon price to guide users to participate in the carbon trading market [15]. The modeling process is:

$$\lambda_{\mathrm{user}}=\begin{cases}\lambda_1,\ E_{\mathrm{Dpf}}(t)\in\left[0,E_{\mathrm{Dpf,min}}\right)\\ \lambda_2,\ E_{\mathrm{Dpf}}(t)\in\left[E_{\mathrm{Dpf,min}},E_{\mathrm{Dpf,mid}}\right)\\ \lambda_3,\ E_{\mathrm{Dpf}}(t)\in\left[E_{\mathrm{Dpf,mid}},E_{\mathrm{Dpf,max}}\right)\\ \lambda_4,\ E_{\mathrm{Dpf}}(t)\in\left[E_{\mathrm{Dpf,max}},\infty\right)\end{cases} \quad (3)$$

where λ_{user} is the carbon price when the user participates in carbon trading, $E_{\mathrm{Dpf}}(t)$ is the carbon emission of users. $E_{\mathrm{Dpf,min}}(t)$, $E_{\mathrm{Dpf,mid}}(t)$ and $E_{\mathrm{Dpf,max}}(t)$ represent carbon emission at different stages.

2.3. Flexible Operation Characteristics of CCPP and CHP

The flexible operation features of CCPP was examined in detail in this paper, such as the coordination between the split-flow flue gas mode and solvent storage mode, thus achieving carbon reduction while enhancing the peak regulation margin of CFPP.

$$E_{\mathrm{cl}}(i,t)=e_{\mathrm{p}}\beta\delta P_{\mathrm{G}}(i,t)+E_{\mathrm{CG}}(i,t) \quad (4)$$

$$E_{\mathrm{pf}}(i,t)=e_{\mathrm{p}}P_{\mathrm{G}}(i,t)-E_{\mathrm{cl}}(i,t) \quad (5)$$

$$E_{\mathrm{CG}}(i,t)=u_1E_{\mathrm{CG,dis}}(i,t)-u_2E_{\mathrm{CG,ch}}(i,t) \quad (6)$$

$$SE_{\mathrm{CG}}(i,t)=SE_{\mathrm{CG}}(i,t-1)+u_2E_{\mathrm{CG,ch}}(i,t)-u_1E_{\mathrm{CG,dis}}(i,t) \quad (7)$$

where $P_{\mathrm{G}}(i,t)$ is the total power of CCPP; e_{P} is the carbon emission intensity. $\beta$is the rate of flue gas split-flow. δ is the capture rate. $E_{\mathrm{cl}}(i,t)$ is the CO_2 stripped. $E_{\mathrm{CG}}(i,t)$ is the CO_2 flowing out of the storage tank. u_1, u_2 are 0-1 variables. $E_{\mathrm{CG,ch/dis}}(i,t)$ is the CO_2 stored or released in storage tank. $SE_{\mathrm{CG}}(i,t)$ is CO_2 in storage tank.

In this case, the power consumed $P_{\mathrm{Ge}}(i,t)$ and output $P_{\mathrm{Gh}}(i,t)$ in the CCPP are as follows:

$$P_{\mathrm{Ge}}(i,t)=hE_{\mathrm{cl}}(i,t) \quad (8)$$

$$P_{\mathrm{Gh}}(i,t)=P_{\mathrm{G}}(i,t)-P_{\mathrm{Ge}}(i,t) \quad (9)$$

where h is the energy consumption of CCPP.

In the CHP, the linear coupling connection of thermoelectric power is as follows:

$$P_{\mathrm{CHPe}}=\alpha P_{\mathrm{CHPh}}+\beta \quad (10)$$

where P_{CHPe} and P_{CHPh} are the electric and heat power of CHP. α is the electrothermal elasticity coefficient. The CO_2 generated by CHP actually emitted into the atmosphere is:

$$E_{\mathrm{CHP}}(t)=e_{\mathrm{h}}\left(\varepsilon_{\mathrm{e,h}}P_{\mathrm{CHP,e}}(t)+P_{\mathrm{CHP,h}}(t)\right) \quad (11)$$

where e_h is the carbon emission intensity of CHP, $\varepsilon_{e,h}$ is the electrothermal conversion coefficient.

2.4. ECER Characteristics on User Side

To reduce the energy use, under the power market and carbon trading market, users actively adjust the energy consumption structure through diversified DR strategy, so as to achieve the purpose of ECER. Then, a heat load DR strategy based on layered carbon price is implemented.

$$\min F_{\text{Hload}} = \sum_{t=1}^{T}\left(\lambda_{\text{user}} E_{\text{Hpf}}(t) - c_{\text{HDR}} \cdot \Delta P_{\text{HDR}}(t)\right) \quad (12)$$

$$E_{\text{Hpf}}(t) = e_{\text{Huser}} P_{\text{HDR}}(t) \quad (13)$$

$$P_{\text{HDR}}(t) = P_{\text{H}}(t) + \Delta P_{\text{HDR}}(t) \quad (14)$$

$$\left|\Delta P_{\text{HDR}}(t)\right| \le w_{\text{H}} P_{\text{H}}(t) \quad (15)$$

where c_{HDR} is the unit response reward. $\Delta P_{\text{HDR}}(t)$ is the heat load in response. $E_{\text{Hpf}}(t)$ is the carbon emission of heat load. e_{Huser} is the carbon emission intensity per unit heat load. $P_{\text{HDR}}(t)$ is the heat load after participated in DR. w_{H} is the response coefficient.

In addition, users adjust the electricity consumption structure according to the electricity DR based on TOU.

$$\begin{bmatrix} P_{\text{e}}^{1} \\ P_{\text{e}}^{2} \\ \vdots \\ P_{\text{e}}^{T} \end{bmatrix} = \begin{bmatrix} P_{\text{e0}}^{1} \\ P_{\text{e0}}^{2} \\ \vdots \\ P_{\text{e0}}^{T} \end{bmatrix} + \begin{bmatrix} P_{\text{e0}}^{1}\varepsilon_{\text{e}}^{1,1} & 0 & \cdots & 0 \\ 0 & P_{\text{e0}}^{2}\varepsilon_{\text{e}}^{2,2} & \cdots & 0 \\ \vdots & \vdots & \ddots & \vdots \\ 0 & 0 & \cdots & P_{\text{e0}}^{T}\varepsilon_{\text{e}}^{T,T} \end{bmatrix} \begin{bmatrix} \frac{\partial p_{\text{e}}^{1}}{p_{\text{e0}}^{1}} \\ \frac{\partial p_{\text{e}}^{2}}{p_{\text{e0}}^{2}} \\ \vdots \\ \frac{\partial p_{\text{e}}^{T}}{p_{\text{e0}}^{T}} \end{bmatrix} \quad (16)$$

where ε_{e} is the elastic coefficient between different time period.

2.5. Modeling of Low-carbon Optimization Model for MES

According to the above models, considering the coal-fired unit's operating cost F_{Gop}, the CHP's operating cost F_{CHPop}, the wind waste cost F_{QWind}, and the carbon transaction cost F_{trading}, a high-efficiency and low-carbon MES optimization operation model is as follows:

$$\min F_{\text{total}} = \min(F_{\text{Gop}} + F_{\text{CHPop}} + F_{\text{QWind}} + F_{\text{trading}}) \quad (17)$$

3. Results and Discussion

3.1. Case Introduction

The research object for this calculation is a MES, which is composed of wind farms, improved CCPPs and CHPs. Fig. 2 depicts the predicted wind power and load curves. This paper compares the operation characteristics of the MES under four scenarios to demonstrate the method's effectiveness. Case1: MES without considering carbon capture system. Case2: Carbon capture system in flue gas split mode. Case3: Flexible operation mode of carbon capture system considering solvent storage characteristics. Case4: Apply the diversified DR strategy based on Case3.

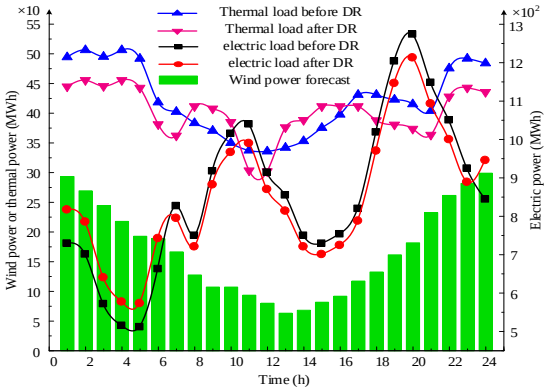

Fig. 2 Load and wind power forecast curve

3.2. Simulation Analysis

Table 1 details the system's cost and utility in four scenarios. Fig. 2 illustrates the load curves following the diversified DR. From Case1 to Case4, the system's total operating cost, total carbon emissions, and wind energy waste all decreased. In comparison to Case1, the overall operating costs for Case2-4 were lowered by 11.07%, 11.39%, and 12.63%, respectively. Total carbon emissions dropped by 4,051.565 tons, 4059.186 tons, 4,169.427 tons, respectively. Carbon trading costs indicate that because the MES cannot manage carbon emissions in Case1, it must acquire carbon credits from the carbon trading market. When the CO_2 emitted is less than the basic carbon credits granted by the market, the MES can sell the excess carbon credits to carbon trading market. Overall, the cost-benefit trend effectively proves that the proposed method can improve economics while lowering carbon emissions and wind power waste.

Table 1. Cost-benefit of MES operation in different cases

Type	F_{Gop}($)	F_{CHPop}($)	F_{QWind}($)	$F_{trading}$($)	F_{total}($)	Total carbon emissions (t)	Total wasted wind power (MW)
Case1	156940	281630	5705.473	16062.859	460330	11289.640	570.547
Case2	227020	248270	3705.802	-69620	409370	7238.075	370.580
Case3	225230	247880	2570.413	-68940	406740	7220.212	257.041
Case4	213770	250650	896.951	-64520	400800	7103.86	89.695

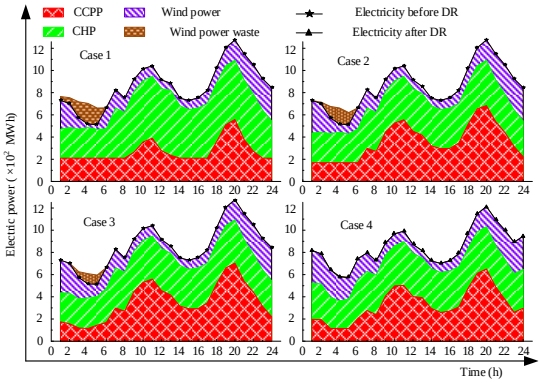

Fig. 3 Electricity supply characteristics of MES

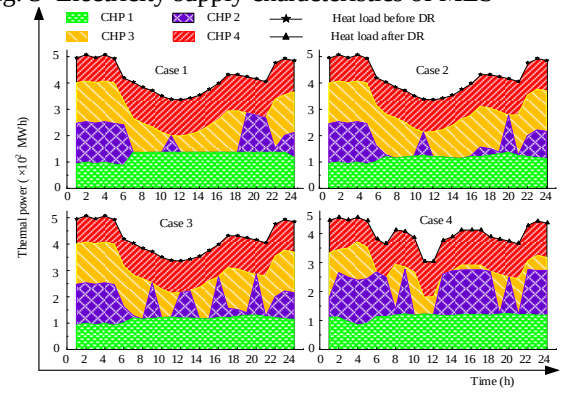

Fig. 4 Heat supply characteristics of MES

The energy supply characteristics of MES in various conditions are shown in Fig. 3-4. Case1 generates a significant amount of wind energy waste. This is because, during low-load periods and in the absence of large-scale energy storage equipment in the MES, there is no insufficient load to consume surplus wind energy. In Case2, after considering carbon capture equipment, wind energy loss has been greatly decreased, but the wind energy that can be consumed is limited due to the coupling of the absorption and the stripper tower in CCPP. Case3 realizes the solvent storage characteristic based on Case2, which decouples the CO_2 absorption and stripping process, hence increasing wind energy consumption. Additionally, in Case4, the deployment of diverse DR effectively altered the energy consumption time relationship for consumers, thereby promoting the wind energy consumption even more. As shown in Fig. 5, due to the coupling characteristic of the absorption and stripping towers, the carbon capture equipment in Case2 consumes more energy during peak-load periods than Case3. This is because the storage characteristics in CCPPs effectively enable virtual peak regulation of MES and minimize the load's peak-to-valley discrepancy. In Case4, the implemented diversified DR facilitates the coordination of the carbon trading market and power market, which effectively decreases the total cost and carbon emissions, and significantly increase users' ECER consciousness. Therefore, the bidirectional connection of ECER capability between supplier and demander contributes to MES' economics and low-carbon.

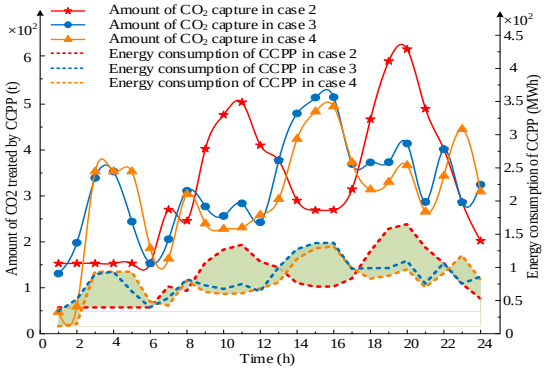

Fig. 5 CO_2 stripping amount and CCPP's energy consumption

4. Conclusions

Multiple demands on human survival, environment and climate make global carbon neutrality imminent. To this end, this paper examined the low-carbon optimization operation of MES, which realizes the dual benefits of economical and low-carbon by implementing MES' operation strategy with coordinated multi-stakeholders. This study found that CCPP is an effective way to address carbon emissions from traditional fossil fuels, and that user responsibility for carbon

emissions can successfully simulate contact between suppliers and demanders in the carbon trading market, hence increasing of both parties' ECEM potential. In the future, we will continue to investigate the complementary influence of user's ECER measures and carbon trading market mechanisms, with the goal of advancing the carbon market's development.

References

[1] M. Manbachi and M. Ordonez, AMI-Based energy management for islanded AC/DC microgrids utilizing energy conservation and optimization, IEEE Trans. Smart Grid, 10(1): 293-304, 2019.

[2] C. Zou, B. Xiong, H. Xue, D. Zheng, Z. Ge, Y. Wang, et al, The role of new energy in carbon neutral, Petroleum Exploration and Development, 48(2): 480-491, 2021.

[3] D. Xu, Q. Wu, B. Zhou, C. Li, Distributed multi-energy operation of coupled electricity, heating, and natural gas networks, IEEE Trans. Sustain Energy, 11(4): 2457-2469, 2020.

[4] H. Wang, P. Hua, X. Wu, R. Zhang, K. Granlund, J. Li, et al., Heat-power decoupling and energy saving of the CHP unit with heat pump based waste heat recovery system, Energy, 250, 2022.

[5] R. Wang, X. Wen, X. Wang, Y. Fu, Low carbon optimal operation of integrated energy system based on carbon capture technology, LCA carbon emissions and ladder-type carbon trading, Appl Energy, 2022.

[6] S. Clegg and P. Mancarella, Integrated electrical and gas network flexibility assessment in low-carbon multi-energy systems, IEEE Trans. Sustain Energy, 7(2): 718-731, 2016.

[7] D. J. Olsen, N. Zhang, C. Kang, M. A. Ortega-Vazquez and D. S. Kirschen, Planning low-carbon campus energy hubs, IEEE Trans. Power Syst, 34(3): 1895-1907, 2019.

[8] X. Zhang, G. Strbac, N. Shah, F. Teng, Whole-system assessment of the benefits of integrated electricity and heat system, IEEE Trans. Smart Grid, 10(1): 1132-1145, 2019.

[9] Z. Ji, C. Kang, Q. Chen, Q. Xia, et al., Low-carbon power system dispatch incorporating carbon capture power plants, IEEE Trans. Power Syst, 28(4): 4615-4623, 2013.

[10] S. Lou, S. Lu, Y. Wu, Optimizing spinning reserve requirement of power system with carbon capture plants, IEEE Trans. Power Syst, 30(2): 1056-1063, 2015

.

[11] P. Martens, E. Delarue, W. D'haeseleer, A mixed integer linear programming model for a pulverized coal plant with post-combustion carbon capture, IEEE Trans. Power Syst, 27(2): 741-751, 2012.

[12] A. Haxhimusa, M. Liebensteiner, "Effects of electricity demand reductions under a carbon pricing regime on emissions: lessons from COVID-19," Energy Policy, 156, 2021.

[13] M. P. Kasmaei, M. Lehtonen, J. Contreras, J. R. et al, Carbon footprint management: A pathway toward smart emission abatement, IEEE Trans. Ind. Inf., 16(2): 935-948, 2020.

[14] K. H.M. Al-Hamed, A comparative review of potential ammonia-based carbon capture systems, Jou. of Environ. Manag., 287, 2021.

[15] Z. Zhao, L. Wu, G. Song, "Convergence of volatile power markets with price-based demand response," IEEE Trans. Power Syst., 29(5): 2107-2118, 2014.

Hongyu Zhu
Currently pursuing the Ph.D in Guangxi University
Research Interests: Smart Energy System, Integrated Demand Response, Energy Conservation

Dr. Dongdong Zhang
Assistant Professor, received Ph.D. degree in Electrical Engineering at the Xi'an Jiaotong University in 2019.
Research Interests: Smart Energy System, Motor Design Intelligent Equipment

Dr. Thomas Wu
Professor, received Ph.D. degree in electrical engineering from the University of Pennsylvania, Philadelphia, PA, USA, in 1999.
Research Interests: Energy Engineering, Intelligent equipment, Motor design, Artificial intelligence.

Recent advances in therapeutic ultrasound

Krit Sujarittam

Department of Mechanical Engineering, Chiang Mai University, TH
E-mail: krit.s@cmu.ac.th

Abstract

In medicine, ultrasound had long been used as a diagnostic tool to visualise inside human bodies. However, recent advancement has seen ultrasound being used as a means to treat illnesses. It has been shown that ultrasound could thermally or mechanically ablate tumours or kidney stones, enhance blood clot dissolution for stroke prevention, or facilitate deliveries of drug into difficult areas such as the brain or tumours – opening doors to new treatments for diseases such as of Alzheimer's, Parkinson's, and many types of cancer. These procedures are targeted and non-invasive, giving ultrasound advantages over most conventional treatments. This manuscript presents a short survey on recent developments in therapeutic ultrasound. Mechanisms and effects of moderate- to high-power ultrasound are described first. Discussions on therapeutic applications utilising these mechanisms and current research focuses follow.

Keywords: Non-invasive therapies, Therapeutic ultrasound, Ultrasound contrast agents

1. Introduction

Modern medicine strives for treatments that cause minimal discomfort and hospital stay, and for many applications, ultrasound has become an effective and attraction option. First adopted as a diagnostic tool, low- to moderate-power ultrasound penetrates human tissue without causing disruption, and has been exploited for various imaging techniques, such as Doppler, power Doppler contrast-enhanced imaging, and functional ultrasound (Hasegawa, 2021; Yusefi and Helfield, 2022; Martinez de Paz and Macé, 2021). However, when the ultrasonic power is increased, ultrasound could induce temporary or permanent effects in tissue and treat various diseases (Xu et al., 2021; ter Haar and Coussios, 2007; ter Haar, 2001; Evans et al., 2007). The field of therapeutic ultrasound, although in its infancy, has been advancing rapidly. Many therapeutic applications, such as thermal ablation and lithotripsy have already been adopted into clinical practice, yet are still being studied and improved upon (Evans et al., 2007; Lingeman et al., 2010; McClain et al., 2013). Others – such as histotripsy and non-invasive drug delivery into the brain and spinal fluid – are being investigated or starting to enter phase-I clinical trials (Vidal-Jove et al., 2022; Xu et al., 2021; Lipsman et al., 2018; Montero et al., 2019).

Several attributes make ultrasound therapies make them attractive, both in the perspectives of medical institutions, personnel, and patients. First, being an imaging tool, ultrasound could simultaneously image and monitor the treatment it performs. This greatly simplifies the equipment and operation procedures, reducing treatment complexity, preparation time, and costs. Second, it is targeted and non-invasive, requiring no incisions and minimal post-treatment recovery. Ultrasound can be applied through the skin and focused onto single points inside the body. Only tissue in the focus would be affected, leaving all surrounding tissue intact. This is very significant for applications such as drug delivery into the brain because, as we will discuss in more detail

later, ultrasound is the only procedure that is both non-invasive and targeted. Other available alternatives will either require penetration of the head and skull bone or cannot localise where therapeutic agent is delivered and spread them across the whole surface of the brain (Pandit et al., 2020; Aryal et al., 2014; Groothuis, 2000; Timbie et al., 2015). Thus, ultrasound is potentially one of the most promising treatment for Alzheimer 's , Parkinson's, and many types of brain cancer (Gandhi et al., 2022; Lipsman et al., 2018; Timbie et al., 2015). Third, ultrasound is non-ionising. This minimises potential long-term side effects compared to many alternative non-invasive procedures such as radiotherapies. Alternatively, ultrasound can also be used to complement these treatments and improve the overall efficacy (Diederich and Hynynen, 1999; Zhu et al., 2019). Uses of ultrasound in therapies have been continuously expanding thanks to the above attributes (Elmansy and Lingeman, 2016; Evans et al., 2007; Xu et al., 2021; Timbie et al., 2015; Aryal et al., 2014).

The purpose of the manuscript is to give an overview of this relatively new and fast-growing field of study. It does not aim to create an exhaustive list of applications and directions of development, however. Instead, we focus here on a broader picture, introducing the main types of therapies while leaving fine details for interested readers as citations. In the sections that follow, we first discuss how ultrasound induces different therapeutic effects. We then move on to discuss different t reatment procedures being developed. Lastly, a comment on the importance of studies that aim to further our understanding of the physics and cellular reactions to ultrasound is given.

2. Effects of Therapeutic Ultrasound

Therapeutic ultrasound generally uses much higher pressures compared to its diagnostic counterparts. Effects resulting from ultrasound are either thermal or mechanical. At moderate pressures, the effects are often thermal. Upon transmission, a portion of ultrasound energy is absorbed by the tissue, heating the latter. The amount of absorbed energy is proportional local intensity of ultrasound being transmitted and the sound frequency, where higher frequencies are more readily absorbed. Thus, by focusing a beam of ultrasound into a single spot inside the body, we could non-invasively and locally heat a region of tissue (Figure 1a). Mode rate he ating coul d com pl ement r adi otherapies, c hemotherapies, immunotherapies and gene therapies (Diederich and Hynynen, 1999; Zhu et al., 2019), and heating to temperatures between approximately 50˚C to 60˚C could permanently destroy malignant tissue, such as tumours (ter Haar, 2001). As the ultrasound pressure increases further, mechanical effects cometo play a more dominant role. When the ultrasound pressure exceeding a level called cavitation threshold (Holland and Apfel, 1989; Apfel and Holland, 1991), the rarefactional pressure is strong enough to either cause dissolved gas to evaporate or pull apart water molecules, forming gas (or vacuum) cavities (Figure 1b). The bubbles expand, driven by the negative pressure, and collapse, driven by the following compressional phase of ultrasound. The collapse is driven by the inertia of the surrounding water rushing towards the bubble centre, and is usually violent (Leighton, 2012; Church and Miller, 2016). It releases a large amount of energy, generating an extreme local temperature and pressure, and radiate shock waves (Leighton, 2012). The effects can disrupt nearby tissue and, at very high sonication pressures, kidney stones or gallstones.

The probability of inducing cavitation depends on both the ultrasound pressure and ultrasound frequency, where the cavitation pressure threshold is lowered with lower ultrasound frequency. A quantity called mechanical index (MI) – defined as the ultrasound pressure amplitude in MPa divided by the square-root of frequency in MHz – is conventionally used to determine a safe ultrasound level. Initially derived under the condition of single-cycle ultrasound pulse

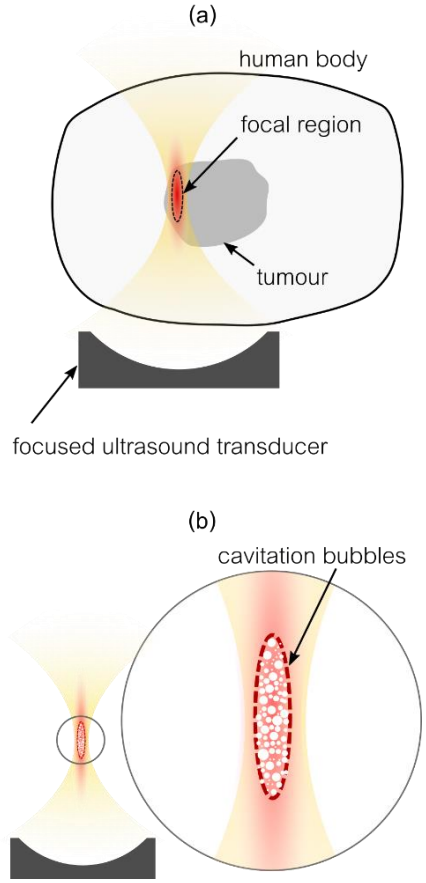

Figure 1. Effects of therapeutic ultrasound can be either thermal or mechanical. (a) At moderate ultrasound pressures, the effects are primarily thermal. Tissue at the focal region of a focused ultrasound beam absorbs the sound energy and heats up. The elevated temperature is used to disrupt the tissue. The focus is then shifted until a whole region to be treated (e.g. whole volume of a tumour) is covered. (b) At higher pressures, effects of ultrasound are primarily mechanical. Once ultrasound pressure exceeds a certain threshold, cavitation bubbles form inside the focal region. The bubbles grow and then violently collapse, releasing a large amount of energy capable of disrupting surrounding tissue.

(Holland and Apfel, 1989; Apfel and Holland, 1991), its use have been extended to multiple-cycle ultrasound and contrast-enhanced ultrasound, and is adopted by safety regulators such as the American Food and Drug Administration (FDA) in guidelines regarding safe acoustic output levels (NEMA, 1996). MI levels where cavitation damage is expected for different types of tissue have been reported in series of studies (O'Brien et al., 2006; Miller and Quddus, 2000; Miller and Dou, 2004; Miller, 2007; Miller et al., 2008; Miller, 2012; Miller et al., 2018).

Recently, it has been found that cavitation could be induced in a more controlled manner and at much lower ultrasound intensity (and MI) by if ultrasound is applied in conjunction with ultrasound contrast agents (Sirsi and Borden, 2009; Frinking et al., 2020). Also known as microbubbles and conventionally used as a diagnostic tool, once injected into the blood stream, these bubbles scatter a large portion of ultrasound impinged on them back to the ultrasound probe and highlight their presence in blood vessels in ultrasound images and greatly facilitate diagnoses of highly-perfused organs such as the heart and liver. However, higher pressure level used in therapies, the bubbles are driven into oscillation. Mechanical effects of these oscillation are used to treat nearby tissue.

The strength of oscillation and effects on surrounding tissue depends on the driving ultrasound's parameter, primarily the pressure. At moderate pressures, the bubbles oscillate stably with the oscillating ultrasound pressure (Sirsi and Borden, 2009). This is often referred to as *stable cavitation*. Stable cavitation produces mild effects around the bubbles. It could stir fluid around it (Maksimov, 2007), gently distend capillaries (Chen et al., 2012), or push against tissue (Bezer et al., 2020). On the other hand, if we increase the ultrasonic pressure, the bubbles behave more violently. At high driving pressures, the main mechanism driving the bubble oscillation switches from the ultrasound to the inertia of the fluid surrounding the bubbles (Leighton, 2012), and they collapse violently and generating much stronger disruption effects to the surrounding tissue (Frinking et al., 2020), similar to when high-intensity ultrasound is applied without

seed bubbles. This kind of bubble oscillation is called *inertial cavitation*. However, it should be noted that it takes a much lower ultrasound pressure to drive existing bubbles into the inertial cavitation regime than it is to generate new bubbles from dissolved gas. The lower ultrasound power required to generate the destructive effects of cavitation makes it easier to treat regions where focusing a high power ultrasound is difficult, such as inside the skull or behind the rib cage (Zubair and Dickinson, 2021; Bobkova et al., 2023).

Various therapeutic uses of ultrasound, applied both with and without microbubbles, have been actively studied in the past few decades (Izadifar et al., 2017; Vidal-Jove et al., 2022; Xu et al., 2021; Lipsman et al., 2018; Montero et al., 2019; Frinking et al., 2020). Applied without contrast agents – ultrasound had been used clinically to destroy tumours (in high-intensity focused ultrasound (HIFU) or in histotripsy) or kidney stones (in lithotripsy). Recent development has focused on refining the procedures, introducing new techniques and new understanding, leading to safer and more effective operations. The application of therapeutic ultrasound in conjunction with contrast agents is a relatively new development. The stirring and destructive effects of microbubble cavitation have been used to enhance the effects of blot clot-dissolving drug (Guan et al., 2020; Chen et al., 2014). Mechanical actions of gently oscillating bubbles have been used to permeabilise biological barriers, allowing drugs to be delivered into regions that they cannot penetrate by themselves, such as cancerous tissue or the brain (Hynynen et al., 2001). At higher ultrasound levels, microbubble could enhance the effects of hyperthermia and ablation therapies (Hynynen, 1991; Clarke and ter Haar, 1997; Luo et al., 2007; Santos et al., 2018). The following sections give overview for each of the procedures above, starting with those that do not involve microbubbles.

3. Therapies Without Microbubbles

Hyperthermia and thermal ablation work by the same principle: turning ultrasonic energy into heat. Both primarily use focused ultrasound to heat a target region deep inside the human body. The efficacy of this treatment depends on the type of tissue and blood perfusion. Different tissue has different thermal and acoustic properties (Azhari, 2010), which dictate the amount of heating and temperature change; and the acoustic frequency, which dictates the relative amount of sound absorption as it travels towards the focus and at the focus; and the amount of perfusion at the target tissue. The tissue with high perfusion is generally require more ultrasound energy to be deposited in a short period of time – often a few seconds – because heat is loss by convection through blood flow. The amount of heating depends on the goal of the treatment. Moderate temperature below that which would cause thermal necrosis could be used to enhance the efficacy of other treatments, such as chemotherapies for cancer (Zhu et al., 2019), or modulate the activities of neurons in treatments of brain diseases (Beisteiner et al., 2023; Hermes et al., 2020).

On the other hand, higher temperatures (i.e. in HIFU) can induce thermal necrosis and are used to for permanent ablation. Current targets for HIFU thermal ablation include tumours in the abdomen, in the brain, and other brain conditions such as Parkinson's (Kennedy, 2005; Evans et al., 2007). For the former, ultrasound is focused into the tumour and used to ablate a small region roughly equal to the size of the ultrasound focus. The ultrasound emitter would then either be moved or, if an array of emitter is used, electrically steered to shift the location of the focus (ter Haar, 2001). The procedure is repeated until the entire volume of the tumour is completely destroyed. Effectiveness of this procedure against prostate tumours and the ability to use either ultrasound elastography or MRI to monitor the progress of the treatment have already been demonstrated in humans (Madersbacher et al., 1995; Beerlage et al., 1999; Souchon et al., 2003). Its

effectiveness against other types of tumours, such as leoimyomata, are currently under investigation (Evans et al., 2007; Keshavarzi et al., 2003). The latter include studies on the effectiveness and suitability of HIFU equipment and monitoring system for specific targets, on measurement of acoustic and/or thermal properties of the target to determine optimal HIFU parameters, on *in vitro* and *in vivo* validations, and human trials.

Brain treatments may be considered its own field given its unique problems associated with focusing ultrasound through the human skull. First, transmission of ultrasound through the human skull is relatively difficult. The human skull is relatively thick and has acoustic properties that are very different from those of other tissue. It thus reflects most of the ultrasound energy impinged on it. Typically, between 75% and 90% of ultrasonic power would be reflected or absorbed by the skull, necessitating a very high ultrasound output. Second, the skull distorts the ultrasound beam, unfocusing the beam as it passes. Corrections for skull aberration is complicated by the large variations of skull properties across both inter- and intra-individuals (Riis et al., 2022; Webb et al., 2018). Current state-of-the-art uses an array of ultrasound emitters capable of producing a high-power output to compensate for the skull reflection and absorption. Aberration is compensated for by activating each element in a sequence which would create a distorted beam before the aberration but would focus correctly after aberration (Kyriakou et al., 2013). CT scan of each patient's skull is used to measure the skull thickness and estimate its acoustic properties, and use the information to correct for the skull distortion. However, the correction is not perfect as the skull acoustic properties and the CT (Hounsfield) values only loose correlate, with significant inter-individual variabilities (Webb et al., 2018).

The difficulties of focusing has implication on treatment safety and efficacy. First, very precise equipment alignment and fixture is required for precise targeting, to ensure that the transmission path through various parts of the skull is the same as those used to calculate aberration correction. This often leads to long treatment preparation time and may require the use of a stereotactic frame. Second, a feedback system is imperative to ensure that the right amount of energy is being deposited as to accurately control the tissue temperature. Current systems (e. g. Insightec System, Insightec Ltd., Tirat Carmel Israel) use MRI to monitor the induced temperature inside the brain, and maintain a high safety profile. As temperatures above physiological state but below thermal necrosis could induce neuromodulation, and temporarily shut down the specific region of the brain within the focus. Current protocol often first uses this level of ultrasound, which allows medical personnel can then verify that the region with elevated temperature is on target and that there is no immediate adverse effect to the patient. After the targeting and safety is verified, higher intensity of ultrasound then follows to permanently ablate the brain region.

As these treatments are based on thermal effects, cavitation is generally avoided for treatment consistency and predictability – antitheses of cavitation. On the other hand, the power of cavitation can also be used as a tool to destroy malignant tissue. This procedure is histotripsy.

Histotripsy uses mechanical effects of ultrasound-induced cavitation bubbles to liquedate a localised region of tissue. Histotripsy can address many limitations of thermal ablation, namely the lack of effectiveness in highly-perfused area and near-target effects. As the primary effect is mechanical, the level of perfusion – and heat convection – does not affect histotripsy and it can effectively ablate highly-perfused tissue. Moreover, since the mechanical effect of bubbles is very localised, only tissue within the region where bubbles are generated is affected. In histotripsy, the boundaries between the treatment and non-treatment region are sharp,

minimising off- and near-target effects (Xu et al., 2021). Histotripsy has implications for treatments of various forms of tumours, hyperplasia, tenson resection, thrombosis, calcified aortic stenosis, as well as some neonatal conditions such as heart syndromes (Xu et al., 2021).

To date, three types of histotripsy have been developed (Xu et al., 2021). At its inception, histotripsy used the power of incident ultrasound to overcome the cavitation threshold of tissue. Called intrinsic threshold histotripsy, a short pulse (1-2 cycles) of high pressure (>26 MPa peak rarefaction pressure) ultrasound focused onto the region to be liquedated. The incident rarefaction pressure generated and drove a cluster of cavitation bubbles at the focus to collapse and mechanically destroy surrounding tissue. The second type – called shock scattering histotripsy – relies on reflection and interference of ultrasound. Here, a pressure below the intrinsic threshold was used but the pulse length was lengthened to ~ 10 cycles. The first few cycles then probabilistically generate few bubbles from existing nuclei. These initial bubbles, having a large acoustic impedance mismatch with tissue like contrast agents, reflect the subsequent ultrasound pulse backwards. The reflected and incident waves interfered at locations just in front of the bubbles, and create in a large local pressure greater than the intrinsic threshold, generating a cloud of cavitation bubbles that is responsible for tissue ablation. Here, the pulse length was kept short to prevent further reflection-interference of ultrasound, which would make the bubble cloud grow towards the transducer. The last kind – boiling histotripsy – first shown in 2011 (Khokhlova, et al., 2011), uses a combination of thermal and mechanical effects. Here, milliseconds (1000s of cycles) of ultrasound is used to create a region of boiling bubbles within the focal region. Mechanical effects caused by the boiling bubbles liquedate nearby tissue.

Developments have been made in the precision of histotripsy, with recent studies showing millimetre- level precision for stationary targets (Sukovich et al., 2019). However, in clinical setting, body movement and respiration may continuously shift the target throughout the course of the treatment, creating a need for an effective targeting that accounts for these movements (Thomas et al., 2021; Miller et al., 2013). There is also a need for a feedback system that informs the operator whether ablation has been done at the correct location and the extent to which the target tissue is liquedated. Ultrasound imaging (Vlaisavljevich et al., 2013), CT (Wagner et al., 2023; Kisting et al., 2023) and MRI (Lu et al., 2021; Gupta et al., 2023) have been used to provide guidance and feedback. The former is relatively economical and real-time. The latter has much implication on safety since cavitation bubbles and ablation zone could be visualise immediately after their inducement. However, certain tumours cannot be discerned clearly using ultrasound imaging as on MRI or CT scans, making targeting difficult for some procedures. MRI, on the other hand, provide a clear image of tumour and post-treatment ablated regions. Recently, a specialised sequence has been developed where ultrasound is synchronised with MRI pulses, allowing cavitation bubble to be visualised and tracked using MRI (Allen et al., 2015). This creates opportunities of using MRI as a precise guidance system for future histotripsy operations.

One barrier to effective histotripsy is the relatively long treatment time. To complete ablate a tissue, multiple ultrasound pulses are needed. The number ranges from tens for soft tissue (such as brain tissue) to hundreds for stiffer tissue, especially those containing a large amount of collagen (Xu et al., 2021). These pulses cannot be applied in rapid succession to avoid activation of residual bubbles from the previous pulse, which could reflect the applied ultrasound and cause new bubbles to form in an off-target regions. Thus, delay between pulses is often limited by the time it takes for the induced bubble to

completely diffuse. In 2012, an innovative solution was proposed (Wang et al., 2012). By emitting low-powered ultrasound between histotripsy pulses, the remaining bubbles are driven into gentle oscillation. The oscillation does not cause major effects on the tissue, but quickens the diffusion process and clear the bubbles. This method has potential to improve future histotripsy protocols.

To date, most histotripsy studies are in the preclinical level – in both large and small animals. Several phase I clinical trials have been conducted to evaluate the safety of histotripsy in humans for prostatic hyperplasia, liver cancer, and calcified aortic stenosis (Xu et al., 2021). In late 2023, the FDA has approved histotripsy for liver treatments in humans.

Lithotripsy uses similar principle as intrinsic threshold histotripsy, but with much larger input pressures to drive extremely destructive bubbles to fracture kidney stones or gallstones (Lingeman et al., 2010; McClain et al., 2013). The technique has already been adopted for clinical uses. Developments have been reported for its hardware, pulse sequence, and treatment protocol (McClain et al., 2013). Hardware development has seen miniaturisation of probes. First generation lithotripters are submersion system, where a patient, anesthetised or sedated, is submerged in a big tank of water and shock wave is generated using surrounding transducers. Later-generation systems, on the other hand, employ more dry probes, coupled to the patient using ultrasound gel similar to that used in diagnostic imaging systems. These simplifies the treatment procedure. The tightness of the focus has also been improved, allowing modern probe to generate a higher pressure by concentrating ultrasound energy into a smaller region (McClain et al., 2013).

Developments in pulse sequence dovetail those of histotripsy. Attempts have been made to optimise the rate of pulsing with highest stone clearance rate (Madbouly et al., 2005; Chacko et al., 2006; Kato et al., 2006). Similar to histotripsy, it was generally agreed that slower pulse rate (60-90 pulses per minute) lead to better stone clearance rate compared to faster pulse rates. Sequences where the power of shock wave is changed during the treatment have also been investigated (Zhou et al., 2004; Maloney et al., 2006), where increasing the shock wave energy as the treatment progress yielded better outcomes compared to if the shock wave energy was constant. Currently, optimal shock and energy ramping rates are determined empirically, as theoretical understanding of the mechanisms of shock-induced stone fragmentation is not understood in detail. It is generally accepted that cavitation generated by the shocks are primary mechanism that fracture the stones (Lingeman et al., 2010). However, it is unclear why having higher-energy shock waves later in the treatment would result in better treatment efficacy (McClain et al., 2013).

4. Microbubble-Mediated Therapies

Hyperthermia, thermal ablation, and histotripsy's effects can be enhanced by the use of microbubbles, allowing the procedure to be performed at a lower ultrasound pressure than conventionally (Hynynen, 1991; Clarke and ter Haar, 1997; Luo et al., 2007; Santos et al., 2018). However, studies in this area are generally limited and is not yet adopted for clinical trials. It could be said that the introduction of microbubbles could further complicated thermal treatments by introducing cavitation, which our understanding of and our ability to control is limited compared to those of ultrasound-induced heating (Evans et al., 2007). However, the use of microbubbles to lower the ultrasound power required for heating may simplifies many hyperthermia procedures, especially for those which target the brain. The human brain absorbs a large amount of ultrasound, requiring brain systems to use very high power to achieve a desired power at the focal spot. This high power could introduce complications, such as burning of the scalp, especially if the coupling between the probe

and the skin is not perfect. Use of microbubbles to lower the required input power has potential to simplify brain hyperthermia procedures and equipment in the future.

Thrombolysis employs microbubbles as a means to increase its efficacy. Ultrasound-driven microbubbles can increase the reach and penetration of thrombolytics, potentially enhancing treatments of acute pulmonary embolism (Engelberger and Kucher, 2014), acute ischemic strokes (Alexandrov et al., 2004; Roos et al., 2014), or myocardial infarction (Roos et al., 2014). The main mechanisms is accepted to be primarily mechanical given that minimal thermal effects are expected from the ultrasound parameters generally used for thrombolysis (Papadopoulos et al., 2017). Micro-circulation of fluid around the oscillating and bubbles and cavitation damage are believed to be the primary mechanisms that enhance blood clot lysis (Bautista et al., 2023). However, quantifying the effects of individual and combination of these mechanisms has not yet been possible. Thus, advances in this field often relies on parameter searches. To this end, an impressive number of studies aiming to optimise the ultrasound parameter have been reported (see Papadopoulos et al., 2017). However, given the wide range of parameter to search from – i.e. combination of concentration and type of microbubbles, ultrasound pressure, frequency, and pulse sequence, thrombolytic drugs, ultrasound applicator – breakthroughs could be difficult. Nevertheless, clinical trials have already been conducted to evaluate the safety and efficacy of this technology with promising results (Eggers et al., 2003; Alexandrov et al., 2004; Eggers et al., 2008).

Drug delivery to the brain. Contrary to high-power cavitation used in the previous procedures to destroy target tissue, lower cavitation power generates a non-destructive effect which could temporarily inhibit physiological functions of certain tissue. This has been used to address a major challenge in medicine – drug delivery to the brain.

The mammalian brain is a highly protected organ shielded from substances by the blood-brain barrier (BBB) – a biological barrier consists of the brain's specialised endothelial cell, astrocytes, pericytes and microglia (Wu et al., 2023). Physiologically, the BBB is a protective mechanism that isolates the brain from blood-borne pathogens, red blood cells (which are neurotoxic), as well as regulates passage of hormones in and out of the brain. However, it also inadvertently prevents most diagnostic and therapeutic agents from reaching brain diseases, complicating the treatments of Alzheimer's, Parkinson's, and brain cancers. Overcoming the BBB is key to future treatments of these diseases.

Microbubble-mediated drug delivery is a promising approach, being the only way to overcome the BBB that is transient, non-invasive, and targeted (Song et al., 2018). Microbubble-mediated procedure involves using focused ultrasound, applied externally without an incision, to excite intravenously-injected microbubbles in the brain. The oscillatory action of the bubbles causes the BBB to temporarily permeabilise, allowing co-injected therapeutics to reach the desired brain regions. The BBB can recover its function after approximately 10s of min or up to 24 h, depending on the protocol being used (Song et al., 2018; Morse et al., 2019). Contrast to conventional invasive procedures, such as direct injection and catheter implantation this procedure requires little recovery time and incurs much smaller risk of post-operation complications (Aryal et al., 2014). Compared to non-invasive conventional treatment – transnasal delivery – microbubble-mediated delivery is capable of delivering drugs to specific region and has potential deliver higher drug doses, addressing the main limitation of transnasal delivery that is poor drug uptake (Timbie et al., 2015).

This procedure has been actively studied since it first demonstration in 2001, when it

was shown that microbubbles temporarily permeabilised rabbit BBB (Hynynen et al., 2001). To date the procedure has been extensively tested in animal model, ranging from mice (Morse et al., 2019) to primates (Kamimura et al., 2018). Different types of microbubbles, ranging from the already clinically approve contrast agents Optison (albumin-shelled C_3F_8; GE Healthcare, Chicago, IL; Raymond et al., 2008), Definity (lipis-shelled C_3F_8; Lipsman et al., 2018), SonoVue (lipid-shelled SF_6; Bracco S.p.A., Milan, Italy; Morse et al., 2019), to custom-made microbubbles (Wang et al., 2014) have been investigated, each at a range of bubble concentrations, ultrasound frequencies, pressures, and pulse lengths.

Despite promising results from multiple animal studies to date (Morse et al., 2019; Kamimura et al., 2018; Wang et al., 2014)more studies are needed before this technology is ready for clinical uses. There are currently two major barriers to clinical adoption of this technology. First is the difficulty of maintaining consistent drug delivery results across different trials. Variations in tissue properties, size, and the stochastic nature of cavitation makes it difficult to control the strength of cavitation to a level strong enough to cause therapeutic effects but not tissue damage. However, we currently lack the complete knowledge of physics that govern cavitation (Leighton, 2012), especially when it is further complicated by the presence of surrounding biological tissue and other oscillating bubbles. New theories and understanding are being developed, but most recent theoretical studies still rely on simplified model of one or a few bubbles oscillating in and/or near a homogenous boundary (Doinikov et al., 2012). Thus, most studies that have been advancing the field have focused on empirical data.

Empirically, different groups have focused on finding new ultrasound sequences that can deliver a more consistent treatment outcomes (Morse et al., 2019) or feedback systems capable of reproducing similar strength of cavitation across different subjects (Kamimura et al., 2018). For the latter, it is generally accepted that the sound signature generated by cavitation is a viable feedback signal that can be used to control cavitation in real-time. Advances have been made both in the theoretical and empirical front (Kaminura et al., 2018; Sujarittam and Choi, 2020; Sujarittam and Choi, 2021). However, advances in the former is limited due to the lack of understanding of the underlying physics and available computation power (Sujarittam and Choi, 2020).

Several clinical trials have been conducted to date (NCT03739905; NCT03119961; NCT03671889). Results of some trials have highlighted the need to improve the procedure's consistency and safety profile. For example, small amount of bleeding in the brain was found post-treatment in one of the first trials (Lipsman et al., 2018). The bleeding recovered and no further complications were reported. However, this suggested that an improvement in safety was needed, especially of the procedure was to be used to treat high-risk patients or children. Studies in this area is active and is ongoing.

5. Fundamental Studies

Recurring themes that come up in the development of various therapeutic ultrasound procedures are the need to develop a deep understanding of (1) ways to precisely control ultrasonic pressure fields and types and strength of microbubble activities; (2) effects that ultrasound or microbubbles induce on tissue, and (3) the tissue response to such effects, including secondary reactions such as chemical signally pathways associated with them. Studies that further our understanding on these fundamentals will help us develop better treatment systems and protocols, and thus have been a focus of many groups. For example, a series of in vitro studies on interactions between microbubble and cultured endothelial cells have elucidated mechanisms that may be responsible in the temporary disruption of the

BBB (Raymond et al., 2007; Cho et al., 2011). These studies observe the interaction between sonicated microbubble and a culture of endothelial cells using either a confocal fluorescent microscope and discovered that there may be at least three separate mechanisms associated with cellmembrane permeabilisation, each could be triggered by different strength of bubble activities and had different probability to cause subsequent cell death. Other studies have focus on dynamics of microbubbles under sonication (Chen et al., 2016; Bezer et al., 2020), and their acoustic emissions (Sujarittam and Choi, 2020; Sujarittam and Choi, 2021) or on other parts of the boundary of our state of the art. Knowledge from these studies will greatly help future experimental and instrument design, as they shed light on what was before a black boxes of microbubble mechanics and microbubble-cell interactions. The key to successful future treatments may be to understand and integrate these newly-discovered information into a system rooted in theoretical and empirical bases.

4. Conclusions

Uses of ultrasound to perform therapies is a young but fast-growing field in medicine and engineering. Ultrasound answers the call of modern medicine for minimal patient disruption, is usually economical, can double as a diagnostic tool used to monitor the progress of the treatments. For many procedures that are still being developed inpre-clinical stages, much effort has been invested to ready them for clinical adoption. For others, refinements have been continuously made to the existing techniques and equipment, to further improve the efficacy and safety of the treatments. Much of these developments have been pushed by large amount of empirical data collected from many longitudinal studies. In the future, it is likely that applications of ultrasound in medicine will further expand. These will require even more pre-clinical studies and clinical trials data to validate. However, advances in our understanding in basic sciences could help us design these new procedures effectively, without as much reliance on trial-and-errors.

References

Alexandrov, A. V., Molina, C. A., Grotta, J. C., Garami, Z., Ford, S. R., Alvarez-Sabin, J., Montaner, J., Saqqur, M., Demchuk, A. M., Moyé, L. A., Hill, M. D., & Wojner, A. W. (2004). Ultrasound- enhanced systemic thrombolysis for acute ischemic stroke. The New England Journal of Medicine, 351(21), 2170–2178. https://doi.org/10.1056/NEJMoa041175

Allen, S. P., Hernandez-Garcia, L., Cain, C. A., & Hall, T. L. (2015). MR-based detection of individual histotripsy bubble clouds formed in tissues and phantoms. Magnetic Resonance in Medicine, 76 (5) , 1486 – 1493 . https://doi.org/10.1002/mrm.26062

Apfel, R. E., & Holland, C. K. (1991). Gauging the likelihood of cavitation from short- pulse, low- duty cycle diagnostic ultrasound. Ultrasound in Medicine & Biology, 17(2), 179–185. https://doi.org/10.1016/0301-5629(91)90125-g

Aryal, M., Arvanitis, C. D., Alexander, P. M., & McDannold, N. (2014). Ultrasound-mediated blood–brain barrier disruption for targeted drug delivery in the central nervous system. Advanced Drug Delivery Reviews, 72. https://doi.org/10.1016/j.addr.2014.01.008

Azhari, H. (2010). Appendix A: TypicalAcoustic Properties of Tissues. Basics of Biomedical Ultrasound for Engineers, 313. https://doi.org/10.1002/9780470561478.app1

Bautista, J. B., Kim, J.-W., Xu, Z., Jiang,X., & Dayton, P. A. (2023). Current status of sub-micron cavitation-enhancing agents for sonothrombolysis. Ultrasound in Medicine and Biology, 49 (5) https://doi.org/10.1016/j.ultrasmedbio.2023.01.018

Beerlage, H. P., van Leenders, G. J. L. H., Oosterhof, G. O. N., Witjes, J. A., Ruijter, E. T., van de Kaa, C. A., Debruyne, F. M. J., & de la Rosette, J. J. M. C. H. (1999). High-intensity focused ultrasound (HIFU) followed after one t o t w o w e e ks by r a di c a l r e t r opubi c prostatectomy: Results of a prospective study. T h e P r o s t a t e , 3 9 (1) , 4 1 – 4 6 . ht t ps : / / doi .org/ 1 0.10 02/ (s i c i) 10 9 7 - 0045(199 904 01) 3 9: 1% 3 C 41 : : a i d - pros7%3E3.0.co;2-5

Beisteiner, R., Hallett, M., & Lozano, A. M. (2023). Ultrasound neuromodulation as a new brain therapy. Advanced Science, 10(14). https://doi.org/10.1002/advs.202205634

Bezer, J. H., Koruk, H., Rowlands, C. J., & Choi, J. J. (2020). Elastic deformation of soft tissue-mimicking materials using a single microbubble and acoustic radiation force. Ultrasound in Medicine & Biology, 46(12), 3 3 2 7 – 3 3 3 8 . https://doi.org/10.1016/j.ultrasmedbio.2020. 08. 012

Bobkova, S., Gavrilov, L. A., Khokhlova, V. A., Shaw, A., & Hand, J. (2010). Focusing of High-Intensity Ultrasound Through the Rib Cage Using a Therapeutic Random Phased Array. Ultrasound in Medicine and Biology, 3 6 (6) , 8 8 8 – 9 0 6 . https://doi.org/10.1016/j.ultrasmedbio.2010. 03. 007

Chacko, J. K., Moore, M., Sankey, N. E., & Chandhoke, P. S. (2006). Does a slower treatment r ate impact the e fficacy of extracorporeal shock wave lithotripsy for solitary kidney or ureteral stones? The Journal of U r ol ogy , 175 (4) , 1370 – 1 3 74 . https://doi.org/10.1016/s0022- 5347(05)00683- x

Chen, H., Brayman, A. A., Evan, A. P., & Matula, T. J. (2012). Preliminary observations on the spatial correlation between short-burst microbubble oscillations and vascular bioeffects. Ultrasound in Medicine and B i o l o g y , 3 8 (1 2) , 2 1 5 1 – 2 1 6 2 . https://doi.org/10.1016/j.ultrasmedbio.2012. 08. 014

Chen, X., Leeman, J. E., Wang, J., Pacella,

J. J., & Villanueva, F. S. (2014). New insights into mechanisms of sonothrombolysis using ultra-high-speed imaging. Ultrasound in Medicine & Biology , 40 (1), 258 – 262. https://doi.org/10.1016/j.ultrasmedbio.2013.0 8. 021

Chen, X., Wang, J., Pacella, J . J., & Villanueva, F. S. (2016). Dynamic behavior of microbubbles during long ultrasound tone-burst excitation: Mechanistic insights into Ultrasound- Microbubble mediated therapeutics using high-speed imaging and cavitation detection. Ultrasound in Medicine & Biology , 40 (1), https://doi.org/10.1016/j.ultrasmedbio.2015.0 9. 017

Cho, E. E., Drazic, J., Ganguly, M., Stefanovic, B., & Hynynen, K. (2011). Two-Photon fluorescence microscopy study of cerebrovascular dynamics in ultrasound-induced blood—brain barrier opening. Journal of Cerebral Blood Flow & Metabolism, 31(9), https://doi.org/10.1038/jcbfm.2011.59

Church, C. C., & Miller, D. L. (2016). A

two-criterion model for microvascular bio- ef f ect s i n d u ced i n vi vo by c ont r a s t microbubbles exposed to medical ultrasound. Ultrasound in Medicine & Biology, 42(6), 1 3 8 5 – 1 3 9 8 . https://doi.org/10.1016/j.ultrasmedbio.201 6.01. 023

Clarke, R. L., & ter Haar, G. R. (1997). Temperature rise recorded during lesion formation by high-intensity focused ultrasound. Ultrasound in Medicine & Biology, 23(2), 299– 306. ht t ps : / / doi .org/ 1 0.1016 / s 03 0 1 - 5629(96)00198-6

Cranston, D., Leslie, T., & ter Haar, G. (2021). A review of high-intensity focused ultrasound in urology. Cancers, 13(22), 5696. https://doi.org/10.3390/cancers13225696

Diederich, C. J., & Hynynen, K. (1999). Ultrasound technology for hyperthermia. Ultrasound in Medicine & Biology, 25(6), 871–

887. ht t ps : / / doi .org/ 1 0.1016 / s 03 0 1 - 5629(99)00048-4

Doinikov, A. A., Aired, L., & Bouakaz, A. (2012). Dynamics of a contrast agent microbubble attached to an elastic wall. IEEE Transactions on Medical Imaging, 31(3), 654–662. https://doi.org/10.1109/tmi.2011.2174647

Eggers, J., Koch, B., Meyer, K., König, I., & Seidel, G. (2003). Effect of ultrasound on thrombolysis of middle cerebral artery occlusion. Annals of Neurology, 53(6), 797–800. https://doi.org/10.1002/ana.10590

Eggers, J., König, I. R., Koch, B., Händler, G., & Seidel, G. (2008). Sonothrombolysis with transcranial color-coded sonography and recombinant tissue-type plasminogen activator in acute middle cerebral artery main stem occlusion. Stroke , 39 (5), 1470 – 1475 . https://doi.org/10.1161/strokeaha.107.503870

Elmansy, H. E., & Lingeman, J. E. (2016). Recent advances in lithotripsy technology and treatment strategies: A systematic review update. International Journal of Surgery, 36, 6 7 6 – 6 8 0 . https://doi.org/10.1016/j.ijsu.2016.11.097

Engelberger, R. P., & Kucher, N. (2014). Ultrasound-assisted thrombolysis for acute pulmonary embolism: a systematic review. European Heart Journal, 35(12), 758–764. https://doi.org/10.1093/eurheartj/ehu029

Evans, K. D., Weiss, B., & Knopp, M. (2007). High-Intensity focused ultrasound (HIFU) for specific therapeutic treatments: A literature review. Journal of Diagnostic Medical Sonography , 23 (6), 319 – 327 . https://doi.org/10.1177/8756479307307268

Frinking, P., Segers, T., Luan, Y., & Tranquart, F. (2020). Three decades of ultrasound contrast agents: a review of the past, present and future improvements. Ultrasound in Medicine & Biology, 46(4), 892–908. https://doi.org/10.1016/j.ultrasmedbio.2019.12.008

Gandhi, K., Barzegar-Fallah, A., Banstola, A., Rizwan, S. B., & Reynolds, J. N. J. (2022). Ultrasound-mediated blood–brain barrier disruption for drug delivery: A systematic review of protocols, efficacy, and safety outcomes from preclinical and clinical studies. P h a r m a c e u t i c s , 1 4 (4) , 8 3 3 . https://doi.org/10.3390/pharmaceutics14040833

Groothuis, D. R. (2000). The blood-brain and blood-tumor barriers: A review of strategies for increasing drug delivery. Neuro-Oncology, 2 (1) , 4 5 – 5 9 . https://doi.org/10.1093/neuonc/2.1.45

Guan, L., Wang, C., Yan, X., Liu, L., Li, Y., & Mu, Y. (2020). A thrombolytic therapy using diagnostic ultrasound combined with RGDS- targeted microbubbles and urokinase in a rabbit m ode l . S c i e n t i f i c R e p o r t s , 10 (1). https://doi.org/10.1038/s41598-020-69202-9

Gupta, D., Choi, D., Lu, N., Allen, S. P., Hall, T. L., Noll, D. C., & Xu, Z. (2023). Magnetic resonance thermometry targeting for magnetic resonance– guided histotripsy treatments. Ultrasound in Medicine and B i o l o g y , 4 9 (5) , 1 1 0 2 – 1 1 0 7 . https://doi.org/10.1016/j.ultrasmedbio.2022.12. 009

Hasegawa, H. (2021). Advances i n ultrasonography: image formation and quality assessment. Journal of Medical Ultrasonics, 4 8 (4) , 3 7 7 – 3 8 9 . https://doi.org/10.1007/s10396-021-01140-z

H e r m e s , C ont i , A ., Tos c hi , N ., & Konofagou, E. E. (2020). Ultrasound neuromodulation: Mechanisms and the potential of multimodal stimulation for neuronal function assessment. Frontiers in P h y s i c s , 8 . https://doi.org/10.3389/fphy.2020.00150

Holland, C. K., & Apfel, R. E. (1989). An improved theory for the prediction of microcavitation thresholds. IEEE Transactions on Ultrasonics, Ferroelectrics and Frequency C o n t r o l , 3 6 (2) , 2 0 4 – 2 0 8 . https://doi.org/10.1109/58.19152

Hynynen, K. (1991). The threshold for thermally significant cavitation in dog's thigh muscle in vivo. Ultrasound in Medicine & B i o l o g y , 1 7 (2) , 1 5 7 – 1 6 9 . https://doi.org/10.1016/0301-5629(91)90123-e

Hynynen, K., McDannold, N., Vykhodtseva, N., & Jolesz, F. A. (2001). Noninvasive MR imaging–guided focal opening of the blood-brain barrier in rabbits. Radiology, 220(3), 640–646. https://doi.org/10.1148/radiol.2202001804

Izadifar, Z., Babyn, P., & Chapman, D. (2017). Mechanical and biological effects of ultrasound: A review of present knowledge. Ultrasound in Medicine & Biology, 43(6), 1085–1104. https://doi.org/10.1016/j.ultrasmedbio.2017.01.023

Izadifar, Z., Izadifar, Z., Chapman, D., & Babyn, P. (2020). An introduction to high intensity focused ultrasound: Systematic review on principles, devices, and clinical applications. Journal of Clinical Medicine, 9(2). https://doi.org/10.3390/jcm9020460

Kamimura, H. A., Flament, J., Valette, J., Cafarelli, A., Aron Badin, R., Hantraye, P., & Larrat, B. (2018). Feedback control of microbubble cavitation for ultrasound- mediated blood–brain barrier disruption in non- human primates under magnetic resonance guidance. Journal of Cerebral Blood Flow & Metabolism , 39 (7) , 1 191 – 1 203. https://doi.org/10.1177/0271678x17753514

Kato, Y., Yamaguchi, S., Hori, J., Okuyama, M., & Kakizaki, H. (2006). Improvement of stone comminution by slow delivery rate of shock waves in extracorporeal lithotripsy. International Journal of Urology, 13(12), 1461–1465. https://doi.org/10.1111/j.1442-2042.2006.01609.x

Kennedy, J. E. (2005). High-intensity focused ultrasound in the treatment of solid tumours. Nature Reviews Cancer, 5(4), 321–327. https://doi.org/10.1038/nrc1591

Keshavarzi, A., Vaezy, S., Noble, M. L., Paun, M. K., & Fujimoto, V. Y. (2003). Treatment of uterine fibroid tumors in an in situ rat model using high-intensity focused ultrasound. Fertility and Sterility, 80, 761–767. https://doi.org/10.1016/s0015-0282(03)00783- 0

Khokhlova, T. D., Canney, M. S., Khokhlova, V. A., Sapozhnikov, O. A., Crum, L. A., & Bailey, M. R. (2011). Controlled tissue emulsification produced by high intensity focused ultrasound shock waves and millisecond boiling. The Journal of the Acoustical Society of America, 130(5), 3498–3510. https://doi.org/10.1121/1.3626152

Kisting, M. A., Jentink, M. S., Wagner, M., Xu, Z., Hinshaw, J. L., Laeseke, P. F., Ziemlewicz, T. J., Koepsel, E. K., & Lee, F. T. (2023). Imaging for targeting, monitoring, and assessment after histotripsy: A non-invasive, non- thermal therapy for cancer. EMJ Radiology. https://doi.org/10.33590/emjradiol/10308529

Kyriakou, A., Neufeld, E., Werner, B., Paulides, M. M., Székely, G., & Kuster, N. (2013). A review of numerical and experimental compensation techniques for skull-induced phase aberrations in transcranial focused ultrasound. International Journal of Hyperthermia , 30 (1) , 36 – 46 . https://doi.org/10.3109/02656736.2013.861519 Leighton, T. (2012). The Acoustic Bubble. Academic Press.

Lingeman, J. E., McAteer, J. A., Gnessin, E., & Evan, A. P. (2009). Shock wave lithotripsy: advances in technology and technique. Nature Reviews Urology, 6(12), 660–670. https://doi.org/10.1038/nrurol.2009.216

Lipsman, N., Meng, Y., Bethune, A. J., Huang, Y., Lam, B., Masellis, M., Herrmann, N., Heyn, C., Aubert, I., Boutet, A., Smith, G. S., Hynynen, K., & Black, S. E. (2018). Blood– brain barrier opening in Alzheimer's disease using MR-guided focused ultrasound. Nature Communications , 9 (1) . https://doi.org/10.1038/s41467-018-04529-6

Lu, N., Hall, T. L., Choi, D., Gupta, D., Daou, B., Sukovich, J. R., Fox, A. D., Gerhardson, T., Pandey, A. S., Noll, D. C., & Xu, Z. (2021). Transcranial mr- guided histotripsy system. IEEE Transactions on Ultrasonics Ferroelectrics and Frequency

Control, 68(9), 2917–2929. https://doi.org/10.1109/tuffc.2021.3068113

Luo, W., Zhou, X., Zhang, J., Qian, Y., Zheng, M., Yu, M., & Gong, X. (2007). Analysis of apoptosis and cell proliferation after high intensity-focused ultrasound ablation combined with microbubbles in rabbit livers. European Journal of Gastroenterology & Hepatology, 19(11), 962–968. https://doi.org/10.1097/meg.0b013e3282cfb6f0

Madbouly, K., El-Tiraifi, A. E., Seida, M. A., El-Faqih, S. R., Atassi, R., & Talic, R. F. (2005). Slow versus fast shock wave lithotripsy rate for urolithiasis: A prospective randomized study. The Journal of Urology, 173(1), 127–130. https://doi.org/10.1097/01.ju.0000147820.3699 6.86

Madersbacher, S., Pedevilla, M., Vingers, L., Susani, M., & Marberger, M. (1995). Effect of high-intensity focused ultrasound on human prostate cancer in vivo. Cancer Research, 55(15), 3346–3351.

Maksimov, A. O. (2007). Viscous streaming from surface waves on the wall of acoustically-driven gas bubbles. European Journal of Mechanics - B/Fluids, 26(1), 28–42. https://doi.org/10.1016/j.euromechflu.2006.03.008

Maloney, M. E., Marguet, C. G., Zhou, Y., Kang, D. E., Sung, J. C., Springhart, W. P., Madden, J. F., Zhong, P., & Preminger, G. M. (2006). Progressive increase of lithotripter output produces better in-Vivo stone comminution. Journal of Endourology, 20(9), 603–606. https://doi.org/10.1089/end.2006.20.603

Martinez de Paz, J. M., & Macé, E. (2021). Functional ultrasound imaging: A useful tool for functional connectomics? NeuroImage, 245, 118722. https://doi.org/10.1016/j.neuroimage.2021.118 722

McClain, P. D., Lange, J. N., & Assimos, D. G. (2013). Optimizing shock wave lithotripsy: a comprehensive review. Reviews in Urology, 15(2).

Miller, D. L. (2007). Overview of experimental studies of biological effects of medical ultrasound caused by gas body activation and inertial cavitation. Progress in Biophysics and Molecular Biology, 93(1), 314–330. https://doi.org/10.1016/j.pbiomolbio.2006.07.0 27

Miller, D. L. (2012). Induction of pulmonary hemorrhage in rats during diagnostic ultrasound. Ultrasound in Medicine & Biology, 38(8), 1476–1482. https://doi.org/10.1016/j.ultrasmedbio.2012.04. 004

Miller, D. L., Dong, Z., Dou, C., & Raghavendran, K. (2018). Pulmonary capillary hemorrhage induced by different imaging modes of diagnostic ultrasound. Ultrasound in Medicine and Biology, 44(5), 1012–1021. https://doi.org/10.1016/j.ultrasmedbio.2017.11. 006

Miller, D. L., & Dou, C. (2004). Membrane damage thresholds for pulsed or continuous ultrasound in phagocytic cells loaded with contrast agent gas bodies. Ultrasound in Medicine & Biology, 30(3), 405–411. https://doi.org/10.1016/j.ultrasmedbio.2003.11. 013

Miller, D. L., Dou, C., & Wiggins, R. C. (2008). Frequency dependence of kidney injury induced by contrast-aided diagnostic ultrasound in rats. Ultrasound in Medicine and Biology, 34(10), 1678–1687. https://doi.org/10.1016/j.ultrasmedbio.2008.03. 001

Miller, D. L., & Quddus, J. (2000). Diagnostic ultrasound activation of contrast agent gas bodies induces capillary rupture in mice. Proceedings of the National Academy of Sciences, 97(18), 10179–10184. https://doi.org/10.1073/pnas.180294397

Miller, R. M., Kim, Y. S., Lin, K. W., Cain, C. A., Owens, G. E., & Xu, Z. (2013). Histotripsy cardiac therapy system integrated with real-time motion correction. Ultrasound in Medicine and Biology, 39(12), 2362–2373.

https://doi.org/10.1016/j.ultrasmedbio.2013.08. 004

Montero, A.-S., Franck Bielle, Lauriane Goldwirt, Adrien, L., Guillaume Bouchoux, Canney, M., Belin, F., Beccaria, K., Pierre-François Pradat, François Salachas, Séverine Boillée, Lobsiger, C. S., Lafon, C., Jean-Yves Chapelon, & Carpentier, A. (2019). Ultrasound-induced blood–spinal cord barrier opening in rabbits. Ultrasound in Medicine and Biology, 45(9), 2417–2426. https://doi.org/10.1016/j.ultrasmedbio.2019.05. 022

Morse, S. V., Pouliopoulos, A. N., Chan, T. G., Copping, M. J., Lin, J., Long, N. J., & Choi, J. J. (2019). Rapid short-pulse ultrasound delivers drugs uniformly across the murine blood-brain barrier with negligible disruption. Radiology, 291(2), 459–466. https://doi.org/10.1148/radiol.2019181625

NEMA. (1996). Standard for real-time display of thermal and mechanical acoustic output indices on diagnostic ultrasound equipment. American Institute of Ultrasound in Medicine and the National Electrical Manufactures Association.

O'Brien, W. D., Yang, Y., Simpson, D. G.,

Frizzell, L. A., Miller, R. J., Blue, J. P., & Zachary, J. F. (2006). Threshold estimation of ultrasound-induced lung hemorrhage in adult rabbits and comparison of thresholds in mice, rats, rabbits and pigs. Ultrasound in Medicine & Biology, 32(11), 1793–1804. https://doi.org/10.1016/j.ultrasmedbio.2006.03. 011

Pandit, R., Chen, L., & Götz, J. (2020). The blood-brain barrier: Physiology and strategies for drug delivery. Advanced Drug Delivery Reviews, 165-166, 1–14. https://doi.org/10.1016/j.addr.2019.11.009

Papadopoulos, N., Kyriacou, P. A., & Damianou, C. (2017). Review of protocols used in ultrasound thrombolysis. Journal of Stroke and Cerebrovascular Diseases, 26(11), 2447–2469. https://doi.org/10.1016/j.jstrokecerebrovasdis.2017.07.032

Raymond, S. B., Skoch, J., Hynynen, K., & Bacskai, B. J. (2006). Multiphoton imaging of ultrasound/optison mediated cerebrovascular effects in vivo. Journal of Cerebral Blood Flow & Metabolism, 27(2), 393–403. https://doi.org/10.1038/sj.jcbfm.9600336

Raymond, S. B., Treat, L. H., Dewey, J. D., McDannold, N. J., Hynynen, K., & Bacskai, B.

J. (2008). Ultrasound enhanced delivery of molecular imaging and therapeutic agents in alzheimer's disease mouse models. PLoS ONE, 3(5), e2175. https://doi.org/10.1371/journal.pone.0002175

Riis, T. S., Webb, T. D., & Kubanek, J. (2022). Acoustic properties across the human skull. Ultrasonics, 119, 106591. https://doi.org/10.1016/j.ultras.2021.106591

Roos, S. T., Juffermans, L. J. M., Slikkerveer, J., Unger, E. C., Porter, T. R., & Kamp, O. (2014). Sonothrombolysis in acute stroke and myocardial infarction: A systematic review. IJC Heart & Vessels, 4, 1–6. https://doi.org/10.1016/j.ijchv.2014.08.003

Santos, M. A., Wu, S.-K., Li, Z., Goertz, D. E., & Hynynen, K. (2018). Microbubble-assisted MRI-guided focused ultrasound for hyperthermia at reduced power levels. International Journal of Hyperthermia, 35(1), 599–611. https://doi.org/10.1080/02656736.2018.1511468

Sirsi, S. R., & Borden, M. A. (2009). Microbubble compositions, properties and biomedical applications. Bubble Science, Engineering & Technology, 1(1-2), 3–17. https://doi.org/10.1179/175889709x446507

Song, K.-H., Harvey, B. K., & Borden, M.

A. (2018). State-of-the-art of microbubble- assisted blood- brain barrier disruption. Theranostics, 8(16), 4393–4408. https://doi.org/10.7150/thno.26869

Souchon, R., Rouvière, O., Gelet, A., Detti, V., Srinivasan, S., Ophir, J., & Chapelon, J.-Y. (2003). Visualisation of HIFU lesions using elastography of the human prostate in vivo: preliminary results. Ultrasound in Medicine and Biology, 29(7), 1007–1015.

https://doi.org/10.1016/s0301-5629(03)00065- 6

Sujarittam, K., & Choi, J. J. (2020). Angular dependence of the acoustic signal of a microbubble cloud. The Journal of the Acoustical Society of America, 148(5), 2958–2972. https://doi.org/10.1121/10.0002490

Sujarittam, K., & Choi, J. J. (2022). The relationship between bubble concentration and the acoustic emission energy of separate frequency bands. JASA Express Letters, 2(2), 022002. https://doi.org/10.1121/10.0009394

Sukovich, J. R., Cain, C. A., Pandey, A. S., Chaudhary, N., Camelo-Piragua, S., Allen, S. P., Hall, T. L., Snell, J., Xu, Z., Cannata, J. M., Teofilovic, D., Bertolina, J. A., Kassell, N., & Xu, Z. (2019). In vivo histotripsy brain treatment. Journal of Neurosurgery, 131(4), 1 3 3 1 – 1 3 3 8 . https://doi.org/10.3171/2018.4.jns172652

ter Haar, G. (2001). High intensity focused ultrasound for the treatment of tumors. E c hoc ar di o gr ap h y - a J o u r n al of Cardiovascular Ultrasound and Allied T e c h n i q u e s , 1 8 (4) , 3 1 7 – 3 2 2 . ht t ps : / / doi .or g/ 10.1046/ j .1 5 4 0 - 8175.2001.00317.x

ter Haar, G., & Coussios, C. (2007). High intensity focused ultrasound: Physical principles and devices. International Journal o f H y p e rt h e rm i a , 23 (2) , 89 – 104. https://doi.org/10.1080/02656730601186138

Thomas, G. P. L., Khokhlova, T. D., & Khokhlova, V. A. (2021). Partial respiratory m ot i on c om pe ns a t i on f or a bdo m i n a l extracorporeal boiling histotripsy treatments with a robotic arm. IEEE Transactions on Ultrasonics, Ferroelectrics, and Frequency C o n t r o l , 6 8 (9) , 2 8 6 1 – 2 8 7 0 . https://doi.org/10.1109/TUFFC.2021.3075938 Timbie, K. F., Mead, B. P., & Price, R. J.

(2015). Drug and gene delivery across the blood–brain barrier with focused ultrasound. Journal of Controlled Release, 219, 61–75. https://doi.org/10.1016/j.jconrel.2015.08.059

Vidal-Jove, J., Serres, X., Vlaisavljevich, E., Cannata, J., Duryea, A., Miller, R., Merino, X., Velat, M., Kam, Y., Bolduan, R., Amaral, J.,

Hall, T., Xu, Z., Lee, F. T., & Ziemlewicz, T. J. (2022). First-in-man histotripsy of hepatic tumors: the THERESA trial, a feasibility study. International Journal of Hyperthermia: The Official Journal of European Society for Hyperthermic Oncology, North American Hyperthermia Group, 39(1), 1115–1123. https://doi.org/10.1080/02656736.2022.2112309

Vlaisavljevich, E., Kim, Y., Allen, S., Owens, G., Pelletier, S., Cain, C., Ives, K., & Xu, Z. (2013). Image-Guided non-invasive ultrasound liver ablation using histotripsy: Feasibility study in an in vivo porcine model. Ultrasound in Medicine & Biology, 39(8), 1 3 9 8 – 1 4 0 9 . https://doi.org/10.1016/j.ultrasmedbio.2013.02. 005

Wagner, M., Periyasamy, S., Kutlu, A. Z., Pieper, A., Swietlik, J. F., Ziemlewicz, T. J., Hall, T. L., Xu, Z., Speidel, M. A., Lee, F. T., & Laeseke, P. F. (2023). An X-ray c-arm guided automatic targeting system for histotripsy. IEEE Transactions on Biomedical Engineering, 7 0 (2) , 5 9 2 – 6 0 2 . https://doi.org/10.1109/tbme.2022.3198600 Wang, S., Samiotaki, G., Olumolade, O.,

Feshitan, J. A., & Konofagou, E. E. (2014). Microbubble type and distribution dependence of focused ultrasound-induced blood–brain barrier opening. Ultrasound in Medicine & B i o l o g y , 4 0 (1) , 1 3 0 – 1 3 7 . https://doi.org/10.1016/j.ultrasmedbio.2013.09. 015

Wang, T.-Y., Xu, Z., Hall, T. L., Fowlkes, J. B., & Cain, C. A. (2012). An efficient treatment strategy for histotripsy by removing cavitation memory. Ultrasound in Medicine & Biology, 3 8 (5) , 7 5 3 – 7 6 6 . https://doi.org/10.1016/j.ultrasmedbio.2012.01. 013

Webb, T. D., Leung, S. A., Rosenberg, J.,

Ghanouni, P., Dahl, J. J., Pelc, N. J., & Pauly,

K. B. (2018). Measurements of the relationship between CT hounsfield units and acoustic velocity and how it changes with photon energy

Designing Modified Covered Lagoon System for Biogas Production from Cassava Starch Wastewater.

Thitipong Thiansem[1], Nithit Pensri[1], Priyaphat Hla-aung [1], Phrommin Phromsen[1], Wiphaphorn Sombat[1] Patiroop Polchan[2] Napat Jakrawatana[2] Saoharit Nitayavardhana[2]

[1]Undergraduate student in Department of Environmental Engineering, Faculty of Engineering, Chiang Mai University, Thailand
[2] Department of Environmental Engineering, Faculty of Engineering, Chiang Mai University, Thailand
Corresponding author, E-mail: nithit_pensri@cmu.ac.th

Abstract: Thailand's agricultural industry, particularly in the production of cassava starch, has been causing significant environmental damage due to the wastewater generated from this production process. However, with the latest advancements in biogas production technology, we can now convert cassava starch wastewater into energy using anaerobic treatment, making it a cost-effective way to utilize wastewater and reduce production costs in the cassava starch industry.
To achieve this goal, we have chosen the Modified Covered Lagoon system for designing a wastewater treatment plant using anaerobic treatment. This system is highly efficient in removing Chemical Oxygen Demand (COD) and operates effectively with an inlet concentration of 20,000 mg/l and a flow rate of 10 m^3 per ton of cassava starch. The result is the production of biogas that can replace fuel oil in the cassava starch production facility, leading to a significant reduction in energy costs and providing an environmentally friendly alternative by utilizing industrial wastewater as an energy source.

Keywords: Biogas, Cassava wastewater, Starch wastewater, Modified Covered Lagoon

1. Introduction

Currently, Thailand has a continuous need for increased energy due to economic and population growth. The trend indicates a growing demand for energy each year. Therefore, developing alternative energy sources could be an option to help reduce production costs in the industrial and business sectors. Biogas is one type of renewable energy derived from the decomposition of organic matter in anaerobic conditions. Waste or wastewater can be used to produce biogas, originating from food processing industries, livestock farms, agricultural residues, or various energy crops. The production of biogas is an effective way to manage organic waste, and the resulting product can be used as a source of electricity and fuel.
Thailand is an agricultural country with a significant number of agro-processing factories. The starch industry, particularly the cassava starch production industry, has grown, leading to an increase in waste and wastewater from these factories. Treating organic wastewater using anaerobic digestion with microorganisms in an anaerobic fermentation system produces biogas, which can serve as a substitute fuel.
The Scope of study is located at Starch Company Limited, Sengsang District, Nakhon Ratchasima Province Thailand. The type of Facility is Cassava Starch Production Plant. Production Capacity was 300 tons/ day, wastewater generation rate was approximately 10 m^3/ton of starch and COD (Chemical Oxygen Demand) indicated 20,000 mg/l.
The factory owner has a desire to treat the wastewater generated from the cassava starch production industry to produce biogas for internal energy consumption within the factory.

This aims to reduce expenses on purchasing fuel from external sources. Additionally, the factory owner intends to replace the waste generated from the production process with raw material fuel to decrease the reliance on imported furnace oil necessary for the cassava starch production process within the factory.

Biogas refers to the gas generated from the anaerobic digestion process, where organic substances are broken down without the presence of oxygen. This process involves two groups of bacteria: acid-forming bacteria and methane-producing bacteria. Generally, biogas is composed of approximately 50-70% methane (CH_4) and around 30-40% carbon dioxide (CO_2). The remaining portion consists of other gases such as ammonia (NH_3), hydrogen (H2), and hydrogen sulfide (H2S), but in smaller quantities. Biogas is considered a clean and renewable energy source that can be utilized in various forms, such as direct heat utilization, as a fuel in engines, or in electricity generation [1].

Anaerobic Digestion within the system, there is a process of anaerobic digestion, where organic substances are broken down without the presence of oxygen. This process involves multiple complex steps that work collaboratively with various groups of bacteria. Each bacterial group has distinct functions in different stages of the digestion process, aiming to produce biogas. Biogas, generated through this intricate process, can be utilized as a renewable energy source including Hydrolysis, Acidogenesis and Methanogenesis [1].

2. Methods

Designing Biogas plant consist of 6 necessity units including Acid Pond (It is a pond that relies on acid-forming bacteria to decompose large molecular organic structures into fatty acids, easily biodegradable organic acids, alcohol, carbon dioxide, and nitrogen gas in an anaerobic environment.), Balancing tank (It is a large collecting tank that ensures a balanced and consistent inflow of wastewater into the normal wastewater treatment system). Modified Covered Lagoon (MCL), Wet Scrubber [8], Dehumidifier (The biogas produced in the production process consists of methane gas (CH_4), carbon dioxide gas (CO_2), hydrogen sulfide gas (H2S), and other gases, including moisture and water vapor. When gases, moisture, and water vapor combine, they form acids that can corrode various equipment materials within the system. This corrosion leads to maintenance costs or the need to replace equipment.) and Closed flare (The system operates with a pipe connected to the waste incineration system, consisting of an isolating valve which is a manual open-close valve. There is also an emergency shut-off valve (Emergency Shut-Off Valve) to prevent direct release of gas into the incineration system. This valve opens only when there is a command to incinerate gas from the automated waste incineration control system.). The tanks in the suspended growth system are designed with the bacteria in a suspended state. In this type of system, the bacteria live and grow in a suspended state, distributed throughout the tank. The suspended bacteria in the tank are evenly dispersed through processes such as mechanical stirring or bacterial agitation. The sludge profile in these tanks follows the water flow, with higher concentrations of bacteria at the bottom compared to the top due to the settling of microorganisms. The tanks in this system are taller at one end than the other, with the lower end being the bottom of the tank. The sludge profile in the tank varies according to the water flow. The concentration of bacteria is higher in the lower part of the tank than the upper part. This is because the process of organic matter decomposition in anaerobic conditions does not use air. Bacteria that grow slowly are those that produce methane. Therefore, it is essential to maintain bacteria in this group in the system for an extended period. (Fig 1)

To achieve this, several methods can be employed with ensuring a high liquid volume in the system to increase the Hydraulic Retention Time (HRT). Separating sludge from bacteria and returning sludge to the tank. This

allows for a longer Solid Retention Time (SRT) compared to the Hydraulic Retention Time (HRT). Creating granules by making bacteria form aggregates and facilitating their separation from the tank. This promotes a longer Solid Retention Time (SRT) than Hydraulic Retention Time (HRT). The Modified Anaerobic Covered Lagoon (MCL) system features large earthen pits, typically with a depth of no less than 6 meters, covered with a plastic sheet made of PVC or HDPE on top to capture and contain biogas. The gas is stored under slightly higher pressure than atmospheric pressure (causing the plastic sheet to inflate). The pit walls and floor are lined to prevent wastewater from contaminating the groundwater. Materials such as PVC or HDPE plastic are commonly used for lining the floor [1].

The plastic sheet can be secured by pressing the edges into the soil or using water seals by submerging the edge of the plastic in a water trough. This modified lagoon system addresses limitations of the anaerobic covered lagoon by improving efficiency and reducing the pit volume. Modifications can take various forms, including adding additional pits and allowing sequential flow based on anaerobic digestion processes (e.g., acidogenesis pit, methane-producing pit). Installing additional pits for purposes like backflow mixing (adding sludge pits and backflow pumping pipes). Adding distribution pipes to evenly distribute water throughout the pit, enhancing water circulation and mixing. Introducing collection points for scum and effluent drainage pipes.

The biogas generated is collected at the top of the digestion pit, covered with a plastic sheet made of PVC or HDPE. This captured biogas can then be utilized as an alternative energy source for various applications.

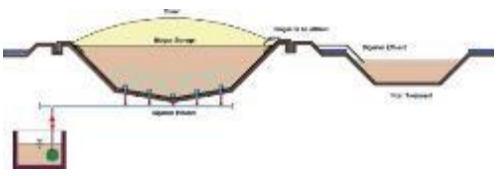

Figure 1: Modified Covered Lagoon

The data suggests that the suitable concentration of solids in wastewater for a Covered Lagoon system is between 0.5-3.0%. This concentration would result in a system efficiency in organic matter removal exceeding 60%. Considering investment and operational costs, it is evident that the Covered Lagoon system is priced in the low to mid-range, with an investment ranging from 250-1300 Baht/ m^3 and operational costs ranging from 0.9-3 Baht/ m^3 of wastewater. This makes it economically viable and cost-effective for investment. Additionally, developing the system to reduce the accumulation of sludge at the bottom of the lagoon would further enhance its efficiency in organic matter removal, making it a Modified Covered Lagoon system in the present context.

3. Results and Discussion

The design of the plant results in three units: Acid Pond, Balancing Tank, and Modified Covered Lagoon.

3.1 Designing Acid Pond.

Starting with the Acid Pond is designed with a Hydraulic Retention Time (HRT) of 1 day [2], an Organic Loading Rate (OLR) of 16.67 KgCOD/m^3·d, a depth of 5 meters, width of 27 meters, length of 54 meters, a slope of 2 meters (30 degrees), and a total pond volume of approximately 3906.67 m^3. (Fig 2)

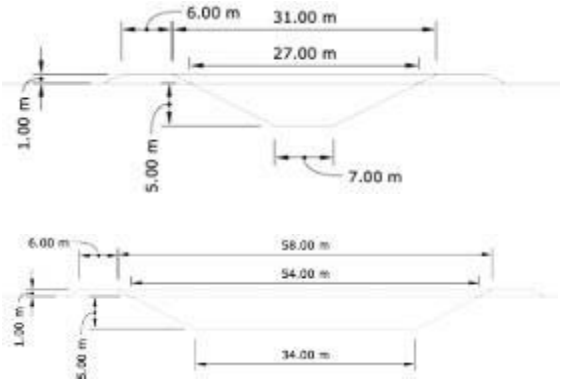

Figure 2: a cross-section of Acid Pond

3.2 Designing Balancing Tank.

The Balancing Tank is designed to handle a total inlet flow of 9,600 m³, inclusive of 3,600 m³/day for inlet flow and 6,000 m³/day for flow return. It has an HRT of 1 day [6], a depth of 3 meters, width of 13 meters, length of 26 meters, a slope of 30 degrees, and a total tank volume of 456 m³[7].(Fig 3)

Figure 3: a cross-section of a Balancing Tank

3.3 Designing Modified Covered Lagoon.

The Modified Covered Lagoon is designed with an inlet flow of 3,600 m³/day (factored by a safety factor of 1.2), an Organic Loading Rate (OLR) of 1.99 kg COD/m³·d, an HRT of 10 days [5], a depth of 5 meters, width of 70 meters, length of 140 meters, a slope of 30 degrees, and a total MCL volume of 39,166.67 m³.(Fig 4)

Figure 4: a cross-section of MCL

3.4 Biogas production calculation.

In terms of gas production (Fig 5), the inlet flow is 3,000 m³/day, with a COD inlet of 20,000 mg/l. The COD removal efficiency is 80%, resulting in a gas yield of 0.31 [4]. The biogas generation is estimated at 24,800 m³/day, serving as a potential replacement for fuel gas.

To assess the economic impact, calculate the potential replacement of fuel. The factory produces 300 tons of starch per day, requiring 38 liters of fuel oil per ton. Therefore, the fuel oil required is 11,400 liters/day. At a cost of 20 Baht per liter, the daily cost of fuel oil is 228,000 Baht. Given that 1.1 liters of fuel oil is equivalent to 2 m³ of biogas, the biogas equivalent to fuel oil is 20,728 m³. The MCL system can produce 24,800 m³ of biogas per day. This results in an excess of biogas, with 4,072 m³ sent to the flare daily.

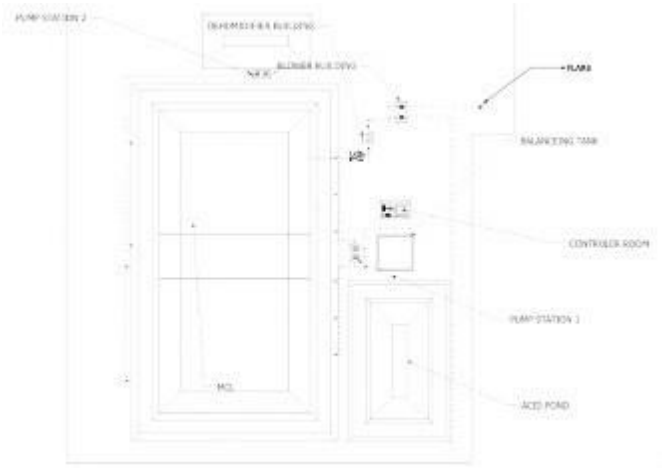

Figure 5: Biogas Plant design

4. Conclusions

The design of this biogas production system plant can replace the use of fuel oil with wastewater from cassava flour production. The designed plant includes various gas-generating units with the following capacities: an Acid Pond with an approximate volume of 3,900 m³, a Balancing Tank with a volume of 456 m³, and an MCL (Modified Covered Lagoon) with a volume of around 39,000 m³. The system is intended to efficiently produce biogas for substituting fuel oil used in the cassava flour industry within the factory.

References

[1] Handbook on Operations Related to Design, Production, Quality Control, and Utilization of Biogas by Department of industrial works, Thailand.

[2] Lettinga and Hulshoff (1991) suggested that for acidogenic reactor should be 6-24 hours.

[3] Thanapat T, Pariraya C, Krit C, Kabuki S, Treating Tapioca Starch

Industrial Wastewater Using Two-Phase (MS-USSB) Environmental and Natural Resources Jounal 2023; 21(1): 78-79

[4] K.Peerawat, K.Prawit, O Sompong, Hydrogen and Methane Production from Starch Processing Wastewater by Thermophilic Two-Stage Anaerobic Digestion in 2015 International Conference on Alternative Energy Procedia 79 827-832

[5] HRT Value provided on this slide are for high-rate complete-mix mesophilic anaerobic digestion (Metcalf & Eddy, page 1513 and 1514)

[6] Assoc. Prof. Dr. Saneh Kanjanawong, Wastewater Engineering Book, along with the year 2543.

[7] Water Research Commission on Balancing Tank Control Application Book.

[8] Water Scrubbing for Removal of Hydrogen Sulfide (H2S) in biogas from Hog Farms.

Thitipong Thiansem
Born on 28th June 2000
Majoring in environmental engineering, Chiang Mai University, Thailand.

Nithit Pensri

Born on 3rd April 2001
Majoring in environmental engineering, Chiang Mai University, Thailand.

Priyaphat Hla-aung
Born on 27th May 2001
Majoring in environmental engineering, Chiang Mai University, Thailand.

…

…
Phrommin Phromsen
Born on 6th April 2002
Majoring in environmental engineering, Chiang Mai University, Thailand

Dr. Napat Jakrawatana
B.Eng., M.Eng, PhD
Associate Professor
Research Interests: Circular Economy; Material Flow Analysis for Waste and Resource management; Greenhouse Gas Management

Dr. Saoharit Nitayavardhana
B.Sc., M.Sc, PhD
Assistant Professor
Research Interests: Biorefinery; Biological biomass conversion; Sustainable waste management and value added process

Experimental Study on the Effect of Elliptical Hole Nozzle on Flash Boiling Spray of High Pressure Liquid Ammonia

Yizhou Yang[1], Zhixia He[1], Chen Li1,[2], Jiafeng Chen[2], Wenjun Zhong[2]

[1] Institute for Energy Research, Jiangsu University, Zhenjiang 212013, China
[2] School of Energy and Power Engineering, Jiangsu University, Zhenjiang 212013, China
*Corresponding author, *Zhixia He, Email: zxhe@ujs.edu.cn

Abstract. Ammonia is an ideal alternative fuel for mitigating carbon emissions. High-pressure direct injection of liquid ammonia (LNH3) offers significant advantages in enhancing energy efficiency and minimizing emissions. Due to the high saturation vapor pressure, the injection of LNH3 is susceptible to flash boiling. This study established a high-pressure common-rail LNH3 jet experimental platform and investigated the flash boiling spray characteristics of round and elliptical hole nozzles, by using the high-speed micro-imaging technology with backlight lighting. The results demonstrate that under non-flash boiling conditions, the residual LNH3 in the SAC chamber and nozzle can rapidly corrode the acrylic material of the nozzle, leading to deformation and failure of the nozzle structure. Under flash boiling conditions, LNH3 ejected from the hole will produce spherical macroscopic spray morphology. Then the spray gradually transitions from an elliptical profile to a conical profile as back pressure increases. Compared with round hole nozzles, elliptical hole nozzles exhibit higher flow velocity which enhances oil-gas mixing and promotes more pronounced flash boiling phenomena. Flash boiling occurs at an earlier stage with increased spray cone angle thereby improving atomization characteristics both during flash and non-flash boiling conditions. The tail jet of elliptical hole nozzles terminates earlier while exhibiting a higher rate decrease in average gray value, which improves the atomization quality in the tail spray stage and meets the requirements of timing, quantification, and precise control of the fuel injection system.

Keywords: Liquid ammonia jet, Elliptical hole, Flashing boiling spray, Common rail

1. Introduction

Liquid ammonia has emerged as a highly promising alternative fuel in the absence of widespread hydrogen energy[1]. However, due to its corrosiveness and toxicity, there is limited research on the direct injection of liquid ammonia, with most studies focusing on low-pressure injection and prototype nozzles [2-3]. Reliable experimental data is necessary to calibrate numerical simulations. Enhancing the atomization quality of the liquid ammonia jet through optimized elliptical orifice structures can help mitigate its high NOx emission issue. Additionally, the characteristics of the liquid ammonia jet under flash-boiling conditions have yet to be investigated. Therefore, the objective of this study is to examine the influence of superheating and orifice structure on high-pressure direct injection of liquid ammonia spray.

2. Experimental setup and methodology

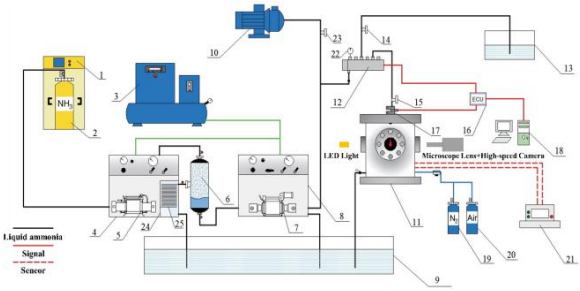

Fig. 1. High-pressure common rail liquid ammonia jet visualization experimental platform.

Fig. 1 presents the high-pressure common rail liquid ammonia jet visualization experimental platform. It comprises three components: an ammonia liquefaction system, a fuel injection system, and an image acquisition system.To visualize the internal flow and near-field spray of the nozzle structure, the needle valve inside the fuel injector was extracted and the head portion was cut off as illustrated in Fig. 2A, Fig. 2 illustrate the visualization images of circular and elliptical holes under high-speed microscopy and show the images of the exit of the round and elliptical holes obtained using a metallographic microscope.

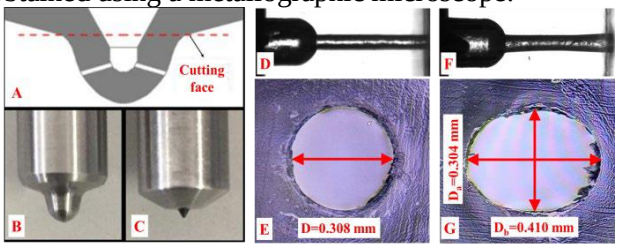

Fig. 1 Metal nozzle cutting process and transparent nozzle images

2.2. Image post-processing and repeatability analysis

In prior research, the near-field atomization characteristics have frequently been characterized using the spray cone angle, which has been widely believed to indicate a greater atomization effect with a greater spray cone angle. Under non-flashing boiling conditions, liquid jets exhibit a near-field spray that possesses a cone-shaped shape, featuring a linear distribution of the spray edge. This allows for the use of the spray cone angle to describe the macroscopic morphology of the spray. However, for near-field

sprays in flashing or excessively flashing boiling states, as illustrated in Fig. 3B, the macroscopic morphology of the near-field sprays appears to be spherical, with a parabolic distribution of the spray edge. In such scenarios, the macroscopic morphology of the spray cannot be effectively described using the spray cone angle. Hence, the average grayscale value is determined to describe the spray development process, as outlined in the following equation:

$$\alpha = \frac{\sum \frac{\gamma}{255}}{N}$$

Where γ represents the grayscale value of a pixel, ranging from 0 to 255, with 0 corresponding to black areas and 255 corresponding to white areas in the image. The $\gamma/255$ represents the normalized grayscale value. N represents the number of pixels in the solving region. By summing up the normalized grayscale values of all pixels within the solving region and dividing it by the number of pixels, the average grayscale value is obtained. This value indicates the liquid phase concentration within the solving region, and a higher value indicates a higher liquid phase concentration.

In the present study, the MATLAB software was utilized for post-processing of the visual images. As illustrated in Fig. 3A, the visual image was instantaneously subtracted from the image without injection to obtain the spray morphology. After applying an inversion process, the average grayscale value was determined. Additionally, in order to analyze the development of spray during the jet process, two consecutive images from the transient injection process were selected and subtracted, as depicted in Fig. 3B. The resulting image was subsequently subjected to an inversion process to obtain the image of spray expansion. The gray area in the image depicts the area where the spray develops within a unit time.

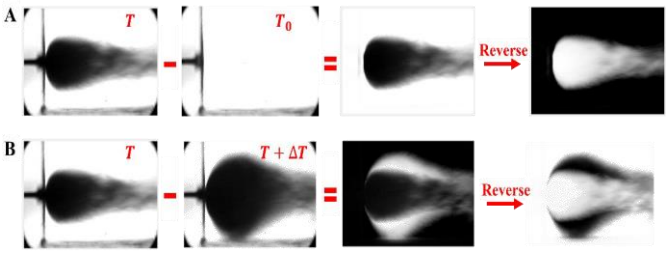

Fig. 2 Image post-processing methodology.

To verify the stability and repeatability of the experimental setup, the post-processing of the spray images was performed for three independent injections. The resulting transient variations in the average grayscale value and their standard deviation are depicted in Fig. 4. The capture rate of 100,000 frames per second was achieved with a resolution of 640×280.

Observing the figure, it can be observed that the primary deviation among the three independent injections occurs during the rapid increase and decrease of the average grayscale value, corresponding to the stages when the needle valve lifts and seats. When the needle valve stabilizes at its maximum lift, the macroscopic spray morphology remains consistent for the three injections. In general, the experimental setup used for LNH3 jet visualization in this particular study exhibits excellent repeatability.

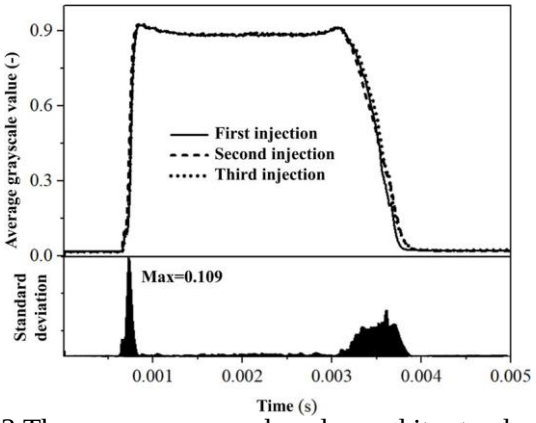

Fig. 3 The average grayscale value and its standard deviation under three independent injections.

3. Results and Discussion

3.1 Spray expansion images under different back pressures

Fig 3 shows the spray expansion image of the liquid ammonia jet at the initial stage, with an injection pressure of 30 MPa and varying back pressures (0.1, 0.3, and 0.6 MPa). At low back pressure, a near-spherical spray morphology forms downstream of the orifice. As the back pressure increases, the superheat of liquid ammonia decreases, leading to a decrease in the phase change mass transfer rate during the flash-boiling process. This weakening of the expansion effect causes the initially spherical spray to gradually transform into an ellipsoidal shape and eventually into a conical spray profile under non-flash conditions.

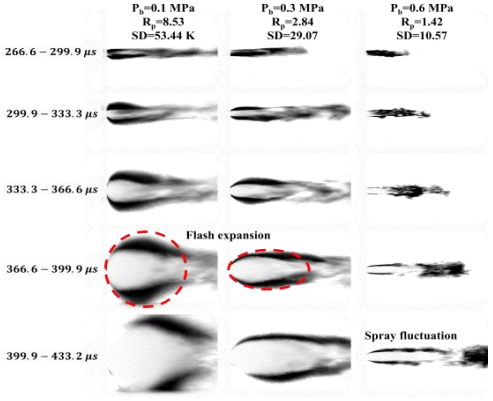

Fig. 3 Spray expansion images under different back pressures.

3.2 Spray characteristics of liquid ammonia jet under elliptical hole nozzle

Fig 4 presents the transient visualization images depicting the development of the near-field spray for both an elliptical hole nozzle and a circular nozzle under the same back pressure.

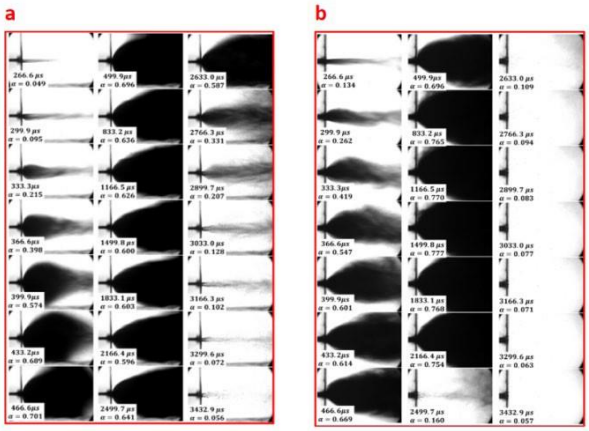

Fig. 4 Spray transient images from a circular nozzle（a）and a elliptical nozzle（b）

In Fig. 5a, the transient development of the average grayscale value of the spray from the elliptical hole nozzle is shown under an injection pressure of 30 MPa and back pressures of 0.1, 0.2, 0.3, 0.4, and 0.5 MPa, respectively. To directly compare the circular and elliptical nozzles, Fig. 5b illustrates the average grayscale value changes at back pressures of 0.1 and 0.6 MPa. The turbulent disturbances at the exit of the elliptical nozzle are observed to be higher compared to those at the circular nozzle exit, as seen in Fig. 5b. The liquid ammonia jet emitted from the elliptical nozzle demonstrates improved atomization characteri -stics, both under flashing and non-flashing conditions. Additionally, the elliptical nozzle structure enhances the atomization performance during the tail spray stage.

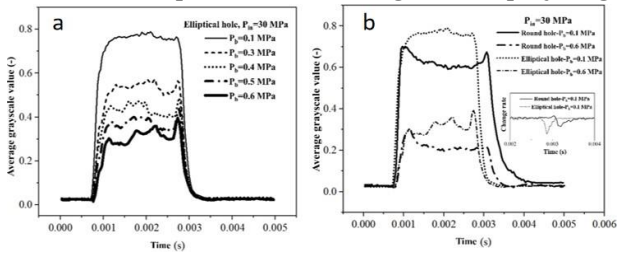

Fig. 5 Variations in average grayscale value from a elliptical nozzle under different back pressures.（a）and from circular and elliptical nozzles under different back pressures.（b）

4. Conclusion

A high-pressure common rail liquid ammonia jet visualization experimental platform was established in this study. Transparent nozzle technology and high-speed photography microscopy imaging technology were utilized to capture images of the flow inside the transparent nozzle and the near-field spray of the liquid ammonia jet under backlight illumination. The main conclusions are as follows:

(1) Under flashing conditions, liquid ammonia sprayed from the spray hole forms a macroscopic spray shape close to a sphere at the beginning of the spray. With increasing back pressure, the spray shape gradually transforms from an ellipsoidal contour to a conical spray shape under non-flashing conditions.

(2) The elliptical orifice nozzle has a higher flow rate than the circular orifice nozzle, and its better oil and gas mixing effect leads to more extensive flashing.

(3) The tail spray under the elliptical orifice nozzle ends earlier and has a higher rate of decrease in macroscopic liquid phase fraction, thereby improving the atomization effect in the tail spray stage and meeting the requirements of timing, quantification, and precise control of the fuel injection system.

5. Reference

1. Li Y, et al., Explosion hazard evaluation of renew able hydrogen/ammonia/air fuels. Energy 2018;159:252–63
2. Colson, S., et al., Study on the effect of injection temperature and nozzle geometry on the flashing transition of liquid ammonia spray. Fuel, 2023. 348: p. 128612.
3. Li, S., et al., An investigation on near-field and far-field characteristics of superheated ammonia spray. Fuel, 2022. 324: p. 124683
4. An Z.,et al., Numerical study on the phase change andspray characteristics of liquid ammonia flash spray[J]. Fuel,2023,345.
5. Chai, W.S., et al., A review on ammonia, ammonia-hydrogen and ammonia-methane fuels. Renewable and Sustainable Energy Reviews, 2021. 147(39): p. 111254.
6. Dimitriou, P. and R. Javaid, A review of ammonia as a compression ignition engine fuel. International Journal of Hydrogen Energy, 2020. 45(11): p. 7098-7118.
7. Gross, C.W. and S.C. Kong, Performance characteristics of a compression-ignition engine using direct-injection ammonia–DME mixtures. Fuel, 2013. 103(none).
8. Li, T., X. Zhou, and N. Wang, A comparison between low- and high-pressure injection dual-fuel modes of diesel-pilot-ignition ammonia combustion

engines. Journal of the Energy Institute, 2022(102-): p. 102.
9. Zhang, Z., et al., Performance characteristics of a two-stroke low speed engine applying ammonia/diesel dual direct injection strategy. Fuel, 2023. 332: p. 126086.
10. Pelé, R., et al., First Study on Ammonia Spray Characteristics with a Current GDI Engine Injector. Fuels, 2021. 2(3): p. 253-271.
11. Zeng, W., et al., Atomization and vaporization for flash-boiling multi-hole sprays with alcohol fuels. Fuel, 2012. 95: p. 287-297.
12. Li, S., et al., An investigation on near-field and far-field characteristics of superheated ammonia spray. Fuel, 2022. 324: p. 124683.

Yizhou Yang
Master student

Research interests:
experiment of nozzle flow and spray

Prof. Dr. Zhixia He

Research interests:
Thermal fluid theory in utilization of Energy

Innovation technology for encapsulation of bioactive compounds from marigold extract.

Nipathon Wilailak, Sarunthorn Jaikaew, Nukrob Narkprasom, Phanat Saengcharoenratt, Kanjana Narkprasom*

Faculty of Engineering and Argo-Industry, Maejo University, Chiang Mai, Thailand
*E-mail: aoikanjana63@gmail.com

Abstract: The aim of this research was to study the optimal conditions for encapsulation efficiency of phenolic compounds and antioxidant activity effects of marigold (*Tagetes erecta L*) beads by encapsulation technique. The optimal condition for encapsulation efficiency of phenolic compounds and antioxidant activity effects from marigold bead using response surface method. The variables were used to study the optimal conditions of ratio of sodium alginate content to marigold extract, encapsulation frequency, and concentration of calcium chloride. The results showed that all three factors impacted encapsulation efficiency of phenolic compounds and antioxidant activity. Statistical analyses indicated that the experimental data were best fitted to a quadratic polynomial equation with high decision coefficient (R^2) at 0.9174 and 0.9121 for total encapsulation efficiency of phenolic compounds and antioxidant activity, respectively. The optimum conditions were at 1.5% ratio of sodium alginate to marigold extract (w/v%) at 1400 Hz of encapsulation frequency and at 5% of calcium chloride solution concentration (w/v%) resulting in the highest encapsulation efficiency of phenolic compounds and antioxidant activity effects of marigold beads were 49.72±0.511% and 64.698%±0.375%, respectively.

Keywords: *Tagetes erecta L*, Encapsulation, Response surface method, Phenolic compounds, Antioxidant activity

1. Introduction

At present it is found that Due to the COVID-19 outbreak situation, many educational institutions in the area have adjusted their teaching methods to teaching via the internet (online) 80%, while the other 20% may use other forms of teaching. including work There is a distance to prevent the spread of COVID-19, so there is work from home or residence (Work from home). Working and studying via the internet involves spending time with media such as television, computers, and tablets. tablet or mobile phone close-up for a long time You must use your eyes to look at the information on the screen. This may affect vision in the long term. And looking for things that help boost immunity, "food" is another matter that consumers know and consider. Therefore, choosing to eat foods that are beneficial Clean and safe Therefore, it is an additional factor in choosing food.

Marigold is one of the important economic flowering plants in Thailand. It is a native plant of Mexico. The scientific name is Tagetes erecta L. and the common name is Marigold. It is classified as an herbaceous plant. It is widely grown throughout Thailand. Because the seeds are large, easy to grow, strong, rarely affected by disease or insects. and can be grown all year round You can set the flowering period to coincide with important festivals. Because marigolds have auspicious meanings because the color of the flowers is golden yellow, which means prosperity and stability. Therefore, people like to use it for auspicious ceremonies and decorate places on important occasions. In addition, marigold flowers also have many good properties for the body, such as substances

that help nourish eyesight, namely lutein and zeaxanthin. which is classified as an eye nourishing substance from colored plants Both of these substances have properties that help prevent macular degeneration [1]. They are compounds in the carotenoid group (Carotenoid), which is a type of antioxidant. According to a study by the Office of Herbal Information, Faculty of Pharmacy, Mahidol University, it was found that water extracts of 4 types of flowers, such as marigold, cosmos, pink rose, and bougainvillea, had the best antioxidant effects. The substances found in these 4 types of flowers are mostly phenolic acids and flavonoids. And in marigold flowers, phenolic acids are 3-4 times higher than other flowers. These substances have the effect of inhibiting the division of colon cancer cells. bile duct cancer and stomach cancer, etc. However, marigold flowers are still not a favorite to eat. Because it has a bitter taste and has a pungent odor that is unique to marigold flowers

The objective of this research project is to develop marigold flowers into "beads" through the encapsulation process. Which is a technology for encapsulating important substances that are solid, liquid, or gas inside a capsule. The encapsulated substance can be made of polymers or substances that can form walls or sheaths. It depends on the desired product characteristics and uses in the food industry. The wall helps control the speed at which important substances are released.

2. Materials and Methods

2.1 Materials

Yellow Queen (Tagetes erecta) was cultivated at the Faculty of Agricultural Production, Maejo University, Chiang Mai, Thailand. Dried using a microwave vacuum rotary dryer (Marchcool co., LTd) until the moisture content is less than 6%. The dried marigold flower petals were then grinded in a laboratory grinder and the fraction was passed through a 40-mesh sieve to obtain a reduced particle size.

2.2 Chemicals

Folin- Ciocalteu phenol, DPPH (2 , 2 - diphenyl-1-picrylhydrazyl), Na_2CO_3, and ethanol were purchased from Union Science (Chiang Mai, Thailand).

2.3 Preparation of marigold flower extract

The extraction of phenolic compounds and antioxidant activity using the microwave-assisted extraction to a modified method of from Anong et al. (2014) [2]. Dried marigold powder of 6.25 g was mixed a water 100 ml in a round bottom. Extract with microwave oven (Samsung, ME711K) and Soxhlet extractor set. The microwave oven was connected to a cooling system (Thermo Electron Haake WKL 25 Recirculator Chiller) to control the temperature of circulated water was set to 30°C. The extraction time was 25 minutes, and the microwave power was 700 watts. The extracts obtained were then centrifuged (Universal centrifuge, model PLC – 012E, Taiwan) at a speed of 6000 rpm for 15 minutes to remove coarse impurities before analysis.

2.4 Encapsulation of marigold flower extract.

The extrusion method is used to encapsulate marigold flower extract by encapsulator B390 (BUCHI Labortechnik AG 9230 Flawil, B-390). Take the sodium alginate solution and mix it with marigold flower extract. Frequency set in the range of 1000-2000 Hz with 1000 micrometer nozzle. The encapsulated marigold beads were dropped into a bath of calcium chloride solution of various concentrations, stirring gently with a magnetic wand all the time. After that 10 minutes filtered and washed with distilled water three times to remove the remaining calcium chloride.

2.5 Experimental design

The response surface methodology (RSM) is an efficient statistical technique for the optimization of multiple variables experiments allowing the determination of optimum process parameters with a minimum number of runs.

Table 1. Sets of Independent variables selected in the Box–Behnken design (BBD).

Independent variables	Symbols	Value of levels		
		-1	0	1
The ratio of sodium alginate to marigold extract (w/v%)	X_1	1	1.5	2
Frequency (Hz)	X_2	1000	1400	1800
Calcium chloride solution concentration (w/v% $CaCl_2$)	X_3	2.5	5	7.5

2.5.1 Box–Behnken design (BBD)

A Box– Behnken design (BBD) was implemented to check the influence of independent factors are the ratio of sodium alginate to calendula extract (X_1), frequency (X_2), and calcium chloride solution concentration (X_3) on the encapsulation efficiency of phenolic compounds and antioxidant activity effects from marigold bead. Three varying independent parameters were encrypted to three levels as -1, 0, and 1 (Table 1). A total of fifteen experimental runs measured in a randomized order were conducted to maximize the response value. The obtained data was analyzed using a second-order polynomial equation. (Equation 1)

$$YY = \beta\beta_0 + \beta\beta_1 XX_1 + \beta\beta_2 XX_2 + \beta\beta_3 XX_3 + \beta\beta_{12} XX_1 XX_2 + \beta\beta_{13} XX_1 XX_3 + \beta\beta_{23} XX_2 XX_3 + \beta\beta_{11} XX_1^2 + \beta\beta_{22} XX_2^2 + \beta\beta_{33} XX_3^2 \quad (1)$$

Where:

Y = The measured responses
X_1, X_2, *and* X_3 = The independent variables
β_0 = The model constant
β_1, β_2 and β_3 = The linear coefficients
β_{12}, β_{13} and β_{23} = The interacted coefficients
β_{11}, β_{22} and β_{33} = The quadratic coefficients

Design Expert 7.0.0 software (Stat-Ease Inc., Minneapolis, USA) was used for the generation and analysis of the experimental design and data.

2.6 Analysis of total phenolic content

Total phenolic content was determined by the Folin–Ciocalteu reagent method. 0.1 ml of marigold flower bead extract was mixed with 2 ml Sodium carbonate solution (Na_2CO_3) in test tube. After a 30-minute reaction in the dark at room temperature. The measure the absorbance at 750 nm to determine the quantity of phenolic content present. All results were compared with the gallic acid standard curve. Expressed in milligrams (mg/gram or GAE gallic acid equivalent) per gram of gallic acid.

2.7 Analysis of antioxidant activity

Antioxidant activity was measured using by DPPH assay according to a modified method of Shimada et al. (1992) [3].0.1 ml of marigold flower bead extract was mixed with 2.9 ml of 0.1 mM DPPH in methanol. After a 30-minute reaction in the dark at room temperature. The measure the absorbance at 515 nm. The antioxidant activity was calculated according to the following Equation 2:

$$\%\text{inhibition} = \left(1 - \frac{\text{absorbance of sample}}{\text{absorbance of control}}\right) \times 100 \quad (2)$$

2.8 Statistical Analysis

The response surface data obtained were analyzed by Analysis of Variance (ANOVA). Differences were considered significant at a confidence level of 95% ($p < 0.05$) using statistical softwere SPSS version 26.

3. Results and Discussion

3.1 Effect of the ratio of sodium alginate to marigold extract on encapsulation efficiency of phenolic compounds.

In all the tested runs, the encapsulation efficiency of phenolic compounds was most dependent on the ratio of sodium alginate to marigold extract (w/ v%). and showed a decreasing trend when the shape of the beads changed. As observed in Fig xx. The highest encapsulation efficiency of phenolic compounds was 1.5% ratio of sodium alginate to marigold extract (w/v%). The reason behind this may be Polyphenol structure, the size of the molecule or the moieties of the specific polyphenolic compounds (i.e. hydroxylic or carboxylic group) can affect the yield of encapsulation [4]. The viscosity of sodium alginate affects the flow through the encapsulator nozzle, causing the marigold extract beads to be spherical, which affects the

Table 2 Box-Behnken Design matrix and experimentally obtained results of investigated responses.

RUN	Independent variables			Responses	
	X_1	X_2	X_3	Y_1	Y_2
1	1(-1)	1000(-1)	5(0)	45.22^{cde}±0.661	55.457^{g}±0.071
2	2(1)	1000(-1)	5(0)	47.47^{abc}±1.018	58.801^{f}±0.166
3	1(-1)	1800(1)	5(0)	45.47^{cde}±1.288	55.686^{g}±0.427
4	2(1)	1800(1)	5(0)	48.04^{ab}±0.385	59.952^{e}±0.200
5	1(-1)	1400(0)	2.5(-1)	43.53^{e}±0.995	51.179^{k}±0.070
6	2(1)	1400(0)	2.5(-1)	48.54^{ab}±1.245	61.547^{bc}±0.132
7	1(-1)	1400(0)	7.5(1)	44.12^{de}±1.563	54.168^{h}±0.114
8	2(1)	1400(0)	7.5(1)	48.14^{ab}±0.638	60.963^{cd}±0.065
9	1.5(0)	1000(-1)	2.5(-1)	48.08^{bcd}±2.270	60.563^{d}±0.742
10	1.5(0)	1800(1)	2.5(-1)	46.27^{bcd}±0.439	52.412^{j}±0.066
11	1.5(0)	1000(-1)	7.5(1)	46.01^{bcde}±0.905	53.545^{i}±0.486
12	1.5(0)	1800(1)	7.5(1)	46.32^{bcd}±1.262	58.797^{f}±0.274
13	1.5(0)	1400(0)	5(0)	49.72^{a}±0.511	64.698^{a}±0.375
14	1.5(0)	1400(0)	5(0)	49.04^{a}±0.515	61.608^{b}±0.205
15	1.5(0)	1400(0)	5(0)	49.06^{a}±1.303	62.101^{b}±0.214
Predicted value	1.82	1377.24	4.78	49.51	63.84
Experimental value	1.5	1400	5	49.72	64.70

encapsulation process of important substances [5]. When increasing the ratio of sodium alginate to marigold extract, the encapsulation efficiency of phenolic compounds will decrease. Because there is too much viscosity, the shape of the beads is similar to water droplets.

3.2 Effect of frequency on encapsulation efficiency of phenolic compounds.

To encapsulate important substances in addition to the materials used in the coating. Determining the independent factors that arise from the instrument is also important. The shape of the bead affects the frequency. Moura et al. (2018) [6] determined that a higher frequency (of 1150 Hz) provides stability to the bead. Therefore, a study of frequencies in the range 1000-1800 of encapsulation revealed no significant effect on the encapsulation efficiency of phenolic compounds.

3.3 Effect of calcium chloride solution concentration on encapsulation efficiency of phenolic compounds.

The concentration of calcium chloride solution influenced the encapsulation efficiency of phenolic compounds. Because the concentration of calcium chloride solution causes sodium alginate to increase the chance of agglomeration [7], which results in increased encapsulation efficiency of phenolic compounds when used in the appropriate ratio.

3.4 Effect of encapsulation parameters of antioxidant activity.

According to the optimized results, the highest antioxidant activity
of 94.70% was reported at optimum conditions of ultrasonic the optimum conditions were at 1.5% ratio of sodium alginate to marigold extract (w/v%) at 1400 Hz of encapsulation frequency and at 5% of calcium chloride solution concentration (w/v%) pertaining to conditions where the maximum encapsulation efficiency of phenolic compounds (experiment 8 of Table 1). The ratio of sodium alginate to marigold extract was most related. followed by frequency were the highly influencing parameters on of encapsulation efficiency antioxidant activity similar to that of encapsulation efficiency of phenolic compounds.

Table 3. Analysis of variance and model regression coefficient of independent variables (The ratio of sodium alginate to marigold extract (w/v%), Frequency (Hz), and Calcium chloride solution concentration (w/v% CaCl2))

Factor	Efficiency of phenolic compounds (%)					Efficiency of antioxidant activity (%)				
	Coefficient	Standard error	P-value	Lower 95%	Upper 95%	Coefficient	Standard error	P-value	Lower 95%	Upper 95%
Intercept	49.273	0.528	0.000	47.916	50.630	62.802	1.165	0.000	59.807	65.797
X_1	1.733	0.323	0.003	0.902	2.564	3.097	0.713	0.007	1.263	4.931
X_2	-0.127	0.323	0.711	-0.957	0.704	-0.190	0.713	0.801	-2.024	1.644
X_3	-0.268	0.323	0.444	-1.099	0.562	0.222	0.713	0.769	-1.613	2.056
X_1X_2	0.081	0.457	0.865	-1.093	1.256	0.231	1.009	0.828	-2.363	2.824
X_1X_3	-0.247	0.457	0.613	-1.421	0.928	-0.893	1.009	0.417	-3.487	1.701
X_2X_3	0.608	0.457	0.241	-0.566	1.783	3.351	1.009	0.021	0.757	5.945
X_1^2	-1.694	0.476	0.016	-2.917	-0.471	-2.347	1.050	0.076	-5.046	0.353
X_1^3	-1.027	0.476	0.083	-2.250	0.195	-2.982	1.050	0.036	-5.681	-0.282
X_2^3	-1.496	0.476	0.026	-2.719	-0.274	-3.491	1.050	0.021	-6.191	-0.792

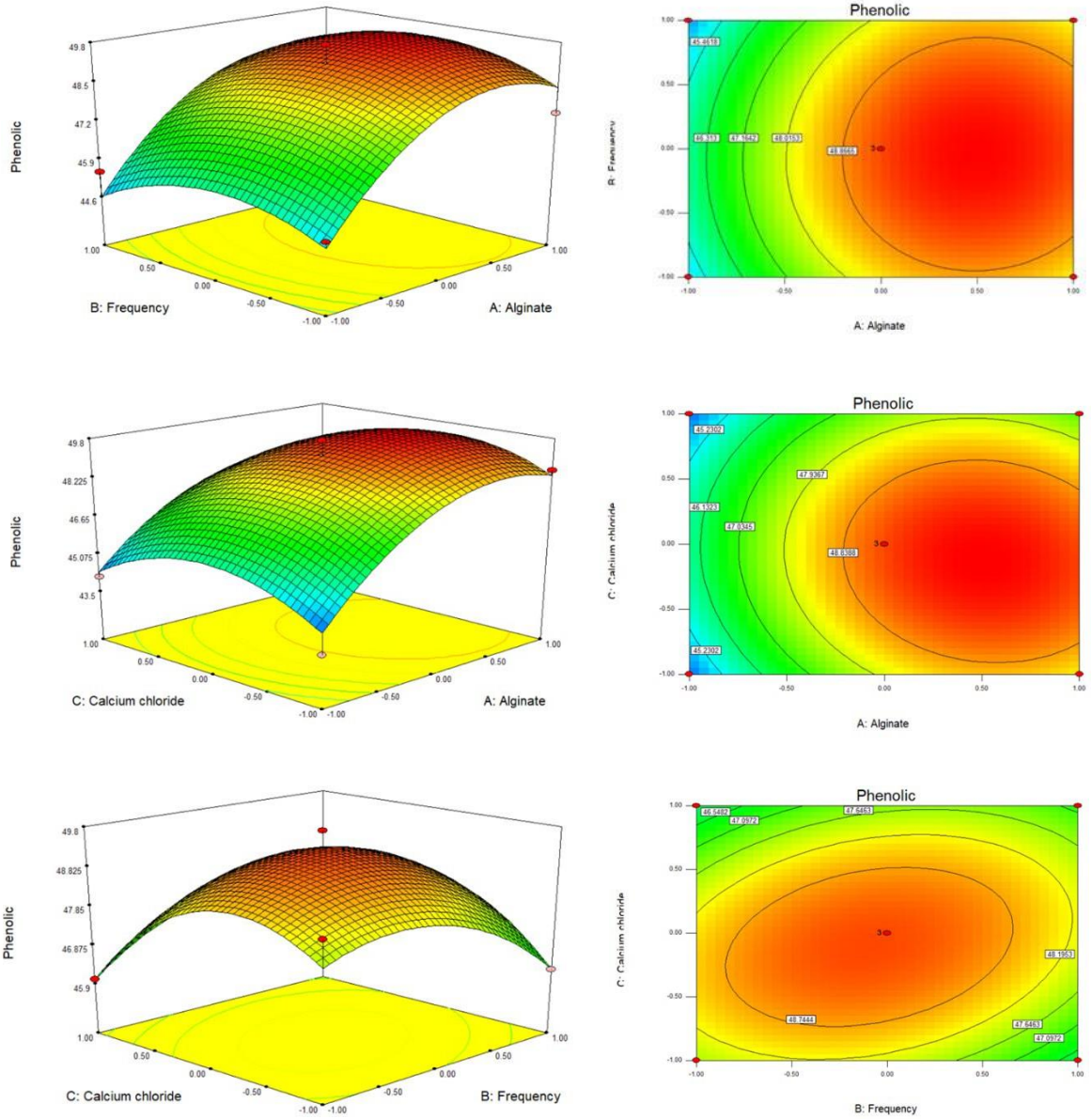

Fig. 1. 3D Response plots and 2D contour plots of encapsulation efficiency of phenolic compounds
Footnote: 3D response surface plots (A, B, C) and 2D contour plots (A', B', C') of the encapsulation efficiency of phenolic compounds (%) as the ratio of sodium alginate to marigold extract (w/v%), Frequency (Hz) and Calcium chloride solution concentration (w/v% $CaCl_2$)

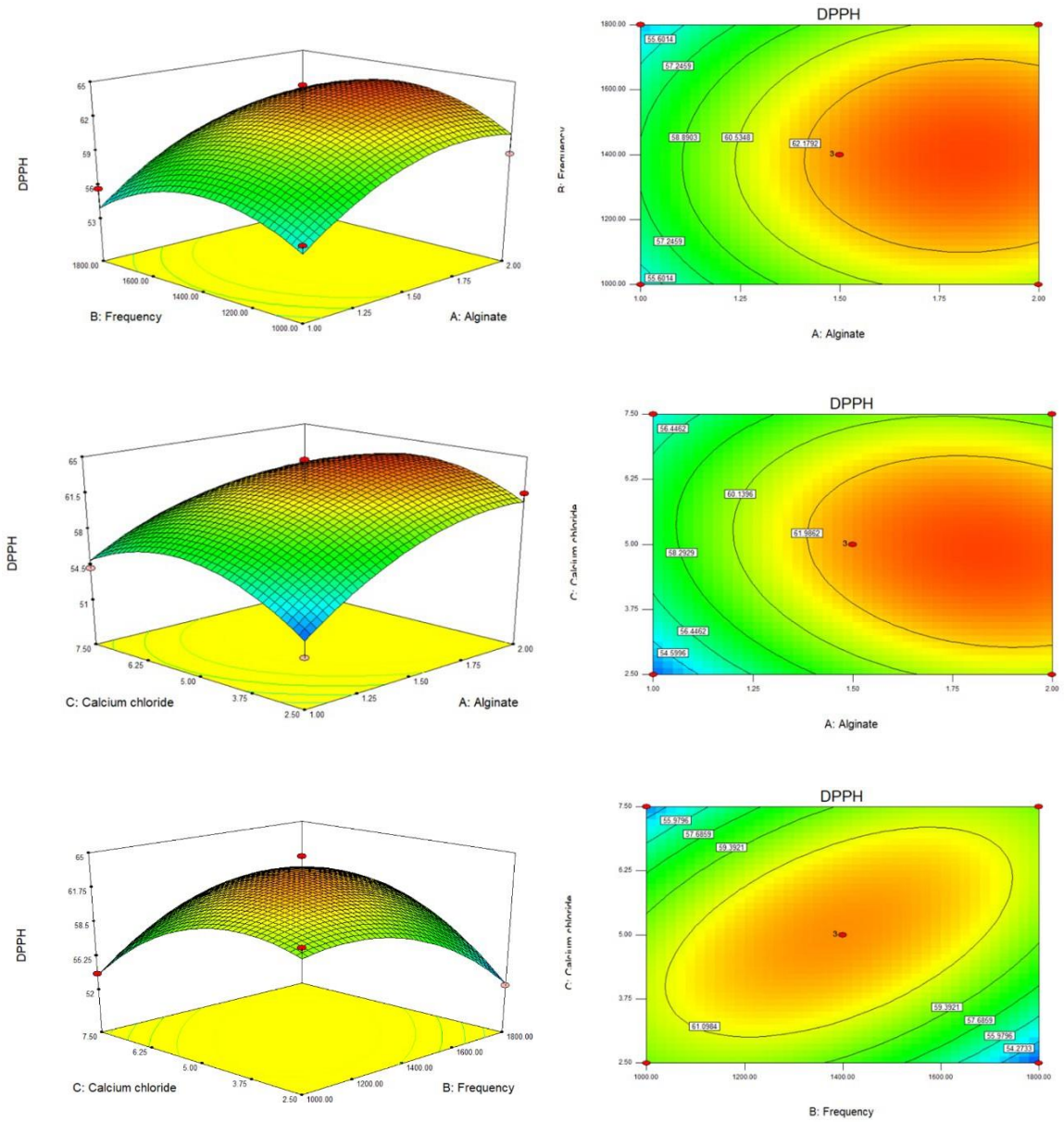

Fig. 1. 3D Response plots and 2D contour plots of encapsulation efficiency of antioxidant activity
Footnote: 3D response surface plots (A, B, C) and 2D contour plots (A', B', C') of the encapsulation efficiency of phenolic compounds (%) as the ratio of sodium alginate to marigold extract (w/v%), Frequency (Hz) and Calcium chloride solution concentration (w/v% $CaCl_2$)

3.5 Optimization for encapsulation efficiency of phenolic compounds and antioxidant activity.

The influence of the studied parameters indicates that the optimum conditions were at 1.5% ratio of sodium alginate to calendula extract (w/v%) at 1400 Hz of encapsulation frequency and at 5% of calcium chloride solution concentration (w/v%) (Table 2). By applying regression analysis on the experimental data, the independent variables and dependent variable are related by the following second-order polynomial equation:

Phenolic compounds:

$$YY = 49.273 + 1.733XX_1 - 0.127XX_2 - 0.268XX_3 + 0.081XX_1XX_2 - 0.247XX_1XX_3aa + 0.608XX_2XX_3 - 1.694XX_1^2 - 1.027XX_2^2 - 1.496XX_3^2 \quad (3)$$

Antioxidant activity:

$$YY = 62.802 + 3.097XX_1 - 0.190XX_2 + 0.222XX_3 + 0.231XX_1XX_2 - 0.893XX_1XX_3aa + 3.351XX_2XX_3 - 2.347XX_1^2 - 2.982XX_2^2 - 3.491XX_3^2 \quad (4)$$

Table 3 The quadratic regression model for phenolic compounds and antioxidant effects resulted in a determination coefficient (R^2) of 0.9174 and 0.9121 respectively. The p-value for the model were less than 0.05, indicating that all models were significant ($p \leq 0.05$). and could be used to predict and obtain the optimization of encapsulation for phenolic compounds and antioxidant effects of marigold beads. Overall, the three independent variables and the quadratic terms brought to bear the significant effects on the encapsulation efficiency of phenolic compounds and the antioxidant effects of marigolds. To confirm the accuracy, an experiment was performed at which conditions the total phenolic content was 49.51% and antioxidant effects 63.84%, which is close to the predicted value.

The estimation of equations 3 and 4 is then generated as a 3D response plot and 2D contour plots (Fig 2 and 3, respectively) to consider the interaction between the independent variables and the response of the dependent variable.

4. Conclusions

Development of the process of processing marigold flowers into beads by encapsulation. Study the optimal conditions for encapsulation efficiency of phenolic compounds and antioxidant activity effects using Box–Behnken design (BBD). From this research, it was found that the retention of phenolic compounds was most related to the ratio of sodium alginate to marigold extract. As for the frequency of encapsulation and the concentration of calcium chloride solution had a correspondingly less relationship. Marigold flowers can be added to add value in the functional food market. They are foods that contain important substances that have both basic nutritional values that are beneficial to the body. It also helps prevent and reduce the risk of developing various diseases.

References

[1] Alves- Rodrigues A, Shao A. The science behind lutein. Toxicol Lett. 2004 Apr 15;150(1):57-83. DOI: 10.1016/j.toxlet.2003.10.031.

[2] Srisopa, A., Nakaew, N., and Srisayam, M. (2016). Chemical and biological properties of marigold extracts obtained by organic solvent- free extraction. Pibulsongkram Rajabhat University.

[3] Shimada, K., K. Fujikawa, K. Yahara and T. Nakamura. (1992). Antioxidative properties of xanthan on the autoxidation of soybean oil in cyclodextrin emulsion. J. Agric. Food Chem., 40: 945-948. DOI: 10.1021/jf00018a005

[4] Viktor, N., Ana Kalusevic, V., Manojlovic, Steva, L., Branko, B. (2011). An overview of encapsulation technologies for food applications, Procedia Food Science, Volume 1

[5] Sharmaine, A., Alicia, M., Esther S., José, M, G., Carmen G. (2020). Encapsulation of ginger oil in alginate-based shell materials, Food Bioscience,

Volume 37.

[6] Sílvia C. S. R. de Moura1,2 & Gabriela N. Schettini3 & Aline O. Garcia2 & Darlila A. Gallina2 & Izabela D. Alvim2 &Miriam D. (2019). Stability of Hibiscus Extract Encapsulated by Ionic Gelation Incorporated in Yogurt. Food and Bioprocess Technology, 12:1500–1515

[7] Tunsirikongkon, A., Yong, C, P.,Dong-H, K., Phuong, T, Jeong, S, K., (2020). Effect of calcium chloride on the protein encapsulation and stability of pro liposomal granules, Journal of Drug Delivery Science and Technology, Volume 57.

Ms. Nipathon Wilailak Master student, Master of Engineering (Renewable Food Engineering). **Research Interests:** Extraction and Green technology.

Ms. Sarunthorn Jaikaew Bachelor's Degree of Engineering (Renewable Food Engineering).

Dr. Kanjana Narkprasom Assistant Professor **Research Interests:** Product research and development and Innovation food.

Dr. Nukrob Narkprasom Assistant Professor **Research Interests:** Food Engineering and Fermentation process.

Dr. Phanat Saengcharoenratt Lecturer **Research Interests:** Food Science and Technology.

Medicaments Recovery and Recycling Efforts to Avoid Ecosystem Pollution Caused by the Inappropriate Disposal of Unused/Expired Pharmaceuticals.

Li Ruihan[1*]

[1]School of Pharmacy, Jiangsu University, Zhenjiang, China

*E-mail: 3211603004@stmail.ujs.edu.cn,

Abstract: With the increment of the drugs consumption, pharmaceutical waste has become an indisputable fact today, resulting from the inproper practices of abundant medicines. As a global problem, it has contribute to environmental pollution. The objective of the study was to summarize the international evidences of the expired medicines management and disposal, and propose some suggestions to change the current conditions and improve the public awareness of it. This review referred to 35 articles from different continents and different countries with uneven levels of economic development. This review takes as its starting point a study of cumulative active drug concentrations in rivers on a global scale, reflecting the differences in drug disposal methods and the factors influencing them around the world. And then the article mainly suggests that people tend to treat the unwanted drugs as daily household waste and make them present in natural environment through the sewage system. Consequently, it bring the hazardous influences to the ecosystem, because of drug toxicity. Reducing the pharmaceutical waste and negative impacts on nature is a all-round and multi-stage process, which may contains the common dissemination, the selection and accesses, drug recovery systems and the environmental measures to waste management and wastewater treatment after recycling.

Keywords: Disposal of pharmaceutical waste, Household drug storage, Take-back medication program, Drug pollution, Pharmaceuticals in the environment.

1. Introduction

Advances in medicine, public health, and living standards have led to the increase of life expectancy.According to the United Nations' World Population Prospects (UN WPP) data,the global average life expectancy was just over 70 years,while it was less than half two years ago. [1]The development of the times has brought about sweeping changes in our world, with economic, social and cultural changes accompanied by civilization diseases, such as cancers, cardiovascular and respiratory diseases and obesity, which were all manifested in medicaments consumption. [2]If expressed in defined daily does (DDD), antibiotic consumption increased 65% between 2000 from 2015, from 21.1 to 34.8 billion DDDs, and the antibiotic consumption rate increased 39%, from 11.3 to 15.7 DDDs per 1,000 inhabitants per day over the study period.[3] Taking antibiotics for example, the annual antibiotics consumption was determined by the Defined Daily Dose (DDD)/1000 inhabitants/day (DID). Even before the the COVID-19 pandemic**,** results total consumption of antibiotics in the Lebanese community, measured by DDD/1000 inhabitants/day (DID), significantly increased from 18.71 in 2004 to 31.26 in 2016.[4] Antibiotic sales increased at an alarming rate during the epidemic. In the study of the Crolia region, it was measured as days of therapy (DOT) and reported as per 1000 inhabitants or per 1000 inhabitant-days. total azithromycin DOT in Croatia increased in 2017, 2018, 2019, and 2020 (1.76, 1.91, 1.91 and 2.01/1000 inhabitant-days, respectively).[5] Using another, more intuitive representation, estimates the number of prescriptions written indicate that approximately 100 tonnes of drugs were prescribed in Germany in 1995 . In 2000, the top 25 compounds were all used in the UK in quantities greater than 10 tonnes/year, and the top 3 compounds prescribed [acetaminophen (paracetamol), metformin hydrochloride and ibuprofen] were all used in quantities >100 tonnes/year. In fact, not only antibiotics, but also psychotropic and other drugs have shown an increase under the influence of the new coronary pneumonia.[6, 7]

Except increasing the economic burden and inducing drug resistance, the environmental pollution of drug wastage cannot be ignored. An increase in their presence in the environment is the consequence of medicaments increment , which may affect the survival, reproduction, metabolism and populations of organisms and alter the community structure and ecological functions of ecosystems, including biomass production and biodiversity.[8] A carps study from the Zhudong Veterans' Hospital (24°43′22.9″N, 121°05′59.4″E) and the Toucian River in Taiwan shows that pharmaceutical contaminants exhibit acute toxicity to vertebrate organisms.[9] As for how drugs enter the environment, there are two main pathways. The first is through human excretion and then discharged into the environment via wastewater treatment plants, as it is likely that a large portion of the drug cannot be fully metabolised in the body and is excreted in prototype form via the urine. The second way is that people dispose of expired/unused drugs as household waste and enter the environment through landfill or incineration, where some of the drugs will be biodegraded, but some will still be present.

Given above,the objectives of this review are to analylise environmental impacts of improper disposal of unused/expired pharmaceuticals, summarize disposal methods around the world, and propose some suggestions.

2. Methods

The review is based on 40 papers from databases such as Web of Science, China National Knowledge Internet(CNKI) and PubMed, as well as references from these articles. The articles were searched with 'Disposal of pharmaceutical waste', 'Take-back medication programme'; 'Drug pollution',. 'Pharmaceuticals in the environment' as the keywords, articles were selected that examined the disposal of pharmaceutical waste in different time periods, on different continents, and in countries with different levels of economic development.And then, it is followed by the use of visual analyses and flow charts to present the results of the analyses and discussions

3. Results

3.1 A global-scale study of API pollution

Active pharmaceutical ingredients（API) can be harmful to ecosystems and human health. Although there have been many studies on the detection of pharmaceuticals in the aquatic environment, most of them have used different assays for different subjects, with small, regionalised and individualised samples that lack representativeness, while ignoring many countries in the world.These are unsuitable for global-scale problems and strategies。[10-13]

The researchers conducted a global assay of drug concentrations in rivers covering 104 countries, 137 sampling operations, 1052 sampling sites, and 61 active ingredients, which included areas with different population densities, different topography, and located in different climatic zones. The samples were randomised, representative and feasible.

Figure 1: detection frequencies for contaminants detected

Cumulative pharmaceutical concentrations are measured at each sampling site as the sum of all API residues . The most contaminated samples were mainly from African (e.g. Ethiopia > Tunisia > Democratic Republic of Congo > Kenya > Nigeria) and Asian countries (Pakistan > India > Armenia > Palestine > China). The data indicates that many of the samples with high cumulative drug concentrations came from low- and middle-income countries, while samples from countries in other regions had much lower concentrations.[14]

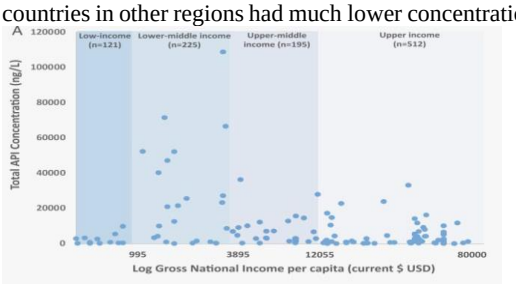

Figure 2: Cumulative concentration of APIs observed across respective river catchments organized by World Bank GNI per capita

3.2 Collection of Unused/Expired Pharmaceuticals

The way i n which the population disposes of expired/unused drugs depends to a large extent on the socio-economic development and the level of education of the population.

In low-income and lower-middle-income countries, there are often no guidelines on the disposal of medicines by the population, and there is limited knowledge of optimal disposal methods, leading to inappropriate disposal of unused medicines .[15] In Malasia , half of the participants disposed of their drug waste in the rubbish bin. Some 2.9 per cent of respondents dumped household drug waste directly down the drain, while 8.8 per cent dumped it down the kitchen or toilet sink.[16] The situation in the Johannesburg area of South Africa was similar to that of Malaysia, but the majority of respondents were strongly opposed to the disposal, for example, storing medicines indefinitely at home (42.3 %), throwing them outside (55%), burning them (61%) or returning them to the local pharmacy (68%). And yet they still choose to landfill without sorting.[17] Unlike the previous two surveys, the Ethiopian survey covered training in drug waste management, yet nearly two thirds of the respondents indicated that they had not received training on drug waste management.[18]

On the other hand, in Australia since 1998, there have been project to address the safe disposal of medicines, a survey conducted in 2016 showed that less than 18% had heard of the program and that most people dispose of unwanted medicines in their household rubbish or into the sewerage.[19] In Kuwait, guidelines issued by the Ministry of Health state that pharmacies must return surplus medicines to health centres.[20] In the UK study, respondents also mentioned that they had previously disposed of their medication, with 48 per cent sending it back to the GP hospital, giving it to a family member or friend, 27 per cent throwing it in the bin, and 25 per cent dumping it down sinks and toilets.[21] It is reassuring to note that when checking the management of medicines in the homes of Portuguese residents, the return of surplus medicines to the pharmacy was the most common answer, accounting for 69 per cent of cases, for reasons related to the availability of containers and recycling bins for packaging waste in separate mobile phones.[22]

With the exception of a few countries mentioned above, most high-income countries are equipped with collection systems for return to pharmacy or centralised recycling, the details of which depend on the different policies of each country. Where pharmacies are involved, in some countries they organise their own take-back schemes, while in others they need to follow legal requirements to participate in the take-back of medicines. In Lebanon, for example, the Ministry of Public Health has issued several decrees regulating medical waste generated by hospitals, but not by the general population, in accordance with the law and international conventions, but it is not yet officially operational.[23]The Article 127b of the European Union Directive 2004/27/EC (2004)of the European Parliament and of the Council requires that member States shall have appropriate collection systems in place for unused or expired medicinal products. A survey conducted by the European Federation of Pharmaceutical Industry Association reported that, 3 years later, 20 of the 28 nations surveyed established a pharmaceutical waste collection scheme, most of which were pharmacy-based collection systems .[24]

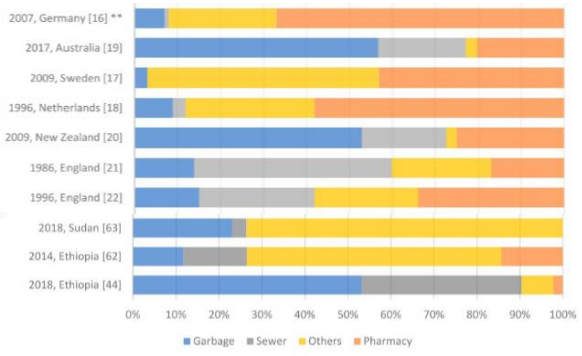

Figure 3: Drug waste disposal practices in other highly developed countries favour recycling of unused drugs rather than just throwing them away or flushing them away[25]

4. Discussion

Drugs in the environment pose a range of health problems, most notably ecological and human health. Pharmaceuticals, which are essential for human survival and development, have been in existence for more than 40 years now, so they should be minimised in the environment through the adoption of practical measures.

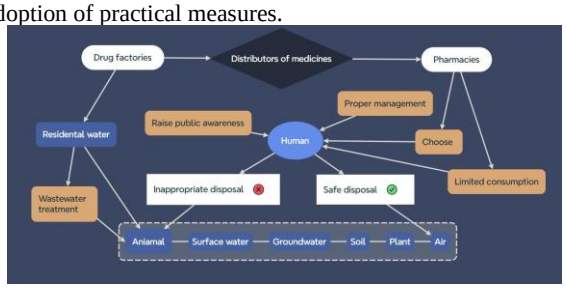

Figure 4: The life cycle of pharmaceuticals

Measures to deal with pharmaceutical waste contamination are related to the life cycle of English medicines. The entire life cycle of pharmaceuticals can be divided into upstream, which is primarily concerned with design, synthesis and production within the pharmaceutical plant, and drug selection and purchase, and downstream, which highlights wastewater from residences, hospitals and livestock, as well as advanced pollutant treatment technologies.[26]

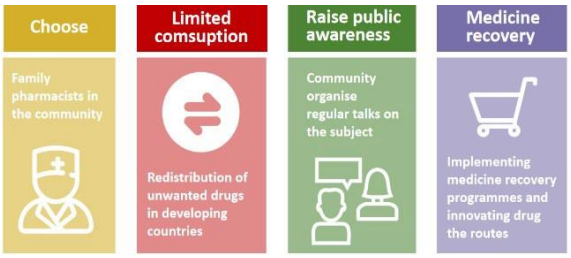

Figure 5: Measures to deal with pharmaceutical waste contamination

The composition of drugs in the environment is very complex, and likewise reducing the amount and negative effects of the drugs that afflict the Admiral's Bell is a process that involves a number of stages

4.1 Raise public awareness

Some data prove that families in low- and middle-income countries are using expired drugs. Australian families even believe that these drugs can be used for a year or more after their expiry date. Therefore, there is a need for public education and public awareness on the rational use of medicines and expiry dates of medicines.[27-29]

4.2 Limit to prescribe and Purchase Pharmaceuticals

There is a need for adequate numbers of pharmacists in the community; limiting the amount of medicines prescribed by health-care workers who are authorised to prescribe medicines to the amount needed, and strengthening the management and education of health-care workers and pharmacists. Improve regulations on the promotion of medicines and adopt appropriate sanctions to prevent violations. Although the law cannot reduce patient demand, it can raise social awareness and safeguard the drug market for ecologically healthy and sustainable development.[30]

4.3 New wastewater and solid waste treatment

The common methods of disposal of pharmaceutical wastes, whether incineration or landfill, inevitably cause harm to the environment. Wastewater treatment, another important area, is an innovative and effective method for the disposal of pharmaceutical residues. Among them, photocatalysis plays an important role and is considered to be one of the most promising methods for eliminating organic pollutants from the environment.[31-33]

4.4 Pharmaceutical recovery

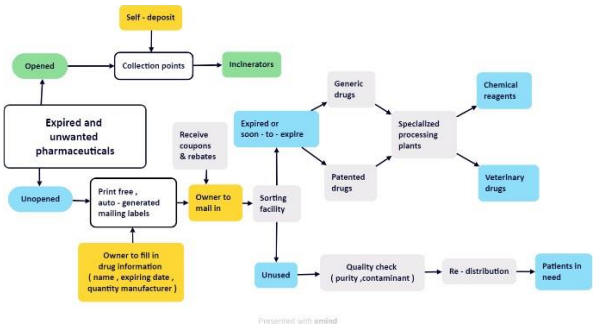

Figure 5:Framework diagram for recovery and recycling of expired/unused medicines in the home

In this medication recovery and recycling process, residents first need to separate unwanted medications into opened and unopened medications. Opened medications need to be stored or mailed to a centralised medication collection point. The collection point is responsible for delivering the medication to the waste incineration plant. Unopened medicines are transported by special logistics lines. Users do not need to transport the medicines, but only need to fill in the accurate information about the medicines, including the trade name, expiry date, quantity and manufacturer of the medicines, and scan the barcode on the product package to fill in the information automatically. The system will automatically generate free postcode labels, which are printed and affixed to the medicines. In-person pick-ups or other human contact should be avoided during the COVID-19 pandemic to reduce the risks of viral transmission.[34, 35] Once arrived at sorting facilities, packages are further categorized by automatic sorting facilities after reading the printed codes and retrieving the information from an internet-based database. Based on the information submitted by owners, products are categorized by their active ingredients, expiration dates, and forms, i.e., pills, capsules, powders, or gels. Unopened, non-expiring pharmaceuticals that are in shortages of supply are preserved for further quality check and potential re-distribution to patients in need. Other pharmaceuticals are sorted and prepared before being sent to specialized processing plants for subsequent extraction, recovery, and purification of their active ingredients into various products such as chemical reagents, veterinary drugs, or agrochemicals. Products with proprietary formulations are sent back to their manufacturers in bulk quantities for deformulation and reuse. After processing, quality checks are implemented to ensure the purity and safety of products for their prospective use. Such an integrated policy and technology framework will not only reduce the entry of bioactive pharmaceutical compounds into the environment, but alleviate the shortage and costs of pharmaceuticals and raw ingredients by tapping into the vast amounts of expired and unwanted pharmaceuticals that are left from the current pandemic and beyond.

5. Conclusion

The present review shows that, globally, the improper disposal of pharmaceutical wastes poses a threat to the ecosystem and human health. A survey of drug waste disposal methods in various locations found that, with the

exception of a few highly developed countries, the most common way of disposing of unused/expired drugs in low-, middle- and high-income countries was to throw them directly into the rubbish or pour them down the sink. Although drug take-back programmes are practised in some of those countries, the actual situation varies greatly, owing to the complexity of their respective social, economic and cultural circumstances. The main objective of exploring this issue is to reduce the harms such as environmental pollution caused by drug wastage, which can be intervened in the life cycle of drugs in the environment, for example, by conducting public education science on how to use drugs rationally, restricting the choice and purchase of medicines to reduce the storage of medicines in the home, improving the waste treatment technology to reduce the hazardous pollutants, and conducting drug recycling to improve the utilisation of medicines to reduce the wastage of medicines, so as to reduce the Drugs enter the environment. Drugs help people to regain their health, and human beings cannot live without them. To achieve this ultimate goal, it is necessary to take measures to reduce the health threat posed by drug wastage.

References

[1]. Rueda HernÁNdez, L.V., *Esperanza de vida e inicio de la etapa de adulto mayor.* Revista Salud Uninorte, 2022. **38**(1): p. 5-20.

[2]. Góralczyk, K. and A. Majcher, *Are the civilization diseases the result of organohalogen environmental pollution?* Acta Biochimica Polonica, 2019. **66**(2): p. 123-127.

[3]. Klein, E.Y., et al., *Global increase and geographic convergence in antibiotic consumption between 2000 and 2015*. Proceedings of the National Academy of Sciences of the United States of America, 2018. **115**(15): p. E3463-E3470.

[4]. Lahoud, N., et al., *Trends in the consumption of antibiotics in the Lebanese community between 2004 and 2016.* International Journal of Clinical Pharmacy, 2021. **43**(4): p. 1065-1073.

[5]. Bogdanic, N., et al., *Azithromycin consumption during the COVID-19 pandemic in Croatia, 2020.* Plos One, 2022. **17**(2).

[6]. Díaz, M.S., M.L. Martín-Calvo, and R. Mateos-Campos, *Trends in the Use of Anxiolytics in Castile and Leon, Spain, between 2015-2020: Evaluating the Impact of COVID-19.* International Journal of Environmental Research and Public Health, 2021. **18**(11).

[7]. Vukicevic, T., et al., *Consumption of psychotropic drugs in Croatia before and during the COVID-19 pandemic: a 10-year longitudinal study (2012-2021).* Social Psychiatry and Psychiatric Epidemiology, 2023.

[8]. Shao, S., et al., *Research progress on distribution, migration, transformation of antibiotics and antibiotic resistance genes (ARGs) in aquatic environment.* Critical Reviews in Biotechnology, 2018. **38**(8): p. 1195-1208.

[9]. Li, S.-W. and A.Y.-C. Lin, *Increased acute toxicity to fish caused by pharmaceuticals in hospital effluents in a pharmaceutical mixture and after solar irradiation.* Chemosphere, 2015. **139**: p. 190-196.

[10]. Cantwell, M.G., et al., *SELECTED PHARMACEUTICALS ENTERING AN ESTUARY: CONCENTRATIONS, TEMPORAL TRENDS, PARTITIONING, AND FLUXES.* Environmental Toxicology and Chemistry, 2016. **35**(11): p. 2665-2673.

[11].Kairigo, P., et al., *Contamination of Surface Water and River Sediments by Antibiotic and Antiretroviral Drug Cocktails in Low and Middle-Income Countries: Occurrence, Risk and Mitigation Strategies.* Water, 2020. **12**(5).

[12].Martin, J., et al., *Monitoring of pharmaceutically active compounds on the Guadalquivir River basin (Spain): occurrence and risk assessment.* Journal of Environmental Monitoring, 2011. **13**(7): p. 2042-2049.

[13].Suzuki, T., et al., *Environmental Risk Assessment of Active Human Pharmaceutical Ingredients in Urban Rivers in Japan.* Chemical & Pharmaceutical Bulletin, 2021. **69**(9): p. 840-853.

[14].Wilkinson, J.L., et al., *Pharmaceutical pollution of the world's rivers.* Proc Natl Acad Sci U S A, 2022. **119**(8).

[15].Gwenzi, W., T.T. Simbanegavi, and P. Rzymski, *Household Disposal of Pharmaceuticals in Low-Income Settings: Practices, Health Hazards, and Research Needs.* Water, 2023. **15**(3).

[16]. Ariffin, M. and T. S. T. Zakili, *Household Pharmaceutical Waste Disposal in Selangor, Malaysia-Policy, Public Perception, and Current Practices.* Environmental Management, 2019. **64**(4): p. 509-519.

[17].Magagula, B.K., I.T. Rampedi, and K. Yessoufou, *Household Pharmaceutical Waste Management Practices in the Johannesburg Area, South Africa.* International Journal of Environmental Research and Public Health, 2022. **19**(12).

[18].Mohammed, S.A., M.H. Kahissay, and A.D. Hailu, *Pharmaceuticals wastage and pharmaceuticals waste management in public health facilities of Dessie town, North East Ethiopia.* Plos One, 2021. **16**(10).

[19].Hanning, S.M., et al., *Quantification and composition of pharmaceutical waste in New Zealand.* Journal of Material Cycles and Waste Management, 2022. **24**(4): p. 1603-1611.

[20].Abahussain, E., M. Waheedi, and S. Koshy, *Practice, awareness and opinion of pharmacists toward disposal of unwanted medications in Kuwait.* Saudi Pharmaceutical Journal, 2012. **20**(3): p. 195-201.

[21]. Watkins, S., et al., *Household disposal of pharmaceuticals: attitudes and risk perception in a UK sample.* Journal of Material Cycles and Waste Management, 2022. **24**(6): p. 2455-2469.

[22].Dias-Ferreira, C., S. Valente, and J. Vaz, *Practices of pharmaceutical waste generation and discarding in households across Portugal.* Waste Management & Research, 2016. **34**(10): p. 1006-1013.

[23].Hajj, A., et al., *Assessment of knowledge, attitude, and practice regarding the disposal of expired and unused medications among the Lebanese population.* J Pharm Policy Pract, 2022. **15**(1): p. 107.

[24].Glassmeyer, S.T., et al., *Disposal practices for unwanted residential medications in the United States.* Environment International, 2009. **35**(3): p. 566-572.

[25].Alnahas, F., et al., *Expired Medication: Societal, Regulatory and Ethical Aspects of a Wasted Opportunity.* International Journal of Environmental Research and Public Health, 2020. **17**(3).

[26].Caban, M. and P. Stepnowski, *How to decrease pharmaceuticals in the environment? A review.* Environmental Chemistry Letters, 2021. **19**(4): p. 3115-3138.

[27].Dayom, D., et al., *Expired and leftover medicines in the home: potentials for accidental drug poisoning in children.* Int J Pharm Ther, 2014. **5**(4): p. 283-288.
[28].Kelly, F., et al., *'You don't throw these things out:'an exploration of medicines retention and disposal practices in Australian homes.* BMC Public Health, 2018. **18**(1): p. 1-12.
[29].Kumar, C., et al., *Drugs at Home: A Source of Potential Health Threats.* A Community-based Exploratory Study on the Patterns of Home Drug Storage Practices in South India, 2020. **8**(04): p. 7.
[30] . Naser, A. Y., et al., *Medications disposal and medications storage in Jordan: A cross‐sectional study.* International Journal of Clinical Practice, 2021. **75**(3): p. e13822.
[31].Li, S., et al., *Constructing Cd0. 5Zn0. 5S/Bi2WO6 S-scheme heterojunction for boosted photocatalytic antibiotic oxidation and Cr (VI) reduction.* Advanced Powder Materials, 2023. **2**(1): p. 100073.
[32].Oluwole, A.O., E.O. Omotola, and O.S. Olatunji, *Pharmaceuticals and personal care products in water and wastewater: A review of treatment processes and use of photocatalyst immobilized on functionalized carbon in AOP degradation.* BMC chemistry, 2020. **14**(1): p. 1-29.
[33].Wang, C., et al., *A novel organic/inorganic S-scheme heterostructure of TCPP/Bi12O17Cl2 for boosting photodegradation of tetracycline hydrochloride: Kinetic, degradation mechanism, and toxic assessment.* Applied Surface Science, 2023. **610**: p. 155346.
[34].Dai, H., J. Han, and E. Lichtfouse, *Who is running faster, the virus or the vaccine?* 2020, Springer. p. 1761-1766.
[35].Sun, S., J. Li, and J. Han, *How human thermal plume influences near-human transport of respiratory droplets and airborne particles: a review.* Environmental Chemistry Letters, 2021. **19**: p. 1971-1982.

The Cross-species Adaptation of Influenza A Virus from Pet Dogs

Min Zhu*, Ying Chen

College of Animal Science and Technology, Guangxi University, Nanning, 530000, P.R. China
*E-mail: minzhu0907@st.gxu.edu.cn

Abstract: Influenza A viruses (IAVs) are highly contagious pathogen that could infect a wide range of mammalian hosts, including humans, pigs and dogs. The production of novel IAVs through reassortment between subtypes results in the cross-species transmission from avian to mammals, which poses a risk for public health. Previous studies have found that the swine-origin influenza A virus (H1N1/2009) crossed species barriers successfully to infect humans and caused pandemic worldwide through human-to-human transmission. When the reassortment happens between animal influenza viruses, the novel viruses could cross species barriers to infect humans, leading to the emergence of viruses with pandemic potential. This article demonstrates the novel mechanism of cross-species adaptation of swine-origin H1N1 canine influenza virus (CIV) to new host by serial lung-to-lung passages in mice. Reverse genetic substitution of the viral genes and mutation experiments demonstrated that the mutations in PA-T97I could enhance the polymerase activity. Furthermore, a combination of HA (N198D and A227E) with NS(A53D) in the rLZ57-WT backbone resulted in efficient replication and a significant increase in virulence, which highlights the importance of surveillance programs in pet dogs to monitor the emergence of IAVs carrying the adaptive mutations.

Keywords: adaptation, cross-species, humans, influenza A virus, pet dogs

1. Introduction

Influenza A virus (IAV) is an important pathogen that infect a wide range of mammalian and avian species. In particular, the acquisition of adaptive mutations by repeated infection and replication could accelerate the evolution of the viral genome and help it adapt to new hosts. During the last two decades, IAVs have jumped from horses to dogs (H3N8) and birds to dogs (H3N2) (Crawford et al., 2005; Zhu et al., 2015), and viral adaptation is primarily responsible for the jump across these species. In addition, there were spillover subtypes found in dogs, including H5N1, H5N2, H6N1 and H9N2 avian influenza virus, as well as H1N1, H3N2, and pandemic 2009 H1N1 human influenza viruses(Chen, 2010; Lin et al., 2015; Sun, 2013; Wasik et al., 2021; Zhan et al., 2012). In our previous study, two reassortant Eurasian avian-like (EA) H1N1 swine influenza virus genotypes possessing four internal segments from the pandemic H1N1 2009 influenza virus (H1N1 pdm/09) lineage (PB2, PB1, PA and NP) were individually introduced from pigs into dogs. These had the potential to infect and be transmitted to humans(Chen et al., 2018; Wang, 2019). However, little is known about the mutations required for H1N1 influenza viruses that originate in pigs to overcome the species barrier and their ability to adapt to new hosts.

Adaptation is considered to be a primary impetus during evolution, and the process of natural selection in IAVs can be mimicked by their experimental adaptation in mice(Brown et al., 2001). Numerous studies have shown that the amino acid substitutions associated with HA, NP, NA, M and NS genes and the polymerase genes during mouse adaptation could be critical determinants of virulence, tissue tropism and pathogenicity(Evseev and Magor, 2021; Hu and Liu, 2015; Paterson and Fodor, 2012; Taubenberger and Kash, 2010). The HA protein determined the binding specificity by mediating the attachment of viruses to host-cell sialyloligosaccharide receptors via binding sites, and this was a primary determinant for mouse lung virulence(Ward, 1997). The viral ribonucleoprotein (vRNP) complex contributed to the host species adaptation by increasing the polymerase activity and virus replication efficiency in mammals. For example, the Glu-to-Lys substitution at position 627 (E627K)(Subbarao et al., 1993) and the Asp-to-Asn substitution at position 701 (PB2-D701N) were identified as key determinants for adaptation of avian influenza virus to a new host species(Gabriel et al., 2005). The mouse-adapted 2009 pandemic influenza virus (H1N1 pdm/09) became pathogenic in mice and demonstrated polymerase-activity-enhancing mutations (PB2-E158G and PA-L295P)(Ilyushina, 2010; Zhou et al., 2011).

In order to understand the cross-species adaptation mechanism of the novel swine-origin H1N1 canine influenza virus bearing H1N1 pdm/09 segments in a mammalian model, we generated a mouse-adapted variant, A/canine/Guangxi/LZ57/2015 (H1N1) (LZ57). This involved serial lung-to-lung passages in mice which resulted in six adaptive mutations, located in the PB2 (E578D) and PA (T97I) of the polymerase complex, the HA (N198D and A227E), NS1 (A53D) and NEP (R42K). This paper will provide new insights into the cross-species adaptation mechanism and factors that affect the virulence and replication capacity of IAVs in mammals.

2. Methods

2.1. Virus and cells

Madin-Darby canine kidney (MDCK) cells, human embryonic kidney cells (293T) and adenocarcinomic human alveolar basal epithelial cells (A549) were maintained in Dulbecco's Modified Eagle's Medium (DMEM, Corning) supplemented with 10 % fetal bovine serum (FBS, Gibco) and 1×penicillin-streptomycin liquid (Solarbio, Beijing, China) at 37℃, 5 % CO_2. The H1N1 A/Canine/Guangxi/LZ57/2015(H1N1) (LZ57) influenza virus was originated from the purification of A/Canine/Guangxi/LZ56/2015(H1N1) (LZ56) by plaque assay for three times. The LZ57 virus naturally harbored a 135-amino acid truncation in the effector domain of NS1 protein, which exibited low pathogenicity in mice based on previous studies (data not shown).

2.2. Mouse experiments

To determine the lethal mouse-adapted variant viruses and evaluate the pathogenicity of different recombinant viruses, groups of 6-week-old female BALB/c mice (Charles River, Beijing) were lightly anesthetized and inoculated intranasally with 10^6 PFU/50 μL of five H1N1 mouse-adapted variant viruses in a volume of 50 μL. The control group was inoculated intranasally with 50 μL phosphate-buffered saline (PBS). Three mice in each group

were euthanized and lung tissues were collected to assess viral replication in MDCK cells on 3 dpi. Clinical symptoms, body weight and survival rate were monitored and recorded until 14 dpi. Mice were humanely euthanized when the body weight loss was above 25 % of the pre-inoculation weight. The virus stock with the highest virulence in mice was designated as the mouse-adapted virus (LZ57-MA).

The 50 % mouse-lethal dose (MLD_{50}) was determined by inoculating groups of five BALB/c mice intranasally with 10-fold serial dilutions of each viruses (from 10^1 to 10^6 PFU per mouse). As described above, the healthy status and body weight were monitored daily for 14 dpi. The MLD_{50} were calculated by the method of Reed-Muench.

2.3. Genome sequencing and alignment

Total viral RNA of the LZ57-WT and LZ57-MA variant (the 13th passage purified by plaque assay) was extracted using QIAmp Viral RNA Mini Kit (Qiagen Germantown, MD, USA) following manufacturer's instructions. Reverse transcription and amplification of the full-length genome were performed using segment-specific primers(Chen et al., 2018). The PCR products were purified and sequenced by the method of Sanger (Shanghai, China) and nucleotide sequences were aligned using the Lasergene sequence analysis software package (DNAStar, Madison, WI).

2.4. Construction of plasmids and virus rescue

All nucleotide sequences of LZ57-WT and LZ57-MA viruses were amplified and digested with *Sap* I, and then cloned into the *Sap* I site of ambisense plasmids (pDZ), which was kindly provided by Dr. Adolfo García-Sastre (Icahn School of Medicine at Mount Sinai, New York, USA). Mutations in HA and NS genes were introduced by PCR-based site-directed mutagenesis with primer pairs containing point mutations. All of the constructs were confirmed by sequencing. Consequently, eight plasmids of about 4 μg (~0.5 μg per plasmid) were transfected into 293T cells by using 12 μL Lipofectamine 2000 (Invitrogen) according to the manufacturer's instructions. After 24 hours post-transfection (hpt), the supernatant was harvested and inoculated in MDCK cells and passaged for three times until the obvious cytopathic effect (CPE). All rescued viruses were completely sequenced to confirm the absence of unwanted mutations. Virus titers were determined by plaque assay three replicate for each sample on MDCK cells and calculated by Reed-Muench method.

2.5. Viral growth kinetics

The wild-type and mouse-adapted viruses were inoculated into MDCK cells at a multiplicity of infection (MOI) of 0.01. The mutated viruses were inoculated in monolayer MDCK or A549 cells at a MOI of 0.01 and 0.1, respectively. Cells were cultured with serum-free DMEM including 1μg/mL of TPCK trypsin. After incubation at 37℃ for 1 h, the cell supernatants were harvested at 12, 24, 36, 48, 60 and 72 hours post-infection (hpi) and titrated in MDCK cells by plaque assays. Each sample consisted to three replicates and analyzed using the Reed-Muench method.

2.6. Minigenome assay

To compare the activities of viral ribonucleoprotein (RNP) complexes (PB2, PB1, PA and NP), the four plasmids (PB2, PB1, PA and NP genomes in pDZ) (500 ng each), 100 ng of the luciferase reporter plasmid (pLuci) and 50 ng of the internal control plasmid (pRL-TK) were co-transfected into 293T cells at 37 ℃. After 24 hpt, the cell lysates were collected for measuring luciferase activity using the Dual-Luciferase activity Reporter Assay System (Promega, USA). The polymerase activity was

normalization by firefly luciferase activity to Renilla luciferase activity. There were two replicates for each complex combination each time, and all experiments were performed three times.

2.7. Prediction of HA protein structure

To understand the effect of mutations of HA protein to the structure and function, the partial structure models of HA complex of LZ57-WT and LZ57-MA were generated by the online prediction platform I-TASSER (https://zhanglab.dcmb.med.umich.edu/I-TASSER/). PyMOL software (http://www.pymol.org/pymol/) was used to analysis the predicted result and form the visual images.

2.8. Statistical analyses

All statistically analyses were performed using GraphPad Prism 6.0 (GraphPad Software, San Diego, CA, USA). Statistically significant differences among groups were determined using analysis of variance (ANOVA). Differences were considered Statistically significant at a *P* value by * ($P < 0.05$), ** ($P < 0.01$), *** ($P < 0.001$), **** ($P < 0.0001$)

3. Results and Discussion

3.1 Adaptation of an H1N1 influenza virus in mice

In our previous study, a selected swine-origin EA H1N1 virus was originally isolated from domesticated dogs (LZ57), and it was derived from A/Canine/Guangxi/LZ56/2015 (LZ56)(Chen et al., 2018). It had a similar internal gene lineage to G4 EA H1N1. In particular, this EA H1N1 canine virus was found to predominantly bind to the human receptor and efficiently transmit between guinea pigs via direct contact(Wang, 2019). Notably, this virus differed from those in the majority of EA H1N1 viruses, which contained a deletion of amino acids at position 81–126 in NS1. Although this virus could replicate efficiently in the lungs, it was found to be less virulent in mice inoculated with 10^5 PFU/50 μL (data not shown). Whether this could adapt to mice thus resulting in the enhanced virulence and replication-capable virus is poorly understood. Herein, we serially passaged the LZ57 virus by lung-to-lung transfer in BALB/c mice in order to study the molecular basis of adaptation to new host species. The body weights of the mice and virus titers in lungs were evaluated from the 1st to 13th passage (Fig. 1a). After ten passages, the mice displayed a continuous trend of body weight loss and high replication ability in mouse lung. In order to obtain a more stable mouse-adapted virus, the H1N1 influenza virus was passaged until the 13th passage. As a result, the weight loss, survival rate and viral titers in mouse lungs exhibited markedly virulence, compared to the wild-type virus, indicating that virus populations of the mouse-adapted variants had acquired mutations that affected the increased virulence (Fig. 1b).

There were five plaques with different sizes (MAP13-A, MAP13-B, MAP13-C, MAP13-D and MAP13-E), that were cloned and inoculated into cultures of MDCK cells in order to prepare a virus stock for testing in mice. The MAP13-A virus exhibited the largest plaques when compared to the other four. Five plaques with a single phenotype were selected and tested in mice (Figs. 1c and 1d). Finally, MAP13-A virus which displayed the highest virulence when compared to the other cloned viruses, was sequenced and the consistency of genome sequences determined was confirmed and it was designated as the LZ57-MA virus.

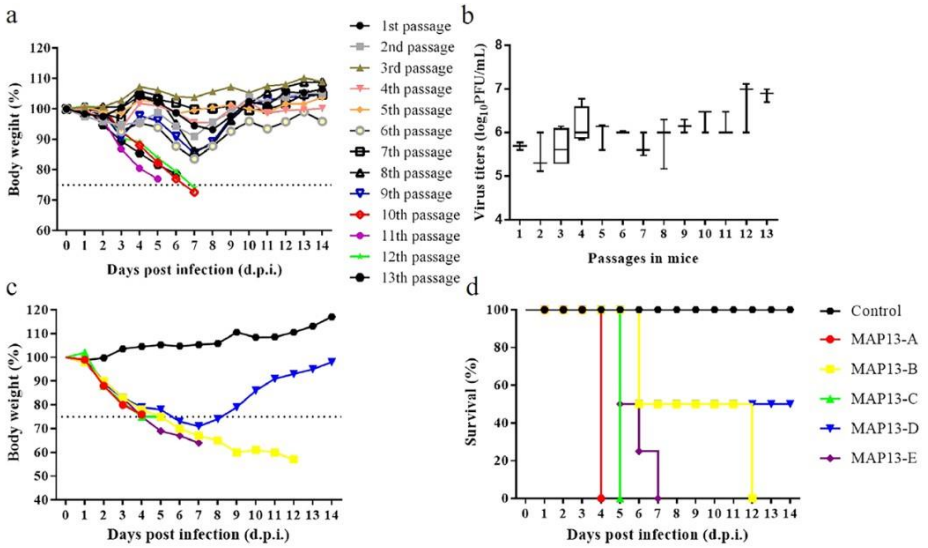

Fig. 1. The generation of the mouse-adapted H1N1 influenza virus. Six-week-old female BALB/c mice (n = 6 per group) were inoculated intranasally with a dose of 10^5 PFU/50 µL of LZ57-WT virus and passaged from lung-to-lung until the 13th passage.
(a) The changes in body weights (from the 1st to 13th passage) and (b) the viral titers of mouse-adapted isolates in the lungs were determined by using the plaque assay. (c) The changes in body weights of five purified-plaques of the mouse-adapted viruses and (d) the mouse mortality in the five groups was determined by survival rate.

3.2 Pathogenicity and replication of the wild-type and mouse-adapted H1N1 viruses in vitro and in vivo

Two groups of BALB/c mice were infected with 10^6 PFU of LZ57-WT and LZ57-MA viruses. The mice inoculated with LZ57-WT displayed a slight weight loss and died at 7 dpi (33% survival). In contrast, severe clinical signs including decreased general activity, ruffled fur and huddling were observed in the group LZ57-MA-inoculated group. All the mice in this group lost weight progressively and died before 5 dpi (Figs. 2a and 2b) and they had a higher virus titer of 6.87 Log_{10} PFU/mL in the lungs at 3 dpi ($P < 0.01$) (Fig. 2c). Growth kinetics in vitro revealed that there was an obvious replicative advantage compared to the wild-type virus (Fig. 2d), suggesting the mouse-adapted H1N1 virus exhibited enhanced virulence in mice and they were able to replicate efficiently in MDCK cells.

To understand the molecular basis that was responsible for the increased virulence during the adaptation of a swine-origin H1N1 canine virus to mice, the full-length genome sequences of both the LZ57-WT and LZ57-MA were compared. Sequence analysis identified six acquired mutations in the mouse-adapted virus and these were in the polymerase proteins (PB2-E578D and PA-T97I), hemagglutinin (HA- N198D and HA-A227E), NS1 (NS1-A53D) and nuclear export protein (NEP-R42K). The statistical results of influenza viruses of different origins at specific positions showed that the residues of PB2-578E, PA-97T and NEP-42R were commonly present in most of the influenza viruses that still had advantageous selection. All of six adaptive mutations could be found in the swine H1N1 virus, but some of them were rare, including PB2-578D, PA-97I, HA-198D and NEP-42K (Table 1). In particular, the residues in PA-97I had previously been detected in some human, swine and equine isolates. Interestingly, the amino acids present in HA-227 varied depending on the origin of virus. The glutamic acid residue at position 227 in HA was detected in the majority of human (99.6%) and swine viruses (26.3%), but most of the canine, avian and equine viruses possessed a serine residue at this position, suggesting that this amino acid might be involved in host specificity.

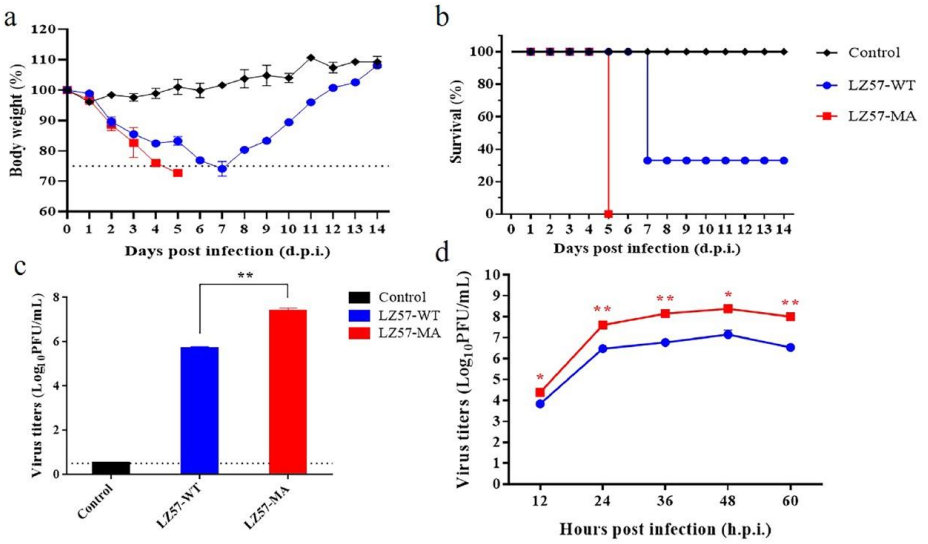

Fig. 2. The increased virulence of the mouse-adapted H1N1 influenza virus in mice. Six-week-old female BALB/c mice were inoculated intranasally with a dose of 10^6 PFU/50 μL of each virus or PBS which was used as the control. (a) The changes in body weights and (b) the mortality of LZ57-MA was evaluated based on the survival rates. The replication of viruses in mouse lungs was titrated by using the plaque assay (c). Viral growth kinetics of LZ57-WT and LZ57-MA viruses in cultured MDCK cells (MOI=0.01) (d). The asterisks indicate the P-values (* $P < 0.05$; ** $P < 0.01$; *** $P < 0.001$) compared to the wild-type viruses.

Table 1
Amino acid substitutions identified in LZ57-MA virus protein during mouse adaptation.

Protein	Position	Changes of amino acids in influenza viruses[a]						
		LZ57-WT	LZ57-MA	Human (H1N1) (2009–2020)	Swine (H1N1) (2009–2020)	Canine	Avian (H3N2)	Equine (H3N8)
PB2	578	E	D	E(3983/3988) G(4/3988) Q(1/3988)	E(1575/1576) D(1/1576)	E(152/152)	E(263/263)	E(120/120)
PA	97	T	I	T(4266/4273) I(7/4273)	T(1598/1615) A(12/1615) S(3/1615) I(1/1615) K(1/1615)	T(162/164) A(1/164) N(1/164)	T(291/291)	T(108/109) I(1/109)
HA[b]	198	N	D	A(11357/11957) E(534/11957) T(25/11957) V(25/11957) N(7/11957) G(4/11957) S(4/11957) P(1/11957)	A(3076/3891) E(177/3891) N(572/3891) T(27/3891) S(17/3891) V(12/3891) D(4/3891) K(4/3891) I(1/3891) P(1/3891)	H3N2: A(153/155) V(2/155) H3N8: A(1/196) E(195/196) H5:P(3/3) H9N2:T(1/1) H6N1:G(1/1) H1N1:A(2/2)	A(381/389) T (5/389) N(1/389) S (1/389) V (1/389)	E(818/844) A(13/844) G(13/844)
	227	A	E	E(11815/11863) A(20/11863) K(10/11863) G(9/11863) D(3/11863) Q(3/11863) P(2/11863) H(1/11863	A(2698/3889) E(1022/3889) T(94/3889) S(57/3889) G(12/3889) V(3/3889) K(2/3889) Q(1/3889)	H3N2:S(155/155) H3N8:S(196/196) H5:S(5/5) H9N2:Q(1/1) H6N1:R(1/1) H1N1:E(2/2)[c]	S(386/389) P(3/389)	S(832/843) P(9/843) A(1/843) T(1/843)
NS1	53	A	D	D(2490/2607) N(101/2607) E(11/2607) Y(2/2607) G(2/2607) A(1/2607)	D(870/1243) E(313/1243) N(40/1243) K(8/1243) G(7/1243) A(2/1243) S(2/1243) Y(1/1243)	D(163/163)	D(228/230) N(2/230)	D(86/96) N(7/96) G(3/96)
NEP	42	R	K	R(792/801) G(3/801) K(3/801) T(2/801) I(1/801)	R(693/697) G(2/697) K(2/697)	R(95/97) K(1/97) G(1/97)	R(119/120) K(1/120)	R(43/43)

[a] The isolates observed in nature containing specific amino acids, which come from Influenza Research Database (https://www.fludb.org/).
[b] H3 numbering.
[c] A/canine/Beijing/cau2/2009(H1N1)(JN540086); A/canine/Beijing/cau9/2009(H1N1)(JN540094).

3.3 The HA and NS genes played a key role in the higher virulence of LZ57-MA

Reverse genetics was employed to investigate the differences in the virulence between LZ57-WT and LZ57-MA. Eight gene segments from LZ57-WT and LZ57-MA were inserted into the pDZ vector and the LZ57- WT and LZ57-MA viruses were rescued. These were designated as rLZ57-WT and rLZ57-MA, respectively. After confirmation by sequence analysis, the rescued viruses were added to cultured MDCK cells for the subsequent experiments. After infecting mice with serial 10-fold dilutions of the recombinant viruses as shown in Fig. 3, the MLD_{50} of the wild-type and mouse-adapted viruses were found to be 5.75 (rLZ57-WT) and 2.75 Log_{10} PFU (LZ57-MA), respectively. This suggested that there was a clear disparity in their virulence. When the recombinant rLZ57-WT viruses were replaced with the PB2, PA, HA and NS genes, they showed a moderate increase in virulence (ranging from 4.25 to 4.5 log_{10} PFU). When either two or three segments replaced the rLZ57-WT segments, the recombinant viruses showed higher pathogenicity levels relative to the MA viruses, except for rLZ57-ma (PA+NS) and rLZ57-ma (PB2 +PA+NS) which showed a slightly lower virulence. Notably, the greatest effects were seen upon introduction of the HA and NS segments (MLD_{50}, 1.5 versus 2.75 log PFU/mL), relative to the MA virus (>101.25- fold increase in MLD_{50}). These combined results indicated that the mutant HA and NS genes played an important role in the increased virulence of these viruses, no matter whether they interacted with PA or PB2 gene.

Although the single mutation in PA-T97I and PB2-E578D did not show obvious increase in virulence, they interacted individually with these two genes to significantly enhanced their virulence in mice. PA-97I has been identified as a key factor for adaptation and virulence in mice(Song, 2009), which was also shown to produce a higher polymerase activity in our study. Similarly, the PB2-E578D was also found in the Song's experiments, but it did not have any effect on virulence. Interestingly, the efficient polymerase activity was suppressed by a combination of PB2-578D and PA-97I in the wild-type virus (Fig. S1), and this was consistent with a lower virulence in mice. In contrast, this underlined the importance of virulent determinants of the HA and NS genes in the MA virus.

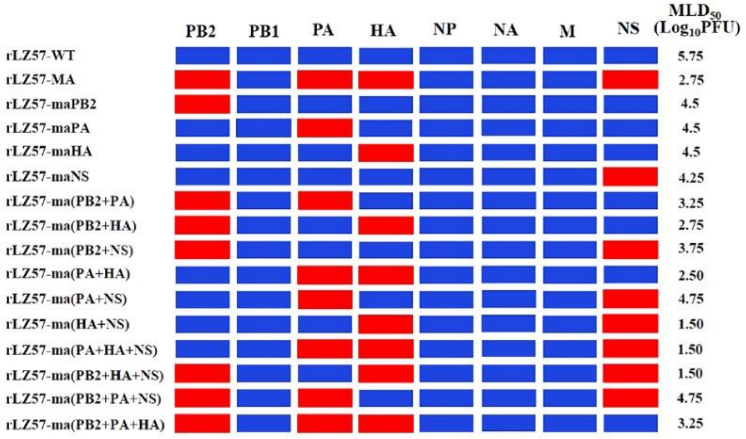

Fig. 3. Virulence of the recombinant viruses (rLZ57-WT and rLZ57-MA) in mice. The gene segments of rLZ57-WT virus were exchange on the rLZ57-MA backbone. Gene segments derived from the wild-type and mouse-adapted viruses are shown in blue and red, respectively. The MLD_{50} values were determined by inoculating groups of five BALB/c mice with 10-fold serial dilutions of the stock recombinant viruses (from 10^1 to 10^6 PFU per mouse).

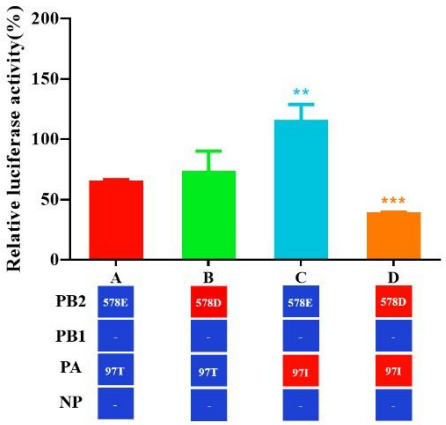

Supplementary Figure 1 Effects of the mouse-adapted mutations on polymerase activity. The polymerase activity of reconstituted RNP complexes composed of the PB2, PB1, PA, and NP plasmids of the wild-type (rLZ57-WT) and mouse-adapted virus (rLZ57-MA). The NP plasmid in these complexes is the same. Luciferase activity values were measured at least three times. The asterisk indicates a *P*-value (**P<0.01, ***P<0.001) compared to the polymerase activity of the reconstituted RNP of the wild-type virus.

3.4 A combination of HA (N198D A227E) and NS1 (A53D) had a significantly enhanced virulence and replication capacity

Recombinant viruses with single or multiple different point mutations in the HA, NS1 and NEP proteins were generated to assess the key roles of these substitutions in virulence (Fig. 4) and replication in cultured MDCK and A549 cells (Fig. 5). The rLZ57 recombinants with single-point mutations of HA and NS genes, except for the N198D mutations (MLD_{50}, >5.0 versus 2.5), showed some increased virulence, but this was still less than that of the MA virus. Surprisingly, the eight recombinants with the combined mutations of HA and NS gene exhibited a level of virulence similar to that of the rLZ57-MA, except for rLZ57-ma [HA(N198D) +NS(R42K)] (MLD_{50}, 4.25 versus 2.5, respectively). In particular, the combination of HA (N198D A227E) gene with NS1 (A53D) could produce a synergistic effect on the significantly increased virulence when compared to the MA virus (>10-fold increase in MLD_{50}).

The growth yields of these recombinant viruses containing different mutations displayed a trend of increased yields in MDCK and A549 cells (Fig. 5a). In MDCK cells, the HA (N198D A227E) and NS (A53D) substitutions produced maximum yields (6.0 and 6.9 $\log_{10}$ PFU/mL, respectively) when compared to other viruses at the early time point (12 and 24 hpi). In A549 cells, the HA (N198D) and NS (R42K) produced a maximum yield at 36 hpi (6.29 $\log_{10}$ PFU/mL), but this was reduced after that point time when compared to the other viruses. In contrast, both the mutations with HA (N198D A227E) and NS (A53D)/(R42K) as well as HA (A227E) and NS (R42K) were synergistic after their combination, resulting in enhanced replication at a later point time (60 hpi). Consistent with the growth curve, the plaque size changed due to individual mutations of the HA and NS genes (Figs. 5b and 5c). Interestingly, there were similar plaque sizes between the MA and wild-type viruses, but the combination of HA (A227E) and NS (R42K) formed the largest plaques among these substitutions ($P < 0.0001$). This suggested that the reassortant viruses containing these mutations could be the key determinants for controlling the plaque size.

Viruses	PB2	PA	HA		NS1	NEP	MLD_{50} (Log_{10} PFU)
	578	97	198	227	53	42	
rLZ57-WT	E	T	N	A	A	R	5.75
rLZ57-MA	D	I	D	E	D	K	2.75
rLZ57-maHA(N198D)	E	T	D	A	A	R	>5.0
rLZ57-maHA(A227E)	E	T	N	E	A	R	NA[a]
rLZ57-maNS(A53D)	E	T	N	A	D	R	3.25
rLZ57- maNS(R42K)	E	T	N	A	A	K	3.5
rLZ57-ma[HA(N198D)+NS(A53D)]	E	T	D	A	D	R	2.5
rLZ57- ma[HA(N198D)+NS(R42K)]	E	T	D	A	A	K	4.25
rLZ57-ma[HA(A227E)+NS(A53D)]	E	T	N	E	D	R	2.25
rLZ57-ma[HA(A227E)+NS(R42K)]	E	T	N	E	A	K	2.25
rLZ57-ma[HA(N198D)+NS]	E	T	D	A	D	K	2.75
rLZ57-ma[HA(A227E)+NS]	E	T	N	E	D	K	2.5
rLZ57-ma[HA+NS(A53D)]	E	T	D	E	D	R	1.5
rLZ57- ma[HA+NS(R42K)]	E	T	D	E	A	K	1.75

Figure 4 Virulence in mice with HA and NS mutations. The colors indicate the encoded amino acids from wild-type (blue) and mouse-adapted (red) viruses. The amino acid differences between PB2, PA, HA, and NS of virus strains rLZ57-WT and rLZ57-MA are shown as single letters with position indicated at the top. The MLD_{50} was determined by inoculating groups of five BALB/c mice intranasally with 10-fold serial dilutions of each viruses (from 10^1 to 10^6 PFU per mouse).[a]NA represents the virus with A227E mutation can not be rescued and the MLD_{50} is not applicable.

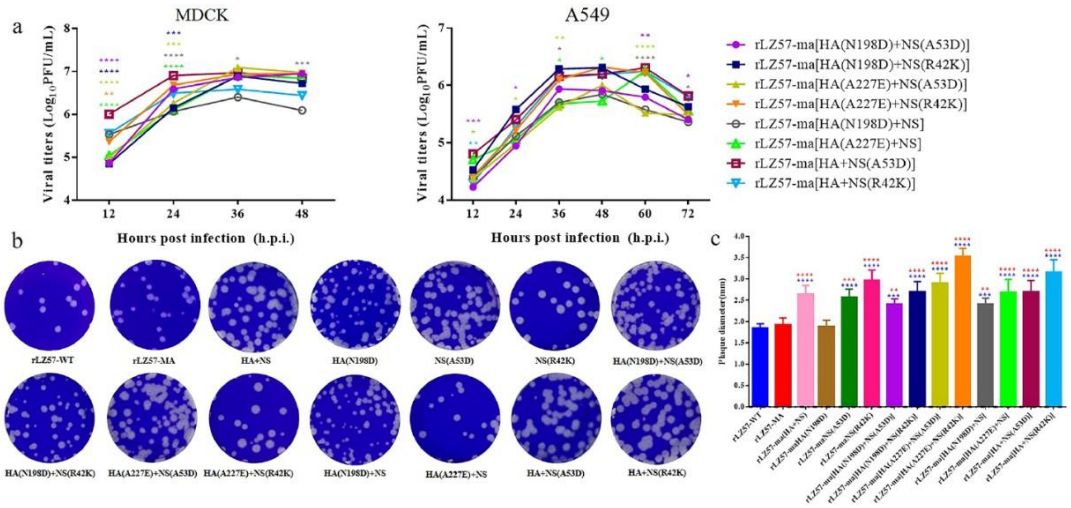

Fig. 5. Growth properties of the mutated viruses. (a) Growth curves after inoculation of mutated viruses at MOIs of 0.01 and 0.1 into MDCK and A549 cell, respectively (** $P < 0.01$; *** $P < 0.001$; **** $P < 0.0001$). (b) Plaque phenotypes of the viruses with wild-type, mouse-adapted, HA and NS mutations. The viruses were inoculated with 10-fold serial dilutions of the different viruses at 37 ℃ for 1 h in cultured MDCK cells. Infected cells were incubated for 60 hpi before staining with 0.8% (w/v) crystal violet solution. (c) The areas with individual plaques were measured from scanned images using ImageJ software. The diameters of selected plaques were calculated and the data collected. They were analyzed by GraphPad Prism 6.0 and normalized to the wild-type virus.

The HA protein is the key determinant for mouse lung virulence. A number of studies have shown that the mutations in the HA protein conferred its pathogenicity/virulence, transmissibility and host adaptation by changes in its biological properties(Gao et al., 2009; Keleta et al., 2008; Kong et al., 2021; Matrosovich et al., 2000; Tumpey et al., 2007; Wang et al., 2017; Yang et al., 2013; Zheng et al., 2010). The mouse-adapted rLZ57-MA acquired N198D and A227E mutations within the receptor binding site (RBS) of the HA protein. The amino acid residues in the RBS region were critical for the recognition of different-origin influenza viruses and alterations in the cell receptor(Matrosovich et al., 2000; Stevens et al., 2006). The mutation of Asn-to-Asp at position 198 (H3 numbering) in the H1 HA1 domain of the mouse-adapted virus resulted in the loss of a glycosylation site, which is known to be a common mechanism for acquisition of virulence(Ward, 1997). Ilyushina et al. found that the amino acid changes at position 198 (N198D) in the H9 HA protein might contribute to the restoration of virulence that is associated with the loss of the

glycosylation(Ilyushina, 2010).

Residue 227 is commonly alanine (A) in swine H1 influenza viruses. However, H1N1 pdm/09 contains a glutamic acid (E) residue at this position. In addition, residue 227 E occurs frequently in the human seasonal viruses (Table 1), suggesting that this position could serve as the interaction between the virus and its human host(van Doremalen et al., 2011). de Vries et al. found that the introduction of a E227A mutation into swine-origin HA protein could result in more efficient binding to α2,6-linked sialic acid. However, a combination of T200A and E227A mutations in the swine H1 protein had a synergistic effect that mainly contributed to the receptor binding affinity(de Vries et al., 2011). Nevertheless, the combination of 219I and 227E in the new pandemic H1 protein resulted in the disruption of interaction with the α2–6 sialylatedglycans(Maines et al., 2009). However, the mutations of 219K and 227E corrected this interaction network and played an important role in binding to sialic acid and increasing its transmissibility(Jayaraman et al., 2011). In our study, the location of the RBS in the crystal structure showed that the substitution of the residues at positions 198 (N198D) and 227 (A227E) resulted in interactions between A227E and 220R (220-loop) as well as 198D and 199H (190-helix) by potential hydrogen bonds (Fig. 6). This suggests that the double mutations in HA might play a crucial role in the receptor binding specificity. More biological properties of the receptor-binding and tissue tropism need to be investigated in future studies.

Our study clarified that NS1 was a multifunctional protein that played a key role in the inhibition of the host innate immune response and viral replication(Evseev and Magor, 2021; Forbes et al., 2012; Hale et al., 2008; Jiao et al., 2008; Selman et al., 2012). In our study, the NS1-A53D and NEP-R42K substitutions were found in the mouse-adapted virus, and they contributed to the enhanced virulence. The NS1-A53D substitution commonly exists in all species and are highly conserved. The NEP-R42K mutation can also be observed in other species, including avian-origin canine and H3N2 avian influenza viruses (Table 1). These were not previously implicated in increased virulence. The acquisition of adaptive mutations in NEP facilitated the avian influenza viruses escape the restrictions of the vial genome by enhancing the polymerase activity in order for them to cross the species barrier(Mänz et al., 2012). Whether these adaptive mutations that led to increased virulence and replication were caused by participating directly in RNA binding, interferon suppression and overcoming the restriction in the polymerase activity still need to be further investigated.

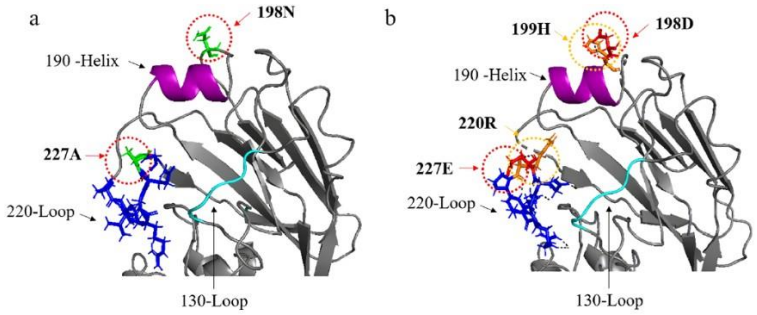

Fig. 6. Comparison of the amino acid mutations between the (a) wild-type and (b) mouse-adapted canine H1N1 viruses. Three components of the HA receptor-binding pocket: the 130-loop (131–135aa), 190-helix (184–191aa) and 220-loop (218–225aa) are shown in cyan, purple and blue, respectively. The amino acids at positions 198 and 227 that were identified in the LZ57-MA virus were mapped on the HA crystal structure. The red arrow indicates the mutation of amino acids.

4. Conclusions

We obtained a highly pathogenic adaptive virus through lung-to-lung passage in mice, which contained six adaptative mutations, and found that the combination of the HA and NS genes resulted in a virulent phenotype in mice. This paper provides new insights into the cross-species adaptation of IAV from pet dogs and the potentially novel virulent determinants of the H1N1 influenza virus.

References

Brown, E.G., Liu, H., Kit, L.C., S. Baird*§, a.M.N., 2001. Pattern of mutation in the genome of influenza A virus on adaptation to increased virulence in the mouse lung identification of functional themes. Proc Natl Acad Sci U S A. 98, 6883-6888.

Chen, Y., Trovão, N.S., Wang, G., Zhao, W., Ouyang, K., Huang, W., García-Sastre, A., He, P., Zhou, H., Nelsond, M. I., 2018. Emergence and Evolution of Novel Reassortant Influenza A Viruses in Canines in Southern China. mbio 9, e00909-00918.

Chen, Y., Zhong, G., Wang, G., Deng, G., Li, Y., Shi, J., Zhang, Z., Guan, Y., Jiang, Y., Bu, Z., Kawaoka, Y., Chen, H., 2010. Dogs are highly susceptible to H5N1 avian influenza virus. Virology 405, 15-19.

Crawford, P.C., Dubovi, E.J., Castleman, W.L.S., Iain.; Gibbs, E. P. J.; Chen, Limei.; Smith, Catherine.; Hill, Richard C.; Ferro, Pamela.; Pompey, Justine.; Bright, Rick A.; Medina, Marie-Jo.; Influenza Genomics Group; Johnson, Calvin M.; Olsen, Christopher W.; Cox, Nancy J.; Klimov, Alexander I.; Katz, Jacqueline M.; Donis, Ruben O., 2005. Transmission of equine influenza virus to dogs. Science (New York, N.Y.) 310, 482-485.

de Vries, E., Tscherne, D.M., Wienholts, M.J., Cobos-Jiménez, V., Scholte, F., García-Sastre, A., Rottier, P.J.M., de Haan, C.A.M., 2011. Dissection of the Influenza A Virus Endocytic Routes Reveals Macropinocytosis as an Alternative Entry Pathway. PLoS Pathog 7.

Evseev, D., Magor, K.E., 2021. Molecular Evolution of the Influenza A Virus Non-structural Protein 1 in Interspecies Transmission and Adaptation. Frontiers in microbiology 12, 693204.

Forbes, N.E., Ping, J., Dankar, S.K., Jia, J.-J., Selman, M., Keleta, L., Zhou, Y., Brown, E.G., 2012. Multifunctional Adaptive NS1 Mutations Are Selected upon Human Influenza Virus Evolution in the Mouse. PloS one 7.

Gabriel, G., Dauber, B., Wolff, T., Planz, O.H.-D.K., J. Stech and Peter Palese, 2005. The viral polymerase mediates adaptation of an avian influenza virus to a mammalian host. Proc. Natl. Acad. Sci. USA 102, 18590-18595.

Gao, Y., Zhang, Y., Shinya, K., Deng, G., Jiang, Y., Li, Z., Guan, Y., Tian, G., Li, Y., Shi, J., Liu, L., Zeng, X., Bu, Z., Xia, X., Kawaoka, Y., Chen, H., 2009. Identification of Amino Acids in HA and PB2 Critical for the Transmission of H5N1 Avian Influenza Viruses in a Mammalian Host. PLoS Pathogens 5.

Hale, B.G., Randall, R.E., Ortín, J., Jackson, D., 2008. The multifunctional NS1 protein of influenza A viruses. J Gen Virol 89, 2359-2376.

Hu, J., Liu, X., 2015. Crucial role of PA in virus life cycle and host adaptation of influenza A virus. Med. Microbiol, Immunol 204, 137-149.

Ilyushina, N.A., Khalenkov, A. M., Seiler, J. P., Forrest, H. L., Bovin, N. V., Marjuki, H., Barman, S., Webster, R. G., Webby, R. J., 2010. Adaptation of pandemic H1N1 influenza viruses in mice. Journal of virology 84, 8607-8616.

Jayaraman, A., Pappas, C., Raman, R., Belser, J.A., Viswanathan, K., Shriver, Z., Tumpey, T.M., Sasisekharan, R., 2011. A Single Base-Pair Change in 2009 H1N1 Hemagglutinin Increases Human Receptor Affinity and Leads to Efficient Airborne Viral Transmission in Ferrets. PloS one 6.

Jiao, P., Tian, G., Li, Y., Deng, G., Jiang, Y., Liu, C.,

Liu, W., Bu, Z., Kawaoka, Y., Chen, H., 2008. A Single-Amino-Acid Substitution in the NS1 Protein Changes the Pathogenicity of H5N1 Avian Influenza Viruses in Mice. Journal of virology 82, 1146-1154.

Keleta, L., Ibricevic, A., Bovin, N.V., Brody, S.L., Brown, E.G., 2008. Experimental Evolution of Human Influenza Virus H3 Hemagglutinin in the Mouse Lung Identifies Adaptive Regions in HA1 and HA2. Journal of virology 82, 11599-11608.

Kong, X., Guan, L., Shi, J., Kong, H., Zhang, Y., Zeng, X., Tian, G., Liu, L., Li, C., Kawaoka, Y., Deng, G., Chen, H., 2021. A single-amino-acid mutation at position 225 in hemagglutinin attenuates H5N6 influenza virus in mice. Emerging Microbes & Infections 10, 2052-2061.

Lin, H.-T., Wang, C.-H., Chueh, L.-L., Su, B.-L., Wang, L.-C., 2015. Influenza A(H6N1) Virus in Dogs, Taiwan. Emerging infectious diseases 21, 2154-2157.

Maines, T.R., Jayaraman, A., Belser, J.A., Wadford, D.A., Pappas, C., Zeng, H., Gustin, K.M., Pearce, M.B., Viswanathan, K., Shriver, Z.H., Raman, R., Cox, N.J., Sasisekharan, R., Katz, J.M., Tumpey, T.M., 2009. Transmission and Pathogenesis of Swine-Origin 2009 A(H1N1) Influenza Viruses in Ferrets and Mice. Science. 325, 484-487.

Mänz, B., Brunotte, L., Reuther, P., Schwemmle, M., 2012. Adaptive mutations in NEP compensate for defective H5N1 RNA replication in cultured human cells. Nature communications 3, 802.

Matrosovich, M., Tuzikov, A., Bovin, N., Gambaryan, A., Klimov, A., Castrucci, M.R., Donatelli, I., Kawaoka, Y., 2000. Early alterations of the receptor-binding properties of H1, H2, and H3 avian influenza virus hemagglutinins after their introduction into mammals. Journal of virology 74, 8502-8512.

Paterson, D., Fodor, E., 2012. Emerging roles for the influenza A virus nuclear export protein (NEP). PLoS Pathogens 8, e1003019.

Selman, M., Dankar, S.K., Forbes, N.E., Jia, J.-J., Brown, E.G., 2012. Adaptive mutation in influenza A virus non-structural gene is linked to host switching and induces a novel protein by alternative splicing. Emerg. Microbes Infect. 1.

Song, D., Lee, C., Kang, B., Jung, K., Oh, T., Kim, H., Park, B., Oh, J., 2009. Experimental infection of dogs with avian-origin canine influenza A virus (H3N2). Emerging infectious diseases 15, 56-58.

Stevens, J., Ola Blixt, Terrence M. Tumpey, J.K.T., 5 James C. Paulson,1,2 Ian A. Wilson1,3*, 2006. Structure and Receptor Specificity of the Hemagglutinin from an H5N1 Influenza Virus. Science (New York, N.Y.) 312, 404-410.

Subbarao, E.K., London, W., Murphy, B.R., 1993. A single amino acid in the PB2 gene of influenza A virus is a determinant of host range. J. Virol 67, 1761-1764.

Sun, X., Xu, X., Liu, Q., Liang, D., Li, C., He, Q., Jiang, J., Cui, Y., Li, J., Zheng, L., Guo, J., Xiong, Y., Yan, J., 2013. Evidence of avian-like H9N2 influenza A virus among dogs in Guangxi, China. Infection, Genetics and Evolution 20, 471-475.

Taubenberger, J.K., Kash, J.C., 2010. Influenza Virus Evolution, Host Adaptation, and Pandemic Formation. Cell host & microbe 7, 440-451.

Tumpey, T.M., Maines, T.R., Hoeven, N.V., Laurel Glaser, A.S., 2 Claudia Pappas,1,2 Nancy J. Cox,1 David E. Swayne,3 Peter Palese,2 Jacqueline M. Katz,1 Adolfo García-Sastre, 2007. A two-amino acid change in the hemagglutinin of the 1918 influenza virus abolishes transmission. Science (New York, N.Y.) 315, 655-659.

van Doremalen, N., Shelton, H., Roberts, K.L., Jones, I.M., Pickles, R.J., Thompson, C.I., Barclay, W.S., 2011. A Single Amino Acid in the HA of pH1N1 2009 Influenza Virus Affects Cell Tropism in Human Airway Epithelium, but

Not Transmission in Ferrets. PloS one 6.

Wang, C., Wang, Q., Hu, J., Sun, H., Pu, J., Liu, J., Sun, Y., 2017. A Multiplex RT-PCR Assay for Detection and Differentiation of Avian-Origin Canine H3N2, Equine-Origin H3N8, Human-Origin H3N2, and H1N1/2009 Canine Influenza Viruses. PloS one 12, e0170374.

Wang, G., Dos Anjos Borges, L. G., Stadlbauer, D., Ramos, I., Bermudez Gonzalez, M. C., He, J., Ding, Y., Wei, Z., Ouyang, K., Huang, W., Simon, V., Fernandez-Sesma, A., Krammer, F., Nelson, M. I., Chen, Y., Garcia-Sastre, A., 2019. Characterization of swine-origin H1N1 canine influenza viruses. Emerg Microbes Infect 8, 1017-1026.

Ward, A.C., 1997. Virulence of influenza A virus for mouse lung. Virus Genes 14, 187-194.

Wasik, B.R., Voorhees, I.E.H., Parrish, C.R., 2021. Canine and Feline Influenza. Cold Spring Harbor perspectives in medicine 11.

Yang, G., Li, S., Blackmon, S., Ye, J., Bradley, K.C., Cooley, J., Smith, D., Hanson, L., Cardona, C., Steinhauer, D.A., Webby, R., Liao, M., Wan, X.F., 2013. Mutation tryptophan to leucine at position 222 of haemagglutinin could facilitate H3N2 influenza A virus infection in dogs. J Gen Virol 94, 2599-2608.

Zhan, G.j., Zong-shuai, L., Yan-li, Z., Shi-jin, J., Zhi-jing, X., 2012. Genetic characterization of a novel influenza A virus H5N2 isolated from a dog in China. Veterinary Microbiology 155, 409-416.

Zheng, B., Chan, K.-H., Zhang, A.J.X., Zhou, J., Chan, C.C.S., Poon, V.K.M., Zhang, K., Leung, V.H.C., Jin, D.-Y., Woo, P.C.Y., Chan, J.F.W., To, K.K.W., Chen, H., Yuen, K.-Y., 2010. D225G mutation in hemagglutinin of pandemic influenza H1N1 (2009) virus enhances virulence in mice. Exp. Biol. Med 235, 981-988.

Zhou, B., Li, Y., Halpin, R., Hine, E., Spiro, D.J., Wentworth, D.E., 2011. PB2 residue 158 is a pathogenic determinant of pandemic H1N1 and H5 influenza a viruses in mice. Journal of virology 85, 357-365.

Zhu, H., Hughes, J., Murcia, P.R., 2015. Origins and Evolutionary Dynamics of H3N2 Canine Influenza Virus. J Virol. 89, 5406-5418.

Min Zhu

Changzhou, Jiangsu province, China
Majoring in the canine influenza virus

Ying Chen

Liuzhou, Guangxi province, China
Majoring in the influenza A virus

New Method for Measuring Water Flow Rate in Plant Stems Using Thermoelectric Cooling Techniques

Kritsada Sompan, Thongchai Maneechukate*, Chawaroj Jaisin, Parin Kongkraphan

School of Renewable Energy, Maejo University, Chiang Mai, Thailand
**Corresponding author, E-mail: kritsadasompan@gmail.com*

Abstra ct: This research introduces thermoelectric cooling to analyze the mass flow rate of water in plant stems as a novel measurement method employing the heat balance approach. The equipment comprises a thermoelectric module, copper plate, thermocouple, thermopile, and heat insulator. This innovative technique for measuring water flow rates in plant stems is suitable for small-sized plants with stem diameters not less than 5 mm. The water flow rate is measured by applying a 4V direct current to the thermoelectric module, resulting in a suitable temperature of -4.8 °C Without loading. The position of the temperature sensor placement will be aligned with the flow direction of water in plant stems. It will be positioned 8 mm away from the thermoelectric module along the direction of water flow into the plant stem and 4 mm away in the direction of water flow out. Experimental results from testing water flow in plant stems at 0.67 g, 1.14 g, and 1.60 g per 4 minutes, respectively, using the designed and analyzed sensor, showed actual flow rates of 0.50 g, 1.00 g, and 1.40 g per 4 minutes. The absolute errors were 0.17 g, 0.14 g, and 0.21 g, respectively, with relative errors of 25.38%, 14.35%, and 14.90%, and accuracies of 74.61%, 85.64%, and 85.09%, respectively. The sensor's accuracy in measuring water flow rates in plant stems falls within an acceptable range and provides a promising direction for agricultural applications.

Keywords: Heat balance, Heat flux, Sap flow meter, Thermoelectric

1. Introduction

The measurement of water flow rates in plant stems has been continuously developed and refined, utilizing the theory of heat balance to analyze the mass flow rate of water in plant stems. This involves supplying heat to the plant stem to maintain a temperature higher than the surrounding environment, typically by 5-7 ºC. The heating system loses energy to the plant stem due to the conduction of heat from the flowing water within the plant stem's xylem vessels. Addressing this energy loss has led to the development of sensors for measuring water flow rates in plant stems [11]. The primary equipment for measuring the mass flow rate of water in plant stems includes a heating device, temperature sensor, and heat-insulating material. These components are crucial for analyzing the mass flow rate of water. Researchers have developed heating devices specifically for small-sized plant stems. The heating element can be made from materials such as copper or Teflon wire, allowing it to be easily shaped to match the form of the plant stem. This characteristic facilitates the uniform distribution of heat around the plant stem [1-9]. The heating device must be covered with insulation to prevent heat loss to the environment and to prevent external factors from interfering with the sensor. Commonly used insulation materials include polyethylene, aluminum foil, and others that are flexible and can be shaped to match the form of the plant stem [1-3-10-13]. Furthermore, there has been an application of 3D printing technology to shape sensors that are suitable for plants of various sizes [2]. Sensors measuring the mass flow rate of water in plant stems are not commonly used in agriculture due to their high cost, which may not be feasible for farmers. However, Thai researchers have studied and developed these sensors for application in agriculture, particularly for fruit trees with large stems such as durian, mangosteen, longan, lychee, and mango. This research focuses on horticultural and orchard crops, aiming to apply the technology in the management and control of irrigation systems in agricultural fields [5]. Sensors measuring the mass flow rate of water in these plant stems have employed the theory of heat balance. This method is widely favored for analysis because it allows observation of the water flow rate behavior in the plant stems at different time intervals [8].

This research has developed a mass flow rate water sensor for plant stems with diameters ranging from 5 to 40 mm. The focus was on developing a sensor to measure the water flow rate in small-sized plant stems using the heat balance technique for analysis. In this technique, heat is supplied to the plant stem to analyze the flow rate. However, in the climatic conditions of Thailand, supplying heat to plant stems may cause damage due to the tropical climate prevalent in the country, with an average temperature ranging from 18 to 38 °C. To address this issue, the sensor was developed to supply cool temperatures to the plant stems instead of heat. The use of cooling for analyzing flow rates with the heat balance technique has not been developed or explored in Thailand. The sensor is composed of readily available materials in the market, making it cost- effective and easily maintainable. The sensor includes a thermoelectric, an Aeroflex, a thermopile, and a temperature-sensitive sensor of type k and copper. The copper sheet functions to dissipate heat from the thermoelectric. The sensor is assembled to measure the water flow rate in plant stems and is designed to be flexible to adapt to the shape of the plant stem. The sensor's operation starts with the thermoelectric generating coolness, and the brass sheet transports the coolness to the plant stem. The Aeroflex serves as insulation to prevent the loss of temperature to the environment. When the plant stem receives the cooling, the temperature-sensitive resistor measures the temperature, and the sensor analyzes the temperature difference to determine the mass flow rate of water in the plant stem. The development of this sensor is inspired by the concepts presented by [1-13-3-10]. This flow rate sensor has been developed as a practical solution, and it is

intended to be applied widely. It is designed to be accessible to general farmers, allowing them to benefit from this technology.

2. Methods

The development of the water flow rate sensor in plant s tems employs the technique of supplying cold temperature to the plant stem for the analysis of water flow rate or plant water consumption. The analysis principle considers the length, cross-sectional area, and radius of the plant stem. The measurement of the flow rate involves selecting a point on the plant stem for analysis. Using the sensor, the analysis of the flow rate is carried out by supplying cold temperatures or transferring energy to the plant stem. When water flows through the point where energy is supplied to the plant stem, the water receives energy, resulting in the transfer of cold energy along with the mass of water. This process involves either gaining energy through the mass of water or losing heat energy through the transfer of heat. There is energy loss in the radial direction and the cross-sectional area of the plant stem, leading to energy loss in the cooling temperature device, as illustrated in Figure 1 [11-12]. The explanation of energy loss in the form of cooling is described by the following mathematical equation [9].

$$Q = Q_v + Q_r + Q_f + S \quad (1)$$

When Q is the total heat energy supplied to the plant stem (W), Q_v is the heat energy transferred to the plant stem in the cross-sectional area direction (W), Q_r is the heat transfer in the radial direction of the plant stem (W), and Q_f is the heat energy loss due to carrying heat with the mass of water inside the plant stem (W) S stands for the rate of change of heat storage per unit temperature change in the stem, measured in watts (W).

The loss of heat energy due to carrying heat can be explained as follows [9].

$$Q_f = C_{pw}F(T_u - T_d) \quad (2)$$

When c_{pw} is the specific heat capacity of water ($J \bullet kg^{-1} \bullet °C^{-1}$), F is the mass flow rate of water in the plant stem ($kg \bullet s^{-1}$), Tu is the temperature of water in the plant stem in the inflow direction to the refrigeration unit (°C), and Td is the temperature of water in the plant stem in the outflow direction from the refrigeration unit (°C).

The analysis to determine the mass flow rate of water in the plant stem involves substituting Equation 2 into Equation 1, resulting in the mathematical relationship between the mass flow rate of water and the time the water flows through the cross-sectional area of the plant s tem, which can be described by the following mathematical equation:

$$F = (Q - Q_v - Q_f) / c_{pw}(T_u - T_d) \quad (3)$$

The analysis of the mass flow rate of water in plant stems using Equation 3 involves supplying heat energy to the plant stem. When water flows through, it induces a thickness of heat flow. In analyzing the flow rate, initially setting F = 0, when heat energy is supplied, the heat energy is divided by the specific heat capacity of water and the temperature difference of water in the plant stem. Solving the equation yields the mass of water (in kilograms). In the case of nighttime flow rate measurements, the flow rate is at its minimum when F approaches 0 or F = 0. By analyzing and approximating the water flow rate in the plant stem, expressed in kilograms, this method can be compared with other measurement methods, providing reliable results[9-3-10].

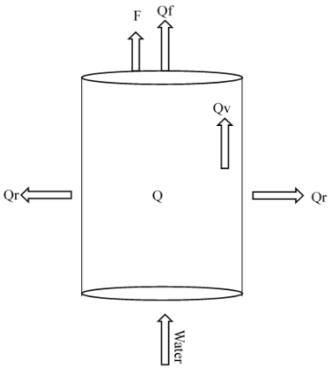

Figure 1 Method Related to the Analysis of the Heat Energy Balance in the Plant Stem, Involving the Loss of Heat Energy to the Plant Stem.

The technical design utilizes the cold generated by the thermoelectric unit for heat balance analysis to determine the flow rate of water in the stems of small-sized plants. The concept for this measurement technique is drawn from studies conducted by [3-9-2]. The sensor is flexible, allowing it to conform to the shape of the plant stem. The refrigeration unit for the plant stem consists of a thermoelectric element with a copper sheet attached to the cold side of the thermoelectric and a thermopile attached to the copper sheet, as shown in Figure 2.

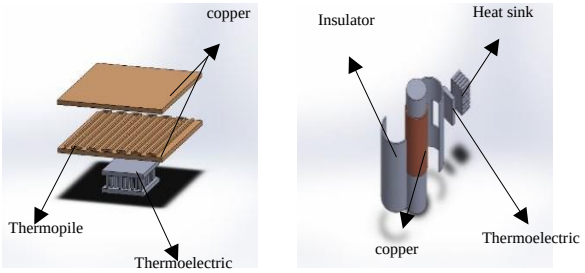

Figure 2 The material of the refrigeration unit with the thermoelectric and the design of the sensor are tailored to conform to the shape of the plant stem.

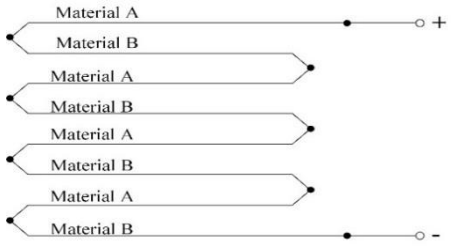

a) Connecting two types of materials in series to form a thermopile.

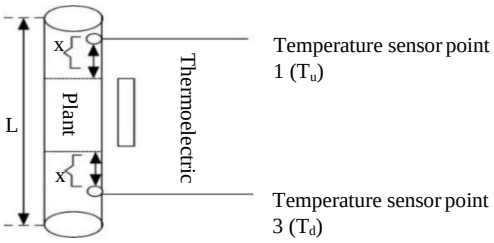

b) Testing the distance of the temperature sensor from the temperature supply device

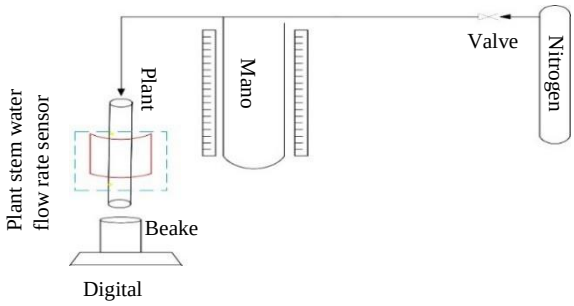

c) Testing the flow rate of water in plant stems and assessing the accuracy of the water flow rate sensor.

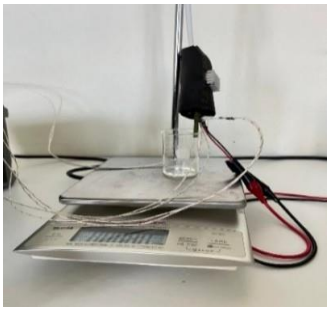

d) Testing the mass flow rate of water in plant stems.

Figure 3 Designing the thermopile and designing the testing method for analyzing the mass flow rate of water in plant stems.

The design of the cooling technique for the plant stem, used for measuring the water flow rate in the plant stem, employs the principles of the Peltier effect from the thermoelectric circuit. Applying a direct current voltage into the thermoelectric circuit induces a temperature difference on both sides. One side functions as a heat absorber, causing a decrease in temperature, while the other side acts as a heat rejecter, leading to an increase in temperature [6]. The basic principles of refrigeration, have been applied in testing a refrigeration sensor using a thermoelectric element with dimensions of 20 x 20 x 5 mm. The experiment involves applying electrical voltage in the range of 3 to 12 V to determine the suitable voltage for achieving the desired cooling temperature without any load. The testing methodology is outlined in [4]. Once the appropriate electrical voltage for refrigeration is obtained, it is applied to the cold side of a 50 x 50 x 1 mm copper sheet attached to the thermoelectric element. The thermoelectric element then transfers the cold temperature to the plant stem. The copper sheet also has a thermopile attached, serving the purpose of measuring the temperature at the contact surface of the brass sheet. The thermopile is composed of two different types of metal conductors, with their ends sequentially connected, totaling 14 connection points, as illustrated in Figure 3(a). Temperature measurements are taken at the contact surface of the copper sheet and the contact surface of the thermoelectric element to test the rate of heat transfer from the thermoelectric element to the copper sheet.

When the thermoelectric element cools one side, the other side of the thermoelectric becomes hot. To effectively achieve cooling, heat dissipation is necessary. Without proper heat dissipation, heat from the hot side may transfer to the cold side, hindering the cooling process. Heat dissipation is achieved by attaching a finned heat sink, utilizing the natural principle of releasing energy. The heat dissipation rate of the finned heat sink is then tested for the hot side of the thermoelectric element.

From the testing of the optimal cooling for the thermoelectric element for plant stems to analyze the water flow rate in the plant stems, a test was conducted to install a temperature sensor to measure the water temperature before entering and after exiting the refrigeration unit. There needs to be an appropriate distance for temperature measurement. The testing involved measuring the distance from the refrigeration unit at intervals of 0, 4, 8, 12, and 16 mm. The test results are shown in Figure 3(b). After conducting the tests for installing the water temperature sensor in the plant stem, suitable for flow rate analysis, the next step is to test the water flow rate in the plant stem at three different rates. This is done by forcing nitrogen gas to push the water out at the end of the plant stem, as shown in Figure 3(c). The flow rate of water was measured using an electronic balance for comparison with the water flow rate in the plant stem obtained from the sensor. An analysis was conducted to determine the error and accuracy of the sensor measurements. The plant stem used in the test had a circumference of 5 mm and belonged to an avocado plant. The testing methodology was derived from [7].

3. Results and Discussion

3.1 Testing to Determine the Suitable Electrical Voltage for Thermoelectric Cooling and Heat Sink Heat Dissipation

Testing to find the cooling temperature of the thermoelectric can be conducted with voltages ranging from 3 to 12 V. The suitable voltage for cooling can be determined by testing at room temperature. The voltages capable of achieving cooling temperatures are 4 V, 5 V, and 6 V, resulting in cooling temperatures of -4.8°C, -4.5°C, and -3.5°C, respectively. The corresponding hot-side temperatures are 38.2°C, 39.2°C, and 47.6°C, as shown in Figure 4. From the graph, it can be observed that the voltage at 6 V can achieve the lowest temperature, followed by the voltage at 5 V, but it is not suitable for cooling because the heat generated on the hot side is significant, causing quick reflection of heat to the cold side, which may result in inefficient cooling. The suitable voltage is 4 V, which can achieve a cooling temperature of -4.8 °C. The temperature on the hot side at 4 V is lower than that at 5 V and 6 V, and the reflection of heat back to the cold side is slower, making it the appropriate voltage for the cooling performance of the thermoelectric module.

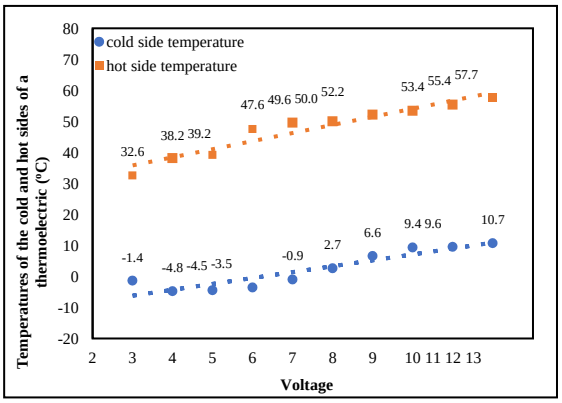

Figure 4 The relationship between the temperatures on the hot and cold sides of the thermoelectric module.

From the cooling process of the other side of the thermoelectric module, heat may be generated or cooling and heat can occur simultaneously. However, the sensor measuring the flow rate of water in the plant stem needs to utilize the cooling effect on one side only. Therefore, the hot side is not utilized and heat needs to be dissipated using a heat sink to prevent excess heat from reflecting to the cold side too quickly. The heat dissipation relies on natural convection. The test results shown in Figure 5 indicate that during the time interval of 5 to 55 seconds, heat dissipation results in a temperature drop of 3-4 °C. In the time interval of 60 to 120 seconds, heat dissipation leads to a temperature drop of 5-6 °C. As time progresses beyond 120 seconds, the temperature on the hot side increases. Increased heat dissipation also occurs, and part of the heat that cannot be dissipated in time is reflected to the cold side of the thermoelectric module, causing an increase in the cold-side temperature. For effective cooling with the thermoelectric module, the operation should not exceed 120 seconds, followed by a pause to allow both sides' temperatures to return to ambient levels for 300-600 seconds before starting another cooling cycle.

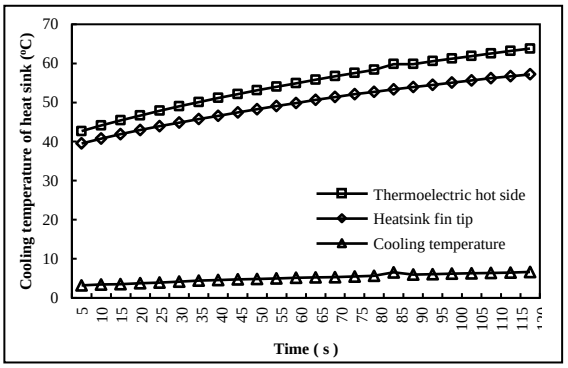

Figure 5 Heat dissipation of the heat sink compared over a period of 120 seconds.

Heat dissipation with a heat sink involves taking a sample temperature to simulate the heat dissipation scenario using a temperature simulation program for the base temperature of the heat sink at 42.67 °C and the temperature at the end of the heat sink fins at 39.50 °C. The heat dissipation achieved is 3.17 °C. The simulated heat dissipation scenario is illustrated in Figure 6.

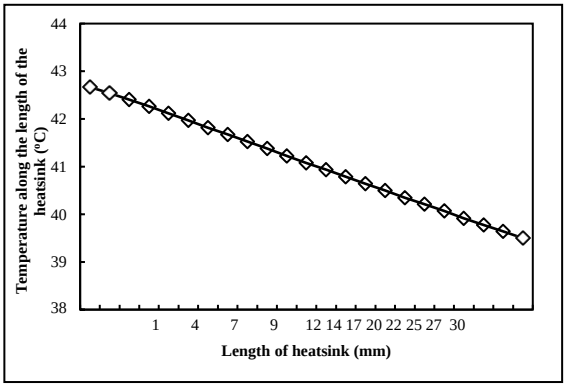

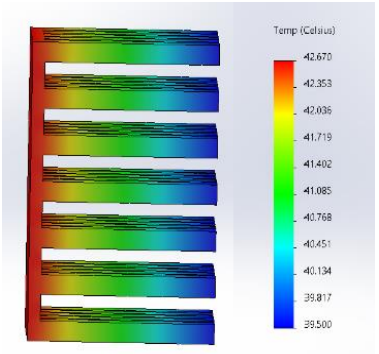

Figure 6 Heat dissipation of the thermoelectric device with a heat sink is modeled using an analysis program to simulate the scenario.

The suitable electrical voltage for cooling the thermoelectric is 4 V. Therefore, a copper plate with dimensions of 50 x 50 x 1 mm was placed on the cold side of the thermoelectric. The test aimed to examine the heat transfer from the thermoelectric to the copper plate. The copper plate has a thermal conductivity of 401 W/m^2•K and a heat transfer resistance of 1496x10^{-3} K/W. The

testing duration was 120 seconds. The initiation of the cooling process of the thermoelectric has a temperature of 2.49 °C, while the temperature at the contact surface of the copper plate is 12.16 °C. The temperature difference is 9.67 °C, resulting in a heat transfer to the copper plate of 6462.783 W, as shown in Figure 7. It can be observed that as time increases, the cool side temperature of the thermoelectric and the copper plate start to approach each other, causing the temperature difference to decrease toward zero. This results in a reduction in the rate of heat transfer, following the law of heat balance. This phenomenon occurs because the heat from the hot side of the thermoelectric reflects towards the cold side, causing the temperature on the cold side to increase. Consequently, the temperature of the copper plate also increases accordingly.

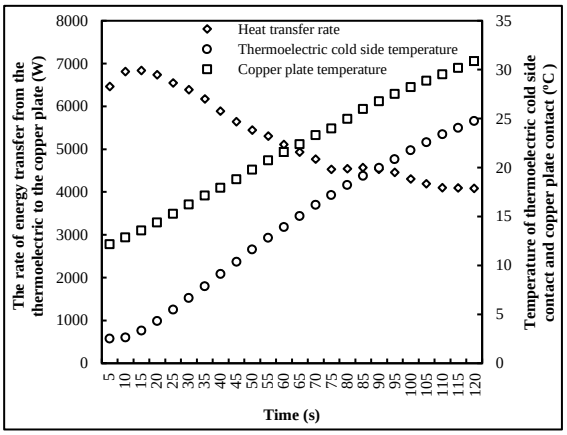

Figure 7 The relationship of the heat transfer rate between the cold side of the thermoelectric and the copper plate

3.2 Testing to determine the installation distance of the temperature sensor for measuring water temperature in plant stems away from the cooling temperature control unit.

Measuring the water flow rate in plant stems using the supplied cold temperature is crucial for obtaining water temperature data in plant stems, which is essential for analyzing the water flow rate in plant stems. The installation distance of the temperature sensor was tested before water entered and exited the cooling unit, as shown in Figure 9(f). Introducing nitrogen gas into the tube connected to the experimental plant stem, where water is present in the tube. The nitrogen pressure acts on the water, causing it to flow out from the end of the plant stem. The mass of the flowing water is measured using an electronic scale, as shown in Figure 3(c). From the test results, the installation distance of the temperature sensor before entering the refrigeration unit is in the range of 8-10 mm. This is because the temperature of the water before entering is approximately equal to the ambient temperature. Subsequently, the installation distance of the temperature sensor after exiting the refrigeration unit is crucial. Testing was conducted at distances of 0, 4, 8, 12, and 16 mm. The optimal installation distance is found to be 4 mm, as shown in Figure 9(b). It can be observed that when the temperature T2 is low, it results in a decrease in temperature T3, as it receives cooling from T2. This leads to the transfer of coldness to T3, causing a temperature difference between T1 and T3. At a distance of 4 mm, there is greater accuracy in measuring the temperature of the water exiting the refrigeration unit compared to other distances. At a distance of 0 mm, it is not suitable because T3 is too close to the refrigeration unit, causing T3 not to decrease below T1. The temperature measurement is prone to error, as shown in Figure 9(a). At a distance of 8 mm, the temperature T3 exhibits uncertainty due to temperature fluctuation, making it less reliable for flow rate analysis, as shown in Figure 9(c). At distances of 12 and 16 mm, the temperature T3 gradually decreases as T2 increases. T3 does not show a clear trend to follow T2 because the temperature sensor is too far away. This introduces uncertainty to the measurements, possibly due to measurement errors or external factors, making it unsuitable, as illustrated in Figures 9(d) and 9(e). Therefore, the distance of 4 mm is suitable for analyzing the flow rate of water in plant stems.

From the temperature measurement test of water in plant stems after exiting the refrigeration unit, the suitable distance for installation is found to be 4 mm. Subsequently, a flow rate analysis of water in plant stems was conducted at every sensor distance after water flowed out of the refrigeration unit. The distances analyzed were 0, 4, 8, 12, and 16 mm, respectively. The results of the analysis for the flow rate of water in plant stems were as follows: 1.32 g, 1.14 g, 1.29 g, 1.32 g, and 1.31 g, respectively, for 240 seconds. The actual measured flow rate of water in the plant stems was 1 g. The absolute errors were 0.32 g, 0.14 g, 0.29 g, 0.32 g, and 0.31 g, respectively, with absolute error percentages of 32.27%, 14.35%, 23.10%, 32.29%, and 31.10%. The accuracy percentages in measurement were 67.72%, 85.65%, 70.89%, 67.70%, and 68.89%, respectively. As shown in Figure 8, the calculated accuracy values indicate that the 4 mm distance is within an acceptable range and has higher accuracy compared to other distances. Therefore, the 4 mm distance is suitable for analyzing the mass flow rate of water in plant stems.

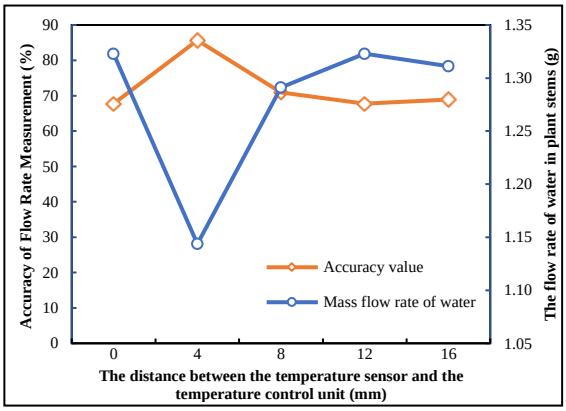

Figure 8 The analysis of the water flow rate in plant stems and the accuracy of temperature sensor installations at various distances.

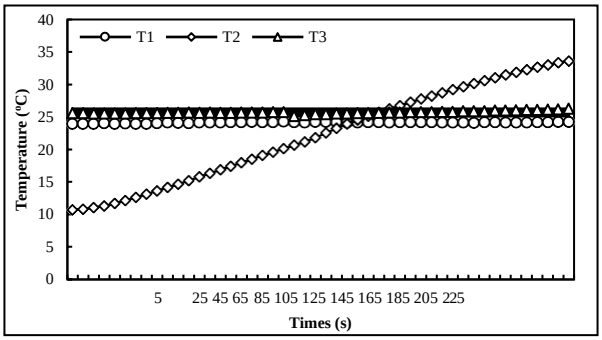

a) Distance of the temperature sensor from the measuring point is 0 mm

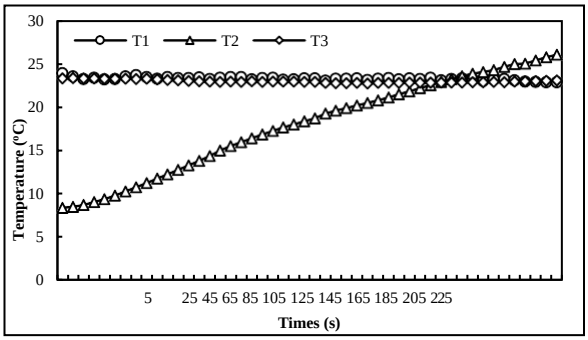

b) Distance of the temperature sensor from the measuring point is 4 mm

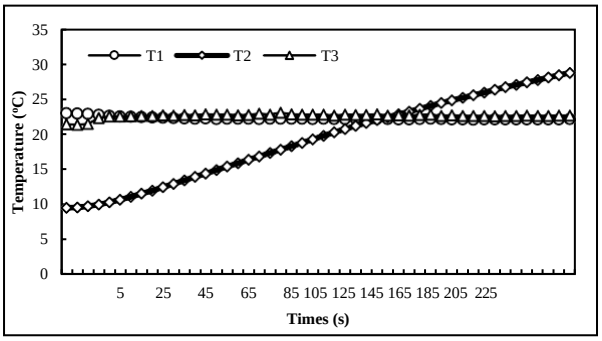

c) Distance of the temperature sensor from the measuring point is 8 mm

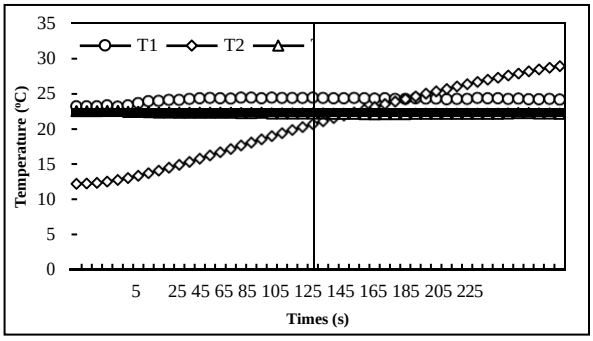

d) Distance of the temperature sensor from the measuring point is 12 mm

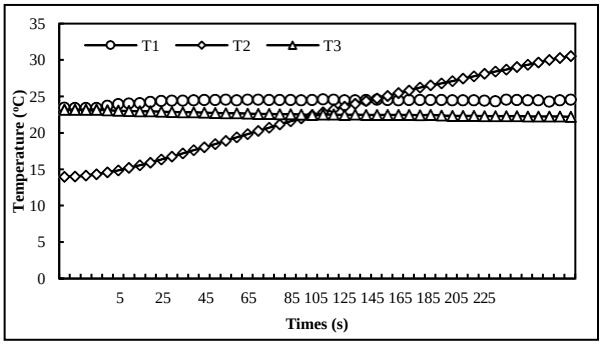

e) Distance of the temperature sensor from the measuring point is 16 mm

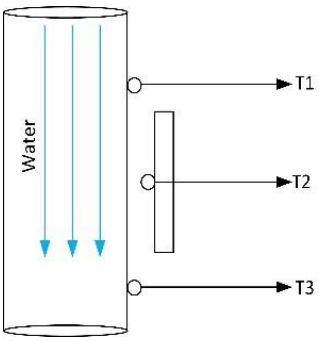

f) The temperature measuring point of the water in the plant's stem.

Figure 9 Testing to measure water temperature in plant stems involved determining the installation distance of the temperature sensor from the cooling temperature apparatus.

3.3 The analysis of the rate of heat transfer to plant stems for the analysis of water flow rate in plant stems.

The analysis of the water flow rate in plant stems during the sensor installation phase suitable for measuring water temperature in the stem involves analyzing the heat balance or the transfer of cold energy to the plant stem. When the cooling device starts working and delivers cold to the plant stem, the temperature difference between sensor points T1 and T3 occurs, resulting in the cooling device losing total energy of 3584.102 W. This energy loss is divided into energy loss in the radial direction of the plant stem (Q_r) at 1878.140 W, energy loss in the cross-sectional area of the plant stem (Q_v) at 0.20906 W, and energy loss due to cooling by the mass flow of water in the plant stem (Q_f) at 1705.748 W, as shown in Figure 10. It can be observed that there is a maximum energy loss in the radial direction of the plant stem due to the dispersion of energy around the plant stem. The downward loss is attributed to cooling effects when water receives cold. Water molecules carry the cold along the direction of water flow. From the variable Q_f, it is possible to understand the flow of water inside the plant stem. By considering the energy loss to the plant stem, the value can be used to calculate the flow rate of water within the plant stem using the heat balance technique.

3.4 Testing the flow rate of water in plant stems and analyzing the measurement accuracy of the sensor.

Measuring the flow rate of water in plant stems involved testing three flow rates. The method used was to force the flow of water out of the plant stem by applying nitrogen pressure gas. The actual measured flow rates were 0.5 g, 1 g, and 1.14 g, respectively. The flow rates analyzed by the sensor were 0.67 g, 1.14 g, and 1.61 g, respectively. The absolute errors were 0.17 g, 0.14 g, and 0.20 g, respectively. The relative errors were 25.38%, 14.35%, and 14.90%, respectively. The accuracy of measurements was 74.62%, 85.65%, and 85.10%, respectively. The test results, as shown in Figure 11, provide insights into the accuracy of f low rate measurements. Slower flow rates in plant stems lead to higher measurement errors, while flow rates equal to or greater than 1 g exhibit measurements with an accuracy of over 80%, which is an acceptable range for measuring the water flow rate in plant stems.

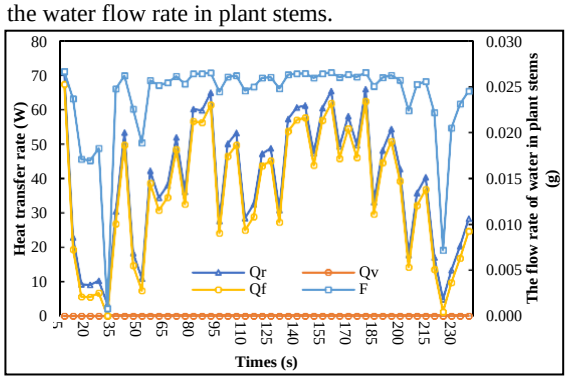

Figure 10 Transfer rate of cooling to the plant stem.

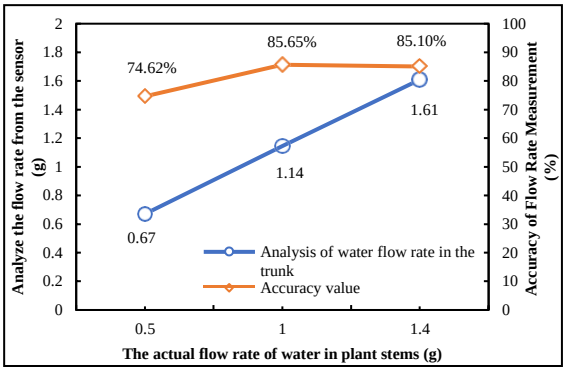

Figure 11 Analyzing the accuracy in measuring the flow rate of water within plant stems with increasing flow rates

4. Conclusions

The measurement of the water flow rate in plant stems utilizes the theory of heat balance to analyze the water flow rate within plant stems. In this research, a sensor was developed using the technique of delivering cold to plant stems for analyzing the heat balance in plant stems. The cooling technique is a new development designed to suit the climate of Thailand, minimizing damage to plant stems during sensor installation. The sensor measures the water flow rate in plant stems and is suitable for plants with stem diameters ranging from 5 mm to 40 mm. The sensor is flexible and adapts to the shape of the plant s tem. The materials used in the sensor include thermoelectric, copper sheet, aeroflex, thermophile, and thermocouple type K. These materials are combined to form the sensor, as shown in Figure 2. The cooling of plant stems uses a 20 x 20 x 5 mm thermoelectric with a rectangular fabric shape, which is not suitable for distributing temperature around the plant stem. Therefore, a 50 x 50 x 1 mm red brass sheet is attached to distribute the cold temperature around the plant stem. It is covered with a 9 mm thick heat-insulating material to prevent loss or interference from the environmental temperature, as shown in Figure 3(b). The sensor measuring the flow rate was developed and tested in the laboratory as a guideline for practical application in the actual environment.

From the test of the water flow rate sensor in plant stems in the laboratory, the suitable cooling was tested by using the thermoelectric and appropriate electrical voltage. At 4 V, the thermoelectric was capable of achieving a temperature of -4.8 °C. The hot side temperature was lower than the voltages of 5 V and 6 V, and the heat reflection back to the cold side was delayed, making it the appropriate voltage for thermoelectric cooling. After determining the suitable voltage, a red brass sheet was attached to the cold side of the thermoelectric to distribute the cold temperature around the plant stem. The energy transfer test was conducted to transfer heat energy from the thermoelectric to the red brass sheet. The red brass sheet had a heat conductivity value of 401 W/m²•K and a heat transfer resistance of 1496x10⁻³ K/W. The test duration was 120 seconds. The cooling process of the thermoelectric started with a temperature of 2. 49 ° C, and the contact surface temperature of the red brass sheet was 12.16 °C, resulting in a temperature difference of 9.67 °C. The heat transfer to the red brass sheet was 6462.783 W, as shown in Figure 7. It can be observed that as time increases, the cold temperature of the thermoelectric and the copper sheet begins to approach each other. This leads to the temperature difference approaching zero, resulting in a reduction in the rate of heat transfer according to the heat balance law. This phenomenon occurs because the heat from the hot side of the thermoelectric reflects back to the cold side, causing the temperature on the cold side to increase. This, in turn, leads to an increase in temperature on the copper sheet. On the other s ide of the thermoelectric, the cooling process results in either heating up or cooling down simultaneously. However, the water flow rate sensor needs to benefit from the cooling side only. Therefore, the hot side does not contribute to the cooling and needs to dissipate heat using heat fins to prevent excessive heat reflection to the cold side. The heat dissipation relies on natural heat convection. The test results, as shown in Figure 5, indicate that during the time interval of 5 – 55 seconds, the heat dissipation is 3 – 4 °C. In the time interval of 60 – 120 seconds, the heat dissipation is 5 – 6 °C. After more than 120 seconds, the temperature on the hot side increases significantly. For effective thermoelectric cooling, the system should operate for no more than 120 seconds, followed by a rest

period to allow both sides' temperatures to equalize with the ambient temperature. This rest period typically takes 300 – 600 seconds before starting the cooling process again.

The analysis of the water flow rate in plant stems involved testing the installation distance of the water temperature sensor before entering and exiting the refrigeration unit. Nitrogen gas was introduced into the tube connected to the plant stem within the experimental setup. Water was present inside the tube, and the nitrogen pressure exerted force on the water, causing it to flow out from the end of the plant stem. The mass of the flowing water was then measured using an electronic balance. The testing duration was 240 seconds. The results of the test for the installation distance of the water temperature sensor before entering the refrigeration unit ranged from 8 to 10 mm. This is because the water temperature before entering closely approximated the environmental temperature. Subsequently, the installation distance of the water temperature sensor after exiting the refrigeration unit is a crucial part of the experiment. By conducting tests at distances of 0, 4, 8, 12, and 16 mm, it was found that the optimal testing distance is 4 mm. It can be observed that when the temperature (T2) is low, it results in a reduction in temperature at T3 because it receives cooling from T2. This leads to the transfer of cold to T3, causing a temperature difference between T1 and T3. At the 4 mm distance, there is greater accuracy in measuring the temperature of the water coming out of the cooling system compared to other distances. After determining the optimal installation distance for measuring water temperature in the plant stem as 4 mm, further tests were conducted to analyze the water flow rate in the plant stem at various sensor installation distances after the water flowed out of the cooling system. The analyzed distances were 0, 4, 8, 12, and 16 mm, listed in sequential order. The analysis results for finding the water flow rate in the plant stem are as follows: 1.32 g, 1.14 g, 1.29 g, 1.32 g, 1.31 g over 240 seconds. The actual water flow rate in the plant stem, as measured, was 1 g. The absolute errors are 0.32 g, 0.14 g, 0.29 g, 0.32 g, 0.31 g, in sequence. The relative errors are 32.27%, 14.35%, 23.10%, 32.29%, 31.10%, in sequence. The accuracy in measurements is 67.72%, 85.65%, 70.89%, 67.70%, 68.89%, in sequence. Upon calculating the accuracy in measurements, it is evident that the 4 mm distance has an accuracy within an acceptable range and exhibits higher accuracy compared to other distances. The analysis of heat balance begins when the refrigeration unit starts working, supplying cold to the plant stem. The temperature sensor measures the water temperature in the plant stem at points T1 and T3, resulting in a temperature difference. The refrigeration unit loses a total of 3584.102 W of energy, distributed as follows: energy loss in the radial direction of the plant stem (Q_r) at 1878.140 W, energy loss in the cross-sectional area of the plant stem (Q_v) at 0.20906 W, and energy loss for cooling through the mass flow of water in the plant stem (Q_f) at 1705.748 W. The maximum energy loss occurs in the radial direction of the plant stem due to the distribution of energy around the plant stem. The downward loss is a result of cooling, where the molecules of water carry the coldness along the flow direction of the water. The variable Q_f provides information about the flow of water within the plant stem. The measurement of the water flow rate in plant stems was conducted by testing three flow rates: 0.5 g, 1 g, and 1.14 g, in sequential order. The testing method involved forcing nitrogen gas to make the water flow out of the plant stems, and the actual measured flow rates were 0.5 g, 1 g, and 1.14 g, respectively. The analyzed flow rates by the sensor were 0.67 g, 1.14 g, and 1.61 g, respectively. The absolute errors were 0.17 g, 0.14 g, and 0.20 g, in sequential order. The relative errors were 25.38%, 14.35%, and 14.90%, and the accuracies of the measurements were 74.62%, 85.65%, and 85.10%, respectively. These test results provide insights into the accuracy of f low rate measurements. When the water flow rate in plant stems is slow, the measurements tend to have higher errors, exceeding 80%. For water flow rates greater than or equal to 1 g, the measurement accuracy is higher than 80%, which is within an acceptable range.

The testing of the water flow rate measurement technique in plant stems using cold temperatures for mass flow rate analysis is an experimental and developmental effort conducted in a laboratory setting. The goal is to enhance precision in measurements for future applications in real agricultural conditions. The aim is to develop a more accurate and cost-effective sensor that utilizes readily available market equipment. This technology can be easily adopted by farmers for implementing controlled irrigation systems based on the specific water and nutrient needs of crops, reducing costs in the production process, improving the quality of the yield, and serving as a guideline for energy efficiency in agricultural systems.

5. Acknowledge

This work was supported by the School of Renewable Energy, the school of renewable energy, Maejo University Chiangmai Thailand in the facilities laboratory and the scholarship. We would l ike to thank you for the scholarship in the project to produce and develop graduates in renewable energy ASEAN countries for graduate students year 2021.

References

[1] Arthur Groot., Kenneth M. King. (1992). Measurement of sap flow by the heat balance method: numerical analysis and application to coniferous seedlings. Agricultural and Forest Meteorology, 59, 289-308.

[2] Gracee Lloyd Miner., Jay M. Ham., Gerard J. Kluitenberg. (2017). A heat-pulse method for measuring sap flow in corn and sunflower using 3D printed sensor bodies and low-cost electronics. Agricultural and Forest Meteorology, 246, 86-97.

[3] J . M. Baker., C. H. M. Van Bavel. (1987). Measurement of mass flow of water in the stems of

herbaceous plants. Plant cell and environment, 10, 777-782.
[4] Jensak Ekburanawat. (2019). Desig n and development of a thermoelectric pan for heating and chilling application. RMUTI Journal science and technology. Vol. 12, No. 3, (2019). ISSN 2672-9369 (Online). Thailand. https://www.tci-thaijo.org/index.php/rmutijo/index.
[5] Jessada Sopharat., Charturong Chanseetis, Aussanee Pichakum., Nilubol Nuanjunkong., Wichittra Chueapram. (2019 November 5-7). Introduction and development of sap flow probe for transpiration measurement of perennial trees [Paper Presentation]. The 18th National Horticulture Conference, Thailand. doi: 10.14457/KU.res.2020.37
[6] Jirayutsawat Prasom., Sittichoke Subteatakul., Taweedej Sirithanapipat. (2019, July 2-5). Study on Characteristics of Thermoelectric Cooling. Thailand Mechanical Engineering Network Academic Conference, Udon Thani Province, Thailand.
[7] Kathy Steppe., Dirk J.W. De Pauw., Tanya M. Doody., Robert O. Teskey. (2010). A comparison of sap flux density using thermal dissipation, heat pulse velocity and heat field deformation methods. Agricultural and forest meteorology, 150, 1046-1056.
[8] Piyarose Maleecharoen., Chonnathat Boonchaliaw., Taweedej Sirithanapipat. (2020 February 5-7). Plant water and nutrients uptake activity via temperature measurement [Paper Presentation]. The 58th Kasetsart University Academic Conference, Thailand.
[9] R. S. Senock., J. M. HAM. (1993). Heat balance sap flow gauge for small diameter stems. Plant cell and Environment, 16, 593-601.
[10] S.L. Steinberg., C.H.M. Van Bavel., M.J. Mcfarland. (1990). Improved sap flow gauge for woody and herbaceous plant. Agronomy Journal. Vol. 82, 851-854.
[11] Sakuratani, T. (1981). A heat balance method for measuring water flux in the stems of intact plants. J. Agric. Meteorol. 37 (1), 9-17.
[12] Sakuratani, T., Jiro ABE., (1985). A heat balance method for measuring water flow rate in stems of intact plants and its application to sugarcane plants. JARQ. Vol. 19, No. 2, (1985). Japanese
[13] Susan Steinberg., Cornelius H.M. van Bavel., Marshall J. McFarland. (1989). A gauge to measure mass flow rate of sap in stems and trunks of woody plants. American society for horticultural science. Vol. 114(3), 466-472.

Mr. Kritsada Sompan
Master's student, Master of Engineering (Renewable Energy Engineering).
Research Interests: Smart energy management systems.

Dr. Thongchai Maneechukate
PhD Assistant Professor
Research Interests: Electrical Engineering, Control Systems Engineering and Smart Farm.

Dr. Chawaroj Jaisin
PhD Associate Professor
Research Interests: Embedded technology, Postharvest technology, and Energy conservation,

Dr. Parin Khongkrapan
PhD Assistant Professor
Research Interests: Plasma technology, Drying technology, Machine design, Energy

Guidelines for Potential Management of the Natural Tourism Destination: Tad-Kamuet Waterfall, Nong Luang Village, Paksong District, Champasak Province, Lao People's Democratic Republic

Sengdaeth Touysimeuang[1*], Wutthipong Chuatrakul[2], Keerati Trakansiriwanich[3], Yutthakarn Waiapha[4]

[1]Master Student, School of Tourism Development, Maejo University, Thailand
[2]Ph.D. Lecturer, School of Tourism Development, Maejo University, Thailand
[3]Ph.D. Lecturer, School of Tourism Development, Maejo University, Thailand
[4]Ph.D. Lecturer, School of Tourism Development, Maejo University, Thailand
[*]Corresponding author: Email: sengdaeth1011@gmail.com

Abstract: This study was conducted to: 1) measure potential level of the natural tourism destination: Tad-Kamuet waterfall, Nong Luang village, Paksong district, Champasack province, Lao PDR and determine guidelines for potential development of the natural tourism destination. A set of questionnaires was used for data collection administrated with 157 respondents consisting of 3 groups: local people, community leaders and representatives of connected public organizations. Obtained data were analyzed by using descriptive statistics: mean and standard deviation. Results of the study revealed that, as a whole, the potential of the natural tourism destination or Tad-Kamuet waterfall was found at a moderate level (χ = 3.14). This covered 5 elements: accommodation, tourism activity, accessibility, and amenity. Based on its detail, however, only attraction was found at a high level (χ = 3.58). For the potential development guidelines, the following should be done: 1) improving the quality of infrastructure there; 2) creating more responsible tourism activities and routes; 3) restructuring the tourism information center; and 4) controlling service change and product prices in the natural tourism destination areas.
Keywords: Potential, Natural Tourism Destination, Tad-Kamuet Waterfall, Lao PDR

1. Introduction

Lao People's Democratic Republic (Lao PDR) has determined the tourism sector as crucial to develop the country's economy since 1975. In 1990, more than 14,000 foreign tourists visited Lao PDR which generated revenue for more than 2.2 million U.S. dollars. The number of foreign tourists increased to 1,407 million foreign in 2018 with an average income of 1,462 billion U.S. dollars earning from the country's tourism (LNTA, 2007; MoICT, 2021). In fact, Lao PDR is rich in biodiversity with an estimated 10,000 species of flowering plants; 166 reported species of reptiles and amphibians; 700-800 species of birds; at least 90 species of bats; over 100 species of large mammals; and 500 species of fish (WB, 2019a, 2019b).

Nong Luang village is located in Paksong district, Champasack province, southern Lao PDR. This village is about 12 kilometers from an urban area and its' southern part is close to Dong Hua Sao National Park. Nong Luang village is famed for its beautiful waterfall called Tad-Kamuet waterfall where there are a lot of tourism visiting there. Main occupations of local people there are coffee cultivation and animals domestication for household consumption (Chanpaseuth Xaiyapath, 2018). Aside from the reputation in its coffee and waterfall, Nong Luang is well-known as a natural tourism destination. Since it is the location of Dong Hua Sao National Biodiversity Conservation Area (DHSNBCA) (GoL, 2021). Many people claim that it is "the mysterious land's ancient heritage amazed nature wonders waterfalls". Location, a new flora named 'Mouk Nong Luang' (*Camchaya bolavenensis*) is found in this village (Noyori et al., 2022).

Nowadays, Nong Luang village faces problems in forest encroachment, deforestation and destruction of tourism resources due to poverty and lack of employment opportunities. Importantly, local people there are not encouraged to take part in local tourism activities for income generating. Thus, the local people there do not have an idea about benefits of community -based tourism and they even are not aware of laws associated with forest encroachment and destruction. This includes deforestation for coffee plantation and wildlife hunting for food or even forest product gathering. These human activities consequently lead to habitat loss and decreased biodiversity (Lee et al., 2021). In addition, there is no local tourists guide training there, community-based tourism, and awareness of

forest/ natural resources conservation. It can be said that poverty, education, community-based tourism, etc. have impacts on forest/ natural resource conversation and livelihoods (WB, 2019: 54).

According to the reasons as mentioned above, the researcher chose to conduct a study related to the potential management of a natural tourism destination- Tad Kamuet waterfall in Nong Luang village. It aimed to: 1) measure potential level of the natural tourism destination- Tad Kamuet waterfall and 2) determine guidelines for potential development of the natural tourism destination.

Review of Related Literature

The potential of natural tourism destination included 5 elements (Punyavee Visadsoontornsaku & Chawalee na Thalang, 2020); 1) accessibility means transportation ability to reach the tourism destination; 2) activity which means tourism activities related to the participation in a tourism destination; 3) amenity which means facilities to support the tourist at tourism destination;
4) attraction meaning the attractions for the tourist required to visit; and 5) accommodation mean homestays and resorts.

The potential of natural tourism destination included 4 elements (Boonlert Chittangwattana, 2005); 1) Attraction meaning the natural resources have interesting waterfall; 2) Accessibility mean the infrastructure is facilities; 3) Amenity meaning tourism destinations are impressive in various aspects such as ethnic traditions, archeology, or antiques; and 4) Ancillary service means add-tourism activities such as internet café, banks, and hospitals.

From the reviewed concepts related to the potential of natural tourism destinations mentioned above, the researcher determined the potential natural tourism destination of Punyavee Visadsoontrnku & Chawalee na Thalang (2020) and Boonlert Chittangwattana (2005). The researcher chose the potential the natural tourism destination's Punyavee Visadsoontrnku & Chawalee na Thalang (2020); 1) accessibility, 2) activity, 3) amenity, 4) attraction, and 5) accommodation. These variables were chosen in this study.

Figure 1. Conceptual framework.

2. Research Methodology

This study employed quantitative research method and a set of questionnaires was used for data collection. The sample group consisted of 157 respondents consisting of 3 groups: 1) local people in locate of this study; 2) community leaders; and 3) representative of connected public organizations. Obtained data were analyzed by using descriptive statistics: mean and standard deviation.

3. Results and Discussion

According to the first objective, results of the study showed that, as a whole, potential of the natural tourism destination on Tad Kamuet waterfall was found at a moderate level (χ = 3.14). This was on the basis of the following 5 elements: accessibility (χ = 3.03, moderate level); activity (χ = 3.17, moderate level); amenity (χ = 2.70, moderate level); accommodation (χ = 3.22, moderate level); and attraction (χ = 3.58) which was found at a high level (Table 1). For the second objective, it was found that guidelines for developing potential of the natural tourism destination- Tad Kamuet waterfall included improvement of the following: 1) the quality of infrastructure at the natural tourism destination; 2) creating more responsible tourism activities and routes; 3) restructuring of the tourism information center; and 4) controlling service charges and product prices in the natural tourism destination area. In other words, the following should be avoided: forest encroachment /deforestation and too much natural resources utilization; ignorance of knowledge and understanding dissemination about the importance of community -based tourism and natural resources conservation; and service charges /product prices are set alone by entrepreneurs.

Levels of potential natural tourism destination based on the following:
1. Accessibility
2. Activity
3. Amenity
4. Attraction
5. Accommodation

→ **Guidelines for potential management of the natural tourism destination; Tad- Kamuet waterfall, Nong Luang village, Paksong district, Champasack province, Lao PDR.**

Table 1. Show the levels of potential the natural tourism destination; Tad-Kamuet Waterfall, Nong Luang Village, Paksong District, Champasack Province, Lao PDR.

Segments of potential natural tourism destination		χχ̄	S.D.	Results
1. Accessibility	**Total 9 indicators**	**3.03**	**0.60**	**Moderate**
1.1 The travel distance from the urban to the tourism destination is appropriate.		3.17	0.60	Moderate
1.2 The travel time period from the urban to the tourism destination is appropriate.		3.17	0.56	Moderate
1.3 The cost of traveling from the urban to the tourism destination is appropriate.		3.15	0.47	Moderate
1.4 The tourism destination has buses available.		3.03	0.76	Moderate
1.5 The routes to the tourism destination are safe.		2.98	0.65	Moderate
1.6 The tourism destination area has clear direction sign which are easy to understand.		2.96	0.69	Moderate
1.7 Tourists can walk or drive to the tourism destination.		2.96	0.53	Moderate
1.8 The tourism destination is easily accessible.		2.96	0.59	Moderate
1.9 The tourism destination has enough parking lots.		2.87	0.57	Moderate
2. Activity	**Total 9 indicators**	**3.17**	**0.75**	**Moderate**
2.1 There are many cultural activities such as offering alms to monks.		3.60	0.75	High
2.2 There are many activities to study nature such as hiking to see flower fields, camping, plant viewing, waterfall viewing, etc.		3.50	0.78	High
2.3 There are many tourism activity cares taken.		3.46	0.66	High
2.4 There are many tourism activities that are interesting and creative.		3.37	0.62	Moderate
2.5 There are many companies that provide travel activities such as Green Discovery Company, etc.		3.33	0.79	Moderate
2.6 There are many tourism activities in line with nature and the community.		3.32	0.69	Moderate
2.7 There are many tourism activities that provide opportunities to learn about community lifestyles.		3.06	0.66	Moderate
2.8 There are activities to learn local food cooking with villagers.		2.91	0.69	Moderate
2.9 There are various travel programs.		1.98	1.14	Low
3. Amenity	**Total 9 indicators**	**2.70**	**0.84**	**Moderate**
3.1 There are many porter's services provided for tourists.		4.08	0.91	High
3.2 The tourism destination has adequate trash cans or garbage disposal points.		3.54	0.92	High
3.3 There are many bathrooms to serve tourists.		3.19	0.62	Moderate
3.4 There are many accommodations, enough to accommodate tourists.		3.17	0.64	Moderate
3.5 There is a clear and comprehensive mobile or internet signal.		2.65	0.77	Moderate
3.6 There are enough restaurants, shops, and souvenir shops.		2.42	0.72	Low
3.7 There is an electrical system (small hydropower: Pico-hydropower) to serve tourists.		1.92	1.06	Low
3.8 There is a tourism information center.		1.70	1.00	Lowest
3.9 There are many other utilities such as a gas station, post office, laundromat, hospital, and bank providing adequate services.		1.59	0.89	Lowest
4. Attraction	**Total 9 indicators**	**3.58**	**0.71**	**High**
4.1 The tourism destination has natural scenery and beautiful forests/waterfalls.		4.14	0.65	High
4.2 The tourism destination has outstanding features of interest in landforms such as cliffs, rocks, mountains, plateaus, etc.		4.12	0.63	High

4.3 The tourism destination is complete with forest areas, floras and faunas.	4.11	0.65	High
4.4 The tourism destination is rich of biodiversity that has not been altered or disturbed by humans.	3.97	0.65	High
4.5 The tourism destination has a variety of tourism activities such as hiking, bird watching (wildlife), etc.	3.71	0.74	High
4.6 There is a way of life in the tribe that is in harmony with nature and the environment.	3.19	0.70	Moderate
4.7 Within the tourism destination, there are famous recreational activities such as waterfall viewing, ziplining, etc.	3.18	0.77	Moderate
4.8 The community has culture, unique traditions such as Bai See, natural living, etc.	3.16	0.81	Moderate
4.9 The tourism destination disseminates knowledge about local wisdoms such as handicrafts, weaving, pottery, etc.	2.64	0.82	Moderate
5. Accommodation **Total 9 indicators**	**3.22**	**0.68**	**Moderate**
5.1 There are many officers to provide care and security.	3.41	0.69	High
5.2 Accommodations are located in an area with a good environment and beautiful scenery, with no odors.	3.40	0.69	Moderate
5.3 The accommodations are private; not noisy and there is no bad smell from waste, etc.	3.38	0.70	Moderate
5.4 The accommodations are reasonable for prices and services.	3.23	0.62	Moderate
5.5 The accommodation is clean and beautiful.	3.22	0.61	Moderate
5.6 The accommodation is enough for tourists.	3.22	0.65	Moderate
5.7 There are many types of accommodations to choose: public houses, private accommodations, hotels, homestays, resorts, sleeping in tents, camping, etc.	3.17	0.67	Moderate
5.8 There are clean and adequate bathrooms and toilets.	3.18	0.67	Moderate
5.9 Accommodations have basic amenities such as televisions, telephones, internet, and Wi-Fi adequately provided for services.	2.76	0.78	Moderate
Total	**3.14**	**0.72**	**Moderate**

As a whole, the potential of the natural tourism destination -Tad Kamuet waterfall was found at a moderate level. This was based on opinions of the 157 respondents in i tems of accessibility (χ =3.06, moderate level); activity (χ =3.16, moderate level); amenity (χ= 2.70, moderate level; attraction (χ =3.58, this level; and accommodation (χ = 3.22, moderate level). This conformed to a study of Mexay Tornkham (2017) which showed that, as a whole, a moderate level of potential of the natural tourism attraction in Thakhek District, Khammoune Province, and Lao PDR.

4. Conclusions

As a whole, the natural tourism destination-Tad Kamuet waterfall had a moderate level of potential to cope tourists (χ =3.14). This was based on 5 elements: accessibility, activity, amenity, attraction, and accommodation. Based on its detail, however, only attraction was found at a high level (χ = 3.58).

The following were guidelines for potential development of the natural tourism destination:

1) improving the quality of infrastructure there; 2) creating more responsible tourism activities and routes; 3) restructuring the tourism information center; and 4) controlling service charges and product prices.

References

Boonlert Chittangwattana. (2005). The tourism Industry is the eternal business of Thailand. Bangkok: CP Book standard.

Chanpaseuth Xaiyapath. (2018). The Potentials of Dan Nongluang Natural Tourist Attraction, Nong Luang Village, Paksong District, Champasak Province, Lao People's Democratic Republic. Rajabhat Maha Sarakham University: Master thesis].GoL. (2021). Decree on the creation of Dong Hua Sao National Park. Prime Minister No. 268, Vientiane Capital, Lao PDR. 30 March. Vientiane: Government of Lao PDR.

Lee, J., Kim, D., Nguyen, M. H., Bae, Y. J., &

Manilak, P. (2021). A Checklist of Mushrooms of Dong Hua Sao National Biodiversity Conservation Area (DHSNBCA) of Lao PDR. Journal of Forest and Environmental Science, 37 (2), 163.

LNTA. (2007). Environmental Impacts of Trade Liberalization in the Tourism Sector of the Lao PDR. Lao National Tourism Association. Vientiane: IISD.

MoICT. (2021). Tourism Development Plan 2021-2025 - summary. Ministry Information Culture and Tourism. Vientiane: Ministry Information Culture and Tourism.

Noyori, W., Komada, N., Souladeth, P., & Tagane, S. (2022). Camchaya bolavenensis (asteraceae: vernonieae), a new species from Bolaven Plateau, Southern Laos. Journal of phytotaxa, 536(1), 2.

Punyavee Visadsoontornsaku, & Chawalee na Thalang. (2020). Potentiality Development Approach for Community-basedTourism in Nakhon Ratchasima Province. The Journal of development adminstration research, 10(3), 24-25.

WB. (2019a). Developing Nature Based Tourism as a Strategic Sector for Green Growth in Lao PDR. Vientiane: World Bank in Laos.

WB. (2019b). Lao Biodiversity A Priority for Resilient Green Growth. Vientiane: World Bank in Lao PDR.

Name of authorities

Yutthakarn Waiapha, Ph.D.
School of Tourism Development, Maejo University

Sengdaeth TOUYSIMEUANG, Master Student, School of Tourism Development, Maejo University

Wutthipong Chuatrakul, Ph.D.
School of Tourism Development, Maejo University

Keerati Trakansiriwanich, Ph.D. School of Tourism Development, University

Understanding Non-Communicable Disease Risks in Buddhist Monks: A Review of Lifestyle Factors and Community-Based Solutions

Chimhan Panyacha*, Nitcha Khruekham, Phannason Phankaeo, Khanitta Wisitcharoen and Supawan Jaiboon

[1]Faculty of Nursing, Maejo University, Chiang Mai, Thailand
**Corresponding author, E-mail: Khanitta_ws@mju.ac.th*

Abstract:
An investigation on the difficulties encountered by Buddhist monks in Thailand in upholding a sound way of life, emphasizing the notable occurrence of non-communicable diseases (NCDs) such as hypercholesterolemia, hypertension, diabetes, chronic kidney disease, and osteoarthritis. It highlights that these health problems primarily arise from bad dietary patterns and insufficient physical activity, as monks heavily rely on food donations from laypeople, which often consist of high-calorie and not necessarily health-conscious options. The essay subsequently explores the notion of community empowerment as a tactic to tackle these health issues. The approach encompasses various components, such as personal growth, support groups, identifying and addressing issues, engaging in advocacy through organizations and coalitions, and undertaking collective political and social initiatives. The objective is to enhance knowledge and abilities in order to prevent non-communicable diseases among monks. These endeavors concentrate on enhancing the understanding of the detrimental effects of food offerings on health and advocating for healthier options within the community. This community empowerment strategy prioritizes collective action and education as means to enhance the health and well-being of Buddhist monks. It acknowledges the crucial role they play in Thai society and the necessity of supporting them to lead better lifestyles.

Keywords: Buddhist monks, non-communicable diseases, Thailand

1. Introduction

In Thai society, Buddhist monks are highly regarded as significant figures, providing spiritual guidance and support t o the community. For Buddhist monks to fulfill their obligations they must be in good health and have a high level of well-being. However, a review of the relevant literature indicated that they are less likely to consume healthy food and perform proper exercise [1]. As a result, they are found to be the victims of chronic diseases, especially non- communicable diseases. The evidence showed that many health problems had been discovered among monks during treatments at monastic hospitals. The most prevalent diseases observed are high cholesterol affecting 9,609 individuals, high blood pressure affecting 8,520 individuals, diabetes affecting 6,320 individuals, chronic kidney disease affecting 4,320 individuals, and osteoarthritis affecting 2,600 individuals. Notably, diabetes is one of the predominant diseases found in a considerable number of monks.

Previous studies presented eating behaviors and a sedentary lifestyle as the risk factors for non- communicable diseases. As regards unhealthy eating behavior, Buddhist monks consume food that is calorie-rich because Buddhist monks depend on food offered by people. They have no choice in choosing their food as they cannot prepare food by themselves [2]. Lay people also select food that they believe can bring good fortune to their life, or a dish their passed away relatives particularly enjoyed, so that they are pleased with the food offering. Moreover, the food that people often select for offering would either be relatively

easy to prepare or commercially available [2-3]. Curry and deep-fried foods are mostly found in almsgiving sets, the set usually contains high calories from coconut milk or is very rich in oil from the preparation process [3]. This dietary practice significantly contributes to the onset of these diseases. Moreover, limited physical activity due to the monks' lifestyle increases the risk of developing such illnesses.

Buddhist monks are human resources and are respectful of people in the community. Thus, critical thinking enables communities or lay people to understand the lifestyle of Buddhist monks which helps them make their own decisions leading to the development of confidence, understanding, and effectiveness in addressing non-communicable diseases [4]. Community empowerment has been reported as being an effective strategy in the raising of community awareness and the building of community capacity in the control of non-communicable diseases among Buddhist monks. This initiative aims to raise public awareness that offering food to monks should not merely satisfy their taste preferences but also consider the potential health impacts on the monks. It is essential to contemplate whether the food offerings could have beneficial or adverse effects on the health of the monks. Therefore, increasing knowledge by community empowerment about non-communicable disease prevention among monks becomes pivotal in fostering this understanding.

Community Empowerment on Non - communicable Disease Prevention Among Buddhist Monks

The process of community empowerment, there are five stages) personal development; 2) mutual support group; 3) issue identification and campaigns/organization; 4) participation in organization/coalition advocacy; 5) collective political and social action; 6) outcome of community empowerment [5]. Drawing on information from the situational above, the process of community empowerment can be described to prevent non-communicable disease among Buddhist monks as follows:

1. Personal development by increasing knowledge, skills and abilities are core public health and NCD prevention competencies because personal development builds individual capacity. The health education programs include NCD knowledge, NCD risk factors and complications and community roles in NCD prevention among Buddhist monks. Moreover, the included group discussion method was usually focused on eliciting community' experiences pertinent to the health of Buddhist monks and enhanced critical awareness. This promoted and established critical thinking and analytical understanding of social contexts and developed personal skill collection resources for social action [6].

2. Mutual support group has facilitated all the processes of community empowerment by encouraging participants in mutual decision-making; ensuring crucial decisions are not only in the hands of a few influential members of the community. In their approaches to the mutual support groups meetings and discussions with community members, community leaders and organizations about the NCD issue will be conducted in the community. Therefore, the participation of the community and community leaders is an important factor in making the healthcare process for the monks successful and sustainable in the long term.

3. Issue identification and campaigns/ organization.

Issue identification was responded to by community after community who were critically aware of NCD. There were many different methods used in issue identification. The study of Wisitcharoen et al. [4] showed that the Photovoice method was found to be an excellent method for identifying problems, representing, and enhancing food offerings and physical activity among Buddhist monks through a specific photographic technique. Importantly, the Photovoice method was designed by the process of issue identification and the organization of the campaign process

together with participation in the organization/ coalition advocacy process. These processes were important, and the participants became critically aware of the issue of NCD among Buddhist monks which affects their community [4].

4. Participation in organization/coalition advocacy. Participation in developing problem-solving capacity was presented in community organization approaches. The strengthened existing organizations, such as the Health Promoting Hospital, the Headman organization and the Village Health Volunteers organization provide training skills and knowledge in NCD prevention among Buddhist monks. This process is successful in building the capacity of community organization and good internal functioning in diabetes prevention among Buddhist monks [4].

5. Collective political and social action. The community activity to prevent and delay type 2 diabetes included using media to increase community awareness such as local newspapers and radio announcements [7-9] use of posters in public places and press coverage of events to report results back to the community [8-10]. Moreover, collective partnerships between community organizations have led to the establishment of diabetes schools for diabetes management [7, 10]. For Buddhist monks, the actual visits to the Buddhist monks which aimed to change health determinants, and individual care plans that were specific to each of the Buddhist Monks and provided a supportive environment to sustain NCD prevention among Buddhist monks over time.

4. Conclusions

Communal empowerment helps Buddhist monks prevent non-communicable diseases by developing critical thinking and communal capability. Community empowerment helps Buddhist monks reduce NCDs by encouraging critical thinking and teamwork. Community empowerment provided varied techniques to develop participants' critical consciousness and improve their abilities to avoid diabetes in Buddhist monks in their community. An inactive lifestyle and community-provided unhealthy meals put Thai Buddhist monks at risk. They therefore have high rates of non-NCDs like high cholesterol, hypertension, diabetes, chronic renal disease, and osteoarthritis. To address this issue, community empowerment strategies have been developed, focusing on educating monks and laypeople about healthy eating and exercise. This complete technique includes personal growth, group support, problem recognition, organizational promotion, and joint social intervention. The goal is to improve monks' analytical reasoning and decision-making, improving their well-being and serving as a model for similar public health efforts.

References

[1] Larpthananon, P. (2014). Healthy nutrition practice for healthy monks. Social Research Institute. Bangkok: Charan Sanit Wong Printing.

[2] Srimanee, S., Mantawangkul, C., Phumrittikul, P., Chancharoen, K., Hongkrilert, N., & Romnukul, N. (2013). Factors related to nutrition consumption behaviors of monks and foodstuff dedication behaviors to the Buddhist monks of people in Pasi Charoen District, Bangkok. Research Center for Community Development, Siam University, Thailand.

[3] Angkatavanich, J., Ariyapitipun, T., Wisestrith, W., Prasobtham, J., & Punpanich, D. (2016). Nutritional situation among Buddhist monks from Healthy Monks Healthy Nutrition Project. Bangkok: Panyamit Press.

[4] Wisitcharoen, K., Boonchieng, W., Suwanprapisa, T., & Buddhirakkul, P. (2016). The Effects of a Community Empowerment Program on Community Awareness and Capacity among Stakeholders in Diabetes Prevention in Buddhist Monks. ASR: Chiang Mai University Journal of Social Sciences and

Humanities. 3.10.12982/CMUJASR.2016.0008.
[5] Rissel, C. (1994). Empowerment: The holy grail of health promotion? Health Promotion International, 9(1), 39-47.
[6] Wisitcharoen, K ., Pathike, W. (2019). Community Empowerment to Prevent Non-Communicable Diseases among Thai Buddhist Monks. J Health Sci BCNSP [Internet]. 2019 Sep. 19 [cited 2023 Dec. 9];3(2):1-17. Available from: https://he01.tci-thaijo.org/index.php/bcnsp/article/view/205114
[7] Leesri, T., Vannarit, T., Srisupan, W., Senaratana, W., & Rerkasem, K. (2015). Development of collaborative diabetes management in communities. Chiang Mai University Journal of Natural Sciences, 14(3), 299-312.
[8] Mohan, V., Sandeep, S., Deepa, R., Shah, B., & Varghese, C. (2007). Epidemiology of type 2 diabetes: Indian scenario. The Indian Journal of Medical Research, 125(3), 217-230.
[9] Nield, A., Quarrelle, S., & Myers, S. (2013). Community-based early intervention for the prevention of type 2 diabetes: A case report of the Kahnawake schools diabetes prevention project. Journal of Diabetes & Metabolism, 4(277). doi:10.4172/2155-6156.1000277
[10] Krishnan, A., Ekowati, R., Baridalyne, N., Kusumawardani, N., Kapoor, S. K., & Leowski, J. (2011). Evaluation of community-based interventions for non-communicable diseases: Experiences from India and Indonesia. Health Promotion International, 26(3), 276-289.

Research Interests.

Dr. Khanitta Wisitcharoen
Lecturer
Research Interests.
Community Health, Buddhist Monks Health

Supawan Jaiboon
Lecturer
Research Interests.
Critical Care nursing, Oncology Care nursing.

Mr. Kimhun panyachai
Nursing student
Research Interests.
Community Health, Buddhist Monks Health

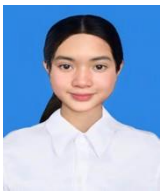

Miss. Nitcha Khruekham
Nursing student
Research Interests.
Interest in community promotion regarding diet and diabetes in monks.

Miss. Phannason Phankaew
Nursing student
Research Interests.
Continuous monitoring of symptomsCulture of Thailand Monk health

Optimizing Hot Water Mass Flow Rates into a Heat Exchanger for Temperature Control in a Cricket Breeding Container

Saowalack Inklam[1], Sarawut Polvongsri[1*]

[1]School of Renewable Energy, Maejo University, Chiang Mai, Thailand
**Corresponding author, E-mail: sarawut-energy@hotmail.com*

Abstract: This research examines the effect of hot water mass flow rate on temperature regulation in a cricket breeding setting, using a heat exchanger originally designed for an automobile air conditioner. The study utilizes a cricket breeding container measuring 1.2 m in width, 2.4 m in length, and 0.6 meters high, with a heat exchanger measuring 0.53 meters wide and 0.35 m in length. A 12V DC pump with 30W power circulates 65°C hot water from a 100-liter tank to a heat exchanger, crucial for optimal temperature in cricket breeding. The system includes three 80 W fans, each generating 1 .5 m/s wind speed for enhanced heat exchange. The experiment investigates three different hot water mass flow rates: 1 L/min, 2 L/min, and 3 L/min. The objective is to determine the most effective flow rate for maintaining the temperature within the desired range of 28 to 32 °C in the cricket breeding container. Experimental results indicate that a flow rate of 1 L/min is optimal, consistently maintaining an average temperature of 32 °C in the container. In contrast, flow rates of 2 L/min and 3 L/min result in temperatures exceeding 32 °C, which are not conducive to efficient cricket farming.

Keywords: Cricket breeding container, Heat exchanger, Hot water mass flow rate, Optimal conditions

1. Introduction: In the present day, there is a continuous and escalating increase in the rate of malnutrition among humans, and it is becoming more severe. [1] According to the report from the Food and Agriculture Organization (FAO) of the United Nations, it has been found that the global population suffering from malnutrition exceeds 820 million people. [2] As a result, the demand for protein sources has increased by 30%. Protein is considered the main source of energy crucial for the body because the body is composed of up to 80% protein, serving as a fundamental component in building various cells. This includes essential amino acids that we need from protein since the body cannot produce them on its own.[3] Due to the increasing problem of nutritional deficiencies and research on protein sources, it has been found that insects are another important source of nutrients for humans. Insects are high in protein content, making them a valuable nutritional resource for addressing the rising issue of nutritional deficiencies. [4] And crickets are currently highly popular both in the Thai market and the global market. [5] In addition, crickets are considered easily accessible and nutritionally diverse insects. They contain carbohydrates, fats, minerals, amino acids, and importantly, have a high protein content of up to 12.9%, which is close to the protein content found in chicken eggs (12.7%). [6] Therefore, during the years 2012 to 2014, there was a promotion to encourage cricket farming. Research has shown that many countries around the world have a cultural tradition of consuming insects as food, primarily found in the regions of Asia, Africa, and South America. [7] While it may be possible to address future food security issues through cricket farming, various challenges are encountered in cricket cultivation. One significant problem is the high mortality rate among crickets due to environmental conditions that cannot be controlled, especially during the winter season when nighttime temperatures average between 10 - 20 °C. [8] This results in slow growth and reduced food consumption by the crickets, leading to a lack of egg production and hindering their ability to reproduce. To address this issue, a solution was implemented by installing a ventilation system and light bulbs to increase warmth in the cricket farming container throughout the night. However, the use of light bulbs proved to be highly energy - consuming.Therefore, a heating pump was introduced to raise the temperature of the water, and the heated water was then used to exchange heat within the cricket farming container. This helped mitigate the problem of low temperatures, maintaining the internal temperature within the range of 28 - 32 °C, and not exceeding 36 °C. This finding aligns with the results of previous research. [9] The study conducted testing and analysis using a small-scale smart cricket farming facility following good agricultural practices standards. The research explored the development of a smart cricket farm by utilizing the internet of things (IoT) in agricultural data analytics. This involved the use of electronic and digital technologies in agriculture to create a smart and efficient cricket farming system. [10]

In this research, the conceptual approach involves designing a cricket farm with temperature control by introducing hot water into a heat exchange system modified from an automobile air conditioner condenser installed in the farm. The study aims to investigate the flow rate of hot water through the heat exchange system, which can be utilized to regulate the temperature in the cricket farm, ensuring it is conducive to the growth and development of crickets.

2. Methods and Materials

2.1 Cricket Farming System

The cricket farming system with temperature control and environmental monitoring is illustrated in Figure 1 . The container is a rectangular box with a lid, constructed using smart boards measuring 1 .2 m in width, 2 .4 m in length, and 0 .6 m in height. The frame is made of square steel tubes with dimensions of 0. 25 m × 0. 25 m and a thickness of 0.06 m. The lid structure uses rectangular steel tubes with dimensions of 0.05 m × 0.025 m and a thickness of 0.006 m. The box's heat exchange panel structure employs square steel tubes measuring 0. 019 m × 0. 019 m with a thickness of 0.002 m. The heat exchange panel, adopting a finned tube design, has a width of 0. 35 m, a length of 0. 53 m, and a thickness of 0. 05 m. Three DC fans, each with a size of 12 V 6 W, are used to distribute temperature inside the cricket container. Additionally, five DC fans with the same specifications are employed

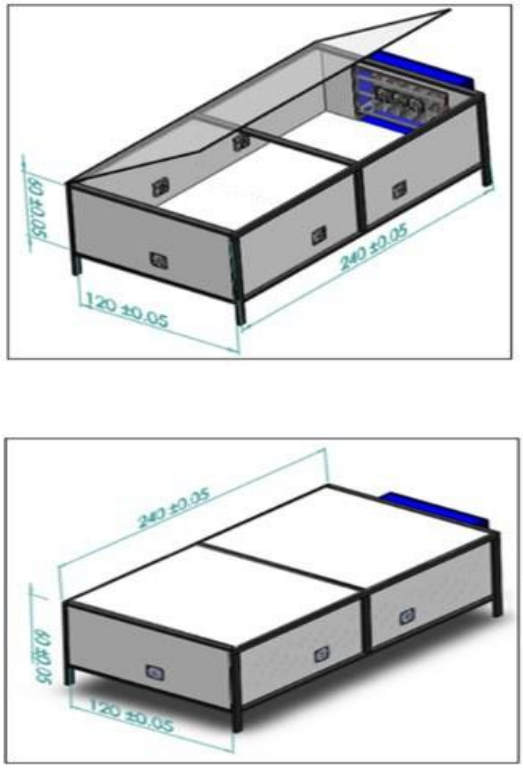

Figure 1: Model of a Cricket Breeding Container with Environmental Temperature Control

To conduct an experiment to connect a cricket breeding box to a system that increases the temperature inside the box, as shown in Figure 2 , comprising a 0. 6 kW heater pump, a 100 L hot water tank containing water at 65 ºC, and a 12 V, 30 W DC water pump. The hot water is drawn from the tank into an air conditioner condenser modified to exchange heat, installed at the front of the cricket breeding box. This system includes three fans with a diameter of 0.15 m, operating at a speed of 1.5 m/s, which function to draw hot air from the heat exchanger and release heat into the cricket breeding box. Install three temperature measurement points as follows: Point 1 (TB1) measures the temperature at the front of the cricket breeding box, 0.20 m away from the fans. Point 2 (TB2) measures the temperature at the center of the box, 1 m away from the fans. Point 3 (TB3) measures the temperature at the rear of the box, 2 m away from the fans.Study the flow rates of hot water at three values: 1 L/min, 2 L/min, and 3 L/min. These flow rates are controlled to maintain the temperature inside the cricket breeding box within the range of 28 – 32 ºC throughout the night.

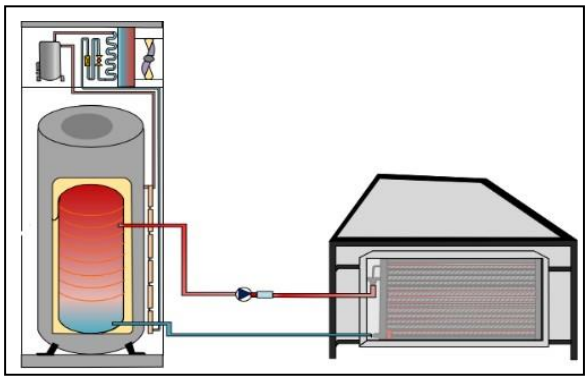

Figure 2: Testing the diagram of the temperature control system inside a cricket breeding container

2.2 The conditions for analysis

The analysis will include the flow rate of water entering the heat exchange unit, the air velocity, and the temperature inside the cricket breeding container.

- The water flow rate must of 0.02 L/min·m^2, 0.03 L/min·m^{2}and 0.05 L/min·m^2
- The air flow rate be constant mass flow 0.30 L/min·m^2
- Determine the inlet water temperature Finned Tube was set at 65 °C
- When the ambient temperature is lower 28 $\pm$ 0.5 °C the system will start.

The rate of heat transfer within the heat exchanger (Q) and the overall heat transfer rate can be calculated using the conservation of energy principle, as expressed in Equation 1.

$$Q_{hx} = UA\Delta T_{LMTD} \quad (1)$$

Where Q_{hx} is heat transfer rate in an exchanger (W). U is the overall heat transfer coefficient (W/m^{2}ºC). A is heat exchanger area (m^2) . ΔT_{LMTD} is Log-mean temperature difference (ºC).

The effectiveness of the heat exchanger can be calculated using Equation 2.

$$\varepsilon = \frac{(T_{a,o} - T_{a,i})}{(T_{w,i} - T_{a,i})} \times 100\% \quad (2)$$

Where ε is heat exchanger effectiveness (%). $T_{a,o}$ is outlet cold fluid temperature (ºC). $T_{a,i}$ is inlet cold fluid temperature (ºC). $T_{w,i}$ is inlet hot fluid temperature (ºC). $T_{w,o}$ is outlet hot fluid temperature (ºC).

The efficiency of the heat exchanger can be calculated from the ratio of the energy gained by the cold fluid to the energy lost by the hot fluid, as expressed in Equation 3.

$$\eta = \frac{T_{a,o} - T_{a,i}}{T_{w,i} - T_{w,o}} \quad (3)$$

Where η is efficiency of heat exchanger (%). $T_{a,o}$ is outlet cold fluid temperature (° C). $T_{a,i}$ is inlet cold fluid temperature (ºC). $T_{w,i}$ is inlet hot fluid temperature (ºC). $T_{w,o}$ is outlet hot fluid temperature (ºC).

3. Result and Discussion

From the test data at a flow rate of 1 L/min, in Figure 3 , the system initiates the supply of hot water from the 100 - liter tank at a temperature of 65 ºC to the heat exchanger when the temperature inside the container is below 28 °C. It stops working when the temperature inside the container exceeds 32. 5 °C. It was found that when the system starts operating, it can control the temperature at every point within the container higher than the environmental temperature consistently. The temperatures at points 1 (TB1), 2 (TB2), and 3 (TB3) start at 29.2 ºC, 28.8 ºC, and 28. 2 ºC, respectively, at 7: 00 PM. As they receive heat from the hot water, the temperature at each point increases until 8:00 PM. The temperatures at various points in the container increase to 33.4 °C, 32.5 °C, and 32.1 °C, respectively. After that, the system stops supplying hot water to the heat exchanger, causing the temperature to decrease again. When it drops to 28 ºC, the system resumes supplying hot water to control the temperature once more. This cycle continues throughout the night. From the test, it was observed that the system can control the temperature in the cricket breeding container to an average of 32. 33 ºC. Meanwhile, the temperature of the hot water in the final storage tank at 6:00 AM is 44°C, which is still sufficient for practical use.

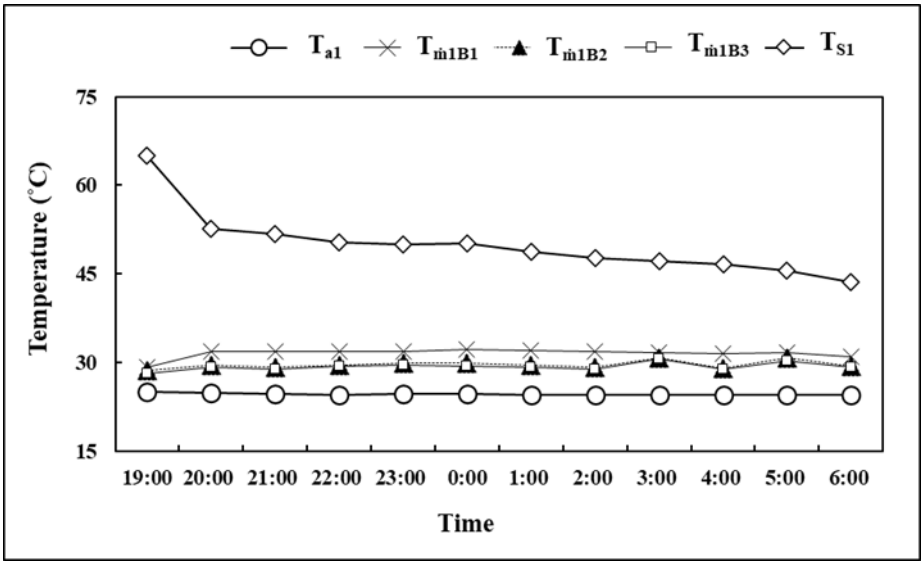

Figure 3: Temperature hot water mass flow rates: 1 L/min

At a flow rate of 2 L/min, based on the test data from Figure 4, the system starts supplying hot water from the 100-liter tank at a temperature of 65 ºC to the heat exchanger when the temperature inside the container is below 28 °C. It stops working when the temperature inside the container exceeds 32.5 °C. It was found that when the system starts operating, it can consistently control the temperature at every point within the container higher than the environmental temperature. The temperatures at points 1 (TB1), 2 (TB2), and 3 (TB3) start at 29. 2 ºC, 28. 8 ºC, and 28. 2 ºC, respectively, at 7:00 PM. As they receive heat from the hot water, the temperature at each point increases until 8:00 PM. The temperatures at various points in the container increase to 34.34 °C, 29.59 °C, and 28.54 °C, respectively. After that, the system stops supplying hot water to the heat exchanger, causing the temperature to decrease again. When it drops to 28 ºC, the system resumes supplying hot water to control the temperature once more. This cycle continues throughout the night. From the test, it was observed that the system can control the temperature in the cricket breeding container to an average of 30. 82 ºC. Meanwhile, the temperature of the hot water in the final storage tank at 6:00 AM is 55.07 °C, which is still sufficient for practical use.

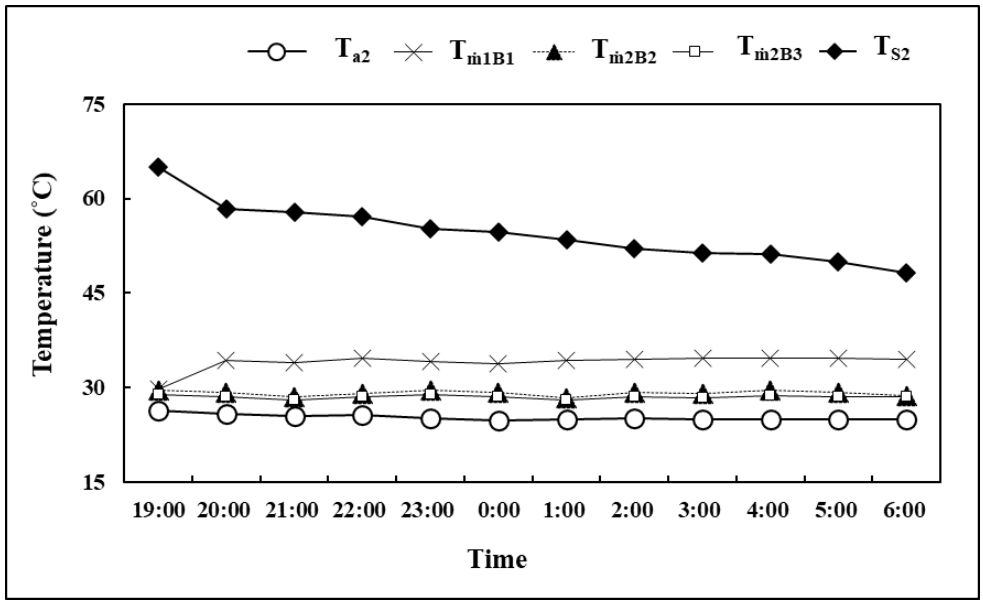

Figure 4: Temperature hot water mass flow rates: 2 L/min

At a flow rate of 3 L/min, based on the test data from Figure 5, the system starts supplying hot water from the 100-liter tank at a temperature of 65 ºC to the heat exchanger when the temperature inside the container is below 28 °C. It stops working when the temperature inside the container exceeds 32. 5 °C. It was found that when the system starts operating, it can consistently control the temperature at every point within the container higher than the environmental temperature. The temperatures at points 1 (TB1), 2 (TB2), and 3 (TB3) start at 29. 2 ºC, 28. 8 ºC, and 28. 2 ºC, respectively, at 7:00 PM. As they receive heat from the hot water, the temperature at each point increases until 8:00 PM. The temperatures at various points in the container increase to 36.86 °C, 29.99 °C, and 26.12 °C, respectively. After that, the system stops supplying hot water to the heat exchanger, causing the temperature to decrease again. When it drops to 28 ºC, the system resumes supplying hot water to control the temperature once more. This cycle continues throughout the night. From the test, it was observed that the system can control the temperature in the cricket breeding container to an average of 31. 11 ºC. Meanwhile, the temperature of the hot water in the final storage tank at 6:00 AM is 54.05 °C, which is still sufficient for practical use.

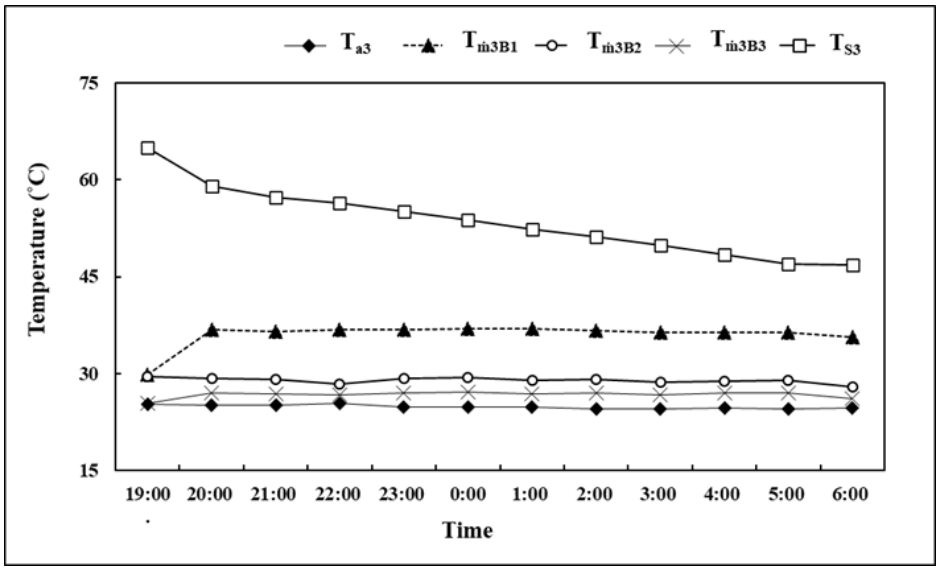

Figure 5: Temperature hot water mass flow rates: 3 L/min

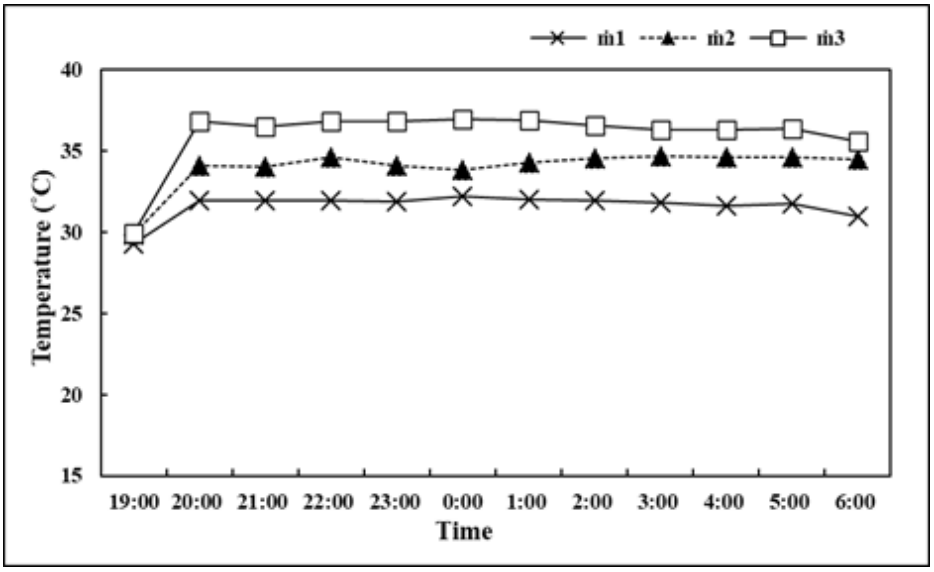

Figure 6: Temperature hot water mass flow rates: 1 L/min, 2 L/min, and 3 L/min.

The passage discusses the temperature control in a rearing tank for beetles (จิงหรีด). At a flow rate of 1 L/min, the average temperature is found to be 32. 06 °C. For the flow rate of 2 L/min, the average temperature is 33.94 °C, and for the flow rate of 3 L/min, the average temperature is 36. 04 °C. It is observed that all flow rates through the heat exchanger can maintain temperatures higher than the ambient temperature.

Among the different flow rates, the flow rate of 1 L/min achieves the best temperature control. This is attributed to the constant temperature control of the rearing tank at 32 °C, which aligns well with the flow rate of 1 L/min. The consistent temperature control ensures that the temperature remains within the suitable range for beetle rearing.

In contrast, the flow rates of 2 L/min and 3 L/min result in higher temperatures, exceeding 3 2 °C. The conclusion drawn is that the flow rate of 1 L/min is the most effective in maintaining the desired temperature for beetle rearing compared to the other flow rates.

4. Conclusion

From a study on adjusting the flow rate of hot water to control the temperature inside different cricket breeding containers, three test values were obtained using an automotive heat exchanger as the main component. The second component is a hot water tank, and a 12V DC water pump is used to circulate hot water and air. The heat exchanger panel size is 0.53 × 0.35 m, and the hot water tank size is 100 L. In this test, the results showed that a flow rate of 1 L/min resulted in relatively stable temperatures at the front of the container (TB1), the middle of the container (TB2), and the back of the container (TB3) at 33.7 °C, 32.5 °C, and 32.1 °C, respectively. The dispersion of hot air remained relatively constant throughout the cricket breeding container. Comparatively, at a flow rate of 2 L/min, the temperatures at the front, middle, and back of the container were 35.8 °C, 32.1 °C, and 29.8 °C, respectively. At a flow rate of 3 L/min, the temperatures at the front, middle, and back of the container were 39.3 °C, 32.3 °C, and 27.8 °C, respectively. It can be observed that the flow rates of 2 L/min and 3 L/min resulted in changes in temperature distribution within the cricket breeding container.

5. Acknowledgements

The authors would like to thank School of Renewable Energy, Macjo University for supporting the study by a grant fund under The Gencrate and Devclopment of Gruduate Students in Renewable Energy Research Fund, in the ASEN Countrics in the graduate.

Nomenclature

Q_{hx}	Heat transfer rate in an exchanger (W)	$T_{w,I}$	Inlet hot fluid temperature (°C)
U	Heat transfer coefficient (W/m²·k	$T_{w,i}$	Inlet hot fluid temperature (°C)
A	Total heat transfer surface area (m²)	$T_{a,I}$	Inlet cold fluid temperature (°C)
ΔT	Log-mean temperature difference (°C)	$T_{a,o}$	Outlet cold fluid temperature (°C)
ε	Heat exchanger effectiveness (%)	η	Efficiency of heat exchanger (%)

6. References

[1] Wendin, K. M. E., & Nyberg, M. E. (2021). Factors influencing consumer perception and acceptability of insect-based foods. Current Opinion in Food Science, 40 , 67 – 71.https://doi.org/10.1016/j.cofs.2021.01.007

[2] Biro, B., Sipos, M. A., Kovacs, A., Badak-Kerti, K., Pasztor-Huszar, K., & Gere, A. (2020).Cricket-enriched oat biscuit: Technological analysis and sensory evaluation. Foods, 9 (11), 1561. https://doi.org/10.3390/foods9111561

[3] Schoenfeld, B. J., & Aragon, A. A. (2018). How much protein can the body use in a single meal for muscle-building? Implications for daily protein distribution. Journal of the International Society of Sports Nutrition, 15(1), 10.

[4] Williams JP, Williams JR, Chester D, Peterson M. (2016) Nutrient content and health benefits of insects. In: Dossey A, Morales-Ramos J, Rojas M, editors. Insects as Sustainable Food Ingredients: Production, Processing and Food Applications. Academic Press: London. p. 61-84.

[5] World Health Organization. (2018) . The nutrition challenge: Food system solutions. WorldHealth Organization. No. WHO/NMH/NHD/18.10

[6] Xiaoming, C., Ying, F., Hong, Z. & Zhiyong, C. (2010). Review of the nuritive value of edible insects. In P.B. Durst, D.V. Johnson, R.L. Leslie. & K. Shono, eds. Forest insects as food: humans bite back, proceedings of a workshop on Asia-Pacific resources and their potential for development. Bangkok, FAO Regional Office for Asia and the Pacific.

[7] Baiano, A. (2020). Edible insects: An overview on nutritional characteristics, safety, farming, production technologies, regulatory framework, and socio- economic and ethical implications. Trend in food science & technology. 100: 35–55

[8] Sun, B.J., Huebner, C., Treidel, L.A., Clark, R.M., Roberts, K.T., Kenagy, G.J.,Williams, C.M. (2 0 2 0). Nocturnal dispersal flight of crickets: Behavioural and physiological responses to cool environmental temperatures. Funct. Ecol. 34 (9), 1907–1920. doi:10.1111/1365-2435.13615.

[9] Thomee, N. (2020). “cricket enemies” National Institute of Animal Health, vol. 20, pp. 1 - 4. (inThai).

[10] Muangprathuba J, Boonnama N, Kajornkasirata S, Lekbangponga N, Wanichsombata A, Nillaor P. (2019). IoT and agriculture data analysis for smart farm. Computers and Electronics in Agriculture. 156: 467 - 74.

The improvement of agricultural production technology can help to solve the problem of food shortage caused by the rapid increase of population

Wang meng[1*]

[1]School of Physics and Electronics,Jiangsu University, China
Wangmeng1206@163.com

Abstract: This article discusses the role of agricultural technological innovation in addressing issues related to population and food. By introducing new drought-resistant agricultural technologies and improving irrigation methods to reduce food loss and enhance agricultural productivity, agricultural technological innovation can effectively boost food production to meet the growing needs of the population while reducing reliance on natural resources and alleviating environmental pressures. Consequently, this article Underscores the significance of agricultural innovation in achieving sustainable development.

Keywords: dryland farming technologies, irrigation methods, population, food.

1. Introduction

Water is an essential input for all agricultural production activities. Crop cultivation relies on freshwater provided by rain, rivers, lakes, and underground aquifers. Currently, the world is facing a severe water crisis. As of March 2020, the United Nations' "World Water Development Report" revealed that approximately 3.6 billion people (almost half of the global population) reside in water-scarce regions, where there is a shortage of water for at least one month each year. It is projected that by 2050, this number will increase to over 5 billion people. The United Nations Water Mechanism report stated that between 2001 and 2018, 74% of natural disasters were related to water. COP27 urges governments worldwide to further integrate water into adaptation efforts, highlighting the critical importance of water in the COP outcomes document. Water scarcity will fundamentally impact agricultural output, trigger food crises, and threaten human survival and development.

According to the report "2020 Global Food and Agriculture Situation: Addressing Water Challenges in Agriculture" released by the Food and Agriculture Organization (FAO) of the United Nations, over the past 20 years, global population has rapidly increased, while per capita freshwater availability has decreased by over 20%. Over 1.2 billion people in global agricultural regions are facing severe water stress and drought issues, with 11% of farmland and 14% of pasture suffering from recurrent drought. More than 60% of irrigated farmland is under significant water pressure. Excluding the impact of extreme weather and locust infestations, the primary cause of global food crises is water scarcity. Future food crises resulting from water scarcity may lead to hunger and malnutrition affecting billions of people. To achieve sustainable development goals, humanity must implement substantial reforms, accelerate the adoption of agricultural water management technologies, and improve water use efficiency.

There are various causes of global water scarcity, and population growth is one of the significant factors. Table 1 illustrates the growth of the world population since the existence of humanity. On November 15, 2022, the United Nations announced that the global population had exceeded 8 billion people. Since the Second World War, global population changes have shown overall stability, transitioning from 7 billion to 8 billion, with both new and old characteristics coexisting. Faced with existing and foreseeable challenges in population development, humanity should scientifically anticipate population changes, tailor responses to specific contexts and times, and formulate rational policies to achieve sustainable human development.

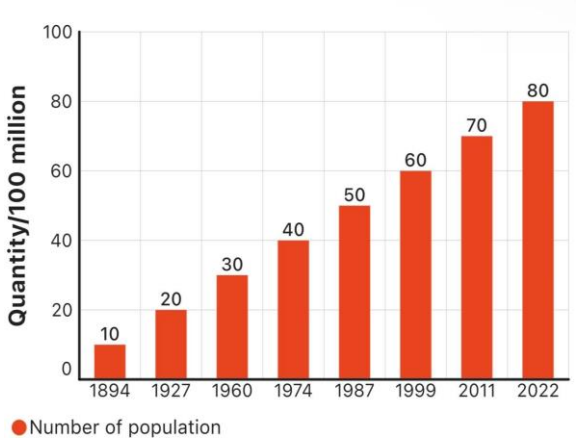

Population growth poses a significant challenge to the carrying capacity of food resources, making food security a globally persistent concern. The "2030 Agenda for Sustainable Development" identifies the elimination of hunger, achieving food security, improving nutritional status, and promoting sustainable agriculture as crucial components among the 17 sustainable development goals. According to the "2021 State of Food Security and Nutrition in the World" report published by the United Nations, an estimated 720million to 811 million people worldwide faced hunger in 2020, an increase of 161 million compared to 2019. In 2020, nearly 2.37 billion people lacked access to adequate food, marking an increase of 320 million within a year (FAO et al., 2020). Additionally, the reduction in agricultural land due to advancing urbanization globally and disruptions in the global food supply chain caused by unforeseen public events exacerbate the risks faced by global food security, bringing new challenges to the stability of the global food security landscape.

Therefore, advanced agricultural irrigation techniques need to be employed to conserve water resources as much as possible, alleviate water stress, and consequently mitigate food shortages.

2. crisis

Rain-fed cultivation refers to farming reliant on natural precipitation. Globally, rain-fed agriculture accounts for 81% of all cultivated land. With climate change intensifying, natural resource depletion, and degradation of agricultural ecosystems, rain-fed agriculture is facing unprecedented challenges globally. In vast arid lands worldwide, which produce 60% of the world's grains and 50% of livestock products, rain-fed agriculture remains the most crucial source of human food.

In 81% of arid regions, not all areas experience water scarcity. Some arid regions practice rainfed agriculture in humid

climatic conditions. Research indicates that in over 80% of global cereal cultivation, rainfall serves as the primary water source, highlighting the significance of both rainwater and land in food production. Vinay Nangia, Chief Scientist of the Soil Water and Agroforestry Team at the International Center for Agricultural Research in Dry Areas (ICARDA), explains, "Over the past 75 years, the global population has doubled, and the demand for food has increased twofold. Simultaneously, accelerated exploitation of natural resources by humans has impacted the regenerative capacity of land and the Earth, exacerbating the challenges of global ecological recovery. In fact, since 1980, human demand has exceeded the Earth's regenerative capacity and land's regenerative capacity. By 1999, human demand surpassed the Earth's regenerative capacity by 20%."

China has achieved leadership in arid agriculture technology. Water scarcity and low precipitation efficiency are global challenges. Data from the World Bank reveals that in some regions, such as the Middle East and North Africa, 82% of water is not efficiently utilized. Globally, the current ratio of irrigated land to arable land is 19%, with China having the highest irrigation ratio at 49.7%, 2.5 times the global average. Despite this, arid land still constitutes a significant portion of global agricultural land. The transition from traditional farming to modern agriculture underscores the constant importance of water in food production. Effectively utilizing water resources is crucial for the 81% of global arable land to produce sufficient food for human survival.

Therefore, employing advanced irrigation techniques to conserve water, reduce evaporation and leakage, and enhance water resource utilization is of utmost importance. I will now introduce some advanced irrigation equipment technologies.

3. Advanced irrigation equipment technologies

3.1. New Low-Energy, Multi-Functional Water-Saving Irrigation Equipment: Key Technology Research and Application

Firstly, the "New Low-Energy, Multi-Functional Water-Saving Irrigation Equipment: Key Technology Research and Application" project, led by researchers Song Weidong and Hong Li from Jiangsu University. This project, supported by the National Water Pump and System Engineering Technology Research Center, has conducted over a decade of in-depth research in water-saving irrigation technology. They have developed a low-energy, lightweight irrigation system and a series of multi-functional spraying devices. The key technologies have reached international leading levels, earning them the National Science and Technology Progress Second Prize. Their research findings have been widely adopted in the water-saving irrigation industry, extensively applied in fields, gardens, and facility agriculture. The technology has been transferred, applied, and radiated to 26 provinces, cities, and autonomous regions in China, covering 22% of China's irrigated area. Major industry enterprises are mass-producing the series, constituting over 55% of the total output of similar domestic products. These products are exported to more than 20 countries and regions, including Europe, the Americas, and Southeast Asia. This project has elevated the level of water-saving irrigation equipment technology, playing a significant role in leading industry development, mitigating drought disasters, and promoting energy conservation and emission reduction.

3.2 key technologies and industrialization of high performance intelligent sprinkler irrigation unit and equipment

The research achievement of Yuan Shouqi's team “key technologies and industrialization of high performance intelligent sprinkler irrigation unit and equipment” won the first prize among the scientific research achievements.

Researcher Yuan Shouqi has organized the group to conduct in-depth analysis and research by the end of “The Eleventh Five-Year Plan”. It was proposed to develop small and medium-sized sprinkler irrigation units and equipment to adapt to the basic agricultural conditions of China. After more than ten years of systematic and in-depth research, breakthroughs have been made in the key technologies of high-performance intelligent sprinkler irrigation units and equipment. They have cultivated the leading enterprises in the sprinkler irrigation machine industry in China, influenced and driven the product upgrading of the mainstream backbone enterprises of sprinkler irrigation machines. The product specifications have grown from the original 4 kinds to more than 50 kinds, and the national ownership has grown from thousands to more than 100000 sets, with a market share of more than 70% of the country. It has made important contributions to promoting China's agricultural water-saving, the technical level of China's water-saving irrigation equipment and the scientific and technological progress of the industry.

4. Conclusions

Water is a critical component of agricultural production, but the world is facing a serious water crisis. Water scarcity is intensified by the combination of a growing population and increasing water demand. Billions of people globally live in water-scarce regions, and it is anticipated that more people will face water resource pressure in the future. Water scarcity significantly impacts agricultural yields, triggering food crises and posing a threat to human survival. Addressing this challenge requires large-scale reform measures, the promotion of agricultural water resource management technologies, and the improvement of water resource efficiency. Utilizing advanced agricultural irrigation techniques to conserve water resources and reduce waste is a crucial step in addressing water resource pressure and food shortages.

References

[1] 李俊海. 全球水资源短缺与粮食危机 [J]. 生态经济,2021,37(03):5-8.

[2]高志民. 新兴技术引领旱作农业生产飞跃[N]. 人民政协报 ,2023-11-02(007).DOI:10.28660/n.cnki.nrmzx.2023.006436.

[3]税纡青,陆杰华.人类步入 80 亿的人口变化特征及其政策性启示[J].人口与健康,2023(01):12- 14.

[4]孔维理.农业水利灌溉中节水的有效措施分析[J]. 河南农业 ,2023(29):59-61.DOI:10.15904/j.cnki.hnny.2023.29.021.

[5].世界气象组织发布首份《全球水资源状况报告》[J].饮料工业,2022,25(06):48.

Green Tourism Development and Practical Types--The Case of Tourist Spots in Guangxi Zhuang Autonomous Region

Tian Jinrong

Guangxi University, China
*E-mail: 865620080@qq.com

Abstract: China's green tourism development concept can be traced back to President Xi Jinping's first scientific assertion that "lucid waters and lush mountains are invaluable assets" when he was the Party Secretary of Zhejiang Province in 2005, and the 18th CPC National Congress was held on November 8, 2012, which brought the concept of lucid waters and lush mountains are invaluable assets into the hearts of the people in the form of formal state documents. The concept of green tourism has also been deepened and enriched from this general idea, and has been applied to the practice of tourism transformation and upgrading. This article takes the green tourism development of attractions in Guangxi Zhuang Autonomous Region as an example, analyzes the more reliable types of green tourism development at present, and provides the development experience of new-style green tourism.

Keywords: Green Tourism; Guangxi Zhuang Autonomous Region; Tourism Type

1. Introduction

On October 18, 2017, President Xi Jinping pointed out in the report of the 19th National Congress that he insisted on the harmonious coexistence of man and nature. President Xi Jinping also said: Guangxi's ecological advantages cannot be exchanged for gold. It is necessary to establish and practice the concept that lucid waters and lush mountains are invaluable assets, and adhere to the basic state policy of saving resources and protecting the environment.

The "Thirteenth Five-Year" Tourism Development Plan requires the full implementation of the tasks of innovation-driven tourism, coordination and promotion, green development, openness and cooperation, and common construction and sharing. These strategic policies provide a good policy basis for Guangxi to transform green tourism and realize consistent development with the environment.

2. Concept and Development of Green Tourism

The purpose of green tourism is to achieve high-quality sustainable development. In 2020, in terms of the development of green tourism in Guilin, Guangxi, Liao Yongyi et al. proposed that green tourism in a narrow sense is a kind of tourism that is far away from the city and close to nature under the premise of not destroying the environment, maintaining ecological balance and rationally developing natural resources. In a broad sense, green tourism refers to all kinds of tourism products and services that are close to nature and have environmental protection functions. Ma Yangmei pointed out that green tourism in the narrow sense refers to the tourism behavior that pays attention to the protection of ecological environment in the process of tourism development, and the main places are located in rural areas and mountain areas. In a broad sense, green tourism refers to tourism products or services in the sense of environmental protection or closeness to nature. Tao Fei believes that the narrow sense of green tourism refers to the development of rural tourism projects and tourism activities in fishing villages, rural areas and mountain areas. Green

tourism in a broad sense means that tourism services and tourism products can meet the different needs of tourists to a certain extent, so as to meet the protection of the ecological environment. During this period, the definition of green tourism was limited to the tourism development in rural and mountain areas, and the cognition of its ecological protection remained in a single link of the development process. With the further implementation of the 14th Five-Year Plan, tourism, as an important industrial carrier for the reform of China's economic system and the adjustment and optimization of industrial structure, is also one of the important industrial sectors responsible for global greenhouse gas emissions. The planning and implementation of green tourism has become more comprehensive, and the definition in 2023 Western Tourism has been updated as follows: Green tourism is a tourism development model with the core of protecting the environment, inheriting culture and promoting social harmony. It emphasizes the balance between economic growth and environmental protection, and effectively reduces the damage to the environment and the waste of resources. It can be seen that with the continuous exploration of economic transformation and tourism, the concept of green tourism development emphasizes the full protection and rational use of natural resources in the process of tourism development and operation to ensure the sustainable development of ecological environment. Participants are no longer limited to the role of developers, and more roles such as operators and tourists are also involved in this comprehensive, coordinated and sustainable model.

3. Guangxi Green Tourism Development Conditions

From the point of view of latitude location, Guangxi is located in the latitude of 21° N to about 26.5° N. The Tropic of Cancer passes through the central region of Guangxi, which belongs to the low latitude region, with higher heat, and the climate type is mainly subtropical monsoon climate. From the point of view of geomorphologic conditions, Guangxi belongs to the high temperature and rainy climate, the external force is dominated by the role of flowing water, the territory of the distribution of flowing water landforms, in the lower topography of Guangxi, the river alluvial action, the formation of flowing alluvial landforms, such as the Xunjiang Plain, the Yujiang Plain, the Binyang Plain and the Nanyujiang delta, and so on. Due to the widespread limestone in Guangxi, the dissolving and eroding action of flowing water is very strong, so the karst landforms in Guangxi are widely distributed in southwest, northwest, central and northeast of Guangxi, accounting for about 37.8% of the total area of Guangxi, and the types of karst landforms developed are also very diverse. Superior climatic conditions, rich geographic environment allows Guangxi to have unique natural characteristics to develop green tourism industry that coexists with nature.

At the same time, 28 ethnic minorities such as Zhuang, Dong, Yao, etc. are gathered in Guangxi, with remarkable ethnic minority characteristics and rich cultural resources, which have great advantages for development. For example: cliff stone carvings, Gui opera, mountain songs, etc., are cultural tourism resources with great regional characteristics; Qingxiu Mountain, Jingjiang Royal Palace, Lingqu, the Red Revolutionary Road, etc., are tourism resources with historical and cultural significance, all of which provide a cultural foundation for the development of green tourism.

Moreover, according to data released by China’s Ministry of Ecology and Environment, Guangxi’s surface water quality ranks first in the country, with Liuzhou City ranking first, Chongzuo City fifth, and Guilin City sixth. Half of the top ten Guangxi cities account for this.

4. The Development Type of Green Tourism

(1)) Botanical Scenic Area-- The Case of Qingxiu Mountain Scenic Area in Nanning City

Located in Nanning City, Qingxiu Mountain Scenic Area is situated on the banks of the Yongjiang River, from Qingshan Road in the west to the ASEAN Business District in the north, and leaning against the Yongjiang River in the south and east, with an area of 13.54 square kilometers. From 1952 to 1960, Qingxiu Mountain was merged into Nanning Farm, and Qingshou Mountain was the first production team of the farm. Until 1985, it was put into use as an agroforestry, production test site and forestry. Subsequently, it was brokenly built for tourism until its overall completion in 2015.

Qingxiu Mountain area is surrounded by hills and mountains, the terrain is high in the north and low in the south, there are more than 200 small and large mountain ranges, and the altitude of the area is 63.9-288.3 meters, the vast mountainous area and the undulating altitude provide a hotbed for the growth of diverse plants. The tourism planning of Nanning City has preserved the places of interest to the greatest extent possible, and on the basis of the original ecological foundation, it has added plants that meet the requirements of the local climate and soil. The overall planning takes ecological construction as the core and plant landscape as the foundation, and the landscape area is divided into two functional areas: the core scenic area and the forest botanical garden area. The core scenic area covers a total area of 518.74 hectares, with the protection of historical relics, ecological protection and restoration as its main functions. Forest Botanical Garden Area is located in the southeastern part of Qingxiu Mountain, with a total area of 835.26 hectares, the scope of which is in addition to the core scenic area, and the main function of this area is to restore forest vegetation.

As of 2015, Nanning Qingxiu Mountain Scenic and Tourist Area has a total of 6128 species of plants belonging to 235 families and 1283 genera, including 202 species of ferns in 30 families and 79 genera; 68 species of gymnosperms in 11 families and 22 genera; 5858 species of angiosperms in 194 families and 1182 genera; there are 232 species of national rare and endangered plants under key protection, among which there are 92 species of first-grade key protection plants, 140 species of second-grade key protection plants, and 142 species of second-grade key protection plants. There are 232 kinds of national-level rare and endangered plants under key protection, including 92 kinds of Grade I plants and 140 kinds of Grade II plants. After years of planning and management, Nanning Qingxiu Mountain is a national AAAAA scenic spot, referred to as 5A scenic spot. There is a Thai garden inside, which reflects the characteristics of transnational. So far, Qingxiu Mountain Scenic Area has become the "green lung" of Nanning City, realizing both tourism and economic benefits on the role of ecological protection, which is an excellent example of green tourism construction in Nanning City.

(2)) Modern Characteristic Agriculture Demonstration Zone - Guilin Green Agricultural Tourism Construction

Modern characteristic agricultural demonstration zone refers to the modern science and technology as the guidance, the use of relevant scientific and technological equipment, the use of scientific management methods and means, the rational planning and layout of agriculture, the efficient use of resources, so as to ensure the safety of supply, material environmental protection, to achieve comprehensive benefits. This kind of modern characteristic agricultural demonstration zone can realize the efficient, convenient and sustainable development of agricultural planting, produce characteristic agricultural products with less area and low side effects of agricultural auxiliary substances, and also use the special landscape formed by agricultural cultivation technology to attract tourists, so that the local natural product sales and local tourism can be coordinated development. The

agricultural strength of Guilin is strong, and the agricultural development conditions are superior. The local government has seized this feature and carried out the comprehensive agricultural demonstration zone planning.

By 2020, a total of 2,302 demonstration zones (parks and sites) at all levels will be built in Guilin, including 35 core demonstration zones at the autonomous district level, 59 demonstration zones at the municipal level, 73 demonstration zones at the county level, 395 demonstration parks at the township level and 1,740 demonstration sites at the village level. From the data point of view, the Guilin municipal government attaches importance to the construction of modern characteristic agriculture demonstration park in Guilin, citrus in Lingui, Yangshuo, grapes in Xing 'an, sand sugar orange in Lipu, persimmon in Gongcheng and Pingle, etc., not only to create a modern characteristic agriculture demonstration zone, but also to combine leisure and sightseeing tourism to attract a large number of tourists, take care of the special crops with planting advantages in different regions, and adapt to local conditions. Gongcheng Hongyan Village is a typical one, which has been rated as one of the top ten rural tourism areas in China.

(3) Nongjiale--Chongzuo City Rural Tourism Innovation

Nongjiale is an emerging form of tourism and leisure, with low development costs and low consumption costs, which can better meet the needs of consumers to get away from the city and experience nature. Nongjiale utilizes the local natural environment, cultural temples, rural cuisine and agricultural activities to attract a large number of tourists to come to experience, and its food ingredients focus on the original ecology, mainly in the direction of the level of service to greatly enhance the local geographic environment, vegetation, ecosystems do not carry out a large transformation, which is more in line with today's consumers to the pursuit of a healthy and green life. Relying on red tourism, Shanglong Village, Shanglong Township, Longzhou County, combines the protection of the Red Army site in Shuilongtun with the transformation of the rural landscape, shaping the travel with culture, highlighting culture with travel, and further transforming the advantages of the red tourism resources into the kinetic energy of development by constructing a development system integrating study, lodging, leisure, and sightseeing experience. At the same time, also organized the masses to participate in the human resources department of the chef training courses, set up a "Red Army canteen", to make a variety of "Red Army meal", so that tourists experience the "red" land of the food culture. Food Culture. Longzhou County, by Bu Township, Langgang Village is located in the periphery of the Langgang National Nature Reserve, a good ecological environment, rich in bird resources. Relying on the advantages, the village built an ecological bird watching science base, and strive for financial support, invested more than 7 million yuan for village roads and parking lots, water supply, power supply, communications and other infrastructure. And under the guidance of the county and township party committees and governments, the village has developed ecological sightseeing tours with the main contents of bird protection and leisure vacation, striving to realize a win-win situation in ecological protection and economic development.

5.Problems in Developing Green Tourism

The main purpose of developing green tourism is to take green, innovation, precise poverty alleviation and rural revitalization as an opportunity to realize effective output and achieve unified development of economic, social and ecological benefits without destroying nature and rationally developing natural resources. However, there are some problems in the development of green tourism at present.

(1) The Fragile Natural Ecological Environment of Guangxi

Guangxi has many fluvial landforms. While the special climate and fluvial alluvial have shaped the unique geographical beauty, the karst landforms and large area of rivers and lakes are prone to soil erosion and water and soil pollution. High temperature and irregular rainfall, urbanization projects and other factors make it more difficult to maintain vegetation and cherish species. Before the development and expansion of green tourism, irrational tourism development will cause great and irreversible damage to the natural environment, which may weaken the self-restoration ability of Guangxi's ecological environment, requiring more human, material and financial resources to be invested in maintenance.

(2)Challenges of Tourism Resource Protection Brought about by the Increase of Tourists

With the concept of green life more and more deeply rooted in people's hearts, tourists from all over China and even international tourists pouring into Guangxi, according to the statistical estimates of Guangxi tourism sample survey, the cumulative number of domestic tourists received by the whole region in 2022 reached 589 million people. This data is also a growing trend, a large number of people in and out of Guilin and its major scenic spots, coupled with the uneven quality of tourists, which brings difficulties to the protection of tourism resources. Tourists' green awareness education needs to be strengthened with the development of tourism, scenic food and drink, souvenirs and other packaging, perhaps investing a lot of money to use environmentally friendly biodegradable materials, scenic areas of environmentally friendly power transportation coverage needs to be improved.

(3)Relative Lag in the Development of Tourism Industry in Non-metropolitan Areas

Despite the long-term development of tourism in Guangxi, as a pillar of the district income, but in addition to the municipal cities of the environmental infrastructure is more perfect, the surrounding counties, townships and other areas of the infrastructure is still relatively backward, can not meet the demand for high-quality green tourism, and the development of green tourism with other mature regions there is still a huge gap. Guangxi green tourism development so far, the tourism model is still upgrading transformation is slow, lack of innovation, low visibility of small places for the use of science and technology is less, publicity is not in place, at home and abroad on mainstream media platforms such as: microblogging, jitterbugs, instagram, etc. on the information basically do not have, the number of tourists relative to the urban areas are small, lack of funds, it is more difficult to keep abreast of the times and development and innovation, and to realize to the green tourism environmental protection Tourism upgrade.

6.Suggestions

For the protection of the natural ecological environment, the government should increase the investment of funds, introduce relevant policies for the protection of the natural environment, and cooperate with relevant departments to strengthen the protection and monitoring of Guangxi waters, plant vegetation in the basin according to local conditions, effectively improve the capacity of water conservation, and reduce the phenomenon of soil erosion and rocky desertification of land. Industrial activities that are not conducive to the protection of the natural environment and harm the natural environment shall be ordered to stop in time, and the environmental pollution and damage that have been caused shall be fully repaired.

Effective protection of relevant historical and cultural resources, certain control of the number of tourists in different scenic spots, real-name reservation system, appropriate closure of business in the middle of the week and other methods can reduce the pressure of scenic spots to a certain extent and increase the time of maintenance work.

Strengthen national literacy education, improve national literacy and expose the criticism of uncivilized behavior.

In addition, the government should further strengthen the construction of infrastructure, train the development and construction of scenic farmhouses in small areas around big cities, so that they can make full use of scientific and technological means for publicity, increase publicity, and keep pace with The Times to create their own characteristics of green brands.

7. Conclusion

The green tourism of Guangxi Zhuang Autonomous Region has achieved certain achievements. For example, the most famous Guilin city has won attention at home and abroad by virtue of its reasonable planning and beautiful landscape. However, the comprehensive upgrading of the tourism industry should not only look at a single achievement, but also comprehensively plan and analyze the construction of scenic spots in various regions to find a suitable local green tourism development road.

In the process of development, we should fully understand the advantages and disadvantages of our own development, closely follow the theme of The Times, rely on policy advantages and scientific and technological strength, always adhere to the road of green development, always adhere to the development concept of "lucid waters and lush mountains are invaluable assets", and adhere to the principle of integrating economic benefits, social benefits and ecological benefits. Only in this way can the green tourism of Guangxi be developed to a new height, and only in this way can the green tourism development suggestions of practical value be provided to all parties.

References

[1]广西壮族自治区文化和旅游厅.2022年旅游主要指标数据通报[EB/OL](2023-01-29).http://wlt.gxzf.gov.cn/zfxxgk/fdzdgknr/sjfb/zbsjt/t15688377.shtml

[2]骆桢荣.绿色旅游供应链视角下乡村旅宿业发展的思考[J].旅游纵览,2023,(17):100- 102.

[3]马扬梅.基于绿色旅游的区域旅游转型研究[J].北京印刷学院学报,2021,29(03): 83- 85.DOI:10.19461/j.cnki.1004-8626.2021.03.023

[4]青秀山政务网.南宁青秀山风景名胜区总体规 划[EB/OL](2016-02-18).http://qxslyfjq.com/qxsfjqzxgg/6513.jhtml

[5]邱丹丹.绿色旅游:可持续发展战略下的生态文明建设路径选 择[J].西部旅游,2023,(16):19-21.

[6]钟林生.“双碳”目标下中国旅游业绿色转型要求与路径[J].旅游学刊,2023,38(11):1-3.DOI:10.19765/j.cnki.1002-5006.2023.11.001

Tian Jinrong

Born on 1999.10.23
Majoring in English Interpretation

Change in phytochemical properties of Kombucha beverage infused with Assam tea and longan juice

Vachira Choommongkol[1], Mathurot Chaiharn[2], and Theeraphol Sanphan[3]*

[1] Programmed in Chemistry, Faculty of Science, Maejo University, Chiang Mai, 50290, Thailand
[2]Programmed in Biotechnology, Faculty of Science, Maejo University, Chiang Mai, 50290, Thailand
[3]Program in Food Science and Technology, Faculty of Engineering and Agro-Industry, Maejo University, Chiang Mai, 50290, Thailand
*E-mail: theeraphol_s@mju.ac.th

Abstract: Kombucha, a fermented tea made with black or green tea and a symbiotic consortium of bacteria and yeasts (SCOBY), offers health benefits due to its rich polyphenol and antioxidant content. This study aims to examine the alterations in phytochemical properties of Kombucha beverage infused with Assam tea and longan juice throughout a 28-day fermentation period. The results revealed a continuous increase in acidity and alcohol content in Kombucha beverage infused with Assam tea and longan juice throughout the fermentation period, spanning from day 0 to day 28**.** Nevertheless, Kombucha beverage infused with Assam tea and longan juice exhibited a consistent decrease in pH value and total soluble solid content throughout the fermentation period, from day 0 to day 28. During fermentation, both Kombucha formulations underwent a transition from a yellow-brown, slightly cloudy solution to a clear, yellow-brown liquid with visible SCOBY bacteria floating on the surface. Therefore, Assam tea and longan, promising ingredients for a novel choice of beverage production for consumers.

Keywords: Assam tea, Kombucha beverage, Longan juice, Phytochemical property

1. Introduction

The consumption of tea has evolved into a prevailing trend embraced by a diverse demographic, spanning from the elderly and working-age individuals to teenagers, owing to its recognized health benefits as part of the beverage category [1]. This popularity among health-conscious consumers has paved the way for innovative tea drinks, including the introduction of Kombucha. Crafted from the infusion of tea and a Scoby microbial leavening agent, a blend of yeast and bacteria from citrus fruits fermented with water for 4-8 months, Kombucha undergoes a meticulous process involving boiling tea, filtering out leaves, adding sugar, and transferring the mix to a fermentation container. After 15 days, the resulting Kombucha boasts a delightful sweet and sour taste, effervescence resembling a carbonated beverage, and an aroma akin to alcoholic drinks, yet it avoids alcoholic classification due to controlled fermentation converting it to acetic acid [2]. Renowned for stimulating the digestive system, maintaining intestinal balance, and reducing cardiovascular risks, Kombucha emerges as a naturally fermented beverage with a nuanced profile of sweet and sour notes, reminiscent of cider, enriched with essential vitamins, minerals, and flavoring substances like fructose, acetic acid, and gluconic acid, catering to holistic well-being [3].

Hence, this study delved into the nuanced quality changes occurring over the 21 -day fermentation period of Kombucha derived from Assam tea leaves and a blend of Assam tea leaves with longan juice. The research team adeptly applied the insights gained to innovate a distinct beverage, thereby diversifying the product range. By enhancing the product's attributes to align with consumer preferences, the resultant kombucha tea, infused with Assam tea and longan juice, not only adopts cost-effective domestic production methods but also ensures consumer

safety and benefits [2, 3]. With its favorable taste profile, this novel product holds significant commercial potential. The research outcomes not only contribute to maximizing the value of Assam tea leaves but also elevate the market worth of longan, fostering a mutually beneficial scenario for stakeholders involved.

2. Methods

2.1 Preparation of Kombucha

The Kombucha Formula 1, a distinctive beverage crafted from Assam tea, involves a meticulous preparation process. Initially,120 g of dried Assam tea leaves are boiled in 6 L of water for 20 min, after which the mixture is filtered. To sweeten and encourage fermentation, 1800 g of brown sugar are added and stirred until fully dissolved. The resulting concoction is strained, and 2 L of the tea are carefully poured into each of the three sterilized tea fermentation jars. The cooled tea, maintained at room temperature (25°C), is then enriched with 500g of the Scoby leavening agent. To facilitate the fermentation process, each jar is covered with cheesecloth and left to incubate at room temperature for an extended period of 28 days.

Kombucha Formula 2 presents a delightful fusion of Assam tea and longan juice, resulting in a unique and flavorful beverage. To create this harmonious blend, 120 grams each of dried Assam leaves and dried longan are boiled in 6 L of water for 20 min. Following the infusion, the mixture is carefully filtered, and 1800 grams of brown sugar are added, stirring until complete dissolution. After straining, 2 L of the infused tea are meticulously poured into each of sterilized tea fermentation jars. Maintaining the temperature at room level (25°C), the tea is complemented with 500 g of the Scoby leavening agent and covered with cheesecloth. The jars are then left to incubate at room temperature for an extensive fermentation period of 28 days. Throughout this process, the quality of the longan leaf kombucha was systematically analyzed.

2.2 Determination of total acid content

The examination of percent acid content on days 0 and 28 involved precise titration using a 0.1 M sodium hydroxide solution and phenolphthalein as the indicator.

2.3 Determination of alcohol content

The determination of content of alcohol percentage on days 0, and 28 was conducted using the Ebulliometer instrument.

2.4 Determination of total soluble solid

The assessment of total soluble solids (°Brix) involved the use of a hand refractometer (Model AR3D-AR64, Abbe, Hamburg, Germany).

2.5 Determination of pH value

The pH values were analyzed on days 0 and 28 using a pH meter (FiveEasy plus, METTLER TOLEDO, Switzerland).

2.6 Determination of color value

The color value analysis was performed using a Colorimeter (HunterLab, ColorFlex® EZ, U.S.A.) in the CIE system, examining L* (brightness), a* (red/green), and b* (yellow/blue) values.

2.7 Statistical Analysis

The experiments were carried out in triplicate. The data underwent analysis of variance (ANOVA), and mean comparisons were conducted using Duncan's multiple range test. The T-test, as described by Steel and Torrie (1980), was utilized for conducting pairwise comparisons. The analysis was conducted utilizing the SPSS software package (SPSS for Windows, SPSS Inc., Chicago, IL, USA).

3. Results and Discussion

3.1 Total acid content

The total acid value of Kombucha beverage infused with Assam tea and Assam tea mixed with longan juice during a 28-day fermentation period showed promising results in Table 1, indicating the development of acidity levels that contribute to the unique taste profile of the beverage. For the

Assam tea Kombucha, the total acid content remained relatively stable from 0.00 at the beginning of fermentation to 0.020 after 28 days. In contrast, the Assam tea mixed with longan juice Kombucha exhibited a noticeable increase in total acid content over the fermentation period, rising from 0.00 at 0 days to 0.031 at 28 days. The observed stability in total acid content for Assam tea Kombucha suggests a controlled and balanced fermentation process. On the other hand, the significant increase in total acid content for the Assam tea mixed with longan juice Kombucha indicates a more pronounced acidity development, possibly influenced by the additional sugars and compounds present in the longan juice. This suggests that t he choice of ingredients, specifically the addition of longan juice, has a discernible impact on the acidification process during Kombucha fermentation [4].

Table 1. Total acid contents of Kombucha beverage infused with Assam tea and Assam tea mixed with longan juice during fermentation time for 28 days.

Kombucha	Total acid content	
	0 day	28 day
Assam tea	0.00 ± 0.00	0.020 ± 0.004
Assam t ea + longan juice	0.00 ± 0.00	0.031 ± 0.003

* Mean ± SD (*n*=3).
** Different letters in the same column indicate significant different (p<0.05).

3.2 Total alcohol content

The total alcohol content of the Kombucha beverages, infused with Assam tea and Assam tea mixed with longan juice during fermentation time for 28 days (Table 2). The total alcohol content remained negligible, registering at 0.00 at the start of fermentation and maintaining a low level of 0.00 after 28 days. In contrast, the Assam tea mixed with longan juice Kombucha exhibited a noticeable increase in total alcohol content, escalating from 0.00 at 0 days to 0.62 at 28 days. The minimal increase in alcohol content for the Assam tea Kombucha suggests a relatively subdued fermentation process, consistent with the traditional low-alcohol nature of Kombucha. Conversely, the Assam tea mixed with longan juice Kombucha displayed a significant rise in alcohol content, indicating a more active fermentation, possibly influenced by the additional sugars and fermentable substrates present in the longan juice [5].

Table 2. Total alcohol contents of Kombucha beverage infused with Assam tea and Assam tea mixed with longan juice during fermentation time for 28 days.

Kombucha	Total alcohol content	
	0 day	28 days
Assam tea	0.00 ± 0.00	0.020 ± 0.004
Assam t ea + longan juice	0.00 ± 0.00	0.031 ± 0.003

* Mean ± SD (*n*=3).
** Different letters in the same column indicate significant different (p<0.05).

3.3 Total soluble solid

Table 3 presents the total soluble solid (TSS) values for Kombucha beverages infused with Assam tea and Assam tea mixed with longan juice at both 0 days and 28 days of fermentation. For the Assam tea Kombucha, the TSS content decreased from an initial value of 16.00 at 0 days to 12.53 at 28 days. Similarly, the Assam tea mixed with longan juice Kombucha also exhibited a reduction in TSS content, decreasing from 16.00 at 0 days to 11.01 at 28 days. The changes in TSS (Table 3) indicated alterations in the concentration of dissolved solids, potentially influenced by fermentation processes and ingredient interactions. The decline in TSS for both Kombucha variants suggests a utilization or breakdown of soluble solids during the 28-day fermentation period. This reduction may be attributed to various factors, including the metabolism of sugars by yeast and bacteria present in the Kombucha culture, leading to the production of organic acids and other fermentation by-products. The decline in TSS content aligns with the typical trend observed in Kombucha fermentation, where sugars are metabolized,

leading to a decrease in sweetness and an increase in acidity [6].

Table 3. Total soluble solid of Kombucha infused with Assam tea and Assam tea mixed with longan juice during fermentation time for 28 days.

Kombucha	Total soluble solid	
	0 day	28 days
Assam tea	16.00 ± 0.00	12.0±0.23
Assam t ea + longan juice	16.00 ± 0.00	11.01±0.18

* Mean ± SD (*n*=3).
** Different letters in the same column indicate significant different ($p<0.05$).

3.4 pH values

Table 4 provides the pH values for Kombucha beverages infused with Assam tea and Assam tea mixed with longan juice at both 0 days and 28 days of fermentation. For the Assam tea Kombucha, the pH decreased from an initial value of 5.54 at 0 days to 2.12 at 28 days. Similarly, the Assam tea mixed with longan juice Kombucha exhibited a decline in pH, moving from 5.68 at 0 days to 2.58 at 28 days. The decline in pH is a characteristic feature of Kombucha fermentation, attributed to the production of organic acids, primarily acetic acid. The decrease in pH values signifies the transformation of sugars into acids by the microbial cultures present in the Kombucha, contributing to the unique tangy flavor associated with the beverage. The decrease in pH is likely influenced by the metabolic activities of acetic acid bacteria and yeast, which thrive in the anaerobic conditions of Kombucha fermentation [6, 7].

Table 4. pH values of Kombucha infused with Assam tea and Assam tea mixed with longan juice during fermentation time for 28 days.

Kombucha	pH values	
	0 day	28 days
Assam tea	5.54 ± 0.03	2.12 ± 0.07
Assam t ea + longan juice	5.68 ± 0.05	2.58 ± 0.03

* Mean ± SD (*n*=3).
** Different letters in the same column indicate significant different ($p<0.05$).

3.5 Color values

Table 5 presents the color parameters, including L*, a*, and b* Kombucha beverages infused with Assam tea and Assam tea mixed with longan juice at both 0 days and 28 days of fermentation. The decrease in L* values for both samples indicates a darkening or reduction in lightness, potentially associated with the accumulation of pigments or changes in the overall color intensity during fermentation. The a* values represent the shift along the red-green axis. The negative a* values observed for both Kombucha variants at 28 days suggest a shift towards the green spectrum, indicating changes in the beverage's color hue. This shift may be attributed to the production of compounds during fermentation that contribute to a greenish tint [8]. The b* values represent the shift along the yellow-blue axis. The decrease in b* values for both Kombucha variants at 28 days suggests a reduction in the yellow component and a shift towards a bluer hue (Fig. 1). These changes in color can be crucial for product aesthetics and consumer acceptance [9].

Table 5. color values of Kombucha beverage infused with Assam tea and Assam tea mixed with longan juice during fermentation for 28 days.

Kombucha	Color values	
	0 day	28 days
Assam tea		
L*	6.58 ± 0.06	2.39 ± 0.02
a*	0.77 ± 0.22	-0.18 ± 0.05
b*	6.57 ± 0.10	1.88 ± 0.03
Assam tea + longan juice		
L*	7.09 ± 0.23	4.98 ± 0.02
a*	3.35 ± 0.06	1.81 ± 0.08
b*	7.94 ± 0.14	6.37 ± 0.08

* Mean ± SD (*n*=3).
** Different letters in the same column indicate significant different ($p<0.05$).

Fig.1. Appearance of Kombucha beverage infused with Assam tea and Assam tea mixed with longan juice during fermentation for 28 days.

4. Conclusions

A continuous increase in acidity and alcohol content in Kombucha infused with Assam tea and longan juice during fermentation. Conversely, pH value and total soluble solid content consistently decreased. The visual transition from a slightly cloudy yellow-brown solution to a clear liquid with visible SCOBY bacteria suggested the fermentation process. The study highlights Assam tea and longan as promising ingredients for novel beverage production, offering consumers an intriguing choice.

Acknowledgement

This work was supported by National Research Council of Thailand and Maejo university for contract No. MJU.-1-65-010.2 to Asst. Prof. Dr. Vachira Choommongkol.

References

[1] Long, X., Waldstein, A., Wu, H., & Geng, Y. (2023). *Centella asiatica* complex health tea: Opportunities and challenges in the development of a commercial product based on indigenous knowledge. Asian Biotechnology and Development Review, 25(1-2), 69-74.

[2] Laureys, D., Britton, S. J., & De Clippeleer, J. (2020). Kombucha tea fermentation: A review. Journal of the American Society of Brewing Chemists, 78(3), 165-174.

[3] Ivanišová, E., Meňhartová, K., Terentjeva, M., Harangozo, Ľ., Kántor, A., & Kačániová, M. (2020). The evaluation of chemical, antioxidant, antimicrobial and sensory properties of kombucha tea beverage. Journal of Food Science and Technology, 57, 1840-1846.

[4] Neffe-Skocińska, K., Sionek, B., Ścibisz, I., & Kołożyn-Krajewska, D. (2017). Acid contents and the effect of fermentation condition of Kombucha tea beverages on physicochemical, microbiological and sensory properties. Cyta-Journal of Food, 15(4), 601-607.

[5] Talebi, M., Frink, L. A., Patil, R. A., & Armstrong, D. W. (2017). Examination of the varied and changing ethanol content of commercial kombucha products. Food Analytical Methods, 10, 4062-4067.

[6] Muhialdin, B. J., Osman, F. A., Muhamad, R., Che Wan Sapawi, C. W. N. S., Anzian, A., Voon, W. W. Y., & Hussin, A. S. (2019). Effects of sugar sources and fermentation time on the properties of tea fungus (kombucha) beverage. International Food Research Journal, 26(2). 481-487.

[7] Hammel, R., Karakilic, V., & Shaw, F. (2016). The affect of temperature and pH on the food safety of kombucha tea. BCIT Environmental Public Health Journal. 1-9.

[8] Pure, A. E., & Pure, M. E. (2016). Antioxidant, antibacterial and color analysis of garlic fermented in kombucha and red grape vinegar. Applied Food Biotechnology, 3(4), 246-252.

[9] Yıkmış, S., & Tuğgüm, S. (2019). Evaluation of microbiological, physicochemical and sensorial properties of purple basil kombucha beverage. Turkish Journal of Agriculture-Food Science and Technology, 7(9), 1321-1327.

Dr. Vachira Choommongkol
Assistant Professor
Research Interests:
Medicinal chemistry,
Phytochemicals,

Dr. Mathurot Chaiharn
Assistant Professor
Research Interests:
Biotechnology, Biochemical extracts,

Dr. Theeraphol Sanphan
Assistant Professor
Research Interests: Food Processing, Value added product from Utilization

The organic economy model: Nurturing sustainability and harmony

Samuel Kwesi Dunyo

Faculty of Business Administration, Maejo University, Chiangmai Thailand
*E-mail: samdunyo@yahoo.com@email.com

Abstract: This study examined the organic economic model with the aim to argue in favor of its full adoption in rapidly growing emerging economics like Thailand. The challenges and benefits of the organic model compared to the market economy model are also highlighted. The study used the opinions of business, policy makers and experts documented in the literature. Basically, the organic economy model seeks to integrate human economic activities with natural processes, fostering a harmonious relationship between economic development and environmental conservation. The investigations revealed some key challenges and merits of the organic economy model relative to the market economy model. One of the primary challenges is the transition from market economic models to the organic model. This requires changes in consumer behavior, business practices, and policy frameworks, which can be met with resistance or inertia. Another challenge is that striking a balance between economic growth and environmental conservation is a delicate task. The challenge lies in developing economic models that support growth without compromising the planet's ecological integrity. The benefits appear to outweigh the challenges. By promoting sustainable practices, the organic economy model aims to mitigate the negative impact of economic activities on the environment and contribute to the overall health of the planet. Additionally, local and community-focused initiatives enhance social cohesion and well-being. By supporting local businesses and economies, the organic economic model contributes to the development of vibrant and resilient communities. Also, sustainability and responsible agricultural resource management contribute to long-term economic stability. By avoiding the depletion of essential resources, the organic economic model seeks to create a foundation for enduring economic prosperity. Finally, various forms of inequality that characterize market economies would reduce significantly with the adoption of the organic model. While challenges exist in its adoption and implementation, the potential benefits make the exploration and pursuit of the organic economic model a worthy endeavor for societies seeking a more balanced and sustainable future.

Key words: Challenges, Organic economy, sustainable development, sufficiency economy philosophy

1. Introduction

Rising Green House Gases (GHG) and its attendant climate change events have rekindled the issue of sustainable economic practices. Some scholars have argued that the market economy championed by economists predominantly in the Western countries may not be helpful in explaining difficult problems faced now by both poor and rich countries.
Market economies may have an initial positive cycle but eventually may end with social polarization, income inequality and subsequently economic growth that compromise environmental quality (Van Bavel, 2019).

In his seminal work, “The Wealth of Nations" (1776), (Smith, 1776) expounded the virtues of free markets, competition, and the invisible hand—the idea that individuals pursuing their self-interest unintentionally contribute to the overall well-being of society. The market economy has not been without its challenges. Economic recessions, inequality, and the ebb and flow of market forces have sparked debates on the role of government intervention (Krueger, Anne O., 1990). Some economists also argued that social policy should play a complementary role in order to translate economic growth generated by the market economy into social welfare (Collier et al,1998) The implication is that the so called social market economy could solve most of the challenges posed by the market economy (Wohlgemuth, 2008).

The Great Depression of the 1930s prompted a reevaluation of laissez-faire policies, leading to the adoption of Keynesian economics, which emphasized government intervention to stabilize the economy (Keynes, J. M. 1937). Increasing inequality, market failures, and social and environmental externalities have cast doubt on the

government's ability to enact policies that effectively deal with these challenges (Adelman, Irma 1999).

The call for an alternative economy model is rising. As indicated in Karl Polanyi and documented in Maucourant (2001)"To allow the market mechanism to be sole director of the fate of human beings and their natural environment indeed, even of the amount of use of purchasing power, would result in the demolition of society. […] In disposing of a man's labor power the system would, incidentally, dispose of the physical, psychological, and moral entity "man" attached to that tag. […] Nature would be reduced to its elements, neighborhoods and landscapes defiled, rivers polluted, military safety jeopardized, the power to produce food and raw materials destroyed. (Polanyi 2001: 76)"

The complexities of the challenges faced by the global economy is prompting the need to revisit the market economy model. Would a different economy model help? Some proponents of alternative economic model, often associated with sustainability and ethical considerations, use the term "organic economy" to describe a system that prioritizes environmental sustainability, social equity, and community well-being. While the market economy has its challenges, proponents of the organic economy model suggest that it offers potential solutions to address some of these issues. In this essay, we take a look at the organic economy model, its principles and potential implementation challenges. The paper also discussed the sufficiency economy philosophy in comparison to the organic model.

In this section, presented a background that is supported by the brief literature, goals, and scopes. The literatures used must be relevant. The literature review should be integrated in the introduction, methods, and result and discussion.

2. Principles of the organic economy model

One of the key principles of the OEM is environmental sustainability in terms of prudent natural resource management and eco-friendly practices. The OEM emphasizes responsible resource management. For example, sustainable forestry practices ensure that only a portion of the forest is harvested, allowing for regeneration and maintaining biodiversity. Similarly, organic farming practices, such as crop rotation and natural fertilization, reduce reliance on synthetic chemicals, minimizing environmental harm.

The second principle is localism and community empowerment. Community empowerment can occur through local economic development and community engagement. Community-supported agriculture (CSA) programs connect local farmers directly with consumers, promoting local economic development and reducing the environmental impact of long-distance transportation.
Community engagement encourages worker cooperatives, where employees have a say in decision-making, empower local communities by fostering a sense of ownership and collaboration.

Thirdly, the OEM promotes fair trade and ethical practices. For instance, fair trade coffee ensures that farmers receive a fair price for their product, promoting economic equity and better living conditions in coffee-producing regions. At the same time companies committed to ethical sourcing of materials for products, such as fair trade clothing, ensure that workers are treated fairly and work in safe conditions.

Another principle is the diversification and resilience which involves transitioning from a monoculture agriculture system to agroforestry, where different crops and trees are cultivated together, promotes biodiversity and reduces the risk of crop failure due to pests or climate changes. Resilience planning also ensures that local food hubs that bring together small-scale farmers, processors, and distributors enhance the resilience of local food systems and reduce vulnerability to disruptions in the global supply chain.

A fifth principle of the OEM is consumer education and empowerment. Eco-labeling on products, such as the Fair Trade or USDA Organic label, provides consumers with transparent information about the social and environmental practices of the products they purchase. Educational campaigns on sustainable consumption empower consumers

to make choices that align with their values, such as reducing single-use plastic consumption.

The OEM also brings along decentralization and democratic decision-making. Participatory budgeting allows community members to have a direct say in allocating local funds, promoting local decision-making and community engagement. Also worker cooperatives operate on democratic principles, with employees participating in decision-making processes, ensuring a more equitable distribution of power within the organization.

OEM promotes sustainable development. Cities that incorporate green infrastructure planning ensure a sustainable and resilient urban environment, considering long-term ecological health and the well-being of future generations. Intergenerational land trusts protect natural resources for future generations, ensuring that land is used in a way that benefits both current and future communities.

Businesses are able to balance profit-making with a commitment to social and environmental responsibility, exemplifying a balanced approach to business.

Finally, OEM embraces innovation and adaptation in terms of technological innovation and climate adaptation. Sustainable technology, such as solar-powered water pumps for agriculture or eco-friendly building materials, represents innovations aligned with the principles of the organic economy model. Community-based climate adaptation projects, like flood-resilient infrastructure or sustainable water management, demonstrate the capacity to adapt to changing environmental conditions.

3. Potential Implication and Challenges

While the organic economy model presents a promising framework for addressing sustainability, ethical concerns, and community well-being, it is not without its potential implications and challenges. Implementation of this model may face hurdles and necessitate careful consideration of various factors. A major implementation challenge of the OEM is the Transition Costs. Implementing the OEM may require a significant transition from existing economic structures. Businesses and communities may face initial costs associated with adopting sustainable practices, ethical sourcing, and decentralized decision-making. Managing this transition effectively is crucial to ensure a smooth shift toward the organic model.

The second challenge is competitive disadvantages. Businesses adhering to organic and ethical practices may face challenges competing with conventional counterparts that prioritize short-term profits over sustainability. Higher production costs associated with environmentally friendly and fair labor practices could place organic businesses at a competitive disadvantage, especially in price-sensitive markets.

Another challenge is consumer awareness and behavior. The success of the organic economy model depends on consumer awareness and willingness to support sustainable and ethical products. Educating consumers about the environmental and social impact of their choices is a continuous challenge. Convincing individuals to prioritize values over lower prices may require extensive marketing and educational efforts.

Globalization and Supply Chain Complexity also poses a great challenge. In a globalized economy, supply chains are often complex and interconnected. Ensuring ethical sourcing and sustainable practices throughout the entire supply chain can be challenging, especially when dealing with multinational corporations or navigating international regulations. Coordinating efforts on a global scale is necessary for the model's success.

Small-Scale Agriculture Limitations. While localism is a key principle of the organic economy model, it may face limitations in certain sectors, such as agriculture. Scaling up sustainable and organic agriculture to meet the demands of growing populations can be challenging, especially when compared to large-scale conventional farming practices.

Policy and Regulatory Support. The success of the organic economy model may hinge on the development of supportive policies and regulations. Governments play a crucial role in incentivizing sustainable practices, promoting fair trade, and ensuring a level playing field for businesses committed to ethical principles. Lack of regulatory support can hinder the widespread adoption of the model.

Economic incentives and financial models. Creating financial models that incentivize businesses to adopt the organic economy model is essential. Governments, financial institutions, and investors need to provide support and incentives for businesses that prioritize sustainability and ethical practices. Aligning economic incentives with long-term environmental and social goals may require innovative financial mechanisms.

Measurement and Certification Challenges. Ensuring the authenticity of organic and sustainable claims requires robust certification and labeling systems. Establishing and maintaining these systems can be challenging, as they must account for various factors such as fair labor practices, environmental impact, and supply chain transparency.

Social Equity Considerations. While the organic economy model aims to address social equity, there is a risk that certain communities or groups may be left behind in the transition. Ensuring that the benefits of the model reach marginalized or economically disadvantaged populations is critical to prevent exacerbating existing inequalities.

Technological Innovation. Embracing sustainable technologies and innovations is a key component of the organic economy model. However, the pace of technological development and the affordability of green technologies may pose challenges. Access to and adoption of these innovations need to be widespread to achieve the model's sustainability goals.

Interconnectedness of Challenges. The challenges associated with the organic economy model are interconnected and multifaceted. Addressing one challenge often requires consideration of others, requiring a comprehensive and integrated approach.
Balancing economic, social, and environmental goals while navigating these interconnections poses a significant ongoing challenge.

Despite these challenges, the organic economy model offers a compelling vision for a more sustainable and equitable future.
Overcoming these obstacles requires collaboration among businesses, governments, consumers, and other stakeholders. As societies strive to balance economic prosperity with environmental and social responsibility, addressing these implications and challenges will be crucial for the successful implementation of the organic economy model.

4. The organic economy model and the sufficiency economy philosophy

The Organic Economy Model and the Sufficiency Economy Philosophy are two distinct approaches to economic and societal development, each with its unique principles and emphasis. This section explores the key characteristics of both models to understand their similarities and differences:

4.1 Organic Economy Model

Foundation
Focus: The organic economy model places a strong emphasis on sustainability, ethical practices, and community well-being.
Environmental Considerations: It prioritizes environmental sustainability through practices such as organic farming, renewable energy, and eco-friendly production methods.

Economic Structure
Localism: The model promotes localism, encouraging the development of resilient, community-centric economies that prioritize the well-being of local residents.
Fair Trade: It emphasizes fair trade and ethical practices, ensuring fair compensation for workers and ethical sourcing of materials throughout the supply chain.

Consumer Involvement
Consumer Education: The model emphasizes consumer education, aiming to empower individuals to make informed choices aligned with sustainability and ethical considerations.
Transparency: There is a focus on transparent information about products and services, often through eco-labeling, to allow consumers to make responsible purchasing decisions.

Decentralization and Democracy
Local Decision-Making: The model supports decentralized decision-making, empowering local communities to shape their economic futures.
Participatory Governance: There is an emphasis on participatory governance, involving stakeholders in decision-making processes, which can include community members and workers in cooperatives.

Holistic Approach
Triple Bottom Line: The model adopts a triple bottom line approach, considering social, environmental, and economic factors in decision-making.
Long-Term Perspective: It prioritizes long-term sustainability, ensuring that economic activities meet present needs without compromising the ability of future generations to meet their own needs.

4.2 The Sufficiency Economy Philosophy
Foundation
Focus: The Sufficiency Economy Philosophy (SEP), developed by His Majesty King Bhumibol Adulyadej of Thailand, emphasizes moderation, self-reliance, and resilience.
Scholars have since studied the SEP to see its practical relevance in various parts of Thailand (Mongsawad, P. 2010; Piboolsravut, P. 2004). This essay outline core parts of the SEP and its differences and similarities with OEM.
Moderation: It encourages individuals and communities to avoid excess and live within their means.

Economic Structure
Balanced Development: The philosophy advocates for balanced and sustainable development, avoiding overreliance on external factors.
Diversification: It encourages a diversified economic portfolio to reduce vulnerability to external shocks.

Individual and Community Values
Self-Sufficiency: Individuals and communities are encouraged to be self-sufficient, meeting their basic needs without relying excessively on external resources.
Community Values: The philosophy promotes a sense of community and mutual support, emphasizing the well-being of the collective.

Principles of Sufficiency Economy
Moderation: Encourages individuals and businesses to avoid excess and extravagant behavior.
Reasonableness: Promotes reasoned and considerate decision-making in both personal and business matters.
Risk Management: Advocates for cautious and prudent risk management to ensure resilience in the face of uncertainties.

Adaptability and Resilience
Adaptability: The philosophy encourages adaptability and flexibility in the face of changing circumstances.
Resilience: It aims to build resilience at both individual and community levels, enabling them to withstand external economic shocks.

4.3 Similarities between SEP and OEM
Environmental Focus: Both SEP and OEM recognize the importance of environmental considerations, but the organic model places a stronger emphasis on sustainable and eco-friendly practices in production.

Community-Centric Approach: Both SEP and OEM value community well-being, but the sufficiency economy philosophy emphasizes self-reliance and moderation within the community.

Decentralization: Both SEP and OEM support decentralized decision-making, but the sufficiency economy philosophy may place more emphasis on individual and household self-sufficiency.

Risk Management: The sufficiency economy philosophy explicitly emphasizes prudent risk management, while the organic economy model often addresses risk indirectly through sustainable practices.

In short, while both the OEM and the SEP share common principles of sustainability, community well-being, and decentralized decision-making, they differ in their emphasis on environmental practices, self-sufficiency, and the philosophical principles guiding economic decisions. Each model provides a unique perspective on creating a more balanced and resilient approach to economic development.

5. Conclusion

The OEM presents a compelling vision for a sustainable and harmonious future. By prioritizing environmental stewardship, community well-being, and long-term economic stability, this model offers an alternative approach to traditional economic systems. While challenges exist in its adoption and implementation, as is the case SEP, the

potential benefits make the exploration and pursuit of the organic economic model a worthy endeavor for societies seeking a more balanced and sustainable future.

References

[1] Adelman, Irma (1999). The role of government in economic development. Department of Agricultural and Resource Economics and Policy, Working Paper No. 890. California: University of California.

[2] Collier, Paul (1998). Social capital and poverty. Social Capital InitiativeWorking Paper No. 4. Washington, D.C.: World Bank, Social Development Department.Available from http://siteresources.worldbank.org/INTRANETSOCIALDEVELOPMENT882042-1111750197177/20502364/SCI-WPS-04.pdf

[3] Keynes, J. M. (1937). The general theory of employment. The quarterly journal of economics, 51(2), 209-223.

[4] Krueger, Anne O. (1990). Government failures in development. Journal of Economic Perspectives, vol. 4, No. 3, pp. 9-23.

[5] Maucourant, J. r. m. (2001). Une lecture de Karl Polanyi. L'Ã? conomie politique, 12(2001/4), 90-106.

[6] Mongsawad, P. (2010). The philosophy of the sufficiency economy: a contribution to the theory of development. Asia Pacific Development Journal, 17(1), 123.

[7] Piboolsravut, P. (2004). Sufficiency economy. ASEAN Economic Bulletin, 21(1), 127-134.

[8] Smith, A. (1776). An inquiry into the nature and causes of the wealth of nations: Volume One. In. London: printed for W. Strahan; and T. Cadell, 1776.

[9] Van Bavel, B. (2019). The invisible hand?: how market economies have emerged and declined since AD 500. Oxford University Press.

[10] Wohlgemuth, M. (2008). A European social model of state-market relations: the ethics of competition from a neo-liberal perspective.

Dr. Samuel Kwesi Dunyo
Research Interest: Fiscal and monetary Policy analysis, financial markets, innovation, and sustainable development.

Uncovering the potentials of long-term straw return and nitrogen supply on subtropical maize (*Zea mays* L.) photosynthesis and grain yield

Fei Gao[1*], Rayyan Khan[1], Li Yang[1], Xun Bo Zhou[1,*]

[1]Guangxi Key Laboratory of Agro-environment and Agro-products Safety, Key Laboratory of Crop Cultivation and Physiology, College of Agriculture, Guangxi University, Nanning 530004, China.
*E-mail: xunbozhou@gmail.com

Abstract: In China, the practice of returning straw to the soil stands as a pivotal technique for managing agricultural waste. Beyond waste utilization, it significantly contributes to soil enrichment and amplifies grain yield. A five-year (2018–2022) field experiment was designed to investigate the impact of varied straw treatment methods and optimal nitrogen (N) application rates on maize's photosynthesis process and grain yield. Main plots were allocated different straw treatments, including straw return (SR) and the traditional practice (TP) of no straw return, while sub-plots were subjected to varying N levels: 100, 150, 200, 250 and 300 kg N ha^{-1}. The findings revealed a proportional increase in gaseous exchange parameters, relative chlorophyll content (SPAD), leaf area index (LAI), dry matter (DM), and grain yield corresponding to elevated N levels. Similarly, SR exhibited a notable enhancement in these parameters compared to TP. Following a five-year duration, SR combined with the optimal N level (250 kg ha^{-1}) exhibited a 2% increase in SPAD values and an 8% surge in Pn, consequently yielding a 27% higher LAI compared to TPN300. Notably, while the SPAD, Pn, LAI, DM, and grain yield peaked at the higher 300 kg N ha^{-1} level, statistically, results were akin to those obtained with 250 kg N ha^{-1}. Hence, this study delineates that SR coupled with 250 kg N ha^{-1} stands as the optimal approach, fostering superior photosynthetic efficiency, robust dry matter production, and amplified grain yield.

Keywords: Maize (*Zea mays* L.); Nitrogen fertilizer; Photosynthesis; Straw return; Grain yield

1. Introduction

Maize (*Zea mays* L.) is one of the most important grain crops in the world including in China (Fan et al., 2022). Plant genetics, nitrogen, and water resources are viewed as paths to increase grain yields. However, nitrogen resource availability is the main impediment to grain yield increase in many cropping systems (Sinclair and Rufty, 2012). Additionally, nitrogen is overused causing soil degradation and water pollution, and endangering the environment (Wang et al., 2021).

Straw is a by-product of crops that are rich in nitrogen, phosphorous, potassium, and other trace elements (Wang et al., 2020). Straw return (SR) is a green agricultural technology that reduces environmental pollution (straw burning) and improves soil health and grain yields (He et al., 2022). China is a vast agricultural country that yielded a respective 797 million tons and 802 million tons in 2020 and 2021 of different types of crop straw ((Chen et al., 2022); National Bureau of Statistics data, http://www.stats.gov.cn/). It has been highly advocated straw utilization in China due to the prohibition of straw burning causing environmental pollution.

Guangxi is a subtropical monsoon humid region with maize as the top food crop growing in a double cropping system. Indeed, N is the most limiting nutrient for tropically produced maize (Osmond and Riha, 1996), nitrogen application along with straw return improves soil fertility via improved soil enzyme activities and microbial community composition (Yang et al., 2022). The nitrogen uptake and grain yield were boosted due to straw incorporation plus N application (150−225 kg ha^{-1}) and also prevented N loss.

To sum up, previous studies mainly focused on the effect of straw returning application in different crops, cropping systems, different regions, and different fertilizers. It is noteworthy, that rice straw returning is especially common in southern regions of China, apart from this, a large amount of maize straw is also produced. However, there is a lack of knowledge on maize straw returning in

combination with nitrogen fertilizer application in improving subtropical grain yield.

2. Methods

The experiment was carried out at the Agriculture Research Farm of Guangxi University (22°50′N, 108°17′E) from 2018 to 2022. It had a warm and subtropical monsoon climate, and the average monthly rainfall and temperature during the growth period of maize are shown in the Fig. 1.

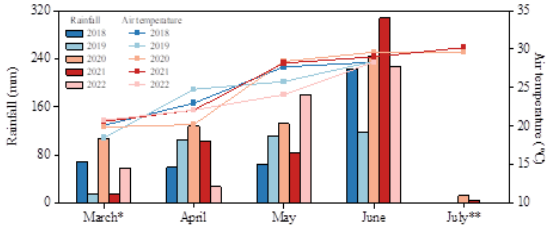

Fig. 1. Monthly rainfall and air temperature during the years 2018–2022. *From sowing to March 31; **From July 1 to harvest.

The experiment was carried out in a randomized complete block design with a split-plot arrangement having three replications. The experiment was comprised of two cultivation systems such as SR and traditional practice (TP) (no straw return) that were assigned to the main plot and five nitrogen fertilization rates (100, 150, 200, 250, and 300 kg ha^{-1}) were allotted to sub-plots. All the maize straws from the previous crop were harvested, chopped, mixed, and incorporated into the field with the help of a rotavator. Traditional practice was to manually remove the straw from the field plots before fertilization and preparation of the land. Maize variety Zhengda 619 was manually sown with 0.3 m plant-to-plant spacing and 0.6 m row spacing with 2–3 seeds per hole, the seedlings were thinned to one seedling at the 2–3 leaf stage. The population density was 55556 plants ha^{-1}. 2/3 of N (46.4% urea), 100 kg ha^{-1} of P (P_2O_5 as18.0% calcium magnesium phosphate fertilizer), and 100 kg ha^{-1} K (K_2O as 60.0% potassium chloride) were used as base fertilizers at the time of sowing. The remaining nitrogen fertilizer was applied as the top dressing during the 12th leaf stage (V12). The photosynthesis rate (Pn), intercellular carbon dioxide concentration (Ci), stomatal conductance (Gs), and transpiration rate (Tr) of the leaves were measured with LI-6800 Portable Photosynthesis System (LI-COR, Lincoln, NE, USA). SPAD-502 Plus chlorophyll meter (Konica Minolta, Tokyo, Japan) was used to determine the relative chlorophyll content (SPAD values) on maize plants. Furthermore, the leaf length and width were measured using a measuring tape. Three maize plants divided into stem, leaf, and ear. The samples were placed in the oven at 105 ℃ for one hour and then achieve a constant drying weight. After drying in the oven the samples were weight to get the biomass. For grain yield determination, an area of 2 m^2 in each plot was selected for threshing and after threshing, the grain yield was measured.

3. Results and Discussion

3.1. Gaseous exchange parameters

The analysis of the results showed that the gas exchange parameters was significantly affected by straw treatments (ST), nitrogen (N) levels, and Years (Y) (Fig. 2). Among the ST, SR increased the gas exchange parameters to varying degrees compared with TP. Such as, photosynthesis rate (Pn) was increased by 13% in SR compared with TP. Similarly, different N levels also enhanced gas exchange parameters, as we witnessed that stomatal conductance (Gs) was 90% and 105% increase in N250 and N300 compared with N100, respectively. Furthermore, the gas exchange parameters was higher in SRN250 combination compared with TPN300 treatments combination. Intercellular CO_2 (Ci) was 5% higher in SRN250 in comparison with TPN300. Across ST and N, the transpiration rate (Tr) was increased from the first year to the fifth year. Overall the results showed that the gas exchange parameters was improved in the fifth year under SRN250 in comparison with TPN300.

Previous studies have shown that both N supply and SR can effectively improve the photosynthetic capacity and grain yield (Guo et al., 2021; Liu et al., 2018; Wang et al., 2021). Similarly to Wang et al.'s (2022) findings, but Gs showed an opposite trend with increasing nitrogen application rates. Similarly, in treatments combination, SRN250 enhanced the aforementioned parameters compared with TPN300 (Fig. 2). The reason behind the improvement of the maize gaseous exchange parameters may be that straw returning to the field and applying N fertilizer can effectively supply nutrients needed for maize photosynthetic metabolism, and the SPAD values increase which promotes the photosynthesis process.

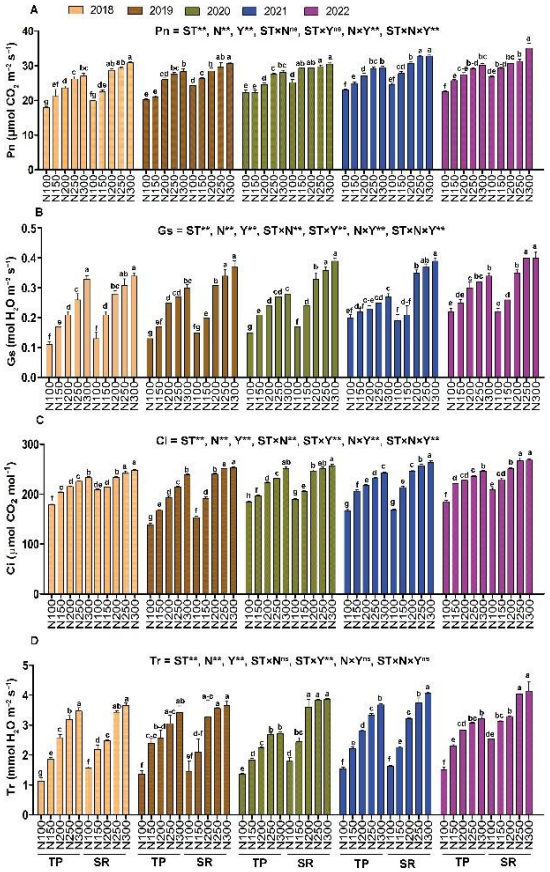

Fig. 2. Photosynthetic characteristics of maize under straw treatments and different nitrogen levels application during the years 2018–2022. Different lowercase letters indicate significant differences (** indicate significant differences at 0.01 probability level while ns stands for nonsignificant). Photosynthesis rate (Pn, A), stomatal conductance (Gs, B), intercellular CO_2 concentration (Ci, C), and transpiration rate (Tr, D) represents means ± standard errors of three replications. ST: straw treatments; N: nitrogen; Y: year; TP: traditional practice (no straw return); SR: straw return.

3.2. SPAD values and leaf area index

The chlorophyll content traps sunlight energy and convert atmospheric carbon dioxide into sugars via photosynthesis. Additionally, Hawkins et al. (2009) proved that SPAD values are used for an effective estimation of the total chlorophyll content, and showed a strong positive correlation with maize grain yield (Kandel, 2020). The results showed that the relative chlorophyll content (SPAD values) and LAI was significantly affected by ST, N, and Y (Fig. 3). The SPAD and LAI showed a total of 9% and 21% increment from TP to SR, respectively. The LAI was increased by 33%, 45%, and 49% in N200, N250, and N300 compared with N100. Moreover, the SPAD values were 2% and 6% higher in SRN200 and SRN250 compared with TPN300, respectively. Finally, the SR showed a prominent effect in the last year that resulted various increment in LAI and SPAD value under SRN200 and SRN250 in comparison with TPN300.

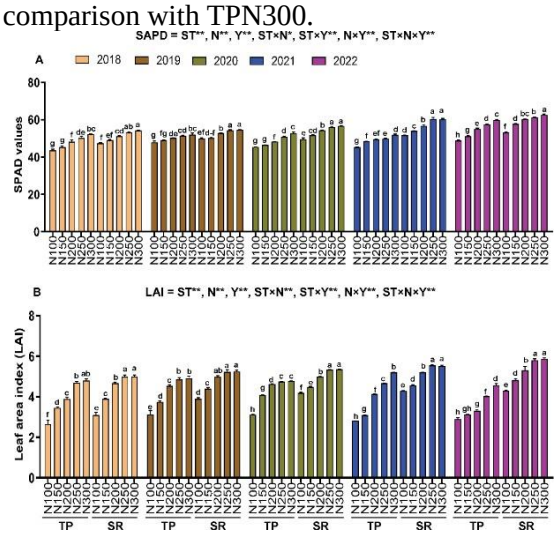

Fig. 3. Relative chlorophyll content and leaf area index of maize under straw treatments and different nitrogen levels application during the years 2018–2022. Different lowercase letters indicate significant differences (** indicate significant differences at 0.01 probability level while ns stands for nonsignificant). Relative chlorophyll content (SPAD values, A) and leaf area index (LAI, B) represents means ± standard errors of three replications. ST: straw treatments; N: nitrogen; Y: year; TP: traditional practice (no straw return); SR: straw return.

3.3. Dry matter and grain yield

The dry matter (DM) of maize was significantly affected by ST, N, and Y (Fig. 4A). The DM was increased by 14% in SR (1662.0 g m^{-2}) compared with TP (1453.6 g m^{-2}). Similarly, N application also increased DM and the analysis of the results showed a respective increase of 27%, 39%, and 43% in N200 (1591.1 g m^{-2}), N250 (1736.3 g m^{-2}), and N300 (1787.0 g m^{-2}) compared with N100 (1251.5 g m^{-2}). The DM content was 9% more in the fifth year (1617.0 g m^{-2}) compared with the first year (1477.4 g m^{-2}). Moreover, in treatments combination, the DM was increased by 2% and 13% in SRN200 (1695.2 g m^{-2}) and SRN250 (1881.3 g m^{-2}) compared with TPN300 (1658.7 g m^{-2}), respectively. Overall, the results showed that the DM content was improved by SR after five years as a 6% and 15% increment was observed in the last year (fifth year) under SRN200 (1802.0 g m^{-2}) and SRN250 (1946.4 g m^{-2}) compared with TPN300 (1698.0 g m^{-2}), respectively.

Finally, grain yield was also significantly affected by ST, N, and Y (Fig. 4B). Among the ST, SR (6407 kg ha^{-1}) increased the grain yield by 10% compared with TP (5840 kg ha^{-1}). N application also improved grain yield and showed a respective increment of 33%, 39%, and 39% in N200 (6481 kg ha^{-1}), N250 (6796 kg ha^{-1}), and N300 (6819 kg ha^{-1}) compared to N100 (4890 kg ha^{-1}). In treatments combination, the grain yield was 7% higher under SRN250 (7064 kg ha^{-1}) compared with TPN300 (6583 kg ha^{-1}). Altogether, the analysis of the results showed that yield was increased by SR after five years as a 7% increment was observed in the fifth year under SRN250 (7088 kg ha^{-1}) compared with TPN300 (6616 kg ha^{-1}).

Our result revealed that grain yield increased by 10% in SR compared with TP. Moreover, after five years of straw returning, we witnessed a 7% increment in grain yield under SRN250 compared with TPN300 (Fig. 4). The possible reason may be, first, the straw return might change the nitrogen and microbial activities that can improve the root growth environment (Hu et al., 2021). This create favorable soil moisture conditions for grain yield and production (Jin et al., 2020; Zhang et al., 2023). Second, adding nitrogen fertilizer and straw returning to the field jointly improve the leaves' capacity to produce and transport photosynthates (Meng et al., 2021). In the nutshell, an appropriate amount of N (200–250 kg ha^{-1}) plus the straw return is a good one instead of a higher N dose (300 kg ha^{-1}) plus no straw return.

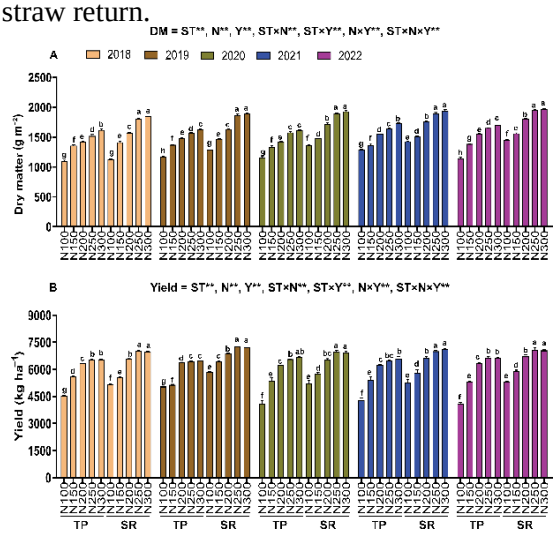

Fig. 4. Dry matter and yield of maize under straw treatments and different nitrogen levels application during the years 2018–2022. Different lowercase letters indicate significant differences (** indicate significant differences at 0.01 probability level while ns stands for nonsignificant). Dry matter (A) and yield (B) represents means ± standard errors of three replications. ST: straw treatments; N: nitrogen; Y: year; TP: traditional practice (no straw return); SR: straw return.

4. Conclusions

Straw return (SR) significantly improved SPAD values, photosynthesis rate, dry matter, soil nitrogen content, maize grain nitrogen content, and grain yield as compared to traditional practice (TP) (no straw return). An increase was observed in gaseous exchange parameters, leaf area index, dry matter, and grain yield at N200, N250, and N300 (kg ha^{-1}) levels. However, nitrogen application of 250 kg ha^{-1} in the SR cultivation system remained higher for a better photosynthesis process, dry matter accumulation, and grain yield than in the TP cultivation system. The regression and correlation analyses also favored SR cultivation over than TP cultivation system. The correlation analysis showed that grain yield and dry matter were highly correlated with each other in the SR cultivation system compared with the TP cultivation system. Therefore, it depicted that optimum nitrogen application (250 kg ha^{-1}) along with straw incorporation into a field has proved the best strategy for better maize grain yield. More research on long-term trails are still needed to understand how it impacts the soil physio-chemical properties, soil nutrients status, soil enzyme activities, and microbial community structure. These findings offer helpful information when addressing significant concerns about straw use in China. Therefore, balancing straw integration practices with nitrogen fertilizer consumption is essential and the cornerstone of sustainable agricultural development.

References

[1] Fan, Y. fang, Gao, J. lin, Sun, J. ying, Liu, J., Su, Z. jun, Hu, S. ping, Wang, Z. gang, Yu, X. fang, 2022. Potentials of straw return and potassium supply on maize (*Zea mays L.*) photosynthesis, dry matter accumulation and yield. Sci. Rep. 12, 799.

[2] Sinclair, T.R., Rufty, T.W., 2012. Nitrogen and water resources commonly limit crop yield increases, not necessarily plant genetics. Glob. Food Secur. 1, 94–98.

[3] Wang, G.Y., Hu, Y.X., Liu, Y.X., Ahmad, S., Zhou, X.B., 2021. Effects of

supplement irrigation and nitrogen application levels on soil carbon–nitrogen content and yield of one-year double cropping maize in subtropical region. Water 13, 1180.

[4] Wang, W., Cheng, Z., Cong, Q., 2020. The comprehensive utilization technology of crop straw. IOP Conf. Ser.: Earth Environ. Sci. 446, 032047.

[5] He, J., Zhou, W., Guo, S., Deng, X., Song, J., Xu, D., 2022. Effect of land transfer on farmers' willingness to pay for straw return in Southwest China. J. Clean. Prod. 369, 133397.

[6] Chen, L., Sun, S., Yao, B., Peng, Y., Gao, C., Qin, T., Zhou, Y., Sun, C., Quan, W., 2022. Effects of straw return and straw biochar on soil properties and crop growth: A review. Front. Plant Sci. 13, 986763.

[7] Osmond, D.L., Riha, S.J., 1996. Nitrogen fertilizer requirements for maize produced in the tropics: A comparison of three computer-based recommendation systems. Agric. Syst. 50, 37–50.

[8] Yang, L., Muhammad, I., Chi, Y.X., Wang, D., Zhou, X.B., 2022. Straw return and nitrogen fertilization to maize regulate soil properties, microbial community, and enzyme activities under a dual cropping system. Front. Microbiol. 13, 823963.

[9] Guo, Y., Yin, W., Fan, H., Fan, Z., Hu, F., Yu, A., Zhao, C., Chai, Q., Aziiba, E.A., Zhang, X., 2021. Photosynthetic physiological characteristics of water and nitrogen coupling for enhanced high-density tolerance and increased yield of maize in arid irrigation regions. Front. Plant Sci. 12, 726568.

[10] Liu, Z., Gao, J., Gao, F., Liu, P., Zhao, B., Zhang, J., 2018. Photosynthetic characteristics and chloroplast ultrastructure of summer maize response to different nitrogen supplies. Front. Plant Sci. 9, 576.

[11] Wang, J., Ma, Y., Di, L., Qian, X., Wang, G., 2021. Straw incorporation with nitrogen amendment shapes bacterial community structure in an iron-rich paddy soil by altering nitrogen reserves. Microorganisms. 9, 988.

[12] Hawkins, T.S., Gardiner, E.S., Comer, G.S., 2009. Modeling the relationship between extractable chlorophyll and SPAD-502 readings for endangered plant species research. J. Nat. Conserv. 17, 123–127.

[13] Kandel, B.P., 2020. Spad value varies with age and leaf of maize plant and its relationship with grain yield. BMC Res. Notes 13, 13–16.

[14] Hu, W., Yu, C., Zhao, W., Liu, R., Yang, C., Zhou, Z., 2021. The effects of straw-returning and inorganic K fertilizer on the carbon–nitrogen balance and reproductive growth of cotton. J. Cotton Res. 4, 31.

[15] Jin, Z., Shah, T., Zhang, L., Liu, H., Peng, S., Nie, L., 2020. Effect of straw returning on soil organic carbon in rice–wheat rotation system: A review. Food and Energy Secur. 9, e200.

[16] Zhang, H., Liu, Q., Liu, S., Li, J., Geng, J., Wang, L., 2023. Key soil properties influencing infiltration capacity after long-term straw incorporation in a wheat (Triticum aestivum L.)–maize (*Zea mays L.*) rotation system. Agric. Ecosyst. Environ. 344, 108301.

[17] Meng, X., Guo, Z., Yang, X., Su, W., Li, Z., Wu, X., Ahmad, I., Cai, T., Han, Q., 2021. Straw incorporation helps inhibit nitrogen leaching in maize season to increase yield and efficiency in the Loess Plateau of China. Soil Till.e Res. 211, 105006.

Ms. Fei Gao
Master student, Majoring in Crop Science （Crop cultivation and farming）

Dr. Rayyan Khan
DOB: Feb 10, 1991
Major: Crop Cultivation and Farming System
Current status: Postdoctoral Fellow
College of Agriculture, Guangxi University

Dr. Li Yang
Lecturer
Majoring in Crop cultivation physiology and field ecology

Dr. Xunbo Zhou, PhD,
Professor

Majoring in Crop physiology and ecology

Experimental Study on the Effect of Stepped Vertical Greening Based on the Spray System on Outdoor Thermal Environment: A Case Study of Nanning City, China

Xinyi Lu, Peisi Chen , Yutao Chen , Junli Wang, Xiu Yang*

School of Civil Engineering and Architecture, Guangxi University, China

*E-mail: 79926885@qq.com

Abstract: Stepped vertical greening is a popular garden landscape technique for both indoor and outdoor viewing. Under the background of advocating energy conservation and emission reduction, improving the effect of stepped vertical greening on the thermal environment has become a hot research issue. This study proposed the stepped vertical greening cooling measure based on the spray system, which was tested under various working conditions on the steps of a teaching building in Nanning, Guangxi Province during the summer. The study compared temperature and humidity data at measurement points between a test and a control group. According to the study's findings, the temperature of the site with stepped vertical greening based on the spray system was reduced by an average of 3.2 °C, with a temperature difference rate of change of up to 0.25 °C per minute. The humidity was also increased by an average of 12.8%RH, with a humidity difference rate of change of up to 0.79%RH per minute. These results indicate that the improvement effect is obvious and it is conducive to the realization of energy saving and emission reduction. The stepped vertical greening based on the spray system has good feasibility in Nanning City, which provides a reference for its popularization and application in South China and even Southeast Asia area.
Keywords: stepped vertical greening, spray system, outdoor thermal environment, Nanning

1. Introduction

As the issue of global warming becomes increasingly pressing, countries are strongly supporting the development of energy-saving and emission-reducing technologies and policies. For urban managers and planning workers, how to incorporate carbon peak and carbon neutrality requirements into landscape design work is an important subject [1]. Stepped vertical greening is a popular indoor and outdoor landscaping technique, but also a way of vertical greening. Under the background of energy-saving and emission reduction, the effect of stepped vertical greening on the thermal environment has become a hot research issue. L H Phin et al (2018) have proposed that landscape design could reduce the impact of climate and carried out a study on improving energy efficiency and microclimate in urban areas [2]. Li He ping et al (2023) have quantitatively studied the carbon sink effect of landscape patterns in urban agglomerations, providing an effective reference for China to achieve the goal of "double carbon" from the perspective of low-carbon urban agglomerations[3]. Vertical greening is one of the most important technologies for energy-saving and emission-reduction in buildings and has experienced rapid development in recent years. Irina Susorova et al (2013) have developed a method for predicting and evaluating the thermal effect of vertical greening systems and proposed a mathematical model of a facade covered with climbing plants to assess the thermal effect of plants on heat transfer through the building facade[4]. Senlin Zheng et al (2016) have developed a simulation method for predicting and evaluating the outdoor thermal environment, including a three-dimensional vegetation model. They have verified accuracy by comparing the simulation results with data on the site[5].

Cansu Iraz Seyrek Sık et al (2022) have developed a conceptual framework for a design support model of an energy-efficient vertical greening facade system, focusing on its thermal and shading performances[6]. Lan Pan et al (2023) have systematically summarized the four main mechanisms influencing the thermal effect of vertical greening systems and put forward the key direction of future research on vertical greening combined with the existing research[7]. Vertical greening is widely used in public buildings because of its cooling effect and its ability to reduce energy consumption and improve users' comfort[8][9]. Stepped vertical greening has a good landscaping effect. Therefore it is widely used in major public buildings. Nanning City, located in Guangxi, China, has a subtropical monsoon climate with long and hot summers (as shown in Figures 1 and 2)[10]. However, although stepped vertical greening has a better landscape effect than other kinds of vertical greening, its ability to improve the thermal environment is not significant. Chang Yang et al. (2019) established a spray cooling system on the glass roof of a lighted atrium in a building in Guangzhou and tested the effectiveness of the mist layer formed by the system on the glass surface in terms of shading effect and cooling effect, as well as the thermal environment inside the atrium[11]. Xi Meng et al. (2022) focused on the application efficiency of the spray cooling system, the factors affecting the cooling efficiency, optimization measures, and the future development of the spray cooling system to provide a comprehensive and critical review of existing research and suggest future research trends. Provide a comprehensive and critical review of existing research and suggest future research trends[12]. Spray systems have a significant effect on the improvement of the thermal environment. The study proposes an optimized stepped vertical greening method, the stepped vertical greening based on the spray system, which has both good landscape and cooling effects. The study explores its effects on the outdoor thermal environment in Nanning City, which can provide a reference for the application and promotion of stepped vertical greening in South China and even in Southeast Asia.

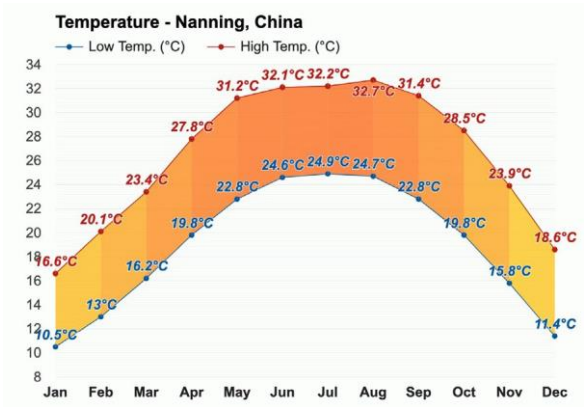

Figures 1. Average temperature of each month Nanning, China[13]

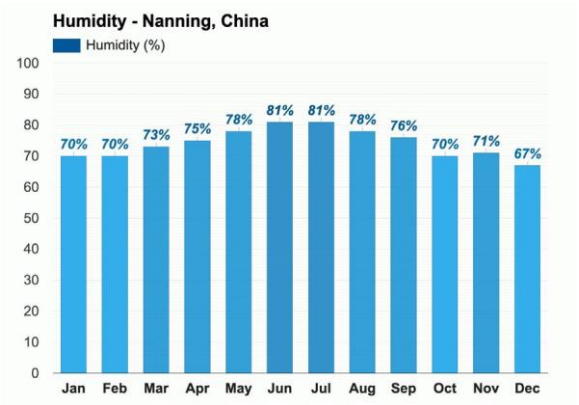

Figures 2. Average humidity of each month Nanning, China[13]

2. Methods

2.1. Experimental site

The study was carried out on the east open-air staircase of Guangxi University's comprehensive teaching building located in Nanning City, which receives the most direct sunlight in the building. The staircase is made of marble and concrete and has a tread width of 300mm and a height of 150mm. For the

experiment, a spray system device was placed on the tenth step of the middle of the staircase, as illustrated in Figures 3 and 4.

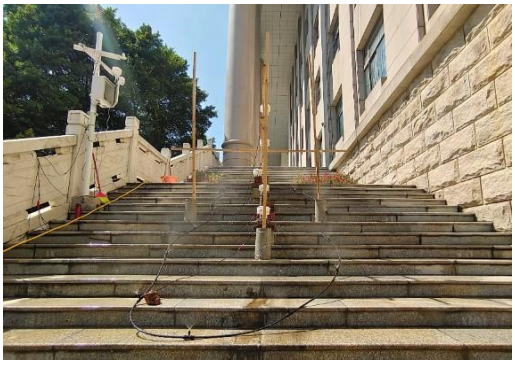

Figures 3. Experimental site (spray system only)

Figures 4. Experimental site (greening + spray system)

2.2. Experimental material and instruments

The setup consists of a collection of 100 potted periwinkle flowers (figure 5.), each with a pot diameter of 200mm. Additionally, there was a compact weather station to measure various meteorological data such as temperature, humidity, solar radiation, wind power, and wind speed. Five temperature and humidity measuring instruments were also included in the system to measure temperature and humidity. All of the instruments provided accurate readings up to one decimal place. There were 12 spray nozzles and a 12V 3A pump(figure 6.). Each nozzle had a water output of 0.8L per minute.

Figures 5. Periwinkle flower

Figures 6. Spray system

2.3. Experimental methodology

Temperature and humidity were the main parameters studied in the experiment. To investigate the effect of stepped vertical greening based on a spray system on the outdoor thermal environment, an experimental group and a control group were established, and the temperature and humidity at different points in the site at the same time of the day (with one minute time interval) were measured and compared.

2.4. Measuring points arrangement

Six temperature and humidity measurement points were set up, in which the temperature and humidity recorder on the meteorological station was the measurement point 1(2.3m from the step), a temperature and humidity re⁴corder was placed 0.5m above the 3rd and 8th steps of the steps (recorded as points 4 and 5). a temperature and humidity recorder was placed 0.5m, 1m and 1.5m above the 5th step, which was recorded as the measurement points 2, 3, and 6. The average values of the measurement points 2, 3, 4, and 5 were taken as the test group data. The data measured at measurement point 1 was used as meteorological data, and the data measured at measurement point 6 was used as control group data. The stepped Vertical greening based on the system was placed as shown in Figures 7-8:

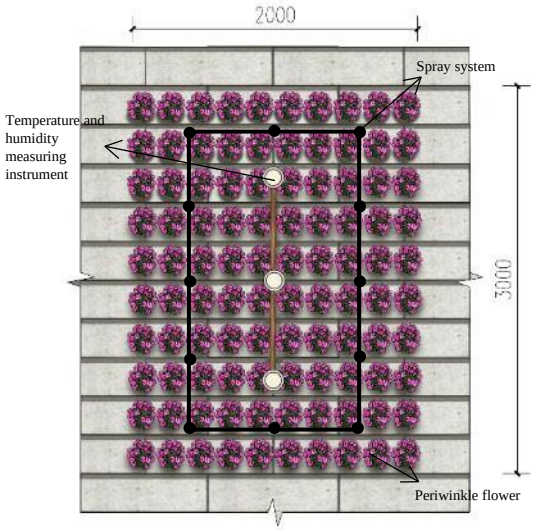

Figures 7. Site layout drawing

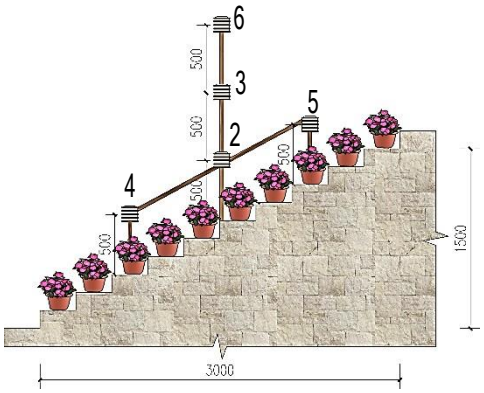

Figures 8. Site layout elevation drawing

3. Results and Discussion

3.1. Data on temperature and humidity (stepped vertical greening+ spray system)

For analysis, the study selected representative data from 11:40-15:00 on October 16, during which time the spray system was open from 12:30-14:00. Figures 9 and 10 display the line graphs of temperature and humidity changes for the step vertical greening based on the spray system, taken from 11:40-15:00 on October 16. Additionally, Figures 11 and 12 display the fitted graphs of temperature and humidity difference from 12:30 to 15:00.

Upon reviewing the figures, several discernible characteristics can be inferred:

1) Between 11:40 and 12:30, the spray system had not yet been turned on.

Regarding temperature, the test group demonstrated higher levels than the control group, with the highest temperature reaching 39.0°C and the lowest at 33.3°C. On average, the temperature difference between the control and test groups was -2.0°C, with the highest difference being 2.9°C.

Regarding humidity, the test group demonstrated lower levels than the control group, with the highest humidity reaching

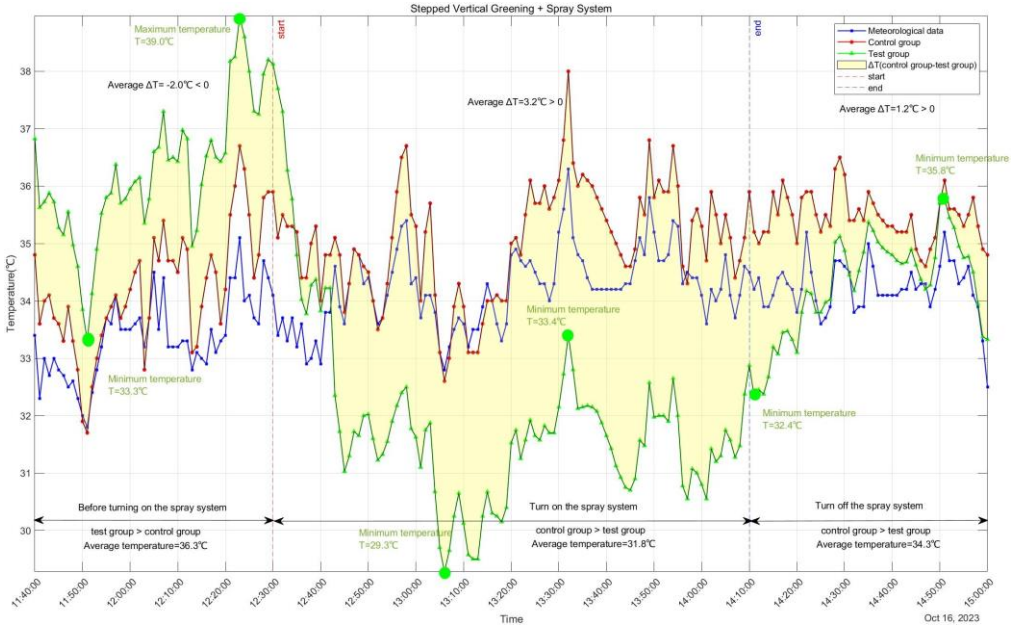

Figures 9. Line graphs of temperature changes from 11:40 to 15:00 (stepped vertical greening +spray system)

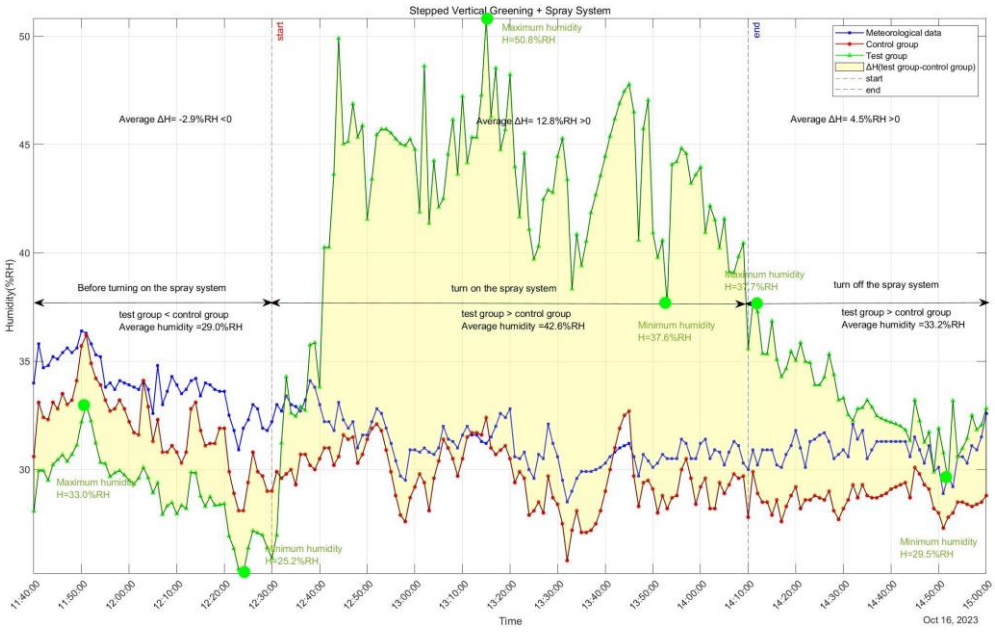

Figures 10. Line graphs of humidity changes from 11:40 to 15:00 (stepped vertical greening +spray system)

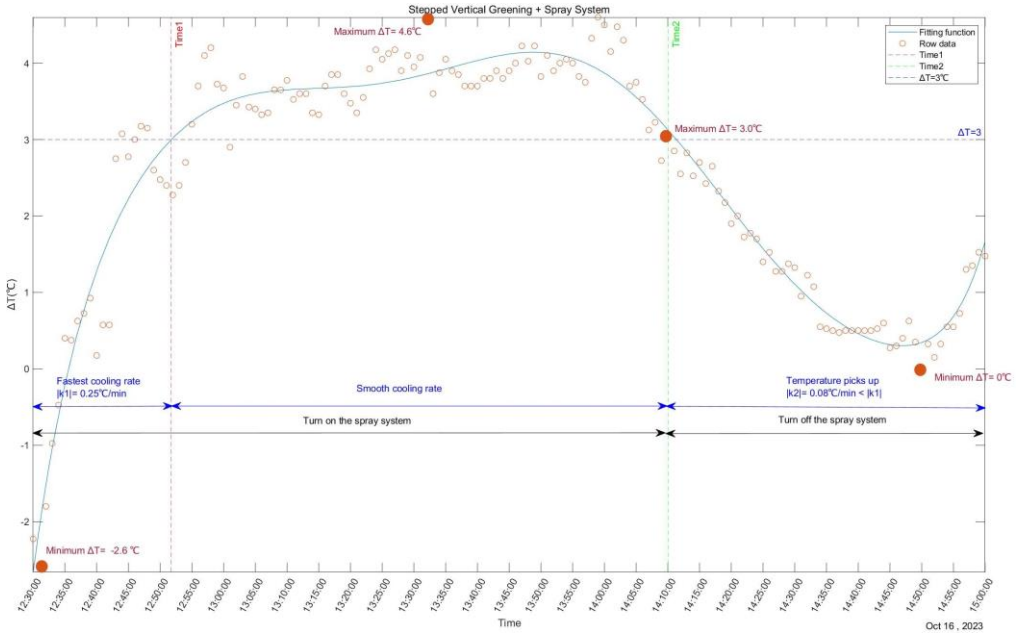

Figures 11. The fitted graphs of temperature difference from 12:30 to 15:00 (stepped vertical greening +spray system)

33.0%RH and the lowest at 25.2%RH. On average, the humidity difference between the test and control groups was -2.9%RH, with the highest difference being 1.9%RH.

2) Between 12:30 and 14:10, the spray system was turned on.

Regarding temperature, the test group demonstrated lower levels than the control group, with the highest temperature reaching 33.4°C and the lowest at 29.3°C. The temperature difference between 12:30 and 12:52 had the fastest rate of change at 0.25℃ /min. On average, the temperature difference between the control and test groups was 3.2°C, with the highest difference being 4.6°C and the lowest at -2.6°C.

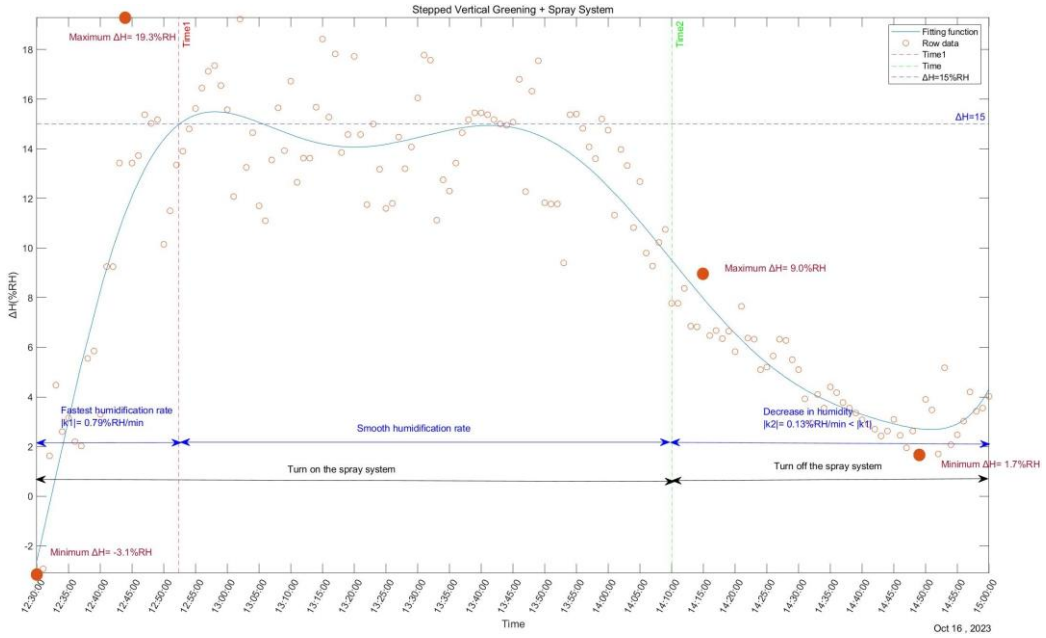

Figures 12. The fitted graphs of temperature difference from 12:30 to 15:00 (stepped vertical greening +spray system)

Regarding humidity, the test group demonstrated higher levels than the control group, with the highest humidity reaching 50.8%RH and the lowest at 37.6%RH. The humidity difference between 12:30 and 12:52 had the fastest rate of change at 0.79%RH/min. On average, the humidity difference between the test and control groups was 12.8%RH, with the highest difference being 19.3%RH and the lowest at -3.1%RH.

3) Between 14:10 and 15:00, for 50 minutes after that the spray system was turned off.

Regarding temperature, the highest temperature reached 35.8°C and the lowest at 32.4°C. The rate of change of the temperature difference was 0.08°C/min. On average, the temperature difference between the control and test groups was 1.2°C, with the highest difference being 3.0°C and the lowest at 0°C.

Regarding humidity, the highest humidity reached 37.7%RH and the lowest at 29.5%RH. The rate of change of the humidity difference was 0.13% RH/min. On average, the humidity difference between the test and control groups was 4.5%RH, with the highest difference being 9.0%RH and the lowest at 1.7%RH.

Temperature and humidity remained essentially at the same frequency, with a significant decrease in temperature and an increase in humidity. On average, the temperature difference improved from -2.0°C to 4.5°C, while the humidity difference improved from -2.9% RH to 12.8% RH. These indicate a significant improvement in the thermal environment of the site compared to the case of stepped vertical greening only.

To further investigate the cooling mechanism of the stepped vertical greening based on the spray system, an experiment with the spray system only was conducted.

3.2. Data on temperature and humidity (spray system only)

This experiment will analyze representative data on October 17th between 11:40 and 15:00. Figures 13 and 14 display the line graphs of temperature and humidity changes for the spray system, taken from 11:40-15:00 on October 17. Additionally, the fitted graphs of temperature and humidity difference from 12:30-15:00 are presented in Figures 15 and 16.

Upon reviewing the f igures, several discernible characteristics can be inferred:

1) Between 11:40 and 12:30, the spray system had not yet been turned on.

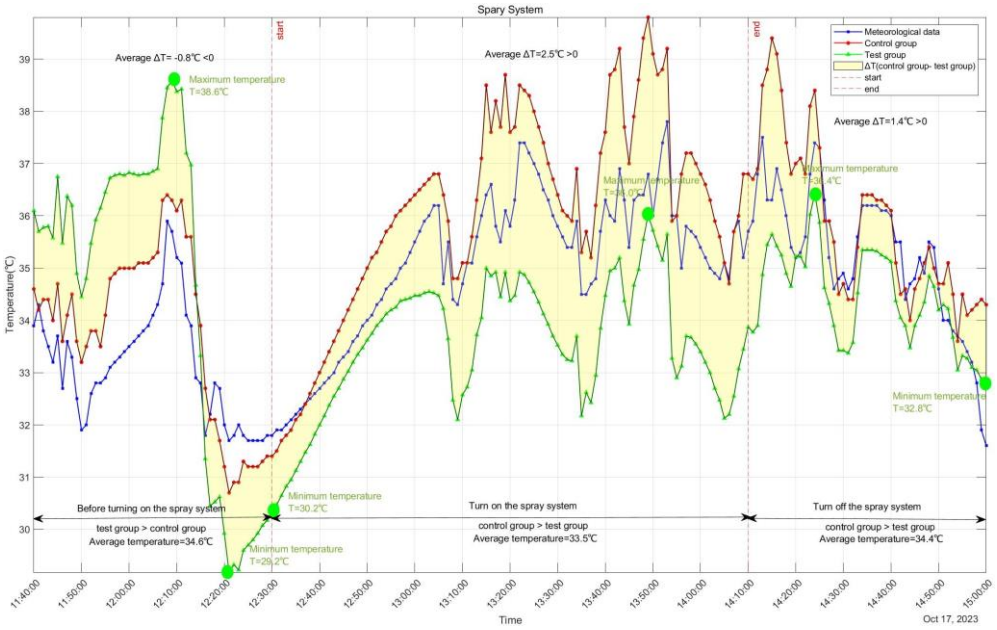

Figures 13. Line graphs of temperature changes from 11:40 to 15:00 (spray system)

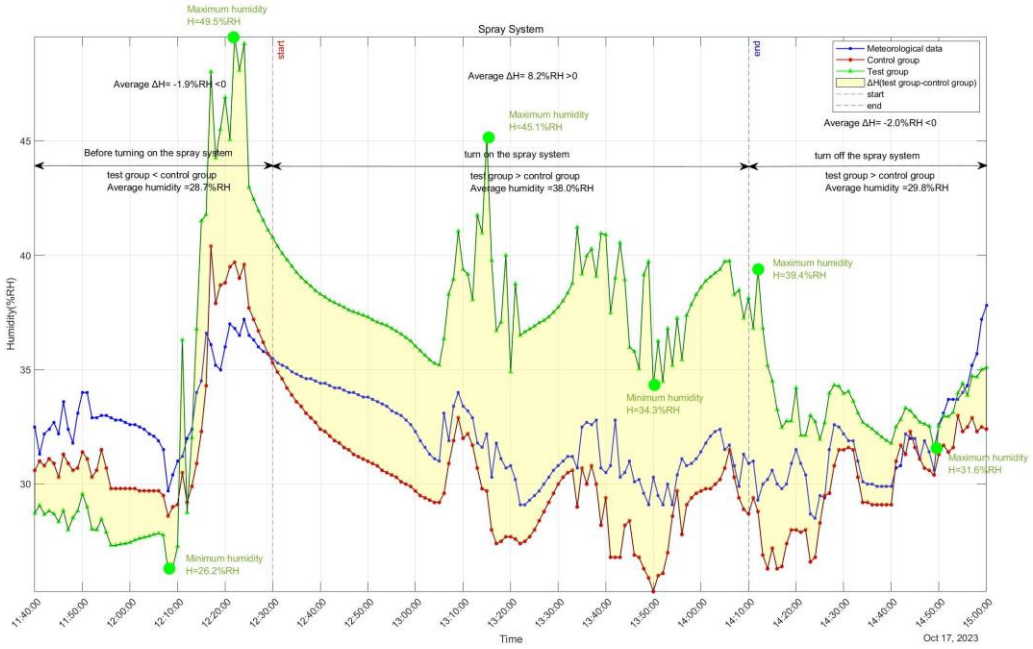

Figures 14. Line graphs of humidity changes from 11:40 to 15:00 (spray system)

Regarding t emperature, the highest temperature reached 38.6°C and the lowest at 29.2°C. On average, the temperature difference between the control and test groups was -0.8°C, with the highest difference being 1.7°C.

Regarding humidity, the highest humidity reached 49.5%RH and the lowest at 26.2%RH. On average, the humidity difference between the test and control groups was -1.9%RH, with the highest difference being 9.9%RH.

2) Between 12:30 and 14:10, the spray system was turned on.

Regarding temperature, the test group demonstrated lower levels than the control group, with the highest temperature reaching 36.0°C and the lowest at 30.2°C. The

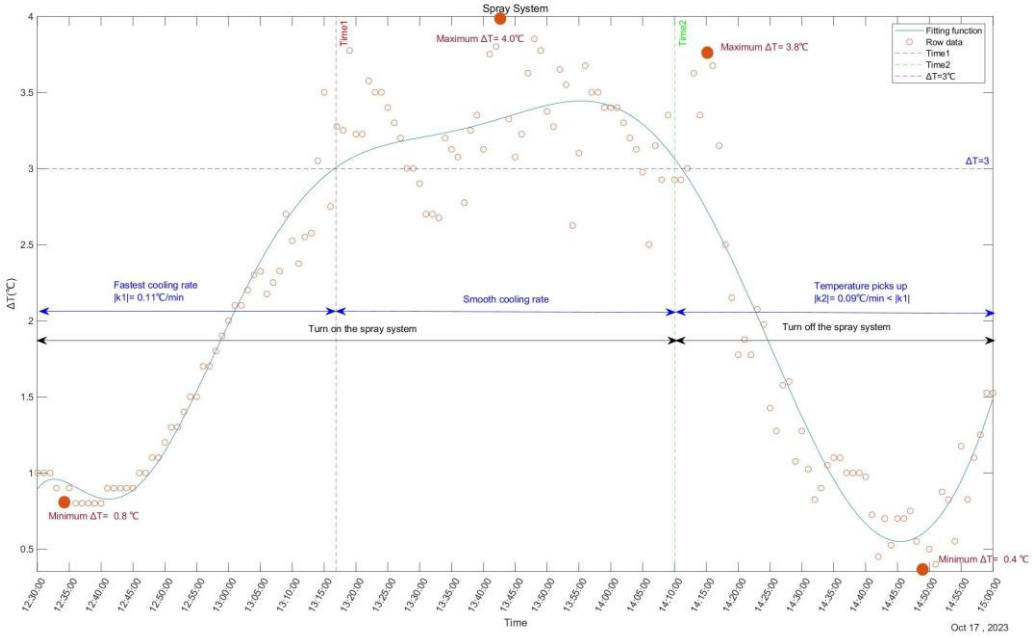

Figures 15. The fitted graphs of temperature difference from 12:30 to 15:00 (spray system)

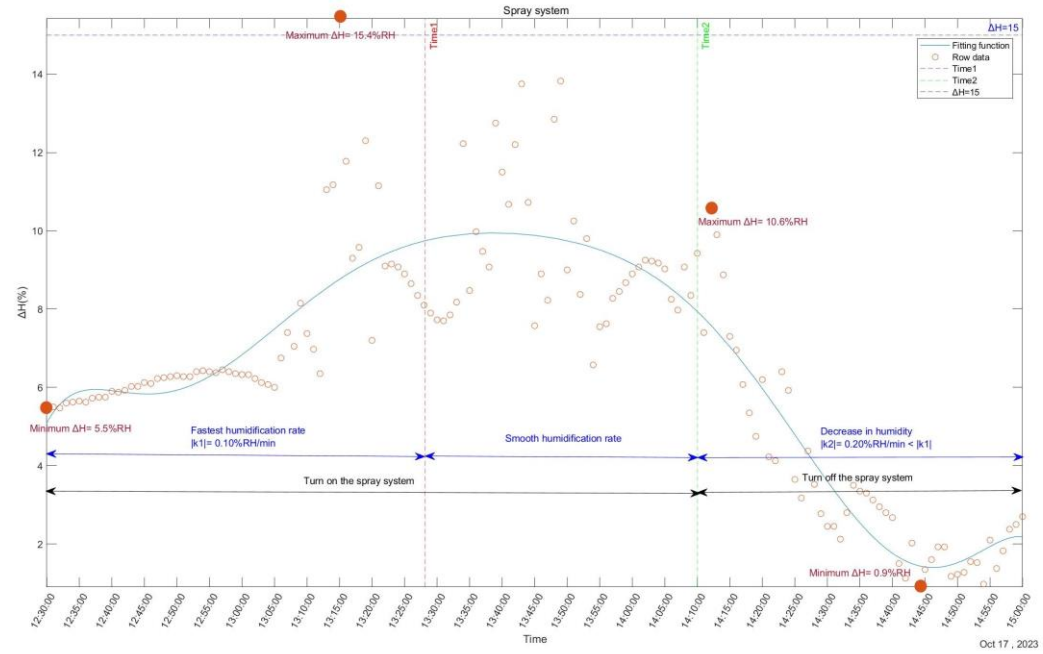

Figures 16. the fitted graphs of humidity difference from 12:30 to 15:00 (spray system)

temperature difference between 12:30 and 12:52 had the fastest rate of change at 0.11℃ /min. On average, the temperature difference between the control and test groups was 2.5°C, with the highest difference being 4.0°C and the lowest at 0.8°C.

Regarding humidity, the test group demonstrated higher levels than the control group, with the highest humidity reaching 45.1%RH and the lowest at 34.3%RH. The humidity difference between 12:30 and 12:54 had the fastest rate of change at 0.10%RH/min. On average, the humidity difference between the test and control groups was 8.2%RH, with the highest difference being 15.4%RH and the lowest at 5.5%RH.

3) Between 14:10 and 15:00, for 50 minutes after that the spray system was turned off.

Regarding temperature, the test group demonstrated lower levels than the control group, with the highest temperature reaching 36.4°C and the lowest at 32.8°C. The rate of change of the temperature difference was 0.09°C/min. On average, the temperature difference between the control and test groups was 1.4°C, with the highest difference being 3.8°C and the lowest at 0.4°C.

Regarding humidity, the test group demonstrated higher levels than the control group, with the highest humidity reaching 39.4%RH and the lowest at 31.6%RH. The rate of change of the humidity difference was 0.20% RH/min. On average, the humidity difference between the test and control groups was –2.0%RH, with the highest difference being 10.6%RH and the lowest at 0.9%RH.

The cooling and humidifying effect of the spray system is much better than that of stepped vertical greening. For the steeped vertical greening based on the spray system, the rate and effect of spray systems in cooling and humidifying at the beginning of the turn-on period, and the ability to moisturize and inhibit the temperature rise after the turn-off period are weaker. The stepped vertical greening based on the spray system is more effective at cooling and humidifying than either spray systems or stepped vertical greening, and both stepped vertical greening and spray systems play an important role in cooling and humidifying.

3.3. Results Analyses

1) When the spray system was not turned on, plants may react to high temperatures and intense light by closing their stomata to minimize water loss and safeguard their well-being. However, this response also led to a significant decrease in the efficiency of photosynthesis and transpiration. As a result, the impact of stepped vertical greening on the thermal environment of the site was considerably limited.

2) When the spray system was turned on, the droplets evaporated and cooled down, increasing the humidity in the air, while at the same time lowering the temperature and saturation difference of the leaves, reducing the pressure of transpiration, partially opening up the stomata of the plants, reducing the consumption of photorespiration, and increasing the photochemical efficiency, which led to a great improvement in the thermal environment of the site.

3) The cooling and humidifying effect of the stepped vertical greening o based on the spray system is more significant than that of the spray system alone. The reason for this is that the plants restore the ability of transpiration, converting the absorbed solar radiation into latent heat, increasing the humidity of the surrounding environment, and absorbing heat when water vapor evaporates, which naturally lowers the air temperature. At the same time, the canopy of the plant shades the sunlight and reduces direct sunlight to the ground, thus lowering the ground temperature. Plants are playing the role of cooling and humidifying, so the cooling and humidifying ability of stepped vertical greening based on the spray system is stronger than that of only a spray system.

4. Conclusions

During the testing period, the implementation of vertical greening based on the spray system had a significant impact on the surrounding thermal environment. The average temperature of the site decreased by 3.2 °C, and the temperature difference rate of change was as high as 0.25 °C per minute. Additionally, the humidity increased by an average of 12.78% RH, with a humidity difference rate of change as high as 0.79% RH per minute. When compared to simple vertical greening and a spray system, the stepped vertical greening based on the spray system demonstrated a stronger ability to reduce

temperature and increase humidity. It is both aesthetically pleasing and socially feasible in Nanning City and can provide considerable economic and social benefits. Given the similar climate characteristics of South China and Southeast Asia to Nanning, the implementation of stepped vertical greening based on the spray system in these areas could be explored and promoted. Because of the l imitation of experimental conditions, there are still some shortcomings in this study. The current study solely focused on measuring the temperature and humidity levels of the outdoor step area. For a more comprehensive analysis, it is recommended to incorporate additional factors such as solar radiation, wind speed, cooling efficiency, and exothermic heat release from the step concrete in future research.

References

[1] Yang, L., & Ye, W. (2022). Landscape design of garden plants based on green and low-carbon energy under the background of big data. *Energy Reports*, 8, 13399–13408.

[2] Phin, L. H., & Krisantia, I. (2018). Microclimate landscape design at southern integrated terminal Bandar Tasik Selatan, Kuala Lumpur. *IOP Conference Series: Earth and Environmental Science*, 012004.

[3] Li, H., Xie, X., & Li, C., . (2023). Carbon Sink Effects and Optimization Suggestions for Landscape Patterns in the Chengdu-chongqing Twin Cities Region: BP Neural Network-based Analysis and Prediction. *Urban Studies*, 30(1), 11.

[4] Susorova, I., Angulo, M., Bahrami, P., & Brent Stephens. (2013). A model of vegetated exterior facades for evaluation of wall thermal performance. *Building and Environment*, 1–13.

[5] Zheng, S., Zhao, L., & Li, Q. (2016). Numerical simulation of the impact of different vegetation species on the outdoor thermal environment. *Urban Forestry & Urban Greening*, 138–150.

[6] Seyrek Şık, C. I., Woźniczka, A., & Widera, B. (2022). A Conceptual Framework for the Design of Energy-Efficient Vertical Green Façades. Energies, 8069.

[7] Pan, L., Zheng, X., Luo, S., Mao, H., Meng, Q., & Chen, J., . (2023). Research Progress on Building Energy Efficiency and Outdoor Cooling Effect of Vertical Greening. *The journal of applied ecology*, *11*.

[8] Sari, A. A. (2017). Thermal performance of vertical greening system on the building façade: A review. *AIP Conference Proceedings*. Presented at the GREEN CONSTRUCTION AND ENGINEERING EDUCATION FOR SUSTAINABL FUTURE: Proceedings of the Green Construction and Engineering Education (GCEE) Conference 2017, East Java, Indonesia.

[9] Wang, P., Wong, Y. H., Tan, C. Y., Li, S., & Chong, W. T. (2022). Vertical Greening Systems: Technological Benefits, Progresses and Prospects. *Sustainability*, 12997.

[10] Li, Y., & He, J. (2021). Evaluating theimprovement effect of low-energy strategies on the summer indoor thermal environment and cooling energy consumption in a library building: A case study in a hot-humid and less-windy city of China. Building Simulation, 14(5), 1423–1437.

[11] Yang, C., Mu, J., & Meng, Q.,. (2019). Thermal Environment Testing and Analysis of Spray Cooling of Lighted Atriums in Buildings. *Building Energy Efficiency*, 47(10), 50 – 55.

[12] Meng, X., Meng, L., Gao, Y., & Li, H. (n.d.). *A comprehensive review on the spray cooling system employed to improve the summer thermal environment: Application efficiency, impact factors, and performance improvement.*

[13] Climate and monthly weather forecast for Nanning, China. (n.d.). *Weather Atlas.* https://www.weather-atlas.com/zh/china/nanning-climate

Xinyi Lu
Guangxi University
Undergraduate student

Research Interests.

1) Green building technology
2) Architecture design

Peisi Chen
Guangxi University
Undergraduate student

Research Interests.

1) Green building technology
2) Architecture design

Yutao Chen
Guangxi University
Undergraduate student

Research Interests.

1) Green building technology
2) Architecture design

Junli Wang
Guangxi University
Undergraduate student

Research Interests.

1) Green building Technology
2) Architecture design

Xiu Yang
Guangxi University
Tutor
South China University of Technology
Ph.D.

Research Interests.

1) Green Building Technology
2) Energy-efficient building design
3) Regional architecture design

Food Loss and Waste in Supply Chain: Challenges and Solutions

Wang Qianyun[1], Guo Yulu[2]

[1]*School of Foreign Languages, Guangxi University, Nanning, China*

[2]*International Cooperation and Exchange Department, Guangxi University, Nanning, China*

E-mail: 18228948021@163.com

Abstract: Food loss and waste in food supply chains pose significant challenges to global food security and sustainable development. As per the Food and Agriculture Organization of the United Nations (FAO), an astonishing 1.6 billion tons of food are wasted worldwide annually, of which 1.3 billion tons are edible. This yearly loss of wasted food is enough to feed 1/8 of the world's population. This paper provides a comprehensive analysis of the complex issues surrounding food loss and waste throughout the various stages of the food supply chain while exploring practical and innovative solutions to address these pressing concerns.

The paper commences by analyzing the FLW in supply chain in China and then primary factors contributing to this phenomenon, ranging from lack of grain storage awareness, low-level cold chain system, overprocessing of grain and consumer expectations. Furthermore, the study explores a series of measures China has made to curb FLW in supply chains, including formulating laws and regulations, promoting technological innovation and FLW reduction education. This paper also studies the cases of other countries to provide reference for China's food security practices. Finally, it puts forward some suggestions on how to reduce the waste of food loss in the supply chain, mainly for government, enterprises and farmers. Addressing food loss and waste is not only crucial for global food security but also vital for achieving broader sustainability goals and building a more resilient and equitable future for all.

Key words: Food loss and waste; SDGs; collaborative cooperation; global crisis; supply chain

1. Introduction

Minimizing food loss and waste is critical in a world where hunger has been steadily increasing since 2014, leading to the daily squandering of vast amounts of edible food. Globally, around 13 percent of food produced is lost between harvest and retail, while an estimated 17 percent of total global food production is wasted in households, in the food service and in retail all together. In 2022, between 691 and 783 million people grappled with hunger, and the lost and wasted food accounted for 38 percent of the total energy used in the global food system1. Specifically, SDG target 12.3 aims “to halve per capita global food waste at the retail and consumer levels and reduce food losses along production and supply chains, including post-harvest losses", by 20302.

The sustainability of our food systems is compromised by food loss and waste. When food is squandered, all the resources utilized in its production—water, land, energy, labor, and capital—are lost. Moreover, disposing of food waste in landfills generates greenhouse gas emissions, furthering climate change. Additionally, food loss and waste can detrimentally affect food security and availability while driving up the overall cost of food.

Resilient food systems rely on sustainability, highlighting the imperative to prioritize integrated strategies aimed at diminishing food loss and waste. Both global and local efforts are necessary to optimize the utilization of our food resources. Introducing technologies, pioneering solutions (such as e-commerce platforms for marketing, adaptable mobile food processing systems), novel operational methodologies, and effective practices for managing food quality are pivotal in ushering in this transformative change, crucial for reducing food loss and waste.

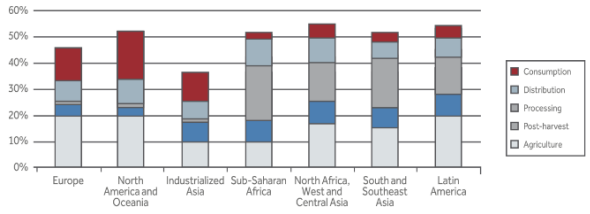

Figure 1. Percentage of the initial production lost or wasted at different stages of the FSC for fruits and vegetables in different

regions.

2. Definitions

Food loss is defined as the decrease in the quantity or quality of food intended for human consumption[3]. It refers to the decrease in edible food throughout the supply chain, from production to retail. Food losses can cover all phases, from production to consumption, but the term generally refers to upstream levels of the value chain, leaving retailing and consumption outside its scope of reference[4]. For instance, vegetables discarded during harvesting or spoiled during transportation are considered food losses, since they are mostly unintended.

Food waste refers to the removal from the food supply chain of food which is still fit for human consumption. This is done either by choice or after the food is spoiled or expired due to poor stock management or neglect.

Food waste typically but not exclusively happens at the retail and consumer levels whereas food loss takes place at the earlier stages of the food supply chain – during production, post-harvest and processing stages[5]. Food loss and food waste come together under the term **food loss and waste (FLW)**, which refers to a decrease in the quantity and quality of food at any stage, from harvest to consumption, regardless of the cause[6]. According to the Coresight Research study, food waste at home accounts for 37% of total FLW while farms is the second biggest culprit at 21%.

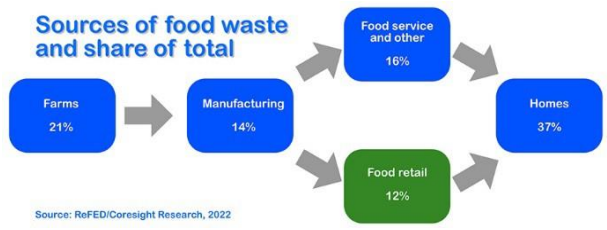

Image 1. From courtesy ReFED Coresight Research

Supply Chain is the network of all the individuals, organizations, resources, activities and technology involved in the creation and sale of a product. A supply chain encompasses everything from the delivery of source materials from the supplier to the manufacturer through to its eventual delivery to the end user. The supply chain segment involved with getting the finished product from the manufacturer to the consumer is known as the distribution channel.

3. FLW in Supply Chain in China

With the rapid development of our China's socio-economy, the swift improvement in people's living standards, and the abundant food supply, food waste has become an increasingly prevalent phenomenon. In China, approximately 27 % of the food produced is lost or wasted, resulting in 30 % of arable land and 34 % of the water for agricultural production being wasted, and approximately 460 million tons of greenhouse gases are emitted in vain[7].

According to a recent study by the Institute of Food and Nutrition Development of Ministry of Agriculture and Rural Affairs in China, the weight weighted average loss and waste rate of seven categories including vegetables, fruits, aquatic products, grain, meat, milk and eggs in China is 22.7% per year, about 460 million tons, of which 300 million tons of food loss in the production and circulation part and 160 million tons of waste in the consumption part. If the waste and loss was reduced by half, China can save 230 million tons of food per year, to meet the nutritional needs of 190 million people for one year[7].

While China's current level of food security does not warrant apprehension (China has sufficient food reserves to meet its internal demand for at least one year), renewed efforts to prevent and reduce food loss and waste would nevertheless generate several economic and environmental benefits that will eventually benefit the entire Chinese society. Locally speaking, reducing food loss and waste would reduce operating costs, and thus – ultimately – prices paid by consumers, and would also reduce the pressure on China's limited land and water resources to produce food that is ultimately not consumed. From a global perspective, China is home to 20 per cent of the world's population but only seven per cent of the world's arable land. By cutting food loss and waste and promoting responsible and sustainable production and consumption, China can significantly contribute to the global battles against poverty, hunger and climate change.

4. Causes of the problems

Lack of Knowledge on efficient grain storage. Some farmers lack grain storage awareness and effective storage space. They put the harvested grain directly on the open courtyard, which may be easy to mildew after rain, snow and other weather, resulting in greater losses, and lowering the quality of food and farmers income.

Infant cold chain logistics. The lack of appropriate Cold Chain Management/Facilities entails a huge loss of perishable food in China: 20%-30% for fruit and vegetables and 12% and

15% for aquatic products and meat respectively. Logistic Costs amount to 18% of GDP in China compared to 8-12% in the EU. Against this background, the needs and constraints of AgriFood Cold Chain Logistic in targeted regions are: 1) Extremely fragmented, poorly organized with fundamental infrastructure and technology, especially in Tibet and Shandong, where few local companies can provide industry-specific logistics services; 2) Dominance of fuel-inefficient fleets, inadequate logistics management and weak driving; 3) Green logistics solutions to reduce energy use/emissions are not being adopted at scale because of low level of confidence on their viability; low level of capacity, skills and cooperation; and 4) Inability to invest in technology/fleet upgrades due the lack of access of MSMEs to financial capital[9].

Overprocessing of food. In order to meet the preferences of consumers, the phenomenon of overprocessing and fine processing is prominent, and the rate of food production continues to decline, resulting in a large number of B vitamins, minerals and other nutritional losses and food waste. Some consumers say that a lot of food in supermarkets is over-cut, such as cutting off most of the leaves of Chinese cabbage to turn it into "baby cabbage". Studies have shown that the nutrient loss of grain finishing can reach up to 80%. Taking rice processing as an example, moderate processing can produce 70 catties of rice per 100 catties, but fine processing can only produce 50 catties.

5. Measures taken by China

At the beginning of this century, China solved the problem of food and clothing and said goodbye to the era of shortage economy. With the increase of economic growth and income, the awareness of food and loss of the whole society gradually faded, especially in the first decade of this century. To solve the problem, China has taken active efforts to reduce food loss and waste. China's food security strategy involves all levels of production, storage, transportation, retail, and consumption. Since this paper focuses on FLW at the supply chain stage, it will focus on initiatives at this stage.

Launch laws and regulations to regulate the public for grain saving and loss reduction. In 2021, the Anti-Food Waste Law of the People's Republic of China was issued, calling for higher standards of food production, storage, transportation, and processing, and the use of new technologies, techniques, and equipment to reduce waste. In the same year, Chinese government issued the *Food Conservation Action Plan* to strengthen savings and losses in all links of the grain industry chain. All these documents demonstrate China's commitment to tackle the problems in food supply chain and create a sound system and policy environment.）

Curb FLW through technological innovation. In recent years, governments at all levels have actively promoted technological food saving actions. In the planting part, we formulated new standards for seeds and sowing. In the harvest part, the government actively promotes intelligent, green and efficient harvesting machinery, decreasing the harvest loss rate; For storage, encourage farmers to apply scientific grain storage technology and enterprises to build smart grain storage. By applying technologies such as air conditioning, low temperature and quasi-low temperature to reduce grain loss in this stage. In the transport sector, actively promote the promotion of special bulk transport trunks and trains as well as loading and unloading machinery and recycling equipment in port are applied. Finally, during processing, it's encouraged to use smart facilitations and equipment.

Promote sustainable production and consumption patterns. Through education and publicity activities, farmers are aware of the importance to reduce FLW in grain storage period. The latest survey shows that the loss rate of farmers' grain storage has dropped from 8% a decade ago to about 3%. Hebei Province applies new models of grain service involves agricultural machinery enterprises, cooperatives and farmers to improve their grain storage efficiency. At the same time, anti-food waste related competitions were held to attract universities to participate. With the theme of "anti-FLW", the students of the Yunnan University team designed the public welfare project called "Food Station", which provides food that would otherwise be wasted to groups in need, such as bread that cannot be sold out in the canteen can be transported to the brewery as raw materials.

Conduct deeper international cooperation. In 2021, together with the Food and Agriculture Organization of the United Nations (FAO), the World Food Programme (WFP), the International Fund for Agricultural Development (IFAD) and the United Nations Centre for the Mechanization of Sustainable Agriculture (CMCSA), China held a webinar themed "Reducing Food Loss and Waste: Promoting Sustainable Food System Transformation in China". Representatives from UN agencies, Chinese governments, banks, universities and research institutions shared and exchanged views on the three themes: Reducing food loss in production and processing; reducing food loss and waste in the supply chain; and financial innovation to reduce food loss and waste.

Through legislation, technology and education, China's FLW has been significantly reduced. In 2022, the national post-production grain service center served more than 17 million rural households and helped farmers reduce food losses by more than 12 million tons. Nevertheless, China's still confronted with enormous FLW in supply chain. As mentioned earlier, the amount of food waste in seven categories of vegetables, fruits, aquatic products, grain, meat, milk and eggs is about 460 million tons every year, of which 300 million tons are lost in the production and transportation process. China still lacks experience in FLW reduction. Next, we will analyze the cases of Thailand, Japan and some western countries in reducing food waste in the supply chain, in order to provide a more comprehensive FLW reduction strategy for China.

6. Cases Study

1. In Thailand

Thailand has long been called "the kitchen of the world" with its abundant natural resources, highly skilled workforce, and strengthening research. The food industry contributed roughly 23% of the country's GDP The value of Thailand's food industry, including local consumption and exports, is expected to reach USD102 billion in 2017. Thailand is also one of the largest net food exporting countries in the world and the second in Asia with a food trade balance at a record value of USD 16.7 billion in 2016[10]. With abundant natural resources, a year-round growing season, relatively low labor costs, and a skilled workforce, Thailand enjoys numerous competitive advantages in the food and agricultural industries.

Packed with micronutrients and vitamins, the germinated brown rice produced by the Ban Lao community-run enterprise in northeastern Thailand's Sakon Nakhon province has long been popular with health-conscious consumers. The processing of this specialty rice product involves soaking and fermentation or germination overnight, followed by steaming to cook the grain before drying it. To reduce the loss in the drying process, Thai government use some simple technologies such as a moisture meter to monitor the drying process and a digital thermometer to reduce losses in processing and improve the quality of the final product. They also cut down losses in transit by using a vacuum sealing machine and transporting the packaged rice in shallow plastic crates. All these measures have helped to lengthen the product's shelf-life, reduce waste in retail and ensure compliance with Thai regulations and standards.

Scholars of Sustenance Thailand (SOS) is now in Chiang Mai to tackle the systemic problems within the food supply chain by operating a Food Rescue Programme with the mission to save surplus food from being wasted while helping the people in need to have equal access to nutritious food. For the past five years, SOS in Bangkok, Phuket and Hua Hin have been able to rescue 3,781 tons of surplus food, reduce 7,940 tons of Co2-eq, and help more than 473,000 people in need by handing over 15.9 million meals. SOS's cold-chain logistic system truck hurls around to rescue surplus food from various sectors from different hotels, supermarkets, food producers, food retailers, and food manufacturers. Along with strict food safety protocol and inspection, rescued food is distributed to beneficiaries in low-income communities, orphanages, shelters, including most of the vulnerable groups in society.

Eden Agritech is a Bangkok-based startup that aims to extend the shelf life of fruits and vegetables with its patented "Naturen" technology. Produce covered in this invisible, chemical-free edible coating lasts up to five times longer than normal while maintaining its nutritional quality.

2. In Japan

There are obvious differences between China and Japan in terms of food industry. China boasts a large territory, abundant resources, and sufficient labor force, so its grain production is as large as possible to meet domestic demand and export to other countries. In contrast, Japan's land resources are limited, and needs to import a lot of food. Japan has a low food self-sufficiency rate at around 37% and depends largely on imports for its food, more than 6.12 million tons thrown away each year. Although China has a large output, the quality of some grain has been questioned due to the excessive use of chemical fertilizers and pesticides in traditional agriculture. On the contrary, Japan focuses on environmental protection and food safety, and adopts organic and ecological agriculture, which makes the food quality relatively high. In recent years, Japan has also taken various measures to reduce FLW in its supply chains.

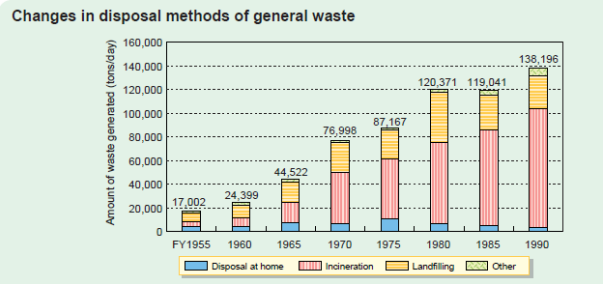

Figure 2. Total waste amount in special cleansing districts in 1970 based on the Public Cleansing Law. Figures for 1975 exclude waste haulage brought in directly upon moving house, etc. Compiled based on: "Annual Report on Health and Welfare" and the "Quality of the Environment in the Japan"

Japanese companies are tackling food waste at their production lines, using artificial intelligence and other technology to reduce the amount of food that never reaches consumers.

Nichirei Foods has developed an AI-powered system for detecting hard-to-remove bones in chicken meat at its plants. The old system, which uses X-rays, sometimes gives false positives, causing the meat to be thrown out instead of processed into fried chicken and other products. The company hopes to slash food waste from chicken processing by 80% in three years. Leading tofu maker Sagamiya Foods is using data from the Japan Weather Association to predict sales, which are affected by temperature. Reducing surplus production will slice annual costs by about 10 million yen ($92,500), the company said. Yamazaki Baking is producing more pastries with creams and jams made from misshapen fruit that cannot be sold at stores. Mayonnaise maker Kewpie devised a different way to wash cabbage leaves, extending the shelf life of its prepackaged shredded cabbage by a day. Kikkoman tweaked its soy sauce containers so they last for 120 days after being opened, while Mizkan Holdings sells snacks online that use vegetable peels and seeds.

In 2019, the Japanese government introduced the Act on Promotion of Food Loss and Waste Reduction to prevent still-edible food from being discarded. The law promotes understanding of food waste and stipulates a basic policy to reduce food loss and waste. All levels of government, businesses and consumers are encouraged to work together to tackle this challenge as a national movement. October is set as the Food Loss Reduction Month. Some key initiatives include: Extending the best before date on consumer products; Recycling food wastes into fertilizer and feed; Creating business incentives for those in the food supply chain; Support food bank activities

3. Other Cases

The measures taken by China in supply chain are mainly for the storage of rice and other grains, while the measures for vegetables, fruits and other food types are less. It is difficult to find relevant cases. In contrast, the efforts of Thailand and Japan to reduce FLW other than rice are also remarkable. The following are some typical cases from other countries.

Apeel from the United States adopted the plant-based products as an alternative to traditional chitosan coating to ensure the humidity of fruits and vegetables and cut off oxygen at the same time. These products, colorless and odorless, can be sprayed directly on the surface of fruits and vegetables, and can help fruits and vegetables to extend the optimal taste time. Apeel's technology is already used in major supermarkets in the United States and some European countries. Another fresh keeping technology enterprise Hazel is changing the nearby air composition of fruit and vegetable during the process of transportation to slow their respiration, and prevent them from the effect of ethylene.

7. Solutions

There has been a lot of discussion about reducing FLW in the supply chain, and most reports focus on the specific stages, including production, storage, transportation. This paper chooses to discuss the important role of different groups in reducing FLW from the four levels of government, enterprises, and producers.

First of all, the government should formulate practical laws with strict supervision. The government can regulate the behavior of producers by making laws and regulations against FLW. Economic incentives could be created, such as lower if food losses decreased to a certain level. In addition, educational programs can be organized to raise public awareness of the urgency to curb FLW. Through advertising, social media and educational programs, the public can realize the importance of reducing food loss and adopting sustainable food consumption behaviors. As consumers become more inclusive, producers and retailers throw away less food before selling to customers.

Second, producers should be involved in reducing food loss. Adopt modern agricultural technologies and methods, such as smart agricultural technology, precision agriculture and water-saving irrigation methods, to reduce resource waste during crop growth. Grow diverse crops and adopt scientific production planning to avoid excessive planting or breeding and avoid producing surplus agricultural products. Strengthen inventory management, check and update inventory regularly, adjust production schedule in time to avoid expiration and wastage.

Companies can also take measures to reduce food losses in the supply chain. For example, shorten the food supply chain: If the food supply chain is long, it means that the food remains in supply chain for a longer period before available to consumers. It is necessary to shorten the food supply chain and establish regulations for purchasing processed food and ingredients. Promote supply chain transparency and enhance information sharing and collaboration to better predict demand and optimize supply chain processes. Train employees to educate them about the impact of food loss and waste and motivate them to participate in FLW reduction practices. At the same time, companies can also work with public welfare organizations to

distribute unsold food that is safe to use to communities, nursing homes or other groups in need of food, so that food can make the most of it.

8. Conclusion

The world today is witnessing serious food security challenges, and food loss and waste in the supply chain has become a pressing issue. This paper analyzes the current situation of FLW in Supply Chain in China and the measures taken by China. After that, this paper introduces typical cases of Thailand, Japan and other countries, in order to provide reference for FLW reduction to China. Through technological innovation, partnership building and policy improvement, we can optimize the supply chain and reduce food loss and waste. From production to transport, storage and consumption, we have a responsibility to ensure that food is fully used. This can not only bring benefits to the economy, but also reduce environmental impact and promote social equity. We must work together for a sustainable future and food security, ensuring that every morsel of food is used to meet people's needs and not wasted.

References

[1] Daniel Ortiz-Gonzalo, Sinne Borby Ørtenblad, et al. (2021). Food loss and waste and the modernization of vegetable value chains in Thailand.

[2] FAO. (2015). Definitional Framework of Food Loss - SAVE FOOD: Global Initiative on Food Loss and Waste Reduction, https://www.fao.org/3/i4068e/i4068e.pdf.

[3] Federica Marra. (2021). Fighting Food Loss and Food Waste in Japan. https://www.academia.edu/8853973/Fighting_Food_Loss_and_Food_Waste_in_Japan.

[4] Gustavsson, J., Cederberg, C., Sonesson, U., van Otterdijk, R., Meybeck, A. (2011). Global food losses and food waste: extent, causes and prevention. Int. Congr. Save Food! https://doi.org/10.1098/rstb.2010.0126, 38.

[5] HLPE. (2014). Food Losses and Waste in the Context of Sustainable Food Systems A Report by the High Level Panel of Experts on Food Security and Nutrition (HLPE), https://www.fao.org/3/i3901e/i3901e.pdf

[6] HUY, ZHOU Y H, HAN Y J, et al. (2013). Resources and economic effects analysis of reducing food waste. China Population, Resources and Environment. 23(12):150-155.

[7] Maryam Rezaei, Bin Liu. (2017). Food Loss And Waste in the Food Supply Chain, https://www.fao.org/3/bt300e/bt300e.pdf.

[8] Ruigang Wang, Shijun Lu, Lin Zhou, et al. (2023). Assessing nutritional and economic aspects of food loss and waste in China, 42, 95-105.

[9] Tianjin Academy of Agriculture Sciences. (Undated). Towards Energy Efficiency in AgriFood Cold Chain Logistic in China, https://www.switch-asia.eu/project/eecho-towards-energy-efficiency-in-agrifood-cold-chain-logistic-in-china/.

[10] United Nations. (Undated). Reducing food loss and waste: Taking Action to Transform Food Systems, https://www.un.org/en/observances/end-food-waste-day.

[11] United Nations General Assembly. (2015). Transforming our world: The 2030 agenda for sustainable development, https://www.unfpa.org/sites/default/files/resource-pdf/Resolution_A_RES_70_1_EN.pdf.

Miss. Wang Qianyun

Master student, Master of Translation and Interpreting

Research Interests:

Tr[illegible]ternational Issues, English Interpreting

Dr. Guo Yulu.

Associate Professor.

Deputy Director of the International Cooperation and Exchange Department, Guangxi University.

Research Interests:

The diplomatic discourse

Interpreting

International Relations (China-ASEAN)

China-Africa Relations

Intercultural communication

International Chinese Language Education

Variation of leaf architecture within F1 maize population for high-density planting

Boonchai Sae-Yang[1*], Piched Khammeekan[1] and Pattama Hannok[1*]
[1]Division of Agronomy, Faculty of Agricultural Production, Maejo University, Chaing Mai, Thailand
**Corresponding author, E-mail: Pattama_h@mju.ac.th*

Abstract: Higher population density is an alternative way to increase maize yield in a limited area. To do so selecting lines with narrow degrees of leaves might be helpful for this purpose since the spacing between plants could be smaller. Therefore, the objective of this study was to estimate the degree of leaves in a breeding population. The experiment was conducted in Randomized Completely Block Design with 4 replications. Twenty-five crosses were planted and tested in the field, in which 20 F1 crosses were developed from 5 parental inbred lines via the Diallel method 3 mating design, and 5 F1 commercial varieties were used as a check. Degrees of 1st to 4th above-ear leaves at R3 stage were collected by using the Angel meter program. The results showed that significant differences in leave degree could be found in all positions of leave (AE1-AE4). Consequently, three schemes of leave degree could be seen e.g., narrow AE1/narrow AE4 (Group 1), large DAE (Group 2), and wide AE1/wide AE4 (Group 3). These 3 groups were significantly different. Group 1 showed the best architecture which should be tested in high-density planting in the field later.

Keywords: Corn, Leaf degree, Breeding material

1. Introduction

Increasing population density in the limited land could improve maize yield. However, in the case of adjusting row spacing and population density, radiation use efficiency and canopy light interception need to be considered to maintain plant yield (Ethridge et al., 2022). Therefore, light emission through the canopy is essential for planting.

Leaf angle is an important trait and causes a unique maize architecture. Erect leaves cause a compact shape of the plant and might be used in high-density planting. Small leaf angle reduces the shade effect between plants, which could increase photosynthetic efficiency and lead to high seed yields (Duan et al, 2022). Increasing population density could be done in many ways e.g., by choosing maize varieties with compact shapes in which leaf angle is small. According to Dzievit *et al*. (2019), many groups of maize scientists have been trying to measure leaf angles from different leaf positions of maize plants. However, it is difficult to know which leaf truly affects the maize architecture. Leaves below-ear leaf and above-ear leaf have been reported in many research articles. Therefore,

our study aimed to observe variation of leaf angles in our breeding population to determine the possibility of conducting a breeding project for high plant density tolerance in the future.

2. Materials and methods

Five parental inbred lines with drought-conferred traits were chosen from the previous project. Twenty F1 crosses (Table 1) were developed via the Diallel method 3 mating design. Five commercial checks (Table 1) were also tested in the field along with those 20 F1 crosses in Randomized Completely Block design with 4 replications. Maize seeds were planted in 25*75 cm. At the milky stage (R3), leaf angle was measured on the 1st - 4th leaves above-ear leaf (AE1-AE4). Angle meter (Kozlov., 2023) was used to measure the obtuse angle as shown in Figure 1. The obtained value was subsequently subtracted from 180° to obtain a leaf angle of AE1-AE4. Furthermore, the leaf angle difference between the 4th and 1st leaves above-ear leaf (DAE) was calculated for all plots.

Descriptive statistics, One- way ANOVA, and Least Significant Difference were done for all 5 traits in R version 4.3.2 (R Core Team, 2023). Three categories (Figure 2) of maize architecture were grouped based on AE1, AE4, and DAE e.g., narrow AE1/narrow AE4 (Group 1), large DAE (Group 2), and wide AE1/wide AE4 (Group 3).

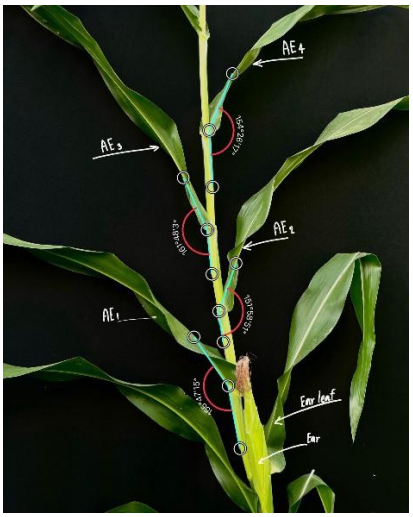

Figure 1 Leaf angle measurement via Angle Meter

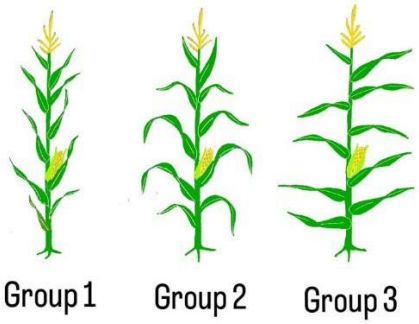

Figure 2 Three categories of maize architecture

Table 1 A list of 20 F1 crosses and five commercial checks

Crosses	Symbols
Nei492006 x Nei492024	C1
Nei492006xNei512008	C2
Nei492006xKei1618	C3
Nei492006xDTMA192	C4
Nei492024xNei492006	C5
Nei492024xNei512008	C6
Nei492024xKei1618	C7
Nei492024xDTMA192	C8
Nei512008xNei492006	C9
Nei512008xNei492024	C10
Nei512008xKei1618	C11
Nei512008xDTMA192	C12
Kei1618xNei492006	C13
Kei1618xNei492024	C14
Kei1618xNei512008	C15
Kei1618xDTMA192	C16
DTMA192xNei492006	C17
DTMA192xNei492024	C18
DTMA192xNei512008	C19
DTMA192xKei1618	C20
Pac789	Chk1
Decarb9979c	Chk2
Suwan5821	Chk3
CPF16	Chk4
P4546	Chk5

3. Result and Discussion

According to the One-way ANOVA result, the effect of cross was significantly found for all leaf angles on AE1- AE4. Moreover, the average leaf angle on AE1-AE4 for all crosses was shown in Table 2. The range of angles on AE1 and AE4 were 21.78-64.87° and 29.28-73.92°, respectively. This result indicated the variation of leaf angle that might affect maize architecture.

Table 2 Leaf angles at different leaf positions (AE1-AE4) and differences between the 4th and 1st leaves above-ear leaf (DAE) of 25 crosses

Crosses	Leaf angles (°) of				
	AE1	AE2	AE3	AE4	DAE
C1	38.55 cdefgh	50.41 bcd	50.49 bcd	59.73 abcdefg	21.19 abcd
C2	45.62 bcd	47.97 cde	52.45 bc	61.40 abcde	15.78 abcdef
C3	41.86 bcdef	47.94 cde	51.26 bcd	64.10 abcd	22.24 abc
C4	36.73 defghi	45.54 cdef	49.05 bcde	62.61 abcde	*25.88* a
C5	43.97 bcde	52.41 bcd	53.42 bc	62.17 abcde	18.20 abcde
C6	48.77 b	57.88 b	54.20 bc	67.72 abc	19.71 abcde
C7	35.07 efghi	39.83 efg	46.55 bcde	48.57 efg	13.50 cdef
C8	64.87 a	70.27 a	65.56 a	73.92 a	9.04 ef
C9	45.25 bcd	48.94 bcd	53.56 bc	67.73 abc	*22.48* abc
C10	49.89 b	55.35 bc	56.67 ab	71.96 ab	22.07 abcd
C11	35.35 efghi	44.44 def	48.27 bcde	60.09 abcdefg	*24.74* ab
C12	40.64 bcdef	53.80 bc	55.67 ab	61.89 abcde	21.25 abcd
C13	35.51 efghi	38.55 fg	41.97 de	57.78 bcdefg	22.27 abc
C14	41.70 bcdef	48.00 cde	51.01 bcd	61.22 abcdefg	19.5 abcde
C15	30.72 ghij	37.89 fg	41.80 de	48.31 efg	17.60 abcdef
C16	27.81 ij	34.48 gh	39.40 ef	46.84 cdefg	19.04 abcde
C17	40.11 bcdefg	45.70 cdef	49.76 bcd	54.96 cdefg	14.86 bcdef
C18	60.31 a	57.37 b	64.98 a	66.65 abc	6.34 f
C19	47.13 bc	54.50 bc	55.57 ab	59.24 abcdefg	12.11 cdef
C20	**27.60 ij**	37.28 fg	38.62 ef	**44.66 gh**	17.06 abcde
Chk1	**21.78 j**	25.46 h	31.05 f	**32.11 h**	10.34 def
Chk2	**22.93 j**	27.34 h	30.02 f	**29.28 h**	6.36 f
Chk3	43.31 bcdef	46.94 cdef	52.41 bcd	61.08 abcdefg	17.76 abcdef
Chk4	30.44 hij	38.15 fg	44.95 cde	50.66 defg	20.23 abcde
Chk5	34.06 fghi	37.50 fg	45.14 cde	50.37 defg	16.32 abcdef
Grand mean	39.60	45.75	48.95	57.00	17.43
F-Test	***	***	***	***	*
%C.V.	16.42	14.14	14.05	18.15	44.33

Note: */**/*** indicate statistical significance at alpha 0.05, 0.01, and 0.001 levels

With the rule of 10% selection, only 9 out of 25 crosses were chosen and categorized based on maize architecture into 3 categories, which were Group 1 (narrow AE1/AE4) as shown in bolded and underlined means in Table 2, Group 2 (large DAE) as shown in italicized and underlined means in Table 2, and Group 3 (wide AE1/ AE4) as shown in underlined means in Table 2. Each group contained 3 crosses. Chk1, Chk2, and C20 showed the narrowest AE1 and AE4 whereas that of C8, C10, and C18 were large on AE1 and AE4. Therefore, they were categorized in Group 1 and 3, respectively (Table 3). Moreover, C4, C11, and C9 were in Group 2 since they showed large DAE values. The concept of grouping maize architecture based on the leaf angle of AE1, AE4, and DAE seemed reasonable because the statistical significance was found among different categories of maize architecture as shown in Table 3

Table 3 Leaf angles of 1st and 4th leaves and their difference for 3 different categories

Group	Crosses	Leaf angle (°) of		
		AE1	AE4	DAE
Group1	C20	27.60 de	44.66 bc	21.51 bc
	Chk1	21.78 e	32.11 c	18.41 bc
	Chk2	22.93 e	29.28 c	10.10 bc
	Average	23.78 c	34.50 b	10.72 a
Group2	C4	36.73 c	62.61 a	25.88 b
	C11	35.35 cd	60.09 ab	24.74 b
	C9	45.25 b	67.73 a	22.48 c
	Average	39.11 b	63.48 a	24.37 a
Group3	C8	64.87 a	73.92 a	4.25 c
	C10	49.89 b	71.96 a	22.07 ab
	C18	60.31 a	66.65 a	6.34 c
	Average	58.56 a	70.42 a	11.86 a
Grand mean		40.52	56.55	16.03
F-test		***	***	*
% C.V.		13.39	17.44	48.28

Note: */**/*** indicate statistical significance at alpha 0.05, 0.01 and 0.001 levels

Furthermore, according to Standard approval for maize characterization by the Department of Agriculture (DOA) of Thailand (2004), five rating scores of leaf angle of the first leaf above the top ear were determined as follows; 1) less than 5° 2) between 6-25° 3) between 26-50° 4) between 51-75° and 5) greater than 76°. It was found that the average AE1 angle of Groups 1 (23.78°), Group 2 (39.11°) and Group 3 (58.56°) from this present study were matched with DOA rating scores of 2, 3 , and 4, respectively.

Therefore, it is very interesting to conduct the field test to observe whether those crosses in Group 1 with the narrowest AE1 and AE4 could give a higher biomass yield than crosses from Group 2 and Group 3.

Conclusion

The variation of leaf angle that causes different maize architecture could be seen in our breeding materials. Therefore, breeding for high population density with improving leaf angle might be possible for future research projects.

Reference

Department of Agriculture (DOA) of Thailand 2004. Standard approval for maize characterization by the Department of Agricultural. [Online]. Available http://lib.doa.go.th/multim/e-book/EB00149.pdf. (7 December 2023)

Duan, H., Li, J., Sun, Y., Xiong, X., Sun, L., Li, W., Gao, J., Li, N., Zhang, J., Cui, J., Fu, Z., Zhang, X., & Tang, J. 2022. Candidate loci for leaf angle in maize revealed by a combination of genome-wide association study and meta-analysis. ORIGINAL RESEARCH article. 13, 1004211,

Dzievit, M., Li, X., & Yu, J. 2019. Dissection of Leaf Angle Variation in Maize through Genetic Mapping and Meta-Analysis. The Plant Genome, 12(1).

Ethridge, R, S., Locke, A, M., Everman, A,M., Jordan, D, V., & Leon, R, G. 2022. Response of Maize, Cotton, and Soybean to Increased Crop Density in Heterogeneous Planting Arrangements. Agronomy. 12(5), 1238.

Kozlov, A. Inc. (©Alexey Kozlov). Angle Meter, Version 1.9.1. November 2023.

R Core Team (2023). _R: A Language and Environment for Statistical Computing_. R Foundation for Statistical Computing, Vienna, Austria.

Mr.Boonchai Sae-Yang
Undergrad student in Agronomy, Faculty of Agricultural Production, Maejo University
Research Interests: Development and improvement of corn varieties.

Mr. Piched Khammeekan
Graduate student in Agronomy, Faculty of Agricultural Production, Maejo University
Research Interests: Low input farming, breeding for low N tolerance

Dr. Pattama Hannok
Assistant Professor
Division of Agronomy, Faculty of Agricultural production, Maejo University
Research Interests: Maize breeding, quantitative genetics

Calorie Detection in Dishes Based on Deep Learning and 3D Reconstruction

Wenjian Gao [1], Xiaobo Zou [1,*], Jiyong Shi [1]

[1] School of Food and Biological Engineering, Jiangsu University, Zhenjiang 212013, China
**Corresponding author, E-mail: zou_xiaobo@ujs.edu.cn*

Abstract: Calories are one of the most important parameters to keep healthy. To realize automatic calorie detection in vegetables and dishes, a depth camera of Intel Realsense was adopted, and deep learning in image classification combined with 3D reconstruction algorithm BundleFusion was applied to the food field. This paper sorted out opening food data sets. In addition, we propose a DenseNet network that combines with spatial attention and channel attention, named CBMA_DenseNet. The optimal performance of top-1 on the test and validation set were 79.15% and 80.02%. And the optimized network has higher accuracy. By verifying the feasibility of the system algorithm and the accuracy of the measurement results, the results show that the minimum and maximum average error were 0.0093 and 0.0429 for single vegetable. For dishes, the minimum and maximum average error were 0.049 and 0.103. In addition, we propose a calorie detection model based on calorie density, considering the error of calorie calculation is the same as that of volume. Calorie counts can be accurately identified. The research has a wide range of applications
Keywords: Calorie calculation, Deep learning, Deep camera, 3D reconstruction.

1. Introduction

The quantitative measurement of calories in food and agricultural products is particularly important. Excessive absorption of calories without corresponding exercise consumption will lead to obesity and other health problems [1]. Currently, intelligent equipment in central kitchens and standardized restaurants has enabled real-time calorie measurement. The method of calorie estimation using only RGB images lacks quantitative control and it has large error in the test process, or only gives the calorie value per unit mass. The calorie detection device based on weight [2] uses an embedded pressure sensor to measure the weight of the food on the current plate, which requires the dishes to correspond to the plate, and the embedded method of the pressure sensor is easy to cause damage. So, we try to use computer vision technology to capture images and detect calorie values.

X.Chen[3] et al. built ChineseFoodNet database, on which different models are adopted and the predicted results of these models are integrated by voting, called "TastyNet". PatrickMc Allister[4] et al. combined deep residual neural network features with supervised machine learning algorithm to classify various food image data sets. Shen Zhidong [5] et al. were engaged in food recognition and nutrition estimation methods based on machine learning CNN model. Ma Peihua [6] et al. engaged in image-based deep learning for nutritional estimation of processed agricultural dishes adopted convolutional neural network for image recognition of processed agricultural dishes, and established the first open access Chinese dish image database named ChinaFood-100 with quantitative nutritional annotations. In 2022, VijayaKumariG et al.[7]used the migration learning technology to classify food, and the model developed Efficientnetb0 was used to classify 101 different foods. In the food calorie estimation method based on deep learning, Liang Yanchao [8] used the three-view method to estimate the volume of a single vegetable individual. Muhammad Fithratur Rahman et al. [9] proposed a convolutional neural network based food recognition method to evaluate the calories of one food picture. They utilize the migration learning and fine-tuning methods of the MobileNetV2 model. Haoyu Hu et al. [10] proposed an object test method to calculate the calorie content of Chinese food and a small amount of western food. They used a single multibox detector (SSD) for real-time food processing test. Isaksen, Runar et al. [11] produced a network to analyze the quality of food from just one image. The working process of the system is mainly divided into three parts, which are image classification, segmentation process, only from the image to separate the main food, estimate the weight of the food. Parisa Pouladzadeh[12] et al. developed a mobile application in their work, which can identify different foods in the same meal and can determine the caloric value of each food.

The value of each pixel in the depth image is the distance between the object corresponding to the pixel and the camera plane. According to the working principle [13], depth cameras can be divided into the following three categories[14]: (1) Based on binocular stereo vision[15]; (2) Based on structured light; (3) Based on the Time of Flight (ToF) method[16]. Virginie Benos[17]et al. designed an object size measuring device based on multi-view 3D reconstruction. The device takes images of the object at multiple angles, and then uses the method of multi-view matching to generate a 3D model of the object for measurement. Li Lingling et al. [18] proposed rapid volume measurement scheme based on Kinect2.0 depth camera. Kinect2.0 depth camera is used to look down at a fixed height to shoot the measured object. After image processing of the depth image, the target contour is located. Serge Thuries et al. from American company Hand Held Products designed a box size measurement system based on ToF depth camera [19]. The system calculates the result after the operator manually delimits the length of the side to be measured on the touch screen.

3D reconstruction algorithm based on depth camera is a research hotspot in recent years. KinectFusion algorithm proposed by Microsoft et al in 2010 [20] and Bundlefusion algorithm proposed by Dai Angela et al in Stanford University in 2017 [21] enable real-time reconstruction of 3D models. With a three-dimensional model of an object, size and volume information can be easily obtained. These 3D reconstruction algorithms tend to study properties and pay more attention to accuracy. They are suitable for fruits, vegetables and dishes with complex surface texture. Therefore, we adopt the deep learning technology to obtain the type information of the image first, and then obtain the 3D information and volume of the image through the 3D reconstruction algorithm of the depth camera. Finally, the quantitative estimation of calories was obtained through the calorie calculation model.

2. Materials and methods

2.1 Sample Selection

Vegetable samples are selected from carrot, tomato, eggplant and other 16 common vegetables, dishes are from Zhenjiang Jimailong Mall. Twenty samples were selected for each vegetable variety. Due to the diversity of vegetable shapes and sizes, vegetable samples were randomly selected to ensure the reliability of the experiment.

Sample dishes Common in restaurants are selected, and some samples are selected as representative dishes for the experiment. This study selected stir-fried green vegetables, diced corn chicken, cabbage vermicelli, fried meat with chili, tomato and egg, potato and beef and other common dishes as our experimental samples.

2.2 Model Selection

Convolutional neural network (CNN) nearly has been the most main-stream method, such as GoogLenet[22], VGG [23], Incepetion and so on. The milestone event in the history of CNN should be the emergence of ResNet[24] model, which can train deeper CNN model to achieve higher accuracy. The core of the ResNet model is to train a deeper CNN network by establishing a "shortcuts, skip connection" between the front layer and the back layer, which could facilitate backpropagation of gradients during training. DenseNet[25] model has the same basic method as ResNet, but it establishes the dense connection between all the front layers and the rear layers. Another feature of DenseNet is feature reuse through concatenation of features on a channel. These features make DenseNet achieve much more better performance than ResNet model with fewer parameters and computational costs.

All our experiments were carried out using the PyTorch deep learning framework. During the training stage, the initial learning rate was set as 0.01, momentum as 0.9 and weight attenuation as 1e-4. Cosine annealing attenuation method is adopted. The epoch number of training is set to 100. The stochastic gradient descent (SGD) method was adopted for training optimization. The images were rotated 90 degrees, randomly cropped, flipped horizontally and flipped vertically. First adjust the training image to 256x256, then apply a horizontal flip random cropping of size 224x224 (probability 0.5). During the test, the image was adjusted to 256x256 and then we used a 224x224 size center cropping to input into the network. All experiments were conducted on Ubuntu operating system, using Intel Xeon Gold 6346 3.1GHz*32 cores, Nvidia A100 Tesla GPU hardware, and 256G memory. In this paper, Intel RealSense D400 Series Dynamic Calibration Tools[27] calibration software is used, and print-target-fixed-width[27] is configured to calibrate the calibration board.

Our data set integrates the Chinese dish data provided by the public data set in today's society, making it more consistent with the content studied in this paper, and more suitable for intelligent Chinese restaurant and intelligent canteen. The whole data set is divided into training, test, and validation sets, with the proportions of about 80%, 10% and 10% respectively. To convert the image to the size required by the network, the model loaded is a fixed input size 224*224. Data sets are randomly selected into training set validation set and test set. There were 108,250 images in the training set. Then, the dataset has 13,531 images in the validation set, and the remaining 13,532 images are used for testing. A variety of popular deep learning network architectures with different structures and different layers are used for comprehensive experiments.

As shown in Figure 1, we try to add optimized attention mechanism CBAM to the existing network. Because the network structure cannot be changed, CBAM cannot be added to each block. Adding CBAM to the last convolution layer and the first convolution layer does not change the network, and pre-trained parameters can be used. CBAM not only improves the original channel attention mechanism, but also adds the spatial attention mechanism.

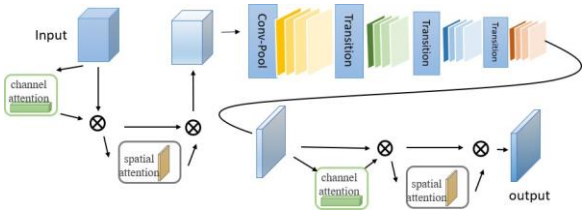

Figure 1. Network flowchart for adding an attention mechanism

2.3 Machine vision system

A RealSense D435i camera is used to acquire the RGB map and depth map of the target [26]. RealSense D435i camera measures 90mm×25mm×25mm, weighs about 75g, and adopts active infrared stereoscopic depth of field technology. The field of view of the depth camera is 65°×40°, the resolution is 1280×720, the frame rate can reach 90fps, and the test depth range is 0.3m-10m. The field of view of the RGB camera is 69°×42°, the resolution is 1920×1080, the frame rate can reach 30fps, the focal length is 1.88mm, and the photosensitive size is 2.73mm×1.55mm[27].

The basic principle of Realsense D435i is to project light with certain structural characteristics through near -infrared laser projection, and then collect it through a special infrared camera. Lights with a specific structure will collect different image phase information of different depth areas of the photo objects, and then convert the change of the structure into deep information by calculating the unit to obtain a three -dimensional structure. Generally, an invisible infrared laser with a specific wavelength is used as a light source, and its light is projected on the object through specific codes. Obtain the position and depth information of the object by calculating the distortion of the coding mode returned by some algorithm. The position of infrared laser projection in the D435i depth camera is only used as a feature point, and the submerged parts in the outdoor sun will only cause less functional points and lower accuracy, but it will not be fully obtained at all depth [28].

As shown in Figure 2(a), 4 coordinate systems of the camera model are given: the world coordinate system(WCS) (Ow), the camera coordinate system(CCS) (O_c), the image coordinate system (ICS)(x',y'), and the pixel coordinate system(PCS) (u,v). Ow-XwYwZw is the WCS used to describe the camera position, O_c-$X_cY_cZ_c$ is the camera coordinate system, optical center is the origin, o-xy is the image coordinate system, optical center is the image midpoint, u-v is the pixel coordinate system, origin is the upper-left corner of the image in unit pixel. P is a point in the WCS , that is, a real point in life. p is the imaging point of point P in the image. The coordinate in the image coordinate system is (x, y), the pixel coordinate is (u, v), and the coordinate in the image coordinate system is (u, v)., f is the camera focal length, is equal to the distance between o and O_c.

2.4 Three-dimensional modeling of dishes

The 3D point cloud model construction module based on Intel RealSense and BundleFusion includes the dish positioning extraction module based on point cloud segmentation, and the 3D reconstruction of positioning dishes. The BundleFusion takes the registered RGB color map and depth map as input. Through this method, real-time 3D mapping can be realized. The process of BundleFusion framework includes RGB color map and depth map as input, consistency test, local pose optimization, global pose optimization, data cache, and finally data integration through block update and pose update.

As shown in Figure 2(b), for the samples of fruits and vegetables, the depth images are obtained above and below the

samples of fruits and vegetables; as shown in Figure 2(c), the depth images are obtained for the two surfaces above the dishes, and on this basis, the BundleFusion 3D modeling is carried out. Configure BundleFusion project environment, including configuring RealSense Sdk local environment and using BundleFusion project code. In order to make D435i work properly in BundleFusion, RealSense D435i driver needs to be developed. This driver is the secondary development based on the API provided by intel official, and on this basis, the BundleFusion depth data interface is called[29]. It can interact with the application program, export the model, and get the 3D reconstruction model.

Furthermore, the measurement system only needs the point cloud model of the measured object itself when measuring the size and volume, so it needs to segment the constructed 3D model. The method adopted by our research group is to first make a rough division to segment the center region of the 3D model, then use statistical filter to remove the outliers in the point cloud model, and finally use RANSAC[29] algorithm to do a plane estimation to segment and remove the background plane. After rough segmentation and filtering [30], the 3D point cloud model contains the measured object and background. After plane estimation and segmentation by RANSAC algorithm, the 3D point cloud model of the object itself is obtained.

2.5 Volume calculation of three-dimensional model of dishes

After obtaining the three-dimensional model, we measured the volume by Monte Carlo algorithm [31] based on principal component analysis (PCA), obtained the three principal directions of the point cloud, obtained the centroid, calculated the covariance, obtained the covariance matrix, and obtained the eigenvalues and long vectors of the covariance matrix. The eigenvector was the main direction. Using the obtained principal direction and center of mass, the input point cloud is converted to the origin, and the principal direction and the coordinate system direction return, and the bounding box of the transformed point cloud to the origin is established. The main direction and surrounding box are set for the input point cloud, which is realized by the inverse transformation from the input point cloud to the original point cloud.

Suppose A is A three-dimensional dish model, A1 is the enclosing cube of dish A, N uniformly distributed pseudo-random points are generated in the reference cube A1, and each random point is detected whether it is located in A. Suppose the number of random points located in dish A is Nin (≤N), Monte Carlo method is applied, then the volume of A is:

$$V \approx V_1\left(\frac{N_{in}}{N}\right)$$

2.6 Dish calorie calculation model

As shown in Figure 2, the samples to be tested are classified by deep learning module. We call MySQL database through Python DB-API, the Python standard database interface, to obtain the pre-designed calorie density (j/cm3) in the database, and then build the calorie calculation model according to the volume data obtained by three-dimensional reconstruction. Calculate the number of calories in a meal.

Suppose a meal contains p portions of Chinese dishes, take k∈ [1, p], the average calorie density ρ_k (J/m3) of the k portion dish, the volume of the k portion dish is V_k, the calorie of the k portion dish is Q_k, $Q_k=\rho_k \cdot V_k$, the total calorie

$$Q=\sum_{k=1}^{p} Q_k \text{ , that is}$$

$$Q = \sum_{k=1}^{p} \rho_k \cdot V_k$$

The caloric value is the total caloric value of p dishes according to the volume data.

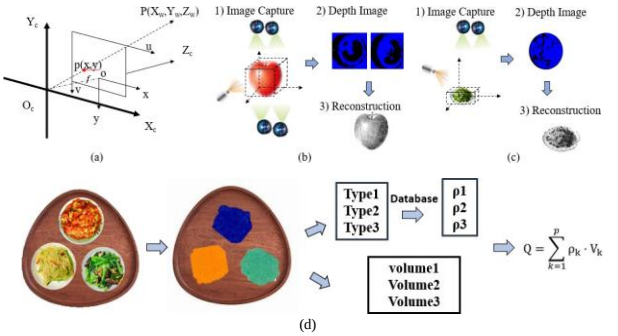

Figure 2. (a)Transformation diagram from pixel coordinate system to camera coordinate system. (b) Depth image acquisition and 3D reconstruction process of vegetable samples. (c) Depth image acquisition and 3D reconstruction process of dishes. Schematic diagram of calorie calculation model of dishes

3. Results and discussion

3.1 Results of dish image classification

The recognition performance of different deep networks is shown in Figure 3(a), which gives the accuracy of top 1 and top 3, respectively. As can be seen from, the best performance of top-1 on the validation set is 80.02%, which is achieved by DenseNet265. As shown in Figure 3(b), in the test set, the recognition rate of DenseNet265 is also the highest, 79.15%. However, each model has a high value in the top3 accuracy, and the model of Densenet265 is still the highest, with 93.66% and 93.73% accuracy in the test set and validation set. It can be seen that considering the relatively large dataset of this study, a deeper model is needed to train. The more complex the model, the better the performance of the model. DenseNet performs better than ResNet for image processing. The essence is that DenseNet can better match the information distribution characteristics of the image, and it uses a multi-scale Kernel. After adding CBAM to ResNet152 and DenseNet265, the accuracy of the network model is improved. After DenseNet265 is added to CBAM, the Top-1 accuracy on the test set reaches 82.47%, and the Top-1 accuracy on the validation set reaches 82.89%.

The deeper the CNN model is, the better the performance is[32][33]. It can be seen from the results that, in the same network architecture, the performance of CNN model has been significantly improved with the increase of the number of layers.

Method	Test		Vaild	
	Top-1 Accuracy/%	Top-3 Accuracy/%	Top-1 Accuracy/%	Top-3 Accuracy/%
VGG19	76.58	90.33	77.69	89.92
ResNet50	74.25	88.06	74.17	88.65
ResNet152	75.61	91.41	75.02	91.56
DenseNet169	77.89	92.03	77.09	92.15
DenseNet201	78.17	92.25	77.88	91.57
DenseNet265	79.15	93.66	80.02	93.73
ResNet152+CBAM	78.21	92.33	77.96	92.71
DenseNet265+CBAM	82.47	94.85	82.89	94.25

(a)

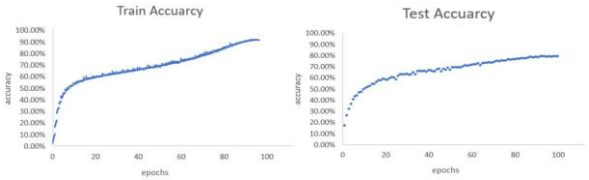

(b)

Figure 3 (a). Top-1 and top-3 recognition rates of different depth networks on food data sets (b). Top-1 accuracy of DenseNet265 training set and test set

3.2 Vegetable and dish volume measurement and calorie calculation results

In this paper, 16 kinds of common vegetable models such as carrot, tomato and eggplant are selected to carry out three-dimensional modeling of vegetable models. The background environment is the indoor wall, the lighting condition is no direct sunlight during the day, and the shooting distance should be kept at about 0.5 meters away from the object. After the measurement system is started, the depth image of fixed D435i depth camera position is acquired, and the depth image of two surfaces is acquired. Figure 4 shows the display interface of the measurement system in the 3D reconstruction stage in the experiment. (a) is the input RGB color map, and (b) is the input depth image. The reconstructed 3D model of the measured object is shown in (c).

After point cloud fusion, each surface of green pepper is completely constructed. Due to the error of IMU pre-integration to determine the camera pose, it can be seen that the surface of the 3D reconstruction model of green pepper has some ups and downs. As shown in (d), after point cloud smoothing, the surface smoothing of green pepper is complete. As shown in (e), the mapping results of point cloud model can be obtained after the registration of RGB image and depth image. Finally, the background is removed to obtain the complete three-dimensional point cloud model diagram of green pepper (f).

After the 3D point cloud model of the image is obtained, the three principal directions of the point cloud are obtained by PCA principal component analysis method. The input point cloud is converted to the origin, and the principal direction and coordinate system direction return, and the bounding box of the point cloud transformed to the origin is established. Set the main direction and bounding box for the input point cloud, as shown in (g). Based on the minimum bounding box volume, Monte Carlo point-casting algorithm was adopted to set a random number of 1000 to calculate the volume of points in the point cloud model, namely, the target point cloud volume, as shown in (h).

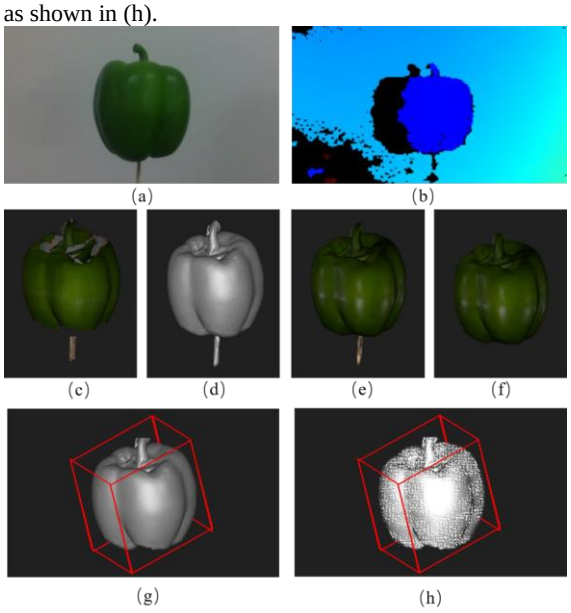

Figure 4(a) RGB color map of vegetables, (b) Depth image of vegetable (c) 3D model after vegetable reconstruction (d) 3D model after point cloud smoothing (e) 3D model after RGB image and depth image registration (f) 3D model after background removal (g) 3D model and minimum envelope box (f) Schematic diagram of volume calculated by Monte Carlo algorithm

The selected samples were combined by species. For example, green pepper and red pepper were grouped together, yellow pumpkin, orange pumpkin and green pumpkin were grouped together, and green, red and yellow bell peppers were grouped together. Finally, 11 varieties were obtained, and 20 samples were tested for each. The vegetable samples and their corresponding reconstruction results were shown in Figure 5(a). Results showed the appearance collection of vegetable samples was complete. After the volume calculation of 20 samples of each variety, the actual volume and the measured volume are shown in Figure 5(b)

Statistical analysis shows that the average deviation of a single vegetable is shown in Figure 5(c). The minimum average deviation of a single vegetable is 0.0093, and the maximum deviation of a single vegetable is 0.0429. The relationship between the measured volume and the actual volume is shown in the figure. Irregular samples of vegetables can lead to a bias in measurement results, considering slight surface shape differences. But it's all within the margin of error. Stir-fried green vegetables, tomato scrambled eggs and other common dishes were used for three-dimensional modeling. Each dish was sampled according to the weight of 60g, 80g, 100g, 120g, 140g, 160g, 180g and 200g, and three-dimensional modeling was carried out for the dishes. The same method was used for three-dimensional modeling for vegetables as above. Compared with vegetables, the difficulty of dish reconstruction is more difficult. In fact, we only shoot on one side, unable to capture the image of the bottom of the dish, so we use flat bottom to simulate the bottom of the dish. In addition, dishes will also have coarser surfaces with complex textures.

Figure 5(c), (d) shows the RGB image and the 3D reconstructed image of the selected dishes. The 3D reconstructed image is the image after point cloud smoothing and background removal. The same method is used to obtain the outsourcing box through the principal component analysis method, and then the volume of the 3D reconstructed model is calculated through the Monte Carlo algorithm. Figure 5(e) shows the calculated volume and actual volume of selected dishes. Figure 5(f) shows the deviation of the experimental dishes. It can be seen that the density of the dishes such as fried green vegetables and fried chicken with corn is higher due to the dense accumulation among the dishes. For example, the dishes with potato and beef have large particles, so the density of the dishes is smaller. These errors are still within the allowable limits.

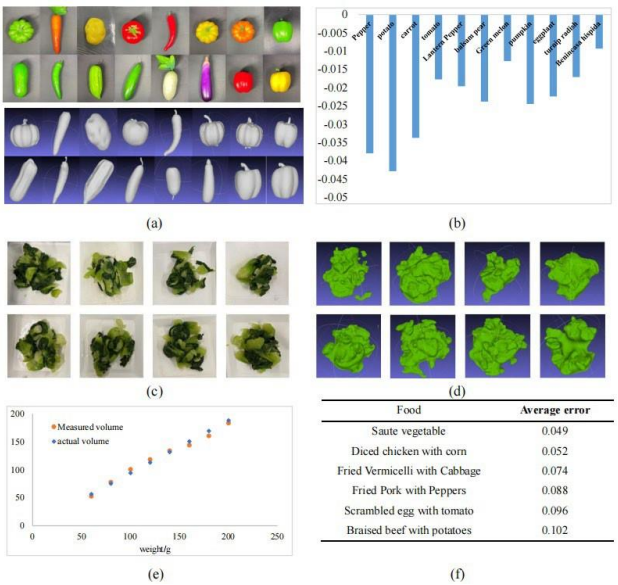

Food	Average error
Saute vegetable	0.049
Diced chicken with corn	0.052
Fried Vermicelli with Cabbage	0.074
Fried Pork with Peppers	0.088
Scrambled egg with tomato	0.096
Braised beef with potatoes	0.102

Figure 5 (a). Sample dishes RGB images (b)Sample dishes 3D reconstructed models (c)Sample dishes and their actual and calculated volumes (d)Deviation of volume measurement of different dishes

4. Conclusions

Nowadays, obesity is a major problem in human life. Therefore, this paper puts forward a novel topic, and with the development of social economy in today's era, it provides a method for fast detection of calories for weight-loss training camps and intelligent restaurants. In our system, deep learning is combined with 3D reconstruction technology and applied to the food field for calorie test. Compared with the popular networks such as VGG, ResNet and DenseNet, the results show that the ideal effect is produced through data enhancement, parameter adjustment and data set fusion. After adding CBAM, the accuracy of the optimal network of ResNet and DenseNet is improved. The addition of 3D reconstruction technology improves the 3D data on the basis of the type data provided by deep learning. The appearance model of the dish is simulated by 3D reconstruction technology, and the outsourced box is established by statistical methods, and the volume is obtained by Monte Carlo method. Finally, the calorie calculation model is established by combining the two technologies. This technology is promising and can be applied well.

References

[1] Mesas, M. Mu˜noz-Pareja, E. López-Garc´ıa, and F. Rodr´ıguezArtalejo, “Selected eating behaviours and excess body weight: a systematic review,” Obesity Reviews, vol. 13, no. 2, pp. 106–135, 2012

[2] Gao Jie, Long Hua, Liu Yongzhao et al. A Method and device for calculating Calorie Intake in meals [P]. YunnanCN106257478A,2016-12-28.]

[3] Chen X , Zhu Y , Zhou H , et al. ChineseFoodNet: A large-scale Image Dataset for Chinese Food Recognition[J]. 2017.

[4] McAllister, Patrick, Zheng, et al. Combining deep residual neural network features with supervised machine learning algorithms to classify diverse food image datasets.

[5] Shen Z , Shehzad A , Chen S , et al. Machine Learning Based Approach on Food Recognition and Nutrition Estimation[J]. Procedia Computer Science, 2020, 174:448-453.

[6] Ma P , Lau C P , Yu N , et al. Image-based Nutrient Estimation for Chinese Dishes Using Deep Learning[J]. Food Research International, 2021(8):110437.

[7] Vkg A , Pv A , Vp B . Food Classification using Transfer Learning Technique[J]. Global Transitions Proceedings, 2022, 3(1):225-229.

[8] Liang Yanchao, Li Jianhua. Food calorie estimation method based on deep learning [J]. Journal of East China University of Science and Technology: Natural Science Edition,2018, 44(2):7.

[9] M.F. Rahman, S.N. Fatihah, Food Calorie Estimation Based on Food Recognition.

[10] H. Hu, Z. Zhang, Y. Song, Image Based Food Calories Estimation Using Various Models of Machine Learning, 2020.

[11] R. Isaksen, E.B. Knudsen, A.I. Walde, A deep learning segmentation approach tocalories and weight estimation of food images, 2019.

[12] P. Pouladzadeh, S. Shirmohammadi, Mobile Multi-Food Recognition Using Deep Learning, ACM Trans. Multimedia Comput. Commun. Appl. 13 (3s)(2017) 1–21.

[13] Lee Seungkyu. Depth camera image processing and applications[C].2012 19th IEEE International Conference on Image Processing. IEEE, 2012.

[14] Xiao Mi binocular camera [EB/OL]. http://www.myntai.com/cn/mynteye/depth/specs, 2019

[15] Intel® Depth Camera SR305[EB/OL]. https://www.intelrealsense.com/depth-camera-sr305, 2019

[16] ESPROS Photonics Corporation,epc600 Datasheet[EB/OL]. http://www.aprizes.com/data/upload/201810/f_06bf5d161bb59897bcd5f9d0787fc04d.pdf, 2019

[17] Benos, Virginie, Vincent Bessettes, and Franck Laffargue.Semi-automatic dimensioning with imager on a portable device[P].U.S. Patent No.8,908,995.9Dec.2014.

[18] Li Lingling, Wang Zhengyong, Qing Linbo, He Haibo. Fast Volume measurement based on Kinect 2.0 depth Image [J]. Microcomputer & Applications,2017,36(07):35-38+42.Thuries Serge, Alain Gillet and Franck Laffargue.Dimensioning system with multipath interference mitigation[P].U.S. Patent No.9,557,166.31 Jan.2017.

[19] Newcombe, Richard A., et al.Kinectfusion: Real-time dense surface mapping and tracking[J].ISMAR. Vol.11.No.2011.2011.

[20] Dai Angela, et al.Bundlefusion: Real-time globally consistent 3dreconstruction using on-the-fly surface reintegration[J].ACM Transactions on Graphics (ToG) 36.3(2017):24.

[21] Szegedy C, Wei L ,Jia Y, et al. Going deeper with convolutions[C]// 2015 IEEE Conference on Computer Vision and Pattern Recognition (CVPR). IEEE, 2015.

[22] K. Simonyan and A. Zisserman, “Very deep convolutional networks for large-scale image recognition,” arXiv preprint arXiv:1409.1556, 2014.

[23] K. He, X. Zhang, S. Ren, and J. Sun, “Deep residual learning for image recognition,” in Proceedings of the IEEE conference on computer vision and pattern recognition, 2016, pp. 770–778.

[24] F. Iandola, M. Moskewicz, S. Karayev, R. Girshick, T. Darrell, and K. Keutzer, “Densenet: Implementing efficient convnet descriptor pyramids,” arXiv preprint arXiv:1404.1869, 2014.

[25] Keselman Leonid, et al.Intel realsense stereoscopic depth cameras[C]. Proceedings of the IEEE Conference on Computer Vision and Pattern Recognition Workshops. 2017.

[26] Intel Realsense D435i depth camera Datasheet [EB/OL] .https://www.intel.com/content/dam/support/us/en/documents/emerging-technologies/intel-realsense-technology/Intel-RealSense-D400-Series-Datasheet.pdf, 2018

[27] Long Y , Wang Y , Zhai Z , et al. Potato volume measurement based on RGB-D camera[J]. IFAC-PapersOnLine, 2018, 51(17):515-520.

[28] Dai A , Niener M , Zollhfer M , et al. BundleFusion: Real-time Globally Consistent 3D Reconstruction using On-the-fly Surface Re-integration[J]. ACM Transactions on Graphics, 2016.

[29] Qu Tianwei, An Bo, Chen Guilan. Application of Improved RANSAC Algorithm in Image Registration [J]. Computer Applications, 2010(7):4.

[30] Uyyala S , Alvarez I J , Jackson B A , et al. High-fidelity 3D reconstruction using facial features lookup and skeletal poses in voxel models:, US10580143B2[P]. 2020.

[31] Jaekel U . A Monte Carlo Method for High-Dimensional Volume Estimation and Application to Polytopes[J]. Procedia Computer Science, 2011, 4(4):1403-1411.

[32] Szegedy, W. Liu, Y . Jia, P . Sermanet, S. Reed, D.

Anguelov, D. Erhan,V . V anhoucke, and A. Rabinovich, “Going deeper with convolutions,”in Proceedings of the IEEE conference on computer vision and patternrecognition, 2015, pp. 1–9.

[33] Szegedy, V . V anhoucke, S. Ioffe, J. Shlens, and Z. Wojna, “Rethinking the inception architecture for computer vision,” in Proceedings of the IEEE Conference on Computer Vision and Pattern Recognition, 2016, pp. 2818–2826.

[34]

Wenjian Gao
Master student, Master of Engineering (Electronic information).
Research Interests: Artificial intelligence, pattern recognition.

Xiaobo Zou
Professor
Research Interests:
Non-destructive testing of agricultural products, food quality and safety, Near infrared, hyperspectral image detection

Jiyong Shi
Professor
Research Interests:
Non-destructive testing of agricultural products, food quality and safety, Near infrared, hyperspectral image detection

The Localization of Thailand Cuisine in China from the Perspective of Globalization—Taking Thai Restaurants in N City as an Example

Zhou Qiaotong[1*]

[1]Guangxi University, China
*E-mail: 478704666@qq.com

Abstract: This thesis aims to analyze the phenomenon of the localization of Thai cuisine in China, involving sociological theory. As a Southeast Asian cuisine, Thai food underwent integration and adaptation upon its introduction to China, resulting in localized dishes with distinctive characteristics that gained popularity among the locals. As globalization progresses, Thai cuisine in China has experienced profound integration, giving rise to exotic local dishes that facilitate friendly cultural exchanges between the two countries. This research focuses on Thai restaurants in N City, China, as the subject of study, exploring how Thai food improved and adapted to a foreign country.

Keywords: Thailand cuisine, globalization, China, food localization

1. Introduction

The tide of globalization has propelled the fusion of cultures worldwide over the past few decades, with food culture standing out as a prominent representative. In this era of globalization, individuals have become more receptive to diverse tastes, actively pursuing novelty and culinary diversity. As an active participant in this global phenomenon, China has undergone significant cultural fusion. Within this process, Thai cuisine has steadily established i tself in China, exhibiting a discernible trend towards localization. This phenomenon not only mirrors the evolution of the restaurant industry but also emerges as a pivotal facet of cultural exchange.

1.1 The Meaning of Studying the Localization of Thailand Cuisine in China

The l ocalization of foreign cuisine represents a form of cultural integration, which can be described as a manifestation of cultural "mix&merge". According to the research conducted by Nie Chunyan and Liu Yingwei, cultural mix&merge influences individuals in five aspects: cultural cognition, cognitive closure needs, intergroup bias, creativity, and organizational change acceptance.[1] Based on this, the study of the localization of Thai cuisine in China can be deemed significant for three main reasons:

I. Promoting Cultural Diversity: The promotion of cultural diversity through the localization of Thai cuisine in China extends beyond mere adjustments in food taste; it encompasses a process of cultural integration and symbiosis. Examining this phe nom e non pr o vi de s a nua nc e d understanding of how globalization fosters c u l t u r a l d i v e r s i t y . T h a i c u i s i n e ' s localization signifies a meaningful dialogue between two distinct cultures, enriching people's cultural choices and actively contributing to the promotion of cultural diversity.

II. Building Cultural Identity: "Culinary culture stands as the most fundamental and distinctive artistic manifestation of cultural identity, capable of accentuating national identity."[2] The construction of social identity undergoes a transformative process with the localization of Thai cuisine in China. Dietary preferences are no longer confined to matters of taste;they

metamorphose into a powerful expression of identity. Research endeavors can uncover the nuanced status and impact of this culinary culture within Chinese society, shedding light on its role in shaping i ndividual and communal identities. This exploration aids in comprehending how individuals interpret and articulate their cultural identity through food in the expansive landscape of globalization.

III. Facilitating China- Thai Cultural Exchange: The localization of Thai cuisine in China stands as a compelling instance of cultural exchange, embodying the outcomes of mutual cultural influence. A thor ough inve stiga tion into this phenomenon unveils t he intricate mechanisms of cultural interaction, fostering deeper understanding and exchange between China and Thailand. Such research holds significant practical implications in the pursuit of constructing a more inclusive and open global society.

Understanding the localization of Thai cuisine in China facilitates further mutual comprehension of each other' s culinary cultures, fostering cultural exchange and promoting integrated development.

1.2 The Concept of Globalization and its Development

As initially defined by Roland Robertson, globalization refers to “think globally and act locally.” Globalization, as a comprehensive concept, embodies the increasing mutual-connection and interdependence of diverse cultures, economies, and societies worldwide. It refers to the interconnected and freely flowing relationships among various regions around the world on a broad global scale.[3] At its core, it signifies the permeation of ideas, goods , and pr actices across bor ders, t ranscending geographical and cultural constraints.

Within the realm of culinary culture, globalization has given rise to transformative trends, influencing the way people eat, experience, and perceive food globally. Firstly, there's a notable trend towards cross-cultural fusion and culinary amalgamation. Different culinary traditions blend, creating a rich tapestry of global f lavors accessible to individuals worldwide. For example, you can see KFCs in countries worldwide, at the same time its counterparts in China sell porridge and Chinese soybean milk. Besides, diverse culinary options become prevalent in cities globally, reflecting a heightened appreciation for and engagement with international food traditions.

Another profound impact of globalization on culinary culture is the heightened emphasis on cultural identity through food. As the world becomes more interconnected, individuals are not only preserving their culinary heritage but also expressing their cultural identity through food choices. This has led to a global culinary landscape that celebrates both the uniqueness of individual food cultures and the willingness to explore and integrate elements from other culinary traditions.

M or e ove r, t he gl oba l exc ha nge of ingredients and culinary techniques has f lourished, enabling unique and exotic foodstuffs to traverse the globe. This ease of access to diverse ingredients has not only enriched local cuisines but has also stimulated international trade in the food industry, leading to an increased availability of globally sourced produce.

In essence, the impact of globalization on culinary culture is a dynamic and multifaceted phenomenon, fostering c ross- cultural connections, diversifying culinary options, and encouraging a nuanced appreciation for cultural identity through food.

1.3 The Introduction of Chinese Culinary Culture

According to the book 《五味杂陈——中国传统饮食文化》(A Medley of Flavors: Traditional Chinese Culinary Culture), over thousands of years of development, China's diverse regions have given rise to eight major culinary styles, namely Shandong, Sichuan, Cantonese, Suzhou, Fujian, Zhejiang, Hunan, and Anhui cuisines.[4] This research focuses on N City in Guangxi Zhuang Autonomous Region of China, primarily featuring Cantonese cuisine. Known for its fresh and delectable taste, this culinary style incorporates distinctive flavors, often enhancing dishes with ingredients such as oyster sauce and shrimp paste. Some scholars argue that geographical factors are crucial in shaping this culinary culture, while simultaneously emphasizing the importance of sustainable development in the realm of gastronomy.

Chinese cuisine has three major characteristics: Rich in content and wide-ranging, this provides abundant material for the construction of discourse on culinary culture. (For example, a rich variety of dishes and diverse ingredients.); Integrative, incorporating exotic ingredients and culinary techniques, continuously enriching Chinese culinary culture; Keeping pace with the times, constantly innovating.[5] These features make Chinese cuisine flexible and open to innovation, allowing it to seamlessly integrate with exotic ingredients and culinary practices.

1.4 The Development of Thai Cuisine in N City

The evolution of Thai cuisine in China has been significantly influenced by strategic policies implemented by Thailand in the late 20th century. The Thai government, recognizing the global appeal of its culinary traditions, initiated a systematic promotion of Thai cuisine on a worldwide scale. This endeavor introduced the plan “The Kitchen of World” of which primary objective was to elevate Thai cuisine to a world-class culinary status through comprehensive global marketing and promotional initiatives.[6]

China, with its unique geographic proximity to ASEAN nations, particularly in the Guangxi region, played a pivotal role in facilitating the growth of Thai cuisine. The strategic location of Guangxi, bordering several ASEAN countries, has fostered a natural synergy in cultural exchange. The hosting of the CAEXPO has further deepened mutual understanding and communication between China and the ASEAN region, providing a fertile ground for Thai restaurants to establish themselves in cities like N City. “Over a decade ago, Southeast Asian restaurants here were few and far between, and sourcing ingredients for Thai cuisine was challenging. Today, Southeast Asian-flavored restaurants are ubiquitous,” said a Ms. from Thailand. To better attract Chinese consumers, she has meticulously recreated the ambiance of Thai streets in the restaurant's decor. She has imported hundreds of sets of Thai clothing and established a dressing experience area, allowing Chinese consumers to experience authentic Thai cultural vibes without leaving the country.[7] The CAEXPO serves as a platform for extensive cross- cultural interactions, contributing to a profound appreciation of Thai culinary traditions among Chinese consumers. The resulting familiarity and understanding have created an opportune environment for the establishment and flourishing of Thai restaurants in N City, exemplifying the harmonious blend of cultural exchange and gastronomic appreciation.

2. The Design and Process of the Research

In my research, I employ a comprehensive methodology that incorporates both interviews and observation to analyze the phenomenon of globalization of Thai cuisine in N City. The interview method involves engaging with key stakeholders in the local Thai restaurant industry, including restaurant owners, chefs, and patrons, to gather firsthand insights into

their perceptions, experiences, and strategies regarding the localization of Thai cuisine.

Within the interview component, a notable case study involves the proprietress of a Thai restaurant, originally from Thailand, who, after years of studying in City N, decided to establish her own Thai restaurant. The interview with her delves into various aspects, including restaurant decor, menu offerings, and strategic adjustments, providing insights into the strategies employed to tailor the dining experience to local tastes. Questions revolve around the rationale behind specific design choices, the selection of menu items, and how the restaurant adapts to local preferences.

Furthermore, this research extends its scope by conducting interviews with customers to gather their opinions and perspectives on the restaurant. This qualitative approach aims to uncover the nuances of customer experiences, preferences, and feedback, contributing valuable qualitative data to the overall analysis of the globalization of Thai cuisine in City N. By combining insights from both restaurant owners and patrons, the research seeks to offer a comprehensive understanding of the intricate dynamics involved in the localization of Thai cuisine within the global context of City N.

Additionally, the observation method entails systematically observing and documenting the operational dynamics, interior designs, menu compositions, and customer interactions within selected Thai restaurants in City N. This approach allows for a nuanced understanding of how Thai culinary traditions adapt and integrate within the local context. By triangulating data obtained from interviews and observations, this research aims to discern the multifaceted aspects of globalization and shed light on the factors influencing the successful adaptation of Thai cuisine in a local context.

3. The Globalization Strategies of Thai Restaurants in N City

In this part, we delve into the intricacies of Thai cuisine localization in N City, focusing on three fundamental aspects: the selection of restaurant names and decor, the adaptations made to menu offerings and the newly innovated Thai dish. These aspects are critical in understanding how Thai restaurants strategically navigate the local landscape, appealing to cultural nuances and consumer preferences.

3.1 Restaurant Name and Decor: A Cultural Expression

The process of Thai cuisine localization in N City begins with a deliberate choice in restaurant name and decor. Most Thai restaurants will have a name that highlights Thai characteristics. Thai restaurant owners in N City often opt for names that resonate with their cultural origins, invoking a sense of authenticity and exoticism. Mr. Ma Yifei noted in his thesis that, Thai restaurants often prefer name that contains the character “泰” (Thai) or incorporate Thai symbols such as Tuk-Tuk , which also can be seen in N City.

For instance, a Thai restaurant might choose a name reminiscent of a specific region in Thailand, bringing forth a narrative that more than mere branding. During an offline investigation, one Thai restaurant located near the school was named “米珰咔,” phonetically transcribed from Thai, meaning “get rich.” According to interview records, the proprietress mentioned that it symbolizes the wish for both herself and the customers dining here to become increasingly prosperous.

Interestingly, this Thai term has gained popularity among the younger demographic in China, making the restaurant’s name an effective means to evoke nostalgic memories of Thai culture among the youth. Besides, its Pattaya-style decor further amplifies this cultural expression. The vibrant colors, traditional Thai artifacts, and distinctive architectural elements create an immersive

experience for diners. This decor not only serves an aesthetic purpose but also contributes to the construction of a cultural narrative within the dining space. The name and decor not only reflect the cultural identity of Thailand but also leave a lasting initial impression on individuals.

Culture and identity frequently intertwine to create a distinct "cultural identity," serving as a recognizable marker for individuals or groups to self-identify, distinguish others, and fortify their sense of belonging.[8] By intertwining cultural representation theories with the practical choices made by Thai restaurants in N City, this thesis aims to unravel the layers of cultural expression embedded in the selection of names and decor. This sets the stage for a comprehensive understanding of how these strategies contribute to the overall localization of Thai cuisine.

3.2 Menu Adaptations: Balancing Familiarity and Authenticity

In the realm of culinary localization, one newly opened Thai restaurant in N City exhibits a nuanced approach to menu adaptations. The relatively minimal changes to traditional Thai dishes may stem from the close alignment of Chinese and Thai culinary habits. The geographical proximity and shared cultural influences between the two nations create a foundation of culinary familiarity.

However, the intricacies emerge when considering the distinct preferences of Chinese and Thai patrons. Chinese customers often gravitate towards Thai dishes that have gained popularity in China, such as curry, pork neck, and Tom Yum soup. On the other hand, Thai patrons display a penchant for authentic Thai dishes less familiar to their Chinese counterparts, including the likes of papaya salad. This also indicates another reason; currently, the process of Thai cuisine localization in N City has, in fact, achieved a certain level of success. People are accustomed to the taste of Thai dishes they have had in other Thai restaurants before, which may be one reason why newly opened Thai restaurants do not need to make extensive modifications to their food recipes.

This dynamic reveals a crucial insight into the localization process: the need to balance offering familiar dishes to cater to local tastes while also promoting lesser-known Thai specialties to encourage culinary exploration. Even with identical recipes, the locally sourced ingredients introduce subtle differences in flavor. For instance, the Chinese variety of small chili peppers may not match the heat of Thailand's devilishly spicy peppers. However, this divergence in spiciness does not hinder people's enjoyment and appreciation of the cuisine.

3.3 An Innovative Thai Dish: A Culinary Fusion

The exploration of Thai cuisine localization in N City extends to the realm of innovative dishes, with a spotlight on the creation of a Thai- inspired spicy chicken pasta. This culinary venture was sparked when the cook, having experienced the rich flavors of Thai sauces in the Thai restaurant, envisioned crafting a pasta dish with a similar taste profile. Drawing inspiration from the palate preferences of the locals in N City, a series of tastings and refinements led to the birth of a mature and distinctive new addition to the menu.

Taking the ubiquitous concept of chicken pasta, the newly crafted dish boasts a robust blend of flavors, featuring the aromatic essence of garlic, stir-fried chicken, and the kick of small chili peppers—delivering a taste reminiscent of traditional Chinese home-cooked meals. However, the innovation doesn't stop there. The dish incorporates Thai elements, such as the infusion of flavors from lemongrass and lime, adding a unique Thai twist to the familiar Chinese taste. This fusion of culinary influences has garnered widespread

appreciation and acceptance among the local populace.

The inception of this Thai-inspired noodle dish exemplifies the adaptive creativity of Thai restaurants in N City. The integration of local taste preferences with Thai culinary elements not only introduces novel and exciting options to the menu but also reflects the dynamic process of cultural exchange and culinary innovation in the local dining scene.

4. Conclusion

This study delves into the localization process of Thai cuisine in N City, yielding significant insights and fulfilling its research significance. In conclusion, the localization of Thai cuisine in this city has achieved notable success. Contrasted with a decade ago when Thai restaurants were virtually non-existent, the majority of the populace has now acclimated to Thai culinary culture. While this success is evident, there remains a need to further promote unfamiliar dishes, encouraging people to venture into novel tastes, such as the papaya salad. Additionally, the entrenched concept of Thai dining has inspired Chinese chefs to innovate, creating Thai-inspired dishes that seamlessly blend the culinary characteristics of both nations.

The research's significance lies in the backdrop of globalization. The localization of Thai restaurants in N City has introduced Chinese citizens to Thai gastronomic culture, fostering a sense of Thai cultural identity.

Moreover, these restaurants have become a cultural haven for Thai expatriates, offering them a sense of home in China. This cultural exchange has enriched local diversity and facilitated deeper cultural ties between the two nations. In essence, the localization of Thai cuisine in N City not only tantalizes taste buds but also serves as a bridge for cross-cultural understanding, symbolizing the harmonious coexistence of global flavors in a localized setting.

References

[1] 聂春艳,and 刘英为.全球化背景下的文化混搭研究.社会科学家 .07(2023):147-153.

[2][8] 位迎苏,李新蕾.全球化视野下我国饮食类纪录片的文化认同建构——以《风味人间》为例[J].中国电视,2019,(09):45-50.

[3] YOUNGJIN(千永真) C .全球本土化视角下韩餐的整合与创造[D].哈尔滨工业大学,2021.DOI:10.27061/d.cnki.ghgdu.2021.006887

[4] 李杨.中国传统饮食文化的起源及价值传承——评《五味杂陈:中国传统饮食文化》[J].食品安全质量检测学报,2023,14(21):309.DOI:10.19812/j.cnki.jfsq11- 5956/ts.2023.21.025

[5] 王笑楠.跨文化视阈下中国饮食文化话语建构研究[J].食品研究与开发,2021,42(16):244-245.

[6] 马一飞.文化认同与在地化[D].云南大学,2021.DOI:10.27456/d.cnki.gyndu.2021.001331

[7]http://www.gx.xinhuanet.com/20230918/f7c7ebaac25f4116bc51e46423319789/c.html

Zhou Qiaotong

Born on China
Majoring in Interpreting

Turning waste into treasure: An eco-friendly cellulose-based hybrid membrane derived from waste bagasse for wearable applications

Yannan Chen[1], Yuhui Jiang[1], Xuejie Yue[1], Fengxian Qiu[1,*], and Tao Zhang[1,*]

[1] *School of Chemistry and Chemical Engineering, Jiangsu University, China*
**Corresponding author, E-mail:* fxqiu@ujs.edu.cn, zhangtaochem@163.com

Abstract: Sugarcane, as one of the most important crops, plays an important role in the economy around the world. However, huge waste and low treatment efficiency put forward new requirements for bagasse treatment. Herein, a wearable eco-friendly cellulose-based hybrid membrane was fabricated with a view to recycling bagasse. Specifically, the cellulose was extracted from waste bagasse, and the CNT/cellulose@Ag nanoparticles (CCAgNP) hybrid membrane was obtained by magnetron sputtering and blending method. The results indicated that benefiting from the high infrared reflectance (0.82) of the AgNP side and the fast absorbance (1.5) of the CCM side, the CCAgNP can achieve a dual thermal insulation due to the synergistic effect of two sides of the membrane. In addition, the asymmetric wettability of both sides of the hybrid membrane enables sweat to be transported unidirectionally, keeps the skin on the surface of the human body dry. More importantly, the hybrid membrane also shows the excellent antibacterial property, air permeability, mechanical property and thermal stability, providing good support for the practical application of the hybrid membrane. This study shows that the fabrication of hybrid membranes with integrated functionalities can be extended for the fabrication of other wearable materials from agricultural wastes for various applications.
Keywords: Agricultural waste, Resource recycling, Thermal management, Sweat unidirectional penetration, Wearing comfort.

1. Introduction

With the reduction of fossil energy and deterioration of ecological environment, considerable attention has been focused on the development of clean energy technologies and renewable materials [1]. At present, the research on clean energy technologies, such as solar energy, wind energy and geothermal energy, have experienced rapid developments during the past decade [2]. However, the applications of these clean energy technologies are not always satisfied partly due to the energy conversion efficiency and large fluctuations by climate and environmental conditions. Biomass resources, which are renewable and inexhaustible, mainly including a series of substances such as crops, trees and their residues, livestock and poultry manure, among which the most affected by human activities are crops and their waste [3, 4]. In 2019, the world has produced about 2 billion tons of agricultural waste with components of cellulose, hemicellulose and lignin. Nowadays, there are four main methods for treating agricultural waste around the world: incineration, fertilizer, feed and fuel, but all four methods have certain shortcomings: incineration will aggravate the greenhouse effect and cause extreme weather. Fertilizers will further increase pest damage, and when used as feed, they are only suitable for ruminants, and as fuel, transportation costs will increase significantly [5]. Therefore, it is desirable to find an economical and environmentally benign approach to fabricate renewable materials for sustainable applications.

The human body exchanges heat with the outside world all the time to maintain a stable body temperature, and relevant studies have shown that under outdoor conditions, radiation heat dissipation is as high as 60% of the total heat loss of the human body [6]. Additionally, thermal management technologies, as a new type of clean energy technologies that can control human temperature, have attracted the attention of many researchers in recent years [7]. Based on Kirchhoff's law of thermal radiation, the exchange of thermal radiation is mainly related to emissivity, reflectivity and transmittance, but ordinary cotton cloth cannot achieve good thermal insulation effect because of its high radiation emissivity and low reflectivity [8]. Hence, it is of great significance to reduce the radiation heat loss of human body to achieve high-efficiency heat preservation. To adapt the future cold environment, researchers have carried out a series of studies on radiation heat loss pathway to enhance the thermal insulation effect of fabrics. For instance, Guo et al. used bacterial cellulose as the substrate and covered Cu nanowires on one side to strengthen the infrared reflectivity to reinforce the radiation insulation effect [9]. Yue et al. took inspiration from polar bear fur and combined cellulose to prepare a coating of CNTs to construct a bionic thermal insulation material [10]. The results can achieve the purpose of energy saving and emission reduction, but the thermal insulation effect is single, and the thermal insulation performance needs to be magnified. Therefore, to solve the problem of poor thermal insulation performance, new thermal management functional materials with integrated functionalities are urgently needed.

The liquid diode is defined as the fluid device which can permeate the liquid from the hydrophobic (LO) surface to the hydrophilic (LI) surface, but can't permeate in the reverse direction [11]. It can rectify the liquid into directional flow and has special selectivity. Nowadays, aiming at the directional rectification characteristics of liquid diodes, many researchers have carried out some researches on the liquid diode and the operating principle. For example, Li et al. successfully prepared Janus PVDF membrane with asymmetric wettability for rapid oil-water separation [12], while Pan et al. obtained the porous photothermal sponge coated with MXene and Polypyrrole using a simple immersion-coating method for portable seawater desalination without salting-out phenomenon [13]. Although some achievements have been made in the study of liquid diodes, the application scenarios are mainly limited to oil-water separation and seawater desalination, and the research on personal thermal management needs to be deepened. At the same time, the high temperature resistance of desert beetles and spider silk in nature has attracted the attention. After a comprehensive bottom-up exploration of such high-temperature resistant organisms, it was found that they can spontaneously realize the efficient delivery of droplets from the inside to the outside of the surface edge, while preventing backflow in the opposite direction. Sweat is produced by sweat glands of human body, and when it accumulates on the skin surface for a long time, it will cause a series of symptoms such as skin allergy and inflammation [14]. Therefore, it is of significance to study whether fabrics can

unidirectionally penetrate sweat to achieve wet comfort.

In this study, the CCAgNP hybrid membrane based on cellulose with dual thermal insulation effect and rapid sweat unidirectional penetration function was designed and prepared using waste bagasse as raw materials for wearable applications. In this design, the introduction of AgNP and CNTs makes the hybrid membrane have dual dynamic thermal insulation performance. In addition, the design of the asymmetric wetting structure of CCAgNP has constructed a water diode that can achieve unidirectional sweat penetration to expand the function of the hybrid membrane. Through a large number of tests and analyses, the composition and structure, thermal management performance, unidirectional sweat penetration performance and wearing comfort of CCAgNP were verified. The work puts forward the construction of an environment-friendly wearable material, which has a potential application prospect in the field of personal thermal management.

2. Materials and methods

2.1. Materials

Sodium hydroxide (NaOH), sodium dodecyl benzene sulfonate (SDBS), acetic acid (CH_3COOH), urea ($CO(NH_2)_2$), sodium chlorite ($NaClO_2$) and sulfuric acid (H_2SO_4) were purchased by Sinopharm Chemical Regent Co., Ltd. (Shanghai, China). Multi-walled carbon nanotubes (MWCNTs) were obtained from Suzhou TANFENG graphene Tech Co., Ltd. Dried sugarcane bagasse was collected from local farms (September, Zhenjiang, China) as the raw materials to extract the bagasse cellulose. All reagents were used directly and without further processing Additionally, the distilled water was used throughout the process.

2.2. Fabrication of CNT/cellulose membrane (CCM)

In this experiment, the bagasse cellulose microfibers were extracted by chlorite and alkaline extraction method, then vacuum filtration method was used to obtain the CNT/cellulose membrane (CCM). As a typical doping process, the CNTs needed to be dispersed into the SDBS solution to form 1.0 wt% CNT dispersion in advance for pretreatment, the ratio of SDBS to CNT was 1.5/1 (w/w), and ultrasonic treatment was carried out at 140 W power for 2 hours. Then 7 g NaOH, 12 g urea, 77 g distilled water, and 4 g CNT aqueous dispersion were mixed to obtain a NaOH/urea/CNTs aqueous system, followed by stirring 10 min and pre-cooled to -6 °C. After that, 4 g of sugarcane bagasse cellulose was added into the mixture to stir vigorously for 5 min to obtain a suspension, subsequently 5 wt% H2SO4 solution was added to prevent cellulose coagulation and regeneration. Finally, the CNT/cellulose membrane was obtained by vacuum filtration, followed by placing the membrane on a glass sheet to avoid shrinkage.

2.3. Fabrication of CNT/cellulose membrane (CCM)

The CNT/cellulose@Ag nanoparticles (CCAgNP) hybrid membrane was successfully fabricated by a controllable magnetron sputtering process. In a typical experiment, the CCM was placed flat on the sample table, and the quartz balance sensor is placed at the same level as the metal clad substrate. Then place the substrate on a rotating stage 10 cm below the metal target, followed by the sample was vacuumized, and Ag nanoparticles were sputtered for 6 minutes with 5 W power. After sputtering, it is worth noting that the silver nanoparticles were uniformly coated on the surface of CCM. Finally, after cooling to the room temperature, the double-layer CCAgNP membrane was obtained.

2.4. Thermal insulation property test

The optical properties of materials are closely related to the thermal insulation property. In order to avoid radiation heat loss, the infrared reflectivity of materials is worth testing. The reflectivity spectra of the CCAgNP was measured by Fourier transform infrared spectroscopy (FT-IR, Nicolet iS50, Nicolet, USA) equipped with an integrating sphere. To compare the difference between CCAgNP and common cotton cloth for thermal management application, an infrared thermal camera (FLIR, T630sc, China) was used to test the thermal images of CCAgNP, CCM and common cotton cloth for more intuitive observation. Concretely, CCAgNP, CCM and common cotton cloth were cut into 1 cm × 1 cm and connected with copper tapes for electrical contacts. And a heater was connected to a power supply, providing a heating power density of about 100 W/m2 to simulate the metabolic heat production rate of the human body. Besides, in order to verify the efficient photo-thermal conversion efficiency of CCAgNP, the thermal insulation property was tested by simulating sunlight irradiation while maintaining a constant temperature of 37 ℃ on the hot stage, and the surface temperature change of the membrane was observed by combining with an infrared thermal camera.

2.5. Sweat unidirectional penetration property test

The sweat accumulated on the skin surface for a long time can't be discharged, which will do harm to human skin. The principle of sweat unidirectional penetration is to conduct human sweat from the inner side to the outer side of clothes through the fiber side, then let the sweat evaporate under the air circulation, thus keeping the skin dry and avoiding the accumulation of moisture and unpleasant odor in the clothes themselves. To investigate wet comfort, the sweat unidirectional penetration property was tested by measuring the contact angle between the two sides of the hybrid membrane and water droplets. As a typical experiment, the CCAgNP was cut into strips 250-mm-wide and 250-mm-long and hang horizontally on the test bench, then dropped the droplet during the test time. A needle tube with a diameter of about 0.2 mm was used to add liquid droplets to the surface of the hybrid membrane at a speed of 40 mL/h, and the penetration of the water droplets was recorded within 60 s. The whole test process was carried out indoors, and the temperature and humidity remained basically unchanged. During the test, the droplets come into contact with the surface of the hybrid film to simulate typical test conditions, and then the wicking performance within 60 seconds is recorded through a microscope camera. After testing, the used membrane can be recycled after rinsing in ethanol to remove the liquid.

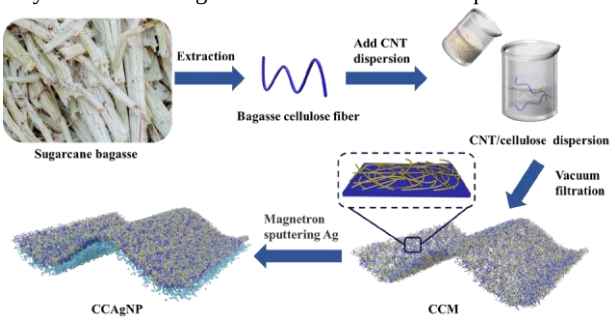

Scheme 1. Illustration of the fabrication procedures of the multifunctional CCAgNP

3. Results and discussion

3.1. Characterizations

The surface morphology of the CCAgNP is determined by using SEM, and the results are shown in Figure 1. It can be seen that the surface becomes rough and there is a bumpy structure after doping with CNTs. And the high magnification map clearly exhibits that CNTs with high aspect ratio are intertwined with each other and distributed on the surface of the fiber in a continuous random network structure, and the

rough surface helps to reduce the infrared transmittance on this side, thereby reducing radiation heat loss, while the existence of CNTs enhances the photothermal conversion efficiency, and efficiently utilizes sunlight to realize thermal energy storage. After magnifying the AgNP layer, it can be observed that AgNP has small diameter, with large gap between particles, uniformly loaded on the base membrane, which indicates that AgNP has been successfully deposited on the surface of CCM.

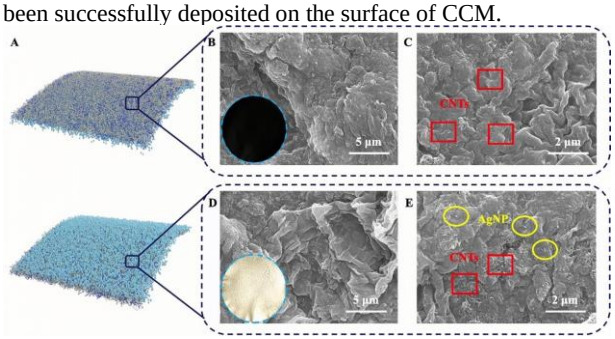

Figure 2. Schematic diagram of the simulation on the (A) CCAgNP, SEM images of (B~C) CCM side, (D~E) AgNP side

X-ray diffraction (XRD) is used to test the material composition and crystal phase structure, and the results are shown in Figure 2. It can be seen that cellulose from bagasse exhibits sharp characteristic peaks at 15.4°, 16.9°, 22.7° and 34.6°, respectively, corresponding to the (1-10), (110), (200) and (004) crystal planes of cellulose Iβ (JCPDS No. 50-2241). The characteristic peaks of CCM are shown at 15° and 22.6°, which can be indexed to the cellulose in bagasse. Among them, the peak at about 15° can be seemed as the (1-10) and (110) overlapped peak. It can be seen that there are four obvious and sharp peaks on one side of AgNP, with 38.3°, 44.4°, 64.7°, and 77.5°, which correspond to the four different crystal planes of (111), (200), (220), and (311), respectively, indicating that the high purity of AgNP. Combining these two results, the content of different components on both sides of the hybrid membrane is displayed, and the hybrid membrane is successfully prepared.

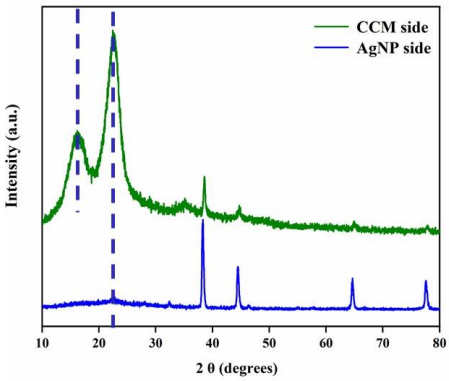

Figure 2. XRD patterns of the two sides of the CCAgNP

3.2 Thermal insulation property

In order to verify the thermal insulation property of CCAgNP, the reflectivity of both sides of the hybrid membrane are measured at first. As shown in Figure 3A, it means the higher the reflectivity of fabric, the better thermal insulation property. Due to the smooth surface of AgNP, the infrared reflectivity of AgNP surface is as high as 0.82, which can effectively reflect infrared radiation back to human body, achieving a more effective warm-keeping effect than common cotton cloth. For further verification of the thermal insulation property of the hybrid membrane, the inside temperature is recorded by a temperature sensor, and its thermal imaging was photographed by an infrared camera (Figure 3B). Correspondingly, the absorbance in the solar radiation region confirms the utilization effect and photothermal conversion degree of CCM side under sunlight (Figure 3C). The higher the photothermal conversion efficiency was, the better the thermal insulation performance would be. As shown in Figure 4C, one side of CCM has a high absorption rate in the visible light range of 380-780 nm, which can efficiently and rapidly convert light energy into heat energy to realize heat preservation. The simulated sunlight experiment proves that CCAgNP has good thermal insulation performance in sunlight. The Figure 3D shows that CCAgNP can heat up to 51.3 ℃ in a short time, which is based on the excellent photothermal conversion performance of CNTs.

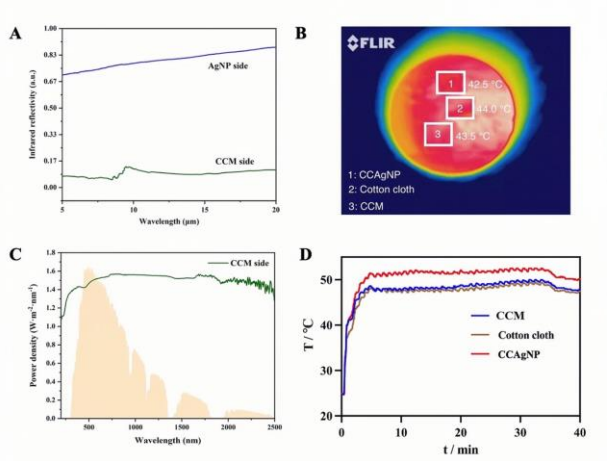

Figure 3. (A) Infrared reflectivity of both sides of CCAgNP, (B) thermal images of common cotton cloth, CCM and CCAgNP, (C) absorbance of CCM side at different wavelengths and (D) temperature change of common cotton cloth, CCM and CCAgNP under the condition of simulating sunlight

3.3 Sweat unidirectional penetration property

According to the theory of liquid diode, liquid can permeate from LO to LI, but not in the opposite direction. In order to verify the directional permeability of CCAgNP, the water contact angle of both sides of the hybrid membrane is measured at first, and the penetration property is shown in Figure 4. When the water droplets fall on both sides of the CCAgNP for an instant, the water contact angles of 53.6° and 116.2° are formed on the CCM side and the AgNP side, respectively.

Furthermore, it can be seen that when the water droplets fall on the CCM side, the water droplets cannot pass through the hybrid membrane, due to the blocking effect of the hydrophobic layer. Instead, the water droplets spread out on the CCM side. And when the water droplets are in contact with the AgNP side, it can be seen that within 60 s, the water droplets are gradually absorbed by the CCM side, then penetrate through the membrane and drip under the action of gravity. The reason for this phenomenon is that the droplet is subjected to hydraulic pressure and Laplace pressure on the membrane surface. When the droplet falls on the hydrophobic side, the upward Laplace pressure is cancelled, and the downward hydraulic pressure and gravity drive the droplet to penetrate. However, when the droplet falls on the hydrophilic side, the hydrophobic upward hydraulic pressure blocks the downward movement of the droplet, thereby spreading on the hydrophilic side.

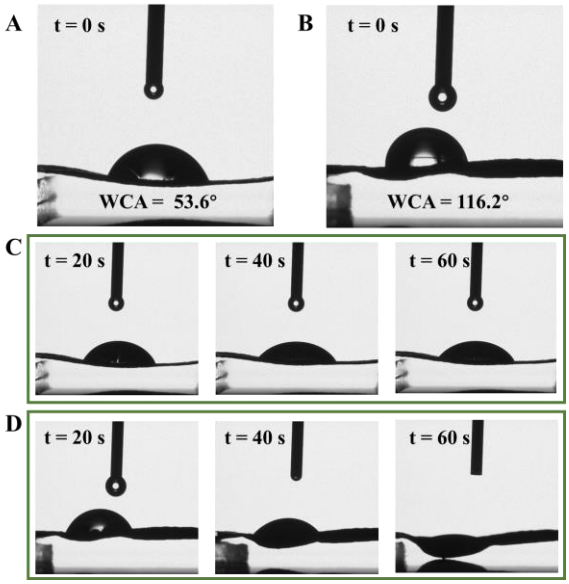

Figure 4. The water contact angle of water droplet on both sides of theCCAgNP at initial:(A) CCM side, (B) AgNP, sweat unidirectional penetration property of the CCAgNP within 60s: (C) from CCM side to AgNP side, and (D) from AgNP side to CCM side

3.4 Wearing comfort properties

Escherichia coli (*E. coli*) and Staphylococcus aureus (*S. aureus*), as two common bacteriums, are harmful to human health, so the antibacterial property of fabrics is particularly important. The antibacterial activities of cellulose and the CCAgNP are evaluated against E. coli and S. aureus under the same condition. As can be seen from Figure 5(A, B), there is no bacteriostatic area around ordinary cotton cloth, but there is obvious bacteriostatic area around the CCAgNP, which indicates that the hybrid membrane has antibacterial property. The results in Figure 5C show that the air permeability of the hybrid membrane is 1.043 mg/(cm^2·h), which is only 0.229 mg/(cm^2·h) lower than that of ordinary cotton cloth. It is evident that the air permeability of CCAgNP is superior to the wearable materials that contain metal in the first two cases, representing a significant improvement. Notably, the air permeability of the third material is even better than cotton cloth, because it contains highly commercialized polyester polyurethane, and the high polymerization and strong intermolecular force characteristics give it excellent air permeability.

Also, it is worth noting in Figure 5D that the mechanical properties of CCAgNP are slightly higher than cellulose, but slightly lower than CCM, but it still retains considerable mechanical strength. This is because the CNTs in the CCM are embedded between the cellulose fibers, forming intermolecular forces to enhance the stress, while the AgNP is small in size and cannot cross-link with the CCM side, thus causing the stress of the CCAgNP to decrease. Meanwhile, in order to verify the thermal stability of CCAgNP, the thermal stability of this sample was tested. The results are shown in Figure 5E. It can be seen that at 200 ℃, the weight of CCAgNP is only reduced by 3%, which is due to the evaporation of bound and free water in the cellulose, and the trend indicates that the hybrid membrane has good thermal stability in the daily temperature environment. With the increase in temperature, cellulose gradually decomposes, and thus it shows a downward trend.

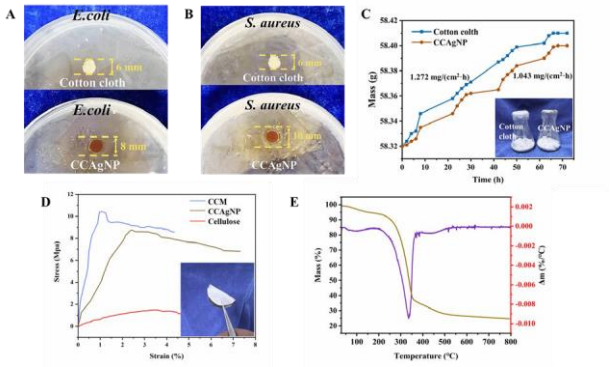

Figure 5. Wearing comfort properties of CCAgNP: (A~B) antibacterial property, (C) air permeability, (D) mechanical property and (E) thermal stability

4. Conclusions

In summary, an eco-friendly cellulose-based hybrid membrane derived from waste bagasse was designed and prepared by one-spot hydrothermal method and magnetron sputtering method, which satisfies the effective recycling of biomass resources. Besides, the hybrid membrane can effectively reflect the human body because of the infrared reflectivity of the AgNP layer up to 0.82, and achieve the purpose of heat preservation with the help of the human body itself. At the same time, based on the excellent photothermal conversion efficiency of CNTs, the temperature can quickly heat up to 51.9 ℃ in 10 minutes under the illumination condition, which forms a dual heat insulation effect when combined with radiation heat preservation. Moreover, the two sides of the hybrid membrane meet the asymmetric wettability, and the water contact angle of CCM side is only 53.6°, while that of AgNP side is as high as 116.2°, thus realizing the unidirectional penetration of sweat and keeping the skin dry to achieve a wet comfortable effect. In addition, the hybrid membrane also shows excellent antibacterial property, air permeability, mechanical property and thermal stability, meeting the requirements of people on fabric comfort. Generally, the results show that the hybrid membrane with integrated functionalization can not only be used in the wearable field, but also provide new strategies in the field of biomass resource recycling.

References

[1] Y. Jin, S. Hu, A.D. Ziegler, L. Gibson, J.E. Campbell, R. Xu, D. Chen, K. Zhu, Y. Zheng, B. Ye, F. Ye, Z. Zeng. (2023) Energy production and water savings from floating solar photovoltaics on global reservoirs, Nature Sustainability, 6 865-874.

[2] H. Shan, P. Poredos, Z. Ye, H. Qu, Y. Zhang, M. Zhou, R. Wang, S.C. Tan. (2023) All-Day Multicyclic Atmospheric Water Harvesting Enabled by Polyelectrolyte Hydrogel with Hybrid Desorption Mode, Adv Mater, 35 e2302038.

[3] N. Gupta, B.K. Mahur, A.M.D. Izrayeel, A. Ahuja, V.K. Rastogi. (2022) Biomass conversion of agricultural waste residues for different applications: a comprehensive review, Environ Sci Pollut Res Int, 29 73622-73647.

[4] F. Xu, C.F. Liu, Z.C. Geng, J.X. Sun, R.C. Sun, B.H. Hei, L. Lin, S.B. Wu, J. Je. (2006) Characterisation of degraded organosolv hemicelluloses from wheat straw, Polymer Degradation and Stability, 91 1880-1886.

[5] E. Capanoglu, E. Nemli, F. Tomas-Barberan. (2022) Novel Approaches in the Valorization of Agricultural Wastes and Their Applications, J Agric Food Chem, 70 6787-6804.

[6] Y. Peng, Y. Cui. (2020) Advanced Textiles for Personal Thermal Management and Energy, Joule, 4 724-742.
[7] Z. Guo, Y. Wang, J. Huang, S. Zhang, R. Zhang, D. Ye, G. Cai, H. Yang, S. Gu, W. Xu. (2021) Multi-functional and water-resistant conductive silver nanoparticle-decorated cotton textiles with excellent joule heating performances and human motion monitoring, Cellulose, 28 7483-7495.
[8] M. He, B. Zhao, X. Yue, Y. Chen, F. Qiu, T. Zhang. (2023) Infrared radiative modulating textiles for personal thermal management: principle, design and application, Nano Energy, 116.
[9] Z. Guo, C. Sun, J. Wang, Z. Cai, F. Ge. (2021) High-Performance Laminated Fabric with Enhanced Photothermal Conversion and Joule Heating Effect for Personal Thermal Management, ACS Appl Mater Interfaces, 13 8851-8862.
[10] X. Yue, M. He, T. Zhang, D. Yang, F. Qiu, Laminated Fibrous Membrane Inspired by Polar Bear Pelt for Outdoor Personal Radiation Management, ACS Appl Mater Interfaces, 12 (2020) 12285-12293.
[11] X. Yu, S. Kang, X. Jiao, H. Lai, R. Wang, Z. Cheng. (2023) A smart underoil“water diode”Janus TiO2 mesh membrane, Chemical Engineering Journal, 456.
[12] T. Li, F. Liu, S. Zhang, H. Lin, J. Wang, C.Y. Tang. (2018) Janus Polyvinylidene Fluoride Membrane with Extremely Opposite Wetting Surfaces via One Single-Step Unidirectional Segregation Strategy, ACS Appl Mater Interfaces, 10 24947-24954.
[13] Y. Pan, E. Li, Y. Wang, C. Liu, C. Shen, X. Liu. (2022) Simple Design of a Porous Solar Evaporator for Salt-Free Desalination and Rapid Evaporation, Environ Sci Technol, 56 11818-11826.
[14] J. Liu, L. Zhang, N. Wang, H. Zhao, C. Li. (2022) Nanofiber-reinforced transparent, tough, and self-healing substrate for an electronic skin with damage detection and program-controlled autonomic repair, Nano Energy, 96.

Ms. Yannan Chen
Master student, Master of Engineering (Chemical Engineering).
Research Interests:
Biomass materials, and Thermal management materials.

Ms. Yuhui Jiang
Master student, Master of Science (Chemistry).
Research Interests:
Recycling of solid waste, and Environmental governance

Dr. Xuejie Yue
Lecturer
Research Interests:
Green separation technology, Infrared energy-saving material

Prof. Fengxian Qiu
Professor
Research Interests:
Biomass materials, Thermal management technology, Green separation technology

Dr. Tao Zhang
Assistant Professor
Research Interests:
Biomass materials, Recycling of solid waste, Thermal management materials

29th TRY-U2023

empowering young researchers for a better future

MAEJO UNIVERSITY
90th ANNIVERSARY